Selected Topics in Superconductivity

Quantum Statistical Theory of Superconductivity

Shigeji Fujita
and
Salvador Godoy

Quantum Statistical Theory of Superconductivity

SELECTED TOPICS IN SUPERCONDUCTIVITY

Series Editor: Stuart Wolf
Naval Research Laboratory
Washington, D. C.

CASE STUDIES IN SUPERCONDUCTING MAGNETS
Design and Operational Issues
Yukikazu Iwasa

INTRODUCTION TO HIGH-TEMPERATURE SUPERCONDUCTIVITY
Thomas P. Sheahen

THE NEW SUPERCONDUCTORS
Frank J. Owens and Charles P. Poole, Jr.

QUANTUM STATISTICAL THEORY OF SUPERCONDUCTIVITY
Shigeji Fujita and Salvador Godoy

STABILITY OF SUPERCONDUCTORS
Lawrence Dresner

Quantum Statistical Theory of Superconductivity

Shigeji Fujita
SUNY, Buffalo
Buffalo, New York

and

Salvador Godoy
Universidad Nacional Autonoma de México
México, D. F., México

Kluwer Academic Publishers

NEW YORK, BOSTON, DORDRECHT, LONDON, MOSCOW

eBook ISBN 0-306-47068-3
Print ISBN 0-306-45363-0

Created in the United States of America

Visit Kluwer Online at: http://www.kluweronline.com
and Kluwer's eBookstore at: http://www.ebooks.kluweronline.com

Preface to the Series

Since its discovery in 1911, superconductivity has been one of the most interesting topics in physics. Superconductivity baffled some of the best minds of the 20th century and was finally understood in a microscopic way in 1957 with the landmark Nobel Prize-winning contribution from John Bardeen, Leon Cooper, and Robert Schrieffer. Since the early 1960s there have been many applications of superconductivity including large magnets for medical imaging and high-energy physics, radio-frequency cavities and components for a variety of applications, and quantum interference devices for sensitive magnetometers and digital circuits. These last devices are based on the Nobel Prize-winning (Brian) Josephson effect. In 1987, a dream of many scientists was realized with the discovery of superconducting compounds containing copper–oxygen layers that are superconducting above the boiling point of liquid nitrogen. The revolutionary discovery of superconductivity in this class of compounds (the cuprates) won Georg Bednorz and Alex Mueller the Nobel Prize.

This series on Selected Topics in Superconductivity will draw on the rich history of both the science and technology of this field. In the next few years we will try to chronicle the development of both the more traditional metallic superconductors as well as the scientific and technological emergence of the cuprate superconductors. The series will contain broad overviews of fundamental topics as well as some very highly focused treatises designed for a specialized audience.

This page intentionally left blank.

Preface

Superconductivity is a striking physical phenomenon that has attracted the attention of physicists, chemists, engineers, and also the nontechnical public. The theory of superconductivity is considered difficult. Lectures on the subject are normally given at the end of Quantum Theory of Solids, a second-year graduate course.

In 1957 Bardeen, Cooper, and Schrieffer (BCS) published an epoch-making microscopic theory of superconductivity. Starting with a Hamiltonian containing electron and hole kinetic energies and a phonon-exchange-pairing interaction Hamiltonian, they demonstrated that (1) the ground-state energy of the BCS system is lower than that of the Bloch system without the interaction, (2) the unpaired electron (quasi-electron) has an energy gap Δ_0 at 0 K, and (3) the critical temperature T_c can be related to Δ_0 by $2\Delta_0 = 3.53\ k_B T_c$, and others. A great number of theoretical and experimental investigations followed, and results generally confirm and support the BCS theory. Yet a number of puzzling questions remained, including why a ring supercurrent does not decay by scattering due to impurities which must exist in any superconductor; why monovalent metals like sodium are not superconductors; and why compound superconductors, including intermetallic, organic, and high-T_c superconductors exhibit magnetic behaviors different from those of elemental superconductors.

Recently the present authors extended the BCS theory by incorporating band structures of both electrons and phonons in a model Hamiltonian. By doing so we were able to answer the preceding questions and others. We showed that under certain specific conditions, elemental metals at low temperatures allow formation of Cooper pairs by the phonon exchange attraction. These Cooper pairs, called the pairons, for short, move as free bosons with a linear energy–momentum relation. They neither overlap in space nor interact with each other. Systems of pairons undergo Bose–Einstein condensations in two and three dimensions. The supercondensate in the ground state of the generalized BCS system is made up of large and equal numbers of ± pairons having charges $\pm 2e$, and it is electrically neutral. The ring supercurrent is generated by the ± pairons condensed at a single momentum $q_n = 2\pi n \hbar L^{-1}$, where L is the ring length and n an integer. The macroscopic supercurrent arises from the fact that ± pairons move with different speeds. Josephson effects are manifestations of the fact that pairons do not interact with each other and move like massless bosons just as photons do. Thus there is a close analogy between a supercurrent and a laser. All superconductors, including high-T_c cuprates, can be treated in a unified manner, based on the generalized BCS Hamiltonian.

Because the supercondensate can be described in terms of independently moving pairons, all properties of a superconductor, including ground-state energy, critical temperature, quasi-particle energy spectra containing gaps, supercondensate density, specific heat, and supercurrent density can be computed without mathematical complexities. This simplicity is in great contrast to the far more complicated treatment required for the phase transition in a ferromagnet or for the familiar vapor–liquid transition.

The authors believe that everything essential about superconductivity can be presented to beginning second-year graduate students. Some lecturers claim that much physics can be learned without mathematical formulas, that excessive use of formulas hinders learning and motivation and should therefore be avoided. Others argue that learning physics requires a great deal of thinking and patience, and if mathematical expressions can be of any help, they should be used with no apology. The average physics student can learn more in this way. After all, learning the mathematics needed for superconductor physics and following the calculational steps are easier than grasping basic physical concepts. (The same cannot be said about learning the theory of phase transitions in ferromagnets.) The authors subscribe to the latter philosophy and prefer to develop theories from the ground up and to proceed step by step. This slower but more fundamental approach, which has been well-received in the classroom, is followed in the present text. Students are assumed to be familiar with basic differential, integral, and vector calculuses, and partial differentiation at the sophomore–junior level. Knowledge of mechanics, electromagnetism, quantum mechanics, and statistical physics at the junior–senior level are prerequisite.

A substantial part of the difficulty students face in learning the theory of superconductivity lies in the fact that they need not only a good background in many branches of physics but must also be familiar with a number of advanced physical concepts such as bosons, fermions, Fermi surface, electrons and holes, phonons, Debye frequency, and density of states. To make all of the necessary concepts clear, we include five preparatory chapters in the present text. The first three chapters review the free-electron model of a metal, theory of lattice vibrations, and theory of the Bose–Einstein condensation. There follow two additional preparatory chapters on Bloch electrons and second quantization formalism. Chapters 7–11 treat the microscopic theory of superconductivity. All basic thermodynamic properties of type I superconductors are described and discussed, and all important formulas are derived without omitting steps. The ground state is treated by closely following the original BCS theory. To treat quasi-particles including Bloch electrons, quasi-electrons, and pairons, we use Heisenberg's equation-of-motion method, which reduces a quantum many-body problem to a one-body problem when the system-Hamiltonian is a sum of single-particle Hamiltonians. No Green's function techniques are used, which makes the text elementary and readable. Type II compounds and high-T_c superconductors are discussed in Chapters 12 and 13, respectively. A brief summary and overview are given in the first and last chapters.

In a typical one-semester course for beginning second-year graduate students, the authors began with Chapter 1, omitted Chapters 2–4, then covered Chapters 5–11 in that order. Material from Chapters 12 and 13 was used as needed to enhance the student's interest. Chapters 2–4 were assigned as optional readings.

The book is written in a self-contained manner so that nonphysics majors who want to learn the microscopic theory of superconductivity step by step in no particular hurry

may find it useful as a self-study reference. Many fresh, and some provocative, views are presented. Researchers in the field are also invited to examine the text.

Problems at the end of a section are usually of a straightforward exercise type directly connected to the material presented in that section. By solving these problems, the reader should be able to grasp the meanings of newly introduced subjects more firmly.

The authors thank the following individuals for valuable criticism, discussion, and readings: Professor M. de Llano, North Dakota State University; Professor T. George, Washington State University; Professor A. Suzuki, Science University of Tokyo; Dr. C. L. Ko, Rancho Palos Verdes, California; Dr. S. Watanabe, Hokkaido University, Sapporo. They also thank Sachiko, Amelia, Michio, Isao, Yoshiko, Eriko, George Redden, and Brent Miller for their encouragement and for reading the drafts. We thank Celia García and Benigna Cuevas for their typing and patience. We specially thank César Zepeda and Martin Alarcón for their invaluable help with computers, providing software, hardware, as well as advice. One of the authors (S. F.) thanks many members of the Deparatmento de Física de la Facultad de Ciencias, Universidad Nacional Autónoma de México for their kind hospitality during the period when most of this book was written. Finally we gratefully acknowledge the financial support by CONACYT, México.

Shigeji Fujita

Salvador Godoy

This page intentionally left blank.

Contents

Constants, Signs, and Symbols

Useful Physical Constants

Quantity	Symbol	Value
Absolute zero on Celsius scale		–273.16°C
Avogadro's number	N_0	6.02×10^{23}
Boltzmann constant	k_B	1.38×10^{-16} erg K^{-1} = 1.38×10^{-23} J K^{-1}
Bohr magneton	μ_B	9.22×10^{-21} erg $gauss^{-1}$
Bohr radius	a_0	5.29×10^{-9} cm = 5.29×10^{-11} m
Electron mass	m	0.911×10^{-27} g = 9.11×10^{-31} kg
Electron charge (magnitude)	e	4.80×10^{-10} esu = 1.6×10^{-19} C
Gas constant	R	8.314 J $mole^{-1}$ K^{-1}
Molar volume (gas at STP)		2.24×10^4 cm^3 = 22.4 liter
Mechanical equivalent of heat		4.186 J cal^{-1}
Permeability constant	μ_0	1.26×10^{-6} H/m
Permittivity constant	ϵ_0	8.85×10^{-12} F/m
Planck's constant	h	6.63×10^{-27} erg sec = 6.63×10^{-34} J s
Planck's constant/2π	$\hbar$	1.05×10^{-27} erg sec = 1.05×10^{-34} J s
Proton mass	m_p	1.67×10^{-24} g = 1.67×10^{-27} kg
Speed of light	c	3.00×10^{10} cm/sec^{-1} = 3.00×10^8 m sec^{-1}

Mathematical Signs and Symbols

$=$	equals
$\simeq$	equals approximately
$\neq$	not equal to
$\equiv$	identical to, defined as
$>$	greater than
$\gg$	much greater than
$<$	less than

$\ll$	much less than
$\geq$	greater than or equal to
$\leq$	less than or equal to
$\propto$	proportional to
$\sim$	represented by, of the order
$\langle x \rangle$, $\bar{x}$	the average value of x
ln	natural logarithm
Δx	increment in x
dx	infinitesimal increment in x
z^*	complex conjugate of a number z
$\alpha^\dagger$	Hermitian conjugate of operator (matrix) α
α^T	transpose of matrix α
P^{-1}	inverse of P
$\delta_{a,b} = \begin{cases} 1 & \text{if } a = b \\ 0 & \text{if } a \neq b \end{cases}$	Kronecker' s delta
$\delta(x)$	Dirac' s delta function
∇	nabla or de1 operator
$\dot{x} \equiv dx/dt$	time derivative
grad $\phi \equiv \nabla\phi$	gradient of ϕ
div $\mathbf{A} \equiv \nabla \cdot \mathbf{A}$	divergence of $\mathbf{A}$
curl $\mathbf{A} \equiv \nabla \times \mathbf{A}$	curl of $\mathbf{A}$
∇^2	Laplacian operator

List of Symbols

The following list is not intended to be exhaustive. It includes symbols of special importance.

Å	Ångstrom (= 10^{-8} cm = 10^{-10} m)
$\mathbf{A}$	vector potential
$\mathbf{B}$	magnetic field (magnetic flux density)
C	heat capacity
c	velocity of light
c	specific heat
$\mathcal{D}(p)$	density of states in momentum space
$\mathcal{D}(\omega)$	density of states in angular frequency
E	total energy
E	internal energy
$\mathbf{E}$	electric field
e	base of natural logarithm
e	electronic charge (absolute value)

F	Helmholtz free energy
f	one-body distribution function
f_B	Bose distribution function
f_F	Fermi distribution function
f_0	Planck distribution function
G	Gibbs free energy
H	Hamiltonian
H_c	critical magnetic field
$\mathbf{H}_a$	applied magnetic field
$\mathcal{H}$	Hamiltonian density
h	Planck's constant
h	single-particle Hamiltonian
$\hbar$	Planck's constant divided by 2π
$i \equiv \sqrt{-1}$	imaginary unit
i, j, k	Cartesian unit vectors
J	Jacobian of transformation
J	total current
j	single-particle current
j	current density
k	angular wave vector $\equiv k$-vector
k_B	Boltzmann constant
L	Lagrangian function
L	normalization length
ln	natural logarithm
$\mathcal{L}$	Lagrangian density
l	mean free path
M	molecular mass
m	electron mass
m^*	effective mass
N	number of particles
$\hat{N}$	number operator
$\mathcal{N}(\epsilon)$	Density of states in energy
n	particle number density
P	pressure
P	total momentum
p	momentum vector
p	momentum (magnitude)
Q	quantity of heat
R	resistance
R	position of the center of mass
r	radial coordinate

$\mathbf{r}$	position vector
S	entropy
T	kinetic energy
T	absolute temperature
T_c	critical (condensation) temperature
T_F	Fermi temperature
t	time
TR	sum of N particle traces $\equiv$ grand ensemble trace
Tr	many-particle trace
tr	one-particle trace
V	potential energy
V	volume
$\mathbf{v}$	velocity (field)
W	work
Z	partition function
$e^{\alpha} \equiv z$	fugacity
$\beta \equiv (k_B T)^{-1}$	reciprocal temperature
Δx	small variation in x
$\delta(x)$	Dirac delta function
$\delta_P = \begin{cases} +1 & \text{if } P \text{ is even} \\ -1 & \text{if } P \text{ is odd} \end{cases}$	parity sign of the permutation P
$\in$	energy
$\in_F$	Fermi energy
η	viscosity coefficient
Θ_D	Debye temperature
Θ_E	Einstein temperature
θ	polar angle
λ	wavelength
λ	penetration depth
κ	curvature
μ	linear mass density of a string
μ	chemical potential
μ_B	Bohr magneton
ν	frequency = inverse of period
Ξ	grand partition function
ξ	dynamical variable
ξ	coherence length
ρ	mass density
ρ	density operator, system density operator
ρ	many-particle distribution function
σ	total cross section

σ	electrical conductivity
$\sigma_x, \sigma_y, \sigma_z$	Pauli spin matrices
τ	tension
τ_d	duration of collision
τ_c	average time between collisions
ϕ	azimuthal angle
ϕ	scalar potential
Ψ	quasi wave function for many condensed bosons
ψ	wave function for a quantum particle
$d\Omega = \sin\theta d\theta d\phi$	element of solid angle
$\omega \equiv 2\pi\nu$	angular frequency
ω_c	rate of collision
ω_D	Debye frequency
[,]	commutator brackets
{, }	anticommutator brackets
{, }	Poisson brackets
$[A]$	dimension of A

This page intentionally left blank.

Introduction

In this chapter we describe basic experimental facts, theoretical background, thermodynamics of superconductors and our microscopic approach to superconductivity including the historical developments.

1.1. BASIC EXPERIMENTAL FACTS

1.1.1. Zero Resistance

Superconductivity was discovered by Kamerlingh Onnes[1] in 1911 when he measured extremely small (zero) resistance in mercury below a certain critical temperature T_c (≈ 4.2 K). His data are reproduced in Fig. 1.1. This *zero resistance* property can be confirmed by a never-decaying supercurrent ring experiment described in Section 1.1.3.

1.1.2. Meissner Effect

Substances that become superconducting at finite temperatures will be called *superconductors* in the present text. If a superconductor below T_c is placed under a weak magnetic field, it repels the magnetic flux (field) **B** completely from its interior as shown in Fig. 1.2 (see the cautionary remark on p. 18). This is called the *Meissner effect,* and

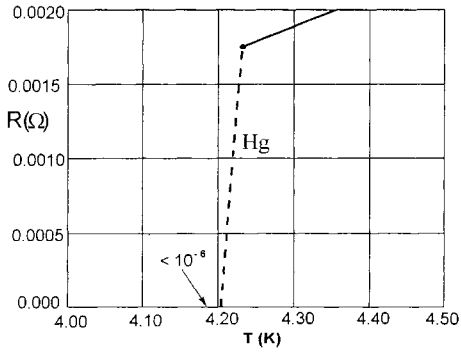

Figure 1. 1. Resistance versus temperature.

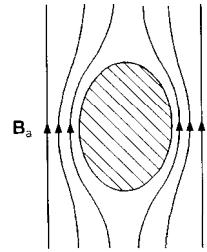

Figure 1.2. A superconductor expels a weak magnetic field (Meissner effect).

it was first discovered by Meissner and Ochsenfeld[2] in 1933.

The Meissner effect can be demonstrated dramatically by a floating magnet as shown in Fig. 1.3. A small bar magnet above T_c simply rests on a superconductor dish. If temperature is lowered below T_c, the magnet will float as indicated. The gravitational force exerted on the magnet is balanced by the magnetic pressure due to the inhomogeneous B-field surrounding the magnet, that is represented by the magnetic flux lines as shown.

1. 1. 3. Ring Supercurrent

Let us take a ring-shaped superconductor. If a weak magnetic field **B** is applied along the ring axis and temperature is lowered below T_c, the field is expelled from the ring due to the Meissner effect. If the field is slowly reduced to zero, part of the magnetic flux lines may be trapped as shown in Fig. 1.4. It was observed that the magnetic moment so generated is maintained by a never-decaying supercurrent around the ring.[3]

1.1.4. Magnetic Flux Quantization

More delicate experiments [4,5] showed that the magnetic flux Φ enclosed by the ring is quantized:

$$\Phi = n\Phi_0, \qquad n = 0, 1, 2, \ldots \tag{1.1.1}$$

$$\Phi_0 \equiv \frac{\pi\hbar}{e} = 2.07 \times 10^{-7} \text{ Gauss cm}^2 \tag{1.1.2}$$

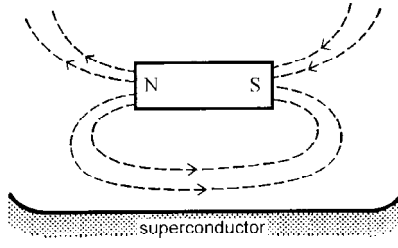

Figure 1.3. A floating magnet.

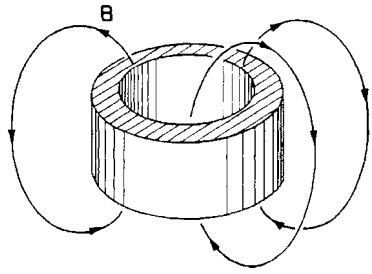

Figure 1.4. A set of magnetic flux lines are trapped in the ring.

Φ_0 is called a *flux quantum.* The experimental data obtained by Deaver and Fairbank[4] is shown in Fig. 1.5. The superconductor exhibits a *quantum state* described by a kind of a macro-wave function. [6,7]

1.1.5. Critical Magnetic Field

If a sufficiently strong magnetic field **B** is applied to a superconductor, superconductivity will be destroyed. The *critical magnetic field* $B_c(T)$, that is, the minimum field that destroys superconductivity, increases as temperature is lowered, so it reaches a maximum value $B_c(0) \equiv B_0$ as $T \to 0$. For pure elemental superconductors, the critical field B_0 is not very high. For example the value of B_0 for mercury (Hg), tin (Sn) and lead (Pb) are 411, 306, and 803 G (Gauss), respectively. The highest, about 2000 G, is exhibited by niobium (Nb). Figure 1.6 exhibits the temperature variation of the critical magnetic field $B_c(T)$ for some elemental superconductors.

1.1.6. Heat Capacity

At very low temperatures, the heat capacity of a normal metal has the temperature dependence $aT + bT^3$, where the linear term is due to the conduction electrons and the cubic term to phonons. The heat capacity C of a superconductor exhibits quite a different behavior. As temperature is lowered through T_c, C jumps to a higher value and then drops like T^3 near T_c.[8] Far below T_c, the heat capacity C_V drops steeply:

$$C_V = \text{constant} \times \exp(-\alpha T_c/T) \tag{1.1.3}$$

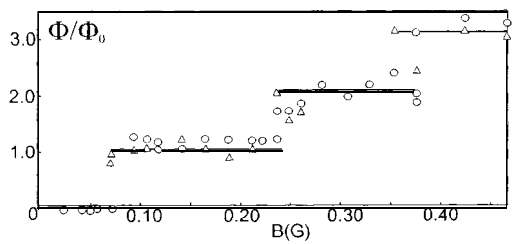

Figure 1.5. The magnetic flux quantization [after Deaver and Fairbank (Ref. 4)].

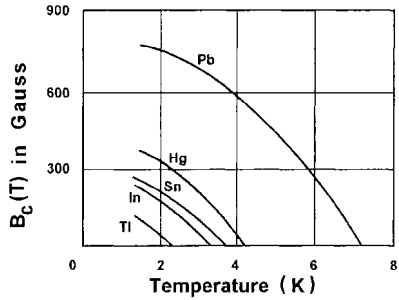

Figure 1.6. Critical fields B_c change with temperature.

where α is a constant, indicating that the elementary excitations in the superconducting state have an energy gap; this will be discussed in Section 1.1.7. The specific heat of aluminum (Al) as a function of temperature[9] is shown in Fig. 1.7.

1.1.7. Energy Gap

If a continuous band of the excitation energy is separated by a finite gap $\in_g$ from the ground-state energy as shown in Fig. 1.8, this gap can be detected by photoabsorption,[10] quantum tunneling,[11] and other experiments. The energy gap $\in_g$ turns out to be temperature-dependent. The energy gap $\in_g(T)$ as determined from the tunneling experiments [12] is shown in Fig. 1.9. Note: The energy gap is zero at T_c and reaches a maximum value $\in_g(0)$ as temperature is lowered toward 0 K.

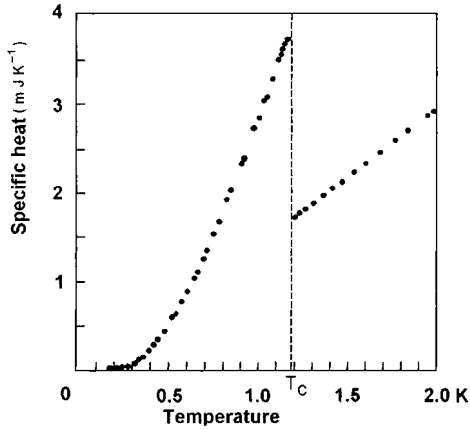

Figure 1.7. Low-temperature specific heat of aluminum.

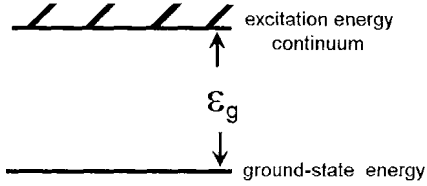

Figure 1.8. Excitation-energy spectrum with a gap.

1.1.8. Isotope Effect

When the isotopic mass M of the lattice ions is varied, T_c changes[13]:

$$T_c \propto M^{-\alpha}, \qquad \alpha \simeq 1/2 \tag{1.1.4}$$

indicating that the lattice vibration plays a role in bringing out superconductivity.

1.1.9. Josephson Effects

Let us take two superconductors separated by an oxide layer of thickness of the order 10 Å, called a Josephson junction. We use this system as part of a circuit including a battery as shown in Fig. 1.10. Above T_c two superconductors S_1 and S_2 and the junction I all show potential drops. If temperature is lowered beyond T_c, the potential drops in S_1 and S_2 disappear because of zero resistance. The potential drop across the junction I also disappears! In other words, the supercurrent runs through the junction I with no energy loss. Josephson predicted, [14]and later experiments [15] confirmed, this effect, called the *Josephson tunneling* or *DC Josephson effect.*

We now take a closed loop superconductor containing two similar Josephson junctions and make a circuit as shown in Fig. 1.11. Below T_c the supercurrent **I** branches out into $\mathbf{I}_1$ and $\mathbf{I}_2$. We now apply a magnetic field **B** perpendicular to the loop lying on the paper. The magnetic flux can go through the junctions, and therefore it can be changed continuously. The total current is found to have an oscillatory component:

$$I = I^{(0)} \cos(\pi\Phi/\Phi_0), \qquad (I^{(0)} = \text{constant}) \tag{1.1.5}$$

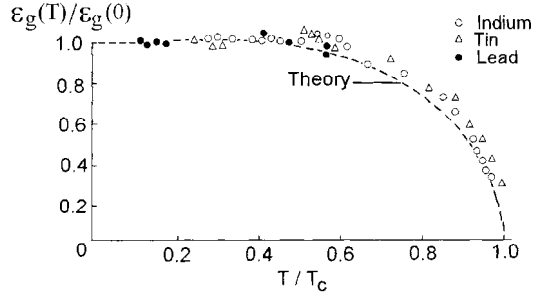

Figure 1.9. The energy gap $\in_g(T)$ versus temperature, as determined by tunneling experiments [after Giaever and Megerle (Ref. 12)].

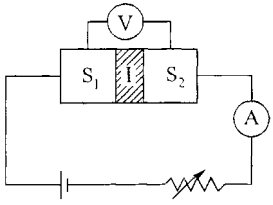

Figure 1.10. Two superconductors S_1 and S_2 and a Josephson junction I are connected with a battery.

where Φ is the magnetic flux enclosed by the loop, indicating that the two supercurrents $\mathbf{I}_1$ and $\mathbf{I}_2$ macroscopically separated (~ 1 mm) interfere just as two laser beams coming from the same source. This is called a *Josephson interference.* A sketch of interference pattern[16] is shown in Fig. 1.12. For various Josephsons effects, Josephson shared the Nobel prize in 1973 with Esaki and Giaever. (Esaki and Giaever are the discoverers of the tunneling effects in semiconductors and in conductor–oxide–superconductor sandwiches.) The circuit in Fig. 1.11 can be used to detect an extremely weak magnetic field, the detector called the *superconducting quantum interference device (SQUID).*

1.1.10. Penetration Depth

In our earlier description of the Meissner effect, we stated that the superconductor expels a (weak) magnetic field **B** from its interior. The finer experiments reveal that the field **B** penetrates into the superconductor within a very thin surface layer. Consider the boundary of a semi-infinite slab. When the external field is applied parallel to the boundary, the B-field falls off exponentially:

$$B(x) = B(0)\, e^{-x/\lambda} \tag{1.1.6}$$

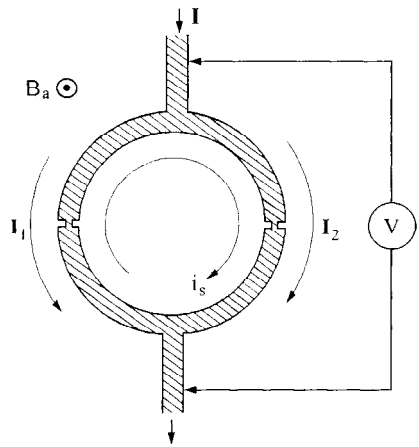

Figure 1.11. Superconducting quantum interference device (SQUID).

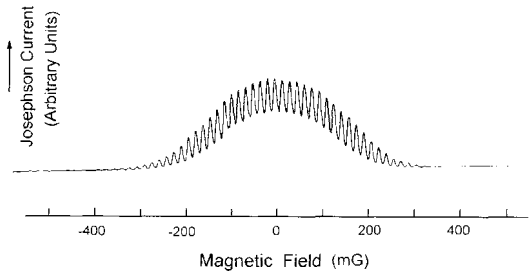

Figure 1.12. Current versus magnetic field [after Jaklevic *et al.* (Ref. 16)].

as indicated in Fig. 1.13. Here λ, called a *penetration depth*, is of order 500 Å in most superconductors at very low temperatures. It is very small macroscopically, which allows us to speak of the superconductor being perfectly diamagnetic. The penetration depth plays a very important role in the description of the magnetic properties.

1.1.11. Occurrence of Elemental Superconductors

More than 40 elements are found to be superconductors. Table 1.1 shows the critical temperature T_c and the critical magnetic field at 0 K, B_0. Most nonmagnetic metals are superconductors, with notable exceptions being familiar monovalent metals such as Li, Na, K, Cu, Ag, Au, and Pt. Some metals can become superconductors under applied pressures and/or in thin films, and these are indicated by asterisks.

1.1.12. Compound Superconductors

Thousands of metallic compounds are found to be superconductors. A selection of compound superconductors with critical temperature T_c are shown in Table 1.2. Note: T_c tends to be higher in compounds than in elements. Nb_3Ge has the highest T_c (~ 23 K).

Compound superconductors exhibit (type II) magnetic behavior different from that of type I elemental superconductors. A very weak magnetic field is expelled from the body (the Meissner effect) just as by the elemental (type I) superconductor. If the field is raised beyond the *lower critical field* H_{c1}, the body allows a partial penetration of the field, still remaining in the superconducting state. A further field increase turns the body into a normal state after passing the *upper critical field* H_{c2}. Between H_{c1} and

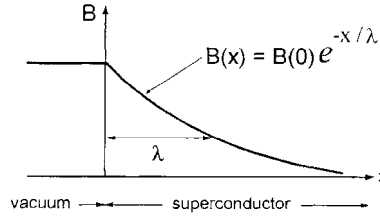

Figure 1.13. Penetration of the field **B** into a superconductor slab.

Table 1.1. Superconductivity Parameters of the Elements

Li	**Be**											**B**	**C**	**N**	**O**	**Ne**
Na	**Mg**											**Al**	**Si***	**P**	**S**	**Ar**
											T_c =	1.18				
											B_c =	105				
K	**Ca**	**Sc**	**Ti**	**V**	**Cr**	**Mn**	**Fe**	**Co**	**Ni**	**Cu**	**Zn**	**Ga**	**Ge***	**As**	**Se***	**Kr**
			0.39	5.38							0.87	1.09				
			100	1420							53	51				
Rb	**Sr**	**Y***	**Zr**	**Nb**	**Mo**	**Tc**	**Ru**	**Rh**	**Pd**	**Ag**	**Cd**	**In**	**Sn**	**Sb***	**Te***	**Xe**
			0.54	9.20	0.92	7.77	0.51				3.40	3.40	3.72			
			47	1980	95	1410	70					293	309			
Cs*	**Ba***	**La**	**Hf**	**Ta**	**W**	**Re**	**Os**	**Ir**	**Pt**	**Au**	**Hg**	**Tl**	**Pb**	**Bi***	**Po**	**Rn**
		6.00		4.48	0.01	1.69	0.65	0.14			4.15	2.39	7.19			
		1100		830	1.07	198	65	19			412	171	803			
Fr	**Ra**	**Ac**														

Ce*	**Pr**	**Nd**	**Pm**	**Sm**	**Eu**	**Gd**	**Tb**	**Dy**	**Ho**	**Er**	**Tm**	**Yb**	**Lu**
Th	**Pa**	**U**	**Np**	**Pu**	**Am**	**Cm**	**Bk**	**Cf**	**Es**	**Fm**	**Md**	**No**	**Lw**
1.36	1.4	0.68											
1.62													

*denotes superconductivity in thin films or under high pressures.
Transition temperature in K and critical magnetic field at 0 K in Gauss.

H_{c2}, the superconductor is in a *mixed state* in which magnetic flux lines surrounded by supercurrents (vortices) penetrate the body. The critical fields *versus* temperature are shown in Fig. 1.14. The upper critical field H_{c2} can be very high ($20T = 2 \times 10^5$ G for Nb_3Sn) Also the critical temperature T_c tends to be high for high-H_{c2} superconductors. These properties make compound superconductors useful materials.

1.1.13. High-T_c Superconductors

In 1986 Bednorz and Müller[17] reported their discovery of the first of the high-T_c cuprate superconductors ($T_c > 30$ K) (La–Ba–Cu–O). Since then many investigations have been carried out on the high-T_c superconductors including Y–Ba–Cu–O with $T_c \approx$

Table 1.2. Critical Temperatures of Selected Compounds

Compound	T_c (K)	Compound	T_c (K)
Nb_3Ge	23.0	MoN	12.0
$Nb_3(Al_{0.8}Ge_{0.2})$	20.9	V_3Ga	16.5
Nb_3Sn	18.05	V_3Si	17.1
Nb_3Al	17.5	UCo	1.70
Nb_3Au	11.5	Ti_2Co	3.44
NbN	16.0	La_3In	10.4

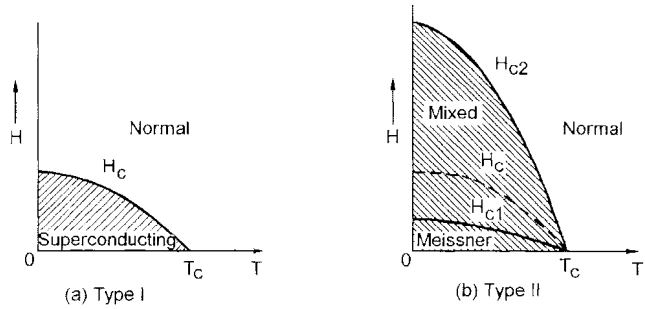

Figure 1.14. Phase diagrams of type I and type II superconductors.

94 K.[17] The boiling point of abundantly available and inexpensive liquid nitrogen (N) is 77 K. So the potential applications of high-T_c superconductors, which are of type II, appear enormous. The superconducting state of these conductors is essentially the same as that of elemental superconductors.

1.2. THEORETICAL BACKGROUND

1.2.1. Metals; Conduction Electrons

All known superconductors are metals or semimetals above T_c. A metal is a conducting crystal in which electrical current can flow with little resistance. This electrical current is generated by moving electrons. The electron has mass m and charge $-e$, which is negative by convention. Their numerical values are $m = 9.109 \times 10^{-28}$ g, $e = 4\ 802 \times 10^{-10}$ esu $= 1.602 \times 10^{-19}$ C. The electron mass is smaller by about 1837 times than the least massive hydrogen atom. This makes the electron extremely mobile. Also it makes the electron's quantum nature more pronounced. The electrons participating in the charge transport, called *conduction electrons*, are those that would have orbited in the outermost shells surrounding the atomic nuclei if the nuclei were separated from each other. Core electrons that are more tightly bound with the nuclei form part of the metallic ions. In a pure crystalline metal, these metallic ions form a relatively immobile array of regular spacing, called a *lattice.* Thus a metal can be pictured as a system of two components: mobile electrons and relatively immobile lattice ions.

1.2.2. Quantum Mechanics

Superconductivity is a quantum effect manifested on a macroscopic scale. This is most clearly seen by a ring supercurrent with the associated quantized magnetic flux. To interpret this phenomenon, a thorough understanding of quantum theory is essential. Dirac's formulation of quantum theory in his book, *Principles of Quantum Mechanics,*[19] is unsurpassed. Dirac's rules that the quantum states are represented by "bra" or "ket" vectors and physical observables by Hermitian operators, are used in the text whenever convenient. Those readers who learned quantum theory by means of wave functions may find Appendix A useful; there the principles of quantum mechanics for a particle are reviewed.

There are two distinct quantum effects, the first of which concerns a single particle and the second a system of identical particles. They are called *first* and *second quantization.*

1.2.3. First Quantization; Heisenberg's Uncertainty Principle

Let us consider a simple harmonic oscillator characterized by the Hamiltonian

$$H = \frac{p^2}{2m} + \frac{kx^2}{2} \tag{1.2.1}$$

where m is the mass and k the force constant. The corresponding energy eigenvalues are

$$\epsilon_n = \hbar\omega_0 \left(n + \frac{1}{2}\right), \qquad \omega_0 \equiv \left(\frac{k}{m}\right)^{1/2}, \qquad n = 0, 1, 2, \cdots \tag{1.2.2}$$

Note: The energies are quantized in Eq. (1.2.2), while the classical mechanical energy can be any positive value; and the lowest quantum energy $\epsilon_0 = \hbar\omega_0/2$, called the *energy of zero-point motion*, is not zero. It is found that the most stable state of *any* quantum system is *not* a state of *static equilibrium* in the configuration of lowest potential energy. It is rather a *dynamic equilibrium* for the zero-point motion, which may be characterized by the minimum total (potential + kinetic) energy under the condition that each coordinate q have a mean range Δq and the corresponding momentum p a range Δp, so that the product $\Delta q\, \Delta p$ satisfy the *Heisenberg uncertainty relation*:

$$\Delta q \Delta p \geq \frac{\hbar}{2} \tag{1.2.3}$$

The most remarkable example of a macroscopic body in dynamic equilibrium is liquid helium (He). This liquid with a boiling point at 4.2 K is known to remain liquid down to 0 K. The zero-point motion of this light atom precludes solidification.

1.2.4. Quantum Statistics; Bosons and Fermions

Electrons are fermions; that is, they are *indistinguishable quantum particles* subject to *Pauli's exclusion principle.* Indistinguishability of the particles is defined by using the permutation symmetry. Permutation operators and their principal properties are surveyed in Appendix B. According to Pauli's principle *no two electrons can occupy the same state*. Indistinguishable quantum particles not subject to Pauli's exclusion principle are called *bosons*. Bosons can occupy the same state multiply. *Every elementary particle is either a boson or a fermion*. This is known as the *quantum statistical postulate*. Whether an elementary particle is boson or fermion is related to the magnitude of its spin angular momentum in units of $\hbar$. *Particles with integer spin are bosons, while those with half-integer spin are fermions*. This is known as the *spin statistics theorem* due to Pauli. According to this theorem and in agreement with all experimental evidence, electrons, protons, neutrons, and μ-mesons, all of which have spin of magnitude $\hbar/2$, are fermions, while photons (quanta of electromagnetic radiation) with spin of magnitude $\hbar$, are bosons. More detailed discussions on bosons and fermions are given in Appendix C.

1.2.5. Fermi and Bose Distribution Functions

The average occupation number at state *a,* denoted by $\langle N_a \rangle$, for a system of free fermions in equilibrium at temperature T and chemical potential μ, is given by the *Fermi distribution function*:

$$\langle N_a \rangle = f_F(\epsilon_a) \equiv \frac{1}{\exp[(\epsilon_a - \mu)/k_B T] + 1} \tag{1.2.4}$$

where ϵ_a is the energy associated with state *a.* The Boltzmann constant k_B has the numerical value $k_B = 1.381 \times 10^{-16}$ erg/deg $= 1.381 \times 10^{-23}$ JK^{-1}.

The average occupation number at state a for a system of free bosons in equilibrium is given by the *Bose distribution function*:

$$\langle N_a \rangle = f_B(\epsilon_a) \equiv \frac{1}{\exp[(\epsilon_a - \mu)/k_B T] - 1} \tag{1.2.5}$$

Note the formal similarity (±) between Eqs. (1.2.4) and (1.2.5).

1.2.6. Composite Particles

Atomic nuclei are composed of nucleons (protons, neutrons), while atoms are composed of nuclei and electrons. It is experimentally found that such composite particles are indistinguishable quantum particles; moreover they move as either bosons or fermions. According to Ehrenfest–Oppenheimer–Bethe's rule,[20] a composite is a fermion *if* it contains an *odd* number of fermions and a boson if the number of fermions in it is *even.* The number of bosons contained in the composite does not matter. Thus He^4 atoms (four nucleons, two electrons) move as bosons and He^3 atoms (three nucleons, two electrons) as fermions. Cooper pairs (two electrons) move as bosons; see Section 9.1.

1.2.7. Superfluids; Bose–Einstein (B–E) Condensation

Liquid He^4 (the most abundant isotope) undergoes a superfluid transition at 2.19 K. Below this temperature, liquid He^4 exhibits frictionless (zero viscosity) flows remarkably similar to supercurrents. The pioneering experimental works on superfluidity were done mostly in the late thirties. In 1938 Fritz London[21] advanced a hypothesis that the superfluid transition in liquid He^4 be interpreted in terms of a B–E *condensation,* [22] where a *finite fraction* of bosons is condensed in the lowest energy state and the rest of bosons have a gas like distribution (see Section 4.2).

1.2.8. Bloch Electrons; The Fermi Liquid Model

In a metal conduction electrons move mainly in a static periodic lattice. Because of the Coulomb interaction among the electrons, the motion of the electrons is correlated. However the crystal electron moves in an extremely weak self-consistent periodic field. Combining this result with the Pauli's exclusion principle, which applies to electrons with no regard for the interaction, we obtain the *Fermi Liquid model* of Landau.[23] (See Section 5.3 and 6.8). In this model the quantum states for the Bloch electron are characterized by k-vector **k,** zone number j, and energy

$$\epsilon = E_j(\mathbf{k}) \tag{1.2.6}$$

At 0 K all of the lowest energy states are filled with electrons, and there exists a *sharp Fermi surface* represented by

$$E_j(\mathbf{k}) = \epsilon_F \tag{1.2.7}$$

where $\in_F$ is the *Fermi energy*. Experimentally all normal conductors are known to exhibit a sharp Fermi surface at 0 K. Theoretically much of the band theory of solids[24] and the microscopic theory of superconductivity are based on this model. The occurrence of superconductors critically depends on the Fermi surface; see Section 8.6.

1.2.9. Electrons and Holes

Electrons (*holes*) in the text are defined as quasi-particles possessing charge (magnitude) that circulate clockwise (counterclockwise) when viewed from the tip of the applied magnetic field vector **B.** This definition is used routinely in semiconductor physics. Holes can be regarded as particles having positive charge, positive mass, and positive energy; holes do not, however, have the same effective mass (magnitude) as electrons, so that holes are not true antiparticles like positrons. Electrons and holes are closely related to the electrons band structures; see Sections 5.7–5.8.

1.2.10. Second Quantization Formalism

In the second quantization formalism, where *creation and annihilation operators* associated with each quantum state are used, a system of identical particles (bosons or fermions) can be treated simply. This formalism also allows us to treat electrons and holes in a parallel manner; this formalism is fully developed in Chapter 6.

1.3. THERMODYNAMICS OF A SUPERCONDUCTOR

We shall briefly discuss the thermodynamics of a superconductor.

1.3.1. Magnetic Flux Density **B** and Magnetic Field **H**

Electric currents necessarily induce magnetic fluxes. Magnetic fields are often externally applied to probe the properties of superconductors. Appreciation of the difference between the *magnetic flux density* **B** and the *magnetic field* **H** is important in understanding the properties of a superconductor. We briefly discuss this subject here. The reader interested in a more detailed description of electromagnetism should refer to the excellent book by Rose-Innes and Rhoderick.[25]

All experiments in electromagnetism support that the magnetic flux density **B** is a basic field just as the electric field **E** is basic. A particle possessing charge q, is subject to a *Lorentz force*:

$$\mathbf{F} = q(\mathbf{E} + \mathbf{v} \times \mathbf{B}) \tag{1.3.1}$$

where **v** is the particle velocity. The B-field satisfies

$$\nabla \cdot \mathbf{B} \equiv \text{div } \mathbf{B} = 0 \tag{1.3.2}$$

which means that the magnetic flux lines in the universe are closed. There are no sources and no sinks for magnetic fluxes. Equation (1.3.2) also implies that the field **B** can be described in terms of a *vector potential* **A** such that

$$\mathbf{B} = \nabla \times \mathbf{A} \equiv \text{curl}\, \mathbf{A} \tag{1.3.3}$$

The B-field satisfies part of Maxwell's equations:

$$\frac{\partial}{\partial t}\mathbf{B}(\mathbf{r}, t) \equiv \dot{\mathbf{B}} = -\nabla \times \mathbf{E} \tag{1.3.4}$$

Formulas (1.3.1)–(1.3.4) are valid in a vacuum. The magnetic field **H** is related to **B** by

$$\mathbf{B} = \mu_0 \mathbf{H} \tag{1.3.5}$$

(μ_0 = permeability of free space).

Let us now consider a magnetizable body. All known superconductors are crystals. We define the magnetic flux density $\bar{\mathbf{B}}$ averaged over the lattice unit cell. (We drop the upper bar indicating the averaging hereafter.) The average field **B** by definition will be connected to the applied magnetic field $\mathbf{H}_a$ and the magnetization (magnetic dipole moment per unit volume) **M** by

$$\mathbf{B} = \mu_0 \mathbf{H}_a + \mu_0 \mathbf{M} \tag{1.3.6}$$

We postulate that the average B-field satisfies Eqs. (1.3.1)–(1.3.4) in a solid just as in a vacuum. The Bloch electron (wave packet) (see Sections 5.8–5.9) can be localized only within the dimension of the lattice constant. Since the B-field enters as part of the Lorentz force and not the H-field, the magnetic flux density **B** is the relevant magnetic quantity in Bloch electron dynamics. In the present text, we shall call the B-field the *magnetic field* just as we call the E-field the *electric field.* On the other hand, the externally applied magnetic field is most often (90% or more) designated in terms of the magnetic field $\mathbf{H}_a$ in solid-state physics. We shall sometimes follow this practice. To convert the units, we simply apply Eq. (1.3.5): $\mathbf{B}_a = \mu_0 \mathbf{H}_a$. The subscript *a,* meaning the applied field, will be omitted when no confusion is feared.

1.3.2. Gibbs Free Energy

In dealing with thermodynamics of a superconductor the Gibbs free energy plays an important role. Let us first review thermodynamics applied to a fluid. The fundamental differential relation representing the First and Second laws of thermodynamics applicable to a reversible process is

$$dE = -PdV + TdS \tag{1.3.7}$$

where P is the pressure, V the volume, and S the entropy. The Gibbs free energy G for the gas is defined by

$$G \equiv E - TS + PV \tag{1.3.8}$$

Using Eqs. (1.3.7) and (1.3.8), we obtain

$$dG = VdP - SdT \tag{1.3.9}$$

which indicates that the Gibbs free energy G is a useful characteristic function of (P, T). In fact we obtain immediately from Eq. (1.3.9):

$$V = \frac{\partial G(P,T)}{\partial P} \equiv \frac{\partial G}{\partial P}\Big)_T, \qquad S = -\frac{\partial G}{\partial T}\Big)_P \tag{1.3.10}$$

where the subscripts denote fixed variables in the partial derivatives.

Solids (and liquids) by definition are in the condensed state. They are characterized by very low compressibility $K_T \equiv -(\partial V/\partial P)_T/V$. Since we deal with superconducting solids exclusively in the present text, we shall drop the effect of the applied pressure hereafter. In other words we assume that

$$K_T = 0 \qquad \text{(incompressible solids)} \tag{1.3.11}$$

Instead we include the effect of a magnetic field in thermodynamics of a superconductor. The fundamental differential relation is given by

$$dE = TdS + \mu_0 H_a dM \tag{1.3.12}$$

where M is the total magnetic moment, meaning that the internal energy E can be changed by supplying heat (first term) and applying a magnetic field $\mu_0 H_a$ (second term). In analogy with Eqs. (1.3.8) and (1.3.9), we define the Gibbs free energy G by

$$G \equiv E - TS - \mu_0 MH \tag{1.3.13}$$

Using Eq. (1.3.12) we obtain

$$dG = -SdT - \mu_0 MdH \tag{1.3.14}$$

implying that the Gibbs free energy G is the characteristic function of the temperature T and the applied magnetic field H. By inspection we obtain from Eq. (1.3.14):

$$S = -\frac{\partial G}{\partial T}\Big)_H, \qquad \mu_0 M = -\frac{\partial G}{\partial H}\Big)_T \tag{1.3.15}$$

1.3.3. Perfect Diamagnetism

We consider a long superconducting rod with a weak magnetic field applied parallel to its length. By the Meissner effect, the magnetic fluxes are expelled from the rod and the B-field inside will be zero. Then from Eq. (1.3.6) the magnetization M must equal $-H_a$:

$$B = \mu_0(H_a + M) = 0, \qquad M = -H_a, \qquad |H_a| < H_c \tag{1.3.16}$$

This state is maintained until the H-field is raised to the *critical field* H_c. By further raising the H-field beyond H_c, the superconductor is rendered normal, in which case:

$$B = \mu_0 H_a, \qquad H_a > H_c \tag{1.3.17}$$

By now reversing the H-field, the B-field retraces the same path. This behavior is shown in Fig. 1.15 (a). The associated magnetization behavior is shown in (b). The sense of

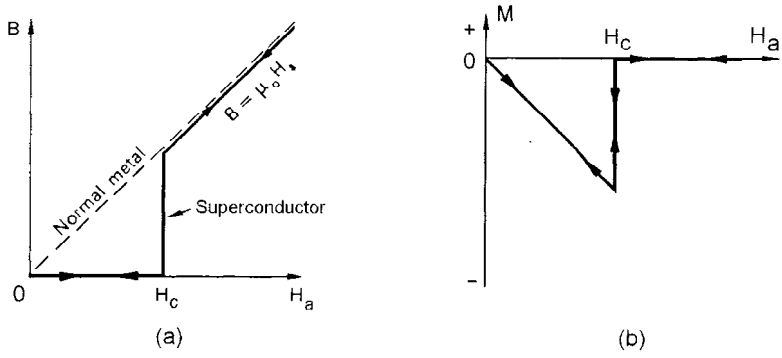

Figure 1.15. Magnetic behavior of a type I superconductor.

the magnetization M is always diamagnetic when the motion of free charges is involved. Since the supercurrent is frictionless, the process occurs in a reversible manner.

The *magnetic susceptibility* χ for a material is defined by

$$M \equiv \chi H \tag{1.3.18}$$

From Eq. (1.3.16) we obtain

$$\chi = -1 \qquad (H_a < H_c) \tag{1.3.19}$$

The material is called paramagnetic or diamagnetic according to whether χ is positive or negative. If $\chi = -1$, it is called a perfect diamagnet. Thus the (type I) superconductor is perfect-diamagnetic below H_c. The magnetization behavior of a type II superconductor is quite different; it will be discussed in Section 12.2.

1.3.4. Isothermal Process; Normal and Super States

Let us take a superconductor and apply a magnetic field isothermally ($dT = 0$). The change in G can be calculated from Eq. (1.3.14)

$$G_S(T,H) - G_S(T,0) = -\mu_0 \int_0^{H_a} M\, dH = \mu_0 \int_0^{H_a} H\, dH = \frac{\mu_0}{2} H_a^2 \tag{1.3.20}$$

by using Eq. (1.3.16). Thus the Gibbs free energy G_S increases quadratically with the applied field H_a. The positive energy $\mu_0 H^2/2$ can be interpreted as the stored magnetic field energy per unit volume needed to generate the deformed magnetic field configuration, [see Fig. 1.2], from the uniform magnetic field configuration. Such a field-theoretical interpretation is useful when a qualitative understanding of a phenomenon is desired.

The state of a superconductor above H_c is characterized by a vanishing magnetization common in nonferromagnetic metals. We may define the hypothetical normal state of the superconductor below H_c to be the state in which $M = 0$. The Gibbs free

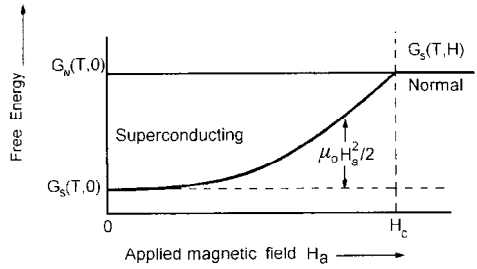

Figure 1.16. Effect of applied magnetic field on Gibbs free energy.

energy $G_N(T, H)$ representing the normal state does not have the magnetization term, and therefore it is independent of H. The Gibbs free energy $G_S(T, H)$ representing the superconducting state must be lower than $G_N(T, H)$. (Only the state with the minimum G is realized in nature.) We may postulate that the Gibbs free energy is the same for both states at the critical field H_c : $G_S(T, H_c) = G_N(T, H_c)$. The behavior of G's versus H is shown in Fig. 1.16. The reader may verify that this behavior of G generates the M–H and B–H curves shown in Fig. 1.15. From the diagram, we obtain

$$G_N(T,0) - G_S(T,0) = \left(\frac{1}{2}\right)\mu_0 H_c(T)^2 \tag{1.3.21}$$

In the zero-temperature limit, the internal energy E is equal to the ground-state energy W of the conductor. Thus we obtain from Eq. (1.3.21):

$$W_N - W_S \equiv E_N - E_S = \left(\frac{1}{2}\right)\mu_0 H_c(0)^2 \equiv \left(\frac{1}{2}\right)\mu_0 H_0^2 \qquad (T = 0) \tag{1.3.22}$$

The critical field H_c can be measured simply by applying a magnetic field parallel to a superconducting rod and observing the field at which resistance appears.

The magnetization M has a jump $-H_c$ at $H = H_c$. The *order of a phase transition* is defined to be the order of the derivative of a free energy whose discontinuity appears for the first time. Since $M = -\mu_0^{-1}(\partial G/\partial H)_T$ from Eq. (1.3.15), the normal-to-super transition here is said to be a phase transition of first order.

1.3.5. Critical Fields; The Phase Diagram

All type I superconductors are found to have similar magnetic behaviors. The critical field H_c depends on the temperature T, and its dependence can be represented within a few per cent by

$$H_c = H_0\left[1 - \left(\frac{T}{T_c}\right)^2\right] \tag{1.3.23}$$

This behavior is illustrated by the H–T (phase) diagram in Fig. 1.14 (a). The values of (H_c, T_c) were given earlier in Table 1.1. The approximate Eq. (1.3.23), called the

Gorter–Casimir formula, was derived by these authors[26] in their phenomenological two-fluid model theory. The fact that the two measurable quantities (T_c, H_c) can be connected with each other independently of the materials is noteworthy. This is often referred to as the *law of corresponding states.* (Such a law is known for a simple liquid whose phase diagrams is represented by a van der Waals equation.) It suggests that a microscopic theory of superconductivity may be developed based on a generic model Hamiltonian.

1.3.6. Superconducting Transition, Supercondensate, and Two Fluid Model

The superconducting transition is a sharp thermodynamic phase transition similar to the vapor–liquid transition of water. But there is a significant difference: In the case of water, the gas and liquid phases are both characterized by two independent thermodynamic variables, such as the number density n and the temperature T. In contrast the superconducting phase has one peculiar component, called a *supercondensate,* which dominates the electrical conduction; and the other component, called the normal component, which behaves normally. The two components are intermixed in space, but they are distinguished in momentum and move distinctly. In other words the superconducting phase can be characterized by the normal thermodynamic variables (n, T) and a macro-wave function Ψ, also called a *Ginzburg–Landau complex order parameter,*[7] which represents the supercondensate. The two-fluid (component) model is applicable only to superconductor and superfluid. The appearance of the supercondensate wave function Ψ below T_c is somewhat similar to the appearance of a spontaneous magnetization M below T_c in a ferromagnet. The Ψ is complex, while the M is real however.

1.3.7. Supercurrents

In true thermodynamic equilibrium, there can be no currents, super or normal. Thus we must deal with a nonequilibrium condition when discussing the main properties of superconductors, such as zero resistance, flux quantization, and Josephson effects. All of these come from the moving supercondensate that dominates the transport and magnetic phenomena. When a superconductor is used to form a circuit with a battery and a steady state is established, all currents passing the superconductor are supercurrents. Normal currents due to the motion of charged particles contributes zero because no voltage difference can be developed in a homogeneous superconductor.

1.3.8. Surface Supercurrents and Meissner State

Experiments show that all supercurrents flow near the type I superconductor's surface within a thin layer characterized by field penetration depth λ. These surface supercurrents run so that the B-field vanishes in the interior of the conductor. We say that the superconductor is in the *Meissner state.* This behavior is shown in Fig. 1.17.

1.3.9. Intermediate State; Thin Films

The applied magnetic field $\mathbf{H}_a$ is a vector field unlike the familiar scalar pressure. Because of this the effect of an applied magnetic field in general depends on the shape of the superconductor. To see this consider the hyperboloidal superconductor shown in Fig. 1.18. If a weak field $\mathbf{H}_a$ is applied along its axis, the closed surface supercurrents

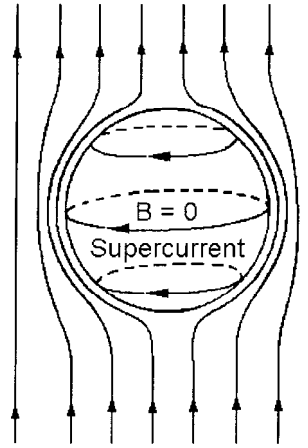

Figure 1.17. Surface supercurrents in a superconductor generate a Meissner state.

may be generated, and the magnetic shielding will be complete inside the body. If however the field $\mathbf{H}_a$ is applied nearly perpendicular to its axis, the surface supercurrents cannot run in closed loops having curvatures of the same sign. Then the magnetic shielding cannot be complete. In other words some magnetic flux must penetrate. For a general direction of the field $\mathbf{H}_a$, some part may be in the Meissner state where the diamagnetic shielding is complete and others in the normal state. We say that the superconductor is in an *intermediate state.* Structures of an intermediate state can be quite complicated, depending on the shape of a conductor and the direction of the magnetic field relative to its geometrical shape. This is true even when a superconductor is made up of homogeneous and isotropic material. Good discussions of the intermediate state can be found in the book by Rose-Innes and Rhoderick.[25] Since we are primarily interested in the microscopic theory of superconductivity, we shall not discuss the intermediate state further. Unless otherwise stated we assume that the magnetic field $\mathbf{H}_a$ is applied to an ideal long cylinder along its axis (see Fig. 1.2). Caution: Strictly speaking the cylinder must not have sharp edge but be of an ellipsoidal shape. We also assume that the superconductor in consideration is great in any dimension (direction) compared with the penetration depth λ This means that we exclude thin films from our consideration.

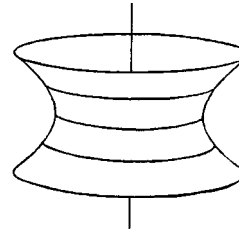

Figure 1.18. A hyperboloid.

Superconductors in thin films in general have higher critical temperatures than in bulk. We are thus omitting an important area of research.

1.4. DEVELOPMENT OF A MICROSCOPIC THEORY

We briefly sketch the historical development of the microscopic theory of superconductivity, including the epoch-making Bardeen–Cooper–Schrieffer (BCS) theory[27] and its subsequent developments.

1.4.1. Phonon Exchange Attraction

As noted earlier in Section 1.2.2, the lattice ions are never strictly at rest even at 0 K because of the quantum zero-point motion. In 1950 Fröhlich proposed a model for a superconductor in which electrons acquire attraction by the exchange of virtual phonons.[28] This was an important step in the construction of a microscopic theory of superconductivity. Experiments indicate an isotope effect on the critical temperature T_c, as described in Section 1.1.8, which can be explained only if the effect of an electron–phonon interaction is included. In fact by using second-order perturbation theory we can show that the interaction is attractive if the pair of electrons between which a phonon is exchanged have nearly the same energies. This kinetic-energy dependence is noteworthy: It reflects the quantum mechanical nature of the phonon-exchange attraction. We shall discuss this attraction in detail in Chapter 7.

1.4.2. The Cooper Pair

In 1956 Cooper demonstrated[29] that however weak the interelectron attraction may be, two electrons just above the Fermi sea could be bound. The binding energy is greatest if the two electrons have opposite momenta ($\mathbf{p}$, $-\mathbf{p}$) and antiparallel spins ($\uparrow,\downarrow$). The lowest bound energy w_0 is given by

$$w_0 = \frac{-2\hbar\omega_D}{\exp[2/\mathcal{N}(0)v_0] - 1} \tag{1.4.1}$$

where ω_D is the Debye frequency, v_0 a positive constant characterizing the attraction, and $\mathcal{N}(0)$ the electron density of states per spin at the Fermi energy. Since the function $\exp(1/x)$ has an essential singularity at $x = 0$, Eq. (1.4.1) cannot be obtained by a perturbation expansion in powers of $x = \mathcal{N}(0)v_0$. If electrons having nearly opposite momenta ($\mathbf{p}, -\mathbf{p} + \mathbf{q}$) are paired, the binding energy is less than $|w_0|$. For small q, which represents the net momentum of a Cooper pair, called a *pairon* for short, the energy momentum relation is

$$w_q = w_0 + \frac{1}{2}v_F q < 0 \tag{1.4.2}$$

where $v_F = (2\epsilon_F/m^*)^{1/2}$ is the Fermi velocity. Equations (1.4.1) and (1.4.2) play very important roles in the theory of superconductivity. We shall derive them from the first principles in Chapter 8.

1.4.3. The Bardeen–Cooper–Schrieffer Theory

In 1957 Bardeen, Cooper, and Schrieffer (BCS) published a classic paper,[27] which is regarded as one of the most important theoretical works in the twentieth century. The Nobel physics prize in 1972 was shared by Bardeen, Cooper, and Schrieffer for this work. (Bardeen was awarded the prize the second time since he shared the 1956 prize with Shockley and Brattain for the invention and development of a transistor.)

In this work BCS assumed a supercondensate made up of ± pairons (pairons having charges $\pm 2e$) and obtained an expression W for the ground-state energy:

$$W = \hbar\omega_D \mathcal{N}(0) w_0 = N_0 w_0 \tag{1.4.3}$$

where

$$N_0 \equiv \hbar\omega_D \mathcal{N}(0) \tag{1.4.4}$$

is the total number of pairons and w_0 the ground pairon energy given by Eq. (1.4.1). In the variational calculation of the ground-state energy BCS found that *unpaired electrons,* often called *quasi-electrons,* have energy

$$E_k = \left(\Delta^2 + \epsilon_k^2\right)^{1/2} \tag{1.4.5}$$

where $\in_k$ the kinetic energy of the Bloch electron measured relative to the Fermi energy $\in_F$. The energy constant Δ, called the *energy gap* in Eq. (1.4.5) is greatest at 0 K and decreases to zero as temperature is raised to the critical temperature T_c, at which the supercondensate ceases to exist. BCS further showed that the energy gap at 0 K, $\Delta(T = 0) = \Delta_0$ and the critical temperature T_c (in the weak coupling limit) are related by

$$2\Delta_0 = 3.53\, k_B T_c \tag{1.4.6}$$

These findings are among the most important results obtained in the BCS theory. A large body of theoretical and experimental work followed several years after the BCS theory. By 1964 the general consensus was that the BCS theory is an essentially correct theory of superconductivity.[30]

1.4.4. Quantum Statistical Theory; Independent Pairon Picture

BCS assumed a free-electron model having a Fermi sphere in their original work. They also assumed the existence of electrons and holes in their model superconductor. These two assumptions however contradict each other. If a Fermi sphere whose inside (outside) is filled with electrons is assumed, there are electrons (holes) only. Besides this logical inconsistency, if we assume a free-electron model, we cannot explain why the law of corresponding states works so well, why monovalent metals like Na are not superconductors, or why compound superconductors including intermetallic, organic, and *high-T_c* superconductors exhibit type II behaviors. Recently Fujita and coworkers[31] proposed a generalized BCS Hamiltonian by incorporating the energy bands of electrons and phonons more explicitly, and they proceeded to calculate thermodynamic and transport properties by a standard method of quantum statistical mechanics. They could solve many puzzling questions left unanswered by the BCS theory including those mentioned earlier, and why

a ring supercurrent does not decay by scattering due to impurities that must exist in any superconductor, why superconductors do not gain energy from an applied static voltage, and why an applied magnetic field eventually destroys the superconducting state. We present in this book this new quantum statistical theory of superconductivity.

If a system-Hamiltonian is composed of single-particle Hamiltonians, the quantum many-body problem can be reduced to a one-body problem by using Heisenberg's equation-of-motion method.[32] All of the properties including the ground-state energy, critical temperature, elementary excitation energy spectra, supercondensate density, specific heat, and supercurrent density can be computed without mathematical complexities.

1.5. LAYOUT OF THE PRESENT BOOK

Chapters 2–4 are preliminaries and deal with the free-electron model of a metal, with quantum theory of lattice vibrations and with the B–E condensation. These are the materials expected of a undergraduate physics major, and they are unlikely to be covered in a one-semester course on superconductivity theory. Readers who are not physics majors will find these preliminary chapters useful. Such concepts as fermions, bosons, Fermi energy, phonons, Debye frequency, B–E condensation, and density of states are discussed and demonstrated. Quantum statistical calculations, starting with a system Hamiltonian and ending with the computation of the measurable quantity (e.g., heat capacity) by means of a grand canonical ensemble are illustrated. Chapters 5 and 6 are also preliminaries. Chapter 5 deals with energy band structures and Bloch electron dynamics. The Bloch theorem, Bloch electrons, Fermi liquid model, electrons and holes, and nonspherical Fermi surfaces are introduced here. These concepts are indispensable in developing the microscopic theory of superconductivity, as is the second quantization formalism, which is fully developed in Chapter 6. The quantum many-body problem can most simply be formulated and treated in the Heisenberg picture. The equation-of-motion method is developed, which will be used repeatedly in the later chapters.

Chapters 7–11 constitute the central core of the present book, and deal with a theory of superconductivity proper. The basic cause for superconductivity is the phonon-exchange attraction, which is derived by employing a time-dependent quantum perturbation method in Chapter 7, where the interaction between electrons and ions is reviewed. For ease of presentation, we discuss the thermodynamic properties of superconductors at 0 K, above and below T_c in Chapters 8–10. In Chapter 8 many important formulas, including those for the binding energy of a Cooper pair, Eq. (1.4.1), the excitation energy of a moving pairon, Eq. (1.4.2), the ground-state energy of the BCS system, Eq. (1.4.3), and the quasi-electron energy with a gap Δ, Eq. (1.4.5), are derived. Our theory is developed by generalizing the BCS theory and incorporating the energy band structures of electrons and phonons. In Chapter 9 we shall see that a system of free pairons having a linear energy–momentum relation undergoes a B–E condensation transition of second order. The critical temperature T_c depends on the pairons density n_0 and on the Fermi velocity v_F. In Chapter 10 we show that quasi-electrons having energy gaps Δ below T_c are bound by the phonon-exchange attraction to form moving pairons having energy gaps $\in_g$. The quantum tunneling data are analyzed based on the pairon transport model. The thermodynamic properties of the superconductor below T_c is calculated under the assumption that moving pairons rather than quasi-electrons are the elementary excitations in

the superconductor. Supercurrents, flux quantization, Josephson effects, Londons' equation, G–L wave function and quasi-wave functions are discussed in Chapter 11 from the many-pairon condensation point of view. In the present text, a quantum statistical theory of superconductivity is presented mainly for elemental superconductors. The theory can be extended to compound superconductors with a slight modification by regarding optical and acoustic phonons as the intermediary for bound pairons. In Chapters 12 and 13, we briefly discuss compound and high-T_c superconductors. Finally summary and remarks are given in Chapter 14.

REFERENCES

1. H. Kamerlingh Onnes, *Akad. V. Wetenschappen* (*Amsterdam*) **14**, 113 (19 11).
2. W. Meissner and R. Ochsenfeld, *Naturwiss.* **21**, 787 (1933).
3. J. File and R. G. Mills, *Phys. Rev. Lett.* **10**, 93 (1963).
4. B. S. Deaver and W. M. Fairbank, *Phys. Rev. Lett.* **7**, 43 (1961).
5. R. Doll and M. Näbauer, *Phys. Rev. Lett.* **7**, 51 (1961).
6. F. London and H. London, *Proc. Roy. Soc.* (*London*)**A149**, 71 (1935);*Physica* **2**, 341 (1935).
7. V. L. Ginzburg and L. D. Landau, *J. Exp. Theor. Phys.* (*USSR*) **20**, 1064 (1950).
8. W. H. Keesom and J. H. Van den Ende, *Commun. Phys. Lab. Univ. Leiden,* **No. 2196** (1932); W. H. Keesom and J. A. Kok, *Physica* **1**, 175 (1934).
9. N. E. Phillips, *Phys. Rev.* **114**, 676 (1959).
10. R. E. Glover III and M. Tinkham, *Phys. Rev.* **108**, 243 (1957); M. A. Biondi and M. Garfunkel, *Phys. Rev.* **116**, 853 (1959).
11. I. Giaever, *Phys. Rev. Lett.* **5**, 147, 464 (1960).
12. I. Giaever and K. Megerle, *Phys. Rev.* **122**, 1101 (1961).
13. C. A. Reynolds, *et al., Phys. Rev.* **122**, 1101 (1950).
14. B. D. Josephson, *Phys. Lett.* **1**, 251 (1962).
15. P. W. Anderson and J. M. Rowell, *Phys. Rev. Lett.* **10**, 486 (1963).
16. R. C. Jaklevic, *et al., Phys. Rev.* **140**, A1628 (1965).
17. J. G. Bednorz and K. A. Müller, *Z. Phys. B* **64**, 189 (1986).
18. M. K. Wu, *et al., Phys. Rev. Lett.* **58**, 908 (1987).
19. P. A. M. Dirac, *Principles of Quantum Mechanics,* 4th ed. (Oxford University Press, London, 1958).
20. P. Ehrenfest and J. R. Oppenheimer, *Phys. Rev.* **37**, 333 (1931); H. A. Bethe and R. F. Bacher, *Rev. Mod. Phys.* **8**, 193 (1936).
21. F. London, *Nature* (*London*) **141**, 643 (1938); *Superfluids, I and II* (Dover, New York, 1964).
22. A. Einstein, *Sits. Ber. Berl. Akad.* 3 (1925).
23. L. D. Landau, *J. Exptl. Theoret. Physics* (*USSR*)**30**, 1058 (1956); *ibid.* **32,** 59 (1957).
24. A. Haug, *Theoretical Solid-State Physics,* Vol. 1 (Pergamon, Oxford, 1972); C. Kittel, *Introduction to Solid-State Physics,* 6th ed. (Wiley, New York, 1986); N. W. Ashcroft and N. D. Mermin, *Solid-State Physics* (Saunders, Philadelphia, 1976); W. Harrison, *Solid-State Theory* (Dover, New York, 1980).
25. A. C. Rose-Innes and E. H. Rhoderick, *Introduction to Superconductivity,* 2d ed. (Pergamon, Oxford, UK, 1978).
26. C. J. Gorter and H. B. G. Casimir, *Physica* **1**, 306 (1934).
27. J. Bardeen, L. N. Cooper, and J. R. Schrieffer, *Phys. Rev.* **108**, 1175 (1957).
28. H. Fröhlich, *Phys. Rev.* **79**, 845 (1950).
29. L. N. Cooper, *Phys. Rev.* **104,** 1189 (1956).
30. D. J Douglas Jr. and R. W. Schmitt, *Rev. Mod. Phys.* **36**, l–331 (1964); R. D. Park, ed., *Superconductivity* (Marcel Dekker, New York, 1969).
31. S. Fujita, *J. Supercond.* **4**, 297 (1991); *J. Supercond.* **5**, 83 (1992); S. Fujita and S. Watanabe, *J. Supercond.* **5**, 219 (1992); *J. Supercond.* **6**, 75 (1993).
32. S. Fujita and S. Godoy, *J. Supercond.* **6**, 373 (1993).

2

Free-Electron Model for a Metal

In a metal conduction electrons move almost freely. The electrons obey the Fermi–Dirac statistics, and the thermodynamic properties of moving electrons are very different from what classical statistical mechanics predicts. These properties will be discussed based on the free-electron model. Elementary discussions of electrical conduction and the motion of a charged particle in electric and magnetic fields are also included. More advanced treatments of a metal will be given in Chapter 5.

2.1. CONDUCTION ELECTRONS IN A METAL; THE HAMILTONIAN

Let us take a monovalent metal. The Hamiltonian H of the system may be represented by

$$H = \sum_{j=1}^{N} \frac{p_j^2}{2m} + \sum\sum_{j>k} \frac{k_0 e^2}{|\mathbf{r}_j - \mathbf{r}_k|} + \sum_{\alpha=1}^{N} \frac{P_\alpha^2}{2M} + \sum\sum_{\alpha>\gamma} \frac{k_0 e^2}{|\mathbf{R}_\alpha - \mathbf{R}_\gamma|} - \sum_j \sum_\alpha \frac{k_0 e^2}{|\mathbf{r}_j - \mathbf{R}_\alpha|} \tag{2.1.1}$$

$k_0 \equiv (4\pi\epsilon_0)^{-1}$. The sums on the right-hand side (rhs) represent, respectively, the kinetic energy of electrons, the interaction energy among electrons, the kinetic energy of ions, the interaction energy among ions, and the interaction energy between electrons and ions. The metal as a whole is electrically neutral, and therefore the number of electrons should equal the number of ions. Both numbers are denoted by N.

At very low temperatures, the ions will be almost stationary near the equilibrium lattice points. (Because of quantum zero-point motion, the ions are not at rest even at 0 K. But this fact does not affect the following argument in a substantial manner.) Then the system can be viewed as the one in which the electrons move in a periodic lattice potential. The Hamiltonian of this idealized system that now depends on the electron variables only can be written as

$$H = \sum_j \frac{p_j^2}{2m} + \sum\sum_{j>k} \frac{k_0 e^2}{|\mathbf{r}_j - \mathbf{r}_k|} + \sum_j V(\mathbf{r}_j) + C \tag{2.1.2}$$

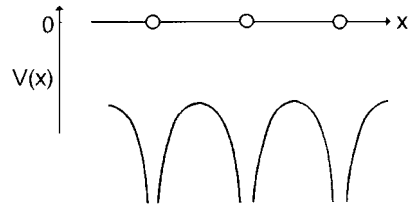

Figure 2.1. A periodic potential in one dimension.

where $V(\mathbf{r}_j)$ represents the lattice potential, and the constant energy C depends on the lattice configuration.

Let us drop the Coulomb interaction energy from Eq. (2.1.2). We then have

$$H = \sum_j \frac{p_j^2}{2m} + \sum_j V(\mathbf{r}_j) + \text{constant} \tag{2.1.3}$$

which now characterizes a system of noninteracting electrons in the lattice. In Fig. 2.1 we draw a typical lattice potential in one dimension.

Quantum mechanical calculations (Bloch's theorem; see Section 5.1) show that the wave function ψ, which satisfies the Schrödinger equation:

$$\left[-\frac{\hbar^2}{2m}\nabla^2 + V(\mathbf{r})\right]\psi(\mathbf{r}) = E\psi(\mathbf{r}) \tag{2.1.4}$$

has the form:

$$\psi_{\mathbf{k}}(\mathbf{r}) = e^{j\mathbf{k}\cdot\mathbf{r}}u_{\mathbf{k}}(\mathbf{r}), \qquad u_{\mathbf{k}}(\mathbf{r}+\mathbf{R}) = u_{\mathbf{k}}(\mathbf{r}) \tag{2.1.5}$$

The absolute square of the wave function:

$$|\psi_{\mathbf{k}}(\mathbf{r})|^2 = |u_{\mathbf{k}}(\mathbf{r})|^2 \tag{2.1.6}$$

then is *lattice-periodic.* That is, the probability distribution function for the electron has the same periodicity as that of the lattice. The associated energy eigenvalues E have *forbidden regions (energy gaps),* and the energy eigenstates are characterized by the *wave vector* $\mathbf{k}$ and the *zone number j,* which enumerates the allowed energy bands:

$$E = \epsilon_j(\hbar\mathbf{k}) \tag{2.1.7}$$

A typical set of the energy bands is shown in Fig. 2.2.

At the absolute zero of temperature, these energy bands are filled with electrons from the bottom up, the upper limit being provided by the *Fermi energy* $\in_F$ This is due to *Pauli's exclusion principle*: No two electrons can occupy the same quantum state.

If the uppermost energy band is completely filled with electrons, no electrons can gain energy in a continuous manner. In this case electrons cannot be accelerated by an applied electric field, and the material having such an electronic band configuration behaves like an insulator. This is true for all crystals formed by inert-gas atoms, such as He.

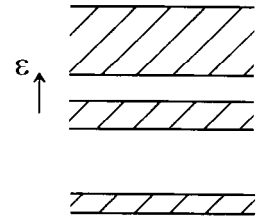

Figure 2.2. A typical set of the energy bands for the electrons in a crystal.

Consider now the case in which the uppermost energy band is partially filled with electrons and the Fermi energy lies in the middle of the band. If a small electric field $\mathbf{E} = -\nabla\phi$ is applied, those electrons having energies close to the Fermi energy can gain the electric energy $-e\phi$ in a continuous manner just as the classical electrons can. This case corresponds to a *metallic material.* The detailed treatments (see Chapter 5) show that those electrons in the partially filled band can flow in much the same manner as electrons in free space, whose energy–momentum relation:

$$E_{\text{free}} = \frac{p^2}{2m} \equiv \frac{\hbar^2 k^2}{2m} \tag{2.1.8}$$

is a simple function of the momentum $\mathbf{p}$ with no energy gap. Only the response to the electric field is different. For most metals, the response of the conduction electrons to the field can adequately be described by the *effective mass approximation.* That is, the conduction electrons respond with a certain effective mass m^*, whose value is of the order of the free electron mass m, the actual value depending on the energy band structures. The dynamic behavior of the conduction electrons can then be characterized by the energy–momentum relation:

$$E_{\text{conduction electron}} = \frac{p^2}{2m^*} \equiv \frac{\hbar^2 k^2}{2m^*} \tag{2.1.9}$$

The foregoing discussions in terms of the energy bands are based on the Hamiltonian in Eq. (2.1.3) with the neglect of the Coulomb interaction among electrons:

$$\sum_{j>k}\sum \frac{k_0 e^2}{|\mathbf{r}_j - \mathbf{r}_k|} \tag{2.1.10}$$

This interaction is very important. However including of this interaction in the quantum mechanical calculations does not destroy such outstanding features as energy bands with gaps and the sharply defined Fermi energy. In this sense the Coulomb interaction plays a secondary role. This interaction introduces a correlation among the electrons' motion, and its proper treatment is quite complicated. Later in Section 5.3, we shall develop a single-electron picture approximation called the Fermi's liquid model.

2.2. FREE ELECTRONS; THE FERMI ENERGY

Let us consider a system of free electrons characterized by the Hamiltonian:

$$H = \sum_j \frac{p_j^2}{2m} \tag{2.2.1}$$

The momentum eigenstates for a quantum particle with a periodic cube box boundary condition are characterized by three quantum numbers:

$$p_{x,j} = \left(\frac{2\pi\hbar}{L}\right)j, \qquad p_{y,k} = \left(\frac{2\pi\hbar}{L}\right)k, \qquad p_{z,l} = \left(\frac{2\pi\hbar}{L}\right)l \tag{2.2.2}$$

where L is the cube side-length, and j, k, and l are integers. For simplicity, we indicate the momentum state by a single Greek letter κ:

$$\mathbf{p}_\kappa \equiv (p_{x,j}, p_{y,k}, p_{z,l}) \tag{2.2.3}$$

The quantum state of our many-electron system can be specified by the set of occupation numbers $\{n_\kappa\}$, with each $n_\kappa \equiv n_{\mathbf{p}_\kappa}$ taking on either one or zero. The ket vector representing such a state will be denoted by

$$|\{n\}\rangle \equiv |\{n_\kappa\}\rangle \tag{2.2.4}$$

The corresponding energy eigenvalue is given by

$$E(\{n\}) = \sum_\kappa \epsilon_\kappa n_\kappa \tag{2.2.5}$$

where $\epsilon_\kappa \equiv p_\kappa^2/2m$ is the kinetic energy of the electron with momentum $\mathbf{p}_\kappa$. The sum of the occupation numbers n_κ equals the total number N of electrons:

$$\sum_\kappa n_\kappa = N \tag{2.2.6}$$

We assume that the system is in thermodynamic equilibrium, which is characterized by temperature $T \equiv (k_B\beta)^{-1}$ and number density n. The thermodynamic properties of the system can then be computed in terms of the grand canonical ensemble density operator:

$$\rho_G = \frac{e^{\alpha N - \beta H}}{\mathrm{TR}\{e^{\alpha N - \beta H}\}} \tag{2.2.7}$$

The ensemble average of n_κ is represented by the *Fermi distribution function* f_F:

$$\langle n_\kappa \rangle \equiv \frac{\mathrm{TR}\{n_\kappa e^{\alpha N - \beta H}\}}{\mathrm{TR}\{e^{\alpha N - \beta H}\}} = [\exp(\beta\epsilon_\kappa - \alpha) + 1]^{-1} \equiv f_F(\epsilon_\kappa) \tag{2.2.8}$$

(Problem 2.2.1.) The parameter α in this expression is determined from

$$n = \frac{\langle N \rangle}{V} = \frac{1}{V}\sum_\kappa \frac{1}{\exp(\beta\epsilon_\kappa - \alpha) + 1} \equiv \frac{1}{V}\sum_\kappa f_F(\epsilon_\kappa) \tag{2.2.9}$$

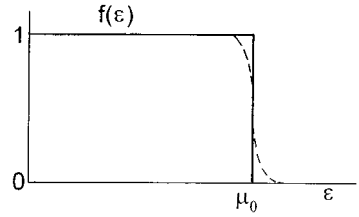

Figure 2.3. The Fermi distribution function against energy $\in$. The solid line is for $T = 0$ and the broken line for a small T.

Hereafter we drop the subscript F on f_F.

We now investigate the behavior of the Fermi distribution function $f(\in)$ at very low temperatures. Let us set

$$\alpha \equiv \beta\mu \equiv \frac{\mu}{k_B T} \tag{2.2.10}$$

Here the quantity μ represents the *chemical potential.* At the low-temperature limit, the chemical potential μ approaches a positive constant $\mu_0 : \mu \to \mu_0 > 0$. We plot the Fermi distribution function $f(\in)$ at $T = 0$ against the energy $\in$ with a solid curve in Fig. 2.3. It is a step function with the step at $\in = \mu_0$. This means that every momentum state $\mathbf{p}_\kappa$ for which $\in_\kappa = p_\kappa^2/2m < \mu_0$ is occupied with probability 1, and all other states are unoccupied. This special energy μ_0 is called the *Fermi energy*; it is often denoted by $\in_F$, and it can be calculated in the following manner:

From Eq. (2.2.9) we have

$$n = V^{-1} \sum_\kappa [f(\epsilon_\kappa)]_{T=0} = V^{-1} \qquad \text{(the number of states } \kappa \text{ for which } \in_\kappa \leq \mu_0) \tag{2.2.11}$$

The momentum eigenstates in Eq. (2.2.2) can be represented by points in the three-dimensional momentum space, as shown in Fig. 2.4. These points form a simple cubic

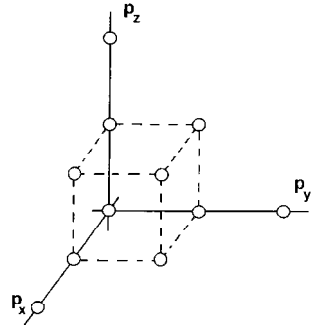

Figure 2.4. The momentum states for a periodic cubic boundary condition form a simple cubic lattice with the lattice constant $2\pi\hbar/L$.

(sc) lattice with the lattice constant $2\pi\hbar/L$. Let us define the *Fermi momentum* p_F by

$$\mu_0 \equiv \epsilon_F \equiv \frac{p_F^2}{2m} \tag{2.2.12}$$

The number of occupied states will be equal to the number of lattice points within the sphere of radius p_F. Since one lattice point corresponds to one unit cell for the sc lattice, this number is equal to the volume of the sphere, $(4\pi/3)p_F^3$, divided by the volume of the unit cell, $(2\pi\hbar/L)^3$:

$$\text{number of occupied states} = \left(\frac{4\pi}{3}\right)\frac{p_F^3}{(2\pi\hbar/L)^3} \tag{2.2.13}$$

Introducing this into Eq. (22.11), we obtain

$$n = \left(\frac{4\pi}{3}\right)\frac{p_F^3}{(2\pi\hbar/L)^3/L^3} = \left(\frac{4\pi}{3}\right)\frac{p_F^3}{(2\pi\hbar)^3} \tag{2.2.14}$$

This result was obtained under the assumption of a periodic cube-box boundary condition. The result obtained in the *bulk limit,* where

$$L^3 = V \to \infty, \qquad N \to \infty \text{ such that } \qquad n \equiv \frac{N}{V} = \text{Constant} \tag{2.2.15}$$

is valid independent of the shape of the boundary (see Problem 2.2.2).

In our discussion so far, we have neglected the fact that an electron has a *spin angular momentum* (or simply *spin*) as additional degrees of freedom. It is known that any quantum state for an electron must be characterized not only by the quantum numbers $(p_{x,j}, p_{y,k}, p_{z,l})$ describing its motion in the ordinary space, but also by the quantum numbers describing its spin. It is further known that the electron has a permanent magnetic moment associated with its spin and that the eigenvalues s_z of the z-component of the electronic spin are discrete and restricted to the two values $\pm\hbar/2$. In the absence of a magnetic field, the magnetic potential energy is the same for both spin states. In the grand canonical ensemble, the states with the same energy are distributed with the same probability. In taking account of the spins, we must then multiply the rhs of Eq. (2.2.14) by the factor 2, called the *spin degeneracy factor.* We thus obtain

$$n = \frac{8\pi}{3}\frac{1}{(2\pi\hbar)^3}p_F^3 \tag{2.2.16}$$

(including the spin degeneracy). After solving this equation for p_F, we obtain the Fermi energy as follows:

$$\boxed{\epsilon_F = \frac{\hbar^2(3\pi^2 n)^{2/3}}{2m}} \tag{2.2.17}$$

Let us estimate the order of magnitude for ϵ_F by taking a typical metal, Cu. This metal has a specific weight of 9g cm^{-3} and a molecular weight of 63.5, yielding the number density $n = 8.4 \times 10^{22}$ electrons/cm^3. Using this value for n, we find that

$$\epsilon_F \equiv k_B T_F, \qquad T_F \cong 80{,}000 \text{ K} \tag{2.2.18}$$

This T_F is called the *Fermi temperature.* The value found for the Fermi energy $\epsilon_F \equiv k_B T_F$ is very high compared to the thermal excitation energy of the order $k_B T$, which we shall see later in Section 2.4. This makes the thermodynamic behavior of the conduction electrons at room temperature drastically different from that of a classical gas.

The Fermi energy by definition is the chemical potential at 0 K. We may look at this relation in the following manner. For a box of a finite volume V, the momentum states form a simple cubic lattice as shown in Fig. 2.4. As the volume V is made greater, the unit-cell volume in the momentum space, $(2\pi\hbar/L)^3$, decreases like V^{-1}. However in the process of the bulk limit, we must increase the number of electrons N in proportion to V. Therefore the radius of the *Fermi sphere* within which all momentum states are filled with electrons neither grows nor shrinks. Obviously this configuration corresponds to the lowest energy state for the system. The Fermi energy $\epsilon_F \equiv p_F^2/2m$ represents the electron energy at the surface of the Fermi sphere. If we attempt to add an extra electron to the Fermi sphere, we must bring in an electron with an energy equal to ϵ_F, indicating that $\epsilon_F = \mu_0$.

Problem 2.2.1. Verify Eq. (2.2.8).

Problem 2.2.2. The momentum eigenvalues for a particle in a periodic rectangular box with sides of unequal lengths (L_1, L_2, L_3) are given by $p_{x,j} = 2\pi\hbar j/L_1, p_{y,k} = 2\pi\hbar k/L_2, p_{z,l} = 2\pi\hbar l/L_3$. Show that the Fermi energy ϵ_F for free electrons is still given Eq. (2.2.17) in the bulk limit.

2.3. DENSITY OF STATES

In many quantum statistical calculations, we must convert the sum over quantum states into an integral. This conversion becomes necessary when we first find discrete quantum states for a periodic box, then seek the sum over states in the bulk limit. This conversion is a welcome procedure because the resulting integral is easier to handle than the sum. The conversion is of a purely mathematical nature, but it is an important step in carrying out statistical mechanical computations.

Let us first examine a sum over momentum states corresponding to a one-dimensional motion. We take

$$\sum_k A(p_k) \tag{2.3.1}$$

where $A(p)$ is an arbitrary function of p. The discrete momentum states are equally spaced, as shown by short bars in Fig. 2.5. As the normalization length L is made greater, the spacing (distance) between two successive states $2\pi\hbar/L$ becomes smaller. This means that the number of states per unit momentum interval increases with L. We denote the number of states within a small momentum interval Δp by Δn. Consider the ratio $\Delta n/\Delta p$. Dividing both the numerator and denominator by Δp, we obtain

$$\frac{\Delta n}{\Delta p} = \frac{1}{\text{momentum spacing per state}} = \frac{L}{2\pi\hbar} \tag{2.3.2}$$

This ratio $\Delta n/\Delta p$ increases linearly with the normalization length L.

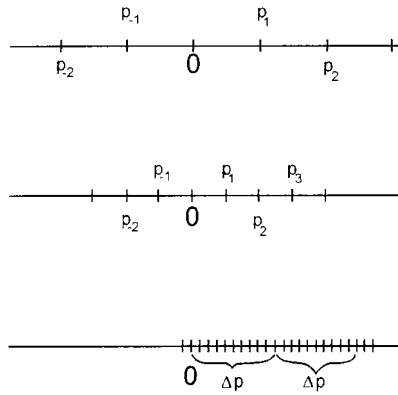

Figure 2.5. The linear momentum states are represented by short bars forming a linear lattice with unit spacing equal to $2\pi\hbar/L$.

Let us now consider a sum:

$$\sum_l A(p_l)\frac{\Delta n}{\Delta_l p}\Delta_l p \tag{2.3.3}$$

where $\Delta_l p$ is the lth interval and p_l represents a typical value of p within the interval $\Delta_l p$, say the p-value at the midpoint of $\Delta_l p$. The two sums Eqs. (2.3.1) and (2.3.3) have the same dimension, and they are close to each other if (i) the function $A(p)$ is a smooth function of p, and (ii) there exist many states in $\Delta_l p$ so that $\Delta n/\Delta_l p$ can be regarded as the *density of states*. The second condition is satisfied for the momentum states $\{p_k\}$ when the length L is made sufficiently large. In the bulk limit, Eqs. (2.3.1) and (2.3.3) will be equal:

$$\lim_{L\to\infty}\sum_{k(\text{states})} A(p_k) = \sum_{\Delta_l p} A(p)\frac{\Delta n}{\Delta_l p}\Delta_l p \tag{2.3.4}$$

In the small interval limit the sum on the rhs becomes the integral $\int dp\, A(p) dn/dp$, where [using Eq. (2.3.2)]

$$\frac{dn}{dp} \equiv \lim_{\Delta p\to 0}\frac{\Delta n}{\Delta p} = \frac{L}{2\pi\hbar} \tag{2.3.5}$$

is the density of states in the momentum space (line). In summary we therefore have

$$\boxed{\sum_k A(p_k) \to \int_{-\infty}^{\infty} dp\, A(p)\frac{dn}{dp}} \tag{2.3.6}$$

We stress that condition (i) depends on the nature of the function A. Therefore if $A(p)$ is singular at some point, this condition is not satisfied, which may invalidate the

limit in Eq. (2.3.6). Such exceptional cases do occur. (See Section 4.2.) We further note that the density of states $dn/dp = L(2\pi\hbar)^{-1}$ does not depend on the momentum.

The sum-to-integral conversion, which we have discussed, can easily be generalized for a multidimensional case. For example we have

$$\sum_{\mathbf{p}_k} A(\mathbf{p}_k) \to \int d^3pA(\mathbf{p})\mathcal{D}(\mathbf{p}) \text{ as } V \equiv L^3 \to \infty \tag{2.3.7}$$

The density of states $\mathcal{D}(\mathbf{p}) \equiv dn/d^3p$ can be calculated by extending the arguments leading to Eq. (2.3.2). We choose the periodic cubic box of side length L for the normalization, take the spin degeneracy into account and obtain

$$\mathcal{D}(p) = \frac{dn}{d^3p} = \frac{2L^3}{(2\pi\hbar)^3} \tag{2.3.8}$$

(with spin degeneracy).

Let us use this result and simplify the normalization condition in Eq. (2.2.9). We then obtain

$$n = \text{Lim}(1/V)\int d^3pf(p^2/2m)\mathcal{D}(\mathbf{p}) = 2(2\pi\hbar)^{-3}\int d^3pf(p^2/2m) \qquad (L^3 = V) \tag{2.3.9}$$

Next consider the energy density of the system. Using Eqs. (2.2.5) and (2.2.8) we obtain

$$e \equiv \text{Lim}\,\frac{\langle H\rangle}{V} = \text{Lim}(1/V)\sum_{\kappa}\epsilon_{\kappa}f(\epsilon_{\kappa}) = 2(2\pi\hbar)^{-3}\int d^3p\left(\frac{p^2}{2m}\right)f(p^2/2m) \tag{2.3.10}$$

Equations (2.3.9) and (2.3.10) were obtained by starting with the momentum eigenvalues corresponding to the periodic cube-box boundary conditions. The results in the bulk limit however do not depend on the boundary condition.

The concept of the density of states can also be applied to the energy domain. This is convenient when the sum over states has the form:

$$\sum_{\kappa} g(\epsilon_{\kappa}) \tag{2.3.11}$$

where $g(\epsilon_\kappa)$ is a function of the energy ϵ_κ associated with the state κ. The sums in Eqs. (2.2.5) and (2.2.9) are precisely in this form.

Let dn be the number of the states within the energy interval $d\epsilon$. In the bulk limit, this number dn will be proportional to the interval $d\epsilon$, so that

$$dn = \mathcal{N}(\epsilon)d\epsilon \tag{2.3.12}$$

Here the proportionality factor

$$\mathcal{N}(\epsilon) \equiv \frac{dn}{d\epsilon} \tag{2.3.13}$$

is called the *density of states in the energy domain.* This quantity $\mathcal{N}(\epsilon)$ generally depends on the location of the interval $d\epsilon$, and therefore on a typical energy ϵ within $d\epsilon$, say, the

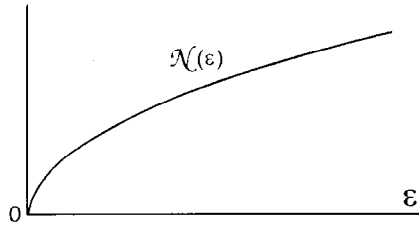

Figure 2.6. The density of states in energy $\mathcal{N}(\epsilon)$ for free electrons in three dimensions grows like $\epsilon^{1/2}$.

energy at the midpoint of the interval $d\epsilon$. If the set of the states $\{\kappa\}$ becomes densely populated in the bulk limit and the function g is smooth, then the sum may be converted into an integral of the form:

$$\boxed{\sum_{\kappa(\text{states})} g(\epsilon_\kappa) \to \int d\epsilon\, g(\epsilon)\mathcal{N}(\epsilon)} \tag{2.3.14}$$

Let us now calculate the density of states $\mathcal{N}(\epsilon)$ for the system of free electrons. The number of states dn in the spherical shell in momentum space is obtained by dividing the volume of the shell $4\pi p^2 dp$ by the unit cell volume $(2\pi\hbar/L)^3$ and multiplying the result by the spin degeneracy factor 2:

$$dn = \frac{2 \times 4\pi p^2 dp}{(2\pi\hbar/L)^3} = V\frac{8\pi p^2}{(2\pi\hbar)^3}dp \tag{2.3.15}$$

Since $p = (2m\epsilon)^{1/2}$, we obtain

$$dp = \frac{dp}{d\epsilon}d\epsilon = \left(\frac{m}{2\epsilon}\right)^{1/2} d\epsilon \tag{2.3.16}$$

Using these equations we obtain

$$dn = V\frac{8\pi(2m\epsilon)}{(2\pi\hbar)^3}\left(\frac{m}{2\epsilon}\right)^{1/2} d\epsilon = V\frac{8\pi 2^{1/2}m^{3/2}}{(2\pi\hbar)^3}\epsilon^{1/2}d\epsilon \tag{2.3.17}$$

or

$$\mathcal{N}(\epsilon) \equiv \frac{dn}{d\epsilon} = V\frac{2^{1/2}m^{3/2}}{\pi^2\hbar^3}\epsilon^{1/2} \tag{2.3.18}$$

The density of states $\mathcal{N}(\epsilon)$ grows like $\epsilon^{1/2}$. Its general behavior is shown in Fig. 2.6.

We may now reexpress the normalization condition (2.2.9) as follows:

$$n = \text{Lim}\,\frac{1}{V}\sum_{\kappa} f(\epsilon_\kappa) = \text{Lim}\,\frac{1}{V}\int_0^\infty d\epsilon f(\epsilon)\mathcal{N}(\epsilon) = \frac{2^{1/2}m^{3/2}}{\pi^2\hbar^3}\int_0^\infty d\epsilon\,\epsilon^{1/2}f(\epsilon) \tag{2.3.19}$$

The density of states in the energy domain, defined by Eq. (2.3.13), is valid even when we have states other than the momentum states. We shall see such cases in later applications (see Sections 3.5).

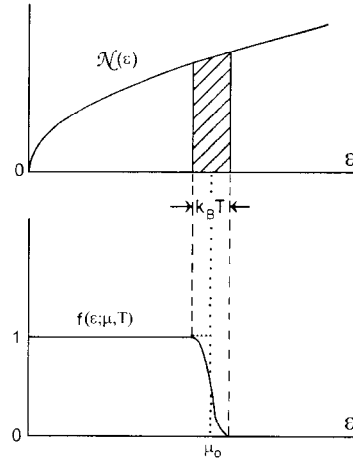

Figure 2.7. The density of states in energy $\mathcal{N}(\epsilon)$ and the Fermi distribution function $f(\epsilon)$ are drawn as functions of the kinetic energy ϵ. The change in f is appreciable only near the Fermi energy μ_0 if $k_B T \ll \mu_0$. The shaded area represents approximately the number of thermally excited electrons.

Problem 2.3.1. Obtain Eq. (2.3.19) directly from Eq. (2.3.9) by using the spherical polar coordinates (p, θ, φ) in the momentum space, integrating over the angles (θ, φ), and rewriting the p-integral in terms of the ϵ-integral.

2.4. HEAT CAPACITY OF DEGENERATE ELECTRONS 1; QUALITATIVE DISCUSSIONS

At room temperature most metals have molar heat capacities of about $3R$ (where R is the gas constant) just as for nonmetallic solids. This experimental fact cannot be explained based on classical statistical mechanics. By applying the Fermi–Dirac statistics to conduction electrons, we can demonstrate the near absence of the electronic contribution to the heat capacity. In the present section, we treat this topic in a qualitative manner.

Let us consider highly degenerate electrons with a high Fermi temperature T_F ($\approx$ 80,000 K). At 0 K the Fermi distribution function:

$$f(\epsilon; \mu, T) \equiv \frac{1}{\exp[(\epsilon - \mu)/k_B T] + 1} \tag{2.4.1}$$

is a step function, as indicated by the dotted line in the lower diagram in Fig. 2.7.

At a finite temperature T, the abrupt drop at $\epsilon = \mu_0$ becomes a smooth drop, as indicated by a solid line in the same diagram. In fact, the change in the distribution function $f(\epsilon)$ is appreciable only in the neighborhood of $\epsilon = \mu_0$. The function $f(\epsilon; \mu, T)$ will drop from 1/2 at $\epsilon = \mu$ to 1/101 at $\epsilon - \mu = k_B T \ln(100)$, [which can be directly verified from Eq. (2.4.1)]. This value $k_B T \ln(100) = 4.6\ k_B T$ is much less than the Fermi energy $\mu_0 = k_B T_F$ (80,000 K). This means that only those electrons with energies

close to the Fermi energy μ_0 are excited by the rise in temperature. In other words the electrons with energies ϵ far below μ_0 are not affected. There are many such electrons, and in fact this group of unaffected electrons forms the great majority.

The number N_X of electrons that are thermally excited can be found in the following manner. In the upper part of Fig. 2.7, the density of states $\mathcal{N}(\epsilon)$ is drawn. Since $\mathcal{N}(\epsilon)d\epsilon$ represents by definition the number of electrons within $d\epsilon$, the integral of $\mathcal{N}(\epsilon)d\epsilon$ over the interval in which the electron population is affected gives an approximate number of excited electrons N_X. This integral can be represented by the shaded area in the diagram. Since we know from the earlier arguments that the affected range of the energy is of the order $k_B T$ ($\ll \mu_0$), we can estimate N_X as

$$N_X = \text{shaded area in the upper diagram} \cong \mathcal{N}(\mu_0) k_B T \tag{2.4.2}$$

where $\mathcal{N}(\mu_0)$ is the density of states at $\epsilon = \mu_0$. From Eqs. (2.3.18) and (2.2.16), we obtain

$$\mathcal{N}(\mu_0) = V \frac{2^{1/2} m^{3/2}}{\pi^2 \hbar^3} \mu_0^{1/2} = \frac{3N}{2\mu_0} \tag{2.4.3}$$

Using this expression, we obtain from Eq. (2.4.2)

$$N_X = \left(\frac{3}{2}\right) \frac{N k_B T}{\mu_0} \tag{2.4.4}$$

The electrons affected will move up with the extra energy of the order $k_B T$ per particle. Therefore the change in the total energy will be approximated by

$$\Delta E = N_X \times k_B T = \left(\frac{3}{2}\right) \frac{N(k_B T)^2}{\mu_0} \tag{2.4.5}$$

Differentiating this with respect to T, for the molar heat capacity, we obtain

$$C_V = \frac{\partial}{\partial T} \Delta E = 3 N_0 k_B^2 \frac{T}{\mu_0} = 3R \frac{T}{T_F} \qquad (\mu_0 \equiv k_B T_F, R \equiv N_0 k_B) \tag{2.4.6}$$

This expression indicates that the molar electronic heat capacity at room temperature (T = 300 K) is indeed small:

$$C_V = 3R \frac{300}{80{,}000} = 0.011\, R$$

It is stressed that the result (2.4.6) was obtained because the number of thermally excited electrons N_X is much less than the total number of electrons N [see Eq. (2.4.4)]. We also note that the electronic heat capacity is linear in the temperature.

2.5. HEAT CAPACITY OF DEGENERATE ELECTRONS 2; QUANTITATIVE CALCULATIONS

Historically Sommerfeld first applied the Fermi–Dirac statistics to the conduction electrons and calculated the electronic heat capacity. His calculations resolved the heat capacity paradox. In this section we calculate the heat capacity quantitatively.

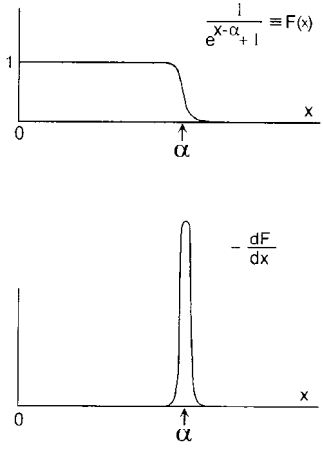

Figure 2.8. The function $F(x)$ and $-dF/dx$ are shown for $x \geq 0$ and $\alpha \gg 1$.

The heat capacity at constant volume, C_v, can be calculated by differentiating the internal energy E with respect to the temperature T:

$$C_V = \frac{\partial E}{\partial T}\Big)_V \tag{2.5.1}$$

The internal energy density for free electrons given by Eq. (2.3.10) can be expressed as

$$\frac{E(T,V)}{V} = \frac{2^{1/2}m^{3/2}}{\pi^2\hbar^3}\int_0^\infty d\epsilon\, \epsilon^{3/2} f(\epsilon;\mu,T) \tag{2.5.2}$$

Here the chemical potential μ is related to the number density n by Eq. (2.3.19):

$$n = \frac{2^{1/2}m^{3/2}}{\pi^2\hbar^3}\int_0^\infty d\epsilon\, \epsilon^{1/2} f(\epsilon) \tag{2.5.3}$$

The integrals on the rhs of Eqs. (2.5.2) and (2.5.3) may be evaluated as follows. Assume

$$\alpha \equiv \beta\mu \gg 1 \tag{2.5.4}$$

Consider

$$F(x) \equiv \frac{1}{e^{x-\alpha}+1}, \qquad -\frac{dF}{dx} \equiv -F'(x) = \frac{e^{x-\alpha}}{(e^{x-\alpha}+1)^2} \tag{2.5.5}$$

whose behaviors are shown in Fig. 2.8. We note that $-dF/dx$ is a sharply peaked function near $x = \alpha$. Let us take the integral:

$$I \equiv \int_0^\infty dx\, F(x)\frac{d\phi(x)}{dx} \tag{2.5.6}$$

where $\phi(x)$ is a certain function of x. By integrating by parts, we obtain

$$I = F(\infty)\phi(\infty) - F(0)\phi(0) - \int_0^\infty dx\,\phi(x)\frac{dF(x)}{dx} = -\phi(0) - \int_0^\infty dx\,\phi(x)\frac{dF(x)}{dx} \tag{2.5.7}$$

using Eqs. (2.5.4) and (2.5.5). We expand the function $\phi(x)$ into a Taylor series at $x = \alpha$

$$\phi(x) = \phi(\alpha) + (x-\alpha)\phi'(\alpha) + \frac{1}{2}(x-\alpha)^2\phi''(\alpha) + \ldots \tag{2.5.8}$$

introduce it into Eq. (2.5.7) and then integrate term by term. If $\alpha >> 1$,

$$-\int_0^\infty dx(x-\alpha)^n\frac{dF(x)}{dx} = \int_{-\alpha}^\infty dy\,y^n\frac{e^y}{(e^y+1)^2} \cong \int_{-\infty}^\infty dy\,y^n\frac{e^y}{(e^y+1)^2} \equiv J_n \tag{2.5.9}$$

The definite integrals J_n vanish for odd n, since the integrands are odd functions of y. For small even n, their numerical values are given by

$$J_0 = 1, \qquad J_2 = \frac{\pi^2}{3} \tag{2.5.10}$$

Using Eqs. (2.5.6)–(2.5.10), we obtain

$$I = \int_0^\infty dx F(x)\frac{d\phi(x)}{dx} = \phi(\alpha) - \phi(0) + \frac{\pi^2}{6}\phi''(\alpha) \tag{2.5.11}$$

Equation (2.5.11) is useful if $\alpha >> 1$ and $\phi(x)$ is a slowly varying function at $x = \alpha$.

We now apply Eq. (2.5.11) to evaluate the ϵ-integral in Eq. (2.5.3)

$$\int_0^\infty d\epsilon\,\epsilon^{1/2}f(\epsilon) = \beta^{3/2}\int_0^\infty dx\,x^{3/2}F(x) \qquad (\beta\epsilon \equiv x)$$

We choose

$$\phi(x) = \frac{2}{3}x^{3/2}, \qquad \frac{d\phi(x)}{dx} = x^{1/2}, \qquad \frac{d^2\phi(x)}{dx^2} = \frac{1}{2}x^{-1/2}$$

and obtain

$$\begin{aligned}\int_0^\infty d\epsilon\,\epsilon^{3/2}f(\epsilon) &= \frac{2}{3\beta^{3/2}}(\beta\mu)^{3/2} + \frac{1}{\beta^{3/2}}\frac{\pi^2}{6}\frac{1}{2}(\beta\mu)^{-1/2} \\ &= \frac{2}{3}\mu^{3/2}\left(1 + \frac{\pi^2}{8}\beta^{-2}\mu^{-2}\right)\end{aligned} \tag{2.5.12}$$

Using Eq. (2.5.12) we obtain from Eq. (2.5.3)

$$n = \frac{2^{3/2}m^{3/2}}{3\pi^2\hbar^3}\mu^{3/2}\left(1 + \frac{\pi^2}{8}\beta^{-2}\mu^{-2}\right) \tag{2.5.13}$$

Similarly we can calculate the ϵ-integral in Eq. (2.5.2) and obtain

$$e \equiv \frac{E(T,V)}{V} = \frac{2^{3/2}m^{3/2}}{5\pi^2\hbar^3}\mu^{5/2}\left(1 + \frac{5\pi^2}{8}\beta^{-2}\mu^{-2}\right) \tag{2.5.14}$$

The chemical potential μ in general depends on density n and temperature T: $\mu = \mu(n, T)$. This relation can be obtained from Eq. (2.5.13). If we substitute $\mu(n, T)$ so obtained into Eq. (2.5.14), we obtain the internal energy density as a function of n and T. By subsequently differentiating this function with respect to T at fixed n, we can obtain the heat capacity at constant volume. We may calculate the heat capacity by taking a route a little different from that just described. The Fermi energy μ_0 is given by $\hbar^2(3\pi^2 n)^{3/2}/2m$ [see Eq. (2.2.16)], which depends only on n. Solving Eq. (2.5.13) for μ and expressing the result in terms of μ_0 and T, we obtain (Problem 2.5.1)

$$\mu = \mu_0\left[1 - \frac{\pi^2}{12}\left(\frac{k_B T}{\mu_0}\right)^2 + \dots\right] \tag{2.5.15}$$

Introducing this expression into Eq. (2.5.14), we obtain (Problem 2.5.1)

$$e = \frac{3}{5}n\mu_0\left[1 + \frac{5\pi^2}{12}\left(\frac{k_B T}{\mu_0}\right)^2\right] \tag{2.5.16}$$

Differentiating this expression with respect to T at constant μ_0, we obtain

$$C_V = \left(\frac{1}{2}\right)\pi^2 N k_B \frac{T}{T_F} \tag{2.5.17}$$

where $T_F \equiv \epsilon_F/k_B$ is the *Fermi temperature*. Here we see that the heat capacity C_V for degenerate electrons is greatly reduced by the factor T/T_F ($\ll 1$) from the ideal-gas heat capacity $3Nk_B/2$. Also note that the heat capacity changes linearly with the temperature T. These findings agree with the results of our previous qualitative calculations.

At the normal experimental temperature the lattice contribution to the heat capacity, which will be discussed in Chapter 3, is much greater than the electronic contribution. Therefore the experimental verification of the linear-T law must be carried out at very low temperatures, where the contribution of the lattice vibration becomes negligible. In this temperature region, the measured molar heat should rise linearly with the temperature T. By comparing the slope with

$$\frac{C_V}{T} = \frac{\pi^2}{2}\frac{R}{T_F} \tag{2.5.18}$$

[using Eq. (2.5.17)], we can find the Fermi temperature T_F numerically. Since this temperature T_F is related to the effective mass m^* by $k_B T_F = (\hbar^2/2m^*)(3\pi^2 n)^{2/3}$ [using Eqs. (2.2.16) and (2.2.17)], we can obtain the numerical value for the effective mass m^* of the conduction electron. Other ways of finding the m^*-value are through the transport and optical properties of conductors, which will be discussed in Chapter 5.

Problem 2.5.1. (a) Use Eq. (2.5.13) to verify Eq. (2.5.15). Hint: Assume $\mu = \mu_0[1 + A(k_B T/\mu_0)^2]$ and find the constant A. (b) Verify Eq. (2.5.16).

2.6. OHM'S LAW, ELECTRICAL CONDUCTIVITY, AND MATTHIESSEN'S RULE

Let us consider a system of free electrons moving in a potential field of impurities, which act as scatterers. The impurities by assumption are distributed uniformly.

Under the action of an electric field **E** pointed along the positive x-axis, a classical electron will move according to Newton's equation of motion:

$$m\frac{dv_x}{dt} = -eE \tag{2.6.1}$$

(in the absence of the impurity potential). This gives rise to uniform acceleration and therefore a linear change in the velocity along the direction of the field:

$$v_x = -\left(\frac{e}{m}\right)Et + v_x^0 \tag{2.6.2}$$

where v_x^0 is the x-component of the initial velocity. For a free electron the velocity v_x increases indefinitely and leads to infinite conductivity.

In the presence of the impurities, this uniform acceleration will be interrupted by scattering. When the electron hits a scatterer (impurity), the velocity will suffer an abrupt change in direction and grow again following Eq. (2.6.2) until the electron hits another scatterer. Let us denote the *average time between successive scatterings* or the *mean free time* by τ_f. The average velocity $\langle v_x \rangle$ is then given by

$$\langle v_x \rangle = -\frac{e}{m}E\tau_f \tag{2.6.3}$$

where we assumed that the electron loses the memory of its preceding motion every time it hits a scatterer, and the average velocity after collision is zero:

$$\langle v_x^0 \rangle = 0 \tag{2.6.4}$$

The charge current density (average current per unit volume) j is given by

$$j = (\text{charge}) \times (\text{number density}) \times (\text{velocity}) = en\langle v_x \rangle = e^2 n\tau_f \frac{E}{m} \tag{2.6.5}$$

where n is the number density of electrons. According to *Ohm's law,* the current density j is proportional to the applied field E when this field is small:

$$j = \sigma E \tag{2.6.6}$$

The proportionality factor σ is called the *electrical conductivity.* It represents the facility with which the current flows in response to the electric field. Comparing the last two equations, we obtain

$$\boxed{\sigma = \frac{e^2 n\tau_f}{m}} \tag{2.6.7}$$

This equation is very useful in the qualitative discussion of the electrical transport phenomenon. The inverse mass-dependence law means that the ion contribution to the

electric transport in an ionized gas will be smaller by at least three orders of magnitude than the electron contribution. Also note that the conductivity is higher if the number density is greater and/or if the mean free time is greater.

The inverse of the mean free time τ_f:

$$\Gamma \equiv \frac{1}{\tau_f} \tag{2.6.8}$$

is called the *rate of collision* or the *collision rate.* Roughly speaking this Γ represents the mean frequency with which the electron is scattered by impurities. The collision rate Γ is given by

$$\Gamma = n_I v A \tag{2.6.9}$$

where n_I, v, and A are, respectively, the density of scatterers, the electron speed, and the scattering cross section.

If there is more than one kind of scatterer, the rate of collision may be computed by the addition law:

$$\Gamma = n_1 v A_1 + n_2 v A_2 + \ldots \equiv \Gamma_1 + \Gamma_2 + \ldots \tag{2.6.10}$$

This is often called *Matthiessen's rule.* The total rate of collision is the sum of collision rates computed separately for each kind of scatterer.

Historically and also in practice, the analysis of resistance data for a conductor proceeds as follows: If the electrons are scattered by impurities and again by phonons (quanta of lattice vibrations), the total resistance will be written as the sum of the resistances due to each separate cause of scattering:

$$R_{\text{total}} = R_{\text{impurity}} + R_{\text{phonon}} \tag{2.6.11}$$

This is the original statement of Matthiessen's rule. In further detail, the electron-phonon scattering depends on temperature because of the changing phonon population while the effect of the electron-impurity scattering is temperature-independent. By separating the resistance in two parts, one temperature-dependent and the other temperature-independent, we may apply Matthiessen's rule. Since the resistance R is inversely proportional to the conductivity σ, Eqs. (2.6.7) and (2.6.10) together imply Eq. (2.6.11).

Problem 2.6.1. Free electrons are confined within a long rectangular planar strip. Assume that each electron is *diffusely scattered* at the boundary so that it may move in all directions without preference after the scattering. Find the mean free path along the long strip. Calculate the conductivity.

Problem 2.6.2. Proceed as in Problem 2.6.1 for the case in which electrons are confirmed within a long circular cylinder.

2.7. MOTION OF A CHARGED PARTICLE IN ELECTROMAGNETIC FIELDS

Let us consider a particle of mass m and charge q moving in given electric and magnetic fields (**E, B**). In this section we shall study the motion of a charged particle, first classically and then quantum mechanically. We shall be interested mainly in those situations for which the electric field **E** is very small and the magnetic field **B** may be arbitrarily large but constant in space and time.

Let us first consider the case in which **E** = 0. Newton's equation of motion for a classical particle having a charge q in the presence of a magnetic field **B** is

$$m\frac{d\mathbf{v}}{dt} = q(\mathbf{v} \times \mathbf{B}) \tag{2.7.1}$$

We take the dot product of this equation with $\mathbf{v}$: $m\mathbf{v} \cdot d\mathbf{v}/dt = q\,\mathbf{v} \cdot (\mathbf{v} \times \mathbf{B})$. The rhs vanishes, since $\mathbf{v} \cdot (\mathbf{v} \times \mathbf{B}) = (\mathbf{v} \times \mathbf{v}) \cdot \mathbf{B} = 0$. We therefore obtain

$$m\mathbf{v} \cdot \frac{d\mathbf{v}}{dt} = \frac{d}{dt}\left(\frac{1}{2}mv^2\right) = 0 \tag{2.7.2}$$

which means that the *kinetic energy* $mv^2/2$ is conserved. This result is valid regardless of how the magnetic field **B** varies in space. If the magnetic field **B** varies in time, an electric field is necessarily induced, and the preceeding result will not hold strictly.

In the case of a constant magnetic field, we can rewrite Eq. (2.7.1) as

$$\frac{d\mathbf{v}}{dt} = \mathbf{v} \times \vec{\omega}_0 \tag{2.7.3}$$

where $\vec{\omega}_0$ is the constant vector pointing along the direction of the magnetic field and having the magnitude:

$$\omega_0 \equiv \frac{qB}{m} \tag{2.7.4}$$

This quantity ω_0 is called the *cyclotron frequency.* It is proportional to the magnetic-field strength and inversely proportional to the mass of the particle. For example for an electron in a field of 1000 Gauss, we have $\omega_0 \sim 10^{10}\ \mathrm{s}^{-1}$.

From Eq. (2.7.3) we can deduce that the motion of the electron consists of the uniform motion along the magnetic field with velocity v_z plus a circular motion with constant speed $v_\perp$ about the magnetic field. The radius R of this circular orbit about the magnetic field, called the *cyclotron radius,* can be determined from

$$\frac{mv_\perp^2}{R} = ev_\perp B \tag{2.7.5}$$

(centripetal force) = (magnetic force). Solving this equation for R, we obtain

$$R = \frac{mv_\perp^2}{eB} = \frac{v_\perp}{\omega_0} \tag{2.7.6}$$

For the case B = 1000 Gauss and $v_\perp = 10^5$ cm/sec, the cyclotron radius R is of the order 10^{-5} cm = 1000 Å. Note: The radius is inversely proportional to B. Thus as

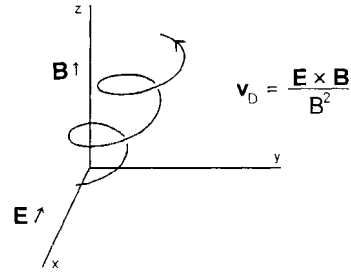

Figure 2.9. A charged particle spirals around a slanted axis under the action of the electric (**E**) and magnetic (**B**) fields, perpendicular to each other.

the magnetic field becomes greater, the electron spirals around more rapidly in smaller circles.

As we saw earlier, the magnetic field **B** does not affect the kinetic energy of the electron. The cyclotron motion then describes an *orbit of constant energy.* This feature is preserved in quantum mechanics. In fact it can be used to explore the Fermi (constant-energy) surface for the conduction electrons in a metal (see Section 5.10).

The motion of an electron in static, uniform electric and magnetic fields is found to be similar to the case we have just discussed. First if the electric field **E** is applied along the direction of **B,** the motion perpendicular to **B** is not affected so that the electron spirals around the magnetic field lines. The motion along **B** is subjected to a uniform acceleration equal to $-e\mathbf{E}/m$.

Let us now turn to the second and more interesting situation in which electric and magnetic fields are perpendicular to each other. Let us introduce $\mathbf{v}_D$ defined by

$$\mathbf{v}_D \equiv \frac{(\mathbf{E} \times \mathbf{B})}{B^2} \tag{2.7.7}$$

which is constant in time and has the dimension of velocity. Let us decompose the velocity **v** in two parts:

$$\mathbf{v} \equiv \mathbf{v}' + \mathbf{v}_D \tag{2.7.8}$$

Substituting this into the equation of motion:

$$m\frac{d\mathbf{v}}{dt} = \text{Lorentz force} = q(\mathbf{E} + \mathbf{v} \times \mathbf{B}) \tag{2.7.9}$$

we obtain

$$\text{lhs} = m\frac{d}{dt}(\mathbf{v}' + \mathbf{v}_D) = m\frac{d\mathbf{v}'}{dt} \tag{2.7.10}$$

$$\text{rhs} = q(\mathbf{E} + \mathbf{v}_D \times \mathbf{B} + \mathbf{v}' \times \mathbf{B}) \qquad \text{[from Eq. (2.7.8)]} \tag{2.7.11}$$

$$= q\left[\mathbf{E} + \frac{(\mathbf{E} \times \mathbf{B}) \times \mathbf{B}}{B^2}\right] + q(\mathbf{v}' \times \mathbf{B}) = q(\mathbf{v}' \times \mathbf{B}) \quad \text{[from Eq. (2.7.7)]} \tag{2.7.12}$$

or

$$m\frac{d\mathbf{v}'}{dt} = q(\mathbf{v}' \times \mathbf{B}) \tag{2.7.13}$$

which has same form as Eq. (2.7.1). The motion can then be regarded as the superposition of the motion in a uniform magnetic field and a drift of the cyclotron orbit with the constant velocity $\mathbf{v}_D$ as given in Eq. (2.7.7). Such a motion is indicated in Fig. 2.9.

The *drift velocity* $\mathbf{v}_D$ in Eq. (2.7.7) is perpendicular to both **E** and **B.** This implies that the weak electric field will induce a macroscopic current **j** in the direction perpendicular to both **E** and **B**:

$$\mathbf{j} = qn\frac{(\mathbf{E} \times \mathbf{B})}{B^2} \tag{2.7.14}$$

where n is the number density of the electrons. This current is called the *Hall current.* We note that drift velocity $\mathbf{v}_D$ is independent of charge and mass. This turns out to be a very important property. The measurement of the Hall effect gives information about the type of the charge carrier (electron or hole) and the number density of carriers.

We have so far discussed the motion of an electron, using classical mechanics. Most of the qualitative features also hold in quantum mechanics. The most important quantum effect is the *quantization of the cyclotron motion.* To see this let us calculate the energy levels of an electron in a constant magnetic field **B.** We choose

$$(A_x, A_y, A_z) = (0, Bx, 0) \tag{2.7.15}$$

which yields a constant field **B** in the z direction, as can easily be verified from $\mathbf{B} = \nabla \times \mathbf{A}$ (Problem 2.7.1). The Hamiltonian H then is given by

$$H = \frac{|\mathbf{p} + e\mathbf{A}|^2}{2m} = \frac{[p_x^2 + (p_y + eBx)^2 + p_z^2]}{2m} \tag{2.7.16}$$

The Schrödinger equation can now be written down as follows:

$$-\frac{\hbar^2}{2m}\left[\frac{\partial^2}{\partial x^2} + \left(\frac{\partial}{\partial y} + \frac{ieB}{\hbar}x\right)^2 + \frac{\partial^2}{\partial z^2}\right]\psi = E\psi \tag{2.7.17}$$

Since the Hamiltonian H contains neither y nor z explicitly, we try the wave function ψ of the form:

$$\psi(x, y, z) = e^{-i(k_y y + k_z z)}\varphi(x) \tag{2.7.18}$$

Substituting this expression into Eq. (2.7.17) yields the following equation for $\varphi(x)$:

$$\left[-\frac{\hbar^2}{2m}\frac{d^2}{dx^2} + \frac{1}{2}m\omega_0^2\left(x - \frac{\hbar k_y}{eB}\right)^2\right]\varphi(x) = E_1\varphi(x) \tag{2.7.19}$$

$$E_1 \equiv E - \frac{\hbar^2 k_z^2}{2m} \tag{2.7.20}$$

(Problem 2.7.2.) Comparison with Eq. (1.2.1) indicates that Eq. (2.7.19) is the wave equation for a harmonic oscillator with the angular frequency $\omega_0 \equiv eB/m$ and the center of oscillation displaced from the origin by

$$X = \frac{\hbar k_y}{eB} \tag{2.7.21}$$

The energy eigenvalues are given by

$$E_1 = \left(n + \frac{1}{2}\right)\hbar\omega_0, \qquad n = 0, 1, 2, \ldots \tag{2.7.22}$$

Combining this with Eq. (2.7.20) we obtain

$$E = \left(n + \frac{1}{2}\right)\hbar\omega_0 + \frac{\hbar^2 k_z^2}{2m} \tag{2.7.23}$$

These energy eigenvalues are called *Landau levels.* The corresponding quantum states, called the *Landau states,* are characterized by the quantum number (n, k_y, k_z). We note that the energies do not depend on k_y, and they are therefore highly degenerate. The Landau states are quite different from the momentum eigenstates. This has significant consequences on magnetization and galvanomagnetic phenomena. The electron in a Landau state may be pictured as a rotation with the angular frequency ω_0 around the magnetic field. If a radiation having a frequency equal to ω_0 is applied, the electron may jump up from one Landau state to another by absorption of a photon energy equal to $\hbar\omega_0$. This generates a phenomenon of *cyclotron resonance,* which will be discussed in Section 5.10.

Problem 2.7.1. Show that the vector potential given by Eq. (2.7.15) generates a magnetic field pointing in the positive z-direction.

Problem 2.7.2. Derive Eq. (2.7.19) from Eqs. (2.7.17) and (2.7.18).

This page intentionally left blank.

3

Lattice Vibrations

Phonons

The heat capacity of a simple insulating crystal is calculated quantum mechanically. Einstein's and Debye's theories are given. Quanta of lattice vibrations are called *phonons.* Phonons of low momenta move like massless bosons. The heat capacity at low temperatures obeys Debye's T^3–law.

3.1. CRYSTAL LATTICES

When a material forms a solid, the atoms align themselves in a special periodic structure called a *crystal lattice.* For example, in rock salt (NaCl), Na^+ and Cl^- ions occupy the sites of a simple cubic (sc) lattice alternately as shown in Fig. 3.1. In sodium (Na), Na^+ ions form a body-centered cubic (bcc) lattice as shown in Fig. 3.2. In solid Ar, neutral atoms form a face-centered cubic (fcc) lattice as shown in Fig. 3.3.

Solids can be classified into metals, insulators, semiconductors, etc., according to the electric transport properties. They can also be classified according to the modes of binding. The readers interested in these aspects are encouraged to refer to elementary solid-state textbooks, such as Kittel's.[1] An overwhelming fact is that almost all materials

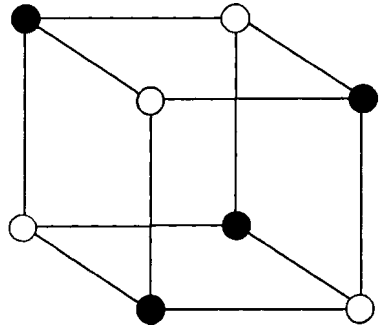

Figure 3.1. A simple cubic lattice. In rock salt, Na^+ and Cl^- occupy the lattice sites alternately.

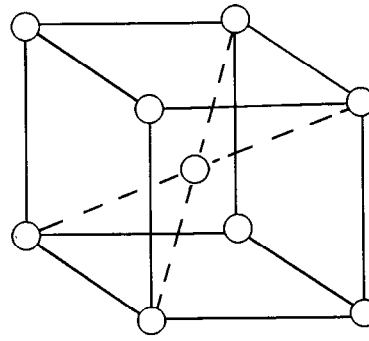

Figure 3.2. A body-centered cubic lattice.

crystallize below a certain temperature. The exceptions are liquid He^3 and He^4, which do not freeze at any temperature at atmospheric pressure. The thermal properties of crystalline solids are remarkably similar for all materials. At high temperatures Dulong–Petit's law for the heat capacity, $C_V = 3Nk_B$, is observed. At low temperatures deviations from this law become significant, which will be shown in the following few sections.

3.2. LATTICE VIBRATIONS; EINSTEIN'S THEORY OF HEAT CAPACITY

Let us consider a crystal lattice at low temperatures. We may expect each atom forming the lattice to execute small oscillations around the equilibrium position. For illustration let us consider the one-dimensional lattice shown in Fig. 3.4. The motion of the jth atom may be characterized by the Hamiltonian of the form:

$$h_j = \frac{p_j^2}{2M} + \left(\frac{1}{2}\right) k_0 u_j^2 \tag{3.2.1}$$

where u_j denotes displacement, and $p_j = M\dot{u}_i$ represents the momentum. Here we assumed a parabolic potential, which is reasonable for small oscillations. If the equipar-

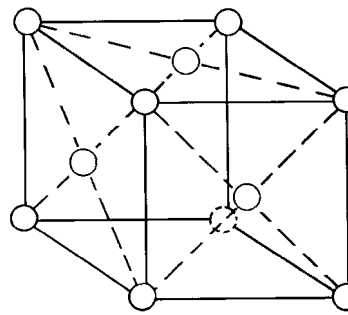

Figure 3.3. A face-centered cubic lattice.

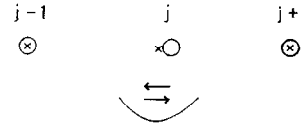

Figure 3.4. The *j*th atom in the linear chain executes simple harmonic oscillations as characterized by the Hamiltonian in Eq. (3.2.1).

tition theorem is applied, the kinetic and potential energy parts each contribute $k_B T/2$ to the average thermal energy. We then obtain

$$\langle h \rangle = \left\langle \frac{1}{2M} p^2 \right\rangle + \left\langle \frac{1}{2} k_0 u^2 \right\rangle = \frac{1}{2} k_B T + \frac{1}{2} k_B T = k_B T \tag{3.2.2}$$

Multiplying Eq. (3.2.2) by the number of atoms N, we obtain $Nk_B T$ for the total energy. By differentiating it with respect to T, we obtain the heat capacity Nk_B for the lattice.

In quantum mechanics the eigenvalues of the Hamiltonian:

$$h = \frac{p^2}{2M} + \left(\frac{1}{2}\right) k_0 u^2 \tag{3.2.3}$$

are given by

$$\epsilon_n = \left(\frac{1}{2} + n\right) \hbar\omega_0, \qquad n = 0, 1, 2, \ldots \tag{3.2.4}$$

$$\omega_0 \equiv \left(\frac{k_0}{M}\right)^{1/2} \tag{3.2.5}$$

The quantum states are characterized by nonnegative integers n. If we assume a canonical ensemble of simple harmonic oscillators with the distribution $\exp[-\beta\epsilon]$, the average energy can be calculated as follows:

$$\langle h \rangle = \frac{\sum_n \epsilon_n e^{-\beta\epsilon_n}}{\sum_n e^{-\beta\epsilon_n}} = -\frac{\partial}{\partial\beta} \ln \left[\sum_n e^{-\beta\epsilon_n}\right] = -\frac{\partial}{\partial\beta} \ln \left[\sum_{n=0}^{\infty} e^{-\beta(1/2+n)\hbar\omega_0}\right]$$

$$= -\frac{\partial}{\partial\beta} \ln \left[\frac{e^{-\beta\hbar\omega_0/2}}{1 - e^{-\beta\hbar\omega_0}}\right] = \left[\frac{1}{2} + f_0(\hbar\omega_0)\right] \hbar\omega_0 \tag{3.2.6}$$

$$f_0(\eta) \equiv \frac{1}{e^{\beta\eta} - 1} \tag{3.2.7}$$

Here f_0 represents the *Planck distribution function.* Notice that the quantum average energy $\langle h \rangle$ in Eq. (3.2.6) is quite different from the classical average energy $k_B T$, see Eq. (3.2.2).

For a three-dimensional lattice with N atoms, we multiply Eq. (3.2.6) by the number of degrees of freedom, $3N$. We then obtain

$$E = 3N \left[\frac{1}{2} + f_0(\hbar\omega_0)\right] \hbar\omega_0 \tag{3.2.8}$$

Differentiating this with respect to T, we obtain the heat capacity (Problem 3.2.1):

$$C_V = \frac{\partial E}{\partial T} = \frac{\partial E}{\partial \beta}\frac{\partial \beta}{\partial T} = \frac{3N(\hbar\omega_0)^2}{k_B T^2}\frac{e^{\beta\hbar\omega_0}}{(e^{\beta\hbar\omega_0}-1)^2}$$

We rewrite this expression in the form (Problem 3.2.1):

$$C_V = 3Nk_B\left(\frac{\Theta_E}{T}\right)^2 e^{\Theta_E/T}\left(e^{\Theta_E/T}-1\right)^{-2} \tag{3.2.9}$$

where

$$\Theta_E \equiv \frac{\hbar\omega_0}{k_B} = \left(\frac{\hbar}{k_B}\right)\left(\frac{k_0}{M}\right)^{1/2} \tag{3.2.10}$$

is the *Einstein temperature.* The function

$$g(x) \equiv x^2 e^x (e^x - 1)^{-2} \qquad \left(x \equiv \frac{\Theta_E}{T}\right) \tag{3.2.11}$$

has the asymptotic behavior (Problem 3.2.2):

$$g(x) \approx \begin{cases} x^2 e^{-x} & \text{for } x \gg 1 \\ 1 & \text{for } x \ll 1 \end{cases} \tag{3.2.12}$$

At very high temperatures ($\Theta_E/T \ll 1$), the heat capacity given by Eq. (3.2.9) approaches the classical value $3Nk_B$:

$$C_V = 3Nk_B g\left(\frac{\Theta_E}{T}\right) \longrightarrow 3Nk_B \tag{3.2.13}$$

At very low temperatures ($\Theta_E/T >> 1$), the heat capacity C_V behaves like:

$$C_V \approx 3Nk_B\left(\frac{\Theta_E}{T}\right)^2 \exp\left(\frac{-\Theta_E}{T}\right) \tag{3.2.14}$$

and approaches zero exponentially as T tends to zero. The behavior of $C_V/3Nk_B$ from Eq. (3.2.9) is plotted against Θ_E/T in Fig. 3.5. For comparison experimental data of C_V for diamond are shown by points with the choice of Θ_E = 1320 K. The fit is quite reasonable for diamond. Historically Einstein obtained Eq. (3.2.9) in 1907[2] before the advent of quantum theory in 1925–26. The discrepancy between experiment and theory (equipartition theorem) had been a mystery.

Einstein's theory explains very well why a certain solid like diamond exhibits a molar heat capacity substantially smaller than $3R$ (the value in accordance with Dulong–Petit's law). It predicts that the heat capacity for any solid decreases as temperature is lowered. This is in agreement with experimental observations. However the temperature dependence at the low temperature end indicates nonnegligible discrepancies. Several years after Einstein's theory, Debye reported a very successful theory of the heat capacity over all temperature range, which will be discussed in Section 3.5.

Problem 3.2.1. Derive Eq. (3.2.9), using Eqs. (3.2.7) and (3.2.8).

Problem 3.2.2. Verify the asymptotic behavior of Eq. (3.2.12) from Eq. (3.2.11).

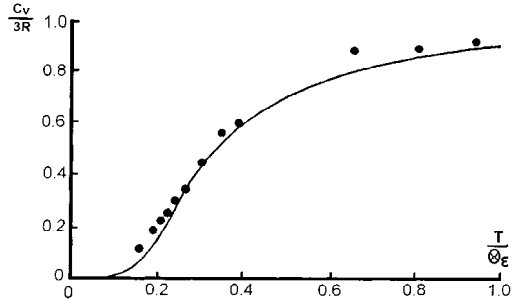

Figure 3.5. The molar heat capacity for Einstein's model of a solid is shown in a solid line. Experimental points are for a diamond with $\Theta_E = 1320$ K.

3.3. OSCILLATIONS OF PARTICLES ON A STRING; NORMAL MODES

Let us consider a set of N particles of equal mass m attached to a light string of length $(N + 1)l$ (in equilibrium), stretched to a tension τ. The masses are equally spaced with a regular separation. We shall look at transverse oscillations of the particles. We denote the transverse displacements by $y_1, y_2, \ldots, y_N$, as indicated in Fig. 3.6.

The kinetic energy of this system is

$$T = \left(\frac{1}{2}\right) m(\dot{y}_1^2 + \dot{y}_2^2 + \ldots + \dot{y}_N^2) \tag{3.3.1}$$

The potential energy for small displacements can be calculated as follows. We look at the length of string between the jth and $(j + 1)$th particles. In equilibrium its length is l, but when the particles are vertically displaced, the increment of the length Δl is

$$\Delta l = [l^2 + (y_{j+1} - y_j)^2]^{1/2} - l \simeq \frac{(y_{j+1} - y_j)^2}{2l} \tag{3.3.2}$$

where we assumed that the displacements are so small that

$$|y_{j+1} - y_j| \ll l \tag{3.3.3}$$

The same expression applies to the sections of the string at both ends if we set

$$y_0 = y_{N+1} = 0 \tag{3.3.4}$$

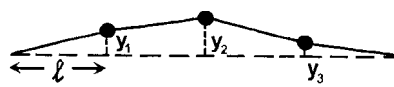

Figure 3.6. Transverse displacements of three particles on a string are represented by y_1, y_2, and y_3.

(fixed-end boundary condition). The work done against the tension τ in increasing the length by Δl is $\tau\,\Delta l$. (We assume that the tension does not change for small displacements.) Thus adding the contributions from each section of the string, we find the potential energy:

$$V = \left(\frac{\tau}{2l}\right)[y_1^2 + (y_2 - y_1)^2 + \ldots + (y_N - y_{N-1})^2 + y_N^2] \tag{3.3.5}$$

The Lagrangian L of our system then is given by

$$L \equiv T - V = \frac{m}{2}\sum_{j=1}^{N}\dot{y}_j^2 - \frac{\tau}{2l}\left[y_1^2 + \sum_{j=1}^{N-1}(y_{j+1} - y_j)^2 + y_N^2\right] \tag{3.3.6}$$

From Lagrange's equations:

$$\frac{d}{dt}\left(\frac{\partial L}{\partial \dot{y}_j}\right) - \frac{\partial L}{\partial y_j} = 0$$

we obtain

$$\frac{d^2y_1}{dt^2} = \frac{\tau}{ml}(-2y_1 + y_2),\ \frac{d^2y_2}{dt^2} = \frac{\tau}{ml}(y_1 - 2y_2 + y_3),\ \cdots,\ \frac{d^2y_N}{dt^2} = \frac{\tau}{ml}(y_{N-1} - 2y_N) \tag{3.3.7}$$

Here we have a set of coupled, linear, homogeneous differential equations. Clearly

$$y_1 = y_2 = \ldots = y_N = 0 \tag{3.3.8}$$

are solutions. This set of solutions corresponds to the trivial case in which all displacements remain zero at all time.

Equations (3.3.7) however allow other solutions, which we discuss now. Let us assume that the solutions of Eqs. (3.3.7) are of the form:

$$y_j(t) = A_j e^{i\omega t}, \qquad j = 1, 2, \ldots, N \tag{3.3.9}$$

Substituting these into Eq. (3.3.7) and dividing the results by $e^{i\omega t}$, we obtain

$$\begin{aligned}
(2\omega_0^2 - \omega^2)A_1 - \omega_0^2 A_2 &= 0 \\
-\omega_0^2 A_1 + (2\omega_0^2 - \omega^2)A_2 - \omega_0^2 A_3 &= 0 \\
&\cdots \\
-\omega_0^2 A_{N-1} + (2\omega_0^2 - \omega^2)A_N &= 0
\end{aligned} \tag{3.3.10}$$

$$\omega_0 \equiv \left(\frac{\tau}{ml}\right)^{1/2} \tag{3.3.11}$$

We note that this quantity ω_0 has the dimensions of a frequency, since

$$[\omega_0] = \left[\left(\frac{\tau}{ml}\right)^{1/2}\right] = \left[\frac{MLT^{-2}}{ML}\right]^{1/2} = [T^{-1}] \tag{3.3.12}$$

where the angular brackets indicate the dimensions of the quantity inside. (M = mass, L = length, and T = time.)

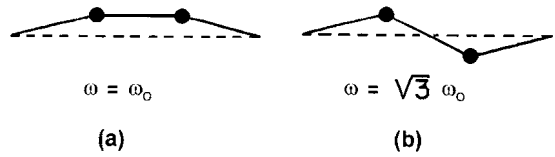

Figure 3.7. The amplitude relations of the two normal modes for a system of two particles.

Let us look at the case of $N = 2$. From Eq. (3.3.10) we have

$$(2\omega_0^2 - \omega^2)A_1 - \omega_0^2 A_2 = 0, \qquad -\omega_0^2 A_1 + (2\omega_0^2 - \omega^2)A_2 = 0 \tag{3.3.13}$$

If we exclude the case in which $A_1 = A_2 = 0$, the solutions of Eqs. (3.3.3) can exist only if the determinant constructed from the coefficients vanishes (Problem 3.3.1):

$$\begin{vmatrix} 2\omega_0^2 - \omega^2 & -\omega_0^2 \\ -\omega_0^2 & 2\omega_0^2 - \omega^2 \end{vmatrix} = 0 \tag{3.3.14}$$

This equation is called the *secular equation.* From this we obtain two solutions (ω_1, ω_2), $\omega_1 = \omega_0$ and $\omega_2 = 3^{1/2}\omega_0$ (Problem 3.3.2). In the first case after substituting $\omega_1 = \omega_0$ into Eq. (3.3.13), we find that the ratio of the coefficients A_1/A_2 equals unity. In the second case of $\omega_2 = 3^{1/2}\omega_0$ the ratio A_1/A_2 is found to be -1. In summary we have

$$\begin{aligned} \omega_1 &= \omega_0, \qquad A_1 : A_2 = 1 : 1 \\ \omega_2 &= 3^{1/2}\omega_0, \qquad A_1 = A_2 = 1 : -1 \end{aligned} \tag{3.3.15}$$

In general we can characterize these special modes of oscillation, called the *normal modes,* by their *characteristic frequencies* and *amplitude relations.* The amplitude relations are schematically shown in Figure 3.7, where we chose a positive A_1. The choice of a negative A_1 generates different figures. Both cases however represent the same normal modes, since only the relative amplitude relation $A_1 : A_2$ is meaningful.

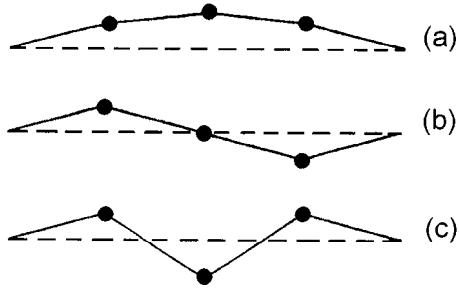

Figure 3.8. The three normal modes with the characteristic amplitude relations.

The case of $N = 3$ can be worked out in a similar manner. The results can be represented by (Problem 3.3.3)

$$\omega_1 = \left(2 - 2^{1/2}\right)^{1/2}\omega_0, \qquad A_1 : A_2 : A_3 = 1 : 2^{1/2} : 1$$
$$\omega_2 = 2^{1/2}\omega_0, \qquad A_1 : A_2 : A_3 = 1 : 0 : -1$$
$$\omega_3 = \left(2 + 2^{1/2}\right)^{1/2}\omega_0, \qquad A_1 : A_2 : A_3 = 1 : -2^{1/2} : 1 \tag{3.3.16}$$

The amplitude relations of these normal modes are illustrated in Fig. 3. 8. For large N the characteristic equation being an algebraic equation of Nth order becomes very difficult to solve. We note however the following general features: For a general N, there are N distinct characteristic frequencies. The mode with the lowest frequency is the one in which all of the particles oscillate in the same direction, while the mode with the highest frequency is the one in which successive masses oscillate in opposite directions.

Let us now take the case of two particles $N = 2$. The Lagrangian L of the system is from Eqs. (3.3.6) and (3.3.11)

$$L = \left(\frac{1}{2}\right)m(\dot{y}_1^2 + \dot{y}_2^2) - \left(\frac{1}{2}\right)m\omega_0^2[y_1^2 + (y_2 - y_1)^2 + y_2^2] \tag{3.3.17}$$

The characteristic frequencies and amplitude relations are given in Eq. (3.3.15). We introduce a new set of generalized coordinates:

$$q_1 \equiv \left(\frac{m}{2}\right)^{1/2}(y_1 + y_2), \qquad q_2 \equiv \left(\frac{m}{2}\right)^{1/2}(y_1 - y_2) \tag{3.3.18}$$

which have the amplitude relations as prescribed in Eq. (3.3.15). Note: These generalized coordinates do not have the dimensions of length. They are nonetheless convenient, as we shall see later. Solving with respect to y_1 and y_2, we obtain

$$y_1 = \left(\frac{2}{m}\right)^{1/2}(q_1 + q_2), \qquad y_2 = \left(\frac{2}{m}\right)^{1/2}(q_1 - q_2) \tag{3.3.19}$$

By differentiation

$$\dot{y}_1 = \left(\frac{2}{m}\right)^{1/2}(\dot{q}_1 + \dot{q}_2), \qquad \dot{y}_2 = \left(\frac{2}{m}\right)^{1/2}(\dot{q}_1 - \dot{q}_2) \tag{3.3.20}$$

Using Eqs. (3.3. 19) and (3.3.20), we can transform the Lagrangian L from Eq. (3.3.17) into

$$\begin{aligned} L &= \frac{1}{2}\dot{q}_1^2 - \frac{1}{2}\omega_0^2 q_1^2 + \frac{1}{2}\dot{q}_2^2 - \frac{3}{2}\omega_0^2 q_2^2 \\ &= \left(\frac{1}{2}\dot{q}_1^2 - \frac{1}{2}\omega_1^2 q_1^2\right) + \left(\frac{1}{2}\dot{q}_2^2 - \frac{1}{2}\omega_2^2 q_2^2\right) = L(q_1, \dot{q}_1, q_2, \dot{q}_2) \end{aligned} \tag{3.3.21}$$

where

$$\omega_1 = \omega_0, \qquad \omega_2 = 3^{1/2}\omega_0 \tag{3.3.22}$$

are characteristic frequencies for the system (Problem 3.3.4). The Lagrangian L in Eq. (3.3.21) can be regarded as a function of the new set of generalized coordinates and velocities $(q_1, \dot{q}_1, q_2, \dot{q}_2)$. From Lagrange's equations $(d/dt)\left(\partial L/\partial \dot{q}_j\right) - \partial L/\partial q_j = 0$, we obtain

$$\frac{d}{dt}(\dot{q}_j) + \omega_j^2 q_j = \frac{d^2}{dt^2} q_j + \omega_j^2 q_j = 0 \tag{3.3.23}$$

which indicates that each coordinate q_j oscillates sinusoidally with the characteristic frequency ω_j. The coordinates (q_1, q_2) that describe the normal modes in this special manner are called the *normal coordinates.*

We note that the choice of a set of normal coordinates is not unique; the factors $(m/2)^{1/2}$ in Eq. (3.3.18) can be chosen in an arbitrary manner. As long as the correct amplitude relations are selected in agreement with Eq. (3.3.15), the generalized coordinates oscillate independently and with the characteristic frequencies. Our particular choice however makes the Lagrangian (and Hamiltonian) formally the simplest.

Let us now introduce a set of canonical momenta in the standard form:

$$p_j \equiv \frac{\partial}{\partial \dot{q}_j} L(q_1, \dot{q}_1, q_2, \dot{q}_2), \qquad j = 1, 2$$

Using Eq. (3.3.21) we obtain

$$p_j \equiv \dot{q}_j \tag{3.3.24}$$

$$H \equiv \sum_p p_j \dot{q}_j - L = \left(\frac{1}{2}p_1^2 + \frac{1}{2}\omega_1^2 q_1^2\right) + \left(\frac{1}{2}p_2^2 + \frac{1}{2}\omega_2^2 q_2^2\right) \tag{3.3.25}$$

[from Eq. (3.3.21)]. Here we see that the Hamiltonian H, which is numerically equal to the total energy $T + V$, is the sum of normal-mode Hamiltonians.

Equations. (3.3.21) and (3.3.25), both expressed in simple forms, can be extended to a general case of N particles. The Lagrangian L for the system was given in Eq. (3.3.6)

$$L = \frac{1}{2}m(\dot{y}_1^2 + \dot{y}_2^2 + \ldots + \dot{y}_N^2) - \frac{1}{2}m\omega_0^2[y_1^2 + (y_2 - y_1)^2 + \ldots + y_N^2]$$

This function L is *quadratic* in $\{y_j, \dot{y}_j\}$. By a suitable choice of normal coordinates $\{q_j\}$, such a Lagrangian can in principle be transformed into

$$L = \frac{1}{2}\sum_{j=1}^{N}(\dot{q}_j^2 - \omega_j^2 q_j^2) \tag{3.3.26}$$

where $\{\omega_j\}$ represent the characteristic frequencies. This is a generalization of Eq. (3.3.21). As stated earlier it is not easy to find characteristic frequencies $\{\omega_j\}$ for the system when N is large. Also finding the relation between $\{y_j\}$ and $\{q_j\}$, like Eq. (3.3.18), is tedious work. The transformation from Eq. (3.3.6) into Eq. (3.3.26) is known as the *principal-axis transformation.* Readers interested in the formal derivation should refer to textbooks on advanced mechanics.[3] Equation (3.3.26) indicates first that there are N characteristic frequencies. This number N is equal to the number of degrees

of freedom of the system. Second each normal coordinate q_j oscillates sinusoidally with its characteristic frequency ω_j.

Let us define the canonical momenta by

$$p_j \equiv \frac{\partial L}{\partial \dot{q}_j} = \dot{q}_j \tag{3.3.27}$$

Now the Hamiltonian H for the system can be written in the simple form:

$$H = \frac{1}{2}\sum_j (p_j^2 + \omega_j^2 q_j^2) \tag{3.3.28}$$

The theory treated in this section is useful in the discussion of lattice vibrations.

Problem 3.3.1. Consider two equations: $ax + by = 0$, $cx + dy = 0$. Show that the necessary and sufficient condition for the existence of a solution other than $x = y = 0$ is

$$\begin{vmatrix} a & b \\ c & d \end{vmatrix} = 0 \tag{1}$$

Remark: To show that it is sufficient, assume (1) and find a solution other than $x = y = 0$. To show that it is necessary, assume a solution for which at least one of (x, y) is nonzero and verify (1).

Problem 3.3.2. (a) Solve Eq. (3.3.14) and find the characteristic frequencies. (b) Find the amplitude relation corresponding to each characteristic frequency obtained in (a).

Problem 3.3.3. Find the characteristic frequencies and the amplitude relations for $N = 3$. Proceed in the same manner as for Problem 3.3.2.

Problem 3.3.4. Using the coordinates (q_1, q_2) in Eq. (3.3.18), derive an expression for the Lagrangian L [see Eq. (3.3.21)].

3.4. TRANSVERSE OSCILLATIONS OF A STRETCHED STRING

Let us consider a string of length L and mass per unit length μ, stretched to a tension τ. In place of a finite set of coordinates $\{y_j(t)\}$, we now have a continuous function $y(x, t)$ to describe the transverse displacement of the string. The equation of motion for the string can be obtained as follows. Consider a small portion of the string between x and $x + dx$ as shown in Fig. 3.9.

The mass of this portion is μdx, and the acceleration along the y-axis is $\partial^2 y/\partial t^2$. The forces acting on the element are the two tensions shown in the diagram. By assumption these tensions have the same magnitude, and they are directed along the tangents of the curve $y = y(x)$ at x and $x + dx$. We now set up Newton's equation (mass × acceleration = net force) for the transverse motion. From the diagram we obtain

$$(\mu dx)\frac{\partial^2 y}{\partial t^2} = \tau \sin\theta(x + dx, t) - \tau \sin\theta(x, t) \tag{3.4.1}$$

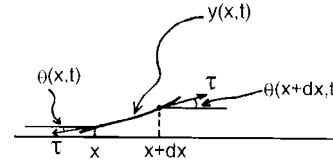

Figure 3.9. The portion of the string between x and $x + dx$ is acted on by the two tensions shown.

where $\theta(x,\ t)$ is the angle between the tangent and the positive x-axis; sin θ appears because we take the y-components of the tensions.

We apply Taylor's expansion formula to sin $\theta(x + dx,\ t)$ and obtain

$$\sin\theta(x+dx,t) = \sin\theta(x,t) + dx\cos\theta\frac{\partial\theta(x,t)}{\partial x} \tag{3.4.2}$$

where we retain terms of up to first order in dx. [This is good enough, since the lhs of Eq. (3.4.1) is of the first order in dx.] Introducing Eq. (3.4.2) into Eq. (3.4.1), and dropping the common factor dx we obtain

$$\mu\frac{\partial^2 y}{\partial t^2} = \tau\cos\theta\frac{\partial\theta}{\partial x} \tag{3.4.3}$$

From the diagram we observe that

$$\frac{\partial y(x,t)}{\partial x} = \tan\theta(x,t) \tag{3.4.4}$$

Differentiating both sides with respect to x, we obtain

$$\frac{\partial^2 y}{\partial x^2} = \left(\frac{d}{d\theta}\tan\theta\right)\frac{\partial\theta(x,t)}{\partial x} = \frac{1}{\cos^2\theta}\frac{\partial\theta}{\partial x} \tag{3.4.5}$$

Now using this we obtain from Eq. (3.4.3):

$$\mu\frac{\partial^2 y}{\partial t^2} = \tau\cos^3\theta\frac{\partial^2 y}{\partial x^2} \tag{3.4.6}$$

If we assume that the slope $\partial y(x,\ t)/\partial x = \tan\theta(x,\ t)$ is small everywhere:

$$|\theta(x,t)| \ll 1 \tag{3.4.7}$$

then we can approximate $\cos\theta = 1 - \theta^2/2 + \ldots$ by 1 and obtain from Eq. (3.4.6):

$$\mu\frac{\partial^2 y}{\partial t^2} = \tau\frac{\partial^2 y}{\partial x^2} \tag{3.4.8}$$

It is convenient to introduce

$$c \equiv \left(\frac{\tau}{\mu}\right)^{1/2} \tag{3.4.9}$$

We can then rewrite Eq. (3.4.8) in the form:

$$\boxed{\frac{\partial^2 y}{\partial t^2} = c^2 \frac{\partial^2 y}{\partial x^2}} \tag{3.4.10}$$

This is the *wave equation* in one dimension. Similar equations occur in many branches of physics, wherever wave phenomena are encountered. Using dimensional analysis,

$$\left[\frac{\tau}{\mu}\right] = \left[\frac{\text{(force)}}{\{\text{mass/length}\}}\right] = \left[\frac{MT^{-2}L}{(M/L)}\right] = L^2T^{-2} \tag{3.4.11}$$

we see that the constant c has the dimensions of a velocity. In fact c is the velocity of the wave propagating along the string [see the paragraphs after Eq. (3.4.20)].

We now wish to find the normal-mode solutions of the wave equation Eq. (3.4.10) with the fixed-end boundary condition, which is represented by

$$y(0, t) = 0, \qquad y(L, t) = 0 \tag{3.4.12}$$

Let us assume solutions of the form:

$$y(x, t) = A(x)e^{i\omega t} \tag{3.4.13}$$

(Notice that the x- and t-dependencies are separated on the rhs.) Introducing Eq. (3.4.13) into Eq. (3.4.10) and dropping the common factor $e^{i\omega t}$, we obtain

$$\frac{d^2A}{dx^2} + k^2A = 0, \qquad k = \pm\frac{\omega}{c} \tag{3.4.14}$$

The general solution of Eq. (3.4.14) is

$$A(x) = a\cos(kx) + b\sin(kx) \tag{3.4.15}$$

where a and b are constants. Substituting Eqs. (3.4.13) and (3.4.15) into the first of Eqs. (3.4.12) yields $(a \cos 0 + b \sin 0)e^{i\omega t} = 0$ or $a = 0$. Thus we obtain from Eq. (3.4.15)

$$A(x) = b\sin(kx)$$

Substituting this expression into the second of Eq. (3.4.12) yields $b \sin(kL) = 0$, whose solution is

$$\text{either} \quad b = 0 \quad \text{or} \quad \sin(kL) = 0 \tag{3.4.16}$$

The first case ($b = 0$) corresponds to the trivial solution where the displacement A remains zero all along the line. In the second case the value of k is limited to

$$\pi n/L = k_n, \qquad n = 1, 2, \ldots \tag{3.4.17}$$

The angular frequency ω is related to k by $\omega = \pm ck$ [see Eq. (3.4.14)]. The characteristic frequencies are therefore also discrete, and they are given by

$$\omega_n = \frac{\pm\pi cn}{L} = \pm ck_n \tag{3.4.18}$$

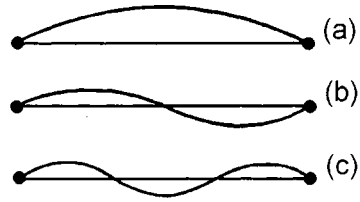

Figure 3.10. The first three normal modes of the stretched string.

These are all multiples of the *fundamental frequency* $\pi c/L$.

Thus we have obtained solutions of the form: $b_n \sin(k_n x)e^{i\omega_n t}$, $n =$ positive integers, where b_n are constants. The solutions with k_n and $k_{-n}(n > 0)$ are *linearly dependent*; they can be obtained from each other by multiplying by a constant factor. We shall take the real part of

$$b_n \sin(k_n x)e^{i\omega_n t}, \qquad n = 1, 2, \ldots \tag{3.4.19}$$

as a set of linearly-independent solutions. Each of these solutions is characterized by the angular frequency $\pm\omega_n$ and the sinusoidal space dependence with wave number k_n. These solutions are called the *normal-mode solutions* for the string. Note: It is much easier to obtain the normal modes of oscillation for a continuous string than for a discrete model of many particles on a stretched string. As we shall see later, these normal modes have many similarities. The space dependence of the first few normal modes, $\sin(k_n x) \equiv \sin(n\pi x/L)$, is shown in Fig. 3.10.

According to Eq. (3.4.19) these normal-mode amplitudes change in time with the characteristic periods given by $T_n \equiv 2\pi\omega_n^{-1}$. Thus the normal modes represent standing waves with a number of fixed nodes, including those modes at both ends. In general the wavelength λ and the wave number k for a sinusoidal wave are related by $\lambda = 2\pi/k$. In the present case the wavelengths are therefore

$$\lambda_n = \frac{2\pi}{k_n} = \frac{2\pi L}{\pi n} = \frac{2L}{n} \tag{3.4.20}$$

Let us now look at the case of $n = 1$. This case corresponds to the minimum k-number (π/L), the maximum wavelength ($2L$), and the minimum frequency ($\pi c/L$). As we see in Fig. 3.10 (a) for all of the range $0 < x < L$, this normal-mode amplitude is similar to that of the minimum frequency for the N particles on the string. Compare Fig. 3.10 (a) with Fig. 3.7 (a) and Fig. 3.8 (a).

A more detailed correspondence can be established in the following manner. Let us take the case of a large number of particles on a stretched string, as indicated in Fig. 3.11 (a). Let us imagine that the mass concentrated on each particle is redistributed along the string uniformly. The resulting case of the mass–string system, shown in Fig. 3.11 (b), can be regarded as the stretched homogeneous string that we are discussing in the present section. An important distinction between the two cases is that the number of normal modes for the stretched string is infinite, since n can be any positive integer. This property arises from the fact that the string is characterized by a continuous function $y(x, t)$ and therefore has infinite degrees of freedom. Another difference related to this

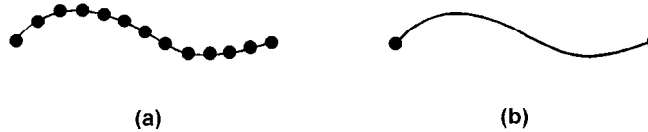

Figure 3.11. If we redistribute the mass in the mass–string system (a) along the string uniformly, we obtain homogeneous string in (b).

is that the stretched string can have a normal mode of extremely great frequency, ($\omega_n = cn\pi/L$), and extremely short wavelength ($\lambda = 2L/n$). Therefore the analogy between the two systems must be discussed with care. This point is relevant in Debye's model of the heat capacity of a solid, which will be discussed in the following section.

3.5. DEBYE'S THEORY OF HEAT CAPACITY

Earlier in Section 3.2, we discussed Einstein's theory of the heat capacity of a solid. This theory explains very well why a certain solid like diamond exhibits a molar heat capacity substantially smaller than $3R$. It also predicts that the heat capacity for any solid should decrease as temperature is lowered. This prediction is in agreement with experimental observations. However the temperature dependence at very low temperatures indicates nonnegligible discrepancies. In 1912 Debye[4] reported a very successful theory of the heat capacity of solids, which we will discuss in this section.

In Einstein's model the solid is viewed as a collection of free harmonic oscillators with a *common* frequency ω_0. This is rather a drastic approximation, since an atom in a real crystal moves under the varying potential field generated by its neighboring atoms. It is more reasonable to look at the crystal as a collection of *coupled* harmonic oscillators. (We can set up a theory from this point of view as we do in Section 7.3) As we saw in the last two sections the motion of a set of coupled harmonic oscillators can be described concisely in terms of the normal modes of oscillations. A major difficulty of this approach however is to find the set of the characteristic frequencies. Debye overcame this difficulty by regarding a solid as a *continuous elastic body* whose normal modes of oscillations are known as elastic waves. This approximation is valid only at low frequencies.

A macroscopic solid can support transverse and longitudinal waves. We first look at the case of the transverse wave. The equation of motion for the transverse elastic wave is

$$\rho \frac{\partial^2 \mathbf{u}}{\partial t^2} = S\nabla^2 \mathbf{u} \tag{3.5.1}$$

where $\mathbf{u}$ is the transverse displacement, and ρ and S are, respectively, the mass density and the shear modulus. Equation (3.5.1) is similar to Eq. (3.4.8) for the transverse oscillation of a stretched string, only the transverse displacement is now a vector $\mathbf{u}$ lying in a plane perpendicular to the direction of the wave propagation. Since the displacement (component) u_j is a continuous-field (opposed to a discrete) variable, the usual Lagrangian formulation does not work. However its generalization is immediate. We use a *Lagrangian field method* as follows.

1. We introduce a Lagrangian density $\mathcal{L}$, which is a function of the displacement-components, their time-derivatives and space-derivatives:

$$\mathcal{L} = \mathcal{L}\left(u_x, u_y, u_z, \frac{\partial u_x}{\partial t}, \frac{\partial u_y}{\partial t}, \frac{\partial u_z}{\partial t}, \frac{\partial u_x}{\partial x}, \ldots\right) \tag{3.5.2}$$

2. We derive the equations of motion by means of *Lagrange's field equations*:

$$\frac{\partial}{\partial t}\left(\frac{\partial \mathcal{L}}{\partial(\partial u_a/\partial t)}\right) + \frac{\partial}{\partial x}\left(\frac{\partial \mathcal{L}}{\partial(\partial u_a/\partial x)}\right) + \frac{\partial}{\partial y}\left(\frac{\partial \mathcal{L}}{\partial(\partial u_a/\partial y)}\right) + \frac{\partial}{\partial z}\left(\frac{\partial \mathcal{L}}{\partial(\partial u_a/\partial z)}\right) - \frac{\partial \mathcal{L}}{\partial u_a} = 0, \quad a = x, y, z \tag{3.5.3}$$

In our case we may choose

$$\mathcal{L} = \frac{1}{2}\rho\left|\frac{\partial \mathbf{u}}{\partial t}\right|^2 - \frac{1}{2}S\left(\left|\frac{\partial \mathbf{u}}{\partial x}\right|^2 + \left|\frac{\partial \mathbf{u}}{\partial y}\right|^2 + \left|\frac{\partial \mathbf{u}}{\partial z}\right|^2\right) \tag{3.5.4}$$

$$= \frac{1}{2}\rho\left[\left|\frac{\partial u_x}{\partial t}\right|^2 + \left|\frac{\partial u_y}{\partial t}\right|^2 + \left|\frac{\partial u_z}{\partial t}\right|^2\right] - \ldots \tag{3.5.5}$$

and verify the correct equation of motion (3.5.1) by using Eqs. (3.5.3) and (3.5.5) (Problem 3.5.1).

Let us assume a cubic box (with the side length L_0) fixed-end boundary condition. The normal modes of oscillations are represented by the amplitude functions:

$$\sin(xk_x)\sin(yk_y)\sin(zk_z) \tag{3.5.6}$$

$$k_a \equiv \frac{\pi n_a}{L_0}, \qquad n_a = 1, 2, \ldots \qquad a = x, y, z \tag{3.5.7}$$

and the angular frequencies:

$$\omega_{t,k} = c_t|\mathbf{k}| = \left(\frac{S}{\rho}\right)^{1/2} k \tag{3.5.8}$$

where c_t is the speed of propagation for the transverse (t) wave. [Eqs. (3.5.6), (3.5.7), and (3.5.8) are straightforward extension of Eqs. (3.4.19), (3.4.17), and (3.4.18).] The wave vector $\mathbf{k}$ is perpendicular to the displacement $\mathbf{u}$:

$$\mathbf{k} \cdot \mathbf{u} = 0 \qquad \text{(transverse wave)} \tag{3.5.9}$$

We now wish to express the Lagrangian density $\mathcal{L}$ in terms of the normal coordinates and velocities. Let us denote the Cartesian components of $\mathbf{u}$ by u_1 and u_2. We follow the standard procedure described in Section 3.3 and introduce the normal coordinates:

$$q_{\mathbf{k},\sigma}(t) = \left(\frac{2}{L_0}\right)^3 \int_0^{L_0} dx \int_0^{L_0} dy \int_0^{L_0} dz u_\sigma \sin(xk_x)\sin(yk_y)\sin(zk_z) \tag{3.5.10}$$

where $\sigma = 1,2$ are called the polarization indices. After lengthy but straightforward calculations, we can then transform $\mathcal{L}$ into (Problem 3.5.2)

$$\mathcal{L} = \sum_{\mathbf{k}} \sum_{\sigma} \left[\frac{1}{4} \rho \dot{q}_{\mathbf{k},\sigma}^2 - \frac{1}{4} S k^2 q_{\mathbf{k},\sigma}^2 \right] \tag{3.5.11}$$

which is the sum of single-mode Lagrangian densities.

The Lagrangian L is defined by the Lagrangian density $\mathcal{L}$ times the volume V:

$$L \equiv V \mathcal{L} \tag{3.5.12}$$

For later convenience we introduce new normal coordinates:

$$Q_{\mathbf{k},\sigma} \equiv \left(\frac{V\rho}{2} \right)^{1/2} q_{\mathbf{k},\sigma} \tag{3.5.13}$$

By using these coordinates, we can reexpress the Lagrangian L as follows:

$$L = \sum_{\mathbf{k}} \sum_{\sigma} \frac{1}{2} [\dot{Q}_{\mathbf{k},\sigma}^2 - \omega_{t,k}^2 Q_{\mathbf{k},\sigma}^2] \tag{3.5.14}$$

an extension of Eq. (3.3.26).

To derive the corresponding Hamiltonian, we define the canonical momenta $\{P_{\mathbf{k},\sigma}\}$ by

$$P_{\mathbf{k},\sigma} \equiv \frac{\partial L}{\partial \dot{Q}_{\mathbf{k},\sigma}} = \dot{Q}_{\mathbf{k},\sigma} \tag{3.5.15}$$

The Hamiltonian H_t for the transverse waves can then be constructed by expressing $\sum_{\mathbf{k}} \sum_{\sigma} P_{\mathbf{k},\sigma} \dot{Q}_{\mathbf{k},\sigma} - L$ in terms of $\{Q_{\mathbf{k},\sigma}, P_{\mathbf{k},\sigma}\}$. The result is given by

$$H_t = \sum_{\mathbf{k}} \sum_{\sigma} \frac{1}{2} [P_{\mathbf{k},\sigma}^2 + \omega_{t,k}^2 Q_{\mathbf{k},\sigma}^2] \tag{3.5.16}$$

The normal modes of oscillations characterized by k-vector $\mathbf{k}$, polarization σ, and frequencies $\omega_{t,k}$, derived here, represent *standing waves,* which arise from the fixed-end boundary condition. If we assume a periodic box boundary condition, the normal modes are the *running waves.* In either case the same results for the heat capacity is obtained.

The energy eigenvalues for the corresponding quantum Hamiltonian for the system are

$$E_t = \sum_{\mathbf{k}} \sum_{\sigma} \left(\frac{1}{2} + n_{\mathbf{k},\sigma} \right) \hbar \omega_{t,k} = E[\{n_{\mathbf{k},\sigma}\}] \tag{3.5.17}$$

$$n_{\mathbf{k},\sigma} = 0, 1, 2, \ldots \tag{3.5.18}$$

It is convenient to interpret Eq. (3.5.17) in terms of the energies of quantum particles called *phonons.* In this view the quantum number $n_{\mathbf{k},\sigma}$ represents the number of phonons in the normal mode ($\mathbf{k}, \sigma$). The energy of the system is then specified by the set of the number of phonons in normal modes (states) $\{n_{\mathbf{k},\sigma}\}$.

By taking the canonical-ensemble average of Eq. (3.5.17), we obtain

$$\langle E_t \rangle = \sum_{\mathbf{k}} \sum_{\sigma} \left(\frac{1}{2} + \langle n_{\mathbf{k},\sigma} \rangle \right) \hbar \omega_{t,k}$$

$$= \sum_{\mathbf{k}} \sum_{\sigma} \left[\frac{1}{2} + f_0(\hbar \omega_{t,k}) \right] \hbar \omega_{t,k} \equiv E_t(\beta) \tag{3.5.19}$$

$$\langle n_{\mathbf{k},\sigma} \rangle = \frac{1}{e^{\beta \epsilon} - 1} \equiv f_0(\epsilon) \tag{3.5.20}$$

When the volume of normalization V is made large, the distribution of the normal-mode points in the k-space becomes dense. In the bulk limit we may convert the sum over $\{\mathbf{k}\}$ in Eq. (3.5.19) into an ω-integral and obtain

$$E_t(\beta) = E_{t,0} + \int_0^\infty d\omega \hbar \omega f_0(\hbar \omega) \mathcal{D}_t(\omega) \tag{3.5.21}$$

$$E_{t,0} \equiv \frac{1}{2} \int_0^\infty d\omega \hbar \omega \mathcal{D}_t(\omega) \tag{3.5.22}$$

where $D_t(\omega)$ is the *density of states (modes) in the frequency domain* defined such that

$$\text{number of modes in the interval } (\omega, \omega + d\omega) \equiv D_t(\omega) d\omega \tag{3.5.23}$$

The $E_{t,0}$ represents the sum of zero-point energies, which is independent of temperature.

The density of states in the frequency domain $D_t(\omega)$ may be calculated as follows. First we note that the angular frequency ω is related to the wave vector $\mathbf{k}$ by $\omega = c_t k$. The constant-ω surface in the k-space is therefore the sphere of radius $k = \omega / c_t$. Consider another concentric sphere of radius $k + dk = (\omega + d\omega)/c_t$. Each mode point is located at the simple cubic lattice sites with unit spacing π / L_0 and only in the first octant $(k_x, k_y, k_z > 0)$. The number of mode points within the spherical shell between the two spheres can be obtained by dividing one-eighth of the k-volume of the shell:

$$\frac{(4\pi k^2 dk)}{8} = \left(\frac{1}{2} \right) \frac{\pi \omega^2 d\omega}{c_t^3}, \qquad (\omega = c_t k)$$

by the unit-cell k-volume, $(\pi / L_0)^3$. Multiplying the result by 2 in consideration of the polarization multiplicity, we then obtain

$$\mathcal{D}_t(\omega) d\omega = \frac{\pi (\omega^2 d\omega / c_t^3)}{(\pi / L_0)^3} = \frac{L_0^3}{\pi^2} \frac{\omega^2 d\omega}{c_t^3} = \frac{V}{\pi^2} \frac{\omega^2 d\omega}{c_t^3} \tag{3.5.24}$$

We may treat the longitudinal waves similarly. The average energy $E_l(\beta) \equiv \langle E_l[\{n_{\mathbf{k}}\}] \rangle$

$$\mathcal{D}_l(\omega) = \frac{V}{2\pi^2} \frac{\omega^2}{c_l^3} \tag{3.5.25}$$

$$c_l \equiv \left[\frac{(B + 3S/4)}{\rho} \right]^{1/2} \tag{3.5.26}$$

is the propagation speed of the longitudinal wave; $B \equiv -V^{-1}\left(\frac{\partial P}{\partial V}\right)_T$ is the bulk modulus. Adding these contributions together, we obtain

$$E \equiv E_t + E_l = E_0 + \int_0^\infty d\omega \hbar\omega f_0(\hbar\omega)\mathcal{D}(\omega), \qquad \text{[Eq. (3.5.31)]} \tag{3.5.27}$$

$$E_0 \equiv \frac{1}{2}\int_0^\infty d\omega \hbar\omega \mathcal{D}(\omega) \tag{3.5.28}$$

where

$$\mathcal{D}(\omega) \equiv \mathcal{D}_t(\omega) + \mathcal{D}_l(\omega) = \frac{V}{2\pi^2}\left(\frac{2}{c_t^3} + \frac{1}{c_l^3}\right)\omega^2 \tag{3.5.29}$$

denotes the density of states in frequency for the combined wave modes.

For a real crystal of N atoms, the number of degrees of freedom is $3N$. Therefore there exist exactly $3N$ normal modes. The elastic body whose dynamic state is described by the vector field $\mathbf{u}(\mathbf{r}, t)$ has an infinite number of degrees of freedom, and therefore it has infinitely many modes. The model of a macroscopic elastic body is a reasonable representation of a real solid for low-frequency modes, that is, long-wavelength modes only. (This property can be demonstrated explicitly as was done in Section 3.4 for a linear chain of coupled harmonic oscillators.) At high frequencies the continuum model does not provide normal modes expected of a real solid. Debye solved the problem by assuming that the "corrected" density of states $D_D(\omega)$ has the same value as given by Eq. (3.5.29) up to the maximum frequency ω_D, then vanishes thereafter:

$$\mathcal{D}_D(\omega) = \begin{cases} \dfrac{V}{2\pi^2}\left(\dfrac{2}{c_t^3} + \dfrac{1}{c_l^3}\right)\omega^2 & \omega < \omega_D \\ 0 & \text{otherwise} \end{cases} \tag{3.5.30}$$

and that the limit frequency ω_D, called the *Debye frequency,* is chosen such that the number of modes for the truncated continuum model equals $3N$:

$$\int_0^\infty d\omega \mathcal{D}_D(\omega) = \int_0^{\omega_D} d\omega \mathcal{D}(\omega) = 3N \tag{3.5.31}$$

Substitution of Eq. (3.5.30) yields (Problem 3.5.3)

$$\omega_D = \left[18\pi^2 n / \left(\frac{2}{c_t^3} + \frac{1}{c_l^3}\right)\right]^{1/3} \tag{3.5.32}$$

where $n \equiv N/V$ is the number density. The density of states $D_D(\omega)$ grows quadratically, reaches the maximum at $\omega = \omega_D$, then vanishes thereafter as shown in Fig. 3.12.

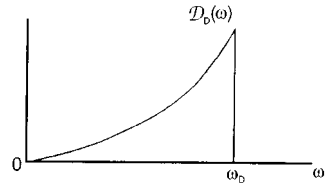

Figure 3.12. The density of modes in angular frequency for the Debye model.

We now compute the heat capacity C_V. Introducing Eq. (3.5.30) into Eq. (3.5.27), we obtain

$$E(T) - E_0 = \int_0^{\omega_D} d\omega \hbar\omega f_0(\hbar\omega) \frac{V}{2\pi^2} \left(\frac{2}{c_t^3} + \frac{1}{c_l^3} \right) \omega^2$$

$$= \frac{9N\hbar}{\omega_D^3} \int_0^{\omega_D} d\omega \frac{\omega^3}{\exp(\hbar\omega/k_B T) - 1} \tag{3.5.33}$$

Introducing the *Debye temperature* Θ_D defined by

$$\Theta_D \equiv \frac{\hbar\omega_D}{k_B} \tag{3.5.34}$$

we can rewrite Eq. (3.5.33) as

$$E(T) - E_0 = 9Nk_B T \left(\frac{T}{\Theta_D} \right)^3 \int_0^{x_D} dx \frac{x^3}{e^x - 1} \tag{3.5.35}$$

$$x_D \equiv \frac{\hbar\omega_D}{k_B T} \equiv \frac{\Theta_D}{T}, \qquad x \equiv \frac{\hbar\omega}{k_B T} \tag{3.5.36}$$

Consider first the high-temperature region where $x \equiv \hbar\omega/k_B T \ll 1$. Then $e^x - 1 \approx x$ and

$$\int_0^{x_D} dx \frac{x^3}{e^x - 1} \simeq \int_0^{x_D} dx\, x^2 = \frac{x_D^3}{3} = \frac{1}{3} \left(\frac{\Theta_D}{T} \right)^3, \qquad x_D \ll 1 \tag{3.5.37}$$

Using this approximation we obtain from Eq. (3.5.35)

$$E(T) = E_0 + 3Nk_B T, \qquad T \gg \Theta_D \tag{3.5.38}$$

Differentiating Eq. (3.5.38) with respect to T, we obtain the heat capacity of the solid: $C_V = \partial E/\partial T = 3Nk_B$, which is in agreement with the classical result.

At very low temperatures, $x_D \equiv \hbar\omega_D/k_B T$ becomes very large. In this limit,

$$\int_0^{\omega_D} dx \frac{x^3}{e^x - 1} \longrightarrow \int_0^{\infty} dx \frac{x^3}{e^x - 1} = \frac{\pi^4}{15} \tag{3.5.39}$$

Table 3.1. Approximate Values for Debye Temperature

Solids	Debye temperature Θ_D in K
NaCl	281
KC1	230
Pb	88
Ag	225
Zn	308
Diamond	1860

We then obtain from Eq (3.5.35)

$$E = E_0 + \left(\frac{3}{5}\right)\frac{\pi^4 N k_B T^4}{\Theta_D^3} \qquad (T \ll \Theta_D) \tag{3.5.40}$$

Differentiating this expression with respect to T, we obtain

$$\boxed{C_V = \frac{12\pi^2}{5} N k_B \left(\frac{T}{\Theta_D}\right)^3} \tag{3.5.41}$$

According to this equation, the heat capacity at very low temperatures behaves like T^3. This is known as the *Debye-T^3 law*. The decrease is therefore slower than the Einstein heat capacity given by Eq. (3.2.14), which decreases exponentially.

At intermediate temperatures the integral may be evaluated as follows. Differentiating Eq. (3.5.33) with respect to T, we obtain

$$C_V = \frac{\partial E}{\partial T} = 9 N k_B \left(\frac{T}{\Theta_D}\right)^3 \int_0^{x_D} dx \frac{x^4 e^x}{(e^x - 1)^2} \qquad \left(x_D \equiv \frac{\Theta_D}{T}\right) \tag{3.5.42}$$

We may compute this integral numerically. We can then express the molar heat of solid as a function of T/Θ_D only. The theoretical curve so obtained is shown in a solid line in Fig. 3.13. The points in the figure are experimental data for various solids. The Debye temperatures adjusted at optimum fitting are also shown in the same figure. Roughly speaking when T/Θ_D is greater than 1 or when the actual temperature exceeds the Debye temperature, the solid behaves classically and the molar heat is nearly equal to $3R$ in agreement with the Dulong–Petit law. When the temperature is less than the Debye temperature, the quantum effect sets in, so the heat capacity is less than $3R$. Thus for lead (a soft metal), with a Debye temperature of only 88 K, room temperature is well above the Debye temperature; therefore its heat capacity is classical, while diamond (a hard crystal), with a Debye temperature of 1860 K, shows a quantum nature in heat capacity even at room temperature. The Debye temperatures for several typical solids are given in Table 3.1.

Debye's theory of the heat capacity gives quite satisfactory results for almost all nonconducting crystals. Exceptions arise if the crystals have striking anisotropies like graphite or if finite-size crystals are considered. For conducting materials we must take into account the electronic contribution to the heat capacity, which was discussed in

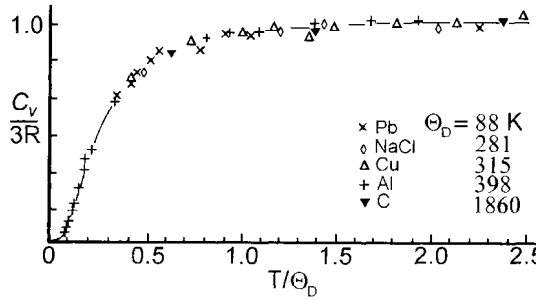

Figure 3.13. The heat capacities of solids. The solid line represents the Debye curve obtained from Eq. (3.5.41). Experimental data for various solids are shown with optimum Debye temperatures [after Sears and Salinger (Ref. 5)].

Chapter 2. We may look at a solid as a collection of coupled harmonic oscillators and develop a theory from this viewpoint. This will be done in Section 7.3.

Problem 3.5.1. Verify Eq. (3.5.1) by using Eqs. (3.5.3) and (3.5.5).

Problem 3.5.2. Verify Eq. (3.5.11).

Problem 3.5.3. Verify Eq. (3.5.32).

REFERENCES

1. C. Kittel, *Introduction to Solid-State Physics,* 6th ed. (Wiley, New York, 1986).
2. A. Einstein, *Ann. Physik* **22,** 186 (1907).
3. H. Goldstein, *Classical Mechanics,* 2d ed. (Addison-Wesley, Reading, MA, 1981).
4. P. Debye, *Ann. Physik* **39,** 789 (1912).
5. F. W. Sears and G. L. Salinger, *Thermodynamics, Kinetic Theory, and Statistical Mechanics,* 3d ed. (Addison-Wesley, Reading, MA, 1975).

This page intentionally left blank.

4

Liquid Helium

Bose–Einstein Condensation

Liquid He^4 undergoes the superfluid transition at 2.2 K. This phenomenon is regarded as a manifestation of the fact that He^4 atoms are bosons and undergo a Bose–Einstein condensation.

4.1. LIQUID HELIUM

In 1925 Einstein showed the possibility of a Bose–Einstein (B–E) condensation[1] such that there exists a condensation temperature T_c below which a macroscopic fraction of free bosons occupies the lowest momentum states. It is now known that a least some of the anomalous properties of liquid helium II, such as the existence of a macroscopic condensate are those that would be expected in completely degenerate bosons.

Helium is the only substance in nature that does not solidify by lowering its temperature under atmospheric pressure. There exist two main isotopes, He^4, the most abundant, and He^3. Interactions between atoms are practically identical for any pair, He^4–He^4, He^3–He^3, or He^3–He^4. (These interactions are mainly determined by the electronic structure that both isotopes share.) The potential has a shallow attractive well such that two He^3 atoms may form a bound state with a very small binding energy. For He^4 the bound state has a 20% greater binding energy. (This difference is due to the

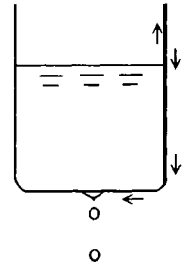

Figure 4.1. Superfluid He in a beaker creeps around the wall and drips down.

difference in mass. Quantum mechanical calculations of the energy eigenvalues involve the total Hamiltonian, that is, the potential plus kinetic energy that contains the mass difference.) The boiling points for liquid He^3 and He^4 are 3.2 and 4.2 K, respectively. These values do reflect the binding energies of the molecules. Liquid He^4 undergoes the so-called λ-transition at 2.2 K into *a superfluid phase* whose flow properties are quite different from those of the ordinary fluid. For example superfluid in a beaker creeps around the walls and drips down, see Fig. 4.1. The reader interested in learning many fascinating properties of liquid He^4 should see Ref. 2. On the other hand, liquid He^3 behaves quite differently. Very recently a phase transition was discovered for this liquid at a temperature of 0.002 K.[3] Its superfluid phase however is quite different from the superfluid phase of liquid He^4, which is commonly called liquid He II. The normal phase of liquid He^4 above the λ-transition, is called liquid He I.

Why does there exist such difference between liquid He^3 and He^4? The He^4 atom has four nucleons (two protons, two neutrons) and two electrons. Since it contains an even number of fermions, it is a boson according to Ehrenfest–Oppenheimer–Bethe's rule (see Chapter 1). Isotope He^3 has three nucleons and two electrons; thus He^3 atom is a fermion. This difference generates a fundamental difference in the macroscopic properties of quantum fluids. To illustrate this point, we study the thermodynamic behavior of a system of free bosons in the following two sections.

4.2. FREE BOSONS; BOSE–EINSTEIN CONDENSATION

Let us consider a system of free bosons characterized by the Hamiltonian:

$$H = \sum_j \frac{p_j^2}{2M} \tag{4.2.1}$$

The equilibrium distribution is represented by the *Bose distribution function:*

$$f_B(\epsilon_p) \equiv \frac{1}{\exp[\beta(\epsilon_p - \mu)] - 1}, \qquad \epsilon_p \equiv \frac{p^2}{2M} \tag{4.2.2}$$

which is subject to the normalization condition:

$$V^{-1} \sum_{\mathbf{p}} f_B(\epsilon_p) = n \text{ (number density)} \tag{4.2.3}$$

Hereafter we drop the subscript B for the Bose distribution function f_B. By definition the Bose distribution function $f(\epsilon_p)$ represents the relative probability of finding a particle with momentum **p.** Therefore the function $f(\epsilon_p)$ must be nonnegative:

$$f(\epsilon_p) = \frac{1}{\exp[\beta(\epsilon_p - \mu)] - 1} \geq 0 \tag{4.2.4}$$

To ensure this property for all $\epsilon_p \geq 0$, the chemical potential μ must be nonpositive:

$$\mu \leq 0 \tag{4.2.5}$$

[or else $f(\epsilon_p)$ would become negative for $0 < \epsilon_p < \mu$]. By the way such a restriction on μ does not apply to the Fermi or Boltzmann distribution function. Why? (Problem 4.2.1.)

In the bulk limit the momentum eigenvalues form a continuous spectrum. For the moment let us replace the sum over momentum states in Eq. (4.2.3) by the momentum integral:

$$n = \text{Lim}\left(\frac{1}{V}\right)\int d^3p\, \mathcal{D}(p) f(\epsilon_p) \tag{4.2.6}$$

The density of states $D(p)$ for free particles (without spin) was calculated in Section 2.3 and it is given by Eq. (2.3.9):

$$\mathcal{D}(p) = \frac{V}{(2\pi\hbar)^3} \tag{4.2.7}$$

Introducing this expression in Eq. (4.2.6), we obtain

$$n = (2\pi\hbar)^{-3}\int d^3p\, f(\epsilon_p) \tag{4.2.8}$$

The momentum-space integration may be carried out in the spherical polar coordinates (p, θ, ϕ) with the momentum-volume element $d^3p = p^2 dp \sin\theta d\theta d\phi$. After performing the angular integration (4π), we may rewrite the result in the form of an energy integral:

$$n = \frac{M^{3/2}}{2^{1/2}\pi^2\hbar^3}\int_0^\infty d\epsilon\, \epsilon^{1/2}\frac{1}{e^{\beta(\epsilon+|\mu|)}-1} \equiv \frac{M^{3/2}}{2^{1/2}\pi^2\hbar^3}F(\beta, |\mu|) \tag{4.2.9}$$

This result can also be obtained by using the density of states in energy:

$$\mathcal{N}(\epsilon) = V\frac{M^{3/2}}{2^{1/2}\pi^2\hbar^3}\epsilon^{1/2} \tag{4.2.10}$$

Let us now consider the ϵ-integral in Eq. (4.2.9):

$$F(\beta, |\mu|) \equiv \int_0^\infty d\epsilon\, \epsilon^{1/2}\frac{1}{e^{\beta(\epsilon+|\mu|)}-1} \tag{4.2.11}$$

which is a function of β and $|\mu|$. For a fixed β the function F is a decreasing function of $|\mu|$ with the maximum occurring at $\mu = 0$:

$$F(\beta, |\mu|) \leq F(\beta, 0) \tag{4.2.12}$$

The maximum value for F can be evaluated by making $\epsilon\beta = x$ as follows:

$$\begin{aligned} F(\beta, 0) &= \int_0^\infty d\epsilon\, \epsilon^{1/2}\frac{1}{e^{\beta\epsilon}-1} \\ &= \beta^{-3/2}\int_0^\infty dx\, x^{1/2}\frac{1}{e^x-1} \end{aligned} \tag{4.2.13}$$

$$\int_0^\infty dx\, x^{1/2} \frac{1}{e^x - 1} = \int_0^\infty dx\, x^{1/2}(e^{-x} + e^{-2x} + \dots)$$
$$= 1.306\pi^{1/2} \tag{4.2.14}$$

We then see that the integral on the rhs of Eq. (4.2.9) has an upper limit. The number density n on the lhs could of course be increased without limit. Something must have gone wrong in our calculations. A closer look at Eq. (4.2.2) shows that the function $f(\epsilon)$ blows up in the neighborhood of $\epsilon = 0$ if $\mu = 0$. This behavior therefore violates the validity condition stated in Section 2.3 for the conversion of the sum-over-states into an integral. In such a case we must proceed more carefully.

Let us go back to Eq. (4.2.3) and break the sum into two parts:

$$\frac{N}{V} = \frac{N_0}{V} + \frac{1}{V} \sum_{\mathbf{p}, \epsilon_p > 0} f(\epsilon_p) \tag{4.2.15}$$

where N_0 is the number of bosons with zero momentum, given by

$$N_0 = \left(e^{\beta|\mu|} - 1\right)^{-1} \tag{4.2.16}$$

This number can be made very large by choosing very small $\beta|\mu|$. For example to have $N_0 = 10^{20}$, we may choose $\beta|\mu| = \ln(1 + N_0^{-1}) = \ln(1 + 10^{-20}) \simeq 10^{-20}$. In fact N_0 can be increased without limit. We note further that because the density of states in energy is proportional to $\epsilon^{1/2}$, see Eq. (4.2.10), the contribution of zero-momentum bosons is not included in the ϵ-integral. We therefore should write the normalization condition in the bulk limit as follows:

$$n = n_0 + \frac{M^{3/2}}{2^{1/2}\pi^2\hbar^3} \int_0^\infty d\epsilon\, \epsilon^{1/2} \frac{1}{e^{\beta(\epsilon + |\mu|)} - 1} \tag{4.2.17}$$

The two terms in Eq. (4.2.17) represent the density $n_0 \equiv N_0/V$ of zero-momentum bosons and the density of moving bosons. The term n_0 is important only when the number of zero-momentum bosons N_0 is a significant fraction of the total number of bosons N. The possibility of such an unusual state, called the *Bose–Einstein (B–E) condensation*, was first recognized by Einstein. (Such possibilities do not exist for fermions.) For low densities or high temperatures, the density of zero-momentum bosons n_0 is negligible compared to the total number density n. By raising the density or by lowering the temperature, the system undergoes a sharp transition into a state in which n_0 becomes a significant fraction of n. At absolute zero all bosons have zero momentum. The sharp change in state resembles the gas-to-liquid condensation but the B–E condensation occurs in the momentum space. Other features of the B–E condensation are discussed in the following section.

Problem 4.2.1. Let us consider a system of free fermions. From the normalization find the range of chemical potential μ that appears in the Fermi distribution function:

$$f_F(\epsilon) \equiv \frac{1}{e^{\beta(\epsilon - \mu)} + 1}$$

Problem 4.2.2. Let us consider a system of free bosons moving in two dimensions. (a) Does the system undergo a transition into a condensed state at low temperatures as in three dimensions? (b) Discuss the heat capacity of the system in all temperature ranges. Calculate explicitly the heat capacity at low- and high-temperature limits.

4.3. BOSONS IN CONDENSED PHASE

At absolute zero all bosons have zero momentum. As temperature is raised, bosons with nonzero momenta emerge. The number of moving or excited bosons given by the volume V times the second term in the rhs of Eq. (4.2.15) can be represented by

$$N_{\epsilon>0} = \sum_{\mathbf{p},\epsilon_p>0} f(\epsilon_p) = \frac{VM^{3/2}}{2^{1/2}\pi^2\hbar^3}\int_0^\infty d\epsilon\,\epsilon^{1/2}\frac{1}{e^{\beta(\epsilon+|\mu|)}-1}$$
$$\equiv \frac{VM^{3/2}}{2^{1/2}\pi^2\hbar^3}F(\beta,|\mu|) \tag{4.3.1}$$

[from Eqs. (4.2.9) and (4.2.11)]. Throughout the condensed phase, the chemical potential μ has an extremely small absolute value (Problem 4.3.1). Since the function $F(\beta,|\mu|)$ is a smooth function of $|\mu|$ for $|\mu| \ll 1$, we may approximate Eq. (4.3.1) by its value at $\mu = 0$:

$$N_{\epsilon>0} \cong \frac{VM^{3/2}}{2^{1/2}\pi^2\hbar^3}F(\beta,0) = 1.306\,\frac{VM^{3/2}}{2^{1/2}\pi^2\hbar^3}(k_BT)^{3/2} \qquad \text{[use of (2.14)]} \tag{4.3.2}$$

Here we see that the total number of bosons in the excited states with positive energies grows like $T^{3/2}$ as temperature is raised. This number may eventually reach the total number N of the system at the *critical temperature* T_c. At and above T_c practically all bosons are in the excited states. This temperature T_c can be obtained from

$$N = \frac{1.306\pi^{1/2}}{2^{1/2}\pi^2}\frac{VM^{3/2}}{\hbar^3}(k_BT_c)^{3/2} = \frac{1}{6.032}\frac{VM^{3/2}}{\hbar^3}(k_BT_c)^{3/2} \tag{4.3.3}$$

Solving for T_c, we obtain

$$\boxed{T_c = 3.31\,\hbar^2(Mk_B)^{-1}n^{2/3}} \tag{4.3.4}$$

Using this relation we can rewrite Eq. (4.3.2) in the form:

$$N_{\epsilon>0} = N\left(\frac{T}{T_c}\right)^{3/2}, \qquad T \le T_c \tag{4.3.5}$$

The number of zero-momentum bosons N_0 can be obtained by subtracting this number from the total number N:

$$N_0 = N - N_{\epsilon>0} = N\left[1 - \left(\frac{T}{T_c}\right)^{3/2}\right], \qquad T \le T_c \tag{4.3.6}$$

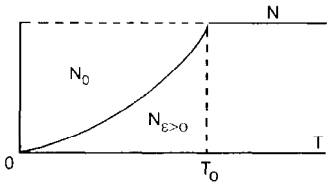

Figure 4.2. The number of condensed bosons N_0 below the critical temperature T_c forms a finite fraction of the total number N.

Here we see that N_0 is in fact a finite fraction of the total number N. The number of bosons in excited states and in the ground state, $N_{\varepsilon>0}$ and N_0, are plotted against temperature in Fig. 4.2.

The thermal energy E of the system comes only from moving bosons. The average energy per unit volume can be calculated as follows:

$$\frac{E}{V} = \text{Lim}\,\frac{1}{V}\sum_{\mathbf{p},\epsilon_p>0}\epsilon_p f(\epsilon_p) = \frac{M^{3/2}}{2^{1/2}\pi^2\hbar^3}\int_0^\infty d\epsilon\,\epsilon^{3/2}\frac{1}{e^{\beta(\epsilon+|\mu|)}-1} \tag{4.3.7}$$

The e-integral here is also a slowly varying function of $|\mu|$ for $|\mu| << 1$. We may therefore approximate it by its value at $\mu = 0$:

$$\int_0^\infty d\epsilon\,\epsilon^{3/2}\frac{1}{e^{\beta(\epsilon+|\mu|)}-1} \cong \int_0^\infty d\epsilon\,\epsilon^{3/2}\frac{1}{e^{\beta\epsilon}-1}$$

$$= \beta^{-5/2}\int_0^\infty dx\,x^{3/2}\frac{1}{e^x-1} \tag{4.3.8}$$

$$\int_0^\infty dx\,x^{3/2}\frac{1}{e^x-1} = 1.342 \tag{4.3.9}$$

Using Eqs. (4.3.8) and (4.3.9) we obtain from Eq. (4.3.7):

$$\frac{E}{V} = \frac{M^{3/2}}{2^{1/2}\pi^2\hbar^3}1.342\,(k_B T)^{5/2} \tag{4.3.10}$$

This result can be rewritten with the aid of Eq. (4.3.3) as follows:

$$\frac{E}{V} = 1.342\,\frac{M^{3/2}}{2^{1/2}\pi^2\hbar^3}(k_B T_c)^{3/2}(k_B T)\left(\frac{T}{T_c}\right)^{3/2} = 0.770\,nk_B T\left(\frac{T}{T_c}\right)^{3/2} \tag{4.3.11}$$

The internal energy density E/V grows like $T^{5/2}$ in the condensed phase.

Differentiating Eq. (4.3.11) with respect to T, we obtain for a mole of the gas

$$C_V = \left(\frac{\partial E}{\partial T}\right)_V = \frac{5}{2}\frac{E}{T} = 1.92\,R\left(\frac{T}{T_c}\right)^{3/2} \tag{4.3.12}$$

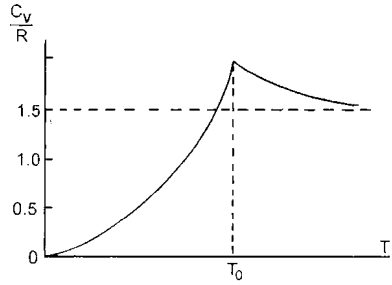

Figure 4.3. The reduced heat capacity C_V/R exhibits a sharp cusp at the critical temperature T_c.

The behavior of the molar heat capacity at constant volume C_V versus temperature T is shown in Fig. 4.3. The molar heat C_V increases like $T^{3/2}$ throughout the condensed phase, and it reaches its maximum value $1.92R$ at the critical temperature T_c. Above T_c it gradually decreases and approaches the classical value $1.50R$ at the high-temperature limit. At the transition point C_V is continuous, but its derivative $\partial C_V/\partial T$ has a jump.

The B–E condensation is similar to the gas–liquid transformation in the sense that it is a sudden macroscopic change of state. It is however quite different in finer detail. The heat capacity of the familiar vapor–liquid transition has a jump. Furthermore there is latent heat at the transition. According to Ehrenfest's classification of phase transition, the B–E condensation is *a phase transition of third order* as $\partial C_V/\partial T$, which is expressed in terms of the third-order derivative of the free energy F, is discontinuous at the transition. For a phase transition of second or higher order, there is no latent heat of condensation. In contrast a phase transition of first order for which the first derivatives of the free energy (volume, entropy, internal energy) have discontinuities between the two phases is accompanied by latent heat. The readers interested in learning more about the general theory of phase transition are encouraged to read the classic book on *Statistical Physics* by Landau and Lifshitz.[4]

To see the relevance of the B–E condensation to the actual liquid helium, let us look at a few properties of this substance. Fig. 4.4 represents the P–T diagram, also called the phase diagram, of pure He^4. Proceeding along the horizontal line at one atmospheric pressure He^4 passes from gas to liquid at 4.2 K. This liquid, called the liquid He I, behaves like any other liquid, and it has finite viscosity. By cooling down further, the substance undergoes a sudden change at 2.18 K. Below this temperature the liquid He II

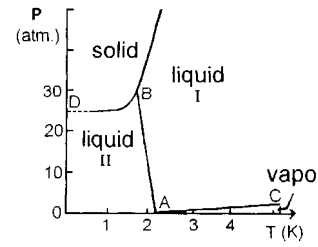

Figure 4.4. The phase diagram of He^4. The line AB, called the λ-line, separates liquid He II from liquid He I. The point C represents the critical point.

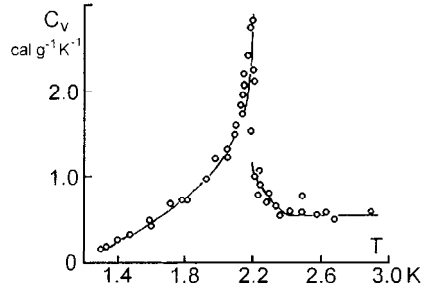

Figure 4.5. Specific heat of liquid He^4 versus temperature [after London (Ref. 2)].

is a superfluid, as mentioned in Section 3.1. The heat capacity of liquid helium measured under its saturated vapor is shown in Fig. 4.5. Because of the similarity between the experimental curve and the inverted Greek letter λ, the transition is often called the λ-*transition.* The heat capacity has an extremely sharp peak of a logarithmic type.[5] The resemblance between this curve and the heat capacity curve of the ideal Bose gas shown in Fig. 4.3 is striking. If we calculate the value of T_c from Eq. (4.2.4) with the use of the mass density of liquid helium $n = 0.145$ g/cm³, we find that $T_c = 3.14$ K, which is remarkably close to the observed λ-transition temperature 2.18 K.

Problem 4.3.1. Assume that free bosons are in the condensed state below the critical temperature T_c. Calculate the pressure P of the system by means of formula:

REFERENCES

1. A. Einstein, *Sits. Ber. Berl. Akad.* **261**, 3 (1925).
2. F. London, *Superfluids*, Vol. 2 (Wiley, New York 1954).
3. D. D. Osheroff, R. C. Richardson, and D. M. Lee, 1972, *Phys. Rev. Lett.* **29**, 920.
4. L. D. Landau and E. M. Lifshitz, *Statistical Physics*, 2d ed. (Addison-Wesley, Reading, MA, 1969).
5. M. J. Buckingham and W. M. Fairbank, "The nature of the λ-transition," in *Progress in low Temperature Physics*, Vol. 3, ed. by C. J. Gorter (North-Holland, Amsterdam, 1961).

5

Bloch Electrons; Band Structures

To properly develop a microscopic theory of superconductivity, a deeper understanding of the properties of normal metals than what is provided by the free-electron model (reviewed in Chapter 3) is required. Based on the Bloch theorem, the Fermi liquid model is derived. At 0 K, the normal metal is shown to have a sharp Fermi surface, which is experimentally supported by the fact that the heat capacity is linear in temperature at the lowest temperatures. Electrons and holes, which appear in the Hall effect measurements, will be connected with the shape of the Fermi surface. Two important experiments to explore the Fermi surface, de Haas–van Alphen oscillations and cyclotron resonance, are discussed in detail. Newtonian equations of motion for a Bloch electron (wave packet) are derived and discussed.

5.1. THE BLOCH THEOREM

Let us consider a periodic potential $V(x)$ in one dimension (see Fig. 2.1), which satisfies

$$V(x + na) = V(x), \qquad -\infty < x < \infty \tag{5.1.1}$$

where a is the lattice constant, and n an integer. The Schrödinger energy-eigenvalue equation for an electron is

$$\left[-\frac{\hbar^2}{2m}\frac{d^2}{dx^2} + V(x)\right]\psi_E(x) = E\psi_E(x) \tag{5.1.2}$$

Clearly $\psi_E(x + na)$ also satisfies the same equation. Therefore the wave function ψ_E is likely to have two values at x and $x + na$, differing only by an x-independent phase:

$$\boxed{\psi_E(x + na) = e^{ikna}\psi_E(x)} \tag{5.1.3}$$

where k is a real number. Equation (5.1.3) represents a form of the *Bloch theorem.*[1] It generates far-reaching consequences in the theory of conduction electrons. Let us prove Eq. (5.1.3). Since $\psi(x)$ and $\psi(x + na)$ satisfy the same equation, they are linearly dependent:

$$\psi(x + na) = c(na)\psi(x) \tag{5.1.4}$$

Hence

$$\psi(x + na + ma) = c(na)\psi(x + ma) = c(na)c(ma)\psi(x) = c(na + ma)\psi(x)$$

Since the wave function $\psi(x)$ does not vanish in general, we obtain

$$c(na + ma) = c(na)c(ma) \text{ or } c(x + y) = c(x)c(y) \tag{5.1.5}$$

Solving this functional equation, we obtain (Problem 51.1)

$$c(y) = \exp(\lambda y) \tag{5.1.6}$$

where λ is a constant. The wave function ψ in Eq. (5.1.4) must be finite for all ranges. Then this constant λ must be a pure imaginary number:

$$\lambda = ik, \qquad k : \text{real} \tag{5.1.7}$$

Combining Eqs. (5.1.4), (5.1.6), and (5.1.7), we obtain Eq. (5.1.3). q.e.d.

Let us discuss a few physical properties of the Bloch wave function ψ. By taking absolute square of Eq. (5.1.3), we obtain

$$|\psi(x+na)|^2 = |\psi(x)|^2 \tag{5.1.8}$$

meaning that:

A) The probability distribution function $P(x)$ is *lattice-periodic*:

$$P(x) \equiv |\psi(x)|^2 = P(x + na), \qquad \text{for any } n \tag{5.1.9}$$

B) The exponential function of a pure imaginary number e^{iky} is periodic: $e^{i(ky+2\pi m)} = e^{iky}$, where m is an integer. We may choose the real number k in Eq. (5.1.3), called the k-number (2π times the wave number), to have a basic range:

$$-\frac{\pi}{a} < k < \frac{\pi}{a} \tag{5.1.10}$$

the two end points are called the *Brillouin boundary* (points).

C) In general there are a number of energy gaps (forbidden regions of energy) in which no solutions of Eq. (5.1.2) exist (see Fig. 2.2 and Section 5.2). The energy eigenvalues E are characterized by the k-number and the *zone number* or *band index* j, which enumerates the *energy bands*:

$$E = E_j(k) \tag{5.1.11}$$

This property is not obvious, and it will be illustrated by examples in Section 5.2.

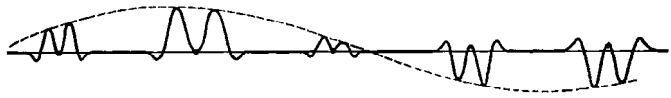

Figure 5.1. Variation of the real (or imaginary) part of the wave function $\psi_E(x)$.

To further explore the nature of the wave function ψ represented by Eq. (5.1.3), let us write

$$\boxed{\psi_E(x) = e^{ikx} u_{j,k}(x)} \tag{5.1.12}$$

and substitute it into Eq. (5.1.3). If the function $u_{j,k}(x)$ is lattice-periodic:

$$u_{j,k}(x + na) = u_{j,k}(x) \tag{5.1.13}$$

the property Eq. (5.1.3) is satisfied (Problem 5.1.2). Equation (5.1.12) represents a second form of the Bloch theorem. In this so-called *Bloch form,* ψ has great similarity with the free-particle wave function:

$$\psi_{\text{free}}(x) = c \exp(ikx) \tag{5.1.14}$$

where c is a constant. The connection may be illustrated as in Fig. 5.1. For the free particle, the k-number can range from $-\infty$ to ∞, and the energy is

$$E_{\text{free}} = \frac{p^2}{2m} \equiv \frac{\hbar^2 k^2}{2m} \tag{5.1.15}$$

with no gaps. These features therefore are different from those stated in properties B and C.

An important similarity arises when we write the time-dependent wave function $\psi(x, t)$ in the running wave form:

$$\psi_E(x, t) = e^{i(kx - \omega t)} U(x) \tag{5.1.16}$$

where the frequency w is defined by

$$\omega = \begin{cases} \hbar^{-1} E_j(k) & \text{for the Bloch electron} \\ \hbar^{-1} E_{\text{free}} & \text{for the free electron} \end{cases} \tag{5.1.17}$$

and the amplitude $U(x)$ is defined by

$$U(x) = \begin{cases} u_{j,k}(x) & \text{for the Bloch electron} \\ c & \text{for the free electron} \end{cases} \tag{5.1.18}$$

Equation (5.1.16) means that the Bloch wave function $\psi_E(x)$ represents a running wave characterized by k-number k, angular frequency w, and wave train $u_{j,k}(x)$.

The group velocity v of the Bloch wave packet is given by

$$v \equiv \frac{\partial \omega}{\partial k} \equiv \hbar^{-1} \frac{\partial E}{\partial k} \tag{5.1.19}$$

By applying the (quantum) principle of wave-particle duality, we then imagine that the Bloch electron moves according to the energy–momentum relation:

$$E = \epsilon_j(\hbar k) \equiv \epsilon_j(p) \tag{5.1.20}$$

and velocity v given by Eq. (5.1.19). This gives a picture of great familiarity. Before fully developing this picture, we generalize our theory to the three-dimensional case.

For definiteness, we consider an infinite orthorhombic (orc) lattice of lattice constants (a, b, c). We choose a Cartesian frame of coordinates (x,y,z) along the lattice axes. The potential $V(x, y, z) = V(\mathbf{r})$ is *lattice-periodic* :

$$V(\mathbf{r} + \mathbf{R}) = V(\mathbf{r}) \tag{5.1.21}$$

$$\mathbf{R} \equiv n_1 a\mathbf{i} + n_2 b\mathbf{j} + n_3 c\mathbf{k} \qquad (n_j : \text{integers}) \tag{5.1.22}$$

Such a vector $\mathbf{R}$ is called a *Bravais lattice vector.* The Schrödinger equation is

$$\left[-\frac{\hbar^2}{2m}\nabla^2 + V(\mathbf{r})\right]\psi_E(\mathbf{r}) = E\psi_E(\mathbf{r}) \tag{5.1.23}$$

The Bloch wave function $\psi_E(\mathbf{r})$ satisfies

$$\boxed{\psi_E(\mathbf{r} + \mathbf{R}) = e^{i\mathbf{k}\cdot\mathbf{R}}\psi_E(\mathbf{r})} \tag{5.1.24}$$

where $\mathbf{k} = (k_x, k_y, k_z)$ are called k-vectors.

The three principal properties of the Bloch wave functions are

A) The probability distribution $P(\mathbf{r})$ is lattice-periodic:

$$P(\mathbf{r}) \equiv |\psi(\mathbf{r})|^2 = P(\mathbf{r} + \mathbf{R}) \tag{5.1.25}$$

B) The k-vector $\mathbf{k} = (k_x, k_y, k_z)$ in Eq. (5.1.24) has the fundamental range:

$$-\frac{\pi}{a} < k_x < \frac{\pi}{a}, \qquad -\frac{\pi}{b} < k_y < \frac{\pi}{b}, \qquad -\frac{\pi}{c} < k_z < \frac{\pi}{c} \tag{5.1.26}$$

the end points, that form a rectangular box are called the *Brillouin boundary.*

C) The energy eigenvalues E have energy gaps, and the allowed energies E can be characterized 'by the zone number j and the k-vectors:

$$\boxed{E = \epsilon_j(\hbar\mathbf{k}) \equiv \epsilon_j(\mathbf{p})} \tag{5.1.27}$$

Eqs. (5.1.24)–(5.1.27) are straightforward extensions of Eqs. (5.1.3), (5.1.8), (5.1.10), and (5.1.11). Using Eq. (5.1.24), we can express the Bloch wave function ψ in the form:

$$\psi_E(\mathbf{r}) \equiv \psi_{j,\mathbf{k}}(\mathbf{r}) = e^{i\mathbf{k}\cdot\mathbf{r}}u_{j,\mathbf{k}}(\mathbf{r}), \qquad u_{j,\mathbf{k}}(\mathbf{r} + \mathbf{R}) = u_{j,\mathbf{k}}(\mathbf{r}) \tag{5.1.28}$$

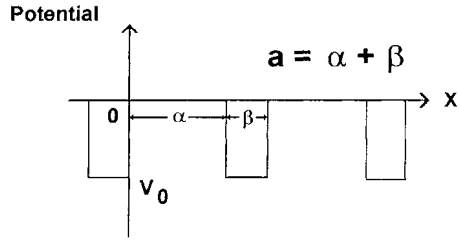

Figure 5.2. A Kronig–Penney potential.

Equations (5.1.27) and (5.1.28) indicate that the Bloch wave function $\psi_E(\mathbf{r})$, associated with quantum numbers (j, $\mathbf{k}$), is a plane wave characterized by k-vector $\mathbf{k}$, angular frequency $w \equiv \hbar^{-1}E_j(\mathbf{k})$ and wave train $u_{j,\mathbf{k}}(\mathbf{r})$.

Problem 5.1.1. Solve: (a) $f(x + y) = f(x) + f(y)$, (b) $f(x + y) = f(x)f(y)$. Hints: Differentiate (a) with respect to x, then convert the result into an ordinary differential equation. Take the logarithm of (b). [Answer: (a) $f(x) = cx$, (b) $f(x) = e^{\lambda x}$.]

Problem 5. 1 .2. (a) Show that a wave equation of the Bloch form [Eq. (5.1.12)] satisfies Eq. (5.1.3). (b) Assuming Eqs. (5.1.3) derive Eq. (5.1.12).

5.2. THE KRONIG–PENNEY MODEL

The Bloch energy-eigenvalues in general have bands and gaps. We show this by taking the Kronig–Penney (K–P) model.[2] Let us consider a periodic square-well potential $V(x)$ with depth V_0 (< 0) and well width $\beta \equiv a - \alpha$ as shown in Fig. 5.2:

$$V(x) = \begin{cases} V_0 & \text{if} \quad na - \beta < x < na \\ 0 & \text{if} \quad na < x < na + \alpha, \end{cases} \qquad \alpha + \beta = a \tag{5.2.1}$$

The Schrödinger energy eigenvalue equation for an electron can be written as Eq. (5.1.2). Since this is a linear homogeneous differential equation with constant coefficients, the wave function $\psi(x)$ should have the form:

$$\psi(x) = ce^{\gamma x}, \qquad (c, \gamma: \text{constants}) \tag{5.2.2}$$

According to the Bloch theorem in Eq. (5.1.12), this function $\psi(x)$ can be written as

$$\psi_k(x) = e^{ikx}u_k(x) \tag{5.2.3}$$

$$u_k(x + a) = u_k(x) \tag{5.2.4}$$

The condition that the function $\psi(x)$ be *continuous* and *analytic* at the well boundary yields the following relation (Problem 5.2.1)

$$\cos ka = \cosh K\alpha \cos \mu\beta - \frac{\mu^2 - K^2}{2K\mu} \sinh K\alpha \sin \mu\beta \equiv f(E) \tag{5.2.5}$$

$$E \equiv -\frac{\hbar^2}{2m}K^2 \equiv V_0 + \frac{\hbar^2}{2m}\mu^2 \qquad (V_0 < 0) \tag{5.2.6}$$

By solving Eq. (5.2.5) with Eq. (5.2.6), we can obtain the eigenvalue E as a function of k. The band edges are obtained from

$$f(E) = \pm 1 \tag{5.2.7}$$

which corresponds to the limits of cos ka. Numerical studies of Eq. (5.2.5) indicate[3] that (1) there are in general a number of negative- and positive-energy bands; (2) at each band edge, an *effective mass* m^* can be defined, whose value can be positive or negative, and whose absolute value can be greater or less than the electron mass m; and (3) the efffective mass is positive at the lower edge of each band and negative at the upper edge. In particular at the lowest band edge ϵ_0 satisfies

$$f(\epsilon_0) = 1 \tag{5.2.8}$$

Near this edge the energy–k relation calculated from Eq. (5.2.5) is (Problem 5.2.2):

$$\epsilon = \epsilon_0 + \frac{\hbar^2}{2m^*}k^2 \qquad (\epsilon_0 < 0) \tag{5.2.9}$$

$$m^* \equiv -\hbar^2 a^{-2} f'(\epsilon_0) \tag{5.2.10}$$

This one-dimensional K–P model can be used to study a simple three-dimensional model. Let us take an orc lattice of unit lengths (a_1, a_2, a_3), with each lattice point representing a short-range attractive potential center (ion). The Schrödinger equation (5.1.23) for this system as it stands is hard to solve.

Let us now construct a model potential V_s defined by

$$V_S(x,y,z) = V_1(x) + V_2(y) + V_3(z) \tag{5.2.11}$$

$$V_j(u) = \begin{cases} V_0 \ (<0) & \text{if } na_j - \beta < u < na_j \\ 0 & \text{otherwise} \end{cases} \tag{5.2.12}$$

where n's are integers. The corresponding two-dimensional model is shown in Fig. 5.3. The domain in which $V_S \neq 0$ are parallel plates of thickness β ($< a_j$) separated by a_j in the direction x_j $(x_1, x_2, x_3) \equiv (x, y, z)$. The intersections of any two plates are straight beams of cross section β^2, where the potential V_s has the value $2V_0$. The intersections of three plates where the potential V_s has the value $3V_0$ are cubes of side length β. The set of these cubes form an orc lattice, a configuration similar to that of the commercially available molecular lattice model made up of balls and sticks. Note: Each square-well potential V_j has three parameters (V_0, β, a_j), and therefore it may represent the true potential fairly we11.[4] The Schrödinger equation for the model Hamiltonian:

$$H_s \equiv \frac{p_x^2 + p_y^2 + p_z^2}{2m} + V_1(x) + V_2(y) + V_3(z) \tag{5.2.13}$$

can now be reduced to three K–P equations (Problem 5.2.3). We can then write an expression for the energy of our model system near the lowest band edge as

$$E = \frac{\hbar^2}{2m_1}k_x^2 + \frac{\hbar^2}{2m_2}k_y^2 + \frac{\hbar^2}{2m_3}k_z^2 + \text{constant} \tag{5.2.14}$$

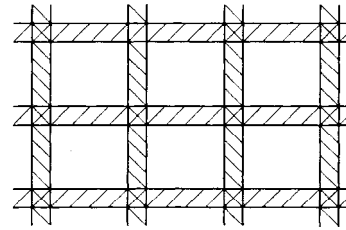

Figure 5.3. A model potential. Each singly-shaded strip has a potential energy (depth) V_0. Each cross-shaded square have a potential energy $2V_0$.

where $\{m_j\}$ are effective masses defined by Eq. (5.2.10) with $a = a_j$.

Equation (5.2.14) is identical to what is intuitively expected of the energy–k relation for electrons in the orc lattice.[3] It is stressed that we *derived* it from first principles assuming a three-dimensional model Hamiltonian H_S. Our study demonstrates qualitatively how electron energy bands and gaps are generated from the Schrödinger equation for a Bloch electron moving in a three-dimensional lattice.

Problem 5.2.1. Derive Eq. (5.2.5).

Problem 5.2.2. Derive Eq. (5.2.10).

Problem 5.2.3. Show that the Schrödinger equation corresponding to the Hamiltonian H_s in Eq. (5.2.13) can be reduced to three one-dimensional K–P equations.

5.3. INDEPENDENT-ELECTRON APPROXIMATION; FERMI LIQUID MODEL

We consider a monovalent metal like Cu. We may assume a Hamiltonian H_A of the form:

$$H_A = \sum_{j=1}^{N} \frac{p_j^2}{2m} + \sum_{j>k}\sum \frac{k_0 e^2}{|\mathbf{r}_j - \mathbf{r}_k|} + \sum_{\alpha=1}^{N} \frac{P_\alpha^2}{2M} + \sum_{\alpha>\gamma}\sum \frac{k_0 e^2}{|\mathbf{R}_\alpha - \mathbf{R}_\gamma|} - \sum_j \sum_\alpha \frac{k_0 e^2}{|\mathbf{r}_j - \mathbf{R}_\alpha|} \tag{5.3.1}$$

which is the same Hamiltonian in Eq. (2.1.1). The motion of the set of N electrons is correlated because of the interelectronic interaction. If we omit the ionic kinetic energy, interionic and interelectronic Coulomb interaction from Eq. (5.3.1), we obtain

$$H_B = \sum_j \frac{p_j^2}{2m} + \sum_j V(\mathbf{r}_j) \tag{5.3.2}$$

which characterizes a system of electrons moving in the *bare lattice potential* V.

Since the metal as a whole is neutral, the Coulomb interaction among the electrons, among the ions, and between electrons and ions, see Eq. (5.3.1), all have the

same order of magnitude, and therefore they are equally important. We now pick one electron in the system. This electron is in interaction with the system of N ions and $N-1$ electrons, the system (medium) having the net charge $+e$. These other $N-1$ electrons should, in accordance with Bloch's theorem be distributed with the lattice periodicity and all over the crystal lattice in equilibrium. This is an important point. We demonstrate it by mathematical induction as follows: (1) For $n = 1$, we have the bare-lattice potential $V(\mathbf{r})$. By applying the Bloch theorem, we obtain a lattice-periodic electron distribution. The static ion lattice is always periodic. We therefore obtain a periodic effective potential $V_1(\mathbf{r})$, which is generated by one electron and N ions. (2) Assume that the nth electron distribution is periodic, so that $V_n(\mathbf{r} + \mathbf{R}) = V_n(\mathbf{r})$. By applying the Bloch theorem to the $(n + 1)$th electron, we see that this electron is distributed lattice periodically. We then obtain a lattice-periodic effective potential $V_{n+1}(\mathbf{r})$, which is generated by $n + 1$ electrons and N ions. The charge per lattice ion is greatly reduced from e to $N^{-1}e$ because the net charge e of the medium is shared equally by N ions. Since N is a large number, the selected electron moves in an *extremely weak effective-lattice-potential field* V_e as characterized by the model Hamiltonian:

$$h_C = \frac{p^2}{2m} + V_e(\mathbf{r}), \qquad V_e(\mathbf{r} + \mathbf{R}) = V_e(\mathbf{r}) \tag{5.3.3}$$

In other words any chosen electron moves in an environment far different from what is represented by the bare-lattice potential V. It moves almost freely in an extremely weak-lattice potential V_e. This picture was obtained with the aid of the Bloch theorem, and therefore it is a result of the quantum many-body theory. To illustrate let us examine the same system from the classical point of view. In equilibrium the classical electron distribution is lattice-periodic, so there should be one electron near each ion. This electron will not move in the greatly reduced field.

We now assume that electrons move independently in the effective potential field V_e. The total Hamiltonian for the idealized system may then be represented by

$$H_C = \sum_j h_C(\mathbf{r}_j, \mathbf{p}_j) \equiv \sum_j \left(\frac{1}{2m}\right) p_j^2 + \sum_j V_e(\mathbf{r}_j) \tag{5.3.4}$$

This Hamiltonian H_C should be a far better approximation of the original Hamiltonian H_A than the Hamiltonian H_B. It is important that both interelectronic and interionic Coulomb repulsion are not neglected but are taken into consideration self-consistently. This model is a *one-electron picture approximation,* but it is hard to improve on by any other simple method. The model in fact forms the basis for the band theory of conduction electrons. We shall assume this model in the present chapter.

We now apply Bloch's theorem to the Hamiltonian H_C composed of the kinetic energy and the interaction energy V_e with the effective lattice having the net charge $+e$. We then obtain the Bloch energy bands $\in_j(\mathbf{k})$ and the Bloch states characterized by band index j and k-vector $\mathbf{k}$. The Fermi–Dirac statistics obeyed by the electrons can be applied to the Bloch electrons with no regard to interaction, which will further be elaborated on in Section 6.8. This means in particular that there should exist a certain Fermi energy $\in_F$ for the ground state of the system similar to what we saw earlier in Section 2.2 for a free-electron model. Let us recall that the energy of the

Bloch electron is characterized by the k-vector and band index j. Thus there is a *sharp Fermi surface* represented by

$$\epsilon_j(\hbar\mathbf{k}) = \epsilon_F \tag{5.3.5}$$

which separates the electron-filled k-space (low-energy side) from the empty k-space (high-energy side). The Fermi surface for a real metal in general is complicated in contrast to the free-electron *Fermi sphere* characterized by

$$\frac{p^2}{2m} \equiv \frac{p_x^2 + p_y^2 + p_z^2}{2m} = \epsilon_F \tag{5.3.6}$$

The independent electron model with a sharp Fermi surface at 0 K is called the *Fermi liquid model* of Landau.[5] As we show later, many thermodynamic and transport properties of conductors are dominated by those electrons near the Fermi surface. The shape of the Fermi surface turns out to be very important for the occurrence of superconductors. In the following section, we shall examine the Fermi surfaces of some metals.

The Fermi liquid model was obtained in the static-lattice approximation in which the motion of the ions is neglected. If the effect of moving ions (phonons) is taken into account, this model must be modified. The electron–phonon interaction turns out to be very important in the theory of superconductivity, and it will be discussed in Chapter 7.

5.4. THE FERMI SURFACE

Why does a particular metal exist with a particular crystalline state? This is a good but very hard question. The answer must involve the composition and nature of the molecules constituting the metal and the interaction between the component particles. To illustrate let us take sodium, which is known to form a bcc lattice. This monovalent metal may be thought of as an ideal composite system of electrons and ions. The system Hamiltonian may be approximated by H_A in Eq. (5.3.1), which consists of the kinetic energies of electrons and ions and the Coulomb interaction energies among and between electrons and ions. This is an approximation since the interaction between electron and ion deviates significantly from the ideal Coulomb law at short distances because each ion has core electrons. At any rate the study of the ground-state energy of the ideal model favors a fcc lattice structure, which is not observed for this metal. If multivalent metals like Pb and Sn are considered, the situation becomes even more complicated, since the core electrons forming part of ions may have anisotropic charge distribution. Because of this it is customary in solid-state physics to assume the experimentally known lattice structures first, then proceed to study the Fermi surface.

Once a lattice is selected, the Brillouin zone is fixed. For an orc lattice the Brillouin zone is a rectangular box defined by Eq. (5.1.26). We now assume a large periodic box of volume

$$V = (N_1 a)(N_2 b)(N_3 c), \qquad N_1, N_2, N_3 \gg 1 \tag{5.4.1}$$

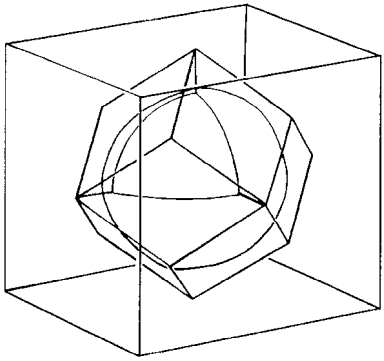

Figure 5. 4. The Fermi surface of sodium (bcc) is nearly spherical within the first Brillouin zone.

Let us find the number N of the quantum states within each Brillouin zone. With the neglect of the spin degeneracy, the number N is equal to the total phase-space volume divided by unit phase-cell volume

$$\left(\frac{2\pi\hbar}{a}\right)\left(\frac{2\pi\hbar}{b}\right)\left(\frac{2\pi\hbar}{c}\right) \div \left(\frac{2\pi\hbar}{N_1 a}\right)\left(\frac{2\pi\hbar}{N_2 b}\right)\left(\frac{2\pi\hbar}{N_3 c}\right) = N_1 N_2 N_3 \qquad (5.4.2)$$

The spin degeneracy doubles this number. We note that the product $N_1N_2N_3$ simply equals the number of the ions in the normalization volume. It is also equal to the number of the conduction electrons in a monovalent metal. In other words *the first Brillouin zone can contain twice the number of conduction electrons for the monovalent metal.* This means that at 0 K, half of the Brillouin zone may be filled by electrons. For example if an energy–momentum relation Eq. (5.2.14) is assumed, the Fermi surface is an ellipsoid. Something similar to this actually happens to alkali metals including Li, Na, K. These metals form bcc lattices. All experiments indicate that the Fermi surface is nearly spherical and entirely within the Brillouin zone. The Fermi surface of sodium is shown in Fig. 5.4.

The *nearly free electron model* (NFEM) developed by Harrison[6] can predict a Fermi surface in the first approximation for any metal. (The interested readers are referred to the book by Harrison.[7]) This model is obtained by applying Heisenberg's uncertainty principle and Pauli's exclusion principle to a solid, therefore it has a general applicability unhindered by the complications due to particle–particle interaction. Briefly in the NFEM, the first Brillouin zone is drawn for a selected metal. Electrons are filled starting from the center of the zone, with the assumption of a free-electron energy–momentum relation [Eq. (5.1.15)]. If we apply the NFEM to alkali metals, we simply obtain the Fermi sphere as shown in Fig. 5.4.

Noble metals, including copper (Cu), silver (Ag), and gold (Au), are monovalent fcc metals. The Brillouin zone and Fermi surface of copper are shown in Fig. 5.5. The Fermi surface is far from spherical. (How such a Fermi surface is obtained after the analyses of the de-Haas–van-Alphen effect will be discussed in Section 5.6.) Notice that the *Fermi surface approaches the Brillouin boundary at right angles.* This

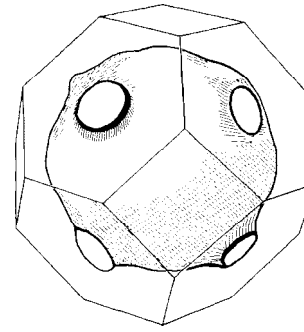

Figure 5. 5. The electron sphere bulges out in the ⟨111⟩ direction to make contact with the hexagonal zone faces.

arises from the mirror symmetry possessed by the fcc lattice, which will be shown here. From Eq. (5.1.24) we obtain

$$\psi_E(\mathbf{r}+\mathbf{R}) = e^{i(\mathbf{k}+\mathbf{G})\cdot\mathbf{R}}\psi_E(\mathbf{r}) \tag{5.4.3}$$

where $\mathbf{G}$ is any reciprocal lattice vector satisfying

$$\exp(i\mathbf{G}\cdot\mathbf{R}) = 1 \tag{5.4.4}$$

Equation (5.4.3) means that the energy $E = \epsilon_j(\hbar\mathbf{k})$ is periodic in the k-space:

$$\epsilon_j(\hbar\mathbf{k}+\hbar\mathbf{G}) = \epsilon_j(\hbar\mathbf{k}) \tag{5.4.5}$$

If the lattice has a mirror symmetry, we can choose the symmetry plane as the y–z plane and express the symmetry by

$$V(x,y,z) = V(-x,y,z) \tag{5.4.6}$$

The Schrödinger equation (5.1.23) is invariant under the mirror reflection $(x \to -x)$. This means that $\psi_E(x)$ and $\psi_E(-x)$ satisfy the same equation, where we omitted the y- and z-dependence. According to the Bloch theorem (5.1.24)

$$\psi_E(-x-a) = e^{-ika}\psi_E(-x) \tag{5.4.7}$$

Taking a mirror reflection of this equation, we obtain

$$\psi_E(x+a) = e^{-ika}\psi_E(x) \tag{5.4.8}$$

Combination of Eqs. (5.1.24) and (5.4.8) means that the energy $\epsilon_j(\hbar\mathbf{k})$ is an even function of k:

$$\epsilon_j(-\hbar k) = \epsilon_j(\hbar k) \tag{5.4.9}$$

The opposing faces of the Brillouin boundary are often separated by the fundamental reciprocal-lattice constants, and the mirror symmetry planes are located in the middle of these faces. This is true for many familiar lattices, including fcc, bcc, sc,

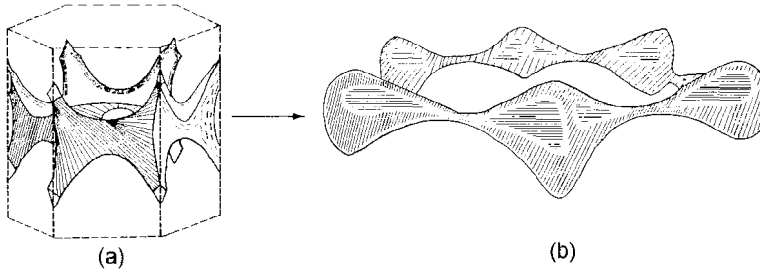

Figure 5.6. The Fermi surfaces in the second zone for Be. (a) NFEM monster (b) measured coronet. The coronet encloses unoccupied states.

diamond, orc, hexagonal closed-pack (hcp). Differentiating Eq. (5.4.9) with respect to k, we obtain

$$\epsilon_j'(k) \equiv \frac{d}{dk}\epsilon_j(k) = -\epsilon_j'(-k) \tag{5.4.10}$$

By setting $k = \pi/a$, we have $\epsilon_j'(\pi/a) = -\epsilon_j'(-\pi/a) = -\epsilon_j'(\pi/a)$, where the last equality follows from Eq. (5.4.5). We thus find that

$$\epsilon_j'\left(\frac{\pi}{a}\right) = 0 \qquad \text{q.e.d.} \tag{5.4.11}$$

For a divalent metal like calcium (Ca) (fcc), the first Brillouin zone can in principle contain all of the conduction electrons. However, the Fermi surface must approach the zone boundary at right angles, which distorts the ideal configuration considerably. Thus the real Fermi surface for Ca has a set of unfilled corners in the first zone, and the overflow electrons are in the second zone. As a result Ca is a metal, and not an insulator. Besides Ca has electrons and holes (see Section 5.8).

Divalent beryllium (Be) forms a hcp crystal. The Fermi surfaces in the second zone (a) constructed in the NFEM and (b) observed,[8] are shown in Fig. 5.6. The reason why the monster having sharp corners must be smoothed out is explained in Section 5.9.

Transition metal tungsten (W), which contains d-electrons [(xenon) $4f^{14}5d^46s^2$], forms a bcc crystal. The conjectured Fermi surface is shown in Fig. 5.7.

Let us now consider trivalent aluminum (Al), which forms a fcc lattice. The first Brillouin zone is entirely filled with electrons. The second zone is half filled with electrons, starting with the zone boundary as shown in Fig. 5.8. As the last example, we examine the Fermi surface of lead (Pb), which also forms a fcc lattice. Since this metal is quadrivalent and therefore has a great number of conduction electrons, the Fermi surface is quite complicated. The conjectured Fermi surface in the third zone is shown in Fig. 5.9. For more detailed description of the Fermi surface of metals see standard texts on solid-state physics (Refs. 3, 7, 11, and 12). Al, Be, W, and Pb are superconductors, while Na and Cu are not, which will be discussed further in Chapter 8.

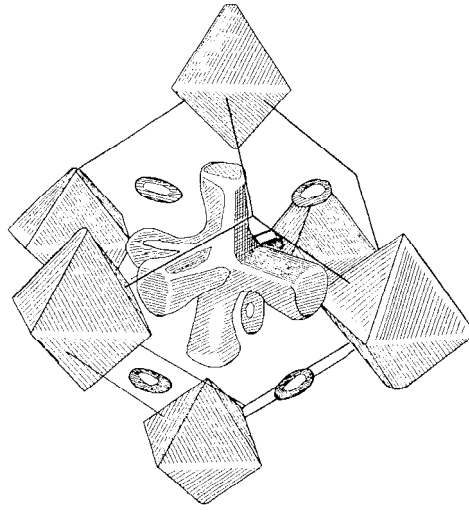

Figure 5.7. The Fermi surface for bcc tungsten. The central figure contains electrons and all other figures contain vacant states [after Schönberg and Gold (Ref. 9)].

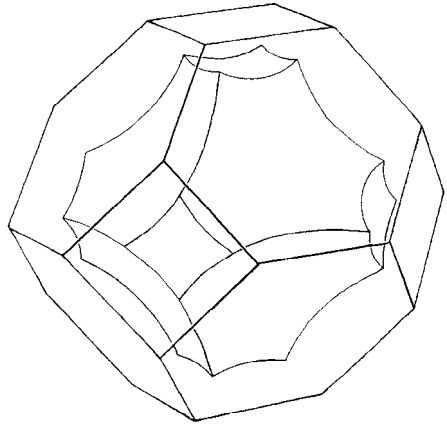

Figure 5.8. The Fermi surface constructed by Harrison's model (NFEM) in the second zone for Al. The convex surface encloses vacant states.

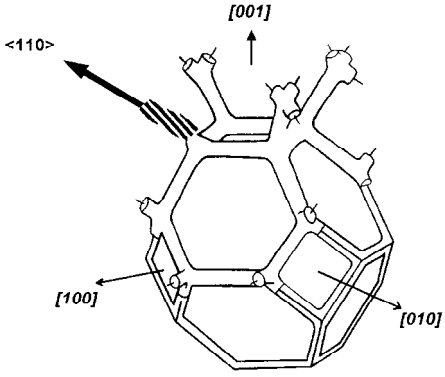

Figure 5.9. The conjectured Fermi surface in the third zone for fcc Pb. The cylinder encloses electrons.

5.5. ELECTRONIC HEAT CAPACITY; THE DENSITY OF STATES

The band structures of conduction electrons are quite different from metal to metal. In spite of this, the electronic heat capacities at very low temperatures are all similar, which is shown in this section.

In Sections 2.4–2.5, we saw that the heat capacity of free electrons has a linear-T dependence at lowest temperatures. We first show that *any normal metal having a sharp Fermi surface must have a linear-T heat capacity.* Let us follow the approximate calculations described in Section 2.4. The number of excited electrons N_x is estimated by [see Fig. 2.7 and Eq. (2.4.2)]

$$N_x = \mathcal{N}(\epsilon_F) k_B T \tag{5.5.1}$$

where $\mathcal{N}(\epsilon_F)$ is the density of states at the Fermi energy ϵ_F. Each thermally excited electron will move up with extra energy of the order $k_B T$. The approximate change in the total energy ΔE is given by multiplying these two factors:

$$\Delta E = N_x k_B T = \mathcal{N}(\epsilon_F)(k_B T)^2 \tag{5.5.2}$$

Differentiating this with respect to T, we obtain an expression for the heat capacity:

$$C_V \cong \frac{\partial}{\partial T}\Delta E = 2k_B^2 \mathcal{N}(\epsilon_F) T \tag{5.5.3}$$

which indicates the linear-T dependence. This temperature dependence comes from the Fermi distribution function. We can therefore improve our calculation by following Sommerfeld's method outlined in Section 2.5. Comparing Eq. (2.4.6) with Eq. (2.5.18), the correction factor is $(\pi^2/2)/3 = \pi^2/6$. Using this factor we obtain from Eq. (5.5.3)

$$\boxed{C_V = \left(\frac{1}{3}\right)\pi^2 k_B^2 \mathcal{N}(\epsilon_F) T} \tag{5.5.4}$$

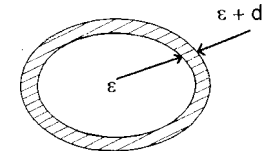

Figure 5.10. Two constant-energy curves at ϵ and $\epsilon + d\epsilon$ in the two-dimensional k-space.

which allows a quantitative comparison with experiments, since the coefficient $[\pi^2 k_B^2 \mathcal{N}(\epsilon_F)/3]$is calculated exactly.

The density of states $\mathcal{N}(\epsilon_F)$ for any normal metal can be expressed by

$$\boxed{\mathcal{N}(\epsilon_F) = \sum_j \frac{2}{(2\pi\hbar)^3} \int dS \frac{1}{|\nabla \epsilon_j(\hbar\mathbf{k})|}} \tag{5.5.5}$$

where 2 is the spin degeneracy factor, and the surface integration is carried out over the Fermi surface represented by

$$\epsilon_j(\hbar\mathbf{k}) = \epsilon_F \tag{5.5.6}$$

Equation (5.5.5) may be proved as follows. First consider the two-dimensional case. Assume that the electron moves on the x–y plane only. The constant energy surface is then a closed curve in the k_x –k_y plane. We choose two energy surfaces at ϵ and $\epsilon + d\epsilon$ as shown in Fig. 5.10. Twice the shaded area between the two curves divided by the unit quantum cell area $(2\pi\hbar)^2$ equals the number of the quantum states in the range $(\epsilon, \epsilon + d\epsilon)$. The density of states per unit area $\mathcal{N}(\epsilon)$ is then determined from

$$\mathcal{N}(\epsilon)d\epsilon = \frac{2}{(2\pi\hbar)^2} \text{ (shaded area)} = \frac{2\hbar}{(2\pi\hbar)^2} \int_C dk \frac{d\epsilon}{|\nabla\epsilon(\hbar\mathbf{k})|} \tag{5.5.7}$$

where the integration is carried out along the constant-energy curve C represented by $\epsilon(\hbar\mathbf{k}) = \epsilon$. The equality between the last two members of Eqs. (5.5.7) can be seen from the ϵ–k diagram shown in Fig. 5.11:

$$d\epsilon = |\nabla\epsilon(\hbar\mathbf{k})|\hbar dk' \qquad \text{q.e.d.} \tag{5.5.8}$$

This graphic method can simply be extended to three dimensions. If the Fermi surface extends over two zones, the total density of states is the sum over zones (j).

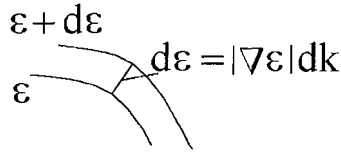

Figure 5.11. A diagram indicating the relation $d\epsilon = |\nabla\epsilon(\hbar\mathbf{k})|\hbar dk'$.

As an illustration, consider a free electron system having the Fermi sphere:

$$\epsilon = (p_x^2 + p_y^2 + p_z^2)/2m \equiv \epsilon_F \tag{5.5.9}$$

The gradient $\nabla\epsilon(\mathbf{p})$ at any point of the surface has a constant magnitude p_F/m, and the surface integral is equal to $4\pi p_F^2$. Equation (5.5.5) then yields

$$\mathcal{N}(\epsilon_F) = V[2(2\pi\hbar)^{-3}]\left[\frac{4\pi p_F^2}{(p_F/m)}\right] = V\left[\frac{2^{1/2}m^{3/2}}{\pi^2\hbar^3}\right]\epsilon_F^{1/2} \tag{5.5.10}$$

see Eq. (2.3.18). As a second example, consider the ellipsoidal surface represented by Eq. (5.2.14). After elementary calculations we obtain (Problem 5.5.1)

$$\mathcal{N}(\epsilon) = V\left(\frac{2^{1/2}}{\pi^2\hbar^3}\right)(m_1 m_2 m_3)^{1/2}\epsilon^{1/2} \tag{5.5.11}$$

which shows that the density of states still grows like $\epsilon^{1/2}$, but the coefficient depends on the three effective masses (m_1, m_2, m_3).

Problem 5.5.1. (a) Compute the momentum-space volume between the surfaces represented by

$$\epsilon = p_x^2/2m_1 + p_y^2/2m_2 + p_z^2/2m_3 \quad \text{and} \quad \epsilon + d\epsilon = p_x'^2/2m_1 + p_y'^2/2m_2 + p_z'^2/2m_3$$

By counting the number of quantum states in this volume in the bulk limit, obtain Eq. (5.5.11). (b) Derive Eq. (5.5.11), starting from the general formula (5.5.5). Hint: Convert the integral over the ellipsoidal surface into that over a spherical surface.

5.6. DE-HAAS-VAN-ALPHEN OSCILLATIONS; ONSAGER'S FORMULA

An important way of studying the Fermi surface in a metal is to measure and analyze the magnetic susceptibility χ defined by

$$M = \chi B \tag{5.6.1}$$

where M is the magnetization (magnetic moment per unit volume) and B the applied magnetic field (magnitude). When the experiments are done on pure samples and at very low temperatures, the susceptibility χ in some metals is found to exhibit oscillations with varying magnetic field strength B. This phenomenon was first discovered in 1930 by de Haas and van Alphen[13] in a study of bismuth (Bi), and it is called *de-Haas–van-Alphen (dHvA) effect* (oscillations). As we shall see presently, these oscillations have a quantum mechanical origin. The analyses of the dHvA oscillations nowadays are done routinely in terms of Onsager's formula [Eq. (5.6.2)]. According to Onsager's theory[14] the nth maximum (counted from $1/B = 0$) occurs for a field B given by the relation:

$$n + \gamma = \frac{1}{2\pi\hbar e}\frac{A}{B} = \frac{1}{(2\pi\hbar)^2}\Phi_0\frac{A}{B} \tag{5.6.2}$$

where A is any extremal area of intersection between the Fermi surface and the family of planes $\mathbf{B} \cdot \mathbf{p} \equiv \mathbf{B} \cdot (\hbar \mathbf{k})$ = constant, and γ is a phase (number) less than unity. The constant

$$\Phi_{el} \equiv \frac{2\pi\hbar}{e} \equiv \frac{h}{e} = 4.135 \times 10^{-1} \text{ gauss-cm}^2 \tag{5.6.3}$$

is called the *electron flux quantum.* For example, consider an ellipsoidal Fermi surface:

$$\epsilon_F = \frac{p_1^2}{2m_1} + \frac{p_2^2}{2m_2} + \frac{p_3^2}{2m_3}, \qquad m_1, m_2, m_3 > 0 \tag{5.6.4}$$

Assume that the field $\mathbf{B}$ is applied along the p_3-axis. All the intersections are ellipses represented by

$$\epsilon - \frac{p_3^2}{2m_3} = \frac{p_1^2}{2m_1} + \frac{p_2^2}{2m_2} \tag{5.6.5}$$

(p_3 = constant). The maximum area of the intersection occurs at $p_3 = 0$, (belly, see Fig. 5.12), and its area A equals:

$$A = \pi(2m_1\epsilon)^{1/2}(2m_2\epsilon)^{1/2} = 2\pi(m_1m_2)^{1/2}\epsilon \tag{5.6.6}$$

Using Eq. (5.6.2) and solving for ϵ, we obtain

$$\epsilon = eB(m_1m_2)^{-1/2}(n + \gamma)\hbar \tag{5.6.7}$$

which indicates that the energy ϵ is quantized as the energy of the simple harmonic oscillator with the angular frequency:

$$\omega_0 \equiv \frac{eB}{(m_1m_2)^{1/2}} \tag{5.6.8}$$

As a second example we take a hyperboloidal Fermi surface that can be represented by Eq. (5.6.4) with $m_1, m_2 > 0$ and $m_3 < 0$. Assume the same orientation of **B.** Equations (5.6.5) and (5.6.6) then hold, where the area A represents the minimal area of the intersection at $p_3 = 0$ (neck, see Fig. 5.12). As a third example assume that $m_3 = \infty$ in Eq. (5.6.4), which represents a Fermi cylinder. In this case also the area A is given by Eq. (5.6.6) for the same orientation of **B.**

All three geometrical shapes are discussed by Onsager[14] in his short correspondence. At the time of his writing in 1952, only the ellipsoidal Fermi surface was known in experiments. All three cases do occur in reality. When tested by experiments, the agreements between theory and experiment are excellent. The cases of ellipsoidal and hyperboloidal surfaces were found, e.g., in noble metals Cu, Ag, and Au. dHvA oscillations in silver (Ag) are shown in Fig. 5.12, where the susceptibility χ is plotted against B^{-1} in arbitrary units. The magnetic field $\mathbf{B}$ is along a $\langle 111 \rangle$ direction. The two distinct periods are due to the "neck" and "belly" orbits indicated, the high-frequency oscillations coming from the larger belly orbit. By counting the number of high-frequency periods in a single low-frequency period, e.g., between the two arrows, we can deduce directly that $A_{111}(\text{belly})/A_{111}(\text{neck})=51$.

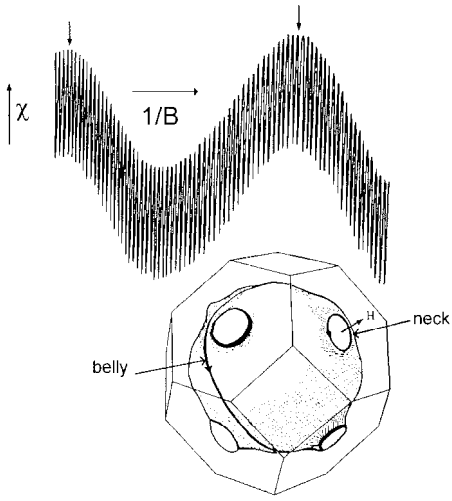

Figure 5.12. DHvA oscillations in silver with the magnetic field along a ⟨111⟩ direction. The two distinct periods are due to the neck and belly orbits indicated in the inset.

Onsager's derivation of Eq. (5.6.2) in his original paper is illuminating; let us follow his arguments. For any closed k-orbit, there should be a closed orbit in the position space, called a closed r-orbit. The periodic component of the motion, which involves the components of $\mathbf{p} \equiv \hbar\mathbf{k}$ and $\mathbf{r}$ perpendicular to $\mathbf{B}$, is quantized. We apply the Bohr–Sommerfeld quantization rule:

$$\oint \mathbf{p} \cdot d\mathbf{r} = (n + \gamma)2\pi\hbar \tag{5.6.9}$$

to the r-orbit. The cross section of the helical orbit Ω is determined such that the enclosed magnetic flux Φ equals $(n + \gamma)$ times the magnetic flux quantum $\Phi_{el} \equiv h/e$:

$$\Phi = (n + \gamma)\Phi_{el}, \qquad \Phi_{el} \equiv \frac{h}{e} \equiv \frac{2\pi\hbar}{e} \tag{5.6.10}$$

Since the magnetic flux Φ is given by $B\Omega$, we obtain

$$(n + \gamma)\Phi_{el} = B\Omega \tag{5.6.11}$$

For a free electron the closed circular path in the p-space perpendicular to the field becomes a similar path in the r-space, turned through a right angle, and with dimensions changed in the ratio $(eB)^{-1}$ (see Problem 5.6.1). This may also hold for nearly circular closed orbits. If we assume this relation for a Bloch electron, the area enclosed by the closed p-orbit A is proportional to that enclosed by the closed r-orbit Ω:

$$A = (eB)^2 \Omega \tag{5.6.12}$$

Combining the last three equations we obtain Eq. (5.6.2). q.e.d.

The remarkable argument advanced by Onsager is that an electron in a closed r-orbit may move, keeping a finite number n of flux quantum $\Phi_{el} \equiv h/e$ within the orbit. This comes from a physical principle that the magnetic field **B** does not work on the electron and therefore does not change its kinetic energy. This property should hold for any charged particle, electron, or Cooper pair. Such a flux quantization in a superconductor was observed later in 1961 by Deaver and Fairbank,[15] and Doll and Näbauer.[16] Because the Cooper pair has charge (magnitude) $2e$, the observed flux quantum is found to be $h/2e$, that is, half the electron flux quantum Φ_{el} defined in Eq. (5.6.3). We shall discuss this topic in more detail in Sections 11.1 and 11.4. The phase γ in Eq. (5.6.9) can be set equal to 1/2. This may be deduced by taking the case of a free electron for which quantum calculations are carried out exactly. The quantum number n can be large. Thus Onsager's formula with $\gamma = 1/2$ can be applied for any strength of field if Eq. (5.6.12) holds true (Problem 5.6.1).

Equation (5.6.12) however turns out to contain a certain limitation, because the equation of motion for the Bloch electron is similar to, yet quite different from, that for a free electron, which will be discussed in Section 5.8.

Problem 5.6.1. Consider a free electron having mass m and charge q subject to a constant magnetic field **B.** (a) Write down Newton's equation of motion. (b) Show that the magnetic force $q\mathbf{v} \times \mathbf{B}$ does not work on the electron; that is, the kinetic energy $E \equiv m v^2/2$ does not change in time. (c) Show that the component of **v** parallel to **B** is a constant. (d) Show that the electron spirals about the field **B** with the angular frequency $\omega = eB/m$. (e) Show that the orbit projected on a plane perpendicular to the field **B** is a circle of radius $R = v_\perp/\omega = m v_\perp/eB$, where $v_\perp$ represents the speed of the circular motion. Find the maximum radius R_m. (f) Define the *kinetic momentum* $\mathbf{p} = m\mathbf{v}$ and express the energy $\in$ in terms of p_j. (g) Choose the $x_3(= z)$-axis along **B.** Show that the curve represented by $E(p_1, p_2, 0) = \in$ is a circle of radius $(2m\in)^{1/2} = p$. (h) Show that the areas of the circles obtained in (e) and (g) differ by the scale factor $(eB)^2$.

5.7. THE HALL EFFECT; ELECTRONS AND HOLES

In this section we discuss the Hall effect. As we see later electrons and holes play very important roles in the microscopic theory of superconductivity.

Let us consider a conducting wire connected with a battery. If a magnetic field **B** is applied, the field penetrates the wire. The Lorentz force:

$$\mathbf{F} = q\mathbf{v} \times \mathbf{B} \tag{5.7.1}$$

where q is the charge of the carrier, may then affect the electron's classical orbit. If so the picture of the straight line motion of a free electron in kinetic theory has to be modified significantly. If the field (magnitude) B is not too high and the stationary state is considered, the actual physical situation turns out to be much simpler.

Take the case in which the field **B** is applied perpendicular to the wire of a rectangular cross-section as shown in Fig. 5.13.

Experiments show that a voltage V_c is generated perpendicular to the field **B** and the electric current **J** such that a steady current flows in the wire apparently

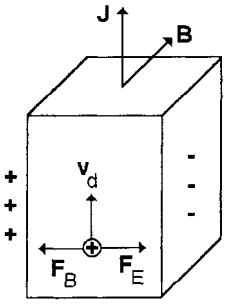

Figure 5.13. The magnetic and electric forces ($\mathbf{F}_B, \mathbf{F}_E$) balance to zero in the Hall-effect measurement.

unhindered. We may interpret this condition as follows. Let us write the current density j as

$$\mathbf{j} = q n \mathbf{v}_d \tag{5.7.2}$$

where n is the density of conduction electrons and $\mathbf{v}_d$ the *drift velocity.* A charge carrier having a velocity equal to the drift velocity $\mathbf{v}_d$ suffers the Lorentz force:

$$\mathbf{F} = q(\mathbf{E}_c + \mathbf{v}_d \times \mathbf{B}) \tag{5.7.3}$$

where $\mathbf{E}_c$ is the electric field due to the cross voltage V_c. In the geometry shown only the x-component of the force $\mathbf{F}$ is relevant. If the net force vanishes:

$$q(E_c + v_d B) = 0 \tag{5.7.4}$$

the carrier can proceed along the wire z-direction unhindered.

Let us check our model calculation. We define the *Hall coefficient* R_H by

$$R_H \equiv \frac{E_c}{jB} \tag{5.7.5}$$

where the three quantities on the rhs can be measured. Using Eqs. (5.7.2) and (5.7.4), we obtain

$$R_H = -\frac{1}{qn} \tag{5.7.6}$$

The experimental values for $-qnR_H$ in some metals are given in Table 7.1.

For alkali metals the agreement between theory and experiment is nearly perfect. This is quite remarkable. Equation (5.7.4) means a zero net balance between the magnetic force $F_B = q v_d B$ and the electric force $F_E = qE_c$ only in the average sense through the drift velocity v_d. In real metals there must be a great number of electrons moving under the action of unbalanced forces. Do these electrons move in curved orbits? The concept of classical electron orbits must be abandoned in quantum theory. However a rigorous quantum treatment of the Hall effect is still lacking.

The measured Hall coefficients R_H for most metals are negative. This can be understood by assuming that the charge carriers are *electrons having a negative charge*

Table 5.1. Hall Coefficients of Selected Metals

Metal	Valence	$-1/nqR_H$
Li	1	0.8
Na	1	1.2
K	1	1.1
Cu	1	1.5
Ag	1	1.3
Au	1	1.5
Be	2	−0.2
Mg	2	−0.4
In	3	−0.3
Al	3	−0.3

$q = -e$. There are exceptions however. As we see in Table 5.1, A1, Be and others exhibit positive Hall coefficients. This can be explained only by assuming that in these metals the main charge carriers are *holes possessing a positive charge* $q = +e$. This is a quantum many-body effect. As we shall see in Section 5.8, the existence of electrons and holes is closely connected with the shape of the Fermi surface. Nonmagnetic metals that have holes tend to be superconductors, which will be explained in Section 8.6.

5.8. NEWTONIAN EQUATIONS OF MOTION FOR A BLOCH ELECTRON

In Section 5.5 we saw that the electronic heat capacity is generated by the thermal excitation of the electrons near the Fermi surface. In Section 5.6 we observed that those electrons near the Fermi surface are also responsible for the dHvA oscillations in the susceptibility. These same electrons also participate in transporting charge. We discuss here and in following sections how these electrons respond to the applied electromagnetic fields.

Let us recall that in the Fermi liquid model each electron in a crystal moves independently in an extremely weak lattice-periodic effective potential V_e (r):

$$V_e(\mathbf{r}+\mathbf{R}) = V_e(\mathbf{r}) \tag{5.8.1}$$

We write down the Schrödinger equation corresponding to the single-electron Hamiltonian:

$$\left[-\frac{\hbar^2}{2m}\nabla^2 + V_e(\mathbf{r})\right]\psi(\mathbf{r}) = E\psi(\mathbf{r}) \tag{5.8.2}$$

According to Bloch's theorem, the wave function ψ satisfies

$$\psi_{j,\mathbf{k}}(\mathbf{r}+\mathbf{R}) = e^{i\mathbf{k}\cdot\mathbf{R}}\psi_{j,\mathbf{k}}(\mathbf{r}) \tag{5.8.3}$$

The Bravais vector **R** can take on only discrete values, and its minimum length can equal the lattice constant a_0. This generates a limitation on the domain in **k.** For example the values for each k_a $(a = x,y,z)$ for a sc lattice are limited to $(-\pi/a_0, \pi/a_0)$.

This means that the Bloch electron's wavelength $\lambda \equiv 2\pi/k_a$ has a lower bound:

$$\lambda > 2a_0 \tag{5.8.4}$$

The Bloch electron state is characterized by k-vector **k,** band index j, and energy

$$\epsilon = \epsilon_j(\hbar\mathbf{k}) \equiv \epsilon_j(\mathbf{p}) \tag{5.8.5}$$

The energy–momentum relation represented by Eq. (5.8.5) can be probed by transport measurements. A metal is perturbed from the equilibrium condition by an applied electric field; the deviations of the electron distribution from the equilibrium move in the crystal to reach and maintain a stationary state. The deviations, that is, the *localized Bloch wave packets,* should extend over several or more lattice sites. This is so because no wave packets constructed from waves of the wave vectors (k_x, k_y, k_z) whose magnitudes have the upper bounds (π/a_0) can be localized within distances less than a_0.

Dirac demonstrated,[17] that for any p-dependence of the kinetic energy [$\epsilon = \epsilon_j(\mathbf{p})$] the center of a quantum wave packet, identified as the position of the corresponding particle, moves in accordance with Hamilton's equations of motion. Thus *the Bloch electron representing the wave packet should move classical mechanically under the action of the force averaged over the lattice constants.* The lattice force $-\partial V_e/\partial x$ averaged over a unit cell vanishes

$$\left\langle -\frac{\partial}{\partial x}V_e \right\rangle_{\text{unit cell}} \equiv -a_0^{-3}\int\int dydz \int_0^{a_0} dx \frac{\partial}{\partial x}V_e(x,y,z) = 0 \tag{5.8.6}$$

Thus only important forces acting on the Bloch electron are electromagnetic forces.

We now formulate dynamics for a Bloch electron as follows. First from the quantum principle of *wave–particle duality,* we postulate that

$$(\hbar k_x, \hbar k_y, \hbar k_z) = (p_x, p_y, p_z) \equiv (p_1, p_2, p_3) \equiv \mathbf{p} \tag{5.8.7}$$

Second we introduce a model Hamiltonian:

$$H_0(p_1, p_2, p_3) \equiv \epsilon_j(\hbar k_1, \hbar k_2, \hbar k_3) \tag{5.8.8}$$

Third we generalize our Hamiltonian H to include the electromagnetic interaction energy:

$$H = H_0(\mathbf{p} - q\mathbf{A}) + q\phi \tag{5.8.9}$$

where (**A,** ϕ) are vector and scalar potentials generating electromagnetic fields (**E,** **B**):

$$\mathbf{E} = -\nabla\phi(\mathbf{r},t) - \frac{\partial \mathbf{A}(\mathbf{r},t)}{\partial t}, \qquad \mathbf{B} = \nabla \times \mathbf{A}(\mathbf{r},t), \qquad \mathbf{r} \equiv (x_1, x_2, x_3) \tag{5.8.10}$$

By using the standard procedures, we then obtain Hamilton's equations of motion:

$$\dot{\mathbf{r}} \equiv \mathbf{v} = \frac{\partial H}{\partial \mathbf{p}} = \frac{\partial}{\partial \mathbf{p}}H_0(\mathbf{p} - q\mathbf{A}), \qquad \dot{\mathbf{p}} = -\frac{\partial H}{\partial \mathbf{r}} = -\frac{\partial}{\partial \mathbf{r}}H_0 - q\frac{\partial}{\partial \mathbf{r}}\phi \tag{5.8.11}$$

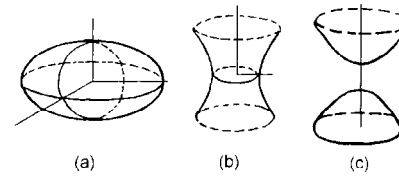

Figure 5.14. (a) Ellipsoid, (b) hyperboloid of one sheet (neck); (c) hyperboloid of two sheets (inverted double caps).

The first equation defines the velocity $\mathbf{v} \equiv (v_1, v_2, v_3)$. Notice that in the zero-field limit these equations are in agreement with the general definition of a group velocity:

$$v_{g,i} \equiv \frac{\partial \omega(\mathbf{k})}{\partial k_i}, \qquad \omega(\mathbf{k}) \equiv \frac{\epsilon(\mathbf{p})}{\hbar} \qquad \text{(wave picture)} \tag{5.8.12}$$

$$v_i \equiv \frac{\partial \epsilon(\mathbf{p})}{\partial p_i} \qquad \text{(particle picture)} \tag{5.8.13}$$

In the presence of magnetic field, the first of Eqs. (5.8.11) gives the velocity $\mathbf{v}$ as a function of $\mathbf{p} - \mathbf{q}\,\mathbf{A}$. Inverting this functional relation, we have

$$\mathbf{p} - q\,\mathbf{A} = \mathbf{f}(\mathbf{v}) \tag{5.8.14}$$

Using Eq. (5.8.14) and Eq. (5.8.11), we then obtain (Problem 5.8.2)

$$\frac{d\mathbf{f}}{dt} = q(\mathbf{E} + \mathbf{v} \times \mathbf{B}) \tag{5.8.15}$$

Since the vector $\mathbf{f}$ is a function of $\mathbf{v}$, Eq. (5.8.15) describes how the velocity $\mathbf{v}$ changes by the action of the Lorentz force (the right-hand term). To see the nature of Eq. (5.8.15), let us take a quadratic energy–momentum relation represented by

$$\epsilon = \frac{p_1^2}{2m_1^*} + \frac{p_2^2}{2m_2^*} + \frac{p_3^2}{2m_3^*} + \epsilon_0 \tag{5.8.16}$$

where $\{m_j^*\}$ are *effective masses* and ϵ_0 is a constant. The effective masses $\{m_j^*\}$ may be positive or negative. Depending on their values the energy surface represented by Eq. (5.8.16) is ellipsoidal or hyperboloidal see Fig. 5.14. If the Cartesian axes are taken along the major axes of the ellipsoid, Eq. (5.8.15) can be written as

$$m_j^* \frac{dv_j}{st} = q(\mathbf{E} + \mathbf{v} \times \mathbf{B})_j \tag{5.8.17}$$

(see Problem 5.8.1). These are *Newtonian equations of motion*: (mass) × (acceleration) = (force). Only a set of three effective masses (m_j^*) are introduced. The Bloch electron moves in an anisotropic environment if the effective masses are different.

Let us now go back to the general case. The function $\mathbf{f}$ may be determined from the energy–momentum relation as follows. Take a point A at the constant-energy surface represented by Eq. (5.8.5) in the k-space. We choose the positive normal vector to point in the direction that energy increases. A normal curvature κ is defined to

be the inverse of the radius of the contact circle at A, R_A, in the plane containing the normal vector times the sign of curvature δ_A:

$$\kappa \equiv \delta_A R_A^{-1} \tag{5.8.18}$$

where the sign of the curvature, δ_A, is +1 or −1 according to whether the center of the contact circle is on the positive side (which contains the positive normal) or not. In space-surface theory,[18] the two planes that contain the greatest and smallest normal curvatures are known to be mutually orthogonal. They are by construction orthogonal to the contact plane at A. Therefore, the intersection of these two planes and the contact plane can form a Cartesian set of orthogonal axes with the origin at A, called the *principal axes of curvatures.* By using this property, we define *principal masses* m_i by

$$\boxed{\frac{1}{m_i} \equiv \frac{\partial^2 \epsilon}{\partial p_i^2}} \tag{5.8.19}$$

where dp_i is the differential along the principal axis i. If we choose a Cartesian coordinate system along the principal axes, Eq. (5.8.15) can be written as

$$\boxed{m_i \frac{dv_i}{dt} = q(\mathbf{E} + \mathbf{v} \times \mathbf{B})_i} \tag{5.8.20}$$

These equations are similar to the equation of motion Eq. (5.8.17). The principal masses $\{m_i\}$ however are defined at each point on the constant-energy surface, and therefore they depend on $\mathbf{p}$ and $\epsilon_j(\mathbf{p})$. Let us take a simple example: The ellipsoidal constant-energy surface represented by Eq. (5.8.16) with all positive m_i^*. At extremal points, e.g., $(p_{1,\max}, 0, 0) = ([2(\epsilon - \epsilon_0)m_1^*]^{1/2}, 0, 0)$, the principal axes of curvatures match the major axes of the ellipsoid. Then the principal masses $\{m_i\}$ can simply be expressed in terms of the constant effective masses $\{m_j^*\}$ (Problem 5.8.3).

The formal proof of the equivalence between Eqs. (5.8.15) and (5.8.20) can be carried out as follows. Since f_j are functions of (v_1, v_2, v_3), we obtain

$$\frac{df_i}{dt} = \sum_j \frac{\partial f_i}{\partial v_j} \frac{dv_j}{dt} = \sum_j \frac{1}{\partial v_j / \partial f_i} \frac{dv_j}{dt} \tag{5.8.21}$$

The velocities v_i from Eq. (5.8.11) can be expressed in terms of the first p-derivatives. Thus in the zero-field limit:

$$\boxed{\frac{\partial v_j}{\partial f_i} \to \frac{\partial^2 \epsilon}{\partial p_i \partial p_j} \equiv \frac{1}{m_{ij}}} \tag{5.8.22}$$

which defines the *mass tensor elements* $\{m_{ij}\}$. By using Eqs. (5.8.21) and (5.8.22), we can reexpress Eq. (5.8.15) as

$$\boxed{\sum_j m_{ij} \frac{dv_j}{dt} = q(\mathbf{E} + \mathbf{v} \times \mathbf{B})_i} \tag{5.8.23}$$

which is valid in any Cartesian frame of reference. The mass tensor $\{m_{ij}\}$ in Eq. (5.8.23) is real and symmetric:

$$m_{ij} = m_{ji} \tag{5.8.24}$$

Such a real symmetric tensor can always be diagonalized by a principal-axes transformation (see Section 3.3). The principal masses $\{m_i\}$ are given by Eq. (5.8.19) and the principal axes are given by the principal axes of curvature. q.e.d.

In Eq. (5.8.19) the third principal mass m_3 is defined in terms of the second derivative $\partial^2\epsilon/\partial p_3^2$, in the energy-increasing (p_3-) direction. The first and second principal masses (m_1, m_2) can be connected with the two principal radii of curvature (P_1, P_2), which by definition equal the inverse of the two principal curvatures (κ_1, κ_2) (Problem 5.8.4):

$$\frac{1}{m_j} = -\kappa_j v \equiv -\frac{v}{P_j}, \qquad v \equiv |\mathbf{v}|, \qquad \frac{1}{P_j} \equiv \kappa_j \tag{5.8.25}$$

Equations (5.8.25) are very useful relations. The signs (definitely) and magnitudes (qualitatively) of the first two principal masses (m_1, m_2) can be obtained by a visual inspection of the constant-energy surface, an example of which is the Fermi surface. The sign of the third principal mass m_3 can also be obtained by inspection: the mass m_3 is positive or negative according to whether the center of the contact circle is on the negative or the positive side. For example the system of free electrons has a spherical constant-energy surface represented by $\epsilon = p^2/(2m)$ with the normal vector pointing outward. By inspection the principal radii of curvatures at every point of the surface are negative, and therefore according to Eq. (5.8.25), the principal masses (m_1, m_2) are positive and equal to m. The third principal mass m_3 is also positive and equal to m.

Equation (5.8.20) was derived from the energy–k relation [Eq. (5.8.5)] without referring to the Fermi energy. It is valid for all wave vectors $\mathbf{k}$ and all band indices j. Further discussion of Eq. (5.8.20) will be given in Section 5.9.

Problem 5.8.1. Assume a quadratic energy–momentum relation [Eq. (5.8.16)] and derive Eq. (5.8.17).

Problem 5.8.2. Assume a general energy–momentum relation [Eq. (5.8.8)] and derive Eq. (5.8.15).

Problem 5.8.3. Consider the ellipsoidal constant-energy surface represented by Eq. (5.8.16) with all $m_i^* > 0$. At the six extremal points, the principal axes of curvatures match the major axes of the ellipsoid. Demonstrate that the principal masses $\{m_i\}$ at one of these points can be expressed simply in terms of the effective masses $\{m_j^*\}$.

Problem 5.6.4. Verify Eq. (5.8.25). Use a Taylor expansion.

5.9. BLOCH ELECTRON DYNAMICS

Our Newtonian equations of motion Eq. (5.8.20):

$$m_i \frac{dv_i}{dt} = q(\mathbf{E} + \mathbf{v} \times \mathbf{B})_i \tag{5.9.1}$$

are distinct from the equation of motion:

$$\hbar \frac{d\mathbf{k}}{dt} = q(\mathbf{E} + \mathbf{v} \times \mathbf{B}) \tag{5.9.2}$$

found in the standard textbooks on solid state physics.[4,7,11,12] In this section we show that Eqs. (5.9.1) are the correct ones to use in Bloch electron dynamics. As we shall see later, a correct knowledge of Bloch electron dynamics is essential in developing the theory of superconductivity.

The velocity $\mathbf{v}$ is defined in terms of the derivatives of $\in_j(\mathbf{p}) \equiv \in_j(\hbar\mathbf{k})$, which are the energy eigenvalues of the zero-field Schrödinger equation (5.8.2). If a high-constant magnetic field is applied, the quantum states are characterized by the Landau-like quantum numbers (n, k_y, k_z) (see Section 2.7) quite distinct from the Bloch quantum numbers $(j, \mathbf{k})$. The principal masses and effective masses are defined at the low-field limit. The validity of Eqs. (5.9.1) and (5.9.2) is therefore limited to low fields. Microwaves and visible lights, which are used to probe the states of conduction electrons, have wavelengths much greater than the lattice constants. The Bloch electron should then respond to the electromagnetic fields carried by the radiation, as represented by Eq. (5.9.1). If radiations, such as x-rays and γ-rays, whose wavelengths are comparable to, or smaller than, the lattice constant are applied to a solid, the picture of the interaction between Bloch electron (spread over several lattice sites) and radiation should break down. Rather, the picture of the interaction between free electron and radiation should prevail; this picture is routinely used for theory of the photoelectric effect and Compton scattering. In other words, Eq. (5.9.1) is valid for the fields varying slowly over the lattice constant.

In the presence of a static magnetic field, a free classical charge spirals around the field, keeping its kinetic energy unchanged. The motion of a Bloch electron in a metal is more complicated. But *its kinetic energy is conserved.* This is supported by the experimental fact that no Joule heating is detected in any metals under static magnetic fields. (We caution here that if the applied magnetic field is changed, certain electric fields are necessarily generated, and these electric fields can cause a Joule heating.)

The energy conservation law under a static magnetic field can be derived as follows. From Eq. (5.8.9) with $\mathbf{E} = \Phi = 0$, we obtain

$$\frac{d}{dt} H_0(\mathbf{p} - q\mathbf{A}) = \sum_j \frac{\partial H_0}{\partial p_j} \frac{df_j}{dt} = \mathbf{v} \cdot q(\mathbf{v} \times \mathbf{B}) = 0 \tag{5.9.3}$$

[from Eqs. (5.8.11) and (5.8.15)]. If we choose the Cartesian coordinates along the principal axes of curvature, we have

$$\frac{df_j}{dt} = m_j \frac{dv_j}{dt}, \qquad \sum_j \frac{\partial H_0}{\partial p_j} \frac{df_j}{dt} = \frac{d}{dt}\left(\sum_j \frac{1}{2} m_j v_j^2\right) = 0 \tag{5.9.4}$$

We can then write the kinetic energy H_0 in the form:

$$\boxed{H_0 = \sum_j \frac{1}{2} m_j v_j^2} \tag{5.9.5}$$

which is reduced to the familiar expression $E = mv^2/2$ in the free-particle limit. This conservation law represented by Eq. (5.9.3) cannot be derived from Eq. (5.9.2), since the energy–momentum relation is not incorporated in this equation.

The principal masses $\{m_j\}$ defined by Eq. (5.8.19) depend on $\mathbf{p} = \hbar\,\mathbf{k}$ and $\in_n(\mathbf{p})$. No m_j can be zero. Otherwise according to Eq. (5.8.20) the acceleration becomes ∞ in the j-direction in the presence of the Lorentz force. This means that the Fermi surface cannot have cusps, which is in accord with all known experiments. This result is significant since the NFEM Fermi surface for a multivalent metal (see Section 5.4 and Fig. 5.8) contains cusps; these cusps must be smoothed out.

Although Eq. (5.8.19) is equivalent to Eq. (5.8.23) the former is much simpler to solve, and it can be interpreted in terms of the principal masses. This is somewhat similar to the situation in which Euler's equations of motion for a rigid body are set up in the body's frame of coordinates and are expressed in terms of principal moments of inertia.

In our earlier discussion of the Hall effect in Section 5.7, we saw that in some metals there are holes and/or electrons. Their existence is closely connected with the actual Fermi surface of a chosen metal. To illustrate let us consider two cases:

(1) The case of a free electron. The constant-energy surface is a sphere whose outward normal corresponds to the energy-increasing direction. The principal masses at any surface point are all equal to m_A^*, and they are positive according to Eq. (5.8.20):

$$m_1 = m_2 = m_3 = m_A^* > 0 \tag{5.9.6}$$

(2) The case of a constant-energy sphere whose *inward* normal corresponds to the energy-increasing direction. The principal masses are all equal and negative:

$$m_1 = m_2 = m_3 = m_B^* < 0, \qquad |m_B^*| = m_A^* \tag{5.9.7}$$

If we apply a constant magnetic field $\mathbf{B}$ in the positive x_3-direction, we observe from

$$m^* d\mathbf{v}/dt = (-e)(\mathbf{v} \times \mathbf{B}) \tag{5.9.8}$$

that the electron moves clockwise (counterclockwise) in the x_1–x_2 plane for case 1 (case 2).

The concept of a negative mass is a little strange. It is convenient to introduce a new interpretation as in the case in which Dirac discussed a positron in his prediction of this particle. In the Newtonian equation (5.9.8), the effective mass m^* and the electron charge $-e$ appear on the opposite sides. In the new interpretation (picture), we say that the hole has a positive mass $|m^*| = -m^*$ and a positive charge $+e$. In this new picture, the linear momentum $|m^*|\mathbf{v}$ has the same direction as the velocity $\mathbf{v}$, and the kinetic energy $T = |m^*|v^2/2$ is positive. In summary the dynamics of electrons and holes can be discussed in a parallel manner, only we must remember

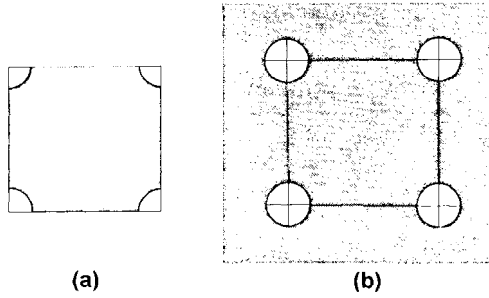

Figure 5.15. (a) Vacant states at the corners of an almost filled band in the reduced zone scheme. (b) The same states in the extended zone scheme.

that holes have charge $+e$. We introduced electrons and holes by using the special constant-energy surfaces (spheres). To apply these concepts to a metal, we have to merely extend our theory to *local* Fermi surfaces, a few examples of which follow.

We emphasize that we could discuss electrons and holes only through Eq. (5.9.1) and not through Eq. (5.9.2). Other shortcomings of the latter equation include the following. Equation (5.9.1) does not depend on the choice of the auxiliary field $(\mathbf{A}, \phi)$ and therefore they are gauge-invariant. On the other hand, Eq. (5.9.2) is not gauge-invariant. A further difficulty of Eq. (5.9.2) arises when we consider inhomogeneous electromagnetic fields $[\mathbf{E}(\mathbf{r}), \mathbf{B}(\mathbf{r})]$. Since the vector $\mathbf{k}$ is Fourier-conjugate to the position $\mathbf{r}$, it cannot depend on this variable. Thus Eq. (5.9.2) may be valid for homogeneous fields only, a severe limitation. Even then the solution of Eq. (5.9.2) indicates a further limitation. Consider the case of $\mathbf{B} = 0$. Assuming $\mathbf{E} = (E, 0,0)$, we have a solution: $\hbar k_x = qEt + p_0$, where p_0 is a constant. This solution does not depend on the energy–momentum relation, and it is material- and orientation-independent. It does not allow us to discuss anisotropic electron motion in layered conductors, such as graphite and high-T_c superconductors.

Further tests will be made by comparing the theoretical prediction with experiments. Let us take a square lattice. According to Harrison's construction of a NFEM Fermi surface,[6,7] the first Brillouin zone for a divalent metal may be filled with Bloch electrons everywhere except near the four corners as shown in Fig. 5.15 (a). A possible electron orbit in the presence of a magnetic field $\mathbf{B}$ may be a circle in the extended-zone scheme shown in (b). By inspection the curvature $\kappa \equiv P^{-1}$ is positive, and therefore the principal mass m^* is negative according to Eq. (5.8.25). Applying Eq. (5.9.1) we then observe that the Bloch electron moves like a hole, that is, clockwise in the x–y plane if $\mathbf{B}$ is directed in the z-direction. The corresponding orbit in the position (or r-) space is a circle directed clockwise, which is in accord with the fact that the centripetal force must act for a circular motion. If we adopt Eq. (5.9.2) with $q = -e$, the k-vector changes clockwise in the k_x–k_y plane. To obtain a circular motion with the centripetal force, we must still assume that this hypothetical electron carries a negative mass. In other words, Eq. (5.9.1) give a complete dynamics, while Eq. (5.9.2) does not. Thus the known experimental fact that holes exist in some metals cannot be explained from Eq. (5.9.2) alone.

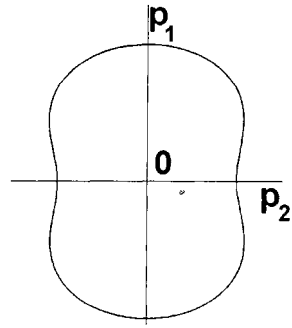

Figure 5.16. An oval of Cassini.

Significantly different predictions arise when we consider a closed Fermi curve (an oval of Cassini) represented by

$$(p_1^2 + p_2^2)^2 + a^4 - 2a^2(p_1^2 - p_2^2) = b^2, \qquad 2^{1/2}a > b \equiv \left(2m\epsilon_F\right)^{1/2} > a \quad (5.9.9)$$

See Fig. 5.16. This curve contains arcs of negative curvatures where electrons with energies higher than the Fermi energy ϵ_F can move and arcs of positive curvatures where holes with energies less than ϵ_F can move. Since the magnetic field cannot supply energy, this is not a physically executable orbit. More generally if any constant-energy curve contains arcs of curvatures of different signs, the Bloch electron cannot travel along it. The currently prevailing equation (5.9.2) does not inhibit such motion.

One of the most important ways of studying the Fermi surface is to measure and analyze dHvA oscillations in terms of Onsager's formula (5.6.2). As stated earlier a physically executable Bloch electron k-orbit must consist of arcs of curvatures of the same sign according to Eq. (5.9.1). Onsager's formula may be applied only to those k-orbits.

5.10. CYCLOTRON RESONANCE

The most direct way of exploring the Fermi surface is to perform and analyze cyclotron resonance experiments. As we shall see later, the concepts of electrons and holes play essential roles in the microscopic theory of superconductivity. Because of this relevance we discuss the cyclotron resonance in some depth in this section.

The operating principle of cyclotron resonance is simple. Take a free-electron model. If a magnetic field **B** is applied, all electrons near the Fermi sphere represented by

$$\frac{1}{2m^*}(p_1^2 + p_2^2 + p_3^2) = \epsilon_F \quad (5.10.1)$$

will move, keeping the magnetic flux inside intact. These electrons have different circulating speeds:

$$v_\perp \equiv (v_1^2 + v_2^2)^{1/2} \quad (5.10.2)$$

But all electrons move about the B-field with the same angular frequency

$$\omega_0 \equiv \frac{qB}{m^*} \tag{5.10.3}$$

called the *cyclotron frequency.* If a monochromatic radiation (microwave) with the matching frequency ω:

$$\omega = \omega_0 \tag{5.10.4}$$

is applied, a significant absorption peak should be observed. The peak position (frequency) directly gives the value of the effective mass m^* according to Eq. (5.10.3).

To observe actually the resonance peak, certain experimental conditions must be met: (1) the sample must be pure, (2) experiments should be performed at the liquid He temperature, and (3) the operating frequency ω must be reasonably high. These conditions ensure that the resonance width (frequency) arising from the electron-impurity and the electron-phonon interaction are much smaller than the peak frequency. In 1955 Dresselhaus, Kip, and Kittel (DKK)[19] reported a full account of their first observation of the cyclotron resonance in Ge and Si. They found electrons and holes in both semiconductors and that resonance peaks change with the orientation of the field relative to the crystal axes. After analyzing the data, they obtained the electron-type ellipsoidal Fermi surfaces with the effective masses:

$$(m_1^*, m_2^*, m_3^*) = (0.082, 0.082, 1.58)m \text{ for Ge} \tag{5.10.5}$$

$$(m_1^*, m_2^*, m_3^*) = (0.19, 0.19, 0.97)m \text{ for Si} \tag{5.10.6}$$

This has been considered an important event in the history of solid-state physics. The effective mass m^* is a material constant distinct from the gravitational electron mass m, which is a constant. The m^* appears in the kinetic-theoretical discussion of the electrical resistance (see Section 2.6). It enters as a phenomenologic parameter in free-electron model of a metal. It also appears in the discussion of the extreme low temperature behavior of the heat capacity. The fact that the effective mass m^* can be measured directly by the cyclotron resonance experiments is the most remarkable.

Figure 5.17 represents typical experimental data obtained by DKK. In the abscissa, the magnetic field rather than the microwave frequency is taken. In normal experimental runs, the magnetic field is varied. The charge carriers can be identified by applying circularly polarized microwaves. If the field orientation is varied, all peak positions were found to move. In their controlled experiments, field **B** is rotated in a (110) plane from [001] to [110]. The reduced inverse-resonance frequency versus the angle from the [001] axis is shown in Fig. 5.18. The solid lines are theoretical curves computed in terms of the DKK formula:

$$\omega = \left(\omega_t^2 \cos^2\theta + \omega_t\omega_l \sin^2\theta\right)^{1/2}, \qquad \omega_t \equiv \frac{eB}{m_t}, \qquad \omega_l \equiv \frac{eB}{m_l} \tag{5.10.7}$$

where θ is the angle between the field and the normal to the cyclotronic (circulating) plane. Formula (5.10.7) was derived with the assumption of a spheroidal Fermi surface represented by

$$\epsilon = \frac{p_1^2}{2m_t} + \frac{p_2^2}{2m_t} + \frac{p_3^2}{2m_l} \tag{5.10.8}$$

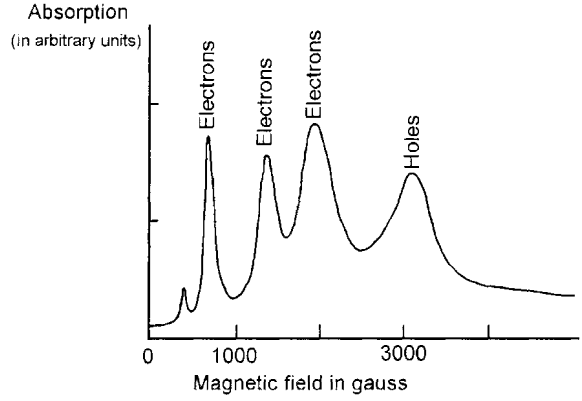

Figure 5.17. Cyclotron resonance absorption for Ge at $\nu = 24 \times 10^9$ cycles sec^{-1} at $T = 4$ K [after Dresselhaus *et al.* (Ref. 19)].

If the set of the four spheroidal surfaces is assumed to be located at the centers of the Brillouin-boundary hexagons whose normal points in the ⟨l11⟩ directions, the three lines of numerical fits are obtained all at once with the choice of the mass parameters (m_t, m_l). Notice the excellent agreement between theory and experiment. Germanium (Ge) and silicon (Si) share the same diamond-lattice structure. Yet the cyclotron resonance peaks observed in Si were found to be very different from those in Ge. The number of peaks and the orientation dependence of each peak can however be fitted within the experimental errors in terms of Eq. (5.10.7) under the assumption that three spheroidal Fermi surfaces are located at the centers of the Brillouin-boundary squares whose normal vectors point in the ⟨100⟩ directions. Thus if cyclotron resonance experiments are performed and analyzed properly, we can obtain a detailed information of the local Fermi surfaces. Metals have high carrier density, and generally greater effective masses, and reflect the applied radiation at the surface. All of these make it more difficult to observe cyclotron resonance peaks. The difficulties

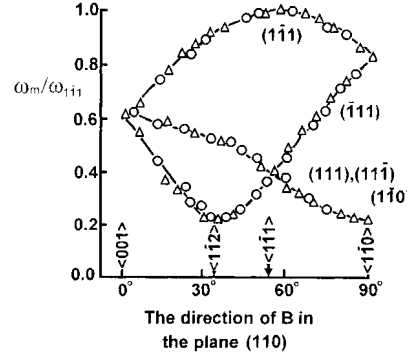

Figure 5.18. The orientation dependence of the resonance maxima ω_m for electrons Ge. Theoretical curves are obtained from Eq. (5.10.7) and experimental data from Ref. 19.

can however be overcome by using an Azbel–Kaner geometry[20] in which the field **B** is applied in the plane of a well-prepared sample surface. Khaikin and Minas[10] and Onuki, Suematsu, and Tamura[21] made extensive cyclotron resonance studies in lead (Pb), using this geometry. Watanabe and Fujita[22] analyzed these data in terms of Shockley's formula[23]:

$$\frac{\omega}{eB} = \left\{ \frac{[m_2 m_3 \cos^2(\mu, x_1) + m_3 m_1 \cos^2(\mu, x_2) + m_1 m_2 \cos^2(\mu, x_3)]}{m_1 m_2 m_3} \right\}^{1/2} \tag{5.10.9}$$

where $\cos(\mu, x_j)$ are the directional cosine between the B-field pointing in the direction μ and the x_j-axes. Watanabe and Fujita[22] found that the most prominent peaks come from the set of neck-like Fermi surfaces with axes pointing in $\langle 110 \rangle$, represented by

$$\epsilon = \frac{p_1^2}{2m_1^*} + \frac{p_2^2}{2m_2^*} + \frac{p_3^2}{2m_3^*} \tag{5.10.10}$$

where $(m_1^*, m_2^*, m_3^*) = (1.18, 0.244, -8.71)m$ are effective masses along the axes: $(x_1, x_2, x_3) = ([001], [110], [1\bar{1}0])$. Thus, the mid-sections of the cylinders shown in Fig. 5.9, are found to be *hyperboloidal*. Electrons and holes co-exist near the neck.

Shockley's formula (5.10.9) may be derived as follows. After substituting

$$v_j(t) = \exp(i\omega t)\, v_j \tag{5.10.11}$$

into Eq. (5.8.18) with $\mathbf{E} = 0$, we obtain a secular equation from the condition that (v_1, v_2, v_3) are not identically zero. Solving the secular equation we obtain the desired expression [Eq. (5.10.9)] for the cyclotron frequency ω (Problem 5.10.1). The obtained frequency ω does not depend on the circulating speed nor therefore on the energy of the circulating motion. This means that all the electrons resonate at the same frequency if the energy–momentum relation is quadratic; the observed peak should therefore be strong and sharp in the absence of scatterers (impurities, phonons). Further note that if $m_1^* m_2^* m_3^* < 0$, as for a neck, no real ω exist satisfying Shockley's formula (5.10.9) for some range of the magnetic field direction. This corresponds to a forbidden region of the peaks in the experiments.

By assuming $m_1 = m_2$, Eq. (5.10.9) is reduced to Eq. (5.10.7). If $m_3 = \infty$, formula (5.10.9) is reduced to a *cosine law* formula:

$$\omega = eB(m_1 m_2)^{-1/2} \cos\theta \tag{5.10.12}$$

where θ is the angle between the field and the c-axis. Such a case occurs for layered organic superconductors and it will be discussed in Section 13.2.

Problem 5.10.1. Derive Shockley's formula (5.10.9).

REFERENCES

1. F. Bloch, *Z. Phys. 52,* 555 (1928).
2. R. L. Kronig and W. G. Penney, *Proc. Roy. Soc.* (*London*) **130,** 499 (1931).
3. A. Haug, *Theoretical Solid-State Physics,* vol. 1 (Pergamon, Oxford, UK, 1972), pp. 64–69.

4. K. Shukla, *Kronig–Penney Models and their Applications to Solids,* Doctoral Diss., State University of New York at Buffalo (1990).
5. L. D. Landau, *J. Exptl . Theoret . Phys* (*USSR*) **30,** 1058 (1956).
6. W. A. Harrison, *Phys. Rev.* **118,** 1190 (1960).
7. *ibid., Solid-State Theory* (Dover, New York, 1979).
8. T. L. Loucks and P. H. Cutler, *Phys. Rev.* **133,** A819 (1964).
9. D. Schönberg and A. V. Gold, "Physics of Metals- 1" in *Electrons*, ed. J. M. Ziman (Cambridge University Press, Cambridge, UK, 1969), p. 112.
10. M. S. Khaikin and R. T. Minas, *Sov. Phys. JETP* **15** (1962).
11. C. Kittel, *Introduction to Solid-State Physics,* 6th ed. (Wiley, New York, 1986).
12. N. W. Ashcroft and N. D. Mermin, *Solid-State Physics* (Saunders, Philadelphia, 1976).
13. W. J. de Haas and P. M. van Alphen, *Leiden Comm.,* 208d, 212a (1930); *Leiden Comm.,* 220d (1932).
14. L. Onsager, *Phil. Mag.* **43,** 1006 (1952).
15. B. S. Deaver and W. M. Fairbank, *Phys. Rev. Lett.* **7,** 43 (1961).
16. R. Doll and M. Näbauer, *Phys. Rev. Lett.* **7,** 51 (1961).
17. P. A. M. Dirac, *Principles of Quantum Mechanics,* 4th ed. (Oxford University Press, London, 1958).
18. For example see L. P. Eisenhart, *Introduction to Differential Geometry* (Princeton University Press, Princeton, 1940).
19. G. Dresselhaus, A. F. Kip, and C. Kittel, *Phys. Rev.* **98,** 368 (1955).
20. M. Y. Azbel and E. A. Kaner, *J. Phys. Chem Solids* **6,** 113 (1958).
21. Y. Onuki, H. Suematsu, and S. Tamura, *J. Phys. Chem Solids* **38,** 419, 431 (1977).
22. S. Watanabe and S. Fujita, *J. Phys. Chem Solids* **52,** 985 (1991).
23. W. Shockley, *Phys. Rev.* **90,** 491 (1953).

This page intentionally left blank.

6

Second Quantization; Equation-of-Motion Method

The most remarkable fact about a system of fermions is that no more than one fermion can occupy a single-particle quantum state because of Pauli's exclusion principle. For bosons no such restrictions apply; that is, any number of bosons can occupy the same state. According to the quantum statistical postulate, an elementary particle is either a boson or a fermion. We shall discuss in the present chapter the second quantization formalism in which creation and annihilation operators associated with each quantum state are used. This formalism is, as we shall see later, extremely useful in treating of many-boson or many-fermion systems. We also develop Heisenberg's equation-of-motion method for many-particle systems. This method allows us to obtain the energy of a quasi-particle in a many-particle system.

6.1. CREATION AND ANNIHILATION OPERATORS FOR BOSONS

In the following theoretical developments, the reader is expected to know the fundamentals of quantum mechanics. Dirac's formulation of quantum mechanics[1] is unsurpassed; it is summarized in Appendix A. Basic concepts of bosons and fermions are reviewed in Appendix C.

The quantum state for a system of bosons (or fermions) can most conveniently be represented by a set of occupation numbers $\{n_a'\}$, where n_a' are the numbers of bosons (or fermions) occupying the quantum states a. This representation is called the

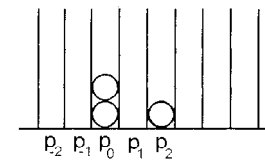

Figure 6.1. A many-boson state is described by a set of occupation numbers $\{n_j\}$.

occupation number representation or simply the *number representation.* For bosons the possible values for n_a' are zero or any positive integers:

$$n_a' = 0, 1, 2, \ldots \tag{6.1.1}$$

The many-boson state can best be represented by the distribution of particles (balls) in the states (boxes) as shown in Fig. 6.1.

Let us introduce operators whose eigenvalues are given by Eq. (6.1.1). We denote these operators by n_a without prime. Since Eq. (6.1.1) is meant for each and every state a independently, we assume that

$$[n_a, n_b] \equiv n_a n_b - n_b n_a = 0 \tag{6.1.2}$$

It is convenient to introduce complex dynamic variables η and $\eta^\dagger$ instead of directly dealing with the number operators n. We attach state labels *a, b,* . . . to the variables η and $\eta^\dagger$, and assume that they satisfy the following *Bose commutation rules*:

$$\boxed{[\eta_a, \eta_b^\dagger] = \delta_{ab}, \qquad [\eta_a, \eta_b] = [\eta_a^\dagger, \eta_b^\dagger] = 0} \tag{6.1.3}$$

Let us set

$$\eta_a^\dagger \eta_a \equiv n_a \ (= n_a^\dagger) \tag{6.1.4}$$

which is Hermitian. Clearly operators $n_a \equiv \eta_a^\dagger \eta_a$ satisfy Eq. (6.1.2). We shall show that $\eta_a^\dagger \eta_a$ has as eigenvalues all nonnegative integers. Let n' be an eigenvalue of $n \equiv \eta^\dagger \eta$ (dropping the suffix a) and $|n'\rangle$ an eigenket belonging to it. By definition

$$\langle n'|\eta^\dagger \eta|n'\rangle = n'\langle n'|n'\rangle \tag{6.1.5}$$

Now $\langle n'|\eta^\dagger \eta|n'\rangle$ is the squared length of the ket $\eta|n'\rangle$ and therefore

$$\langle n'|\eta^\dagger \eta|n'\rangle \geq 0 \tag{6.1.6}$$

Also by definition $\langle n'|n'\rangle > 0$; thus from Eqs. (6.1.5) and (6.1.6), we obtain

$$n' \geq 0 \tag{6.1.7}$$

The case of equality occurs only if

$$\eta|n'\rangle = 0 \tag{6.1.8}$$

Consider now $[\eta, n] \equiv [\eta, \eta^\dagger \eta]$. We may use the following identities:

$$[A, BC] = B[A,C] + [A,B]C, \qquad [AB, C] = A[B,C] + [A,C]B \tag{6.1.9}$$

and obtain

$$[\eta, \eta^\dagger \eta] = \eta^\dagger [\eta, \eta] + [\eta, \eta^\dagger]\eta = \eta, \qquad \eta n - n\eta = \eta \tag{6.1.10}$$

Hence

$$n\eta|n'\rangle = (\eta n - \eta)|n'\rangle = (n' - 1)\eta|n'\rangle \tag{6.1.11}$$

Now if $n' > 0, \eta|n'\rangle$ is not zero [from Eqs. (6.1.7) and (6.1.8)], then it is, according to Eq. (6.1.11), an eigenket of n belonging to the eigenvalue $n' - 1$. Therefore with n' any eigenvalue not equal to zero, $n' - 1$ is another eigenvalue. We can repeat the argument and deduce that if $n' - 1 \neq 0$, $n' - 2$ is another eigenvalue of n. Continuing this way we obtain a series of eigenvalues n', $n' - 1$, $n' - 2, \cdots$ that can terminate *only* with the value 0 in view of Eq. (6.1.7). By a similar process, we can show from the Hermitian conjugate of Eq. (6.1.10) that the eigenvalue of n has no upper limit (Problem 6.1.1). Hence the eigenvalues of n are nonnegative integers 0, 1, 2, $\cdots$. q.e.d.

Let $|\phi_a\rangle$ be a normalized eigenket of n_a belonging to the lowest eigenvalue 0, so that

$$\eta_a|\phi_a\rangle = 0 \tag{6.1.12}$$

By multiplying all these kets $|\phi_a\rangle$ together, we can construct a normalized eigenket:

$$|\Phi_0\rangle \equiv |\phi_a\rangle|\phi_b\rangle \cdots \tag{6.1.13}$$

which is a simultaneous eigenket of all n belonging to the eigenvalues zero. This ket is called the *vacuum ket*; it has the following property:

$$\eta_a|\Phi_0\rangle = 0 \text{ for any } a \tag{6.1.14}$$

Using the commutation rules Eqs. (6.1.3) we obtain a relation (dropping suffix a)

$$\eta(\eta^\dagger)^{n'} - (\eta^\dagger)^{n'}\eta = n'(\eta^\dagger)^{n'-1} \tag{6.1.15}$$

which may be proved by induction (Problem 6.1.2). Using Eqs. (6.1.12) and (6.1.15), we see that

$$n(\eta^\dagger)^{n'}|\phi\rangle = n'(\eta^\dagger)^{n'}|\phi\rangle \tag{6.1.16}$$

indicating that $(\eta^\dagger)^{n'}|\phi\rangle$ is an eigenket belonging to the eigenvalue n'. The square length of $(\eta^\dagger)^{n'}|\phi\rangle$ is

$$\langle\phi|\eta^{n'}(\eta^\dagger)^{n'}|\phi\rangle = n'\langle\phi|\eta^{n'-1}(\eta^\dagger)^{n'-1}|\phi\rangle = \cdots = n'! \tag{6.1.17}$$

We see from Eq. (6.1.11) that $\eta|n'\rangle$ is an eigenket of n belonging to the eigenvalue $n' - 1$ if $n' \neq 0$. Similarly we can show from the conjugate of Eq. (6.1.10) that $\eta^\dagger|n'\rangle$ is an eigenket of n belonging to the eigenvalue $n' + 1$. Thus operator η acting on the number eigenket annihilates one particle, while operator $\eta^\dagger$ creates one particle. Therefore η and $\eta^\dagger$ are called *annihilation* and *creation operators,* respectively.

From Eqs. (6.1.16) and (6.1.17) we can infer that if $n'_1, n'_2, \cdots$ are any nonnegative integers

$$(n'_1!n'_2!\cdots)^{-1/2}(\eta_1^\dagger)^{n'_1}(\eta_2^\dagger)^{n'_2}\cdots|\Phi_0\rangle \equiv |n'_1, n'_2, \cdots\rangle \tag{6.1.18}$$

is a normalized simultaneous eigenket of all the n belonging to the eigenvalues $n'_1, n'_2, \cdots$. Various kets [Eq. (6.1.18)] obtained by taking different n' form a complete set of kets all orthogonal to each other.

Following Dirac,[1] we postulate that the quantum states for N bosons can be represented by *symmetric kets*:

$$S[|\alpha_a^{(1)}\rangle|\alpha_b^{(2)}\rangle \cdots |\alpha_g^{(N)}\rangle] \equiv |\alpha_a\alpha_b \cdots \alpha_g\rangle_S \tag{6.1.19}$$

where S is the *symmetrizing operator,* defined by

$$S \equiv (N!)^{-1/2} \sum_P P \tag{6.1.20}$$

and P are permutation operators for the particles indices $(1,2,\cdots,N)$. The definition and the main properties of permutation operators are summarized in Appendix B. These kets in Eq. (6.1.19) are not normalized but:

$$(n_1!n_2!\cdots)^{-1/2}|\alpha_a\alpha_b\cdots\alpha_g\rangle_S \equiv |\{n\}\rangle \tag{6.1.21}$$

are normalized kets representing the same states. Comparing Eqs. (6.1.21) and (6.1.18), we obtain

$$\boxed{|\alpha_a\alpha_b\cdots\alpha_g\rangle_S = \eta_a^\dagger\eta_b^\dagger\cdots\eta_g^\dagger|\Phi_0\rangle} \tag{6.1.22}$$

That is, unnormalized symmetric kets $|\alpha_a\alpha_b\cdots\alpha_g\rangle_S$ for the system can be constructed by applying N creation operators $\eta_a^\dagger\eta_b^\dagger\cdots\eta_g^\dagger$ to the vacuum ket $|\Phi_0\rangle$. So far we have tacitly assumed that the total number of bosons is fixed at N'. If this number is not fixed but is variable, we can easily extend the theory to this case. Let us introduce a Hermitian operator N defined by

$$N \equiv \sum_a \eta_a^\dagger\eta_a = \sum_a n_a \tag{6.1.23}$$

the summation extending over the whole set of boson states. Clearly the operator N has eigenvalues 0, 1, 2, $\cdots$, and the ket $|\alpha_a\alpha_b\cdots\alpha_g\rangle_S$ is an eigenket of N belonging to the eigenvalue N'. For example we may arrange such kets in the order of N', i.e., zero-particle state, one-particle states, two-particle states, $\cdots$:

$$|\Phi_0\rangle, \qquad \eta_a^\dagger|\Phi_0\rangle, \qquad \eta_a^\dagger\eta_b^\dagger|\Phi_0\rangle, \qquad \cdots \tag{6.1.24}$$

These kets are all orthogonal to each other; two kets referring to the same number of bosons are orthogonal as before, and two referring to different numbers of bosons are orthogonal because they have different eigenvalues N'. By normalizing the kets [Eq.(6.1.21)], we obtain a set of kets like Eq. (6.1.21) with no restriction on $\{n'\}$. These kets form the basic kets in a representation where $\{n_a\}$ are diagonal.

Problem 6.1.1. (a) Show that $n\eta^\dagger - \eta^\dagger n = \eta^\dagger$. (b) Use this relation in (a) to obtain a series of eigenvalues n', $n'+1$, $n'+2, \cdots$, where n' is an eigenvalue of n.

Problem 6.1.2. Prove Eq. (6.1.15) by mathematical induction. Hint: use Eq. (6.1.9).

6.2. PHYSICAL OBSERVABLES FOR A SYSTEM OF BOSONS

We wish to express observable physical quantities for the system of identical bosons in terms of η and $\eta^\dagger$. These observables are by postulate symmetric functions of the single-boson variables. A general observable may be written in the form:

$$\sum_j y^{(j)} + \sum_i \sum_j z^{(ij)} + \cdots \equiv Y + Z + \cdots \tag{6.2.1}$$

where $y^{(j)}$ is a function of the dynamic variables of the jth boson, $z^{(ij)}$ is that of the dynamic variables of the ith and jth bosons, and so on.

We first show that the observable

$$Y \equiv \sum_j y^{(j)} \tag{6.2.2}$$

is expressed in terms of η and $\eta^\dagger$. Since $y^{(j)}$ acts only on the ket $|\alpha^{(j)}\rangle$ of the jth boson, we have

$$y^{(j)}(|\alpha_{x_1}^{(1)}\rangle|\alpha_{x_2}^{(2)}\rangle \cdots |\alpha_{x_j}^{(j)}\rangle \cdots) = \sum_a (|\alpha_{x_1}^{(1)}\rangle|\alpha_{x_2}^{(2)}\rangle \cdots |\alpha_a^{(j)}\rangle \cdots)\langle\alpha_a^{(j)}|y^{(j)}|\alpha_{x_j}^{(j)}\rangle$$

Summing this equation over all j and applying operator S to the result, we obtain

$$SY(|\alpha_{x_1}^{(1)}\rangle|\alpha_{x_2}^{(2)}\rangle \cdots) = \sum_j \sum_a S(|\alpha_{x_1}^{(1)}\rangle|\alpha_{x_2}^{(2)}\rangle \cdots |\alpha_a^{(j)}\rangle \cdots)\langle\alpha_a^{(j)}|y^{(j)}|\alpha_{x_j}^{(j)}\rangle \tag{6.2.3}$$

The matrix element $\langle\alpha_a^{(j)}|y^{(j)}|\alpha_{x_j}^{(j)}\rangle \equiv \langle\alpha_a|y|\alpha_{x_j}\rangle$ does not depend on the particle index j. Since Y is symmetric, we can replace SY by YS for the lhs of Eq. (6.2.3). After straightforward calculations, we obtain from Eq. (6.2.3)

$$\begin{aligned} Y\eta_{x_1}^\dagger \eta_{x_2}^\dagger \cdots |\phi_0\rangle &= \sum_j \sum_a \eta_{x_1}^\dagger \eta_{x_2}^\dagger \cdots \eta_{x_{j-1}}^\dagger \eta_a^\dagger \eta_{x_{j+1}}^\dagger \cdots |\Phi_0\rangle\langle\alpha_a|y|\alpha_{x_j}\rangle \\ &= \sum_a \sum_b \eta_a^\dagger \sum_j \eta_{x_1}^\dagger \eta_{x_2}^\dagger \cdots \eta_{x_{j-1}}^\dagger \eta_{x_{j+1}}^\dagger \cdots |\Phi_0\rangle\delta_{bx_j}\langle\alpha_a|y|\alpha_b\rangle \end{aligned} \tag{6.2.4}$$

From the commutation rules [Eqs. (6.1.3)] and the property in Eq. (6.1.14) we can show that

$$\eta_b \eta_{x_1}^\dagger \eta_{x_2}^\dagger \cdots |\Phi_0\rangle = \sum_i \eta_{x_1}^\dagger \eta_{x_2}^\dagger \cdots \eta_{x_{j-1}}^\dagger \eta_{x_{j+1}}^\dagger \cdots |\Phi_0\rangle\delta_{bx_j} \tag{6.2.5}$$

(Problem 6.2.1). Using this relation we obtain

$$Y\eta_{x_1}^\dagger \eta_{x_2}^\dagger \cdots |\Phi_0\rangle = \sum_a \sum_b \eta_a^\dagger \eta_b \langle\alpha_a|y|\alpha_b\rangle[\eta_{x_1}^\dagger \eta_{x_2}^\dagger \cdots |\Phi_0\rangle] \tag{6.2.6}$$

Since the kets $\eta_{x_1}^\dagger \eta_{x_2}^\dagger \cdots |\Phi_0\rangle$ form a complete set, we obtain

$$\boxed{Y = \sum_a \sum_b \eta_a^\dagger \eta_b \langle\alpha_a|y|\alpha_b\rangle} \tag{6.2.7}$$

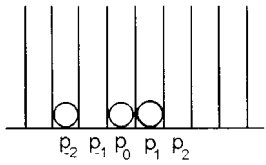

Figure 6.2. A many-fermion state can be represented by occupation numbers $\{n_j\}$.

In a similar manner Z in Eq. (6.2.1) can be expressed by (Problem 6.2.2)

$$Z = \sum_a \sum_b \sum_c \sum_d \eta_a^\dagger \eta_b^\dagger \eta_d \eta_c \langle \alpha_a \alpha_b | z | \alpha_c \alpha_d \rangle$$

$$\langle \alpha_a \alpha_b | z | \alpha_c \alpha_d \rangle \equiv \langle \alpha_a^{(1)} | \langle \alpha_b^{(2)} | z^{(12)} | \alpha_d^{(2)} \rangle | \alpha_c^{(1)} \rangle \tag{6.2.8}$$

Problem 6.2.1. Prove Eq. (6.2.5). Hint: Start with cases of one- and two-particle state kets.

Problem 6.2.2. Prove Eq. (6.2.8) by following those steps similar to Eqs. (6.2.3)–(6.2.7).

6.3. CREATION AND ANNIHILATION OPERATORS FOR FERMIONS

In this section we treat a system of identical fermions in a parallel manner.

The quantum states for fermions by postulate are represented by *antisymmetric kets*:

$$|\alpha_a \alpha_b \cdots \alpha_g\rangle_A \equiv A(|\alpha_a^{(1)}\rangle |\alpha_b^{(2)}\rangle \cdots |\alpha_g^{(N)}\rangle) \tag{6.3.1}$$

where A is the *antisymmetrizing operator* defined by

$$A \equiv (N!)^{-1/2} \sum_P \delta_P P \tag{6.3.2}$$

with δ_p being +1 or –1 according to whether P is even or odd (see Section B.2). Each antisymmetric ket in Eq. (6.3.1) is characterized so that it changes its sign if an odd permutation of particle indices is applied to it and the individual fermion states $a, b, \cdots, g$ are all different. Just as for a boson system, we can introduce observables $n_1\ n_2, \cdots$ each with eigenvalues 0 or 1 representing the number of fermions in the states $\alpha_1, \alpha_2, \cdots$ respectively. The many-fermion occupation number state can be represented as in Fig. 6.2.

We can also introduce a set of linear operators $(\eta, \eta^\dagger)$, one pair $(\eta_a, \eta_a^\dagger)$ corresponding to each particle state α_a, satisfying the *Fermi anticommutation rules*:

$$\boxed{\{\eta_a, \eta_b^\dagger\} \equiv \eta_a \eta_b^\dagger + \eta_b^\dagger \eta_a = \delta_{ab}, \qquad \{\eta_a, \eta_b\} = \{\eta_a^\dagger, \eta_b^\dagger\} = 0} \tag{6.3.3}$$

The number of fermions in the state α_a is again represented by

$$n_a \equiv \eta_a^\dagger \eta_a = n_a^\dagger \tag{6.3.4}$$

We see from Eq. (6.3.3) that

$$n_a^2 \equiv \eta_a^\dagger \eta_a \eta_a^\dagger \eta_a = \eta_a^\dagger (1 - \eta_a^\dagger \eta_a) \eta_a = \eta_a^\dagger \eta_a = n_a \text{ or } n_a^2 - n_a = 0 \tag{6.3.5}$$

If an eigenket of n_a belonging to the eigenvalue n_a' is denoted by $|n_a'\rangle$, Eq. (6.3.5) yields

$$(n_a^2 - n_a)|n_a'\rangle = (n_a'^2 - n_a')|n_a'\rangle = 0$$

Since $|n_a'\rangle \neq 0$, we obtain $n_a'(n_a' - 1) = 0$, meaning that the eigenvalues n_a' of n_a are either 0 or 1 as required:

$$n_a' = 0 \text{ or } 1 \tag{6.3.6}$$

Similarly to the case of bosons, we can show (Problem 6.6.1) that

$$|\alpha_a \alpha_b \cdots \alpha_g\rangle_A = \eta_a^\dagger \eta_b^\dagger \cdots \eta_g^\dagger |\Phi_0\rangle \tag{6.3.7}$$

which is normalized to unity. Physical observables can be expressed in the same form as Eqs. (6.2.7) and (6.2.8) as in the case of bosons.

In summary, both states and physical observables for a system of identical particles can be expressed in terms of creation and annihilation operators. This new formalism, called the *second quantization formalism,* has great advantages over the usual Schrödinger formalism. First the permutation symmetry property of the quantum particles is represented simply in the form of Bose commutation (or Fermi anticommutation) rules. Second physical observables in second quantization are defined independently of the number of particles, so that the formalism may apply to systems in which the number of particles is not fixed but variable. Third and most importantly, all relevant quantities (states and observables) can be defined referring only to the single-particle states, thus enabling us to describe the many-body system in three-dimensional space. This is a natural description since all particles in nature move in three dimensions. In fact, *relativistic quantum field theory* can be developed only in second quantization.

Problem 6.3.1. Prove Eq. (6.3.7).

6.4. SECOND QUANTIZATION IN THE MOMENTUM (POSITION) SPACE

Creation and annihilation operators can be defined for *any* particle states. For familiarity and later use, we shall discuss second quantization in the momentum and the position space. Suppose we have a system of N identical particles interacting with each other. Each particle is assumed to have no internal degrees of freedom. The Hamiltonian of the system consists of the kinetic energies and the pairwise potential energies:

$$H = \sum_j \epsilon^{(j)} + \frac{1}{2}\lambda \sum_j \sum_{j \neq k} v^{(jk)} \equiv H_0 + \lambda V \tag{6.4.1}$$

where $\epsilon^{(j)} \equiv p_j^2/(2m)$ is the kinetic energy of the jth particle, $v^{(jk)} \equiv v(\mathbf{r}_j - \mathbf{r}_k)$ the potential energy between the jth and kth particle, and λ the coupling constant. If the interaction λV is absent, then the Hamiltonian depends only on the momenta of the particles. In this case the momentum representation will be the simplest choice for the treatment of the system. In the presence of the pairwise interaction, which is not in general diagonal in the momentum representation, the momentum representation will lose its unique advantage. Nevertheless it turns out to be as convenient a representation as the position representation. Corresponding to these two representations, we may introduce two kinds of creation and annihilation operators.

Let us start with the momentum representation. We assume that all of the eigenvalues of the single-particle momentum are discrete. This can be achieved by assuming that the particles are contained in a periodic box of volume L^3. The momentum ket representing a symmetric or an antisymmetric system-state can be obtained by introducing a product of momentum kets for the single particle, then properly symmetrizing the product

$$|\mathbf{p}^N\rangle = \begin{cases} S(|\mathbf{p}_a^{(1)}\rangle|\mathbf{p}_b^{(2)}\rangle \cdots |\mathbf{p}_g^{(N)}\rangle) & \text{for bosons} \\ A(|\mathbf{p}_a^{(1)}\rangle|\mathbf{p}_b^{(2)}\rangle \cdots |\mathbf{p}_g^{(N)}\rangle) & \text{for fermions,} \end{cases} \tag{6.4.2}$$

where the upper indices denote particles and the lower indices momentum states. (Read $|\alpha_{\mathbf{p}_a}^{(j)}\rangle = |\mathbf{p}_a^{(j)}\rangle$.) In view of Eqs. (6.1.21) and (6.3.7) the momentum ket [Eq. (6.4.2)] and its adjoint for the system can be expressed as

$$|\mathbf{p}^N\rangle \equiv b_a^\dagger b_b^\dagger \cdots b_g^\dagger |\Phi_0\rangle, \qquad \langle \mathbf{p}^N| \equiv \langle \Phi_0| b_g \cdots b_b b_a \tag{6.4.3}$$

where b and $b^\dagger$ satisfy the following commutation (anticommutation) rules:

$$[b_1, b_2^\dagger] = \delta_{\mathbf{p}_1,\mathbf{p}_2}, \qquad [b_1, b_2] = [b_1^\dagger, b_2^\dagger] = 0 \text{ for bosons} \tag{6.4.4}$$

$$\{b_1, b_2^\dagger\} = \delta_{\mathbf{p}_1,\mathbf{p}_2}, \qquad \{b_1, b_2\} = \{b_1^\dagger, b_2^\dagger\} = 0 \text{ for fermions.} \tag{6.4.5}$$

Using Eqs. (6.2.7) and (6.2.8) we can express the Hamiltonian H as

$$H = \sum_{\mathbf{p}_1} \sum_{\mathbf{p}_2} b_1^\dagger b_2 \langle \mathbf{p}_1 | c | \mathbf{p}_2 \rangle + \frac{1}{2}\lambda \sum_{\mathbf{p}_1} \cdots \sum_{\mathbf{p}_4} b_1^\dagger b_2^\dagger b_4 b_3 \langle \mathbf{p}_1 \mathbf{p}_2 | v | \mathbf{p}_3 \mathbf{p}_4 \rangle \tag{6.4.6}$$

The matrix elements of the kinetic energy ϵ and the potential energy v are calculated as

$$\langle \mathbf{p}_1 | \epsilon(\mathbf{p}) | \mathbf{p}_2 \rangle = \epsilon_1 \delta_{\mathbf{p}_1,\mathbf{p}_2} \tag{6.4.7}$$

$$\langle \mathbf{p}_1 \mathbf{p}_2 | v | \mathbf{p}_3 \mathbf{p}_4 \rangle = V^{-1} \delta^{(3)}_{\mathbf{p}_1+\mathbf{p}_2,\mathbf{p}_3+\mathbf{p}_4} v(\mathbf{p}_1 - \mathbf{p}_2), \qquad v(\mathbf{q}) \equiv \int d^3 r e^{-i\mathbf{q}\cdot\mathbf{r}/\hbar} v(\mathbf{r}) \tag{6.4.8}$$

Substituting Eqs. (6.4.7)–(6.4.8) in Eq. (6.4.6), we obtain

$$H = \sum_{\mathbf{p}_1} \epsilon_1 b_1^\dagger b_1 + \frac{\lambda}{2V} \sum_{\mathbf{p}_1 \cdots \mathbf{p}_4} \cdots \sum v(\mathbf{p}_1 - \mathbf{p}_3) \delta^{(3)}_{\mathbf{p}_1+\mathbf{p}_2,\mathbf{p}_3+\mathbf{p}_4} b_1^\dagger b_2^\dagger b_4 b_3 \tag{6.4.9}$$

The total number of particles is represented by

$$N = \sum_{\mathbf{p}_1} b_1^\dagger b_1 \tag{6.4.10}$$

The second quantization formulation in the position space is similar. We introduce *quantum field* operators $\psi(\mathbf{r})[\psi^\dagger(\mathbf{r})]$ labeled by continuous eigenvalues $\mathbf{r}$, satisfying the following commutation (or anticommutation) rules:

$$\begin{aligned} [\psi(\mathbf{r}), \psi^\dagger(\mathbf{r}')] &= \delta^{(3)}(\mathbf{r} - \mathbf{r}') \\ [\psi(\mathbf{r}), \psi(\mathbf{r}')] &= [\psi^\dagger(\mathbf{r}), \psi^\dagger(\mathbf{r}')] = 0 \qquad \text{(bosons)} \end{aligned} \tag{6.4.11}$$

$$\begin{aligned} \{\psi(\mathbf{r}), \psi^\dagger(\mathbf{r}')\} &= \delta^{(3)}(\mathbf{r} - \mathbf{r}') \\ \{\psi(\mathbf{r}), \psi(\mathbf{r}')\} &= \{\psi^\dagger(\mathbf{r}), \psi^\dagger(\mathbf{r}')\} = 0 \quad \text{(fermions)} \end{aligned} \tag{6.4.12}$$

The number of particles in an arbitrary volume V is given by

$$N(V) = \int_V d^3 r \psi^\dagger(\mathbf{r})\psi(\mathbf{r}) \tag{6.4.13}$$

The Hamiltonian H can be expressed by

$$H = -\frac{\hbar^2}{2m} \int d^3 r\, \psi^\dagger(\mathbf{r})\nabla^2\psi(\mathbf{r}) + \frac{1}{2}\int\int d^3 r_1 d^3 r_2\, \psi^\dagger(\mathbf{r}_1)\psi^\dagger(\mathbf{r}_2)\psi(\mathbf{r}_2)\psi(\mathbf{r}_1)v(\mathbf{r}_1 - \mathbf{r}_2) \tag{6.4.14}$$

Properly symmetrized kets and bras for the system of bosons (or fermions) are given by

$$|\mathbf{r}^N\rangle \equiv \psi^\dagger(\mathbf{r}_1)\psi^\dagger(\mathbf{r}_2)\cdots\psi^\dagger(\mathbf{r}_N)|\phi_0\rangle, \quad \langle\mathbf{r}^N| \equiv \langle\phi_0|\psi(\mathbf{r}_N)\cdots\psi(\mathbf{r}_2)\psi(\mathbf{r}_1) \tag{6.4.15}$$

Problem 6.4.1. Verify Eq. (6.4.8).

6.5. REDUCTION TO A ONE-BODY PROBLEM

Let us consider a system for which the total Hamiltonian H is the sum of single-electron energies h:

$$H = \sum_j h^{(j)} \tag{6.5.1}$$

For example the *single-electron* Hamiltonian h for an electron may contain the kinetic energy and the potential energy due to an external electric field. We assume that the Hamiltonian H does not depend on the time explicitly. In the Schrödinger Picture (SP) (see Section A.3), the energy eigenvalue problem is formulated by

$$H|E\rangle = E\,|E\rangle \tag{6.5.2}$$

where E is the eigenvalue. In the position representation this equation is written as

$$H(x_1, -i\hbar\partial/\partial x_1, x_2, -i\hbar\partial/\partial x_2, \cdots)\Psi(x_1, x_2, \cdots) = E\Psi \tag{6.5.3}$$

where Ψ is the wave function for the system. We consider a one-dimensional motion for conceptional and notational simplicity. [For a three-dimensional motion, (x,p) should be replaced by $(x, y, z, p_x, p_y, p_z) = (\mathbf{r}, \mathbf{p})$.] If the number of electrons N is large, the wave function ψ contains numerous electrons variables $(x_1, x_2, \cdots)$. This complexity needed in dealing with many electron variables can be avoided if we use the second quantization formulation and the Heisenberg Picture (HP), which will be shown later in this section.

As a preliminary, we consider an electron is characterized by the Hamiltonian

$$h(x,p) = \frac{1}{2m}p^2 + u(x) \tag{6.5.4}$$

We may set up the eigenvalue equations for the position x, the momentum p, and the Hamiltonian h as follows:

$$x|x'\rangle = x'|x'\rangle \tag{6.5.5}$$

$$p|p'\rangle = p'|p'\rangle \tag{6.5.6}$$

$$h|\epsilon_\nu\rangle = \epsilon_\nu|\epsilon_\nu\rangle \equiv \epsilon_\nu|\nu\rangle \tag{6.5.7}$$

where x', p', and ϵ_v are eigenvalues.

The total Hamiltonian H can be represented by

$$H = \sum_a \sum_b \langle\alpha_a|h|\alpha_b\rangle \eta_a^\dagger \eta_b \equiv \sum_a \sum_b h_{ab}\eta_a^\dagger \eta_b \tag{6.5.8}$$

where $\eta_a(\eta_a^\dagger)$ are annihilation (creation) operators associated with the particle state a and satisfying the Fermi anticommutation rules [Eq. (6.3.3)].

In the HP a variable $\xi(t)$ changes following the *Heisenberg equation of motion:*

$$\boxed{-i\hbar\frac{d\xi(t)}{dt} = [H,\xi] \equiv H\xi - \xi H} \tag{6.5.9}$$

Applying Eq. (6.5.9) for $\xi = \eta_a^\dagger$, we obtain

$$-i\hbar\frac{d\eta_a^\dagger}{dt} = [H, \eta_a^\dagger] \tag{6.5.10}$$

whose Hermitian conjugate is given by

$$i\hbar\frac{d\eta_a}{dt} = ([H,\eta_a^\dagger])^\dagger = -[H,\eta_a] \tag{6.5.11}$$

Note: By quantum postulate the physical observable ξ is Hermitian: $\xi^\dagger = \xi$. Variables η_a and $\eta_a^\dagger$ are not Hermitian, but both obey the same Heisenberg equation of motion [Eq. (6.5.9)].

We introduce Eq. (6.5.8) into Eq. (6.5.10), then calculate the commutator $[H,\eta_a^\dagger]$. In such a commutator calculation, the following identities:

$$[A, BC] = \{A, B\}C - B\{A, C\}, \qquad [AB, C] = A\{B, C\} - \{A, C\}B \tag{6.5.12}$$

are often very useful. These formulas are similar to Eqs. (6.1.9). Note: The negative signs on the right-hand terms occur when the cyclic order is destroyed. We obtain

$$-i\hbar\frac{d\eta_a^\dagger}{dt} = \sum_c\sum_b h_{cb}[\eta_c^\dagger\eta_b, \eta_a^\dagger] = \sum_c\sum_b h_{cb}\eta_c^\dagger\{\eta_b, \eta_a^\dagger\} = \sum_c \eta_c^\dagger h_{ca} \quad (6.5.13)$$

which means that the change of the one-body operator $\eta_a^\dagger$ is determined by the one-body Hamiltonian h. This is one of the main advantages of working with second quantization operators in the HP. Equation (6.5.13) is valid for *any* particle states $\{a\}$. If we choose the energy states $\{\varepsilon_\nu\}$ for $\{a\}$, we have

$$h_{\nu\nu'} \equiv \langle\nu|h|\nu'\rangle = \epsilon_\nu\delta_{\nu,\nu'} \quad (6.5.14)$$

Denoting the energy state creation operator by $\psi_\nu^\dagger$, we obtain from Eq. (6.5.14)

$$-i\hbar\frac{d\psi_\nu^\dagger}{dt} = \epsilon_\nu\psi_\nu^\dagger, \quad \text{or} \quad i\hbar\frac{d\psi_\nu}{dt} = \epsilon_\nu\psi_\nu \quad (6.5.15)$$

From Eqs. (6.5.10), (6.5.13), and (6.5.15), we obtain

$$\epsilon_\nu\psi_\nu^\dagger = \sum_\mu \psi_\mu^\dagger h_{\mu\nu} \quad (6.5.16)$$

which is formally similar to Eq. (6.5.7). We shall later in Section 6.7 use this property to set up an energy eigenvalue problem for a quasi-particle.

So far we have dealt with the system of electrons (fermions). All formulas are valid for bosons, for which creation and annihilation operators should be defined to satisfy the Bose commutation rules [Eq. (6.1.3)].

Here we make a small digression. In the field operator language the Hermitian conjugate of Eq. (6.5.13) reads

$$i\hbar\frac{\partial\Psi(\mathbf{r}, t)}{\partial t} = h\left(\mathbf{r}, -i\hbar\frac{\partial}{\partial\mathbf{r}}\right)\Psi(\mathbf{r}, t) \quad (6.5.17)$$

which is formally identical to the Schrödinger equation of motion. Note: This is obtained under Eq. (6.5.1). If the system Hamiltonian H contains an interparticle interaction, the evolution equation for $\Psi(\mathbf{r}, t)$ is nonlinear (see Problem 6.5.2):

$$\begin{aligned} i\hbar\frac{\partial\Psi(\mathbf{r}, t)}{\partial t} &= h\left(\mathbf{r}, -i\hbar\frac{\partial}{\partial\mathbf{r}}\right)\Psi(\mathbf{r}, t) \\ &\quad + \int d^3r'\, v(\mathbf{r}-\mathbf{r}')\Psi^\dagger(\mathbf{r}', t)\Psi(\mathbf{r}', t)\Psi(\mathbf{r}, t) \end{aligned} \quad (6.5.18)$$

In quantum field theory the basic dynamical variables are particle-field operators. The quantum statistics of the particles are given by the Bose-commutation or the Fermi-commutation rules satisfied by the field operators. The evolution equations of the field operators are intrinsically nonlinear when the interparticle interaction is present.

Problem 6.5.1. Verify that the equation of motion (6.5.13) holds for bosons.

Problem 6.5.2. Use Eq. (6.5.9) to verify Eq. (6.5.18).

6.6. ONE-BODY DENSITY OPERATOR; DENSITY MATRIX

Physical observables X for the system, such as total momentum, total angular momentum, and total charge current, can be expressed as the sum of the corresponding single-particle observables ξ:

$$X = \sum_{j=1}^{N} \xi^{(j)} \tag{6.6.1}$$

In second quantization the observable X can be expressed by

$$X = \sum_a \sum_b \langle \alpha_a | \xi | \alpha_b \rangle \eta_a^\dagger \eta_b \tag{6.6.2}$$

This is the same form as Eq. (6.5.8). Also note that this form does not depend on the number N of fermions (or bosons) of the system, an advantage.

We now take a system-ensemble average of Eq. (6.6.2) and obtain

$$\langle X \rangle \equiv \mathrm{Tr}\{X\rho\} = \sum_a \sum_b \xi_{ab} \langle \eta_a^\dagger \eta_b \rangle \tag{6.6.3}$$

where ρ is a system-density operator, normalized to unity: $\mathrm{Tr}\{\rho\} = 1$. For later convenience we note an important property (Problem 6.6.1):

$$\mathrm{Tr}\{X\rho\} = \mathrm{Tr}\{\rho X\} \tag{6.6.4}$$

That is, two linear operators commute under the trace.

Let us now examine

$$\langle \eta_a^\dagger \eta_b \rangle \equiv \mathrm{Tr}\{\eta_a^\dagger \eta_b \rho\} \equiv \langle \alpha_b | n | \alpha_a \rangle \tag{6.6.5}$$

The lhs is a (complex) number, and it depends on the state variables (α_a, α_b). By considering all sets of states $\{\alpha_a\}$ and $\{\alpha_b\}$, we may define a single-particle operator n through Eq. (6.6.5). This operator n so defined is called the *one-body density operator* or *number-density operator* and

$$\langle \alpha_b | n | \alpha_a \rangle \equiv n_{ba} \tag{6.6.6}$$

are called *b-a* elements of the *one-body density matrix.* Note: The order of (a, b) is reversed in going from the lhs to the rhs in Eq. (6.6.5). Introducing Eq. (6.6.5) into Eq. (6.6.3), we obtain

$$\boxed{\langle X \rangle \equiv \mathrm{Tr}\{X\rho\} = \sum_a \sum_b \xi_{ab} n_{ba} \equiv \mathrm{tr}\{\xi n\}} \tag{6.6.7}$$

where the symbol tr means a one-body trace; that is, the many-body average can be computed in terms of the one-body average, a great convenience.

We now study the properties of the density operator n. By postulate the system-density (or probability-density) operator ρ is Hermitian:

$$\rho^\dagger = \rho \tag{6.6.8}$$

By straightforward calculations, we obtain

$$n^*_{ba} = [\langle \alpha_b | n | \alpha_a \rangle]^* = [\mathrm{Tr}\{\rho \eta_a^\dagger \eta_b\}]^* = \mathrm{Tr}\{\eta_b^\dagger \eta_a \rho^\dagger\} = \mathrm{Tr}\{\rho \eta_b^\dagger \eta_a\} = n_{ab}$$

or

$$n^\dagger = n \tag{6.6.9}$$

That is, the one-body density operator n is Hermitian.

The system density operator ρ by definition can be expressed in the form:

$$\rho = \sum_m |m\rangle P_m \langle m|, \qquad \sum_m P_m = 1 \tag{6.6.10}$$

where $\{P_m\}$ denote the probabilities that the system is in many-particle states $\{m\}$. Using Eq. (6.6.10), we can show (Problem 6.6.2) that the diagonal elements

$$n_{aa} \equiv n_a \equiv \langle \alpha_a | n | \alpha_a \rangle \quad (\geq 0) \tag{6.6.11}$$

are nonnegative, and they represent the (relative) occupation probabilities at the states $\{a\}$. If the states are continuously distributed, n_a can be regarded as the *particle number density*. Summing Eq. (6.6.11) over all particle states $\{a\}$, we obtain

$$\sum_a n_a = \sum_a \langle \alpha_a | n | \alpha_a \rangle = \left\langle \sum_a \eta_a^\dagger \eta_a \right\rangle = \langle \hat{N} \rangle \tag{6.6.12}$$

The system-density operator ρ(t) in the SP obeys the *quantum Liouville equation:*

$$\boxed{i\hbar \frac{\partial \rho}{\partial t} = [H, \rho]} \tag{6.6.13}$$

By using this equation and assuming Eq. (6.5.1), we can show (Problem 6.6.3) that the one-body density operator $n(t)$obeys the one-body Liouville equation:

$$\boxed{i\hbar \frac{\partial n}{\partial t} = [h, n]} \tag{6.6.14}$$

Equation (6.6.14) was obtained under the condition that the system Hamiltonian H is the sum of particle Hamiltonians h. If H contains an interparticle interaction, the evolution equation of $n(t)$ is more complicated.

In equilibrium quantum statistical mechanics, the grand canonical ensemble is most useful. This ensemble is characterized by

$$\rho_{gc} \equiv \Xi^{-1} \exp(\alpha N - \beta H_N) \tag{6.6.15}$$

where H_N is the N-particle Hamiltonian and Tr_N denotes the N-particle ensemble trace. The quantity Ξ

$$\Xi \equiv \sum_{N=0}^{\infty} \mathrm{Tr}_N \{\exp(\alpha N - \beta H_N)\} \equiv \mathrm{TR}\{\exp(\alpha N - \beta H)\} \tag{6.6.16}$$

is called the *grand partition function.* The one-body density matrix n_{ba} is defined by

$$n_{ba} \equiv \frac{\mathrm{TR}\{\eta_a^\dagger \eta_b \exp(\alpha N - \beta H)\}}{\mathrm{TR}\{\exp(\alpha N - \beta H)\}} \tag{6.6.17}$$

If the Hamiltonian H is of the form Eq. (6.5.1), we can simply compute all matrix elements in the energy-state number representation and obtain (Problem 6.6.4)

$$n_{\nu\lambda} = \frac{1}{\exp(\beta\epsilon_\nu - \alpha) \pm 1}\delta_{\nu\lambda} \tag{6.6.18}$$

where $\{\varepsilon_\nu\}$ are the energy eigenvalues defined by Eq. (6.5.7) and the upper (lower) signs correspond to the cases of fermions (bosons). Then the particle number (or unnormalized one-body) density operators n is represented by

$$n = \frac{1}{\exp(\beta h - \alpha) \pm 1} \tag{6.6.19}$$

which are called the Fermi or the Bose density operator. The single-particle Hamiltonian h may contain the kinetic and potential energy as represented by Eq. (6.5.4).

Problem 6.6.1. Prove Eq. (6.6.4). Use a matrix representation.

Problem 6.6.2. Verify Eq. (6.6.11).

Problem 6.6.3. Prove Eq. (6.6.14) by using Eqs. (6.6.13) and (6.5.1). Hint: Take (a, b) matrix elements and establish the equality.

Problem 6.6.4. Prove Eq. (6.6.18).

6.7. ENERGY EIGENVALUE PROBLEM

We set up an energy eigenvalue problem for a quasi-particle in this section.

We first reexamine the one-body problem. By multiplying Eq. (6.5.7) from the left by $\langle x'|$, we obtain

$$h(x, -i\hbar\partial/\partial x)\phi_\nu(x) = \epsilon_\nu\phi_\nu(x) \tag{6.7.1}$$

$$\phi_\nu(x') \equiv \langle x'|\epsilon_\nu\rangle \equiv \langle x'|\nu\rangle \tag{6.7.2}$$

Equation (6.7.1) is just the Schrödinger energy-eigenvalue equation, and $\phi_\nu(x)$ is the quantum wave function. If we know with certainty that the system is in the energy eigenstate ν, we may choose a one-body density operator ρ_1 to be

$$\rho_1 = |\nu\rangle\langle\nu|, \qquad \mathrm{tr}\{\rho_1\} = 1 \tag{6.7.3}$$

Let us now consider $\mathrm{tr}\{|\nu\rangle\langle x|\rho_1\}$ which can be transformed as follows:

$$\mathrm{tr}\{|\nu\rangle\langle x|\rho_1\} = \sum_\alpha \langle\alpha|\nu\rangle\langle x|\nu\rangle\langle\nu|\alpha\rangle = \sum_\alpha \langle x|\nu\rangle\langle\nu|\alpha\rangle\langle\alpha|\nu\rangle = \langle x|\nu\rangle$$

or

$$\mathrm{tr}\{|\nu\rangle\langle x|\rho_1\} \equiv \langle x|\rho_1|\nu\rangle = \phi_\nu(x) \tag{6.7.4}$$

This means that the wave function $\phi_\nu(x)$ can be regarded as a *mixed representation* of the density operator ρ in terms of the states (ν, x). In a parallel manner, we can show (Problem 6.7.1) that the wave function in the momentum space $a_\nu(p) \equiv \langle p|\nu\rangle$ can be regarded as a mixed representation of ρ_1 in terms of the energy state ν and the momentum state p:

$$a_\nu(p) = \mathrm{tr}\{|\nu\rangle\langle p|\rho_1\} = \langle p|\rho_1|\nu\rangle \tag{6.7.5}$$

In analogy with Eq. (6.7.5) we introduce a *quasi-wave function* $\Psi_\nu(p)$ through

$$\Psi_\nu(p) \equiv \mathrm{Tr}\{\psi_\nu^\dagger a_p \rho\} \tag{6.7.6}$$

where a_p is the annihilation operator for the momentum state p, and ρ a many-body or system density operator that commutes with the Hamiltonian:

$$[\rho, H] = 0 \tag{6.7.7}$$

[This is the necessary condition that ρ be a stationary density operator, which can be seen at once from the quantum Liouville equation (6.6.13).] For example we may take ρ to be the canonical density operator:

$$\rho_c \equiv \frac{\exp(-\beta H)}{\mathrm{Tr}\{\exp(-\beta H)\}} = \frac{\exp(-\beta H)}{Z} \tag{6.7.8}$$

where

$$Z \equiv \mathrm{Tr}\{\exp(-\beta H)\} \tag{6.7.9}$$

is the partition function. We multiply Eq. (6.5.16) by $a_p\rho$ from the right, take a many-body trace and obtain

$$\boxed{\sum_\mu \Psi_\mu(p) h_{\mu\nu} = \epsilon_\nu \Psi_\nu(p)} \tag{6.7.10}$$

which is formally identical to the Schrödinger energy-eigenvalue equation for the one-body problem (Problem 6.7.2):

$$\sum_\mu \phi_\mu(p) h_{\mu\nu} = \epsilon_\nu \phi_\nu(p), \qquad \phi_\nu(p) \equiv \langle p|\nu\rangle \tag{6.7.11}$$

We reformulate Eq. (6.7.10) for a later use. Using Eqs. (6.5.13) and (6.5.16), we obtain

$$\mathrm{Tr}\{[H, \psi_\nu^\dagger] a_p \rho\} = \mathrm{Tr}\{\psi_\nu^\dagger [a_p, H]\rho\} = \epsilon_\nu \Psi_\nu(p) \tag{6.7.12}$$

whose complex conjugate is

$$\epsilon_\nu \Psi_\nu^*(p) = \mathrm{Tr}\{[H, a_p^\dagger]\psi_\nu \rho\} \tag{6.7.13}$$

where we used Eq. (6.7.7) and the following general property (Problem 6.7.3):

$$\mathrm{Tr}\{AB\rho\} = \mathrm{Tr}\{\rho AB\} = \mathrm{Tr}\{B\rho A\} \tag{6.7.14}$$

(cyclic permutation under the trace).

Either Eq. (6.7.12) or its complex conjugate Eq. (6.7.13) can be used to formulate the energy-eigenvalue problem. If we choose the latter, we may proceed as follows: (1) Given H in the momentum space, compute $[H, a_p^\dagger]$; the result can be expressed as a linear function of $a^\dagger$. (2) Multiply the result by $\psi_\nu \rho$ from the right, then take a trace; the result is a linear function of Ψ^*; (3) use Eq. (6.7.13); the result is a linear homogeneous equation for Ψ^*, a standard form of the energy eigenvalue equation. The energy eigenvalue problem discussed here will be used later to find the excitation energy of a quasi-particle in a many-body system. Earlier we saw that the ordinary wave function $a_\nu(p)$ can be regarded as a mixed representation of the one-particle density operator $\rho : a_\nu(p) = \langle p|\rho|\nu\rangle$ [see Eq. (6.7.5)]. The quasi-wave function $\psi_\nu(p)$ defined in Eq. (6.7.6) can be regarded as a mixed representation of the one-body density operator n:

$$\boxed{\Psi_\nu(p) = \langle p|n|\nu\rangle} \tag{6.7.15}$$

(This will be used in our later discussion of a supercurrent, see Sections 11.5–11.6).

Problem 6.7.1. Verify Eq. (6.7.5).

Problem 6.7.2. Derive Eq. (6.7.11) from Eq. (6.5.7).

Problem 6.7.3. Verify Eq. (6.7.12).

6.8. QUANTUM STATISTICAL DERIVATION OF THE FERMI LIQUID MODEL

As an application of the equation-of-motion method, we discuss a quantum statistical derivation of the Fermi liquid model.

In Section 5.3 we saw that the Bloch electron moves almost freely in an extremely weak effective lattice potential V_e. The total model Hamiltonian H_C, the subscript C omitted hereafter, may then be represented by

$$H = \sum_j \left(\frac{1}{2m}\right) p_j^2 + \sum_j V_e(\mathbf{r}_j) \tag{6.8.1}$$

$$V_e(\mathbf{r} + \mathbf{R}) = V_e(\mathbf{r}), \qquad (\mathbf{R}: \text{ Bravais vector}) \tag{6.8.2}$$

The Hamiltonian H satisfies Eq. (6.5.1). Thus we can set up a quasi-particle energy eigenvalue problem as described in Section 6.7.

In second quantization we may write the Hamiltonian H as

$$H = \int d^3r \left[-\frac{\hbar^2}{2m}\phi^\dagger(\mathbf{r})\nabla^2\phi(\mathbf{r}) + V_e(\mathbf{r})\phi^\dagger(\mathbf{r})\phi(\mathbf{r})\right] \tag{6.8.3}$$

where $\phi(\mathbf{r})[\phi^{\dagger}(\mathbf{r})]$ represent the annihilation (creation) field operators satisfying the Fermi anticommutation rules [Eq. (6.4.12)]. We now calculate the commutator $[\phi(\mathbf{r}),H]$. After using Eqs. (6.8.3), (6.4.12), and (6.5.11), we obtain (Problem 6.7.1)

$$i\hbar\frac{d\phi}{dt} = [\phi(\mathbf{r}), H] = \left[-\frac{\hbar^2}{2m}\nabla^2 + V_e(\mathbf{r})\right]\phi(\mathbf{r}) \tag{6.8.4}$$

which has the same form as the Schrödinger equation of motion. We multiply Eq. (6.8.4) from the left by $\rho\psi_{\nu}^{\dagger}$ then take a grand ensemble trace. By introducing the quasi-wave function [see Eq. (6.7.6)]:

$$\Psi_{\nu}(\mathbf{r}) \equiv \mathrm{TR}\{\psi_{\nu}^{\dagger}\phi(\mathbf{r})\rho\} \tag{6.8.5}$$

We can write the result as

$$\boxed{\epsilon_{\nu}\Psi_{\nu} = -\frac{\hbar^2}{2m}\nabla^2\Psi_{\nu}(\mathbf{r}) + V_e(\mathbf{r})\Psi_{\nu}(\mathbf{r})} \tag{6.8.6}$$

which is identical to the Schrödinger eigenvalue equation for the one-electron Hamiltonian $h = p^2/2m + V_e(\mathbf{r})$. Equation (6.8.6) is an energy eigenvalue equation for a *single* quasi-particle. The quasi-particles in our model system are independently moving Bloch electrons characterized by quantum numbers $(j, \mathbf{k})$. They are fermions because of Eq. (6.4.12). Therefore at 0 K all of the Bloch states of lowest energies are filled with electrons, and there will be a sharp Fermi surface in the k-space represented by $\epsilon_F = \epsilon_j(\hbar\mathbf{k})$. Thus the sharp Fermi surface is obtained in a general manner without specifying the effective lattice potential V_e. Only a periodic crystal lattice must be assumed.

Problem 6.8.1. Verify Eq. (6.8.4).

REFERENCE

1. P. A. M. Dirac, *Principles of Quantum Mechanics,* 4th ed. (Oxford University Press, London, UK, 1958).

This page intentionally left blank.

7

Interparticle Interaction; Perturbation Methods

The Coulomb interaction between an electron and an ion is attractive and long-ranged. This interaction at distances in a metal is greatly reduced because of the screening of other conduction electrons. For the same reason, the repulsive Coulomb interaction between two electrons is also greatly reduced. The crystal electron must move in a varying electric field generated by the ionic-lattice vibration. The Fröhlich Hamiltonian representing an interaction between electron and phonon is derived. By exchanging a virtual phonon, two electrons can gain an attraction if the difference between the electron energies on emission (absorption) of a phonon is less than the phonon energy. This is shown by using a quantum perturbation theory. Fermi's golden rule for the rate of a transition between two quantum states is derived.

7.1. ELECTRON–ION INTERACTION; THE DEBYE SCREENING

The Coulomb interaction is the best understood of the four fundamental interactions in nature. The other three are the gravitational interaction, the strong interaction which holds nucleons together and the weak interaction which allows a neutron to decay into a proton with emission of an electron and a neutrino. In atomic and solid-state physics, the Coulomb interaction and its derivatives play by far the most important roles. It is customary to neglect the other three interactions.

Let us take two particles with charge q_1 and q_2, separated by a distance r. The Coulomb force acting on one particle points along the line connecting the two. Its magnitude is

$$F = k_0 q_1 q_2 \frac{1}{r^2} \qquad [k_0 \equiv (4\pi\epsilon_0)^{-1}] \tag{7.1.1}$$

The Coulomb force $\mathbf{F}$ acting on the particle with charge q_1 can be described by the electrostatic potential field φ such that

$$\mathbf{F} = -q_1 \nabla \varphi(\mathbf{r}) \tag{7.1.2}$$

For example if the particle with charge q_2 is at the origin, the potential φ is given by

$$\varphi(r) = k_0 q_2 \frac{1}{r} \tag{7.1.3}$$

Let us now consider an ion with charge e, fixed at the origin and surrounded by a system of free electrons. We may expect that the electron density n is no longer constant and that in equilibrium it is perturbed such that the electric potential field φ far from the origin is essentially canceled by the induced electron density variation. We say that the ionic charge is *screened* by the electron gas. There will be a distance within which the screening is ineffective and outside which the screening is almost complete. We treat this screening effect in the present section.

Poisson's equation in electrostatics is given by

$$\nabla^2\varphi = \left(\frac{e}{\epsilon_0}\right)[n(\mathbf{r}) - n_0] \tag{7.1.4}$$

where $n(\mathbf{r}) - n_0$ is the deviation from the uniform density n_0 very far from the origin. In equilibrium the chemical potential μ must be constant in space:

$$\mu(\mathbf{r}) = \text{constant} \tag{7.1.5}$$

We consider the system at 0 K. At a distance very far from the origin, where φ is regarded as zero, we set μ to equal the Fermi energy:

$$\mu = \epsilon_F = \left(\frac{\hbar^2}{2m}\right)(3\pi^2 n_0)^{2/3} \tag{7.1.6}$$

where we used Eq. (2.2.17). In a region where φ is nonzero, we may assume that

$$\mu = \left(\frac{\hbar^2}{2m}\right)[3\pi^2 n(\mathbf{r})]^{2/3} - e\varphi(\mathbf{r}) \tag{7.1.7}$$

Using Eq. (7.1.5), we then obtain

$$\left(\frac{\hbar^2}{2m}\right)[3\pi^2 n(r)]^{2/3} - e\varphi(r) = \left(\frac{\hbar^2}{2m}\right)[3\pi^2 n_0]^{2/3} \tag{7.1.8}$$

where we omitted the angular dependence; n and φ now depend only on the distance r from the origin. If the potential energy $e\varphi$ is not large compared with the Fermi energy ϵ_F, we may expand $n(r)$ in powers of $e\varphi/\epsilon_F$ and keep the linear term n_1 only, obtaining

$$n(r) - n_0 \cong n_1(r) = \left(\frac{3}{2}\right) n_0 e \frac{\varphi(r)}{\epsilon_F} \tag{7.1.9}$$

(Problem 7.1.1). Using Eqs. (7.1.4) and (7.1.9), we obtain

$$\left(\frac{d^2}{dr^2} + \frac{2}{r}\frac{d}{dr}\right)\varphi(r) = q_D^2\varphi \tag{7.1.10}$$

$$q_D^2 \equiv \frac{6\pi n_0 e^2}{\epsilon_F} = \frac{4me^2 n_0^{1/3}}{\hbar^2}\left(\frac{3}{\pi}\right)^{1/3} = \frac{4n_0^{1/3}}{a_0}$$

$$a_0 \equiv \text{Bohr radius} = 0.529\ \text{Å} \tag{7.1.11}$$

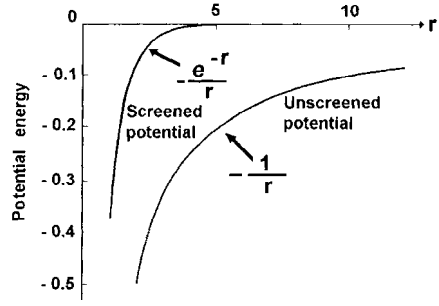

Figure 7.1. Comparison of screened and unscreened Coulomb potential. $q_D = 1$.

Equation (7.1.10) can be solved simply, yielding (Problem 7.1.2)

$$\boxed{\varphi(r) = k_0 \frac{e}{r} \exp(-q_D r).} \tag{7.1.12}$$

This is called the *screened Coulomb potential.* Compared with Eq. (7.1.3), it has the factor of an exponential-decay type. It is plotted in Fig. 7.1 as a function of r. The inverse of q_D:

$$r_D \equiv \frac{1}{q_D} \tag{7.1.13}$$

is called the *Debye* or *Thomas–Fermi screening length.* Debye obtained the screened Coulomb potential in the ionic solution problem.[1] Thomas and Fermi obtained Eq. (7.1.12) in theory of metals.[2] For copper with $n_0 = 8.5 \times 10^{22}$ electrons cm^{-3}, the screening length r_D is 0.55 Å. Note: The screening is fully effective in a metal when two electrons are separated by a distance of the order 1 Å.

Problem 7.1.1. Derive Eq. (7.1.9). Hint: Expand: $n = n_0 + n_1 + \cdots$, substitute it in Eq. (7.1.8).

Problem 7.1.2. (a) Verify that $\varphi(r)$ in Eq. (7.1.12) satisfies Eq. (7.1.10). (b) Solve Eq. (7.1.10) by the Fourier transformation method.

7.2. ELECTRON-ELECTRON INTERACTION

We saw in Section 5.3 that each conduction electron moves in an extremely weak lattice field, and therefore it moves almost freely. The electron however has a charge $-e$. It should therefore interact with a second electron in the crystal. These two are in fact moving in a medium consisting of the lattice ions and a great number $(N - 2)$ of other moving electrons. Their mutual Coulomb interaction will therefore be screened by

the motion of the other electrons. If the distance between them r is not too small, the interaction should be described by the screened Coulomb interaction

$$k_0 \frac{e^2}{r} \exp(-q_D r) \tag{7.2.1}$$

This interaction may further be reduced by the polarization of the ions surrounding the electron. The net interaction may then be represented by

$$v_D = \frac{k_0}{\kappa} \frac{e^2}{r} \exp(-q_D r) \tag{7.2.2}$$

where κ is the dielectric constant (number). In a pure intrinsic semiconductor like Ge, such polarization effect arising from the core electrons is known to be important.

The total Hamiltonian H is the sum of the kinetic energies $\{\epsilon(\mathbf{p}_j)\}$ and the pair-potential energies $\{v_D(|\mathbf{r}_j - \mathbf{r}_k|)\}$:

$$H = \sum_{j=1}^{N} \epsilon(\mathbf{p}_j) + \sum_{j>k} \sum v_D(|\mathbf{r}_j - \mathbf{r}_k|) = \sum_j \epsilon(\mathbf{p}_j) + \frac{1}{2} \sum_{j \neq k} \sum v_D(|\mathbf{r}_j - \mathbf{r}_k|) \tag{7.2.3}$$

In second quantization the same Hamiltonian H can be expressed as [see : Eq. (6.4.9)]

$$H = \sum_{\mathbf{k}s} \epsilon_k c^\dagger_{\mathbf{k}s} c_{\mathbf{k}s} + \frac{1}{2} \sum_{\mathbf{k}_1 s_1} \cdots \sum_{\mathbf{k}_4 s_4} \langle 12|v_D|34\rangle c^\dagger_1 c^\dagger_2 c_4 c_3 \tag{7.2.4}$$

where $c^\dagger_{\mathbf{k}_1 s_1}$ $(c_{\mathbf{k}_1 s}) \equiv c^\dagger_1$ (c_1) are creation (annihilation) operators satisfying the Fermi anticommutation rules:

$$\{c_{\mathbf{k}s}, c^\dagger_{\mathbf{k}'s'}\} \equiv c_{\mathbf{k}s} c^\dagger_{\mathbf{k}'s'} + c^\dagger_{\mathbf{k}'s'} c_{\mathbf{k}s} = \delta_{\mathbf{k},\mathbf{k}'} \delta_{ss'} \tag{7.2.5}$$

$$\{c_{\mathbf{k}s}, c_{\mathbf{k}'s'}\} = \{c^\dagger_{\mathbf{k}s}, c^\dagger_{\mathbf{k}'s'}\} = 0 \tag{7.2.6}$$

The matrix element $\langle 12|v_D|34\rangle$ can be calculated as shown in Eq. (6.4.7), and it is given by (Problem!7.2.1)

$$\langle 12|v_D|34\rangle = v_D(|\mathbf{p}_1 - \mathbf{p}_3|) \frac{1}{V} \delta_{s_1 s_3} \delta_{s_2 s_4} \delta_{\mathbf{k}_1 + \mathbf{k}_2, \mathbf{k}_3 + \mathbf{k}_4} \tag{7.2.7}$$

$$v_D(q) \equiv \int d^3 r \exp(-i\mathbf{q} \cdot \mathbf{r}\hbar^{-1}) v_D(r) = \frac{4\pi e^2 k_0}{\kappa} \frac{1}{q^2 + q_D^2} \tag{7.2.8}$$

Problem 7.2.1. Verify Eqs. (7.2.7) and (7.2.8).

7.3. MORE ABOUT THE HEAT CAPACITY; LATTICE DYNAMICS

In the present section we review a general theory of heat capacity based on lattice dynamics. Using the results of this theory, we then discuss the basic assumptions of the Debye model,[3] see Section 3.5, and a few related topics.

We first review the dynamics of coupled oscillators. We take a set of N particles of equal mass m attached to a light string of length $(N+1)l$ in equilibrium, stretched to a tension τ, the same system discussed in Section 3.3. The kinetic energy T and the potential energy V for the system were calculated earlier, and they are given by

$$T \equiv \left(\frac{m}{2}\right)(\dot{y}_1^2 + \cdots + \dot{y}_N^2) \tag{7.3.1}$$

$$V \equiv \left(\frac{\tau}{2l}\right)[y_l^2 + (y_2 - y_1)^2 + \cdots + (y_N - y_{N-1})^2 + y_N^2] \tag{7.3.2}$$

where y_j denotes the transverse displacement of the particle j. The Lagrangian L is

$$L = \frac{m}{2}\dot{y}_1^2 - \frac{\tau}{2l}y_1^2 + \sum_{j=2}^{N-1}\left[\frac{m}{2}\dot{y}_j^2 - \frac{\tau}{2l}(y_{j+1} - y_j)^2\right] + \frac{m}{2}\dot{y}_N^2 - \frac{\tau}{2l}y_N^2 \tag{7.3.3}$$

Lagrange's equations of motion generate coupled linear homogeneous differential equations for y_j. The associated characteristic (determinant) equation yields N normal mode frequencies: $\omega_1, \omega_2, \cdots, \omega_N$. By suitably choosing linear combinations of y_j:

$$Q_k \equiv \sum_{j=1}^{N} a_{kj}y_j, \qquad k = 1, 2, \cdots N \tag{7.3.4}$$

we can in principle reexpress the Lagrangian L in the form [see Eq. (3.3.26)]

$$L = \sum_k \left(\frac{1}{2}\right)(\dot{Q}_k^2 - \omega_k^2 Q_k^2) \tag{7.3.5}$$

This Lagrangian is the sum of the harmonic oscillator Lagrangians over all normal modes with the number of the normal modes equaling that of the degrees of freedom for the system. Introducing the canonical momenta:

$$P_k \equiv \frac{\partial L}{\partial \dot{Q}_k} = \dot{Q}_k \tag{7.3.6}$$

we can derive the Hamiltonian H for the system

$$H = \sum_k \left(\frac{1}{2}\right)(P_k^2 + \omega_k^2 Q_k^2) \tag{7.3.7}$$

Let us now take a crystal composed of N molecules. The potential energy V depends on the configuration of N molecules $(\mathbf{r}_1, \mathbf{r}_2, \cdots, \mathbf{r}_N)$. We regard this energy V as a function of the *displacements* of the molecules:

$$\mathbf{u}_j \equiv \mathbf{r}_j - \mathbf{r}_j^{(0)} \tag{7.3.8}$$

measured from the equilibrium positions $\mathbf{r}_j^{(0)}$. Let us expand the potential $V = V(\mathbf{u}_1, \mathbf{u}_2, \cdots, \mathbf{u}_N) \equiv V(u_{1x}, u_{1y}, u_{1z}, u_{2x}, \cdots)$ in terms of small displacements $\{u_{j\mu}\}$:

$$V = V_0 + \sum_j \sum_{\mu=x,y,z} u_{j\mu}\left(\frac{\partial V}{\partial u_{j\mu}}\right)_0 + \frac{1}{2}\sum_j\sum_\mu\sum_k\sum_\nu u_{j\mu}u_{k\nu}\left(\frac{\partial^2 V}{\partial u_{j\mu}\partial u_{k\nu}}\right)_0 + \cdots \tag{7.3.9}$$

where all partial derivatives are evaluated at $\mathbf{u}_1 = \mathbf{u}_2 = \cdots = 0$, which is indicated by subscripts 0. We may set the constant V_0 equal to zero with no loss of rigor. By assumption the lattice is stable at the equilibrium configuration where the potential V must have a minimum; this requires the first-order derivatives to vanish:

$$\left(\frac{\partial V}{\partial u_{j\mu}}\right)_0 = 0 \tag{7.3.10}$$

For small oscillations we may keep terms of the second order in $u_{j\mu}$ only, which is called the *harmonic approximation.* We then have

$$V \cong V' \equiv \sum_j \sum_\mu \sum_k \sum_\nu \frac{1}{2} A_{j\mu k\nu} u_{j\mu} u_{k\nu} \tag{7.3.11}$$

$$A_{j\mu k\nu} \equiv \left(\frac{\partial^2 V}{\partial u_{j\mu} \partial u_{k\nu}}\right)_0 \tag{7.3.12}$$

The prime (′) indicating harmonic approximation will be dropped hereafter. The kinetic energy of the system is

$$T \equiv \sum_j \frac{m}{2} \dot{r}_j^2 = \sum_j \frac{m}{2} \dot{u}_j^2 \equiv \sum_j \sum_\mu \frac{m}{2} \dot{u}_{j\mu}^2 \tag{7.3.13}$$

We can now write the Lagrangian $L \equiv T - V$ as

$$L = \sum_j \sum_\mu \frac{m}{2} \dot{u}_{j\mu}^2 - \sum_j \sum_\mu \sum_k \sum_\nu \frac{1}{2} A_{j\mu k\nu} u_{j\mu} u_{k\nu} \tag{7.3.14}$$

This Lagrangian L in the harmonic approximation is quadratic in $u_{j\mu}$ and $\dot{u}_{j\mu}$ as is the Lagrangian [Eq. (7.3.3)] for the coupled linear chain. According to theory of the *principal-axis transformations*[4], see Section 3.3, we can in principle transform the Hamiltonian (total energy) $H = T + V$ for such a system into the sum of the energies of the normal-modes of oscillations [see Eq. (7.3.7)]:

$$H = \sum_{\kappa=1}^{3N} \frac{1}{2} (P_\kappa^2 + \omega_\kappa^2 Q_\kappa^2) \tag{7.3.15}$$

where $\{Q_\kappa, P_\kappa\}$ are the normal coordinates and momenta [see Eqs. (7.3.4) and (7.3.6)] and ω_κ are characteristic frequencies. Note: There are exactly $3N$ normal modes.

Let us first calculate the heat capacity based on Eq. (7.3.15) by means of classical statistical mechanics. This Hamiltonian H is quadratic in canonical variables (Q_κ, P_κ). Therefore the equipartition theorem holds: We multiply the average thermal energy for each mode $k_B T$ by the number of modes $3N$ and we obtain $3Nk_B T$ for the average energy of the system $\langle H \rangle$. Differentiating this with respect to T, we obtain $3Nk_B$ for the heat capacity, which is in agreement with Dulong–Petit's law. It is interesting to observe that we obtained this result without knowing the actual distribution of normal-mode frequencies. The fact that there are $3N$ normal modes played an important role.

Let us now use quantum theory to calculate the heat capacity based on Eq. (7.3.15). The energy eigenvalues of the Hamiltonian H are given by

$$E[\{n_\kappa\}] = \sum_\kappa \left(\frac{1}{2} + n_\kappa\right) \hbar\omega_\kappa \tag{7.3.16}$$

$$n_\kappa = 0, 1, 2, \cdots \tag{7.3.17}$$

We can interpret Eq. (7.3.16) in terms of phonons as follows: the energy of the lattice vibrations is characterized by the set of the number of phonons $\{n_\kappa\}$ in the normal modes $\{\kappa\}$. Taking the canonical ensemble average of Eq. (7.3.16), we obtain

$$\langle E[\{n_\kappa\}]\rangle = \sum_\kappa \left[\frac{1}{2} + \langle n_\kappa\rangle\right] \hbar\omega_\kappa = \sum_\kappa \left[\frac{1}{2} + f_0(\hbar\omega_\kappa)\right] \hbar\omega_\kappa \equiv E(T) \tag{7.3.18}$$

$$f_0(\epsilon) \equiv \frac{1}{\exp(\epsilon/k_B T) - 1} \tag{7.3.19}$$

Let us digress here. Imagine a case in which all frequencies ω_κ have the same value ω_0. Then Eq. (7.3.18) is reduced to Eq. (3.2.8) in Einstein's theory.

The normal-mode frequencies $\{\omega_\kappa\}$ depend on the normalization volume V, and these will be densely populated for large V. In the bulk limit, we may then convert the sum over the normal modes into a frequency integral and obtain

$$E(T) = E_0 + \int_0^\infty d\omega\, \hbar\omega f_0(\hbar\omega) \mathcal{D}(\omega) \tag{7.3.20}$$

$$E_0 = \frac{1}{2} \int_0^\infty d\omega\, \hbar\omega\, \mathcal{D}(\omega) \tag{7.3.21}$$

where $\mathcal{D}(\omega)$ is the *density of states (modes) in angular frequency* defined such that

$$\text{number of modes in the interval } (\omega,\ \omega + d\omega) \equiv \mathcal{D}(\omega) d\omega \tag{7.3.22}$$

The constant E_0 represents a temperature-independent zero-point energy.

Differentiating $E(T)$ with respect to T, we obtain for the heat capacity

$$\boxed{C_V = \left.\frac{\partial E}{\partial T}\right)_V = \int_0^\infty d\omega\, \hbar\omega \frac{\partial f_0(\hbar\omega)}{\partial T} \mathcal{D}(\omega).} \tag{7.3.23}$$

This expression was obtained by the harmonic approximation only, which is good at very low temperatures, where only small-amplitude oscillations are involved.

To proceed further we have to know the density of normal modes $\mathcal{D}(\omega)$. Let us recall that to find the set of characteristic frequencies $\{\omega_\kappa\}$ requires solving an algebraic equation of $3N$th order, and we need the frequency distribution for large N. This is not a simple matter. In fact a branch of mathematical physics whose principal aim is to find the frequency distribution is called *lattice dynamics*. Figure 7.2 represents a result obtained by Walker[5] after analyzing x-ray scattering data for aluminum based on lattice dynamics. Some remarkable features of the curve are

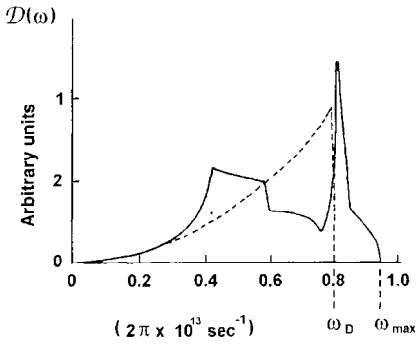

Figure 7.2. The density of normal modes in the angular frequency for aluminum. The solid curve represents the data deduced from x-ray scattering measurements due to Walker (Ref. 5). The broken lines indicate the Debye frequency distribution [Eq. (3.5.30)] with $\Theta_D = 328$ K.

A) At low frequencies:

$$\mathcal{D}(\omega) \propto \omega^2 \tag{7.3.24}$$

B) There exists a maximum frequency ω_m such that

$$\mathcal{D}(\omega) = 0 \quad \text{for } \omega \geq \omega_m \tag{7.3.25}$$

C) A few sharp peaks exist below ω_m.

The feature A is common to all crystals. The low-frequency modes can be described adequately in terms of longitudinal and transverse elastic waves. This region can be represented very well by the Debye's continuum model (see Fig. 7.2), indicated by the broken line. Feature B is connected to the lattice structure. Briefly no normal modes of extreme short wavelengths (extreme high frequencies) exist. There is a limit frequency ω_m. Sharp peaks were first predicted by Van Hove[6] on topological grounds, and these peaks are often referred to as the *van Hove singularities.*

As we demonstrate later in Chapter 8, the cause of superconductivity lies in the electron–phonon interaction. The microscopic theory however can be formulated in terms of the generalized BCS Hamiltonian (see Section 8.2), where phonon variables are eliminated. In this sense the details of lattice dynamics are secondary to our main concern. The following point is noteworthy, however. All lattice-dynamic calculations start with the assumption of a real crystal lattice. For example to treat aluminum, we start with a fcc lattice having empirically known lattice constants. The equations of motion for a set of ions are solved under the assumption of a periodic lattice-box boundary condition. Thus the k-vectors used in both lattice dynamics and Bloch electron dynamics are the same. The domain of the k-vectors can be restricted to the same first Brillouin zone. Colloquially speaking phonons (bosons) and electrons (fermions) live together in the same Brillouin zone, which is equivalent to the statement that electrons and phonons share the same house (crystal lattice). This affinity between electrons and phonons makes the conservation of momentum in the electron–phonon interaction physically meaningful. Thus the fact that the electron–phonon interaction is the cause of superconductivity of all kinds is not accidental.

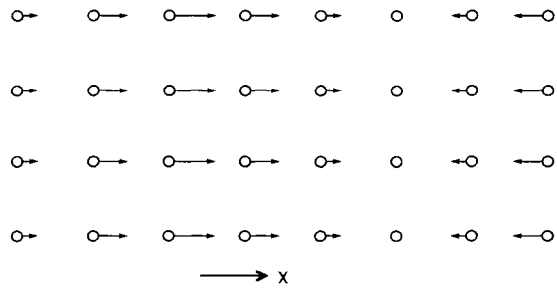

Figure 7.3. A longitudinal wave proceeding in the x-direction. $\lambda = 12a_0$.

7.4. ELECTRON–PHONON INTERACTION; THE FRÖHLICH HAMILTONIAN

A crystal lattice is composed of a regular arrays of ions. If the ions move, then the electrons must move in a varying potential field. In the present section, we derive the Fröhlich Hamiltonian, which is especially suitable for the superconductivity problems.

For simplicity let us take an sc lattice. The normal modes of oscillations for a periodic infinite solid are longitudinal and transverse running waves characterized by wave vector $\mathbf{q}$ and frequency ω_q. First consider the case of a longitudinal wave proceeding in the crystal axis x, which may be represented by

$$u_q \exp(-i\omega_q t + i\mathbf{q}\cdot\mathbf{r}) = u_q \exp(-i\omega_q t + iqx) \tag{7.4.1}$$

where u_q is the displacement in the x-direction. The wavelength

$$\lambda \equiv \frac{2\pi}{q} \qquad (> 2a_0) \tag{7.4.2}$$

is greater than twice the lattice constant a_0. The case: $\lambda = 12a_0$ is shown in Fig. 7.3.

If we imagine a set of parallel plates containing a great number of ions fixed in each plate, we have a realistic picture of the lattice-vibration mode. From Fig. 7.3 we see that density of ions changes in the x-direction. Thus the longitudinal modes are also called the *density wave* modes. The transverse wave modes can also be pictured from Fig. 7.3 by imagining a set of parallel plates containing a great number of ions fixed in each plate and assuming the transverse displacements of the plates. Notice that these modes generate no charge-density variations.

Now the Fermi velocity v_F in a typical metal is on the order of $10^6\ \mathrm{ms}^{-1}$, while the speed of sound is of the order $10^3\ \mathrm{ms}^{-1}$. The electrons are then likely to move quickly to negate any electric field generated by the density variations associated with the lattice waves. Thus the electrons may follow the lattice waves quite easily. Given a traveling normal mode in Eq. (7.4.1), we may assume an electron density deviation of the form:

$$C \exp(-i\omega_q t + i\mathbf{q}\cdot\mathbf{r}) \tag{7.4.3}$$

If electrons follow phonons immediately for all ω_q, the factor C can be regarded as independent of ω_q. We further assume that the deviation is linear in $\mathbf{u_q} \cdot \mathbf{q} = qu_q$ and again the electron density $n(\mathbf{r})$. Thus:

$$C = Aqu_q n(\mathbf{r}) \tag{7.4.4}$$

where A is a constant. This is called the deformation potential approximation.[8] We can express the electron density (field) as

$$n(\mathbf{r}) = \psi^\dagger(\mathbf{r})\psi(\mathbf{r}) \tag{7.4.5}$$

where $\psi(\mathbf{r})$ and $\psi^\dagger(\mathbf{r})$ are annihilation and creation field operators.

We now construct an interaction Hamiltonian H_F, which has the dimension of an energy and which is Hermitian. We propose

$$H_F = \int d^3r \sum_{\mathbf{q}} \left[Aqu_{\mathbf{q}} \exp(i\mathbf{q} \cdot \mathbf{r})\, \psi^\dagger(\mathbf{r})\psi(\mathbf{r}) + \text{h.c.} \right] \tag{7.4.6}$$

(where h.c. is the Hermitian conjugate). Classically, the displacement u_q obeys the harmonic equation of motion:

$$\ddot{u}_{\mathbf{q}} + \omega_q^2 u_{\mathbf{q}} = 0 \tag{7.4.7}$$

Let us write the corresponding Hamiltonian for each mode as

$$H = (2)^{-1}(p^2 + \omega^2 q^2), \qquad q \equiv u,\ p \equiv \dot{q},\ \omega_q \equiv \omega \tag{7.4.8}$$

where we dropped the mode index **q.** If we assume the same Hamiltonian H and the basic commutation relations:

$$[q, p] = i\hbar, \qquad [q, q] = [p, p] = 0 \tag{7.4.9}$$

the quantum description of a harmonic oscillator is complete. The equations of motion are

$$\dot{q} = (1/i\hbar)[q, H] = p, \quad \dot{p} = (1/i\hbar)[p, H] = -\omega^2 q \tag{7.4.10}$$

(Problem 7.4.1). We introduce the dimensionless complex dynamic variables:

$$a^\dagger \equiv (2\hbar\omega)^{-1/2}(p + i\omega q), \qquad a \equiv (2\hbar\omega)^{-1/2}(p - i\omega q) \tag{7.4.11}$$

Using Eq. (7.4.10) we obtain

$$\dot{a}^\dagger = (2\hbar\omega)^{-1/2}(-\omega^2 q + i\omega p) = i\omega a^\dagger, \quad \dot{a} = -i\omega a \tag{7.4.12}$$

We can express (q, p) in terms of $(a^\dagger, a)$:

$$q = -i\left(\frac{\hbar}{2\omega}\right)^{1/2}(a^\dagger - a), \qquad p = \left(\frac{\hbar\omega}{2}\right)^{1/2}(a^\dagger + a) \tag{7.4.13}$$

Thus we may work entirely in terms of these variables. After straightforward calculations, we obtain (Problem 7.4.2):

$$\begin{aligned}\hbar\omega a^\dagger a &= (2)^{-1}(p + i\omega q)(p - i\omega q)\\ &= (2)^{-1}[p^2 + \omega^2 q^2 + i\omega(qp - pq)]\\ &= H - \frac{1}{2}\hbar\omega\end{aligned}$$

$$\hbar\omega a a^\dagger = H + \frac{1}{2}\hbar\omega \tag{7.4.14}$$

$$aa^\dagger - a^\dagger a \equiv [a, a^\dagger] = 1 \tag{7.4.15}$$

$$\begin{aligned}H &= \frac{1}{2}\hbar\omega(a^\dagger a + aa^\dagger)\\ &= \hbar\omega\left(a^\dagger a + \frac{1}{2}\right)\\ &\equiv \hbar\omega\left(n + \frac{1}{2}\right)\end{aligned} \tag{7.4.16}$$

Note: The operators $(a_i^\dagger a)$ satisfy the Bose commutation rules [Eq. (6.1.3)]. We can therefore use operator algebras in Sections 6.1—6.2 and obtain the following results:

- Eigenvalues of $n \equiv a^\dagger a$ [see Eq. (6.1.1): $n' = 0, 1, 2, \cdots$
- Vacuum ket $|\phi\rangle$ [see Eq. (6.1.14)]: $a\,|\,\phi\rangle = 0$
- Eigenkets of n [see Eq. (6.1.16)]: $|\,\phi\rangle, a^\dagger|\phi\rangle, (a^\dagger)^2|\phi\rangle, \cdots$ having the eigenvalues $0, 1, 2, \cdots$
- Eigenvalues of H : $(1/2)\hbar\omega, (3/2)\hbar\omega, (5/2)\hbar\omega, \cdots$

In summary the quantum states of a harmonic oscillator can be described in terms of the occupation numbers of bosons. (The fundamental connection between bosons and harmonic oscillators is discussed in Dirac's book.[9]

We now go back to the case of the lattice-normal modes. Each normal mode corresponds to a harmonic oscillator characterized by $(\mathbf{q}, \omega_q)$. The bosons corresponding to these harmonic oscillators are called *phonons*. The displacements $u_\mathbf{q}$ can be expressed as

$$u_\mathbf{q} = i\left(\frac{\hbar}{2\omega_q}\right)^{1/2}(a_\mathbf{q} - a_\mathbf{q}^\dagger) \tag{7.4.17}$$

where $(a_\mathbf{q}, a_\mathbf{q}^\dagger)$ are creation and annihilation operators satisfying the commutation rules:

$$[a_\mathbf{q}, a_\mathbf{p}^\dagger] \equiv a_\mathbf{q} a_\mathbf{p}^\dagger - a_\mathbf{p}^\dagger a_\mathbf{q} = \delta_{\mathbf{p}q}, \qquad [a_\mathbf{q}, a_\mathbf{p}] = [a_\mathbf{q}^\dagger, a_\mathbf{p}^\dagger] = 0 \tag{7.4.18}$$

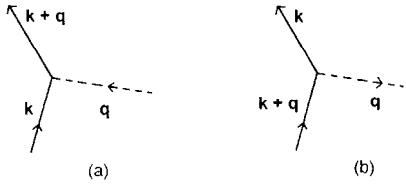

Figure 7.4. Feynman diagrams representing (a) absorption and (b) emission of a phonon by an electron. They correspond to the interaction terms in Eq. (7.4.20).

The field operators ψ ($\psi^\dagger$) can be expanded in terms of the momentum-state electron operators $c_{\mathbf{q}}$ ($c_{\mathbf{q}}^\dagger$):

$$\psi(\mathbf{r}) = \frac{1}{V^{1/2}} \sum_{\mathbf{q}} \exp(i\mathbf{q}\cdot\mathbf{r})\, c_{\mathbf{q}}, \qquad \psi^\dagger(\mathbf{r}) = \frac{1}{V^{1/2}} \sum_{\mathbf{q}} \exp(-i\mathbf{q}\cdot\mathbf{r})\, c_{\mathbf{q}}^\dagger \quad (7.4.19)$$

Using Eqs. (7.4.17) and (7.4.19), we can reexpress Eq. (7.4.6) as (Problem 7.4.3):

$$H_F = \sum_{\mathbf{k}} \sum_{\mathbf{q}} (V_q c_{\mathbf{k}+\mathbf{q}}^\dagger c_{\mathbf{k}} a_{\mathbf{q}} + V_q^* c_{\mathbf{k}}^\dagger c_{\mathbf{k}+\mathbf{q}} a_{\mathbf{q}}^\dagger), \qquad V_q \equiv A \left(\frac{\hbar}{2\omega_q}\right)^{1/2} iq \quad (7.4.20)$$

This is the *Fröhlich Hamiltonian.* Electrons describable in terms of $c_{\mathbf{k}}$'s are now coupled with phonons describable in terms of $a_{\mathbf{q}}$'s. The term

$$V_q c_{\mathbf{k}+\mathbf{q}}^\dagger c_{\mathbf{k}} a_{\mathbf{q}} \quad (V_q^* c_{\mathbf{k}}^\dagger c_{\mathbf{k}+\mathbf{q}} a_{\mathbf{q}}^\dagger)$$

can be interpreted as an interaction process in which a phonon is absorbed (emitted) by an electron as represented by the Feynman diagram[10] in Fig. 7.4 (a) [(b)]. Note: At each vertex the momentum is conserved. The Fröhlich H_F is applicable for longitudinal phonons only. As noted earlier, the transverse lattice normal modes generate no charge density variations, making the electron–transverse-phonon interaction negligible.

Problem 7.4.1. Verify Eq. (7.4.10).

Problem 7.4.2. Verify Eq. (7.4.14).

Problem 7.4.3. Verify Eq. (7.4.20).

7.5. PERTURBATION THEORY 1; THE DIRAC PICTURE

Most quantum problems cannot be solved exactly with the present resources of mathematics. For such problems we can often use a perturbation method. This consists of splitting the Hamiltonian into two parts, one of which must be simple and the other small. The first part may then be considered as the Hamiltonian of a simple or unperturbed system, and the addition of the second then gives rise to small corrections. If the perturbing Hamiltonian contains a small number-parameter λ, we can solve the equation of motion for the perturbed system in a power series in λ.

Suppose we have an unperturbed system characterized by a time-independent Hamiltonian H_0 and a perturbing Hamiltonian V, which can be an arbitrary function of the time t. The Hamiltonian H for the system is

$$H = H_0 + \lambda V(t) \tag{7.5.1}$$

where λ is the coupling constant (number). We assume that at the initial time 0 the system is distributed over various unperturbed states $\{\alpha\}$ with the probabilities $\{Q_\alpha\}$. The density operator corresponding to this distribution is given by

$$\rho(0) = \sum_\alpha |\alpha\rangle Q_\alpha \langle\alpha|, \qquad \sum_\alpha Q_\alpha = 1 \tag{7.5.2}$$

If there were no perturbation, this distribution would be stationary. The perturbation causes it to change. At a later time t, each Schrödinger ket $|\alpha\rangle$ will change, following the Schrödinger equation of motion:

$$i\hbar \frac{\partial}{\partial t}|\alpha, t\rangle = H|\alpha, t\rangle \tag{7.5.3}$$

It is convenient to introduce an evolution operator $U(t)$ such that

$$|\alpha, t\rangle = U(t)|\alpha, 0\rangle \equiv U(t)|\alpha\rangle, \qquad U(0) = 1 \tag{7.5.4}$$

where U satisfies

$$i\hbar \frac{d}{dt} U(t) = [H_0 + \lambda V(t)]U(t) \tag{7.5.5}$$

Each bra $\langle\alpha|$ changes to $\langle\alpha|U^\dagger(t)$. Then the density operator $\rho(t)$ at the time t will be

$$\rho(t) = \sum_\alpha U(t)|\alpha\rangle Q_\alpha \langle\alpha|U^\dagger(t) \tag{7.5.6}$$

The probability of the system being in a state α' is given by

$$\langle\alpha'|\rho(t)|\alpha'\rangle = \sum_\alpha P(\alpha', \alpha, t) Q_\alpha \tag{7.5.7}$$

$$P(\alpha', \alpha, t) \equiv |\langle\alpha'|U(t)|\alpha\rangle|^2 \tag{7.5.8}$$

Thus the problem of calculating the transition probability $P(\alpha', \alpha, t)$ is reduced to determining the probability amplitude $\langle\alpha'|U(t)|\alpha\rangle$.

We can simplify our calculation by working in the *Dirac Picture* (DP). Define

$$U_D(t) \equiv \exp\left(\frac{itH_0}{\hbar}\right) U(t) \tag{7.5.9}$$

After simple calculations we obtain (Problem 7.5.1)

$$i\hbar \frac{d}{dt} U_D(t) = \lambda V_D(t) U_D(t) \tag{7.5.10}$$

$$V_D(t) \equiv \exp\left(\frac{itH_0}{\hbar}\right) V(t) \exp\left(\frac{-itH_0}{\hbar}\right) \tag{7.5.11}$$

Equation (7.5.10) is more convenient to handle than Eq. (7.5.5) because Eq. (7.5.10) makes the change in U_D depend entirely on the perturbation V_D. From Eq. (7.5.9) we obtain

$$\langle \alpha' | U_D(t) | \alpha \rangle = \exp\left(\frac{itE_{\alpha'}}{\hbar}\right) \langle \alpha' | U(t) | \alpha \rangle \tag{7.5.12}$$

where E_α is the eigenvalue of H_0. Using Eqs. (7.5.8) and (7.5.12), we obtain

$$P(\alpha', \alpha, t) \equiv |\langle \alpha' | U_D(t) | \alpha \rangle|^2 \tag{7.5.13}$$

showing that U_D and U are equally good for determining the transition probability P.

From Eqs. (7.5.4) and (7.5.9) we obtain

$$U_D(0) = 1 \tag{7.5.14}$$

We can easily show (Problem 7.5.2) that the solution uniquely determined from Eqs. (7.5.10) and (7.5.14) is the solution of the following integral equation:

$$U_D(t) = 1 - i\lambda\hbar^{-1} \int_0^t d\tau V_D(\tau) U_D(\tau) \tag{7.5.15}$$

This equation allows a solution by iteration (Problem 7.5.3):

$$U_D(t) = 1 - i\lambda\hbar^{-1} \int_0^t d\tau V_D(\tau) + (-i\lambda\hbar^{-1})^2 \int_0^t d\tau \int_0^\tau d\tau' V_D(\tau) V_D(\tau') + \cdots \tag{7.5.16}$$

In some applications it is useful to retain only the first-order term in λ. The transition probability P is then given by

$$P(\alpha', \alpha, t) \cong \left(\frac{\lambda}{\hbar}\right)^2 \left| \int_0^t d\tau \langle \alpha | V_D(\tau) | \alpha' \rangle \right|^2 \tag{7.5.17}$$

The DP is very important in quantum theory. We briefly discuss its connection with the Schrödinger picture (SP). In the SP (see Appendix A) we have observables ξ_s and the time-dependent ket $|\psi, t\rangle_s$, which moves following the Schrödinger equation of motion. The expectation value of ξ at the time t is given by

$$\langle \xi \rangle_t \equiv {}_S\langle \psi, t | \xi_S | \psi, t \rangle_S \tag{7.5.18}$$

In the DP we define the Dirac ket $|\psi, t\rangle_D$ and the Dirac observables $\xi_D(t)$ by

$$|\psi, t\rangle_D \equiv e^{itH_0/\hbar} |\psi, t\rangle_S \tag{7.5.19}$$

$$\xi_D(t) \equiv e^{itH_0/\hbar} \xi_S e^{-itH_0/\hbar} \tag{7.5.20}$$

both of which change in time as follows: (Problem 7.5.4)

$$i\hbar\frac{d}{dt}|\psi,t\rangle_D = \lambda V_D(t)|\psi,t\rangle_D \tag{7.5.21}$$

$$i\hbar\frac{d}{dt}\xi_D(t) = [\xi_D, H_0] \tag{7.5.22}$$

The expectation value of ξ can be expressed in the standard form:

$$\boxed{\langle\xi\rangle_t \equiv {}_S\langle\psi,t|\xi_S|\psi,t\rangle_S = {}_D\langle\psi,t|\xi_D(t)|\psi,t\rangle_D.} \tag{7.5.23}$$

Problem 7.5.1. Derive Eq. (7.5.10) by using Eqs. (7.5.3) and (7.5.9).

Problem 7.5.2. (a) Assume Eq. (7.5.15) and verify Eq. (7.5.10). (b) Integrate Eq. (7.5.10) from 0 to t' and derive Eq. (7.5.15).

Problem 7.5.3. (a) Obtain the first-order and second-order solutions from Eq. (7.5.15). (b) Verify that the expansion solution [Eq. (7.5.16)] satisfies Eq. (7.5.15).

Problem 7.5.4. (a) Verify Eq. (7.5.21). (b) Verify Eq. (7.5.22).

7.6. SCATTERING PROBLEM; FERMI'S GOLDEN RULE

In this section we treat a scattering problem, by using the time-dependent perturbation method. (This method has a wide applicability because it can be applied to nonstationary problems.)

Suppose at the initial time $t = 0$, particles of momenta all nearly equal to a momentum $\mathbf{p}_0$ are distributed uniformly in the whole space except possibly in the neighborhood of the origin, where a fixed scatterer with a short-range potential $v(\mathbf{r})$ is located. Because of this perturbation v, the distribution of particles will change with time. After a long time and at a point far from the origin we may then observe a steady flux of particles with momentum $\mathbf{p}$ deflected by the potential. What will then be the intensity of this flux as a function of $\mathbf{p}$ and $\mathbf{p}_0$? We answer this question by the time-dependent perturbation method. Here we are interested in calculating the following transition probability [see Eq. (7.5.6)]:

$$P(\mathbf{p},\mathbf{p}_0,t) \equiv |\langle\mathbf{p}|U_D(t)|\mathbf{p}_0\rangle|^2 \tag{7.6.1}$$

Let us first consider the lowest (second) order approximation. From Eq. (7.5.15)

$$P(\mathbf{p},\mathbf{p}_0,t) \cong \left(\frac{\lambda}{\hbar}\right)^2 \left|\int_0^t d\tau\langle\mathbf{p}|V_D(\tau)|\mathbf{p}_0\rangle\right|^2 \tag{7.6.2}$$

In our problem the potential v does not depend on the time t. Thus from Eq. (7.5.9)

$$\langle \mathbf{p}|V_D(t)|\mathbf{p}_0\rangle = \exp\left[\frac{it(\epsilon-\epsilon_0)}{\hbar}\right]\langle \mathbf{p}|v|\mathbf{p}_0\rangle,\ \epsilon = \frac{p^2}{2m},\ \epsilon_0 = \frac{p_0^2}{2m} \tag{7.6.3}$$

$$\int_0^t d\tau \langle \mathbf{p}|V_D(\tau)|\mathbf{p}_0\rangle = \langle \mathbf{p}|v|\mathbf{p}_0\rangle \frac{\exp[it(\epsilon-\epsilon_0)/\hbar]-1}{i(\epsilon-\epsilon_0)/\hbar} \tag{7.6.4}$$

provided that $\epsilon \neq \epsilon_0$. Therefore the transition probability P becomes

$$\begin{aligned} P(\mathbf{p},\mathbf{p}_0,t) &= \left(\frac{\lambda}{\hbar}\right)^2 |\langle \mathbf{p}|v|\mathbf{p}_0\rangle|^2 \frac{\{\exp[i(\epsilon-\epsilon_0)t/\hbar]-1\}\{\exp[-i(\epsilon-\epsilon_0)t/\hbar]-1\}}{(\epsilon-\epsilon_0)^2/\hbar} \\ &= 2\left(\frac{\lambda}{\hbar}\right)^2 |\langle \mathbf{p}|v|\mathbf{p}_0\rangle|^2 \frac{1-\cos[(\epsilon-\epsilon_0)t/\hbar]}{(\epsilon-\epsilon_0)^2/\hbar} \end{aligned} \tag{7.6.5}$$

If ϵ differs appreciably from ϵ_0, this probability P is small and remains so for all t, which is required by the law of energy conservation. In fact the small perturbation λv is disregarded, and the energy h_0 is approximately equal to the total energy $h = h_0 + \lambda v$. Since this h is conserved, the energy h_0 must be approximately conserved. This means that if h_0 initially has the numerical value ϵ_0, the probability of its having a value different from ϵ_0 at any later time must be small. On the other hand if there exists a group of states $\{\mathbf{p}\}$ having nearly the same energy as ϵ_0, the probability of a transition to such a group can be quite large. In our scattering problem, there is a continuous range of states $\mathbf{p}$ having a continuous range of energy ϵ surrounding the value ϵ_0.

Let us now introduce a coarse-grained probability distribution function $P_c(\mathbf{p}, \mathbf{p}_0, t)$ and the density of states $\mathcal{D}(\mathbf{p})$ (see Section 2.3) such that the (relative) probability of a transition to a final group of states within the small range $\Delta^3 p$ given by

$$P_c(\mathbf{p},\mathbf{p}_0,t)\mathcal{D}(\hat{\mathbf{p}})\Delta^3 p \equiv \int_{\Delta^3 p} P(\mathbf{p}',\mathbf{p}_0,t)\mathcal{D}(\mathbf{p})d^3p' \tag{7.6.6}$$

where $\Delta^3 p$ is chosen such that the phase-space volume $V\Delta^3 p$ contains a large number of quantum states, and $\hat{\mathbf{p}}$ is a typical value in $\Delta^3 p$.

The momentum state $|\mathbf{p}\rangle$ may alternatively be characterized by energy ϵ and values of polar and azimuthal angles $(\theta, \phi) \equiv \omega : |\mathbf{p}\rangle \equiv |\epsilon, \omega\rangle$. Now the total probability of a transition to the final group of states $\mathbf{p}$ for which the ω have the value ω and the ϵ has any value (there will be a strong probability of its having a value near ϵ_0) will be given by

$$\begin{aligned} \int P(\mathbf{p},\mathbf{p}_0,t)d\epsilon &= 2\int_0^\infty d\epsilon |\langle \epsilon,\omega|v|\mathbf{p}_0\rangle|^2 \frac{1-\cos[(\epsilon-\epsilon_0)t/\hbar]}{(\epsilon-\epsilon_0)^2} \\ &= 2t\hbar^{-1}\int_{-\epsilon_0 t/\hbar}^\infty dx |\langle \epsilon+(\hbar x/t),\omega|v|\mathbf{p}_0\rangle|^2 \frac{1-\cos x}{x^2} \end{aligned} \tag{7.6.7}$$

where we set $\lambda = 1$. For large values of t, this expression reduces to

$$\int P(\mathbf{p}, \mathbf{p}_0, t)d\epsilon = 2\pi t\hbar^{-1}|\langle \epsilon, \omega|v|\mathbf{p}_0\rangle|^2 \qquad \left[\int_{-\infty}^{\infty} dx \frac{1-\cos x}{x^2} = \pi\right] \tag{7.6.8}$$

Thus the total probability up to the time t of the transition to a final group of states $\mathbf{p}$ for which the angles ω have the value ω is proportional to t. There is therefore a finite transition rate (transition probability per unit time) equal to

$$2\pi\hbar^{-1}|\langle \epsilon, \omega|v|\mathbf{p}_0\rangle|^2 = 2\pi\hbar^{-1}|\langle \mathbf{p}|v|\mathbf{p}_0\rangle|^2 \tag{7.6.9}$$

Recalling that the great contribution to this rate comes from the states having energy values near ϵ_0, we may write the transition rate as

$$\lim_{t\to\infty} \frac{P(\mathbf{p}, \mathbf{p}_0, t)}{t} = 2\pi\hbar^{-1}|\langle \mathbf{p}|v|\mathbf{p}_0\rangle|^2\delta(\epsilon - \epsilon_0) \tag{7.6.10}$$

We substitute this into Eq. (7.6.6) and obtain for the *transition rate* R:

$$R = P_c(\mathbf{p}, \mathbf{p}_0, t)\mathcal{D}(\mathbf{p})\Delta^3 p = 2\pi\hbar^{-1}\int_{\Delta^3 p} |\langle \mathbf{p}'|v|\mathbf{p}_0\rangle|^2\delta(\epsilon' - \epsilon_0)\mathcal{D}(\mathbf{p})\, d^3p' \tag{7.6.11}$$

Now the number of states in $\Delta^3 p$ can be expressed by

$$\mathcal{D}(\mathbf{p})\Delta^3 p = \int_{\Delta^3 p} \mathcal{D}(\mathbf{p})\, d^3p' = \int_{\Delta\epsilon} d\epsilon\, \mathcal{N}(\epsilon) \tag{7.6.12}$$

where $\mathcal{N}(\varepsilon)$ is the density of states in energy and $\Delta\epsilon$ the range of energy associated with the momenta in $\Delta^3 p$. Using this identity we obtain from Eq. (7.6.11) (Problem 7.6.1)

$$\boxed{R = 2\pi\hbar^{-1}|\langle \mathbf{p}|v|\mathbf{p}_0\rangle|^2\mathcal{N}_f(\epsilon_0),} \tag{7.6.13}$$

where the subscript f denotes the final state $\mathbf{p}$. For the approximations used in deriving Eqs. (7.6.8) and (7.6.9) be valid, the time t must be neither too small nor too large. It must be large compared with the duration of collision for the approximation evaluation of the integral leading to Eq. (7.6.7) to be valid. It must not be excessively large or else Eq. (7.6.2) will lose the meaning of a transition probability, since we could make the probability Eq. (7.6.7) greater than 1 by making t large enough. However there is no difficulty in t satisfying these restrictions simultaneously if the potential is weak and of short range. Equation (7.6.13) is called *Fermi's golden rule.*

Equation (7.6.13) is valid to the second order in λ. If the potential v is singular in a small region as for a hard-core potential, the Fourier transform of $v(r)$ does not exist. It is however possible to generalize the theory to obtain the following formula:

$$R = 2\pi\hbar^{-1}|\langle \mathbf{p}|T|\mathbf{p}_0\rangle|^2\mathcal{N}_f(\epsilon_0) \tag{7.6.14}$$

where T is the transition operator (see Ref. 9). The T-matrix elements $\langle \mathbf{p}|T|\ \mathbf{p}_0\rangle$ are finite for a hard-core potential, and Eq. (7.6.14) can be used.

Problem 7.6.1. Verify Eq. (7.6.13).

7.7. PERTURBATION THEORY 2; SECOND INTERMEDIATE PICTURE

We saw earlier in Sections 6.5–6.7 that quantum many-body problems can best be treated in the HP. This necessitates solving the equation of motion:

$$-i\hbar\frac{d}{dt}\xi(t) = [H,\xi] \tag{7.7.1}$$

A perturbation theory similar to that used to solve the Schrödinger evolution equation will be developed and discussed in the present section. Let us introduce a *second interaction* (*I*) *picture.* We define a new ket $|\psi, t\rangle_I$ and observables $\xi_I(t)$ by

$$|\psi,t\rangle_I \equiv e^{-itH_0/\hbar}|\psi\rangle_H \tag{7.7.2}$$

$$\xi_I(t) \equiv e^{-itH_0/\hbar}\xi_H(t)e^{itH_0/\hbar} \tag{7.7.3}$$

which change in time, following (Problem 7.7.1):

$$i\hbar\frac{d}{dt}|\psi,t\rangle_I = H_0|\psi,t\rangle_I \tag{7.7.4}$$

$$i\hbar\frac{d}{dt}\xi_I(t) = -\lambda[V_I(t),\xi_I(t)] \tag{7.7.5}$$

$$V_I(t) \equiv e^{-itH_0/\hbar}V(t)e^{itH_0/\hbar} \tag{7.7.6}$$

The expectation value $\langle\xi\rangle_t$ can be expressed in the standard form:

$$\langle\xi\rangle_t \equiv {}_S\langle\psi,t|\xi_S|\psi,t\rangle_S = {}_I\langle\psi,t|\xi_I(t)|\psi,t\rangle_I = {}_H\langle\psi|\xi_H(t)|\psi\rangle_H \tag{7.7.7}$$

To solve Eq. (7.7.5), we introduce script operators $\mathcal{V}_I$, which generate commutators acting on a quantum operator ξ such that

$$\mathcal{V}_I(t)\xi \equiv [V_I(t),\xi] = V_I\xi - \xi V_I \tag{7.7.8}$$

We can then rewrite Eq. (7.7.5) as

$$i\hbar\frac{d}{dt}\xi_I(t) = -\lambda\mathcal{V}_I(t)\xi_I(t), \qquad \xi_I(0) = \xi_H(0) = \xi_S \tag{7.7.9}$$

which can be converted into the following integral equation:

$$\xi_I(t) - \xi_I(0) = \xi_I(t) - \xi_S = i\lambda\hbar^{-1}\int_0^t d\tau\,\mathcal{V}_I(\tau)\xi_I(\tau) \tag{7.7.10}$$

By iteration we obtain

$$\xi_I(t) - \xi_S = i\lambda\hbar^{-1}\int_0^t d\tau\,\mathcal{V}_I(\tau)\xi_S + (i\lambda\hbar^{-1})^2\int_0^t d\tau_1\int_0^{\tau_1} d\tau_2\,\mathcal{V}_I(\tau_1)\mathcal{V}_I(\tau_2)\xi_S + \cdots \tag{7.7.11}$$

Consider a physical property of the form:

$$X = \sum_j \xi^{(j)} \tag{7.7.12}$$

In the HP the variable $X(t)$ changes with the time t following the Heisenberg equation of motion [Eq. (7.7.1)] and the system density operator ρ is stationary. Thus, we may solve Eq. (7.7.1) by the perturbation method and compute the average $\langle X \rangle_t$ via

$$\langle X \rangle_t \equiv \mathrm{Tr}\{X(t)\rho\} = \mathrm{tr}\{\xi(t)n\} \tag{7.7.13}$$

In nonequilibrium quantum statistical mechanics,[9] it is conventional to carry out the computations in the SP, where the system density operator $\rho(t)$ changes in time following the quantum Liouville equation (6.6.13). Then the time-dependent average $\langle X \rangle_t$ can be computed from

$$\langle X \rangle_t \equiv \mathrm{Tr}\{X\rho(t)\} = \mathrm{tr}\{\xi n(t)\} \tag{7.7.14}$$

If the Hamiltonian H is the sum of single-particle Hamiltonian h:

$$H = \sum_j h^{(j)} \tag{7.7.15}$$

then the one-body density operator $n(t)$ defined through [see Eqs. (6.6.6) and (6.6.7)]

$$n_{ba}(t) \equiv \langle \alpha_b | n(t) | \alpha_a \rangle \equiv \mathrm{Tr}\{\eta_a^\dagger \eta_b \rho(t)\} \tag{7.7.16}$$

changes in time following the one-body quantum Liouville equation:

$$i\hbar \frac{\partial n(t)}{\partial t} = [h, n] \tag{7.7.17}$$

Equation (7.7.17) is the same except for the sign as the Heisenberg equation of motion, implying that a similar perturbation method can be used for its solution.

The statistical mechanical method of computing the average $\langle X \rangle_t$ with Eq. (7.7.14) rather than Eq. (7.7.13) has an advantage, since we solve an evolution equation for $n(t)$ only once instead of solving the equation of motion for $\xi(t)$ each time. This method has disadvantages, too. If the Hamiltonian H for the system is not of the form in Eq. (7.7.15), then the evolution equation for $n(t)$ is more complicated than Eq. (7.7.17), and it may be hard to solve. Thus choosing the computation method depends on the physical problem at hand.

Problem 7.7.1. Verify Eqs. (7.7.4) and (7.7.5).

7.8. ELECTRON-IMPURITY SYSTEM; THE BOLTZMANN EQUATION

Let us consider a system of electrons moving independently in a potential field of impurities acting as scatterers. The impurities by assumption are distributed uniformly in space. We introduce a momentum distribution function $\varphi(\mathbf{p}, t)$ such that

$$\varphi(\mathbf{p}, t)\, d^3p \equiv \text{the probability of finding an electron in } d^3p \text{ at time } t \tag{7.8.1}$$

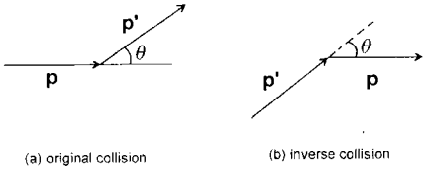

Figure 7.5. In (a) the electron suffers the change in momentum from **p** to **p'** after scattering. The inverse collision is shown in (b).

This function φ will be normalized such that

$$(2\pi\hbar)^{-3}\int d^3p\,\varphi(\mathbf{p},t)=\frac{N}{V}\equiv n \tag{7.8.2}$$

The *electric current density* **j** is given in terms of φ as follows:

$$\mathbf{j}\equiv-\left(\frac{e}{m^*}\right)(2\pi\hbar)^{-3}\int d^3p\,\mathbf{p}\,\varphi(\mathbf{p},t) \tag{7.8.3}$$

The function φ can be obtained by solving the Boltzmann equation, which may be set up as follows. The change in the distribution function φ will be caused by the force acting on the electrons and by collision. We may write this change in the form:

$$\frac{\partial\varphi}{\partial t}=\left(\frac{d\varphi}{dt}\right)_{\text{force}}+\left(\frac{d\varphi}{dt}\right)_{\text{collision}} \tag{7.8.4}$$

The *force term* $(d\varphi/dt)_{\text{force}}$, caused by the force–$e\mathbf{E}$, is given by (Problem 7.8.1):

$$\left(\frac{d\varphi}{dt}\right)_{\text{force}}=-e\mathbf{E}\cdot\frac{\partial\varphi}{\partial\mathbf{p}} \tag{7.8.5}$$

If the density of impurities n_I is low and the interaction between electron and impurity has a short range, each electron will be scattered by one impurity at a time. We may then write the *collision term* in the following form:

$$\left(\frac{d\varphi}{dt}\right)_{\text{collision}}=\int d\Omega\frac{p}{m}n_I I(p,\theta)[\varphi(\mathbf{p}',t)-\varphi(\mathbf{p},t)] \tag{7.8.6}$$

where θ is the *angle of deflection,* i.e., the angle between the initial and final momenta (**p, p'**), as indicated and Fig. 7.5; $I(p, \theta)$ is the differential cross section. In fact the rate of collision is given by the rule: (density of scatterers) × (speed) × (total cross section). If we apply this rule to the flux of particles with momentum **p**, we obtain the second integral of Eq. (7.8.6), the integral with the minus sign. This integral corresponds to the *loss* of flux due to collision. The flux of particles with momentum **p** can *gain* by the *inverse collision,* which is shown in Fig. 7.5(b). The contribution of the inverse collision is represented by the first integral.

So far we have neglected the fact that electrons are fermions. We now look at the effect of quantum statistics. If the final momentum state **p'** was already occupied, the scattering into the state **p'** should not occur. The probability of this scattering therefore must be reduced by the *quantum statistical factor* $1-\varphi(\mathbf{p}', t)$, which represents the

probability that the final state $\mathbf{p}'$ is unoccupied. Pauli's exclusion principle modifies the collision term to

$$\left(\frac{d\varphi}{dt}\right)_{\text{collision}} = \int d\Omega \frac{p}{m} n_I I(p,\theta)\{\varphi(\mathbf{p}',t)[1-\varphi(\mathbf{p},t)] - \varphi(\mathbf{p},t)[1-\varphi(\mathbf{p}',t)]\} \tag{7.8.7}$$

When expanded, the two terms proportional to $\varphi(\mathbf{p},t)\varphi(\mathbf{p}',t)$ in the curly brackets have opposite signs and cancel one other. We then have the same collision term as Eq. (7.8.6).

Gathering the results from Eqs. (7.8.4)–(7.8.6), we obtain

$$\frac{\partial\varphi(\mathbf{p},t)}{\partial t} + (e\mathbf{E})\cdot\frac{\partial\varphi(\mathbf{p},t)}{\partial\mathbf{p}} = n_I \int d\Omega \frac{p}{m} I(p,\theta)[\varphi(\mathbf{p}',t) - \varphi(\mathbf{p},t)] \tag{7.8.8}$$

This is the *Boltzmann equation* for the electron-impurity system.

The usefulness of this equation is well-known.[9] In particular we can solve Eq. (7.8.8) exactly for a small electric field to obtain an expression for the electrical conductivity σ:

$$\sigma = \frac{-e^2}{(2\pi\hbar)^3 m^{*2}} \int d^3p \frac{p_x^2}{\Gamma(p)} \left(\frac{df_F}{d\epsilon_p}\right) \tag{7.8.9}$$

$$\Gamma(p) \equiv \frac{n_I}{m^*} \int d\Omega p I(p,\theta)(1-\cos\theta) > 0 \tag{7.8.10}$$

$\Gamma(p)$ is called the *current relaxation rate.* Earlier in Section 2.6 we discussed the electrical conductivity σ by using a simple kinetic theory. Formula (7.8.9) is a more rigorous result obtained by the Boltzmann equation method. We can show (Problem 7.8.2) that the conductivity due to the neutral impurities is independent of the temperature.

Problem 7.8.1. Derive the force term in Eq. (7.8.5). Use Eq. (7.7.17) and assume a small field **E.**

Problem 7.8.2. Compute the conductivity σ from Eq. (7.8.9) with the assumption that I = constant, and compare the result with $\sigma = e^2 m^{*-1} n_I \tau_f$.

7.9. DERIVATION OF THE BOLTZMANN EQUATION

As an application of the many-body perturbation method, we derive the Boltzmann equation (7.8.8). Let us consider an electron–impurity system characterized by

$$H = \sum_{j=1}^{N} \epsilon(\mathbf{p}_j) + \lambda \sum_j \sum_{\alpha=1}^{N_I} \tilde{v}(\mathbf{r}_j - \mathbf{R}_\alpha) \equiv \sum_j (h_0^{(j)} + \lambda \sum_\alpha \tilde{v}_\alpha^{(j)}) \equiv \sum_j h^{(j)} \tag{7.9.1}$$

where the impurity positions $\{\mathbf{R}_\alpha\}$ are fixed. This Hamiltonian H is the sum of single-electron Hamiltonians:

$$h \equiv h_0 + \lambda v \equiv h_0 + \lambda \tilde{v}_\alpha^{(j)} \tag{7.9.2}$$

The density operator $n(t)$ therefore obeys the one-body quantum Liouville equation:

$$\frac{\partial n(t)}{\partial t} = -\frac{i}{\hbar}[h, n] \equiv -\frac{i}{\hbar}\mathcal{h}\, n \tag{7.9.3}$$

where the commutator-generating script operator $\mathcal{h}$, called the *quantum Liouville operator,* is introduced in the third member of the equations.

From the general theory described in Section 6.6, the diagonal elements of the density matrix in the momentum space yield a momentum distribution function:

$$\langle \mathbf{p}|n(t)|\mathbf{p}\rangle = \varphi(\mathbf{p}, \{\mathbf{R}_\alpha\}) \tag{7.9.4}$$

Since our Hamiltonian h in Eq. (7.9.2) contains the impurity configuration $\{\mathbf{R}_\alpha\}$, we indicated this dependence in this expression.

To compute the electric current, the momentum distribution averaged over the (uniform) impurity configuration, denoted by

$$\bar{\varphi}(\mathbf{p}) \equiv \langle \varphi(\mathbf{p}, \{R_\alpha\})\rangle_{\text{av}} \tag{7.9.5}$$

is required. Let us take momentum-diagonal elements of Eq. (7.9.3) and apply impurity averaging. Noting that

$$\langle \mathbf{p}|[h_0, n]|\mathbf{p}\rangle = \langle \mathbf{p}|(h_0 n - n h_0)|\mathbf{p}\rangle = 0 \tag{7.9.6}$$

we obtain

$$\frac{\partial \bar{\varphi}(\mathbf{p}, t)}{\partial t} = -\frac{i}{\hbar}\langle \mathbf{p}|\langle v\, n\rangle_{\text{av}}|\mathbf{p}\rangle \tag{7.9.7}$$

which is similar to Eq. (7.8.8) but not quite the same. Since we assumed no electric fields, there is no term proportional to $\mathbf{E}$ in Eq. (7.9.7) (see Problem 7.9.1).

The Liouville equation (7.9.3) can be solved formally, yielding:

$$n(t) = \exp(-i\hbar^{-1}\mathcal{h}\, t)\, n(0) \equiv \exp[-i\hbar^{-1}(\mathcal{h}_0 + \lambda v)t]\, n(0) \tag{7.9.8}$$

Using the identity [see Eq. (7.5.15)]:

$$e^{-it\hbar^{-1}\mathcal{h}} = e^{-it\hbar^{-1}\mathcal{h}_0} - i\frac{\lambda}{\hbar}\int_0^t d\tau e^{-i(t-\tau)\hbar^{-1}\mathcal{h}_0} v\, e^{-i\tau\hbar^{-1}\mathcal{h}} \tag{7.9.9}$$

and Eq. (7.9.8), we obtain

$$v\, n(t) = \lambda v e^{-it\hbar^{-1}\mathcal{h}_0} n(0) - i\frac{\lambda^2}{\hbar} v \int_0^t d\tau\, e^{-i(t-\tau)\hbar^{-1}\mathcal{h}_0} v\, n(\tau) \tag{7.9.10}$$

We now substitute Eq. (7.9.10) in Eq. (7.9.7). The linear term in λ should make no contribution, since the effect of the impurity scattering starts with the second order, as we saw in Section 7.6. The double sum coming from the second term in Eq. (7.9.10)

$$\lambda^2 \sum_{\alpha}\sum_{\neq\gamma} \tilde{v}_\alpha \cdots \tilde{v}_\gamma n(\tau) \tag{7.9.11}$$

can be dropped for the same reason. Let us now examine a quantity of the form:

$$A(\mathbf{p}_1, \mathbf{p}_2) = \langle \mathbf{p}_1 | \sum_\alpha \tilde{v}_\alpha a \tilde{v}_\alpha | \mathbf{p}_2 \rangle = \int d^3 p \tilde{v}_{13} a(\mathbf{p}_3) \tilde{v}_{32} \sum_\alpha e^{-i\hbar^{-1}(\mathbf{p}_1 - \mathbf{p}_2)\cdot \mathbf{R}_\alpha} \quad (7.9.12)$$

where a is a quantity independent of the impurity configuration. If we assume a uniform impurity distribution, we may replace the sum over the impurity configuration $\{\mathbf{R}_\alpha\}$ by the following average:

$$\left\langle \sum_{\alpha=1}^{N_I} f(\mathbf{R}_\alpha) \right\rangle_{\text{av}} \to \frac{N_I}{V} \int d^3 R f(\mathbf{R}) \equiv n_I \int d^3 R f(\mathbf{R}) \quad (7.9.13)$$

Using this procedure, we find that

$$\left\langle \sum_\alpha \exp([i\hbar^{-1}(\mathbf{p}_1 - \mathbf{p}_2)\cdot \mathbf{R}_\alpha]) \right\rangle_{\text{av}} = n_I V \delta^{(3)}_{\mathbf{p}_1, \mathbf{p}_2} \quad (7.9.14)$$

meaning that the diagonal elements $A(\mathbf{p}_1, \mathbf{p}_1)$ are finite and proportional to the impurity density n_I, while nondiagonal elements are vanishingly small. We therefore obtain

$$\langle A(\mathbf{p}_1, \mathbf{p}_2) \rangle = n_I \int d^3 p_3 \tilde{v}_{13} a(\mathbf{p}_3) \tilde{v}_{32} \delta^{(3)}_{\mathbf{p}_1, \mathbf{p}_2} \quad (7.9.15)$$

The quantum Liouville operator $\tilde{v}_\alpha$ is linear in the quantum operator $\tilde{v}_\alpha$. Thus Eq. (7.9.15) can be extended to $\tilde{v}_\alpha$. Using Eqs. (7.9.10) and (7.9.15), we obtain from Eq. (7.9.7):

$$\frac{\partial \bar{\varphi}(\mathbf{p}, t)}{\partial t} = -\lambda^2 \hbar^{-2} \left\langle \mathbf{p} \left| \int_0^t d\tau \left\langle \sum_\alpha \tilde{v}_\alpha e^{-i\tau \hbar^{-1} \hbar_0} \tilde{v}_\alpha n(t - \tau) \right\rangle_{\text{av}} \right| \mathbf{p} \right\rangle \quad (7.9.16)$$

The scattering by a fixed impurity is a local event in space and time. The duration of scattering τ_d is much shorter than the mean free time τ_f:

$$\tau_d \ll \tau_f \quad (7.9.17)$$

We may then use the following Markoffian approximation to calculate the rhs of Eq. (7.9.16): we replace $n(t - \tau)$ by $n(t)$ and extend the time (τ) limit to ∞. We then obtain

$$\frac{\partial \bar{\varphi}(\mathbf{p}, t)}{\partial t} = i\lambda^2 \hbar^{-1} \left\langle \mathbf{p} \left| \left\langle \sum_\alpha \tilde{v}_\alpha \frac{1}{\hbar_0 - ia} \tilde{v}_\alpha n(t) \right\rangle_{\text{av}} \right| \mathbf{p} \right\rangle \quad (7.9.18)$$

which is a Markoffian equation. Here a is a small positive constant, which will be set to equal zero at the end of the calculation. (The operator $\hbar_0$ does not have an inverse.) Equation (7.9.18) contains quantum liouville operators $\hbar_0, \tilde{v}_\alpha, v$. Algebras systematically handling these operators are discussed in Appendix D. After straightforward calculations, we can transform Eq. (7.9.18) into

$$\frac{\partial \bar{\varphi}(\mathbf{p}, t)}{\partial t} = \frac{2\pi\lambda^2}{\hbar} n_I \int d^3 p' |v(|\mathbf{p} - \mathbf{p}'|)|^2 [\bar{\varphi}(\mathbf{p}', t) - \bar{\varphi}(\mathbf{p}, t)] \delta(\epsilon_p - \epsilon_{p'}) \quad (7.9.19)$$

This equation can be rewritten in the standard form of a Boltzmann equation:

$$\frac{\partial \varphi(\mathbf{p},t)}{\partial t} = n_I \int d\Omega \frac{p}{m} I(p,\theta)[\varphi(\mathbf{p}',t) - \varphi(\mathbf{p},t)] \tag{7.9.20}$$

$$I(p,\theta)d\Omega \equiv \frac{2\pi}{\hbar}(2\pi\hbar)^3 m^2 |\langle \mathbf{p}|\tilde{v}|\mathbf{p}'\rangle|^2 d\Omega \tag{7.9.21}$$

The detailed derivation of Eqs. (7.9.18)–(7.9.21) are given in Appendix D.

In summary we derived the Boltzmann equation (7.9.20) from the Liouville equation (7.9.3) by using a uniform impurity averaging, weak-coupling, and Markoffian approximations. The impurity averaging represented by Eq. (7.9.13) is important; it allowed us to select the collision term linear in the impurity density n_I. The use of quantum Liouville operators $(\hbar, \hbar_0, v)$ is noted. It allowed us to treat the time-dependent quantum problem simply. In particular the loss and gain collision terms in Eq. (7.8.6) were obtained simultaneously.

Problem *7.9.1.* Assume that a uniform electric field **E** is applied along the *x*-axis. The potential energy $\phi(x) = eEx$ may be assumed. (a) Write down the Hamiltonian including this energy. (b) Derive a quantum Liouville equation for the electron–impurity system [a generalization of Eq. (7.9.3)]. (c) Derive the Boltzmann equation (7.8.8).

7.10. PHONON-EXCHANGE ATTRACTION

By exchanging a phonon, two electrons can gain an attraction under a certain condition. In this section we treat this effect by using the many-body perturbation method.

Let us consider an *electron—phonon system* characterized by

$$\begin{aligned} H &= \sum_{\mathbf{k}}\sum_{s} \epsilon_k c^\dagger_{\mathbf{k}s} c_{\mathbf{k}s} + \sum_{\mathbf{q}} \hbar\omega_q \left(\frac{1}{2} + a^\dagger_{\mathbf{q}} a_{\mathbf{q}}\right) + \lambda \sum_{\mathbf{k}}\sum_{s}\sum_{\mathbf{q}} (V_q a_{\mathbf{q}} c^\dagger_{\mathbf{k}+\mathbf{q}s} c_{\mathbf{k}s} + \text{h.c.}) \\ &\equiv H_{el} + H_{ph} + \lambda V_F \equiv H_0 + \lambda V, \qquad (V \equiv V_F) \end{aligned} \tag{7.10.1}$$

where the three sums represent the total electron kinetic energy (H_{el}), the total phonon energy (H_{ph}), and the Fröhlich interaction Hamiltonian (V_F), respectively [see Eq. (7.4.20)].

For comparison we consider an *electron-gas system* characterized by the Hamiltonian:

$$H_C = \sum_{\mathbf{k}}\sum_{s} \epsilon_k c^\dagger_{\mathbf{k}s} c_{\mathbf{k}s} + \frac{1}{2}\sum_{\mathbf{k}_1 s_1} \cdots \sum_{\mathbf{k}_4 s_4} \langle 34|v_C|12\rangle c^\dagger_4 c^\dagger_3 c_1 c_2 \equiv H_{el} + V_C \tag{7.10.2}$$

$$\begin{aligned} \langle 34|v_C|12\rangle &\equiv \langle \mathbf{k}_3 s_3 \mathbf{k}_4 s_4 |v_C| \mathbf{k}_1 s_1 \mathbf{k}_2 s_2\rangle = \langle \mathbf{k}_3 \mathbf{k}_4 |v_C| \mathbf{k}_1 \mathbf{k}_2\rangle \delta_{s_3 s_1}\delta_{s_4 s_2} \\ &\equiv (4\pi e^2 k_0/V) q^{-2} \delta_{\mathbf{k}_1+\mathbf{k}_2, \mathbf{k}_3+\mathbf{k}_4} \delta_{\mathbf{k}_1-\mathbf{k}_3, \mathbf{q}} \delta_{s_3 s_1}\delta_{s_4 s_2} \end{aligned} \tag{7.10.3}$$

The elementary interaction process may be represented by the diagram in Fig. 7.6. The wavy horizontal line represents the instantaneous Coulomb interaction v_C. The net momentum of a pair of electrons is conserved:

$$\mathbf{k}_1 + \mathbf{k}_2 = \mathbf{k}_3 + \mathbf{k}_4 \tag{7.10.4}$$

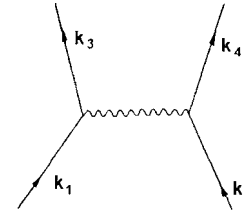

Figure 7.6. The Coulomb interaction represented by the horizontal wavy line generates the change in the momenta of two electrons.

as seen by the appearance of the Kronecker's delta in Eq. (7.10.3). Physically the Coulomb force between a pair of electrons is an internal force, and therefore it cannot change the net momentum.

We wish to find an *effective interaction* Hamiltonian v_e between a pair of electrons generated by a phonon exchange. If we look for this v_e in the second order in the coupling constant λ, the likely candidates may be represented by two Feynman diagrams in Fig. 7.7. Here time is measured upward. (Historically, Feynman represented the elementary interaction processes in the DP by diagrams. Such a diagram representation is very popular and widely used in quantum field theory.[10]) In the diagrams in Fig. 7.7, we follow the motion of two electrons. We may therefore consider a system of two electrons and obtain the effective Hamiltonian v_e by studying of the evolution of the two-electron density operator ρ_2. For brevity we shall hereafter drop the subscript 2 on ρ indicating *two*-body system.

The system density operator $\rho(t)$ changes in time, following the Liouville equation:

$$i\hbar \frac{\partial \rho(t)}{\partial t} = [H, \rho] \equiv \mathcal{H} \rho \tag{7.10.5}$$

We assume the Hamiltonian H in Eq. (7.10.1), and study the time evolution of the two-electron density operator $\rho_2(t)$, using quantum many-body perturbation theory. This study is similar to the previously treated case of the derivation of the Boltzmann equation. Therefore we sketch only the important steps; more detailed calculations are given in Appendix D.

Let us introduce a quantum Liouville operator:

$$\mathcal{H} \equiv \mathcal{H}_0 + \lambda \mathcal{V} \tag{7.10.6}$$

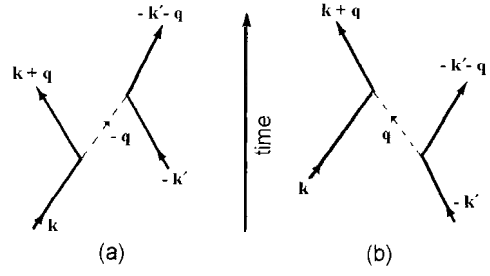

Figure 7.7. A one-phonon exchange process generates the change in the momenta of two electrons similar to that caused by the Coulomb interaction.

corresponding to $H = H_0 + \lambda V$ in Eq. (7.10.1). We assume that the initial-density operator ρ_0 for the combined electron–phonon system can be written as

$$\rho_0 = \rho_{\text{electron}}\,\rho_{\text{phonon}} \tag{7.10.7}$$

which is reasonable in the low-temperature limit ($T \to 0$), where no real phonons are present. In fact only virtual phonons are involved in the dynamic processes. We can then choose

$$\rho_{\text{phonon}} = |0\rangle\langle 0| \tag{7.10.8}$$

where $|0\rangle$ is the vacuum-state ket for phonons:

$$a_{\mathbf{q}}|0\rangle = 0 \text{ for any } \mathbf{q} \tag{7.10.9}$$

The phonon vacuum average will be denoted by an upper bar or angular brackets:

$$\bar{\rho}(t) \equiv \langle 0|\rho(t)|0\rangle \equiv \langle \rho(t)\rangle_{\text{av}} \tag{7.10.10}$$

Using a time-dependent perturbation theory and taking a phonon average, we obtain from Eq. (7.10.5) [compare to Eq. (7.9.16)]:

$$\frac{\partial \bar{\rho}(t)}{\partial t} = -\lambda^2\hbar^{-2}\int_0^t d\tau \langle \mathcal{V}\exp[-i\tau\hbar^{-1}\mathcal{H}_0]\mathcal{V}\rho(t-\tau)\rangle_{\text{av}} \tag{7.10.11}$$

In the weak-coupling approximation, we may calculate the phonon exchange effect to the lowest (second) order, so that

$$\lambda^2\langle \mathcal{V}\exp[-i\tau\hbar^{-1}\mathcal{H}_0]\mathcal{V}\rho(t-\tau)\rangle = \lambda^2\langle \mathcal{V}\exp[-i\tau\hbar^{-1}\mathcal{H}_0]\mathcal{V}\rangle_{\text{av}}\bar{\rho}(t-\tau) \tag{7.10.12}$$

In the Markoffian approximation we may replace $\bar{\rho}(t-\tau)$ by $\bar{\rho}(t)$and take the limit of the τ-integration to ∞. Using these two approximations, we obtain from Eq. (7.10.11)

$$\frac{\partial \bar{\rho}(t)}{\partial t} = i\lambda^2\hbar^{-1}\lim_{a\to 0}\langle \mathcal{V}\,[\mathcal{H}_0 - ia]^{-1}\mathcal{V}\rangle_{\text{av}}\bar{\rho}(t) \tag{7.10.13}$$

Let us now take momentum-state matrix elements of Eq. (7.10.13). The lhs is

$$\frac{\partial}{\partial t}\langle \mathbf{k}_1 s_1, \mathbf{k}_2 s_2|\rho(t)|\mathbf{k}_3 s_3, \mathbf{k}_4 s_4\rangle \equiv \frac{\partial}{\partial t}\rho(1,2;3,4,t) \tag{7.10.14}$$

where we dropped the upper bar indicating the phonon average. The ρ is called the *two-electron density matrix* in the momentum space. The rhs requires more sophisticated computations, since the Liouville operators $(\mathcal{V}, \mathcal{H}_0)$ are involved. After lengthy but straightforward calculations, we obtain from Eq. (7.10.13) (see Appendix D)

$$\begin{aligned}\frac{\partial}{\partial t}\rho(1,2;3,4,t) = \sum_{\mathbf{k}_5 s_5}\sum_{\mathbf{k}_6 s_6} -i\hbar^{-1}[&\langle 1,2|v_e|5,6\rangle\rho(5,6;3,4,t)\\ &-\langle 5,6|v_e|3,4\rangle\rho(1,2;5,6,t)]\end{aligned} \tag{7.10.15}$$

$$\langle 34|v_e|12\rangle \equiv |V_q|^2\frac{\hbar\omega_q}{(\epsilon_3-\epsilon_1)^2-\hbar^2\omega_q^2}\delta_{\mathbf{k}_1+\mathbf{k}_2,\mathbf{k}_3+\mathbf{k}_4}\delta_{\mathbf{k}_3-\mathbf{k}_1,q}\delta_{s_3 s_1}\delta_{s_4 s_2} \tag{7.10.16}$$

Kronecker's delta $\delta_{\mathbf{k}_1+\mathbf{k}_2,\mathbf{k}_3+\mathbf{k}_4}$ in Eq. (7.10.16) means that the net momentum is conserved, since the phonon-exchange interaction is an internal interaction.

For comparison consider the electron-gas system characterized by the Hamiltonian H_C in Eq. (7.10.2). The two-electron density matrix ρ^c for this system changes like

$$\frac{\partial}{\partial t}\rho^c(1,2;3,4,t) = \sum_{\mathbf{k}_5 s_5}\sum_{\mathbf{k}_6 s_6} -i\hbar^{-1}[\langle 1,2|v_c|5,6\rangle\rho^c(5,6;3,4,t) - \langle 5,6|v_c|3,4\rangle\rho^c(1,2;5,6,t)] \tag{7.10.17}$$

which is of the same form as Eq. (7.10.15). The only differences are in the interaction matrix elements. Comparison between Eqs. (7.10.3) and (7.10.16) yields

$$\left(\frac{4\pi e^2 k_0}{V}\right)\frac{1}{q^2} \qquad \text{(Coulomb interaction)}$$

$$|V_q|^2\frac{\hbar\omega_q}{(\epsilon_{\mathbf{k}_1+\mathbf{q}}-\epsilon_{\mathbf{k}_1})^2-\hbar^2\omega_q^2}. \qquad \text{(phonon-exchange interaction)} \tag{7.10.18}$$

In our derivation, the weak-coupling and the Markoffian approximation is justified in the steady state of the electron–phonon system in which the effect of the duration of interaction can be neglected. The electron mass is at least three orders of magnitude smaller than the lattice-ion mass, and therefore the coupling between the electron and ionic motion should be smaller by the mass mismatch. The concept of such a mass mismatch holds in general. In quantum electrodynamics,[9] the electron–photon interaction is represented by terms bilinear in the electron field operators and linear in the photon field operators with a strength *e,* similar to the electron–photon interaction. These two fields are coupled very weakly such that the interaction between two electrons [Eq. (7.4.6)] can be represented by the Coulomb interaction proportional to e^2 in spite of the fact that the photon field can create and annihilate electron–positron pairs any number of times. This is experimentally supported, for example, by the fact that the Coulomb interaction between two electrons and that between two protons are mutually equal within a great precision. That is, the weak coupling approximation is excellent for the photon-exchange interaction since the photon has zero mass. Besides, the Fröhlich electron–phonon interaction is linear in the lattice-vibration amplitude proportional to $(1 + N_q)^{1/2}$ with N_q denoting the phonon number,[9] which is smallest at 0 K ($N_q = 0$). Thus expression (7.10.18) is highly accurate for the effective phonon-exchange interaction at 0 K. This expression has two remarkable features. First note that it depends on the phonon energy $\hbar\omega_q$. Second the sign of the interaction can change. If

$$|\epsilon_{\mathbf{k}_1+\mathbf{q}} - \epsilon_{\mathbf{k}_1}| > \hbar\omega_q \tag{7.10.19}$$

the effective interaction is r*epulsiv*e just as the repulsive Coulomb interaction. If

$$|\epsilon_{\mathbf{k}_1+\mathbf{q}} - \epsilon_{\mathbf{k}_1}| < \hbar\omega_q \tag{7.10.20}$$

the effective interaction is a*ttractive*. In such a case, a bound electron pair may be formed as demonstrated by Cooper,[13] which will be discussed later in Sections 8.3–8.4.

REFERENCES

1. P. Debye and E. Hückel, *Phys. Z.* **24,** 185, 305 (1923).
2. L. H. Thomas, *Proc. Cambr. Phil. Soc.* **23,** 542 (1927); E. Fermi, *Z. Phys.* **48,** 73 (1928); **49,** 550 (1927).
3. P. Debye, *Ann. Physik* **39,** 789 (1912).
4. For example, H. Goldstein, *Classical Mechanics* (Addison-Wesley, Reading, MA, 2d ed., 1980).
5. C. B. Walker, *Phys. Rev.* **103,** 547 (1956).
6. L. Van Hove, *Phys. Rev.* **89,** 1189 (1953).
7. H. Fröhlich, *Phys, Rev.* **79,** 845 (1950); *Proc. R. Soc. London* **A215,** 291 (1950).
8. For example, W. A. Harrison, *Solid-State Theory* (Dover, New York, 1980), pp. 390-93.
9. P. A. M. Dirac, *Principles of Quantum Mechanics,* 4th ed. (Oxford University Press, London, 1958).
10. R. P. Feynman, *Statistical Mechanics* (Addison-Wesley, Reading, MA, 1972); *Quantum Electrodynamics* (Addison-Wesley, Reading, MA, 1961).
11. S. Fujita, *Introduction to Nonequilibrium Quantum Statistical Mechanics,* reprint ed. (Krieger, Malabar, FL, 1983).
12. S. Fujita, *Statistical and Thermal Physics,* part 2 (krieger, Malabar, FL, Ch. 13, 1986).
13. L. N. Cooper, *Phys. Rev.* **104,** 1189 (1956).

8

Superconductors at 0 K

We consider a system of electrons characterized by a generalized BCS Hamiltonian that contains the kinetic energies of electrons and holes and the pairing interaction Hamiltonian arising from phonon-exchange attraction and interelectronic repulsion. If we drop holes from this Hamiltonian, we obtain the Cooper Hamiltonian. In the system characterized by the Cooper Hamiltonian, a bound Cooper pair having antiparallel spins and charge $-2e$ is found. Such a bound quasi-particle, called a pairon, has a linear energy-momentum (Cooper–Schrieffer) relation:

$$w_q = w_0 + \frac{v_F q}{2}, \qquad w_0 = -2\hbar\omega_D \left\{ \exp\left[\frac{2}{v_0 \mathcal{N}(0)} \right] - 1 \right\}^{-1}, \qquad \hbar\omega_D = k_B \Theta_D$$

where $\mathcal{N}(0)$ is the density of states per spin orientation at the Fermi energy and v_0 a positive constant characterizing the phonon-exchange attraction. We follow the original BCS theory to construct a many-pairon ground state of the generalized BCS system, and find a ground-state energy: $W = \hbar\omega_D \mathcal{N}(0) w_0$. In the ground state, all pairons having $\pm 2e$ are condensed at zero momentum. An energy gap Δ is found in the quasi-electron excitation spectrum $E_k \equiv (\epsilon_k + \Delta^2)^{1/2}$.

8.1. INTRODUCTION

The basic experimental facts on superconductors were enumerated in Section 1.1. The purpose of a microscopic theory is to explain all of these facts from first principles, starting with a reasonable Hamiltonian. Besides we must answer such basic questions as:

- What causes superconductivity? The answer is the phonon-exchange attraction. We have discussed this interaction in Chapter 7. It generates Cooper pairs, called pairons for short, under certain conditions.
- Why do impurities not hinder the supercurrent? Why is the supercurrent stable against an applied voltage. Why does increasing the magnetic field destroy the supercurrent?
- Why does the supercurrent flow in the surface layer? Why does the supercurrent dominate the normal current in the steady state?

- What is the supercondensate whose motion generates the supercurrent? How does magnetic-flux quantization arise? Josephson interference indicates that two supercurrents can interfere macroscopically just as two lasers from the same source. Where does this property come from?

- Below the critical temperature T_c, there is a profound change in the behavior of the electrons by the appearance of a temperature-dependent energy gap $\Delta(T)$. This was shown by BCS in their classic work.[1] Why does the energy gap depend on the temperature T? Can the gap $\Delta(T)$ be observed? Is the existence of such an energy gap a necessary condition for superconductivity?

- Phonons can be exchanged between any electrons at all time and at all temperatures. The phonon-exchange attraction can bound a pair of quasi-electrons to form moving (or excited) pairons. What is the energy of excited pairons? How do such electrons affect the low temperature behavior of the superconductor?

- All superconductors behave alike below T_c. Why does the law of corresponding states work here? Why is the behavior of the supercurrent temperature- and material-independent?

- What is the nature of the superconducting transition? Does the transition depend on dimensionality?

- Only about half of elemental metals are superconductors. Why does sodium remain normal down to 0 K? What is the criterion for superconductivity? What is the connection between superconductivity and band structures?

- Compound, organic, and high-T_c superconductors in general show type II behaviors. Why do they behave differently compared with elemental superconductors?

- All superconductors exhibit four main properties: (1) zero resistance, (2) Meissner effect, (3) flux quantization and Josephson effects, and (4) gaps in the elementary excitation energy spectra. Can a quantum statistical theory explain all types of superconductors in a unified manner?

We wish to answer all of these questions in the text. We shall begin with the study of elemental superconductors at 0 K in this chapter. The next three chapters deal with the B–E condensation of pairons, superconductors below T_c, supercurrents, flux quantization and Josephson effects. Compound and high-T_c superconductors will be discussed in Chapters 12 and 13, respectively.

8.2. THE GENERALIZED BCS HAMILTONIAN

In 1957 Bardeen, Cooper, and Schrieffer (BCS) published a classic paper on the theory of superconductivity.[1] In this work they assumed a Hamiltonian containing electron and hole kinetic energies and a phonon-exchange-pairing Hamiltonian. They also assumed a spherical Fermi surface. These two assumptions however contradict each other. If a Fermi sphere whose inside (outside) is filled with electrons is assumed, there

are electrons (holes) only as we saw in Sections 5.8–5.9. Besides this logical inconsistency, if we assume a free electron model having a spherical Fermi surface, we cannot explain why the law of corresponding states works nor why monovalent metals like Na and K are not superconductors. We must incorporate the band structures of electrons and phonons more explicitly. In this section, we set up and discuss a *generalized BCS Hamiltonian.*[2] We assume that

- In spite of the Coulomb interaction among electrons, there exists a sharp Fermi surface for the normal state of a conductor, as described by the Fermi liquid model of Landau,[3] (see Sections 5.3 and 6.8).

- The phonon exchange can generate bound pairs of electrons near the Fermi surface within a distance (energy) equal to Planck's constant $\hbar$ times the Debye frequency ω_D. These pairs having antiparallel spins and charge (magnitude) $2e$ are called *Cooper pairs* or *pairons.* Cooper pair and pairon both denote the same entity. When we emphasize the quasi-particle aspect rather than the two-electron composition aspect, we use the term pairon more often. Under the two conditions, we may write a Hamiltonian H in the form:

$$H = \sum_{\substack{\mathbf{k} \\ \epsilon_k > 0}} \sum_{s} \epsilon_k c^\dagger_{\mathbf{k}s} c_{\mathbf{k}s} + \sum_{\substack{\mathbf{k} \\ \epsilon_k < 0}} \sum_{s} |\epsilon_k| c_{\mathbf{k}s} c^\dagger_{\mathbf{k}s} + \frac{1}{2} \sum_{\mathbf{k}_1} \sum_{s_1} \cdots \sum_{\mathbf{k}_4} \sum_{s_4} \langle 12|U|34\rangle c^\dagger_1 c^\dagger_2 c_4 c_3 \tag{8.2.1}$$

where $\epsilon_{k_1} \equiv \epsilon_1$ is the kinetic energy of a Bloch electron measured relative to the Fermi energy ϵ_F, and $c^\dagger_{\mathbf{k}_1 s_1}$ $(c_{\mathbf{k}_1 s_1}) \equiv c^\dagger_1$ (c_1) are creation (annihilation) operators satisfying the Fermi anticommutation rules:

$$\{c_{\mathbf{k}s}, c^\dagger_{\mathbf{k}'s'}\} = \delta_{\mathbf{k},\mathbf{k}'}\delta_{s,s'}, \qquad \{c_{\mathbf{k}s}, c_{\mathbf{k}'s'}\} = \{c^\dagger_{\mathbf{k}s}, c^\dagger_{\mathbf{k}'s'}\} = 0 \tag{8.2.2}$$

The first (second) sum on the rhs of Eq. (8.2.1) represents the total kinetic energy of electrons with positive ϵ_k (holes with negative ϵ_k). The matrix element $\langle\, 12 \,|\, U \,|\, 34 \,\rangle$ denotes the net interaction arising from the virtual exchange of a phonon and the Coulomb repulsion between electrons. We note that our Hamiltonian H is essentially the same as Eq. (24) of the original BCS paper.[1] We further assume that

- Electrons and holes have different effective masses (magnitude).

- The interaction strengths V_{ij} among and between electron (1) and hole (2) pairons are different so that

$$\langle 12; i|U|34; j\rangle = \begin{cases} -V_{ij} V^{-1} \delta_{\mathbf{k}_1+\mathbf{k}_2,\mathbf{k}_3+\mathbf{k}_4} \delta_{s_1,s_3} \delta_{s_2,s_4} & \text{if } |\epsilon_m| < \hbar\omega_D \\ 0 & \text{otherwise} \end{cases} \tag{8.2.3}$$

Let us introduce the vacuum state $|\phi_1\rangle$, creation and annihilation operators ($c^{(1)\dagger}$, $c^{(1)}$), and the number operators $n^{(1)}_{\mathbf{k}s}$ for electrons ($\varepsilon_k > 0$) such that

$$c^{(1)}_{\mathbf{k}s} \equiv c_{\mathbf{k}s}, \quad c^{(1)\dagger}_{\mathbf{k}s} = c^{\dagger}_{\mathbf{k}s}, \quad n^{(1)}_{\mathbf{k}s} \equiv c^{(1)\dagger}_{\mathbf{k}s} c^{(1)}_{\mathbf{k}s}, \quad c^{(1)}_{\mathbf{k}s}|\phi_1\rangle = 0 \tag{8.2.4}$$

For holes ($\varepsilon_k < 0$), we introduce the vacuum state $|\phi_2\rangle$, creation and annihilation operators ($c^{(2)\dagger}$, $c^{(2)}$), and the number operators $n^{(2)}_{\mathbf{k}s}$ as follows:

$$c^{(2)}_{\mathbf{k}s} \equiv c^{\dagger}_{\mathbf{k}s}, \quad c^{(2)\dagger}_{\mathbf{k}s} = c_{\mathbf{k}s}, \quad n^{(2)}_{\mathbf{k}s} \equiv c^{(2)\dagger}_{\mathbf{k}s} c^{(2)}_{\mathbf{k}s}, \quad c^{(2)}_{\mathbf{k}s}|\phi_2\rangle = 0 \tag{8.2.5}$$

At 0 K there should exist only *zero-momentum (or ground) pairons* of the lowest energy. The ground state Ψ for the system may then be described in terms of a *reduced* Hamiltonian:

$$\begin{aligned} H_0 = &\sum_{\mathbf{k}} \sum_{s} \epsilon^{(1)}_k n^{(1)}_{\mathbf{k}s} + \sum_{\mathbf{k}} \sum_{s} \epsilon^{(2)}_k n^{(2)}_{\mathbf{k}s} \\ &- \sum_{\mathbf{k}}{}' \sum_{\mathbf{k}'}{}' [v_{11} b^{(1)\dagger}_{\mathbf{k}'} b^{(1)}_{\mathbf{k}} + v_{12} b^{(1)\dagger}_{\mathbf{k}'} b^{(2)\dagger}_{\mathbf{k}} + v_{21} b^{(2)}_{\mathbf{k}} b^{(1)}_{\mathbf{k}'} + v_{22} b^{(2)}_{\mathbf{k}'} b^{(2)\dagger}_{\mathbf{k}}] \end{aligned} \tag{8.2.6}$$

where $v_{ij} \equiv V^{-1} V_{ij}$ and $b^{(j)}$ are pair annihilation operators defined by

$$b^{(1)}_{\mathbf{k}} \equiv c^{(1)}_{-\mathbf{k}\downarrow} c^{(1)}_{\mathbf{k}\uparrow}, \qquad b^{(2)}_{\mathbf{k}} \equiv c^{(2)}_{\mathbf{k}\uparrow} c^{(2)}_{-\mathbf{k}\downarrow} \tag{8.2.7}$$

The primes on the last summation symbols indicate the restriction that

$$\begin{aligned} 0 < \epsilon^{(1)}_k \equiv \epsilon_k < \hbar\omega_D \qquad &\text{for electrons} \\ 0 < \epsilon^{(2)}_k \equiv |\epsilon_k| < \hbar\omega_D \qquad &\text{for holes.} \end{aligned} \tag{8.2.8}$$

For the sake of argument, let us drop the interaction Hamiltonian altogether in Eq. (8.2.6). We then have the first two sums representing the kinetic energies of electrons and holes. These energies $(\epsilon^{(1)}_{\mathbf{k}}, \epsilon^{(2)}_{\mathbf{k}})$ are positive by definition. Then the lowest energy of this system, called the Bloch system, is zero, and the corresponding ground state is characterized by zero electrons and zero holes. This state will be called the *physical vacuum state.* In the theoretical developments in this chapter, we look for the ground state of the generalized BCS system whose energy is negative.

The commutation relations for the pair operators can be calculated from Eqs. (8.2.2), (8.2.4), (8.2.5), and (8.2.7). They are given by (Problem 8.2.1)

$$\begin{aligned} [b^{(j)}_{\mathbf{k}}, b^{(i)}_{\mathbf{k}'}] &\equiv b^{(j)}_{\mathbf{k}} b^{(i)}_{\mathbf{k}'} - b^{(i)}_{\mathbf{k}'} b^{(j)}_{\mathbf{k}} = 0 \\ [b^{(j)}_{\mathbf{k}}, b^{(i)\dagger}_{\mathbf{k}'}] &= (1 - n^{(j)}_{\mathbf{k}\uparrow} - n^{(j)}_{-\mathbf{k}\downarrow}) \delta_{\mathbf{k},\mathbf{k}'} \delta_{j,i} \end{aligned} \tag{8.2.9}$$

[In the commutator calculation, Eqs. (6.1.9) and (6.5.12) may be used, e.g.

$$\begin{aligned} [b^{(1)}_{\mathbf{k}}, b^{(1)\dagger}_{\mathbf{k}'}] &\equiv [c_{-\mathbf{k}} c_{\mathbf{k}}, b^{\dagger}_{\mathbf{k}'}] = c_{-\mathbf{k}} [c_{\mathbf{k}}, b^{\dagger}_{\mathbf{k}'}] + [c_{-\mathbf{k}}, b^{\dagger}_{\mathbf{k}'}] c_{\mathbf{k}} \\ &= c_{-\mathbf{k}} (\{c_{\mathbf{k}}, c^{\dagger}_{\mathbf{k}'}\} c^{\dagger}_{-\mathbf{k}'} - c^{\dagger}_{\mathbf{k}'} \{c_{\mathbf{k}}, c^{\dagger}_{-\mathbf{k}'}\}) + (\{c_{-\mathbf{k}}, c^{\dagger}_{\mathbf{k}'}\} c^{\dagger}_{-\mathbf{k}'} - c^{\dagger}_{\mathbf{k}'} \{c_{-\mathbf{k}}, c^{\dagger}_{-\mathbf{k}'}\}) c_{\mathbf{k}} \\ &= (1 - n_{\mathbf{k}} - n_{-\mathbf{k}}) \delta_{\mathbf{k},\mathbf{k}'} \end{aligned}$$

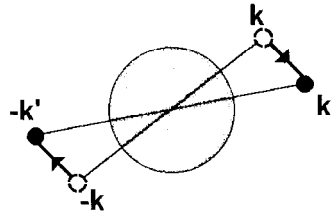

Figure 8.1. An electron-pair transition from $(\mathbf{k}\uparrow,-\mathbf{k}\downarrow)$ to $(\mathbf{k}'\uparrow, -\mathbf{k}'\downarrow)$.

Here spin indices were omitted with the convention that $\mathbf{k}$ has the spin up $\uparrow$ and $-\mathbf{k}$ has the spin down $\downarrow$]. In addition we obtain (Problem 8.2.2)

$$[b_{\mathbf{k}}^{(j)}]^2 \equiv b_{\mathbf{k}}^{(j)} b_{\mathbf{k}}^{(j)} = 0, \qquad [b_{\mathbf{k}}^{(j)\dagger}]^2 = 0 \tag{8.2.10}$$

We now examine the physical meaning of the interaction strengths v_{ij}. Consider part of the interaction terms in Eq. (8.2.6):

$$-v_{11} b_{\mathbf{k}'}^{(1)\dagger} b_{\mathbf{k}}^{(1)}, \qquad -v_{22} b_{\mathbf{k}'}^{(2)} b_{\mathbf{k}}^{(2)\dagger} \tag{8.2.11}$$

The first term generates a transition of the electron pair from $(\mathbf{k}\uparrow, -\mathbf{k}\downarrow)$ to $(\mathbf{k}'\uparrow, -\mathbf{k}'\downarrow)$. This transition may be represented by the k-space diagram in Fig. 8.1. Such a transition may be generated by the emission of a virtual phonon with momentum $\mathbf{q} = \mathbf{k}' - \mathbf{k}$ $(-\mathbf{q})$ by the down (up)-spin electron and subsequent absorption by the up (down)-spin electron, as shown in Fig. 8.2 (a) and (b). Note: These two processes are distinct, but they yield the same net transition. As we saw in Section 7.10, the phonon exchange generates an attractive correlation between the electron-pair states whose energies are nearly the same. The Coulomb interaction generates a repulsive correlation. The effect of this interaction can be included in the strength v_{11}. Similarly the exchange of a phonon (and a photon) induces a correlation between the hole-pair states, and it is represented by the second term in Eq. (8.2.11).

The exchange of a phonon can also pair create or pair annihilate electron (hole) pairons, called –(+) pairons, and the effects of these processes are represented by

$$-v_{12} b_{\mathbf{k}'}^{(1)\dagger} b_{\mathbf{k}}^{(2)\dagger}, \qquad -v_{21} b_{\mathbf{k}'}^{(2)} b_{\mathbf{k}}^{(1)} \tag{8.2.12}$$

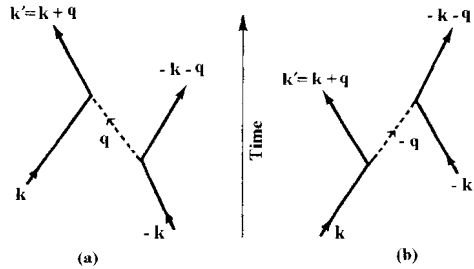

Figure 8.2. Two Feynman diagrams representing a phonon exchange between two electrons.

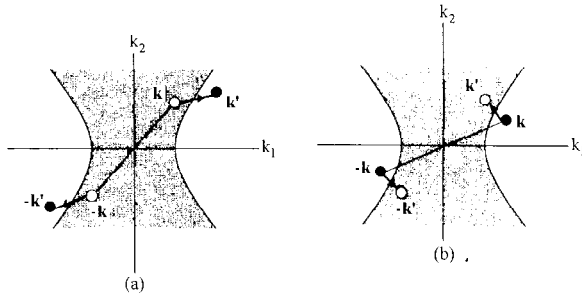

Figure 8.3. k-space diagrams representing (a) pair creation of ± ground pairons and (b) pair annihilation [see the two terms in Eq. (8.2.12)].

These two processes are indicated by k-space diagrams (a) and (b) in Fig. 8.3. The same process can be represented by Feynman diagrams in Fig. 8.4. We assume that time flows upward and that electrons (holes) proceed in the positive (negative) time-directions. We stress that a phonon is electrically neutral; therefore total charge before and after the phonon exchange must be the same. Note: The interaction Hamiltonians in Eqs. (8.2.11) and (8.2.12) all conserve electric charge.

The interaction strength v_{ij} should be the same for all (i, j) if the phonon exchange only is considered. By including the effect of the Coulomb repulsion, only the values of the strengths $v_{11} = v_{22}$ are reduced (see below for an explanation); therefore the following inequalities in general hold:

$$v_{11} = v_{22} < v_{12} = v_{21} \tag{8.2.13}$$

For elemental superconductors, we additionally assume that

- There are only acoustic phonons having a linear energy–momentum relation:

$$\epsilon = c_s q \tag{8.2.14}$$

where c_S is the sound speed.

The two forces, which are generated by the exchange of longitudinal acoustic phonons and photons are both long-ranged. But the speeds of light and sound differ

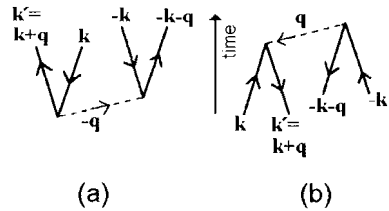

Figure 8.4. Feynman diagrams representing (a) pair creation of ± ground pairons from the physical vacuum and (b) pair annihilation.

by a factor of 10^5. Hence for the same k, the energies of light and sound are different by the same factor of 10^5. It then follows that the photon-exchange interaction acts at a much shorter k-distance than the phonon-exchange interaction. This means that only the phonon-exchange interaction can pair create or pair annihilate ± pairons by emission and absorption of a virtual phonon with momentum $\mathbf{q}$ crossing over the Fermi surface. In other words exchange of a photon with an extremely small q can generate a correlation among pairons, while exchange of an acoustic phonon not only generates a correlation among pairons but also pair creates or pair annihilates pairons of different charge types. This difference generates the inequality in Eq. (8.2.13). The zero-temperature coherence length ξ_0, which is a measure of the Cooper pair size (see Section 8.6) is of the order of 10^4 Å. This may be accounted for by the phonon-exchange attraction of a range of the order of ξ_0, which is much greater than the lattice constant. The bare Coulomb repulsion has an even greater range, but this force can be screened by the motion of other electrons in the conductor. Therefore *the effect of the Coulomb repulsion for the Cooper pair separated by* 10^4 Å *is negligible.* This means that for type I superconductors, the interaction strengths are all equal to each other:

$$v_{11} = v_{22} = v_{12} = v_{21} \equiv v_0 \qquad \text{(type I)} \tag{8.2.15}$$

This assumption simplifies the algebra considerably. In this and the following three chapters, we discuss mainly the case of elemental superconductors. In high-T_c superconductors, the interaction strengths v_{ij} are not equal because the Coulomb repulsion is not negligible and inequalities (8.2.13) hold. This case will be discussed separately in more detail in Chapter 13. The theoretical treatments for both cases are not dissimilar. We shall often develop our theory without assuming Eq. (8.2.15) and derive general results. We then take the limit:

$$v_{11} = v_{22} \to v_{12} \tag{8.2.16}$$

in the final expressions. A further discussion on the nature of the generalized BCS Hamiltonian will be given in Section 8.6.

Problem 8.2.1. Derive Eq. (8.2.9). Use Eqs. (6.1.9) and (6.5.12) effectively.

Problem 8.2.2. Derive Eq. (8.2.10).

8.3. THE COOPER PROBLEM 1; GROUND COOPER PAIRS

In this section we study the Cooper system, which contains only electrons and formally retains the pairing interaction. Such a system was first studied by Cooper.[4] The reduced Hamiltonian H_0 is now given by [see Eq. (8.2.6)]

$$H_0 = \sum_{\mathbf{k}} \sum_{s} \epsilon_k n_{\mathbf{k}s} - v_0 \sum_{\mathbf{k}}{}' \sum_{\mathbf{k}'}{}' b_{\mathbf{k}}^{\dagger} b_{\mathbf{k}'}, \qquad v_0 \equiv V^{-1} V_0 \tag{8.3.1}$$

where the electron indices 1 are dropped throughout. The ground state for the system may be constructed in terms of ground pairons formed by electrons located near the

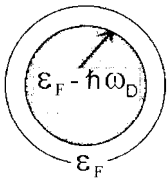

Figure 8.5. Ground pairons are generated from electrons in the ring-shaped region near the Fermi surface. Electrons in the gray area do not participate in the pairon production.

Fermi surface, as shown by the ring-shaped region in the two-dimensional momentum space in Fig. 8.5. The total number of electrons affected by the interaction is

$$2\hbar\omega_D \mathcal{N}(0) \tag{8.3.2}$$

where $\mathcal{N}(0)$ is the density of states at the Fermi energy $\epsilon_F (= 0)$ per spin orientation, and the factor 2 the spin degeneracy factor. Since pairons are formed with electrons of different spin orientations, the number of pairons is given by

$$\boxed{\hbar\omega_D \mathcal{N}(0) = N_0} \tag{8.3.3}$$

Note: The great majority of electrons, that is, all Bloch electrons having energies less than $\epsilon_F - \hbar\omega_D$, located in the gray area in Fig. 8.5, are not affected by the attraction. Excluding these unaffected electrons, all electrons near the Fermi surface may be paired. The total kinetic energy in Eq. (8.3.1) can now be expressed in terms of the pairon occupation numbers represented by $b_{\mathbf{k}}^\dagger b_{\mathbf{k}}$. We may then rewrite the reduced Hamiltonian H_0 in Eq. (8.3.1) as

$$H_0 = \sum_{\mathbf{k}}{}' 2\epsilon_k b_{\mathbf{k}}^\dagger b_{\mathbf{k}} - v_0 \sum_{\mathbf{k}}{}' \sum_{\mathbf{k}'}{}' b_{\mathbf{k}}^\dagger b_{\mathbf{k}'} \tag{8.3.4}$$

where we used the fact that the total kinetic energy of two electrons is $2\epsilon_k$.

We now wish to find the ground-state energy. First note that our Hamiltonian H_0 is a sum of the energies of pairons. This situation is similar to the Hamiltonian in Eq. (6.5.1). Only pairons enter here as quasi-particles in place of electrons. We can therefore set up an energy eigenvalue problem for pairons exactly. We simply follow the steps described after Eq. (6.7.14). Using Eq. (8.2.9) we obtain (Problem 8.3.1)

$$[H_0, b_{\mathbf{k}}^\dagger] = 2\epsilon_k b_{\mathbf{k}}^\dagger - v_0 \sum_{\mathbf{k}}{}' b_{\mathbf{k}'}^\dagger (1 - n_{\mathbf{k}\uparrow} - n_{-\mathbf{k}\downarrow}) \tag{8.3.5}$$

We multiply Eq. (8.3.5) from the right by $\psi_\nu \rho$ and take a grand ensemble trace. After taking the bulk limit, we obtain

$$\begin{aligned} w_\nu \Psi_\nu^*(\mathbf{k}) &= 2\epsilon_k \Psi_\nu^*(\mathbf{k}) - (2\pi\hbar)^{-3} v_0 \int' d^3k' \, \Psi_\nu^*(\mathbf{k}') \\ &\quad + (2\pi\hbar)^{-3} v_0 \int' d^3k' \, \mathrm{TR}\{b_{\mathbf{k}'}^\dagger (n_{\mathbf{k}\uparrow} + n_{-\mathbf{k}\downarrow}) \psi_\nu \rho\} \end{aligned} \tag{8.3.6}$$

$$\Psi_\nu^*(\mathbf{k}) \equiv \mathrm{TR}\{b_{\mathbf{k}}^\dagger \psi_\nu \rho\} \tag{8.3.7}$$

Here $\Psi_\nu(\mathbf{k})$ is the pairon wave function, and w_ν is its energy eigenvalue. The last integral containing $n_{\mathbf{k}\uparrow} + n_{-\mathbf{k}\downarrow}$ can be shown to contribute nothing in the low-temperature limit [see Section 8.4 and Eq. (8.4.17)]. By dropping this integral, we obtain from Eq. (8.3.6)

$$w_0\Psi^*(\mathbf{k}) = 2\epsilon_k\Psi^*(\mathbf{k}) - (2\pi\hbar)^{-3}v_0\int' d^3k'\,\Psi^*(\mathbf{k}') \tag{8.3.8}$$

where we replaced index ν by index 0, indicating the zero-momentum pairon.

Equation (8.3.8) can be solved simply as follows. Consider the last integral:

$$C \equiv (2\pi\hbar)^{-3}v_0\int' d^3k'\,\Psi^*(\mathbf{k}') \tag{8.3.9}$$

which is a constant. Assume that the energy w_0 is negative:

$$w_0 < 0 \tag{8.3.10}$$

Then $2\epsilon_k - w_0 = 2\epsilon_k + |w_0| > 0$. After rearranging the terms in Eq. (8.3.8) and dividing the result by $2\epsilon_k + |w_0|$, we obtain

$$\Psi^*(\mathbf{k}) = \frac{1}{2\epsilon_k + |w_0|}C \tag{8.3.11}$$

Substituting this expression into Eq. (8.3.9) and dropping the common factor C, we obtain

$$1 = (2\pi\hbar)^{-3}v_0\int' d^3k\frac{1}{2\epsilon_k + |w_0|} \tag{8.3.12}$$

By introducing the density of states at the Fermi energy, $\mathcal{N}(0)$, we can evaluate the k-integral as follows (Problem 8.3.2):

$$1 = v_0\mathcal{N}(0)\int_0^{\hbar\omega_D} d\epsilon\frac{1}{2\epsilon_k + |w_0|} = \frac{1}{2}v_0\mathcal{N}(0)\ln[(2\hbar\omega_D + |w_0|)/|w_0|]$$

or

$$\boxed{w_0 = \frac{-2\hbar\omega_D}{\exp[2/v_0\mathcal{N}(0)] - 1}} \tag{8.3.13}$$

We thus found a *negative-energy (or bound) state* for the ground Cooper pair. The v_0-dependence of the energy w_0 is noteworthy. Since $\exp(2/x)$ cannot be expanded in powers of $x = v_0\mathcal{N}(0)$, the energy w_0 cannot be obtained by a perturbation (v_0) expansion method.

If all available electrons are paired, the ground-state energy for the Cooper system, W, is given by the product of w_0 and N_0:

$$W = N_0w_0 = \frac{-2\hbar^2\omega_D^2\mathcal{N}(0)}{\exp[2/v_0\mathcal{N}(0)] - 1} < 0 \tag{8.3.14}$$

Problem 8.3.1. Verify Eq. (8.3.5).

Problem 8.3.2. Verify Eq. (8.3.13).

8.4. THE COOPER PROBLEM 2; EXCITED COOPER PAIRS

Phonons can be exchanged between any pair of electrons. Thus the phonon exchange is in action not only for the ground pairons but also for any pair of electrons near the Fermi surface. These pairons have net momenta and therefore move. They are called *moving* or *excited pairons.* In the present section we examine excited pairons.

Second-quantized operators for a pair of electrons may be represented by

$$B_{12}^{\dagger} \equiv B_{\mathbf{k}_1\uparrow\mathbf{k}_2\downarrow}^{\dagger} \equiv c_1^{\dagger}c_2^{\dagger}, \qquad B_{34} = c_4 c_3 \tag{8.4.1}$$

Odd-numbered electrons carry upward spins $\uparrow$ and the even-numbered carry downward spins $\downarrow$. The commutation relations can be computed using Eq. (8.2.2), and they are given by (Problem 8.4.1)

$$\begin{aligned} [B_{12}, B_{34}] &\equiv B_{12}B_{34} - B_{34}B_{12} = 0 \\ [B_{12}, B_{34}^{\dagger}] &= \begin{cases} 1 - n_1 - n_2 & \text{if } \mathbf{k}_1 = \mathbf{k}_3 \text{ and } \mathbf{k}_2 = \mathbf{k}_4 \\ c_2 c_4^{\dagger} & \text{if } \mathbf{k}_1 = \mathbf{k}_3 \text{ and } \mathbf{k}_2 \neq \mathbf{k}_4 \\ c_1 c_3^{\dagger} & \text{if } \mathbf{k}_1 \neq \mathbf{k}_3 \text{ and } \mathbf{k}_2 = \mathbf{k}_4 \\ 0 & \text{otherwise,} \end{cases} \end{aligned} \tag{8.4.2}$$

$$n_1 \equiv c_{\mathbf{k}_1\uparrow}^{\dagger} c_{\mathbf{k}_1\uparrow}, \qquad n_2 \equiv c_{\mathbf{k}_2\downarrow}^{\dagger} c_{\mathbf{k}_2\downarrow} \tag{8.4.3}$$

where n_j are the number operators for electrons. In addition we obtain

$$[B_{12}]^2 = 0 \tag{8.4.4}$$

Let us now introduce the relative and net momenta (**k, q**) such that

$$\mathbf{k} \equiv \frac{1}{2}(\mathbf{k}_1 - \mathbf{k}_2), \quad \mathbf{q} \equiv \mathbf{k}_1 + \mathbf{k}_2; \qquad \mathbf{k}_1 = \mathbf{k} + \frac{1}{2}\mathbf{q}, \quad \mathbf{k}_2 = -\mathbf{k} + \frac{1}{2}\mathbf{q} \tag{8.4.5}$$

We may alternatively represent pair operators by

$$B'_{\mathbf{kq}} \equiv B_{\mathbf{k}_1\uparrow\mathbf{k}_2\downarrow} \equiv c_{-\mathbf{k}+\mathbf{q}/2\downarrow} c_{\mathbf{k}+\mathbf{q}/2\uparrow}, \qquad B'^{\dagger}_{\mathbf{kq}} = c^{\dagger}_{\mathbf{k}+\mathbf{q}/2\uparrow} c^{\dagger}_{-\mathbf{k}+\mathbf{q}/2\downarrow} \tag{8.4.6}$$

The prime on B will be dropped hereafter. In the k–q representation, the commutation relations (8.4.2) and Eq. (8.4.4) can be reexpressed as

$$[B_{\mathbf{kq}}, B_{\mathbf{k'q'}}] = 0$$

$$[B_{\mathbf{kq}}, B^{\dagger}] = \begin{cases} (1 - n_{\mathbf{k}+\mathbf{q}/2\uparrow} - n_{-\mathbf{k}+\mathbf{q}/2\downarrow}) & \text{if} \quad \mathbf{k} = \mathbf{k}' \text{ and } \mathbf{q} = \mathbf{q}' \\ c_{-\mathbf{k}+\mathbf{q}/2\downarrow} c^{\dagger}_{-\mathbf{k}'+\mathbf{q}'/2\downarrow} & \text{if} \quad \mathbf{k} + \mathbf{q}/2 = \mathbf{k}' + \mathbf{q}'/2 \text{ and} \\ & \qquad -\mathbf{k} + \mathbf{q}/2 \neq -\mathbf{k}' + \mathbf{q}'/2 \\ c_{\mathbf{k}+\mathbf{q}/2\uparrow} c^{\dagger}_{\mathbf{k}'+\mathbf{q}'/2\downarrow} & \text{if} \quad \mathbf{k} + \mathbf{q}/2 \neq \mathbf{k}' + \mathbf{q}'/2 \text{ and} \\ & \qquad -\mathbf{k} + \mathbf{q}/2 = -\mathbf{k}' + \mathbf{q}'/2 \\ 0 & \text{otherwise} \end{cases} \tag{8.4.7}$$

$$[B_{\mathbf{kq}}]^2 = 0 \tag{8.4.8}$$

Using new notation for pairons, we can rewrite the Hamiltonian H as follows:

$$H = \sum_{\mathbf{k}}{}' \sum_{\mathbf{q}}{}' \left[\epsilon\left(|\mathbf{k}+\mathbf{q}/2|\right) + \epsilon\left(|-\mathbf{k}+\mathbf{q}/2|\right)\right] B^{\dagger}_{\mathbf{kq}} B_{\mathbf{kq}} - \sum_{\mathbf{k}}{}' \sum_{\mathbf{q}}{}' \sum_{\mathbf{k}'}{}' v_0 B^{\dagger}_{\mathbf{kq}} B_{\mathbf{k}'\mathbf{q}} \tag{8.4.9}$$

For convenience, we used $\in_P \equiv \in(|\mathbf{p}|)$. Using Eqs. (8.4.7) and (8.4.8), we obtain (Problem 8.4.2)

$$\begin{aligned}[H, B^{\dagger}_{\mathbf{kq}}] = {} & \left[\epsilon\left(|\mathbf{k}+\mathbf{q}/2|\right) + \epsilon\left(|-\mathbf{k}+\mathbf{q}/2|\right)\right] B^{\dagger}_{\mathbf{kq}} \\ & - v_0 \sum_{\mathbf{k}'}{}' B^{\dagger}_{\mathbf{k}'\mathbf{q}} (1 - n_{\mathbf{k}+\mathbf{q}/2\uparrow} - n_{-\mathbf{k}+\mathbf{q}/2\downarrow})\end{aligned} \tag{8.4.10}$$

Note: The net momentum $\mathbf{q}$ is a constant of motion, which arises from the momentum conservation in the phonon exchange processes.

Our Hamiltonian H in Eq. (8.4.9) can be expressed in terms of pair operators (B, $B^{\dagger}$). If we represent the energies of pairons by w_ν and the associated pair-annihilation operators by ϕ_ν, we can in principle reexpress H as

$$H = \sum_{\nu} w_\nu \phi^{\dagger}_\nu \phi_\nu \tag{8.4.11}$$

which is similar to Eq. (6.5.8) with the only difference that here we deal with pair energies and pair-state operators. We multiply Eq. (8.4.10) by $\phi_\nu \rho_{gc}$ from the right and take a grand ensemble trace. After using Eq. (6.7.11), we obtain

$$\begin{aligned}w_\nu a_{\mathbf{kq}} \equiv w_q a_{\mathbf{kq}} = {} & \left[\epsilon\left(|\mathbf{k}+\mathbf{q}/2|\right) + \epsilon\left(|-\mathbf{k}+\mathbf{q}/2|\right)\right] a_{\mathbf{kq}} \\ & - v_0 \sum_{\mathbf{k}'} \langle B^{\dagger}_{\mathbf{k}'\mathbf{q}} (1 - n_{\mathbf{k}+\mathbf{q}/2\uparrow} - n_{-\mathbf{k}+\mathbf{q}/2\downarrow}) \phi_\nu \rangle\end{aligned} \tag{8.4.12}$$

$$a_{\mathbf{kq},\nu} \equiv \mathrm{TR}\{B^{\dagger}_{\mathbf{kq}} \phi_\nu \rho_{gc}\} \equiv a_{\mathbf{kq}} \tag{8.4.13}$$

The energy w_ν can be characterized by $\mathbf{q} : w_\nu \equiv w_q$. In other words excited pairons have momentum $\mathbf{q}$ and energy w_q. We shall omit the subindex ν: $a_{kq,\nu} \equiv a_{kq}$. The angular brackets in Eq. (8.4.12) means the grand canonical ensemble average:

$$\langle A \rangle \equiv \mathrm{TR}\{A \rho_{gc}\} \equiv \frac{\mathrm{TR}\{A \exp(\alpha N - \beta H)\}}{\mathrm{TR}\{\exp(\alpha N - \beta H)\}} \tag{8.4.14}$$

In the bulk limit $N \to \infty$, $V \to \infty$, while $n \equiv N/V =$ finite, where N represents the number of electrons, k-vectors become continuous. Denoting the wave function in this limit by $a(\mathbf{k},\mathbf{q})$, we obtain from Eq. (8.4.12)

$$\begin{aligned}w_q a(\mathbf{k},\mathbf{q}) = {} & \left[\epsilon\left(|\mathbf{k}+\mathbf{q}/2|\right) + \epsilon\left(|-\mathbf{k}+\mathbf{q}/2|\right)\right] a(\mathbf{k},\mathbf{q}) \\ & - (2\pi\hbar)^{-3} v_0 \int' d^3k'\, a(\mathbf{k}',\mathbf{q}) \\ & \times \left\{1 - f_F\left[\epsilon\left(|\mathbf{k}+\mathbf{q}/2|\right)\right] + f_F\left[\epsilon\left(|-\mathbf{k}+\mathbf{q}/2|\right)\right]\right\}\end{aligned} \tag{8.4.15}$$

$$\langle n_p \rangle = \frac{1}{\exp(\beta\epsilon_p) + 1} \equiv f_F(\epsilon_p) \tag{8.4.16}$$

In the low temperature limit ($T \to 0$ or $\beta \to \infty$)

$$f_F(\epsilon_p) \to 0 \qquad (\epsilon_p > 0) \tag{8.4.17}$$

We then obtain

$$w_q a(\mathbf{k}, \mathbf{q}) = \left[\epsilon\left(|\mathbf{k} + \mathbf{q}/2|\right) + \epsilon\left(|-\mathbf{k} + \mathbf{q}/2|\right)\right] a(\mathbf{k}, \mathbf{q}) - (2\pi\hbar)^{-3} v_0 \int' d^3k'\, a(\mathbf{k}', \mathbf{q}) \tag{8.4.18}$$

which is identical with *Cooper's* equation, Eq. (1) of his 1956 letter.[3]

We stress again that the net momentum $\mathbf{q}$ is a constant of motion, which arises from the fact that the phonon exchange is an internal process and therefore cannot change the net momentum. The pair wave functions $a(\mathbf{k}, \mathbf{q})$ are coupled with respect to the other variable $\mathbf{k}$, meaning that the exact (or energy eigenstate) pairon wave functions are superpositions of the pair wave functions $a(\mathbf{k}, \mathbf{q})$.

We note that Eq. (8.4.18) is reduced to Eq. (8.3.8) if the small-q limit is taken; the latter equation was solved earlier in Section 2.3. Using the same technique as in Eqs. (8.3.9–(8.3.12), we obtain from Eq. (8.4.18)

$$1 = (2\pi\hbar)^{-3} v_0 \int' d^3k \left[\epsilon\left(|\mathbf{k} + \mathbf{q}/2|\right) + \epsilon\left(|-\mathbf{k} + \mathbf{q}/2|\right) + |w_q|\right]^{-1} \tag{8.4.19}$$

We now assume a free-electron model. The Fermi surface is a sphere of radius (momentum)

$$k_F \equiv (2m_1\epsilon_F)^{1/2} \tag{8.4.20}$$

where m_1 represents the electron-effective mass. The energy $\epsilon(|\mathbf{k}|)$ is given by

$$\epsilon(|\mathbf{k}|) \equiv \epsilon_k = \frac{k^2 - k_F^2}{2m_1} \tag{8.4.21}$$

Let us recall that the prime on the k-integral in Eq. (8.4.19) means the restriction: $0 < \epsilon[|\mathbf{k} + (\mathbf{q}/2)|], \epsilon[|-\mathbf{k} + (\mathbf{q}/2)|] < \hbar\omega_D$. We may choose the polar axis along $\mathbf{q}$ as shown in Fig. 8.6. The integration with respect to the azimuthal angle simply yields the factor 2π. The k-integral can then be expressed by (Problem 8.4.3)

$$(2\pi\hbar)^3 v_0^{-1} = 4\pi \int_0^{\pi/2} d\theta \sin\theta \int_{k_F + (1/2)q\cos\theta}^{k_F + k_D - (1/2)q\cos\theta} \frac{k^2 dk}{|w_q| + 2\epsilon_k + (4m_1)^{-1}q^2} \tag{8.4.22}$$

$$k_D \equiv m_1\omega_D(\hbar k_F)^{-1} \tag{8.4.23}$$

After performing the integration and taking the small-q and small-(k_D/k_F) limits, we obtain (Problem 8.4.4):

$$\boxed{w_q = w_0 + \frac{v_F q}{2}} \tag{8.4.24}$$

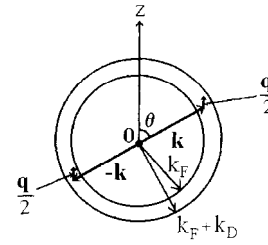

Figure 8.6. The range of the integration variables (k, θ) is limited to a spherical shell of thickness k_D.

where w_0 is given by Eq. (8.3.13). As expected the zero-momentum pairon has the lowest energy. The excitation energy is continuous with no energy gap. Equation (8.4.24) was first obtained by Cooper (unpublished) and it is recorded in Schrieffer's book,[5] Eq. (2-15), and it will be called the *Cooper–Schrieffer relation.* The energy w_q increases *linearly* with momentum q for small q. This behavior arises from the fact that the density of states is strongly reduced with increasing momentum q, dominates the q^2 increase of the kinetic energy. This means that a *pairon moves like a massless particle* with a common speed $v_F/2$. This relation plays a vital role in the B–E condensation of pairons (see Chapter 9).

Such a linear energy–momentum relation is valid for pairons moving in any dimension (D). However the coefficients slightly depend on the dimensions; in fact

$$w_q = w_0 + cq \tag{8.4.25}$$

$c/v_F = 1/2, 2/\pi$, and 1 for three, two, and one dimension, respectively (see Problem 8.4.5). The two-dimensional case is important for high-T_c superconductors (see Section 13.5).

Problem 8.4.1. Verify Eqs. (8.4.2) and (8.4.4).

Problem 8.4.2. Derive Eq. (8.4.10).

Problem 8.4.3. Verify Eq. (8.4.22). Use the diagram in Fig. 8.6.

Problem 8.4.4. Derive Eq. (8.4.24).

Problem 8.4.5. Derive an energy-momentum relation [Eq. (8.4.25)] for two dimensions with the assumption of a Fermi circle. Use the diagram in Fig. 8.6.

8.5. THE GROUND STATE

In this section we look for the ground-state energy of the generalized BCS system. At 0 K there should exist only ± ground pairons. The ground state Ψ for the system may then be constructed based on the reduced Hamiltonian H_0 in Eq. (8.2.6). Following BCS,[1] we assume that the normalized ground-state ket $|\Psi\rangle$ can be written as

$$|\Psi\rangle = \prod_{\mathbf{k}}{}' \frac{1 + g_{\mathbf{k}}^{(1)} b_{\mathbf{k}}^{(1)\dagger}}{(1 + |g_{\mathbf{k}}^{(1)}|^2)^{1/2}} \prod_{\mathbf{k}'}{}' \frac{1 + g_{\mathbf{k}'}^{(2)} b_{\mathbf{k}'}^{(2)\dagger}}{(1 + |g_{\mathbf{k}'}^{(2)}|^2)^{1/2}} |0\rangle \tag{8.5.1}$$

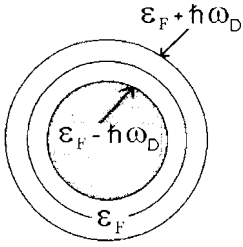

Figure 8.7. The k-space shell in two dimensions where pairons of both charge types are generated and intercorrelated.

Here the ket $|0\rangle$ by definition satisfies

$$c_{\mathbf{k}s}^{(j)}|0\rangle \equiv c_{\mathbf{k}s}^{(j)}|\phi_1\rangle|\phi_2\rangle = 0 \tag{8.5.2}$$

It represents the *physical vacuum state* for electrons and holes, that is, the ground state of the Bloch system (or the Fermi liquid model) with no electrons and no holes present. In Eq. (8.5.1) the product variables $\mathbf{k}$ (and $\mathbf{k}'$) extend over the region of the momenta whose associated energies are within the limit phonon energy $\hbar\omega_D : 0 < \epsilon_k^{(1)}, \epsilon_k^{(2)} < \hbar\omega_D$, and this is indicated by the primes ($'$) on each product symbols. The k-space shell in which $\pm$ pairons are generated and intercorrelated are shown in Fig. 8.7. Since $[b_{\mathbf{k}}^{(j)\dagger}]^2 = 0$ [see Eq. (8.2.10)], only two terms appear for each $\mathbf{k}$ ($\mathbf{k}'$). The quantity $|g_{\mathbf{k}}^{(j)}|^2$ represents the probability that the pair states $(\mathbf{k}\uparrow, -\mathbf{k}\downarrow)$ are occupied. By expanding the product, we can see that the BCS ground state $|\Psi\rangle$ contains the zero-pairon state $|0\rangle$, one-pairon states $b_{\mathbf{k}}^{(j)\dagger}|0\rangle$, two-pairon states $b_{\mathbf{k}}^{(j)\dagger}b_{\mathbf{k}}^{(j)\dagger}|0\rangle$,.... The physical meaning of the state $|\Psi\rangle$ will further be discussed in the paragraph after Eq. (8.5.15) and also in Section 10.4. The ket $|\Psi\rangle$ is normalized such that

$$\langle\Psi|\Psi\rangle = 1 \tag{8.5.3}$$

In

$$\langle\Psi|\Psi\rangle = \left\langle 0 \left| \frac{1 + g_k^{(1)\dagger} b_k^{(1)}}{(1 + |g_k^{(1)}|^2)^{1/2}} \cdot \frac{1 + g_k^{(1)} b_k^{(1)\dagger}}{(1 + |g_k^{(1)}|^2)^{1/2}} \right| 0 \right\rangle = 1$$

the case in which there is only one state $\mathbf{k}$ in the product, we obtain The general case can be worked out similarly (Problem 8.5.1).

Since the ground-state wave function has no nodes, we may choose $g_{\mathbf{k}}^{(j)}$ to be nonnegative with no loss of rigor: $g_{\mathbf{k}}^{(j)} \geq 0$ (see Section 11.1 for further explanation). We now determine $\{g_{\mathbf{k}}^{(j)}\}$ such that the ground-state energy

$$W \equiv \langle\Psi|H_0|\Psi\rangle \tag{8.5.4}$$

has a minimum value. This may be formulated by the extremum condition:

$$\delta W = \delta\langle\Psi|H_0|\Psi\rangle = 0 \tag{8.5.5}$$

The extremum problem implied by Eq. (8.5.5) with respect to variation in g's can more effectively be solved by working with variations in the real probability amplitudes u's and v's defined by

$$u_{\mathbf{k}}^{(j)} \equiv [1 + g_{\mathbf{k}}^{(j)2}]^{-1/2}, \qquad v_{\mathbf{k}}^{(j)} \equiv g_{\mathbf{k}}^{(j)}[1 + g_{\mathbf{k}}^{(j)2}]^{-1/2}, \qquad u_{\mathbf{k}}^{(j)2} + v_{\mathbf{k}}^{(j)2} = 1 \tag{8.5.6}$$

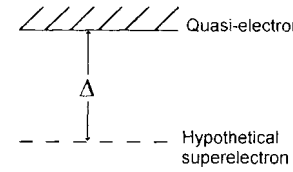

Figure 8.8. Quasi-electrons have an energy gap Δ relative to the hypothetical superelectron energy level.

The normalized ket $|\Psi\rangle$ can then be expressed by

$$|\Psi\rangle \equiv \prod_{\mathbf{k}}{}' (u_{\mathbf{k}}^{(1)} + v_{\mathbf{k}}^{(1)} b_{\mathbf{k}}^{(1)\dagger}) \prod_{\mathbf{k}'}{}' (u_{\mathbf{k}'}^{(2)} + v_{\mathbf{k}'}^{(2)} b_{\mathbf{k}'}^{(2)\dagger}) |0\rangle \tag{8.5.7}$$

The energy W in Eq. (8.5.4) can be written as (Problem 8.5.2)

$$W = \sum_{\mathbf{k}}{}' 2\epsilon_k^{(1)} v_{\mathbf{k}}^{(1)2} + \sum_{\mathbf{k}'}{}' 2\epsilon_{k'}^{(2)} v_{\mathbf{k}'}^{(2)2} - \sum_{\mathbf{k}}{}' \sum_{\mathbf{k}'}{}' \sum_i \sum_j v_{ij} u_{\mathbf{k}}^{(i)} v_{\mathbf{k}}^{(i)} u_{\mathbf{k}'}^{(j)} v_{\mathbf{k}'}^{(j)} \tag{8.5.8}$$

Taking the variations in $\{u\}$ and $\{u\}$ and noting that $u_{\mathbf{k}}^{(j)} \delta u_{\mathbf{k}}^{(j)} + v_{\mathbf{k}}^{(j)} \delta v_{\mathbf{k}}^{(j)} = 0$, we obtain from Eqs. (8.5.5) and (8.5.8) (Problem 8.5.3):

$$2\epsilon_k^{(j)} u_{\mathbf{k}}^{(j)} v_{\mathbf{k}}^{(j)} - (u_{\mathbf{k}}^{(j)2} - v_{\mathbf{k}}^{(j)2}) \sum_{\mathbf{k}'}{}' [v_{j1} u_{\mathbf{k}'}^{(1)} v_{\mathbf{k}'}^{(1)} + v_{j2} u_{\mathbf{k}'}^{(2)} v_{\mathbf{k}'}^{(2)}] = 0 \tag{8.5.9}$$

To simply treat these equations subject to Eq. (8.5.6), let us introduce a set of energy parameters $\Delta_{\mathbf{k}}^{(j)}$, $E_k^{(j)} \equiv \left(\epsilon_k^{(j)2} + \Delta_{\mathbf{k}}^{(j)2}\right)^{1/2}$ such that

$$u_{\mathbf{k}}^{(j)2} - v_{\mathbf{k}}^{(j)2} = \frac{\epsilon_k^{(j)}}{E_k^{(j)}}, \qquad u_{\mathbf{k}}^{(j)} v_{\mathbf{k}}^{(j)} = \frac{\Delta_{\mathbf{k}}^{(j)}}{2E_k^{(j)}} \tag{8.5.10}$$

(Problem 8.5.4). Then Eq. (8.5.9) can be reexpressed as

$$\Delta_{\mathbf{k}}^{(j)} = \sum_{\mathbf{k}'}{}' \sum_{i=1}^{2} v_{ij} \frac{\Delta_{\mathbf{k}'}^{(i)}}{2E_{\mathbf{k}'}^{(i)}} \tag{8.5.11}$$

As we shall see later in Section 8.6.3, $E_k^{(j)}$ can be interpreted as the energy of an unpaired electron or quasi-electron. Quasi-electrons have energy gaps $\Delta_{\mathbf{k}}^{(j)}$ relative to the energy level of the superelectron forming the ground pairon as shown in Fig 8.8.

Since the rhs of Eq. (8.5.11) does not depend on $\mathbf{k}$, the energy gaps

$$\Delta_{\mathbf{k}}^{(j)} \equiv \Delta_j \tag{8.5.12}$$

are independent of $\mathbf{k}$. Thus we can simplify Eq. (8.5.11) to

$$\boxed{\Delta_j = \sum_{\mathbf{k}'}{}' \sum_i v_{ij} \frac{\Delta_i}{2E_{\mathbf{k}'}^{(i)}}} \tag{8.5.13}$$

These are called *generalized energy gap equations* (8.5.20). Notice that there are in general electron and hole energy gaps (Δ_1, Δ_2).

Using Eqs. (8.5.9)–(8.5.13), we calculate the energy W from Eq. (8.5.8) to obtain (Problem 8.5.5)

$$\begin{aligned} W &\equiv \sum_{\mathbf{k}}{}' \sum_{j} 2\epsilon_k^{(j)} v_{\mathbf{k}}^{(j)2} - \sum_{\mathbf{k}}{}' \sum_{\mathbf{k}'}{}' \sum_{i} \sum_{j} v_{ij} u_{\mathbf{k}}^{(i)} v_{\mathbf{k}}^{(i)} u_{\mathbf{k}'}^{(j)} v_{\mathbf{k}'}^{(j)} \\ &= \sum_{\mathbf{k}}{}' \sum_{j} \left\{ \epsilon_k^{(j)} \left[1 - \frac{\epsilon_k^{(j)}}{E_k^{(j)}} \right] - \frac{\Delta_j^2}{2E_k} \right\} \end{aligned} \tag{8.5.14}$$

In the bulk limit the sums over $\mathbf{k}$ are converted into energy integrals, yielding

$$W = \sum_{j=1}^{2} \mathcal{N}_j(0) \int_0^{\hbar\omega_D} d\epsilon \left[\epsilon - \frac{\epsilon^2}{\left(\epsilon^2 + \Delta_j^2\right)^{1/2}} - \frac{\Delta_j^2}{2\left(\epsilon^2 + \Delta_j^2\right)^{1/2}} \right] \tag{8.5.15}$$

The ground state $|\Psi\rangle$ in Eq. (8.5.1) is a superposition of many-pairon states. Each component state can be reached from the physical vacuum state $|0\rangle$ by pair creation and/or pair annihilation of ± pairons and intercorrelation through a succession of phonon exchanges. Since the phonon-exchange processes, as represented by Eq. (8.2.12), can pair-create (or pair-annihilate) ± pairons simultaneously from the physical vacuum, the supercondensate represented by $|\Psi\rangle$ must be composed of *equal* numbers of ± pairons. We see from Fig. 8.7 that the maximum numbers of ± pairons are given by $(1/2)\hbar\omega_D \mathcal{N}_1(0)[(1/2)\hbar\omega_D \mathcal{N}_2(0)]$. We must then have

$$\mathcal{N}_1(0) = \mathcal{N}_2(0) \equiv \mathcal{N}(0) \tag{8.5.16}$$

which appears to be unrealistic, but it will be justified by the assumption that the supercondensate is generated only on part of the Fermi surface (see Section 8.6.8).

Using Eq. (8.5.16), we can rewrite Eq. (8.515) as (Problem 8.5.6)

$$W = \frac{1}{2} N_0 (w_1 + w_2), \qquad w_i \equiv \hbar\omega_D \left\{ 1 - \left[1 + (\Delta_i/\hbar\omega_D)^2 \right]^{1/2} \right\} \ (< 0) \tag{8.5.17}$$

We thus find that the ground-state energy of the generalized BCS system is *lower* than that of the Bloch system without u_{ij}. Further note that the binding energy $|w_i|$ per pairon may in general be different for different charge types.

Let us now find Δ_j from the gap equation (8.5.12). In the bulk limit these equations are simplified to

$$\begin{aligned} \Delta_j &= \frac{1}{2} v_{j1} \mathcal{N}(0) \int_0^{\hbar\omega_D} d\epsilon \frac{\Delta_1}{\left(\epsilon^2 + \Delta_1^2\right)^{1/2}} + \frac{1}{2} v_{j2} \mathcal{N}(0) \int_0^{\hbar\omega_D} d\epsilon \frac{\Delta_2}{\left(\epsilon^2 + \Delta_2^2\right)^{1/2}} \\ &= \frac{1}{2} v_{j1} \mathcal{N}(0) \Delta_1 \sinh^{-1}(\hbar\omega_D/\Delta_1) + \frac{1}{2} v_{j2} \mathcal{N}(0) \Delta_2 \sinh^{-1}(\hbar\omega_D/\Delta_2) \end{aligned} \tag{8.5.18}$$

For elemental superconductors, we assume that the interaction strengths v_{ij} are all equal to each other: $v_{11} = v_{12} = v_{22} \equiv v_0$ [see Eq. (8.2.15)]. Then we see from Eq. (8.5.18) that electron and hole energy gaps coincide

$$\Delta_1 = \Delta_2 \equiv \Delta \tag{8.5.19}$$

Equations (8.5.12) are now reduced to a single equation:

$$\boxed{\Delta = \sum_{\mathbf{k}'}{}' \sum_i v_0 \frac{\Delta}{2E_{\mathbf{k}'}^{(i)}}} \tag{8.5.20}$$

which is called the BCS *energy gap equation.*

After dropping the common factor Δ and taking the bulk limit, we obtain (Problem 8.5.7) $1 = v_0 \mathcal{N}(0) \sinh^{-1}(\hbar\omega_D/\Delta)$ or

$$\boxed{\Delta = \frac{\hbar\omega_D}{\sinh[1/v_0\mathcal{N}(0)]}} \tag{8.5.21}$$

Note: Equation (8.5.21) is similar to Eq. (8.3.13) for the binding energy $|w_0|$ for the ground Cooper pair. The exponential factor is however a little different: The factor $\exp[1/v_0 N(0)]$ appears in Eq. (8.5.21) as opposed to the factor $\exp[2/v_0 N(0)]$ in Eq. (8.3.13).

We now substitute Eq. (8.5.21) into Eq. (8.5.16) and calculate the ground-state energy. After straightforward computation, we obtain (Problem 8.5.8)

$$\boxed{W = \frac{-2\mathcal{N}(0)\hbar^2\omega_D^2}{\exp[2/v_0\mathcal{N}(0)] - 1} \; (= N_0 w_0)} \tag{8.5.22}$$

Equations (8.5.21) and (8.5.22) are the famous BCS formulas for the energy gap and the ground-state energy, respectively. They correspond to Eqs. (2.40) and (2.42) of the original paper.[1] We stress that these results are *exact*, and they were obtained from the reduced BCS Hamiltonian H_0 in Eq. (8.2.6) without assuming the weak coupling limit ($v_0 \to 0$).

Problem 8.5.1. Verify Eq. (8.5.3). Hint: Assume there are only two k-states in the product. If successful, then treat the general case.

Problem 8.5.2. Derive Eq. (8.5.8). Hint: see the hint in Problem 8.5.1.

Problem 8.5.3. Derive Eq. (8.5.9).

Problem 8.5.4. Check the consistency of Eqs. (8.5.6) and (8.5.10). Use the identity $(u^2 + v^2)^2 - (u^2 - v^2)^2 = 4u^2v^2$.

Problem 8.5.5. Verify Eq. (8.5.14).

Problem 8.5.6. Verify Eq. (8.5.17).

Problem 8.5.7. Verify Eq. (8.5.21).

Problem 8.5.8. Derive Eq. (8.5.22).

8.6. DISCUSSION

The most important results of this chapter are formula (8.3.13) for the ground Cooper-pair energy, formula (8.4.24) for the moving pairon energy, formula (8.5.22) for the ground state energy of the BCS system and formula (8.5.21) for a quasi-electron energy gap. We have uncovered several significant features of the ground state of the generalized BCS system, which are now discussed.

8.6.1. The Nature of the BCS Hamiltonian

The generalized BCS Hamiltonian H in Eq. (8.2.1) has a different character from the normal starting Hamiltonian [Eq. (2.1.1)] for a metal, which is composed of interacting conduction electrons and ions. Bardeen, Cooper, and Schrieffer envisioned that there are ground pairons at 0 K and up to the superconducting temperature T_c. Only the basic ingredients required to build up a set of pairons are introduced and incorporated in the BCS Hamiltonian. Electrons and holes are introduced from the outset. These particles are the elementary excitations in the lowest temperatures in the normal state. Their energies are measured relative to the Fermi energy $\in_F$.

Let us consider a bound Cooper pair. The pair distribution function representing the relative probability of finding the two constituting electrons depends on the separation distance r. We shall say that two electrons in the bound state are *correlated.* This correlation arises from the phonon exchange attraction and the Coulomb repulsion, and it may be represented by the pair–pair matrix elements in Eq. (8.2.3).

In a quantum statistical theory, a full justification of the assumed Hamiltonian comes only after calculating all thermodynamic and transport properties and comparing the results with experiments. BCS assumed the Hamiltonian [Eq. (8.2.1)] with a great physical insight and proceeded to compute the main properties of the model superconductor. Our quantum statistical theory will be based on the Hamiltonian H in Eq. (8.2.1), the Hamiltonian of essentially the same form originally proposed by BCS [Eq. (24) of Ref. 1]. There is however a hidden difference: electrons and holes in our theory are defined by referring to a realistic nonspherical Fermi surface. The results arising from this difference will be pointed out in the course of the theoretical development.

8.6.2. Binding Energy per Pairon

Let us examine an exact expression [Eq. (8.5.22)] for the ground-state energy of the BCS system. We may rewrite it in the form:

$$W = N_0 w_0, \qquad N_0 = \hbar\omega_D \mathcal{N}(0), \qquad w_0 = \frac{-2\hbar\omega_D}{\exp[2/v_0\mathcal{N}(0)] - 1} \tag{8.6.1}$$

which may be interpreted as follows: The greatest total number of pairons generated consistent with the BCS Hamiltonian in Eq. (8.2.1) is equal to $\hbar\omega_D\mathcal{N}(0) = N_0$. The k-space shell, shown in Fig. 8.7, in which pairons of both charge types are generated and intercorrelated is twice as large as the corresponding k-shell for the Cooper system, shown in Fig. 8.5. The maximum number of the pairons generated is however given by the same N_0 for both cases. Each Cooper pair contributes a binding energy $|w_0|$, equal to that found in the Cooper problem. This energy $|w_0|$ can be measured directly by quantum-tunneling experiments, as we shall see in Section 10.6. Our interpretation

of the ground-state energy is quite natural, but it is distinct from that of the BCS theory, where the energy gap Δ is regarded as a measure of the binding energy. We shall discuss this point further in Section 10.8.

8.6.3. Critical Magnetic Field B_c and the Energy Gap Δ

By the Meissner effect a superconductor expels a weak magnetic field **B** from its interior. The magnetic energy stored surrounding it should be higher in proportion to $\mathbf{B}^2$ and the excluded volume than that for the uniform B-flux configuration. For a macroscopic superconductor the difference in the energy therefore is given by

$$\frac{VB^2}{2\mu_0} \tag{8.6.2}$$

If this energy exceeds, the difference of the energy between super and normal conductors, $W_S - W_N$, which is equal to $|W_0|$, the superconducting state should break down. The minimum magnetic field B_c that destroys the superconducting state is the *critical magnetic field* at 0 K, $B_c(0) \equiv B_0$. We therefore obtain [see Eq. (1.3.2l)]

$$|W_S - W_N| = |W_0| = N_0|w_0| = \frac{VB_0^2}{2\mu_0} \tag{8.6.3}$$

where we used Eq. (8.6.1). Solving for B_0we obtain

$$B_0 = \left(2n_0|w_0|\mu_0\right)^{1/2} \cong \left[\mathcal{N}(0)V^{-1}\mu_0\right]^{1/2}\Delta \tag{8.6.4}$$

where the weak coupling approximation is used in the last step. Note: The energy gap Δ is approximately proportional to the critical field B_0.

8.6.4. The Energy Gap

In the process of obtaining the ground-state energy W by the variational calculation, we derived energy-gap equations, Eqs. (8.5.13) or (8.5.20), which contain the energy parameters:

$$E_k^{(j)} \equiv \left(\epsilon_k^{(j)2} + \Delta_j^2\right)^{1/2} \tag{8.6.5}$$

The fact that $E_k^{(j)}$ represents the energy of an unpaired electron, more often called a *quasi-electron,* can be seen as follows. The unpaired electron, say, in the state $(\mathbf{k}\uparrow)$, by definition does not have its mate in the state $(-\mathbf{k}\downarrow)$. This electron, which would have the kinetic energy $\epsilon_k^{(1)}$, cannot join the supercondensate, and therefore its total energy should be higher than that of the hypothetical superelectron. The energy difference $\Delta\epsilon$ can be calculated from Eq. (8.5.8) as (Problem 8.7.1)

$$\Delta\epsilon = \epsilon_k^{(1)}[1 - 2v_{\mathbf{k}}^{(1)2}] + 2\left\{\sum_{\mathbf{k}'}{}'[v_{11}u_{\mathbf{k}'}^{(1)}v_{\mathbf{k}'}^{(1)} + v_{12}u_{\mathbf{k}'}^{(2)}v_{\mathbf{k}'}^{(2)}]\right\}u_{\mathbf{k}}^{(1)}v_{\mathbf{k}}^{(1)} \tag{8.6.6}$$

The quantity within the curly brackets is equal to Δ_1 if we use Eqs. (8.5.11) and (8.5.12). Thus we obtain

$$\Delta\epsilon = \epsilon_k^{(1)}[1 - 2v_{\mathbf{k}}^{(1)2}] + 2\Delta_1 u_{\mathbf{k}}^{(1)}v_{\mathbf{k}}^{(1)}$$

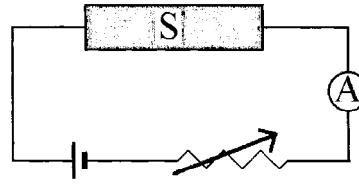

Figure 8.9. A circuit containing superconductor (*S*), battery, and resistance.

If we rewrite $v_{\mathbf{k}}^{(1)}$ and $u_{\mathbf{k}}^{(1)}$ in terms of $E_{\mathbf{k}}^{(1)}$ and Δ_1, we obtain

$$\Delta\epsilon = E_{\mathbf{k}}^{(1)} \tag{8.6.7}$$

Thus the unpaired electron has an energy higher by $E_{\mathbf{k}}^{(1)}$ than the hypothetical superelectron, as shown in Fig. 8.8. The validity domain for the above statement is

$$0 < \epsilon_k^{(1)} < \hbar\omega_D \tag{8.6.8}$$

Only in this domain, there can be superelectrons (part of condensed pairons) with which quasi-e1ectrons are to be compared.

8.6.5. The Energy Gap Equations

The reduced Hamiltonian H_0 in Eq. (8.2.6) can be expressed in terms of pairon operators b's only. In fact we can rewrite H_0 as

$$\begin{aligned} H_0 = &\sum_{\mathbf{k}}{}' 2\epsilon_k^{(1)} b_{\mathbf{k}}^{(1)\dagger} b_{\mathbf{k}}^{(1)} + \sum_{\mathbf{k}}{}' 2\epsilon_k^{(2)} b_{\mathbf{k}}^{(2)\dagger} b_{\mathbf{k}}^{(2)} \\ &- \sum_{\mathbf{k}}{}' \sum_{\mathbf{k}'}{}' [v_{11} b_{\mathbf{k}'}^{(1)\dagger} b_{\mathbf{k}}^{(1)} + v_{12} b_{\mathbf{k}'}^{(1)\dagger} b_{\mathbf{k}}^{(2)\dagger} + v_{21} b_{\mathbf{k}'}^{(2)} b_{\mathbf{k}}^{(1)} + v_{22} b_{\mathbf{k}'}^{(2)} b_{\mathbf{k}}^{(2)\dagger}] \end{aligned} \tag{8.6.9}$$

The ground state Ψ in Eq. (8.5.1) contains pairon variables only. Yet in the energy-gap equations (8.5.13), which result from the extremum condition for the ground-state energy, the energies of quasi-electrons $E_{\mathbf{k}}^{(j)}$ appear. No electron variables however appear in the starting Hamiltonian H_0 in Eq. (8.6.9). Thus it is impossible to guess the existence of any gaps in the quasi-electron energy spectra. Generally speaking the physics is lost in the variational calculation. We shall examine the gap equations from a different angle by using the equation-of-motion method in Sections 10.3–10.4.

8.6.6. Neutral Supercondensate; London Stability

The supercondensate composed of equal numbers of pairons of both charge types is electrically *neutral.* This neutrality explains the stability against a weak electric field because no Lorentz electric force can be exerted on the supercondensate and because the many-pairon supercondensate is in a quantized state. This stability is analogous to that of a stationary excited atomic state, say, the $2p$-state of a neutral hydrogen atom.

A neutral supercondensate is supported by experiments as follows: If a superconducting wire is used as part of a circuit connected to a battery, as shown in Fig. 8.9,

the superconducting wire, having no resistance, generates no potential drop. If a low-frequency *AC* voltage is applied to it, its response becomes more complicated. But the behavior can be accounted for if we assume that it has a normal component with a finite resistance and a super part. This is the *two-fluid model,* which was historically proposed by Gorter and Casimir in the analysis of heat capacity data.[6] The super part, or supercondensate, decreases with rising temperature and vanishes at T_c. The normal part may be composed of any charged elementary excitations including quasi-electrons and excited pairons. At any rate, analyses of all experiments indicate that *the supercondensate is not accelerated by the electric force.* This is a reasonable hypothesis. Otherwise the supercondensate would gain energy without limit, since the supercurrent is slowed down by neither impurities nor phonons, and a stationary state would never have been observed in the circuit.

If a supercondensate has a total charge Q, it suffers the Lorentz force QE, where E is the electric field strength. By applying Newton's equation of motion, (mass) × (acceleration) = force, such a supercondensate must have an infinite mass! But this cannot be a meaningful statement. The assumption of infinite masses for all supercondensates, large or small, does not allow one to discuss the mass's inherent extensive property. The only way out of this difficulty is to assume that the supercondensate has no charge. Then there is no Lorentz force and no acceleration. Finally a number of elemental superconductors exist in nature. If the supercondensate can have a net charge, the charge density should vary in different elements. But all superconducting states in different elements are similar, and no charge-density dependence has been detected. (A further corroboration of the above hypothesis comes from the AC Josephson effect, which will be discussed in Section 11.8.)

8.6.7. Cooper Pairs (Pairons)

The concept of pairons is inherent in the BCS theory, which is most clearly seen in the reduced Hamiltonian H_0 in Eq. (8.6.9), expressed in terms of pairon operators b's only. Phonon-exchange attraction is in action on any pair of electrons if their kinetic energies are nearly equal to zero. Our study in Section 8.4 indicates that a pairon has the energy–momentum (Cooper–Schrieffer) relation [Eq. (8.4.24)]: $w_q = w_0 + v_F q/2 < 0$. Note: The energy is negative; that is, the Cooper pair is bound.

The direct evidence for the fact that a Cooper pair is a bound quasi-particle having charge (magnitude) $2e$ comes from flux quantization experiments, which will be discussed in Section 11.1. The maximum binding energy $|w_0|$ can be measured directly in photoabsorption and quantum tunneling experiments (see Section 10.6).

Roughly speaking a Cooper pair may be pictured as a giant molecule of the size ~ 10^4 Å. The pair distribution function $P(r)$ versus interelectron distance r is shown schematically in Fig. 8.10. This picture may be obtained from Eq. (8.4.24) as follows: If the momentum (magnitude) q is sufficiently large, then the energy w_q of the pair becomes positive, and the pair should break up. The greatest allowable momentum q_0 for the bound pair from Eq. (8.4.24) is

$$q_0 = \frac{2|w_0|}{v_F} \tag{8.6.10}$$

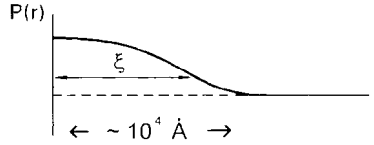

Figure 8.10. A schematic figure indicating the size of a Cooper pair ~ 10^4 Å.

Since $W = N_0 w_0$, the maximum binding energy $|w_0|$ should be on the order of $k_B T_c$:

$$|w_0| \cong k_B T_c \tag{8.6.11}$$

The order of magnitude for the Cooper pair size ξ_1 can be estimated from the uncertainty principle as

$$\xi_1 \cong \frac{\hbar}{q_0} \cong \frac{\hbar v_F}{2k_B T_c}, \tag{8.6.12}$$

[from Eqs. (8.6.10) and (8.6.11)], which is of the order 10^4 Å for typical elemental superconductors. The coherence length ξ_0 over which the G–L wave function (see Section 11.5) should not change appreciably, can be regarded as a measure of the Cooper pair size. This length ξ_0, calculated by the BCS theory,[1] is given by

$$\xi_0 = \frac{\hbar v_F}{\pi \Delta} = \frac{0.18 \hbar v_F}{k_B T_c} \tag{8.6.13}$$

which is of the same order of magnitude as ξ_1 in Eq. (8.6.12). It is customary to describe the Cooper pair size in terms of the BCS (or Pippard) coherence length ξ_0,[1,7] and we shall follow this practice hereafter.

8.6.8. The Cooper System

In the Cooper system, which is characterized by the Hamiltonian H_0 in Eq. (8.4.9), there are only electrons. The Cooper pair formed in the system has a negative energy given by Eq. (8.4.24). Since pairons are bosons (which will be shown in Section 9.1), all pairons can occupy the same zero-momentum state at 0 K. Then the ground-state energy of the system is given by [Eq. (8.3.14)]

$$W_c = N_0 w_0 = \hbar \omega_D \mathcal{N}(0) w_0$$

which is equal to that of the BCS system [see Eq. (8.5.22)].

For the Cooper system, pairons move with the linear energy–momentum relation Eq. (8.4.24) at all temperatures (far below the Debye temperature). The system of free pairons can be shown (see Sections 9.3 and 9.4) to undergo a B–E condensation transition of the second order similar to that observed in a real superconductor. However the condensate for the Cooper system has a finite-charge density, and there is no gap in the pairon energy spectrum. These two facts suggest that dropping the holes contribution from the Hamiltonian in Eq. (8.2.6) to obtain the Cooper Hamiltonian in Eq. (8.3.4) destroys essential elements of superconductivity. After reviewing the basic assumptions

in the generalized BCS Hamiltonian, enumerated in Section 8.1, we discover that the one-phonon exchange process *does* generate pairons of different charges simultaneously from the physical vacuum if the band structures are favorable. Thus there must be pairons of both charge types in any superconductor. In other words the Cooper system cannot be a model of a real superconductor. Despite this limitation the Cooper system is a very useful and exactly solvable auxiliary model in the theory of superconductivity. In fact we shall often use this model to facilitate the calculations needed for the generalized BCS system.

8.6.9. Formation of a Supercondensate; Occurrence of Superconductors

We now discuss the formation of a supercondensate based on the band structures of electrons and phonons. Let us first take lead (Pb), which forms an fcc lattice and which is a superconductor. This metal is known to have a neck-like hyperboloidal Fermi surface represented by[8]

$$E = \frac{p_1^2}{2m_1} + \frac{p_2^2}{2m_2} + \frac{p_3^2}{2m_3}, \quad (m_1, m_2, m_3) = (1.18, 0.244, -8.71)m \tag{8.6.14}$$

We postulate that the supercondensate composed of ± ground pairons is generated near the "necks." The electron transitions are subject to Pauli's exclusion principle, and therefore creating and annihilating ground pairons require a high degree of symmetry in the Fermi surface. A typical way of generating pairons of both charge types by one phonon exchange near the neck is shown in Fig. 8.3. Only part of electrons and holes near the specific region of the Fermi surface are involved in the formation of the supercondensate. The numbers of ± pairons, which are mutually equal by construction, may then be represented by $\hbar\omega_D \mathcal{N}(0)/2$, which justifies Eq. (8.5.16). Next take aluminum (Al), which is also a known fcc superconductor. Its Fermi surface contains inverted double caps characterized by effective masses of different signs ($m_1, m_2 > 0, m_3 < 0$). Acoustic phonons with small momenta may generate a supercondensate near the inverted double caps. Supercondensation occurs *independently of the lattice structure.* Beryllium (Be) forms a hcp crystal. Its Fermi surface in the second zone shown in Fig. 5.6 has necks. Thus Be is a superconductor. Tungsten (W) is a bcc metal, and its Fermi surface, shown in Fig. 5.7 has necks. This metal is also a superconductor. In summary elemental superconductors should have hyperboloidal Fermi surfaces favorable for creating ground pairons of both charge types mediated by small-momentum phonons. All of the elemental superconductors whose Fermi surfaces are known appear to satisfy this condition.

To test further let us consider a few more examples. A monovalent metal, such as sodium (Na), has a nearly spherical Fermi surface within the first Brillouin zone. Such a metal cannot become superconducting at any temperature since it does not have holes to begin with; it cannot have hole pairons and therefore cannot form a neutral supercondensate. A monovalent fcc metal like Cu has a set of necks at the Brillouin boundary. This neck is forced by the inversion symmetry of the lattice (see Section 5.4). The region of the hyperboloidal Fermi surface may be more severely restricted than those necks (unforced) in Pb. Thus this metal may become superconducting at extremely low temperatures, which is not ruled out but unlikely.

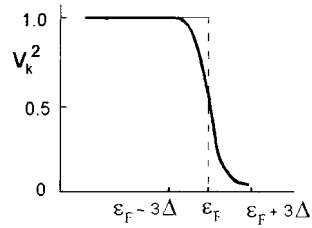

Figure 8.11. The behavior of $v_{\mathbf{k}}^2$ near the Fermi energy.

8.6.10. Blurred Fermi Surface

In Sections 5.3–5.5, we saw that a normal metal has a sharp Fermi surface at 0 K. This fact manifests itself in the linear-T heat capacity universally observed at the lowest temperatures, as shown in Section 5.5. The linear-T law is in fact the most important support of the Fermi liquid model. For a superconductor the Fermi surface is not sharp everywhere. To see this, let us solve Eq. (8.5.11) with respect to $u_{\mathbf{k}}^2$ and $v_{\mathbf{k}}^2$ in the BCS limits. We obtain (Problem 8.7.2)

$$v_{\mathbf{k}}^2 = \frac{1}{2}\left[1 - \frac{\epsilon_k}{\left(\epsilon_k^2 + \Delta^2\right)^{1/2}}\right], \qquad u_{\mathbf{k}}^2 = \frac{1}{2}\left[1 + \frac{\epsilon_k}{\left(\epsilon_k^2 + \Delta^2\right)^{1/2}}\right] \tag{8.6.15}$$

Figure 8.11 shows a general behavior of $v_{\mathbf{k}}^2$ near the Fermi energy. For the normal state $\Delta = 0$, there is a sharp boundary at $\epsilon_k = 0$; but for a finite Δ, the quantity $v_{\mathbf{k}}^2$ drops off to zero over a region on the order of 2–3 Δ. This $v_{\mathbf{k}}^2$ represents the probability that the virtual electron pair at $(\mathbf{k}\uparrow, -\mathbf{k}\downarrow)$ participates in the formation of the supercondensate. It is *not* the probability that either electron of the pair occupies the state **k.** Still the diagram indicates the nature of the changed electron distribution in the ground state. The supercondensate is generated only near the necks and/or inverted double caps. Thus these parts of the Fermi surface are blurred or fuzzy. Elementary excitations near these parts dominate thermodynamic properties of the superconductor below T_c, which will be discussed in Chapter 10.

8.7. CONCLUDING REMARKS

The superconducting state is characterized by the presence of a supercondensate. In this chapter we have seen that the supercondensate at 0 K is composed of equal numbers of pairons of both charge types, the total number being $\hbar\omega_D \mathcal{N}(0)$. The main features of a superconductor (zero resistance, Meissner effect, flux quantization, and Josephson effects) arise directly from the moving supercondensate, which dominates transport and magnetic phenomena. The supercondensate necessarily generates gaps in the elementary excitation energies. All experimental probes are of course done at finite temperatures. At what temperature does a superconducting transition occur? Why and how do the energy gaps change with temperature? To answer these and other questions, we must develop a finite-temperature theory, which will be done in the following chapters.

Problem 8.7.1. (a) Derive Eq. (8.6.6). (b) Verify Eq. (8.6.7).

Problem 8.7.2. Derive Eq. (8.6.15).

REFERENCES

1. J. Bardeen, L. N. Cooper, and J. R. Schrieffer, *Phys. Rev.* **108,** 1175 (1957).
2. S. Fujita, *J. Supercond.* **4,** 297 (1991); *ibid.* **5,** 83 (1992); S. Fujita and S. Watanabe, *J. Supercond.* **5,** 219 (1992); *ibid.* **6,** 75 (1993); S. Fujita and S. Godoy, *J. Supercond.* **6,** 373 (1993).
3. L. D. Landau, *Sov. Phys. JETP* **3,** 920 (1957); *ibid.* **5,** 101 (1957); *ibid.* **8,** 70 (1959).
4. L. N. Cooper, *Phys. Rev.* **104,** 1189 (1956).
5. J. R. Schrieffer, *Theory of Superconductivity,* (Benjamin, New York, 1964).
6. C. J. Gorter and H. G. B. Casimir, *Phys. Z.* **35,** 963 (1934); *Z. Tech. Phys.* **15,** 539 (1934).
7. A. B. Pippard, *Proc. Roy. Soc.* (*London*) **A216,** 547 (1953).
8. Y. Onuki, H. Suematsu, and S. Tamura, *J. Phys. Chem. Solids* **38,** 419 and 431 (experiment) (1977); S. Watanabe and S. Fujita, *J. Phys. Chem. Solids* **52,** 985 (theory) (1991).

This page intentionally left blank.

9

Bose–Einstein Condensation of Pairons

Pairons can multiply occupy one and the same net momentum state. They move as free massless bosons having a linear energy–momentum relation $\epsilon = cp$. The system of pairons undergoes a B–E condensation transition of the second (third) order in three (two) dimensions with the critical temperature $T_c = 1.01\,\hbar v_F k_B^{-1} n^{1/3}$ $(1.24\hbar v_F k_B^{-1} n^{1/2})$, where n is the pairon density.

9.1. PAIRONS MOVE AS BOSONS

By quantum statistical postulate, every elementary particle is either a boson or a fermion. Such composites as He^3, He^4, pairons experimentally are found to be either bosons or fermions. According to Ehrenfest–Oppenheimer–Bethe (EOB)'s rule,[1] a composite is a boson if it contains an even number of fermions, a fermion if the number of fermions in it is odd. Thus, a pairon composed of two electrons (fermions) is a boson. Since this is an important point, we first review the arguments leading to EOB's rule. We follow Bethe's arguments.[1] Take a composite of two identical fermions and study the symmetry of the wave function for two composites, which has four particle-state variables, two for the first composite and two for the second one. Imagine that the exchange between the two composites is carried out particle by particle. Each exchange of fermions (bosons) changes the wave function by the factor – 1 (+1). In the present example, the sign changes twice; therefore the wave function is symmetric. If a composite contains different types of particles, as in the case of He^4, the symmetry of the wave function should be deduced by the interchange within each type. These arguments can clearly be extended to a general case. We note that Feynman used the same arguments to deduce that pairons are bosons.[2]

Since a composite has more degrees of freedom, the correspondence between the symmetry of the wave function and the quantum statistics is not one-to-one. A further work is required. We shall show that pairons can multiply occupy one and the same net momentum state. The total number (operator) of pairons can be represented by

$$\tilde{N}^{(c)} \equiv \sum_{\mathbf{k}_1}\sum_{\mathbf{k}_2} n_{12} = \sum_{\mathbf{q}}\sum_{\mathbf{k}} B^{\dagger}_{\mathbf{kq}} B_{\mathbf{kq}} = \sum_{\mathbf{q}} n^{(c)}_{\mathbf{q}},$$
$$\left[\mathbf{q} \equiv \mathbf{k}_1 + \mathbf{k}_2,\ \ \mathbf{k} \equiv (\mathbf{k}_1 - \mathbf{k}_2)/2\right] \tag{9.1.1}$$

where the superscripts c indicate pairons and

$$n_{\mathbf{q}}^{(c)} \equiv \sum_{\mathbf{k}} B_{\mathbf{kq}}^{\dagger} B_{\mathbf{kq}} \equiv \sum_{\mathbf{k}} n_{\mathbf{kq}} \tag{9.1.2}$$

represents the number (operator) of pairons with momentum $\mathbf{q}$. Using Eqs. (8.4.2), (8.4.4), and (8.2.2), we obtain (Problem 9.1.1)

$$n_{12}^2 \equiv [B_{12}^{\dagger} B_{12}]^2 = B_{12}^{\dagger}[1 - n_1 - n_2 + B_{12}^{\dagger} B_{12}] B_{12} = B_{12}^{\dagger} B_{12} \equiv n_{12} \tag{9.1.3}$$

Hence $(n_{12}^2 - n_{12})|n_{12}'\rangle = n_{12}'(n_{12}' - 1)|n_{12}'\rangle = 0$, indicating that the eigenvalues n_{12}' of the operator n_{12} are 0 or 1. Thus, the number operator in the k–q representation $n_{\mathbf{kq}} = B_{\mathbf{kq}}^{\dagger} B_{\mathbf{kq}}$ with both $\mathbf{k}$ and $\mathbf{q}$ specified has the eigenvalues 0 or 1:

$$n_{\mathbf{kq}}' = 0, 1 \tag{9.1.4}$$

From Eq. (9.1.2) the eigenvalues $n_{\mathbf{q}}'^{(c)}$ of the operator $n_{\mathbf{q}}^{(c)}$ must be nonnegative integers:

$$n_{\mathbf{q}}'^{(c)} = 0, 1, 2, \cdots \qquad \text{q.e.d.} \tag{9.1.5}$$

We may check this result more formally as follows. We introduce

$$B_{\mathbf{q}}^{(c)} \equiv \sum_{\mathbf{k}} B_{\mathbf{kq}} \tag{9.1.6}$$

and calculate $[B_{\mathbf{q}}^{(c)}, n_{\mathbf{q}}^{(c)}]$ to obtain (Problem 9.1.2)

$$[B_{\mathbf{q}}^{(c)}, n_{\mathbf{q}}^{(c)}] = \sum_{\mathbf{k}} (1 - n_{\mathbf{k}+\mathbf{q}/2\uparrow} - n_{-\mathbf{k}+\mathbf{q}\downarrow}) B_{\mathbf{kq}} = B_{\mathbf{q}}^{(c)} \tag{9.1.7}$$

whose Hermitian conjugate is

$$[n_{\mathbf{q}}^{(c)}, B_{\mathbf{q}}^{(c)\dagger}] = B_{\mathbf{q}}^{(c)\dagger} \tag{9.1.8}$$

From these equations we can show [see Eq. (6.1.10) and what follows] that the eigenvalues of $n_{\mathbf{q}}^{(c)}$ are $0, 1, 2, \cdots$ as stated in Eq. (9.1.5). Let us illustrate Eq. (9.1.5) by taking a system of electrons moving in one dimension. The momentum state of an electron pair may be represented by a quantum cell in the k–q space. For a many-electron-pair system, the system state can be represented by the occupation numbers $\{n_{\mathbf{kq}}'\}$ with the restriction that $n_{\mathbf{kq}}' = 0$ or 1, as shown in Fig. 9.1. The number of pairons (characterized by the net momentum q only) $n_{\mathbf{q}}'^{(c)}$ is the sum of pairs at the column q, and clearly it is zero or a positive integer.

The existence of pairons as composites shows up clearly in the flux quantization experiments. The boson nature of pairons appears in the behavior of a supercurrent and particularly in Josephson interference, which will be discussed in Chapter 11.

In the original BCS theory[2] ground pairons were introduced, but their boson nature was not discussed. This appears to have generated much confusion in the literature.[4]

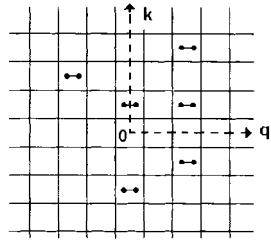

Figure 9.1. The number representation of many electron pairs in the k–q space.

Our bosonic view of pairons does not however contradict the BCS calculations. In fact the total number of ground pairons N_0 in the BCS system at 0 K is represented by

$$N_0 \equiv \sum_{\mathbf{k}} \sum_{i} b_{\mathbf{k}}^{\dagger(i)} b_{\mathbf{k}}^{(i)} \equiv \sum_{\mathbf{k}} \sum_{i} B_{\mathbf{k}0}^{\dagger(i)} B_{\mathbf{k}0}^{(i)} \tag{9.1.9}$$

Its eigenvalues are 0, 1, 2,$\cdots$. In other words there are many pairons all condensed at zero momentum.

If the system in equilibrium is characterized by the grand canonical density operator ρ_{gc}, the ensemble average $\langle n_{\mathbf{q}}^{(c)} \rangle$ can be computed simply in the energy-state occupation number representation. The total energy E for free pairons is given by

$$E = \sum_{\mathbf{q}} w_q n_{\mathbf{q}}^{\prime(c)} \tag{9.1.10}$$

After straightforward calculations, we obtain (Problem 9.1.3):

$$\langle n_{\mathbf{q}}^{(c)} \rangle = \frac{1}{\exp[\beta w_q - \alpha] - 1} \equiv f_B(w_q) \tag{9.1.11}$$

where f_B represents the Bose distribution function. In Chapter 9, we consider mainly bosons and drop the subscript B on f hereafter. The total number of pairons consistent with the Cooper Hamiltonian H in Eq. (8.4.9) is $N_0 = \hbar\omega_D \mathcal{N}(0)$. Thus we have

$$\left(\frac{1}{V}\right) \sum_{\mathbf{q}} \langle n_{\mathbf{q}}^{\prime(c)} \rangle = \left(\frac{1}{V}\right) \sum_{\mathbf{q}} f(w_q) = \frac{N_0}{V} \equiv n_0 \equiv \frac{\hbar\omega_D \mathcal{N}(0)}{V} \tag{9.1.12}$$

We saw in Section 8.4 that pairons have the Cooper–Schrieffer relation:

$$\epsilon_q \equiv w_q - w_0 = cq \tag{9.1.13}$$

where we shifted the energy constant. This relation is similar to that satisfied by acoustic phonons (or photons): $\in = c_s q$; only the speeds are different. A system of pairons undergoes a B–E condensation transition, which we discuss in the following sections.

Problem 9.1.1. Verify Eqs. (9.1.3).

Problem 9.1.2. Use Eq. (8.4.8) to verify Eq. (9.1.7).

Problem 9.1.3. Verify Eq. (9.1.11).

9.2. FREE BOSONS MOVING IN TWO DIMENSIONS WITH $\epsilon = cp$

In this section we consider a system of free massless bosons moving in two dimensions. The system will be shown to undergo a B–E condensation. The B–E condensation of free massive bosons having $\epsilon = p^2/2m$ and moving in three dimensions was discussed earlier in Chapter 4. The following treatment is essentially similar to this case. The results obtained here are useful in the discussion of high-T_c superconductors (see Section 13.5).

The number of bosons N and the Bose distribution function:

$$f(\epsilon;\beta,\mu) \equiv \frac{1}{e^{\beta(\epsilon-\mu)}-1} \equiv f(\epsilon) \quad (>0) \qquad [\alpha \equiv \beta\mu] \tag{9.2.1}$$

are related by

$$N = \sum_{\mathbf{p}} f(\epsilon_p;\beta,\mu) = N_0 + {\sum_{\mathbf{p},\epsilon_p>0}}' f(\epsilon_p) \tag{9.2.2}$$

where:

$$N_0 \equiv (e^{-\beta\mu}-1)^{-1} \tag{9.2.3}$$

is the number of zero-momentum bosons. The prime on the summation indicates the omission of the $p = 0$ state. For notational convenience we write

$$\epsilon = cp \equiv \frac{2}{\pi} v_F p \ (>0) \tag{9.2.4}$$

where $c \equiv 2v_F/\pi$ is the pairon speed in two dimensions.

We divide Eq. (9.2.2) by the normalization area L^2, then take the bulk limit:

$$N \to \infty,\ L \to \infty \text{ while } n_0 \equiv N_0 L^{-2} \equiv n \tag{9.2.5}$$

obtaining

$$n - n_0 \equiv (2\pi\hbar)^{-2} \int d^2p f(\epsilon) \tag{9.2.6}$$

where $n_0 \equiv N_0/L^2$ is the number density of zero-momentum bosons. To avoid confusion we denote the total number density by n hereafter [see Eq. (9.2.5)]. After performing the angular integration and changing the integration variable, we obtain from Eq. (9.2.6) (Problem 9.2.1):

$$2\pi\hbar^2 c^2 \beta^2 (n - n_0) = \int_0^\infty dx \frac{x}{\lambda^{-1}e^x - 1}, \qquad [x = \beta\epsilon] \tag{9.2.7}$$

$$\lambda \equiv e^{\beta\mu} \ (<1) \tag{9.2.8}$$

The fugacity λ is less than unity for all temperatures. After expanding the integrand in Eq. (9.2.7) in powers of λe^{-x} (< 1), then carrying out the x-integration, we obtain

$$n_x \equiv n - n_0 = \frac{k_B^2 T^2 \phi_2(\lambda)}{2\pi\hbar^2 c^2} \tag{9.2.9}$$

$$\phi_m(\lambda) \equiv \sum_{k=1}^{\infty} \frac{\lambda^k}{k^m} \qquad (0 \le \lambda < 1) \tag{9.2.10}$$

Equation (9.2.9) gives a relation among λ, n, and T.

The function $\phi_2(\lambda)$ monotonically increases from zero to the maximum value $\phi_2(1) \cong 1.645$ as λ is raised from zero to one. At the extreme low-temperature region, $\lambda \cong 1$, $\phi_2(\lambda) = \phi_2(1) \cong 1.645$, and the density of excited bosons n_x varies like T^2 as seen from Eq. (9.2.9). This temperature behavior of n_x persists as long as the rhs of Eq. (9.2.9) is smaller than the total density n; the limit or critical temperature T_c is

$$n = \frac{k_B^2 T_c^2 \Phi_2(1)}{2\pi\hbar^2 c^2}$$

or

$$\boxed{k_B T_c = 1.954\,\hbar c n^{1/2} \; [= 1.24\,\hbar v_F n_0^{1/2}].} \tag{9.2.11}$$

If temperature is increased beyond T_c, the density of zero momentum bosons, n_0, becomes vanishingly small compared to n, and the fugacity λ can be determined from

$$n = \frac{k_B^2 T^2 \phi_2(\lambda)}{2\pi\hbar^2 c^2}, \qquad (T > T_c) \tag{9.2.12}$$

In summary fugacity λ is equal to unity in the condensed region $T < T_c$, and it becomes smaller than unity for $T > T_c$, where its value is determined from Eq. (9.2.12).

The internal energy density u, which is equal to the ensemble-average of the system energy per unit area, is given by

$$u = (2\pi\hbar)^{-2} \int d^2p\, \epsilon f(\epsilon) \tag{9.2.13}$$

This can be calculated in the same way as Eq. (9.2.6). We obtain (Problem 9.2.2)

$$u = \frac{\phi_3(\lambda)}{\pi\hbar^2 c^2 \beta^3} = 2nk_B \frac{T^3}{T_c^2} \frac{\phi_3(\lambda)}{\phi_2(1)} \tag{9.2.14}$$

The molar heat capacity at constant density C_n is defined by

$$C \equiv C_n \equiv R(nk_B)^{-1} \frac{\partial u(T,n)}{\partial T} \tag{9.2.15}$$

where R is the gas constant. The partial derivative $\partial u/\partial T$ may be calculated through

$$\begin{aligned} \frac{\partial u(T,n)}{\partial T} &= \frac{\partial u(T,\lambda)}{\partial T} + \frac{\partial u(T,\lambda)}{\partial \lambda} \frac{\partial \lambda(T,n)}{\partial T} \\ &= \frac{\partial u(T,\lambda)}{\partial T} - \frac{\partial u(T,\lambda)}{\partial \lambda} \frac{\partial n(T,\lambda)/\partial T}{\partial n(T,\lambda)/\partial \lambda} \end{aligned} \tag{9.2.16}$$

(Problem 9.2.3). All quantities (n, u, C) can now be expressed in terms of $\phi_m(\lambda)$. After straightforward calculations, the molar heat C becomes (Problem 9.2.4)

$$\begin{aligned} C &= R(\pi\hbar^2 c^2 n k_B)^{-1} k_B^3 T^2 \left[3\phi_3(\lambda) - \frac{2\phi_2^2(\lambda)}{\phi_1(\lambda)} \right] \\ &= 6R \left(\frac{T}{T_c} \right)^2 \frac{\phi_3(\lambda)}{\phi_2(1)} - 4R \frac{\phi_2(\lambda)}{\phi_1(\lambda)} \end{aligned} \tag{9.2.17}$$

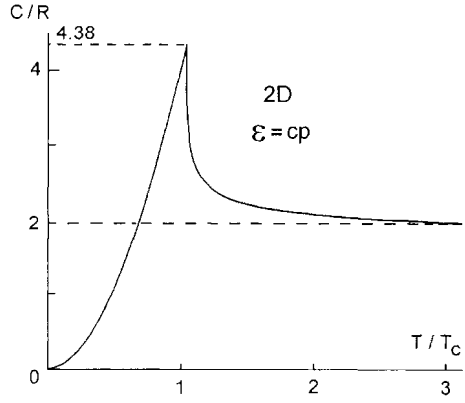

Figure 9.2. The molar heat capacity C for two-dimensional massless bosons rises like T^2, reaches $4.38\,R$ at T_c, and then decreases to $2R$ in the high-temperature limit.

In the condensed region $T < T_c$, $\lambda = 1$. We observe that as $\lambda \to 1$

$$\phi_1(\lambda) \to \sum_1^\infty k^{-1} = \infty, \qquad \phi_2(\lambda) \to \phi_2(1) \cong 1.645$$
$$\phi_3(\lambda) \to \phi_3(1) \cong 1.202, \qquad \phi_4(\lambda) \to \phi_4(1) \cong 1.082 \tag{9.2.18}$$

Using these, we obtain from Eqs. (9.2.14) and (9.2.17)

$$u = 2nk_B \frac{\phi_3(1)}{\phi_2(1)} \frac{T^3}{T_c^2} \tag{9.2.19}$$

$$C = 6R \frac{\phi_3(1)}{\phi_2(1)} \left(\frac{T}{T_c}\right)^2 \qquad (T < T_c) \tag{9.2.20}$$

Observe the quadratic temperature dependence of C; also note that the molar heat capacity C at T_c is given by

$$C(T_c) = 6R \frac{\phi_3(1)}{\phi_1(1)} = 4.38\,R \tag{9.2.21}$$

For $T > T_c$ the temperature dependence of λ, given by Eq. (9.2.12), is quite complicated. We can solve Eq. (9.2.12) for λ numerically by computer, then substitute the solution into Eq. (9.2.17) to obtain the temperature behavior of C. The result is shown in Fig. 9.2. Using Eqs. (9.2.17) and (9.2.16) enables us not only to examine the analytic behavior of C near $T = T_c$ but also to obtain C without numerically computing the derivative $\partial u(T, n)/\partial T$.

In summary the molar heat capacity C for a two-dimensional massless bosons rises like T^2 in the condensed region, reaches 4.38 R at $T = T_c$, then decreases to the high-temperature limit value $2R$. Heat capacity changes continuously at $T = T_c$, but its temperature derivative $\partial C(T, n)/\partial T$ jumps at this point. Thus the B–E condensation is

a third-order phase transition. The condensation of massless bosons in two dimensions is noteworthy[5] since the B–E condensation of massive bosons ($\epsilon = p^2/2m$) is known to occur in three dimensions only. This is not a violation of Hohenberg's theorem[6] that there can be no long-range order in two dimensions, which is derived with the assumption of an f-sum rule representing the mass conservation law. In fact no B–E condensation occurs in two dimensions for finite-mass bosons.[5]

Problem 9.2.1. Verify Eq. (9.2.7).

Problem 9.2.2. Verify Eq. (9.2.14).

Problem 9.2.3. Prove Eq. (9.2.16).

Problem 9.2.4. Verify Eq. (9.2.17).

9.3. FREE BOSONS MOVING IN THREE DIMENSIONS WITH $\epsilon = cp$

The case of free massless bosons moving in three dimensions can be treated similarly. We state the theories and results concisely. The results will be used to describe a B–E condensation of pairons for the BCS system in Section 9.4.

In the bulk limit the normalization condition is given by

$$n - n_0 = (2\pi\hbar)^{-3} \, d^3p f(\epsilon; \beta, \mu) \tag{9.3.1}$$

which reduces to (Problem 9.3.1)

$$n_x \equiv n - n_0 = \frac{k_B^3 T^3 \phi_3(\lambda)}{\pi^2 \hbar^3 c^3} \tag{9.3.2}$$

This equation, similar to Eq. (9.2.9), gives a relation among (n, T, λ).

The function $\phi_3(\lambda)$ has the maximum value of 1.202 at $\lambda = 1$, and it decreases monotonically as λ is reduced from one to zero. Examining Eq. (9.3.2) indicates that

$$\lambda = 1 \text{ for } T < T_c \tag{9.3.3}$$

where the critical temperature T_c is given by

$$k_B T_c = \left[\frac{\pi^2 \hbar^3 c^3 n}{\phi_3(1)} \right]^{1/3} = 2.017 \, \hbar c n^{1/3} \tag{9.3.4}$$

and that λ becomes less than unity for $T > T_c$, where its value is determined from

$$\pi^2 \hbar^3 c^3 n = k_B^3 T^3 \phi_3(\lambda) \qquad (T > T_c) \tag{9.3.5}$$

Substituting Eq. (9.3.3) into Eq. (9.3.2) indicates that the number density of excited bosons n_x in the condensation region ($T < T_c$) rises like T^3 with increasing temperature. This means that the number density of zero-momentum bosons n_0 varies as

$$\frac{n_0}{n} = 1 - \left(\frac{T}{T_c} \right)^3 \text{ for } T < T_c \tag{9.3.6}$$

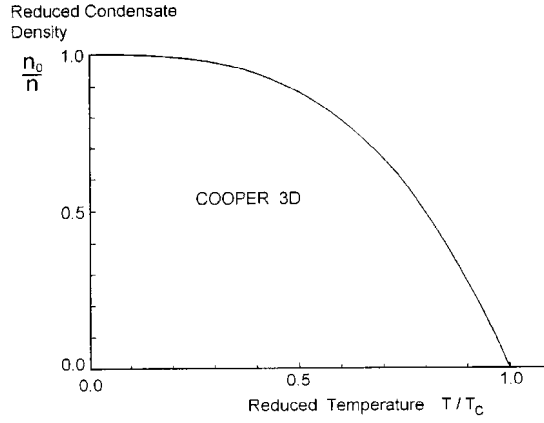

Figure 9.3. The temperature variation of the ground boson density n_0.

which is shown in Fig. 9.3.

The internal energy density u is calculated to be (Problem 9.3.2):

$$u = (2\pi\hbar)^{-3} \int d^3p\, \epsilon f(\epsilon) = \frac{3nk_B T^4 \phi_4(\lambda)}{T_c^3 \phi_3(1)} \tag{9.3.7}$$

This u rises like T^4 in the condensation region:

$$u \propto T^4, \qquad (T < T_c) \tag{9.3.8}$$

in just the same manner as the Stephan-Boltzmann law for black-body radiation. The temperature dependence becomes milder in the nondegenerate region: $T > T_c$, see Fig. 9.4.

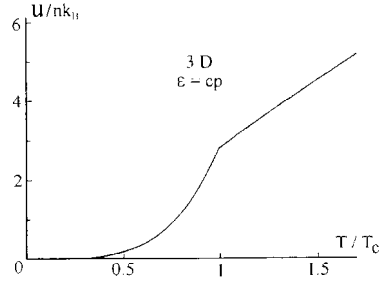

Figure 9.4. The internal energy density u for three-dimensional massless bosons rise like T^4 below T_c and grows less steeply after passing T_c, with a discontinuous change in the slope at $T = T_c$.

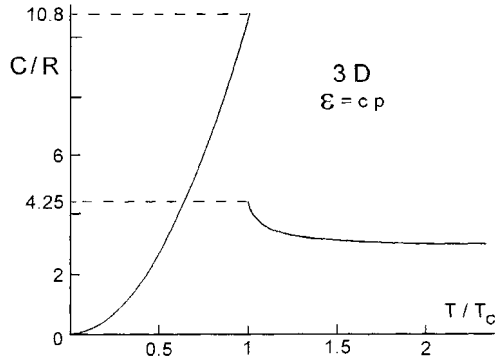

Figure 9.5. The molar heat capacity C for three-dimensional massless bosons rises like T^3, and reaches 10.8 R at the transition temperature $T_c = 2.02\,\hbar c n^{1/3}$. It then drops abruptly by 6.57R and approaches the high-temperature limit value 3R.

The molar heat capacity $C \equiv R(nk_B)^{-1}\partial u(T,n)/\partial T$ is (Problem 9.3.3)

$$C = 12R\left(\frac{T}{T_c}\right)^3 \frac{\phi_4(1)}{\phi_3(1)} = 10.8\,R\left(\frac{T}{T_c}\right)^3, \qquad \text{if } T < T_c \tag{9.3.9}$$

$$C = 12R\left(\frac{T}{T_c}\right)^3 \frac{\phi_4(\lambda)}{\phi_3(1)} - 9R\frac{\phi_3(\lambda)}{\phi_2(\lambda)}, \qquad \text{if } T > T_c \tag{9.3.10}$$

We see immediately that the molar heat C has a discontinuous drop ΔC at T_c equal to

$$\Delta C = \frac{9R\phi_3(1)}{\phi_2(1)} = 6.57\,R \tag{9.3.11}$$

The temperature behavior of C is shown in Fig. 9.5. Thus the phase transition is of second order in contrast to the third-order phase transition obtained for the two-dimensional bosons.

Problem 9.3.1. Verify Eq. (9.3.2).

Problem 9.3.2. Verify Eq. (9.3.7).

Problem 9.3.3. Verify Eqs. (9.3.9) and (9.3.10).

9.4. B–E CONDENSATION OF PAIRONS

In the generalized BCS system there are pairons of two charge types. The energy-momentum relation for each type of pairon above T_c is the same as that for the pairon in the Cooper system. (This relation changes however below T_c because of the presence of the supercondensate, which we discuss in Chapter 10.) In the present section, we treat the B-E condensation of pairons by approaching it from the high temperature side.

Creation operators for electron and hole pairons are defined by

$$B_{12}^{(1)\dagger} \equiv B_{\mathbf{k}_1\uparrow\mathbf{k}_2\downarrow}^{(1)\dagger} \equiv c_1^{(1)\dagger} c_2^{(1)\dagger}, \qquad B_{34}^{(2)\dagger} \equiv c_4^{(2)\dagger} c_3^{(2)\dagger} \tag{9.4.1}$$

The commutation relations can be calculated by using Eqs. (8.2.2) and (8.4.2), yielding:

$$[B_{12}^{(j)}, B_{34}^{(j)\dagger}] = \begin{cases} 1 - n_1^{(j)} - n_2^{(j)} & \text{if } \mathbf{k}_1 = \mathbf{k}_3 \quad \text{and } \mathbf{k}_2 = \mathbf{k}_4 \\ c_2^{(j)} c_4^{(j)\dagger} & \text{if } \mathbf{k}_1 = \mathbf{k}_3 \quad \text{and } \mathbf{k}_2 \neq \mathbf{k}_4 \\ c_1^{(j)} c_3^{(j)\dagger} & \text{if } \mathbf{k}_1 \neq \mathbf{k}_3 \quad \text{and } \mathbf{k}_2 = \mathbf{k}_4 \\ 0 & \text{otherwise} \end{cases}$$
$$[B_{12}^{(j)}, B_{34}^{(j)}] = 0 \tag{9.4.2}$$

subject to the condition that pairon operators of different types j commute. Here

$$n_1^{(j)} \equiv c_{\mathbf{k}_1\uparrow}^{(j)\dagger} c_{\mathbf{k}_1\uparrow}^{(j)}, \qquad n_2^{(j)} \equiv c_{\mathbf{k}_2\downarrow}^{(j)\dagger} c_{\mathbf{k}_2\downarrow}^{(j)} \tag{9.4.3}$$

represent the number operators for electrons and holes. In addition we obtain

$$[B_{12}^{(j)}]^2 = 0 \tag{9.4.4}$$

Equations (9.4.2) and (9.4.4) are generalizations of Eqs. (8.4.2)–(8.4.4).

Let us now introduce the relative and net momenta $(\mathbf{k}, \mathbf{q})$ such that

$$\begin{aligned} \mathbf{k} &\equiv (1/2)(\mathbf{k}_1 - \mathbf{k}_2), & \mathbf{q} &\equiv \mathbf{k}_1 + \mathbf{k}_2; \\ \mathbf{k}_1 &= \mathbf{k} + (1/2)\mathbf{q}, & \mathbf{k}_2 &= -\mathbf{k} + (1/2)\mathbf{q} \end{aligned} \tag{9.4.5}$$

Alternatively we can represent annihilation operators for pairons by

$$B_{\mathbf{kq}}^{\prime(1)} \equiv B_{\mathbf{k}_1\uparrow\mathbf{k}_2\downarrow}^{(1)} \equiv c_{-\mathbf{k}+\mathbf{q}/2\downarrow}^{(1)} c_{\mathbf{k}+\mathbf{q}/2\uparrow}^{(1)}, \qquad B_{\mathbf{kq}}^{\prime(2)} \equiv c_{\mathbf{k}+\mathbf{q}/2\uparrow}^{(2)} c_{-\mathbf{k}+\mathbf{q}/2\downarrow}^{(2)} \tag{9.4.6}$$

The prime on B is dropped hereafter. In this k–q representation the commutation relations [Eq. (9.4.2)] and the Pauli restriction [Eq. (9.4.4)] can be reexpressed as

$$[B_{\mathbf{kq}}^{(j)}, B_{\mathbf{k'q'}}^{(i)\dagger}] = \begin{cases} (1 - n_{\mathbf{k}+\mathbf{q}/2\uparrow} - n_{-\mathbf{k}+\mathbf{q}/2\downarrow})\delta_{ji} & \text{if } \mathbf{k} = \mathbf{k'} \text{ and } \mathbf{q} = \mathbf{q'} \\ c_{-\mathbf{k}+\mathbf{q}/2\downarrow}^{(j)} c_{-\mathbf{k'}+\mathbf{q'}/2\downarrow}^{(j)\dagger} \delta_{ji} & \text{if } \mathbf{k} + \frac{\mathbf{q}}{2} = \mathbf{k'} + \frac{\mathbf{q'}}{2} \\ & \quad \text{and } -\mathbf{k} + \frac{\mathbf{q}}{2} \neq -\mathbf{k'} + \frac{\mathbf{q'}}{2} \\ c_{\mathbf{k}+\mathbf{q}/2\uparrow}^{(j)} c_{\mathbf{k'}+\mathbf{q'}/2\uparrow}^{(j)\dagger} \delta_{ji} & \text{if } \mathbf{k} + \frac{\mathbf{q}}{2} \neq \mathbf{k'} + \frac{\mathbf{q'}}{2} \\ & \quad \text{and } -\mathbf{k} + \frac{\mathbf{q}}{2} = -\mathbf{k'} + \frac{\mathbf{q'}}{2} \\ 0 & \text{otherwise} \end{cases} \tag{9.4.7}$$

$$[B_{\mathbf{kq}}^{(j)}, B_{\mathbf{k'q'}}^{(i)}] = 0, \qquad [B_{\mathbf{kq}}^{(j)}]^2 = 0 \tag{9.4.8}$$

We continue to represent the annihilation operators for ground pairons by $b_{\mathbf{k}}^{(j)}$. Using the new notation, we can rewrite the full Hamiltonian in Eq. (8.2.1) as

$$\begin{aligned} H = {} & \sum_{\mathbf{k},s} \epsilon_k^{(1)} n_{\mathbf{k},s}^{(1)} + \sum_{\mathbf{k},s} \epsilon_k^{(2)} n_{\mathbf{k},s}^{(2)} \\ & - \sum_{\mathbf{k}}{}' \sum_{\mathbf{q}}{}' \sum_{\mathbf{k'}}{}' [v_{11} B_{\mathbf{k'q}}^{(1)\dagger} B_{\mathbf{kq}}^{(1)} + v_{12} B_{\mathbf{k'q}}^{(1)\dagger} B_{\mathbf{kq}}^{(2)\dagger} + v_{21} B_{\mathbf{kq}}^{(2)} B_{\mathbf{k'q}}^{(1)} + v_{22} B_{\mathbf{k'q}}^{(2)} B_{\mathbf{kq}}^{(2)\dagger}] \\ & - \sum_{\mathbf{k}}{}' \sum_{\mathbf{k'}}{}' [v_{11} b_{\mathbf{k'}}^{(1)\dagger} b_{\mathbf{k}}^{(1)} + v_{12} b_{\mathbf{k}}^{(2)\dagger} b_{\mathbf{k'}}^{(1)\dagger} + v_{21} b_{\mathbf{k}}^{(2)} b_{\mathbf{k'}}^{(1)} + v_{22} b_{\mathbf{k'}}^{(2)} b_{\mathbf{k}}^{(2)\dagger}] \end{aligned} \tag{9.4.9}$$

Bilinear terms in b and B do not appear because of momentum conservation:

$$\mathbf{k}_1 + \mathbf{k}_2 - (\mathbf{k}_3 + \mathbf{k}_4) = \mathbf{q} - \mathbf{q}' = 0 \tag{9.4.10}$$

The theory developed so far can be applied for all temperatures. In the remainder of the present section, we consider the system above T_c with no supercondensate ($b = 0$). Then the Hamiltonian H is simplified to

$$H' = \sum_{\mathbf{k},s} \epsilon_k^{(1)} n_{\mathbf{k},s}^{(1)} + \sum_{\mathbf{k},s} \epsilon_k^{(2)} n_{\mathbf{k},s}^{(2)} \tag{9.4.11}$$
$$-\sum_{\mathbf{k}}{}' \sum_{\mathbf{q}}{}' \sum_{\mathbf{k}'}{}' [v_{11} B_{\mathbf{k}'\mathbf{q}}^{(1)\dagger} B_{\mathbf{k}\mathbf{q}}^{(1)} + v_{12} B_{\mathbf{k}'\mathbf{q}}^{(1)\dagger} B_{\mathbf{k}\mathbf{q}}^{(2)\dagger} + v_{21} B_{\mathbf{k}\mathbf{q}}^{(2)} B_{\mathbf{k}'\mathbf{q}}^{(1)} + v_{22} B_{\mathbf{k}'\mathbf{q}}^{(2)} B_{\mathbf{k}\mathbf{q}}^{(2)\dagger}]$$

The prime on H is dropped hereafter. Using Eqs. (9.4.7) and (9.4.11), we obtain (Problem 9.4.1)

$$\begin{aligned}[H, B_{\mathbf{k}\mathbf{q}}^{(1)\dagger}] = {} & [\epsilon^{(1)}(|\mathbf{k} + \mathbf{q}/2|) + \epsilon^{(1)}(|-\mathbf{k} + \mathbf{q}/2|)] B_{\mathbf{k}\mathbf{q}}^{(1)\dagger} \\ & - v_{11} \sum_{\mathbf{k}'} B_{\mathbf{k}'\mathbf{q}}^{(1)\dagger} (1 - n_{\mathbf{k}+\mathbf{q}/2\uparrow}^{(1)} - n_{-\mathbf{k}+\mathbf{q}/2\downarrow}^{(1)}) \\ & - v_{12} \sum_{\mathbf{k}'} B_{\mathbf{k}'\mathbf{q}}^{(2)} (1 - n_{\mathbf{k}+\mathbf{q}/2\uparrow}^{(1)} - n_{-\mathbf{k}+\mathbf{q}/2\downarrow}^{(1)})\end{aligned} \tag{9.4.12}$$

We observe here that the net momentum $\mathbf{q}$ is a constant of motion, which arises from momentum conservation.

We wish to find the energies of excited pairons from Eq. (9.4.12) by using the equation-of-motion method. If we drop the last sum containing v_{12}, the resulting equation is the same as Eq. (8.4.10), yielding the energy-eigenvalue in the bulk limit:

$$\begin{aligned}w_q^{(1)} a_1(\mathbf{k}, \mathbf{q}) = {} & [\epsilon^{(1)}(|\mathbf{k} + \mathbf{q}/2|) + \epsilon^{(1)}(|-\mathbf{k} + \mathbf{q}/2|)] a_1(\mathbf{k}, \mathbf{q}) \\ & - (2\pi\hbar)^{-3} v_{11} \int d^3k' \, a_1(\mathbf{k}', \mathbf{q}) \\ & \{1 - f_F[\epsilon^{(1)}(|\mathbf{k} + \mathbf{q}/2|)] - f_F[\epsilon^{(1)}(|-\mathbf{k} + \mathbf{q}/2|)]\}\end{aligned} \tag{9.4.13}$$

$$\langle n_{\mathbf{p}} \rangle = \frac{1}{\exp(\beta\epsilon_p) + 1} \equiv f_F(\epsilon_p) \tag{9.4.14}$$

In the low-temperature limit ($T \to 0$), $f_F(\epsilon_p) \to 0$. We then obtain for small q

$$w_q^{(1)} = w_0 + \frac{1}{2} v_F^{(1)} q, \qquad v_F^{(1)} \equiv \left(\frac{2\epsilon_F}{m_1}\right)^{1/2} \tag{9.4.15}$$

$$w_0 \equiv -2\hbar\omega_D \{\exp[2/v_0 \mathcal{N}(0)] - 1\}^{-1}, \tag{9.4.16}$$

[from Eq. (8.3.13)], which was obtained after the decoupling in going from Eq. (9.4.12) to Eq. (9.4.13). Similarly we obtain

$$w_q^{(2)} = w_0 + \frac{1}{2} v_F^{(2)} q, \qquad v_F^{(2)} \equiv (2\epsilon_F/m_2)^{1/2} \tag{9.4.17}$$

In practice electron and hole masses (m_1, m_2) may differ greatly. Then the Fermi velocities $v_F^{(1)}$ and $v_F^{(2)}$ are different, yielding different critical temperatures, as seen from Eq. (9.3.4). We call those pairons for which T_c is the higher the *predominant* pairons. If

$$m_1 < m_2, \qquad v_F^{(1)} > v_F^{(2)} \tag{9.4.18}$$

we see in Eq. (9.4.24) that this corresponds to the case where electron pairons are predominant. The opposite case can be worked out in a parallel manner.

Let us now consider the case of finite temperature. If we choose the average kinetic energy of the electron to be $\hbar\omega_D/2$, we obtain (Problem 9.4.2)

$$1 - f_F\left[\epsilon^{(1)}\left(|\mathbf{k}+\mathbf{q}/2|\right)\right] - f_F\left[\epsilon^{(1)}\left(|-\mathbf{k}+\mathbf{q}/2|\right)\right] \simeq 1 - 2f_F\left(\frac{\hbar\omega_D}{2}\right) = \tanh\left(\frac{\hbar\omega_D}{4k_BT}\right) \tag{9.4.19}$$

which is close to unity at temperatures far below the Debye temperature Θ_D:

$$T \ll \Theta_D \equiv \hbar\omega_D k_B^{-1} \tag{9.4.20}$$

Using the approximation [Eq. (9.4.19)], we calculate the excitation energy $w_q^{(1)}$ from Eq. (9.4.13). The result can be expressed as Eq. (9.4.15) with a temperature-dependent band edge:

$$|w_0(T)| = 2\hbar\omega_D\left\{\exp\left[\frac{2}{v_{11}\mathcal{N}_1(0)\tanh(\hbar\omega_D/4k_BT)}\right] - 1\right\}^{-1} \tag{9.4.21}$$

The finite-temperature effect on the excitation energy w_q is very small if $T \ll \Theta_D$, the temperature region of our primary interest. However the fact that we can compute the temperature-dependent excitation energy is interesting and significant. The total number of pairons at 0 K, consistent with the BCS Hamiltonian H in Eq. (9.4.9) is $N_0 = \hbar\omega_D\mathcal{N}(0)$. The total pairon number may decrease when temperature is raised toward the Debye temperature Θ_D and beyond because the magnitude of the temperature-dependent band edge $|w_0(T)|$, given by Eq. (9.4.21), becomes smaller. In fact $|w_0(T)| \to 0$ as $T \to \infty$.

We are primarily interested in the temperature region in which a superconducting transition occurs at T_c much lower than the Debye temperature Θ_D. Thus we hereafter neglect the temperature dependence of the energy–momentum relation. Then the total number density of pairons is still given by N_0:

$$\sum_{\mathbf{q}} n_{\mathbf{q}}^{(pc)} = N_0 = \hbar\omega_D\mathcal{N}(0) \tag{9.4.22}$$

Pairons above T_c move like free massless bosons having energy

$$\epsilon_q \equiv w_q - w_0 = \frac{v_F q}{2} \tag{9.4.23}$$

where we shifted the energy constant and omitted the superscripts denoting predominant pairons. According to our study in Section 8.3, such a system undergoes a B–E condensation transition of the second order at the critical temperature T_c given by

$$\boxed{k_B T_c = 1.01\,\hbar v_F n_0^{1/3},} \tag{9.4.24}$$

which is obtained from Eq. (9.3.4) after setting

$$c \equiv \frac{v_F}{2} \tag{9.4.25}$$

The heat capacity C has a jump ΔC at T_c; the ratio of this jump to the maximum heat capacity $C_{\max}$ is a universal constant:

$$\frac{\Delta C}{C_{\max}} = \frac{6.57\,R}{10.8\,R} = 0.608 \tag{9.4.26}$$

The heat capacity $C(T)$ just below T_c obeys a T^3-law, which is similar to Debye's T^3-law for the heat capacity of phonons at low temperatures.

Problem 9.4.1. Verify Eq. (9.4.12).

Problem 9.4.2. Verify Eq. (9.4.19).

9.5. DISCUSSION

The most important results obtained in this chapter are formulas (9.2.11) and (9.4.24) for the critical temperature T_c for systems of free dominant pairons moving in two and three dimensions with linear energy momentum relation. In the present section we discuss the underlying assumptions and important results.

9.5.1 Pairons are Bosons

Pairons move as bosons. Since this is an important element in the present theory, we elaborate on its physical significance. Let us consider two electrons whose states are specified by $(\mathbf{k}_1\uparrow, \mathbf{k}_2\downarrow)$. These pairs are subject to Pauli's exclusion principle, and the pair-occupation numbers are limited to 1 or 0. We now form a composite particle with the net momentum $\mathbf{k}_1 + \mathbf{k}_2 = \mathbf{q}$ specified. Such composite particles are bosons. By similar arguments we can show that hydrogen atoms are bosons (see Problem 9.5.1).

Let us take a superconductor of macroscopic dimensions at 0 K. There exist a great number of zero-momentum pairons in the system. If the dimension of the system is made ten times greater, the number of zero-momentum pairons will be ten times greater. Thus the occupation number N_0 at zero momentum has no upper limit. Consider now part of the superconductor. The number of zero-momentum pairons per unit volume n_0 is finite, and it is given by $n_0 = \hbar\omega_D \mathcal{N}(0)/V$, see Eq. (9.4.22).

9.5.2. Pairons Move as Massless Particles like Phonons

Pairons move like massless bosons having the linear Cooper–Schrieffer relation:

$$\epsilon_q \equiv w_q - w_0 = \frac{v_F q}{2} \tag{9.5.1}$$

They move with the common speed (Problem 9.5.2):

$$c = \frac{v_F}{2} \tag{9.5.2}$$

regardless of their momenta $\mathbf{q}$ for small q ($< q_0$; see Section 8.6.6). Equation (9.5.1) was obtained in Section 8.4 in the Cooper problem with the assumption of a Fermi sphere and the small-q limit. As we discussed in Section 8.6.8, pairons of two charge types for a type I superconductor are generated near hyperboloidal Fermi surfaces. We must therefore recalculate the energy–momentum relation. The results are however essentially the same, and the linear relation Eq. (9.5.1) still holds (see Problem 9.5.3).

9.5.3. Pairons Do Not Overlap in Space

The pairon size can be estimated from the BCS zero-temperature coherence length:

$$\xi_0 \equiv \frac{\hbar v_F}{\pi \Delta} = 0.18 \frac{\hbar v_F}{k_B T_c} \tag{9.5.3}$$

[see Eq. (8.6.12)]. The average separation r_0 between two pairons may be defined by

$$r_0 \equiv n_0^{-1/3} \tag{9.5.4}$$

where n_0 is the pairon density. By solving Eq. (9.4.24) for n_0 and using Eq. (9.5.4), we obtain

$$r_0 = 1.01 \frac{\hbar v_F}{k_B T_c} = 5.61 \xi_0 \tag{9.5.5}$$

indicating that the interpairon distance is several times greater than the pairon size. Thus pairons do not overlap in space, meaning that the B–E condensation takes place *before* the free pairon picture breaks down. This is why the theory of superconductivity can be developed simply in terms of the independent pairon picture throughout. Pairons condensed at some current-carrying state are discussed in Sections 11.1 and 11.2.

9.5.4. Pairons Move Almost Freely in the Crystal

In Section 5.3 we discussed the Fermi liquid picture in which a Bloch electron moves unhindered by the static-lattice potential. By extending this picture, we can state that a pairon also moves freely in a perfect crystal. (Excited pairons below T_c also move nearly freely, which will be shown in Chapter 10.) Impurities and phonons can affect the free motion of electrons and pairons but they are omitted from our consideration.

9.5.5. Pairons Hardly Interact with Each Other

In the extended Fermi liquid model discussed in Section 7.2, a Bloch electron moves almost freely in the crystal, and two Bloch electrons interact with each other through a screened Coulomb interaction. By extending this last picture, two pairons interact with each other through a screened Coulomb interaction. But the average distance between the two pairons is on the order of 10^4 Å. At this separation the screened Coulomb interaction represented by the Debye potential [Eq. (7.1.12)] is negligible.

9.5.6. B–E Condensation of Massless Bosons

A system of massless bosons characterized by the linear energy–momentum relation $\in = cp$ undergoes a B–E condensation in two dimensions and three dimensions. The two-dimensional case was treated in Section 9.2. The critical temperature T_c is [see Eq. (9.2.11)]

$$k_B T_c = 1.954\,\hbar c n^{1/2} \tag{9.5.6}$$

The phase transition is of the third order. The temperature behavior of the molar heat capacity C is shown in Fig. 9.1. As noted earlier, the B–E condensation transition in two dimensions is not a violation of Hohenberg's theorem.[6] The superconducting transition in high-T_c and layered organic superconductors is related with the B–E condensation of massless bosons moving in two dimensions. We discuss this topic in more detail in Chapter 13.

The three-dimensional case was treated in Section 9.3. The critical temperature T_c is given by Eq. (9.3.4), which can be reexpressed as

$$k_B T_c = 2.017\,\hbar c n^{1/3} \tag{9.5.7}$$

The phase transition is of the second order. The molar heat capacity C versus temperature is shown in Fig. 9.5. The heat capacity has a jump ΔC equal to 6.57 R at T_c [see Eq. (9.3.11)]. The maximum heat capacity at T_c, $C_{\max}$, is equal to 10.8 R according to Eq. (9.3.9). The ratio

$$\frac{\Delta C}{C_{\max}} = \frac{6.57\,R}{10.8\,R} = 0.608 \tag{9.5.8}$$

is a universal constant. Note: This number 0.608 is close to

$$\left(\frac{\Delta C}{C_{\max}}\right)_{\mathrm{BCS}} = 0.588 \tag{9.5.9}$$

obtained in the finite-temperature BCS theory.[1] Table 9.1 shows the measured values of $\Delta C / C_{\max}$ for a selection of elements. The closeness of the measured values to the BCS value 0.588 has been regarded as one of the most important support of the finite-temperature BCS theory. The ratio 0.608 obtained in the three-dimensional B–E condensation of free massless bosons is even closer to the measured values of 0.6 to 0.7. The main reasons for the small but nonnegligible discrepancy are: there are *two* types of pairons, each obeying the linear energy–momentum relation (9.5.1); and the energy–momentum relation changes substantially below T_c, which we discuss in Sections 10.9 and 10.10.

Table 9.1. Measured Ratios $\Delta C/C_{max}$ at the Critical Temperature T_c

Element	$\Delta C/C_{max}$
Hg	0.706
In	0.630
La (hcp)	0.600
Nb	0.655
Pb	0.730
Sn	0.615
Ta	0.615
Tl	0.600
V	0.600

9.5.7. No B–E Condensation in One Dimension

In general the critical temperature T_c for massless bosons moving in D dimensions can be found from

$$n = \frac{1}{(2\pi\hbar)^D} \int d^D p \frac{1}{\exp(\epsilon/k_B T_c) - 1} \qquad \epsilon = cp \tag{9.5.10}$$

The solutions for $D = 2$ and 3 are given in Eqs. (9.5.6) and (9.5.7) respectively. For $D = 1$ Eq. (9.5.10) has no solution. In other words *there is no B–E condensation in one dimension* (Problem 9.5.3).

Let us modify the energy–momentum relation to

$$\epsilon = ap^{\alpha} \tag{9.5.11}$$

where a and α are constants. If we substitute this ϵ into Eq. (9.5.10), we can find a solution if

$$\alpha < 1, \qquad D = 1 \tag{9.5.12}$$

However the index α must be greater than, or equal to, unity; otherwise the boson has an infinite speed at zero momentum. Thus there is no B–E condensation in one dimension.

9.5.8. Critical Temperature T_c; Predominant Pairons

In the present theory the superconducting temperature T_c is identified as the B–E condensation temperature for the predominant pairons. According to Eq. (9.4.24), T_c is proportional to the Fermi speed v_F. Thus if the pairon density is the same for both types, T_c is higher for pairons of that type for which v_F is higher. We call those pairons having higher T_c the *predominant pairons.* The smaller the effective mass m^*, the higher is the Fermi speed $v_F \equiv (2\epsilon_F/m^*)^{1/2}$. Therefore pairons made up of electrons having the smaller effective mass are predominant. For Pb the electron-effective mass m_1 is smaller by a factor of about 35 compared to the hole-effective mass m_2 at the necks (hyperboloidal surface of one sheet); see Eq. (5.10.10). Thus electron pairons are predominant in Pb. Experimentally the predominant type may be determined by examining the Hall voltage. As we discuss in more detail in Section 11.1, the supercurrent is generated by a moving supercondensate composed of equal numbers of ± pairons condensed at a

single momentum. The number density is the same for ± pairons, but they move with different speeds equal to $v_F^{(j)}/2$. The (macroscopic) current is dominated by pairons of that type for which v_F is higher. The predominant pairons in the B–E condensation are also dominant in the supercurrent. In the case of Pb, the Hall voltage is of the electron type, in agreement with experiments.

9.5.9. Law of Corresponding States for T_c 1; Interpairon and Interelectron Distances

The critical temperature T_c for the superconducting transition is much lower than the Fermi temperature T_F. The ratio T_c/T_F can be computed from Eq. (9.4.24). After eliminating the Fermi velocity $v_F \equiv (2\epsilon_F/m^*)^{1/2}$ from this expression, we obtain (Problem 9.5.4)

$$\boxed{\frac{T_c}{T_F} = \frac{2 \times 1.01}{(3\pi^2)^{1/3}} \frac{R_0}{r_0} = 0.653 \frac{R_0}{r_0},} \tag{9.5.13}$$

where

$$R_0 \equiv n_{el}^{-1/3} \tag{9.5.14}$$

is the mean distance between two electrons. Thus the ratio T_c/T_F is proportional to the ratio R_0/r_0. The interelectron distance R_0 can be calculated from data for lattice constants. Therefore the distance r_0 can be calculated from Eq. (9.5.13) accurately with the knowledge of T_c, T_F, and the lattice constants. Table 9.2 shows data on R_0 and r_0 for selected elements. It is quite remarkable that the interpairon distance r_0 for elemental superconductors is much greater than the interelectron distance R_0. Al and Pb are both fcc metals. The significant differences in r_0 must come from the electron energy band structures, which we discuss in the following:

9.5.10. Law of Corresponding States for T_c 2; The Pairon Formation Factor

As discussed in Section 8.5, ± pairons are generated only near specific parts of the Fermi surface. For elemental superconductors these parts are either necks or inverted double caps, which makes the actual number density n_0 of pairons relatively small. We discuss this point here. According to Eq. (8.3.3), the maximum pairon density n_0 is given by

$$n_0 = \hbar\omega_D \mathcal{N}(0) \quad (= r_0^{-3}) \tag{9.5.15}$$

If we assume a Cooper system with a spherical Fermi surface, we can calculate the ratio R^3/r_0^3 and obtain (Problem 9.5.5):

$$\frac{R^3}{r_0^3} = \frac{3}{4} \frac{\Theta_D}{T_F} \tag{9.5.16}$$

Using this, we obtain from Eq. (9.5.13):

$$\frac{T_c}{T_F} = 0.653 \left(\frac{3}{4}\right)^{1/2} \left(\frac{\Theta_D}{T_F}\right)^{1/3} = 0.565 \left(\frac{\Theta_D}{T_F}\right)^{1/3} \tag{9.5.17}$$

Table 9.2. Interpairon Distance r_0 and Pairon Formation Factor α

Elements	Lattice	T_c (K)	T_F (10^4 K)	Θ_D (K)	R_0 Å	r_0^a 10^4 Å	α^b ($\times 10^{-4}$)
Al	fcc	1.14	13.49	428	1.77	13.68	0.97
Pb	fcc	7.193	10.87	105	1.96	1.93	11.29
Zn	hcp	0.875	10.90	327	1.97	16.02	0.94
Sn	diam.	3.722	11.64	200	2.05	4.19	4.51
In	tetr.	3.403	9.98	108	2.06	3.94	5.59
Nb	bcc	9.50	6.18	450	2.62	1.11	13.37
Hg	rhomb.	4.153	8.29	100	2.27	2.96	7.64
Tl	hcp	2.39	9.46	96	2.12	5.48	4.24

[a] $r_0 = 0.653\, RT_F / T_c$.
[b] $\alpha = 1.339\, T_c (T_F^2 \Theta_D)^{-1/3}$.

This represents the corresponding state law for an auxiliary Cooper superconductor. For the actual elemental superconductors, the critical temperature T_c is much less than predicted by Eq. (9.5.17). To facilitate interpretation of the experimental data, we introduce a correction factor α called a *pairon formation factor* such that

$$\frac{T_c}{T_F} \cong 0.565\, \alpha \left(\frac{\Theta_D}{T_F} \right)^{1/3} \tag{9.5.18}$$

Here the factor α represents the ratio of the experimentally observed (T_c/T_F) to the ideal value calculated by Eq. (9.5.17) with the observed Θ_D/T_F. Data for the factor α are given in Table 9.1. Since the Fermi temperature T_F appears on both sides of Eq. (9.5.18), we may rewrite Eq. (9.5.18) as

$$\boxed{T_c = 0.565\, \alpha \Theta_D^{1/3} T_F^{2/3},} \tag{9.5.19}$$

which indicates that the critical temperature T_c is high if the Fermi temperature T_F is high and if the Debye temperature Θ_D is high. But the power laws are different. (We shall obtain different Θ_D and T_c dependence for high-T_c superconductors; see Section 13.7.)

The pairon formation factor α may come from the following three main sources: First, elemental superconductors must have partial hyperboloidal Fermi surfaces where $\pm$ pairons are generated with the help of acoustic phonons. Since these surfaces are only small parts of the total Fermi surface, the factor α is a small fraction. Second, the $\pm$ pairons are generated in equal numbers from the physical vacuum. This means that the density of states for nonpredominant electrons, e.g., holes in Pb, is the relevant density of states that enters in Eq. (9.5.15). This makes α even smaller. Third, necks are more favorable than inverted double caps, since the density of states are by geometry higher around the neck. This feature appears to explain why fcc lead (Pb) has a higher T_c than fcc aluminum (Al). For these and possibly other reasons, the pairon density n_0 in actual superconductors is very small. This makes the interpairon distance r_0 much greater than interelectron distance R_0 as discussed in Section 9.5.9.

In our theory *the existence of $\pm$ pairons is the key criterion for superconductivity.* If the pairon formation factor α that depends on electron and phonon band structures, is small but finite, the material is a superconductor. The value of α can be discussed qualitatively in terms of the Fermi surface. If the Fermi surface is spherical or ellipsoidal

in the first Brillouin zone as in Na and K, $\alpha = 0$. Then the metal remains normal down to 0 K. If a metals' Fermi surface is known to contain necks or inverted double caps as in Al, Pb, Be, W, such a metal has a finite α and it is a superconductor. To find the pairon formation factor α numerically requires a precise knowledge of the Fermi surface, which is beyond the scope of the present theory.

Problem 9.5.1. Show that hydrogens are bosons.

Problem 9.5.2. Derive Eq. (9.5.2). Use Hamilton's equations of motion.

Problem 9.5.3. Show that there are no T_c satisfying Eq. (9.5.10) in one dimension.

Problem 9.5.4. Derive Eq. (9.5.13).

Problem 9.5.5. Derive Eq. (9.5.17).

REFERENCES

1. P. Ehrenfest and J. R. Oppenheimer, *Phys. Rev.* **37,** 333 (1931); H. A. Bethe and R. F. Bacher, *Rev. Mod. Phys.* **8,** 193 (1936).
2. R. P. Feynman, R. B. Leighton, and M. Sands, *Feynman Lectures on Physics,* vol. 3, Ch. 21 (Addison-Wesley, Reading, MA, 1965), pp. 2l–27.
3. J. Bardeen, L. N. Cooper, and J. R. Schrieffer, *Phys. Rev.* **108,** 1175 (1957).
4. See many books cited in the Bibliography, Superconductivity section. About half of them discuss the properties of a superconductor without refering to the boson (pairon) condensate.
5. S. Fujita, T. Kimura, and Y. Zheng, *Found. Phys.* **21,** 1117 (1991).
6. P. C. Hohenberg, *Phys. Rev.* **158,** 383 (1967).

This page intentionally left blank.

10

Superconductors below T_c

Below T_c there is a supercondensate made up of ground pairons of both charge types. The density of condensed pairons n_0 is the greatest at 0 K and monotonically decreases to zero as temperature is raised to T_c. The motion of unpaired electrons (or quasi-electrons) is affected by the presence of a supercondensate. As a result the energy spectra for quasi-electrons have energy gaps $\Delta_j(T)$ that decrease to zero at T_c. By the phonon-exchange attraction, a pair of quasi-electrons are bound to form excited pairons, which have temperature-dependent energy gaps $\in_{g,j}(T)$. These gaps also monotonically decrease to zero at T_c, and they can be measured directly by quantum tunneling and photoabsorption experiments. The *I—V* curves for quantum tunneling are interpreted based on the pairon transport model. Supercondensate density and heat capacity are calculated under the assumption that excited pairons rather than quasi-electrons are predominant.

10.1. INTRODUCTION

Below the critical temperature T_c, there is a supercondensate made up of *ground* pairons of both charge types. The content (density) of the supercondensate is the greatest at 0 K and decreases to zero as temperature is raised to T_c. We see in the present chapter that quasi-electrons have energy gaps Δ_j relative to the hypothetical energy level of the superelectron constituting the supercondensate. These gaps Δ_j depend on the supercondensate density, and therefore they are temperature-dependent. For an elemental superconductor, the gaps for quasi-electrons of both charge types are the same: $\Delta_1 = \Delta_2 \equiv \Delta$. The gap $\Delta(T)$ is greatest at 0 K and declines to zero at T_c. The maximum gap $\Delta_0 \equiv \Delta(T = 0)$ is the gap that appeared in the variational calculation of the BCS ground-state energy in Chapter 8. We derive the famous BCS formula $2\Delta_0 = 3.53\, k_B T_c$,[1] connecting the quasi-electron maximum energy gap Δ_0 and the critical temperature T_c in the weak coupling limit. Quasi-electrons may be bound by the phonon-exchange attraction to form *excited* or *moving pairons*. These excited pairons move with a linear energy-momentum relation just as those pairons above T_c. But they, too, have an energy gap $\in_g(T)$ relative to the energy level of the ground pairons, which constitutes the supercondensate. This pairon energy gap $\in_g(T)$ is the greatest at 0 K, reaching a value equal to the pairon binding energy $|w_0|$; it

decreases to zero as temperature is raised to T_c. It is less than gap $\Delta(T)$ in the range $(0, T_c)$.[2]

Quantum tunneling experiments,[3,4] allow direct measurements of temperature-dependent energy gaps $\epsilon_g(T)$ in the superconductors. Data observed by Giaever and Megerle[4] are interpreted based on the pairon transport model. All elementary excitations, including quasi-electrons and excited pairons, can in principle contribute to the heat capacity. By the *Boltzmann principle* (*Boltzmann factor argument*), excited pairons whose energies are negative are more numerous than quasi-electrons having positive energies. Thus excited pairons dominate the low-temperature behavior of a superconductor. We compute the heat capacity and the supercondensate density of a pure superconductor under the assumption that predominant elementary excitations are excited pairons. All calculations are carried out, starting with the generalized BCS Hamiltonian [Eq. (8.2.1)] and using the equation-of-motion method.

10.2. ENERGY GAPS FOR QUASI-ELECTRONS AT 0 K

Below T_c, where the supercondensate is present, unpaired electrons move differently from those above T_c. In this section we study the energy-momentum relation for quasi-electrons at 0 K. The ground state is describable in terms of the reduced Hamiltonian:

$$H_0 = \sum_{\mathbf{k}} 2\epsilon_k^{(1)} b_{\mathbf{k}}^{(1)\dagger} b_{\mathbf{k}}^{(1)} + \sum_{\mathbf{k}} 2\epsilon_k^{(2)} b_{\mathbf{k}}^{(2)\dagger} b_{\mathbf{k}}^{(2)} - \sum_{\mathbf{k}'}{}' \sum_{\mathbf{k}}{}' [v_{11} b_{\mathbf{k}'}^{(1)\dagger} b_{\mathbf{k}}^{(1)} + v_{12} b_{\mathbf{k}'}^{(1)\dagger} b_{\mathbf{k}}^{(2)\dagger} + v_{21} b_{\mathbf{k}}^{(2)} b_{\mathbf{k}'}^{(1)} + v_{22} b_{\mathbf{k}'}^{(2)} b_{\mathbf{k}}^{(2)\dagger}] \quad (10.2.1)$$

By using this H_0, we obtain (Problem 10.2.1):

$$[H_0, c_{\mathbf{p}\uparrow}^{(1)\dagger}] = \epsilon_p^{(1)} c_{\mathbf{p}\uparrow}^{(1)\dagger} - \left[v_{11} \sum_{\mathbf{k}}{}' b_{\mathbf{k}}^{(1)\dagger} + v_{12} \sum_{\mathbf{k}}{}' b_{\mathbf{k}}^{(2)} \right] c_{-\mathbf{p}\downarrow}^{(1)} \quad (10.2.2)$$

Since the rhs contains $c_{-\mathbf{p}\downarrow}^{(1)}$, we also calculate $[H_0, c_{-\mathbf{p}\downarrow}^{(1)}]$ and obtain

$$[H_0, c_{-\mathbf{p}\downarrow}^{(1)}] = -\epsilon_p^{(1)} c_{-\mathbf{p}\downarrow}^{(1)} - \left[v_{11} \sum_{\mathbf{k}}{}' b_{\mathbf{k}}^{(1)} + v_{12} \sum_{\mathbf{k}}{}' b_{\mathbf{k}}^{(2)\dagger} \right] c_{\mathbf{p}\uparrow}^{(1)\dagger} \quad (10.2.3)$$

These two equations indicate that the dynamics of quasi-electrons describable in terms of c's are affected by ground pairons describable in terms of b's.

To find the energy of a quasi-electron, we follow the equation-of-motion method outlined after Eq. (6.7.14). We multiply Eq. (10.2.1) from the right by $\psi_\nu^{(1)} \rho_0$, where $\psi_\nu^{(1)}$ is the electron energy-state annihilation operator and

$$\rho_0 \equiv |\Psi\rangle\langle\Psi| \equiv \prod_{\mathbf{k}}{}' (u_{\mathbf{k}}^{(1)} + v_{\mathbf{k}}^{(1)} b_{\mathbf{k}}^{(1)\dagger}) \prod_{\mathbf{k}'}{}' (u_{\mathbf{k}'}^{(2)} + v_{\mathbf{k}'}^{(2)} b_{\mathbf{k}'}^{(2)\dagger}) |0\rangle\langle\Psi| \quad (10.2.4)$$

is the density operator describing the supercondensate [see $|\Psi\rangle$ in Eq. (8.5.1)] and take a grand ensemble trace. By using Eq. (6.7.13), the lhs of Eq. (10.2.2) can be expressed as

$$\mathrm{TR}\{[H_0, c^{(1)\dagger}_{\mathbf{p}\uparrow}]\psi^{(1)}_\nu \rho_0\} = \mathrm{TR}\{E^{(1)}_{\nu,\mathbf{p}} c^{(1)\dagger}_{\mathbf{p}\uparrow}\psi^{(1)}_\nu \rho_0\} \equiv E^{(1)}_{\mathbf{p}}\Psi^{(1)*}_\uparrow(\mathbf{p}) \tag{10.2.5}$$

where we dropped the subscript ν; the quasi-electron is characterized by momentum $\mathbf{p}$ and energy $E^{(1)}_{\mathbf{p}}$. The first term on the rhs of Eq. (10.2.2) simply yields $\epsilon^{(1)}_p\Psi^{(1)*}_\uparrow(\mathbf{p})$. Consider now

$$\underline{\mathrm{TR}\{b^{(1)\dagger}_{\mathbf{k}} c^{(1)}_{-\mathbf{p}\downarrow}\psi^{(1)}_\nu \rho_0\} \equiv \mathrm{TR}\{b^{(1)\dagger}_{\mathbf{k}} c^{(1)}_{-\mathbf{p}\downarrow}\psi^{(1)}_\nu |\Psi\rangle\langle\Psi|\}}$$

The state $|\Psi\rangle$ is normalized to unity, and it is the only system state at 0 K, thus

$$\mathrm{TR}\{b^{(1)\dagger}_{\mathbf{k}} c^{(1)}_{-\mathbf{p}\downarrow}\psi^{(1)}_\nu \rho_0\} = \langle\Psi|b^{(1)\dagger}_{\mathbf{k}} c^{(1)}_{-\mathbf{p}\downarrow}\psi^{(1)}_\nu|\Psi\rangle \tag{10.2.6}$$

We note that $\mathbf{k} \neq \mathbf{p}$, which holds, since the state must change after a phonon exchange. We examine the relevant matrix element and obtain (Problem 10.2.2)

$$\langle 0|(u^{(1)}_{\mathbf{k}} + v^{(1)}_{\mathbf{k}} b^{(1)}_{\mathbf{k}})b^{(1)\dagger}_{\mathbf{k}}(u^{(1)}_{\mathbf{k}} + v^{(1)}_{\mathbf{k}} b^{(1)\dagger}_{\mathbf{k}})|0\rangle = v^{(1)}_{\mathbf{k}} u^{(1)}_{\mathbf{k}} \tag{10.2.7}$$

We can therefore write

$$\mathrm{TR}\{b^{(1)\dagger}_{\mathbf{k}} c^{(1)}_{-\mathbf{p}\downarrow}\psi^{(1)}_\nu \rho_0\} = u^{(1)}_{\mathbf{k}} v^{(1)}_{\mathbf{k}}\Psi'^{(1)}_\downarrow(-\mathbf{p}) \tag{10.2.8}$$

$$\Psi'^{(1)}_\downarrow(-\mathbf{p}) \equiv \mathrm{TR}\{c^{(1)}_{-\mathbf{p}\downarrow}\psi^{(1)}_\nu \rho_0\} \tag{10.2.9}$$

Collecting all contributions, we obtain

$$E^{(1)}_{\mathbf{p}}\Psi^{(1)*}_\uparrow(\mathbf{p}) = \epsilon^{(1)}_p\Psi^{(1)*}_\uparrow(\mathbf{p}) - \left[v_{11}{\sum_{\mathbf{k}}}' u^{(1)}_{\mathbf{k}} v^{(1)}_{\mathbf{k}} + v_{12}{\sum_{\mathbf{k}}}' u^{(2)}_{\mathbf{k}} v^{(2)}_{\mathbf{k}}\right]\Psi'^{(1)}_\downarrow(-\mathbf{p}) \tag{10.2.10}$$

Using Eqs. (8.5.10) and (8.5.11), we have

$$\Delta_1 \equiv v_{11}{\sum_{\mathbf{k}}}' u^{(1)}_{\mathbf{k}} v^{(1)}_{\mathbf{k}} + v_{12}{\sum_{\mathbf{k}}}' u^{(2)}_{\mathbf{k}} v^{(2)}_{\mathbf{k}} \tag{10.2.11}$$

We can therefore simplify Eq. (10.2.10) to

$$E^{(1)}_{\mathbf{p}}\Psi^{(1)*}_\uparrow(\mathbf{p}) = \epsilon^{(1)}_p\Psi^{(1)*}_\uparrow(\mathbf{p}) - \Delta_1\Psi'^{(1)}_\downarrow(-\mathbf{p}) \tag{10.2.12}$$

Similarly we obtain from Eq. (10.2.3)

$$E^{(1)}_{-\mathbf{p}}\Psi^{(1)}_\downarrow(-\mathbf{p}) = -\epsilon^{(1)}_p\Psi^{(1)}_\downarrow(-\mathbf{p}) - \Delta_1\Psi^{(1)*}_\uparrow(\mathbf{p}) \tag{10.2.13}$$

The energy $E^{(1)}_{\mathbf{p}}$ can be interpreted as the *positive* energy required to create an up-spin unpaired electron at $\mathbf{p}$ in the presence of the supercondensate. The energy $E^{(1)}_{-\mathbf{p}}$ can be regarded as the energy required to remove a down-spin electron from

the paired state $(\mathbf{p}\uparrow, -\mathbf{p}\downarrow)$. In the pairing approximation, these two energies can be equated:

$$E_{\mathbf{p}}^{(1)} = E_{-\mathbf{p}}^{(1)} \equiv E_p^{(1)} > 0 \tag{10.2.14}$$

In the stationary state, Eqs. (10.2.12) and (10.2.13) must hold simultaneously. Then, the following secular equation holds:

$$\begin{vmatrix} E_p^{(1)} - \epsilon_p^{(1)} & \Delta_1 \\ \Delta_1 & E_p^{(1)} + \epsilon_p^{(1)} \end{vmatrix} = 0 \tag{10.2.15}$$

whose solutions are $E_p^{(1)} = \pm \left(\epsilon_p^{(1)2} + \Delta^2\right)^{1/2}$. Since we know that $E_p^{(1)} > 0$, we obtain

$$\boxed{E_p^{(i)} = \left(\epsilon_p^{(i)2} + \Delta_i^2\right)^{1/2}} \tag{10.2.16}$$

The theory developed here can be applied to holes in a parallel manner. We included this case in the preceding equations. This result confirms our earlier interpretation in Section 8.6.3 that $E_p^{(i)}$ is the energy of the quasi-electron. Since the unpaired electron cannot join the supercondensate, its energy must be higher than the energy of a hypothetical superelectron constituting the supercondensate. In summary unpaired electrons are influenced by the presence of the supercondensate, and have energy gaps.

Problem 10.2.1. Derive Eqs. (10.2.2) and (10.2.3).

Problem 10.2.2. Verify Eq. (10.2.7).

10.3. ENERGY GAP EQUATIONS AT 0 K

In this section we rederive the energy gap equations (8.513) by using the equation-of-motion method.

The supercondensate is made up of ground pairons, which can be described in terms of b's. We calculate $[H_0, b_{\mathbf{k}}^{(1)\dagger}]$ and $[H_0, b_{\mathbf{k}}^{(2)}]$ to obtain (Problem 10.3.1):

$$[H_0, b_{\mathbf{k}}^{(1)\dagger}] = E_1 b_{\mathbf{k}}^{(1)\dagger} = 2\epsilon_k^{(1)} b_{\mathbf{k}}^{(1)\dagger} - \left[v_{11} {\sum_{\mathbf{k}'}}' b_{\mathbf{k}'}^{(1)\dagger} + v_{12} {\sum_{\mathbf{k}'}}' b_{\mathbf{k}'}^{(2)} \right] (1 - n_{\mathbf{k}\uparrow}^{(1)} - n_{-\mathbf{k}\downarrow}^{(1)}) \tag{10.3.1}$$

$$[H_0, b_{\mathbf{k}}^{(2)}] = -E_2 b_{\mathbf{k}}^{(2)} = -2\epsilon_k^{(2)} b_{\mathbf{k}}^{(2)} + \left[v_{21} {\sum_{\mathbf{k}'}}' b_{\mathbf{k}'}^{(1)\dagger} + v_{22} {\sum_{\mathbf{k}'}}' b_{\mathbf{k}'}^{(2)} \right] (1 - n_{\mathbf{k}\uparrow}^{(2)} - n_{-\mathbf{k}\downarrow}^{(2)}) \tag{10.3.2}$$

Equations (10.3.1) and (10.3.2) indicate that the dynamics of ground pairons depend on the presence of quasi-electrons describable in terms of $n^{(j)}$. We now multiply Eq. (10.3.1) from the right by $\phi_1\rho_0$, where ϕ_1 is the electron pairon energy-state annihilation operator, and take a grand ensemble trace. From the first term on the rhs, we obtain

$$2\epsilon_k^{(1)} \,\mathrm{TR}\{b_{\mathbf{k}}^{(1)\dagger}\phi_1\rho_0\} = 2\epsilon_k^{(1)} \langle\Psi|b_{\mathbf{k}}^{(1)\dagger}\phi_1|\Psi\rangle = 2\epsilon_k^{(1)} u_{\mathbf{k}}^{(1)} v_{\mathbf{k}}^{(1)} F_1 \tag{10.3.3}$$

$$F_1 \equiv \langle\Psi|\phi_1|\Psi\rangle \tag{10.3.4}$$

From the first and second sums, we obtain (Problem 10.3.2)

$$-\sum_{\mathbf{k}'}{}' [v_{11} u_{\mathbf{k}'}^{(1)} v_{\mathbf{k}'}^{(1)} + v_{12} u_{\mathbf{k}'}^{(2)} v_{\mathbf{k}'}^{(2)}](1 - v_{\mathbf{k}}^{(1)2} - v_{-\mathbf{k}}^{(1)2}) F_1 \tag{10.3.5}$$

Since we are looking at the ground-state energy, the eigenvalues E_1 and E_2 are zero:

$$E_1 = E_2 = 0 \tag{10.3.6}$$

Collecting all contributions, we obtain

$$\left\{ 2\epsilon_k^{(1)} u_{\mathbf{k}}^{(1)} v_{\mathbf{k}}^{(1)} - (u_{\mathbf{k}}^{(1)2} - v_{\mathbf{k}}^{(1)2}) \sum_{\mathbf{k}'}{}' [v_{11} u_{\mathbf{k}'}^{(1)} v_{\mathbf{k}'}^{(1)} + v_{12} u_{\mathbf{k}'}^{(2)} v_{\mathbf{k}'}^{(2)}] \right\} F_1 = 0 \tag{10.3.7}$$

where we used

$$v_{-\mathbf{k}}^{(1)} = v_{\mathbf{k}}^{(1)} \tag{10.3.8}$$

Since $F_1 \equiv \langle \Psi | \phi_1 | \Psi \rangle \neq 0$, we obtain from Eq. (10.3.7)

$$2\epsilon_k^{(1)} u_{\mathbf{k}}^{(1)} v_{\mathbf{k}}^{(1)} - (u_{\mathbf{k}}^{(1)2} - v_{\mathbf{k}}^{(1)2}) \sum_{\mathbf{k}'}{}' [v_{11} u_{\mathbf{k}'}^{(1)} v_{\mathbf{k}'}^{(1)} + v_{12} u_{\mathbf{k}'}^{(2)} v_{\mathbf{k}'}^{(2)}] = 0 \tag{10.3.9}$$

which is just one of Eqs. (8.5.9), the equations equivalent to the energy gap equations (8.5.13).

As noted earlier in Section 8.2, the ground state Ψ of the BCS system is a superposition of many-pairon states and therefore quantities like

$$\langle \Psi | b_{\mathbf{k}}^{(j)\dagger} | \Psi \rangle, \qquad \langle \Psi | b_{\mathbf{k}}^{(j)\dagger} b_{\mathbf{k}'}^{(j)\dagger} | \Psi \rangle \tag{10.3.10}$$

that connect states of different particle numbers do not vanish. In this sense the state Ψ can be defined only in a grand ensemble.

As emphasized in Section 8.6, the supercondensate is made up of equal numbers of ± pairons, and this state is reachable from the physical vacuum by a succession of phonon exchanges. Since pair creation and pair annihilation of pairons actually lower the system energy [see Eq. (8.2.12)] and since pairons are bosons, all pairons available in the system are condensed into the zero-momentum state; the maximum number of pairons is $\hbar\omega_D \mathcal{N}(0)$. The number of condensed pairons at any one instant may fluctuate around the equilibrium value; such fluctuations are in fact more favorable.

Problem 10.3.1. Derive Eq. (10.3.1).

Problem 10.3.2. Verify Eq. (10.35).

10.4. ENERGY GAP EQUATIONS; TEMPERATURE-DEPENDENT GAPS

In the last two sections we saw that quasi-electron energies and the energy gap equations at 0 K can be derived from the equations of motion for c's and b's, Eqs. (10.2.2) and (10.3.1), respectively. We now extend our theory to a finite temperature.

First we make an important observation. The supercondensate is composed of equal numbers of ground ± pairons condensed at zero momentum. Since there is no distribution, its intensive properties cannot show any temperature variation; only its content (density) changes with temperature. Such a picture of the supercondensate is also known for the superfluid He II. As an experimental corroboration, we cite dripping superfluid from a beaker, as shown in Fig. 4.1. Experiments show that the dripping fluid is colder than the fluid remaining in the beaker, indicating that only the superfluid climbs up the wall and drips down. Second we reexamine Eq. (10.3.1). Combining it with Eq. (10.3.6), we obtain

$$[H_0, b_{\mathbf{k}}^{(1)\dagger}] = 2\epsilon_k^{(1)} b_{\mathbf{k}}^{(1)\dagger} - \left[v_{11} {\sum_{\mathbf{k}'}}' b_{\mathbf{k}'}^{(1)\dagger} + v_{12} {\sum_{\mathbf{k}'}}' b_{\mathbf{k}'}^{(2)} \right] (1 - n_{\mathbf{k}\uparrow}^{(1)} - n_{-\mathbf{k}\downarrow}^{(1)}) = 0 \tag{10.4.1}$$

From our study in Section 10.3 we know that both:

$$\langle \Psi | b_{\mathbf{k}}^{(1)\dagger} | \Psi \rangle = u_{\mathbf{k}}^{(1)} v_{\mathbf{k}}^{(1)} \text{ and } \langle \Psi | b_{\mathbf{k}}^{(2)} | \Psi \rangle = u_{\mathbf{k}}^{(2)} v_{\mathbf{k}}^{(2)} \tag{10.4.2}$$

are finite. The b's refer to pairons constituting the supercondensate while $n_{\mathbf{k}\uparrow}^{(1)}$ and $n_{-\mathbf{k}\downarrow}^{(1)}$ represent the occupation numbers of electrons. This means that unpaired electrons if present can influence the formation and content of the supercondensate. In fact, we see from Eq. (10.4.1) that if $n_{\mathbf{k}\uparrow}^{\prime(1)} = 0$, $n_{-\mathbf{k}\downarrow}^{\prime(1)} = 1$, or if $n_{\mathbf{k}\uparrow}^{\prime(1)} = 1$, $n_{-\mathbf{k}\downarrow}^{\prime(1)} = 0$, terms containing v_{1j} vanish, and there is no attractive correlation; that is, the supercondensate wave function Ψ cannot extend over the pair state $(\mathbf{k}\uparrow, -\mathbf{k}\downarrow)$. Thus as temperature is raised from 0 K, more unpaired electrons are excited, making the supercondensate formation less favorable. Unpaired electrons (fermions) have energies $E_k^{(1)}$. Therefore the thermal average of $1 - n_{\mathbf{k}\uparrow}^{(1)} - n_{-\mathbf{k}\downarrow}^{(1)}$ can be represented by

$$\langle 1 - n_{\mathbf{k}\uparrow}^{(1)} - n_{-\mathbf{k}\downarrow}^{(1)} \rangle = 1 - 2\{\exp[\beta E_k^{(1)}] + 1\}^{-1} = \tanh[\beta E_k^{(1)}/2], \quad (\geq 0) \tag{10.4.3}$$

In the low-temperature limit, this quantity approaches unity from below

$$\tanh[\beta E_k^{(1)}/2] \equiv \tanh[E_k^{(1)}/2k_B T] \to 1 \qquad (T \to 0) \tag{10.4.4}$$

We may therefore regard $\tanh[\beta E_k^{(1)}/2]$ as the probability that the pair state $(\mathbf{k}\uparrow, -\mathbf{k}\downarrow)$ is available for the supercondensate formation at temperature T. As temperature is raised, this probability becomes smaller, making the supercondensate density smaller. Third we make a hypothesis: The behavior of quasi-electrons is affected by the supercondensate only. This is a reasonable assumption at very low temperatures, where very few elementary excitations exist.

We now examine the energy gap equation (8.5.13) at 0 K:

$$\frac{\Delta_j = \sum_{\mathbf{k}}{}' \sum_i v_{ji}\Delta_i}{2E_{\mathbf{k}}^{(i)}} \tag{10.4.5}$$

Here we see that the summation with respect to $\mathbf{k}$ and i extends over all allowed pair-states. As temperature is raised from zero, quasi-electrons are excited, making the physical vacuum less perfect. The degree of perfection at $(\mathbf{k}, i)$ may be represented by the probability $\tanh(\beta E_{\mathbf{k}}^{(i)}/2)$. The supercondensate formation is closely connected with the physical vacuum. Thus we may modify Eq. (10.4.5) as follows:

$$\boxed{\Delta_j = \sum_{\mathbf{k}}{}' \sum_i v_{ji}\Delta_i \frac{\tanh(\beta E_{\mathbf{k}}^{(i)}/2)}{2E_{\mathbf{k}}^{(i)}}} \tag{10.4.6}$$

Equations (10.4.6) are called the *generalized energy-gap equations at finite temperatures.* They reduce to Eqs. (10.4.5) in the zero-temperature limit. In the bulk limit, the sums over $\mathbf{k}'$ can be converted into energy integrals. Equations (10.4.6) become

$$\Delta_j = \frac{1}{2}\sum_{i=1}^{2} v_{ji}\mathcal{N}_i(0) \int_0^{\hbar\omega_D} d\epsilon \frac{\Delta_i}{\left(\epsilon^2 + \Delta_i^2\right)^{1/2}} \tanh\left[\frac{\left(\epsilon^2 + \Delta_i^2\right)^{1/2}}{2k_B T}\right] \tag{10.4.7}$$

For elemental superconductors we assume that $v_{ij} = v_0$ [see Eq. (8.2.15)], and $\mathcal{N}_1(0) = \mathcal{N}_2(0) \equiv \mathcal{N}(0)$ [see Eqs. (8.5.16)]. (See the explanation in Sections 8.5 and 8.6). We then obtain from Eq. (10.4.7) that there is a common energy gap:

$$\Delta_1 = \Delta_2 \equiv \Delta \tag{10.4.8}$$

which can be obtained from

$$\boxed{1 = v_0\mathcal{N}(0) \int_0^{\hbar\omega_D} d\epsilon \frac{1}{\left(\epsilon^2 + \Delta^2\right)^{1/2}} \tanh\left[\frac{\left(\epsilon^2 + \Delta^2\right)^{1/2}}{2k_B T}\right]} \tag{10.4.9}$$

This gap Δ is temperature-dependent. The limit temperature T_c at which Δ vanishes, is defined by

$$\boxed{1 = v_0\mathcal{N}(0) \int_0^{\hbar\omega_D} d\epsilon \frac{1}{\epsilon} \tanh\left[\frac{\epsilon}{2k_B T_c}\right]} \tag{10.4.10}$$

This limit temperature T_c will be identified as the *critical temperature* at which the supercondensate disappears. To see this connection, let us recall the physical meaning of the quasi-particle energies $E_k^{(j)} \equiv (\epsilon_k^{(j)2} + \Delta_j^2)^{1/2}$: $E_k^{(j)}$ is the energy of the unpaired electron of charge type j at $\mathbf{k}$ relative to that of the hypothetical superelectron forming the supercondensate. If there is no supercondensate, no energy gaps can appear.

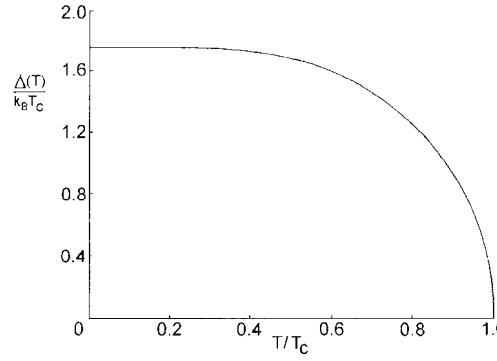

Figure 10.1. Temperature variation of energy gap $\Delta(T)$.

The gap $\Delta(T)$, which is obtained numerically from Eq. (10.4.9) by computer, decreases as shown in Fig. 10.1. In the weak coupling limit:

$$\exp\left[\frac{2}{v_0 \mathcal{N}(0)}\right] \gg 1 \tag{10.4.11}$$

the critical temperature T_c can be computed from Eq. (10.4.10) analytically. The result can be expressed by (Problem 10.4.1)

$$k_B T_c = 1.13\,\hbar\omega_D \exp\left[\frac{1}{v_0 \mathcal{N}(0)}\right] \tag{10.4.12}$$

Comparing Eq. (10.4.12) with the weak coupling limit of Eq. (8.5.21), we obtain

$$\boxed{2\Delta_0 \equiv 2\Delta(T=0) = 3.53\,k_B T_c} \tag{10.4.13}$$

which is the famous BCS formula,[1] expressing a connection between the maximum energy gap Δ_0 and the critical temperature T_c.

As stated earlier in Section 8.6.2, the energy gap Δ is linearly related to the critical field H_c (in the weak coupling limit); see Eq. (8.6.4). A plot of the critical field versus temperature was given in Fig. 1.6. The two curves for $\Delta(T)$ and $H_c(T)$ are similar; but near the critical temperature T_c, $\Delta(T)$ falls off more sharply than $H_c(T)$.

Problem 10.4.1. Obtain the weak-coupling analytical solution [Eq. (10.4.12)] from Eq. (10.4.10).

10.5. ENERGY GAPS FOR PAIRONS

When a phonon is exchanged between two quasi-electrons, these electrons may be bound to form moving pairons. Since quasi-electrons have an energy gap Δ, excited pairons also have an energy gap $\in_g$ relative to the energy of the ground pairons

constituting the supercondensate. We study the energy of excited pairons in this section.

We start with the full Hamiltonian H in Eq. (9.4.9):

$$\begin{aligned} H = {} & c_k^{(1)} n_{\mathbf{k},s}^{(1)} + \sum_{\mathbf{k}}{}' \sum_{s} \epsilon_k^{(2)} n_{\mathbf{k},s}^{(2)} \\ & - \sum_{\mathbf{k}}{}' \sum_{\mathbf{q}}{}' \sum_{\mathbf{k}'}{}' [v_{11} B_{\mathbf{k}'\mathbf{q}}^{(1)\dagger} B_{\mathbf{k}\mathbf{q}}^{(1)} + v_{12} B_{\mathbf{k}'\mathbf{q}}^{(1)\dagger} B_{\mathbf{k}\mathbf{q}}^{(2)\dagger} + v_{21} B_{\mathbf{k}\mathbf{q}}^{(2)} B_{\mathbf{k}'\mathbf{q}}^{(1)} + v_{22} B_{\mathbf{k}'\mathbf{q}}^{(2)} B_{\mathbf{k}\mathbf{q}}^{(2)\dagger}] \\ & - \sum_{\mathbf{k}}{}' \sum_{\mathbf{k}'}{}' [v_{11} b_{\mathbf{k}'}^{(1)\dagger} b_{\mathbf{k}}^{(1)} + v_{12} b_{\mathbf{k}}^{(2)\dagger} b_{\mathbf{k}'}^{(1)\dagger} + v_{21} b_{\mathbf{k}}^{(2)} b_{\mathbf{k}'}^{(1)\dagger} + v_{22} b_{\mathbf{k}'}^{(2)} b_{\mathbf{k}}^{(2)\dagger}] \end{aligned} \tag{10.5.1}$$

Using Eqs. (10.5.1), (8.4.6), and (8.4.7), we obtain (Problem 10.2.1):

$$\begin{aligned} [H, B_{\mathbf{k}\mathbf{q}}^{(1)\dagger}] = {} & [\epsilon^{(1)}(|\mathbf{k} + \mathbf{q}/2|) + \epsilon^{(1)}(|-\mathbf{k} + \mathbf{q}/2|)] B_{\mathbf{k}\mathbf{q}}^{(1)\dagger} \\ & - \left[v_{11} \sum_{\mathbf{k}'}{}' B_{\mathbf{k}'\mathbf{q}}^{(1)\dagger} + v_{12} \sum_{\mathbf{k}'}{}' B_{\mathbf{k}'\mathbf{q}}^{(2)} \right] (1 - n_{\mathbf{k}+\mathbf{q}/2\uparrow}^{(1)} - n_{-\mathbf{k}+\mathbf{q}/2\downarrow}^{(1)}) \\ & - (c_{\mathbf{k}+\mathbf{q}/2\uparrow}^{(1)\dagger} c_{\mathbf{k}-\mathbf{q}/2\uparrow}^{(1)} + c_{-\mathbf{k}-\mathbf{q}/2\downarrow}^{(1)} c_{-\mathbf{k}+\mathbf{q}/2\downarrow}^{(1)\dagger}) \left[v_{11} \sum_{\mathbf{k}'}{}' b_{\mathbf{k}'}^{(1)\dagger} + v_{12} \sum_{\mathbf{k}'}{}' b_{\mathbf{k}'}^{(2)} \right] \end{aligned} \tag{10.5.2}$$

$$\begin{aligned} [H, B_{\mathbf{k}\mathbf{q}}^{(2)}] = {} & - [\epsilon^{(2)}(|\mathbf{k} + \mathbf{q}/2|) + \epsilon^{(2)}(|-\mathbf{k} + \mathbf{q}/2|)] B_{\mathbf{k}\mathbf{q}}^{(2)} \\ & - \left[v_{21} \sum_{\mathbf{k}'}{}' B_{\mathbf{k}'\mathbf{q}}^{(1)\dagger} + v_{22} \sum_{\mathbf{k}'}{}' B_{\mathbf{k}'\mathbf{q}}^{(2)} \right] (1 - n_{\mathbf{k}+\mathbf{q}/2\uparrow}^{(2)} - n_{-\mathbf{k}+\mathbf{q}/2\downarrow}^{(2)}) \\ & - (c_{-\mathbf{k}+\mathbf{q}/2\downarrow}^{(2)} c_{-\mathbf{k}-\mathbf{q}/2\downarrow}^{(2)\dagger} + c_{\mathbf{k}-\mathbf{q}/2\uparrow}^{(2)\dagger} c_{\mathbf{k}+\mathbf{q}/2\uparrow}^{(2)}) \left[v_{21} \sum_{\mathbf{k}'}{}' b_{\mathbf{k}'}^{(1)\dagger} + v_{22} \sum_{\mathbf{k}'}{}' b_{\mathbf{k}'}^{(2)} \right] \end{aligned} \tag{10.5.3}$$

These exact equations indicate that the dynamics of excited pairons depend on excited and ground pairons and quasi-electrons. If we omit interaction terms containing $B_{\mathbf{k}'\mathbf{q}}^{(1)\dagger}$ and $B_{\mathbf{k}\mathbf{q}}^{(2)}$ in Eq. (10.5.2) we obtain

$$\begin{aligned} [H, B_{\mathbf{k}\mathbf{q}}^{(1)\dagger}] = {} & [\epsilon^{(1)}(|\mathbf{k} + \mathbf{q}/2|) + \epsilon^{(1)}(|-\mathbf{k} + \mathbf{q}/2|)] B_{\mathbf{k}\mathbf{q}}^{(1)\dagger} \\ & - (c_{\mathbf{k}+\mathbf{q}/2\uparrow}^{(1)\dagger} c_{\mathbf{k}-\mathbf{q}/2\uparrow}^{(1)} + c_{-\mathbf{k}-\mathbf{q}/2\downarrow}^{(1)} c_{-\mathbf{k}+\mathbf{q}/2\downarrow}^{(1)\dagger}) \left[v_{11} \sum_{\mathbf{k}'}{}' b_{\mathbf{k}'}^{(1)\dagger} + v_{12} \sum_{\mathbf{k}'}{}' b_{\mathbf{k}'}^{(2)} \right] \end{aligned} \tag{10.5.4}$$

This simplified equation is equivalent to a set of two separate equations of motion for a quasi-electron [see Eq. (10.2.2) or Eq. (2-59) in Ref. 6]:

$$[H_0, c_{\mathbf{k}+\mathbf{q}/2\uparrow}^{(1)\dagger}] \equiv [H_0, c_{\mathbf{p}\uparrow}^{(1)\dagger}] = \epsilon_p^{(1)} c_{\mathbf{p}\uparrow}^{(1)\dagger} - c_{-\mathbf{p}\downarrow}^{(1)} \left[v_{11} \sum_{\mathbf{k}'}{}' b_{\mathbf{k}'}^{(1)\dagger} + v_{12} \sum_{\mathbf{k}'}{}' b_{\mathbf{k}'}^{(2)} \right] \tag{10.5.5}$$

In the last three sections, we analyzed Eq. (10.5.5) and its associate $[H_0, c_{-\mathbf{p}\downarrow}^{(1)}]$ and saw that the energy of a quasi-electron is given by

$$E_p^{(j)} = [\epsilon_p^{(j)2} + \Delta_j^2(T)]^{1/2} \tag{10.5.6}$$

Using this knowledge and examining Eq. (10.5.2), we may infer that approximate but good equations of motion for B's are represented by

$$[H, B^{(1)\dagger}_{\mathbf{kq}}] = \left[E^{(1)}\left(|\mathbf{k}+\mathbf{q}/2|\right) + E^{(1)}\left(|-\mathbf{k}+\mathbf{q}/2|\right)\right] B^{(1)\dagger}_{\mathbf{kq}} - \left[v_{11}{\sum_{\mathbf{k}'}}' B^{(1)\dagger}_{\mathbf{k}'\mathbf{q}} + v_{12}{\sum_{\mathbf{k}'}}' B^{(2)}_{\mathbf{k}'\mathbf{q}}\right](1 - n^{(1)}_{\mathbf{k}+\mathbf{q}/2\uparrow} - n^{(1)}_{-\mathbf{k}+\mathbf{q}/2\downarrow}) \tag{10.5.7}$$

Similarly, from Eq. (10.5.3) we obtain

$$[H, B^{(2)}_{\mathbf{kq}}] = -\left[E^{(2)}\left(|\mathbf{k}+\mathbf{q}/2|\right) + E^{(2)}\left(|-\mathbf{k}+\mathbf{q}/2|\right)\right] B^{(2)}_{\mathbf{kq}} - \left[v_{21}{\sum_{\mathbf{k}'}}' B^{(1)\dagger}_{\mathbf{k}'\mathbf{q}} + v_{22}{\sum_{\mathbf{k}'}}' B^{(2)}_{\mathbf{k}'\mathbf{q}}\right](1 - n^{(2)}_{\mathbf{k}+\mathbf{q}/2\uparrow} - n^{(2)}_{-\mathbf{k}+\mathbf{q}/2\downarrow}) \tag{10.5.8}$$

These two equations reduce to the correct limits [Eq. (9.4.12)] at $T = T_c$, where $\Delta_j = 0$ and $E^{(j)}_k = \epsilon^{(j)}_k$. In the other limit, $T \to 0$, they generate Eqs. (10.5.6).

Let us now introduce the energy–(k–q) representation and rewrite Eq. (10.5.7) in the bulk limit. After using the decoupling approximation and taking the low temperature limit, we obtain from Eq. (10.5.7) (Problem 10.5.2):

$$\tilde{w}^{(j)}_q a_j(\mathbf{k},\mathbf{q}) = \left[E^{(j)}\left(|\mathbf{k}+\mathbf{q}/2|\right) + E^{(j)}\left(|-\mathbf{k}+\mathbf{q}/2|\right)\right] a_j(\mathbf{k},\mathbf{q}) - v_{jj}(2\pi\hbar)^{-3}\int' d^3k'\, a_j(\mathbf{k}',\mathbf{q}) \tag{10.5.9}$$

where $\tilde{w}^{(j)}_q$ are the pairon energies and $a_j(\mathbf{k}, \mathbf{q})$ the pairon wave functions. After decoupling ± pairons can be treated separately. We drop the subscript j hereafter. Equation (10.5.9) is reduced to the Cooper equation (8.4.18) in the zero-Δ limit. The same $\mathbf{q}$ appears in the arguments of all a's, meaning that the net momentum $\mathbf{q}$ is a constant of motion; excited pairons move independently. From Eq. (10.5.6), we observe that

$$E\left(|\mathbf{k}+\mathbf{q}/2|\right) + E\left(|-\mathbf{k}+\mathbf{q}/2|\right) \geq 2E_k > 2\epsilon_k \tag{10.5.10}$$

Equation (10.5.9) is similar to Eq. (8.4.18). We can then use the same method to obtain

$$\tilde{w}_q = \tilde{w}_0 + \frac{1}{2}v_F q < 0 \tag{10.5.11}$$

where $\tilde{w}_0(T)$ (< 0) is the solution of

$$1 = \mathcal{N}(0)v_0 \int_0^{\hbar\omega_D} d\epsilon\, [|\tilde{w}_0| + 2\left(\epsilon^2 + \Delta^2\right)^{1/2}]^{-1} \tag{10.5.12}$$

Note: $\tilde{w}_0$ is temperature-dependent, since Δ is; otherwise the excitation energies are similar to those above T_c. Let us write the energy $\tilde{w}_q$ in the form:

$$\tilde{w}_q = w_0 + \epsilon_g(T) + \frac{1}{2}v_F q < 0 \tag{10.5.13}$$

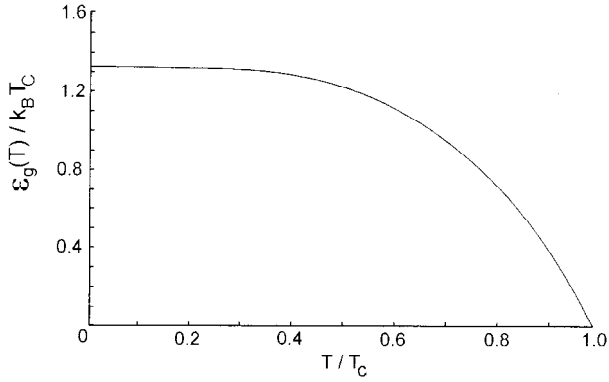

Figure 10.2. Variation of the pairon energy gap $\epsilon_g(T)$ with temperature.

$$\epsilon_g(T) \equiv \tilde{w}_0(T) - w_0 > 0 \tag{10.5.14}$$

where ϵ_g is *the energy gap between excited and ground pairons.* (This gap is shown in the energy diagram in Fig. 1.8.) The gap ϵ_g is nonnegative, as seen by comparing Eq. (10.5.12) and Eq. (8.4.19) and noting inequality Eq. (10.5.10). The gap $\epsilon_g(T)$ depends on the temperature T, and it can be numerically computed from Eq. (10.5.12) as shown in Fig. 10.2.

The temperature behavior of $\epsilon_g(T)$ and $\Delta(T)$ is very similar. Compare Fig. 10.1 and 10.2. Both energy gaps are greatest at 0 K, then monotonically decrease to zero as temperature is raised to T_c. Further note that the pairon energy gap $\epsilon_g(T)$ is smaller than the quasi-electron energy gap $\Delta(T)$ over the entire temperature range:

$$\epsilon_g(T) < \Delta(T), \qquad 0 < T < T_c \tag{10.5.15}$$

an inequality which can be verified from Eq. (10.5.9) (Problem 10.5.3).

Problem 10.5.1. Derive Eqs. (10.5.2) and (10.5.3).

Problem 10.5.2. Derive Eq. (10.5.9).

Problem 10.5.3. Show inequality Eq. (10.5.15) from Eqs. (10.5.9) and (10.5.10).

10.6. QUANTUM TUNNELING EXPERIMENTS 1; S–I–S SYSTEMS

In the last two sections, we have seen that there are two energy gaps (Δ, ϵ_g), one in the quasi-electron and the other in the pairon energy spectrum. Only pairon energy gaps can be observed directly by quantum tunneling techniques. We discuss quantum tunneling in Al–Al_2O_3–Al in this section. A typical experimental set-up is schematically shown in Fig. 10.3. Here S_1 and S_2 are superconductors, and I is an oxide (thin insulator film) of width ~ 20 Å. The system S_1–I–S_2 is connected with a variable resistor and a

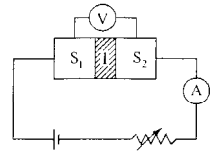

Figure 10.3. A schematic sketch of quantum tunneling circuit.

battery. In the present section, we consider the case in which the same superconductors are used for both S_1 and S_2. Such a system is called an *S–I–S* system.

The operating principles are as follows. If the bias voltage is low, some charged quasi-particles may quantum-tunnel through the oxide; the resulting current is low. When the voltage is raised enough, part of the supercondensate may dissociate, and the resulting quasi-particles may tunnel and generate a sudden increase in the current. By measuring the *threshold voltage* V_t, we obtain information on the energy gaps. The experimental I (current)– V (voltage) curves for Al–Al_2O_3–Al sandwich obtained by Giaever and Megerle[4] are reproduced in Fig. 10.4. The main features of the *I–V* curves (see the two lowest lines at T = 1.10, 1.08, K, T_c = 1.14 K) are

A) An (anti)symmetry with respect to the zero voltage (not shown).

B) A nearly flat small current below some threshold voltage V_t.

C) A sudden current increase near the threshold is temperature-dependent, and the slope $dI\backslash dV$ becomes steeper as temperature is lowered.

D) All *I–V* curves are below the straight line representing Ohm's law behavior.

E) There is no sudden change in the *I–V* curve at the critical temperature (1.14 K).

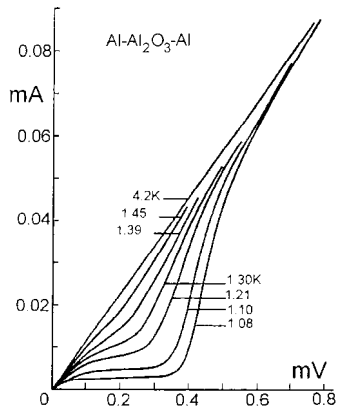

Figure 10.4. Current–voltage characteristics of an Al–Al_2O_3–Al sandwich at various temperatures [after Giaever and Megerle (Ref. 4)].

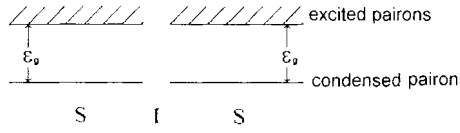

Figure 10.5. Pairon energy diagram for *S–I–S*.

We propose to analyze the experimental data based on the *pairon transport model.* Since Giaever *et al.* interpreted the data based on the quasi-electron transport model,[3,4] we first give some reasons why we choose the pairon transport model. Tunneling experiments are done in a steady-state condition in which all currents in the superconductors S_j are supercurrents; that is, charges are transported by the condensed pairons. Pairons are in negative-energy states, while quasi-electrons have positive energies. By the Boltzmann principle, these pairons are much more numerous than quasi-electrons at 0 K. Our pairon transport model is a natural one, since we deal with pairons throughout in the *S–I–S* sandwich. In Section 11.2 we shall see that the Josephson tunneling, which occurs with no bias, can also be discussed in terms of the pairon motion.

Consider first the low-temperature limit. If the voltage is raised high enough, part of the supercondensate near the oxide may dissociate and some of these pairons gain enough energy to tunnel through the oxide. The threshold voltage V_t times the pairon charge (magnitude) $2e$ should equal twice the binding energy $|w_0|$:

$$(2e)V_t = 2|w_0| \tag{10.6.1}$$

(The factor 2 in front of $|w_0|$ will be explained later.) Such behavior is in accordance with experiments,[5] where an extremely sharp slope is observed in all superconductors.

The behavior shown in Fig. 10.4 is now interpreted with the aid of the diagrams in Fig. 10.5, where the energy spectra for pairons in S_1 and S_2 are shown. Note: Ground pairon energy levels are chosen to have the same height, which represents the fact that with no bias voltage, no supercurrent flows in *S–I–S.* Since we have the same superconductors ($S_1 = S_2$), we have one energy gap $\in_g$. The energy spectra in S_1 and S_2 are symmetric with respect to I (oxide). In such a case, we shall see that the *I–V* curve is *antisymmetric* as stated in A. [In contrast if different conductors are substituted for (S_1, S_2), the *I–V* curve is asymmetric. We discuss this case in Section 10.7].

To see this antisymmetry, first consider the case when a small voltage is applied, as shown in Fig. 10.3. Those quasi-particles carrying the positive (negative) charges on the average tend to move right (left). Second, if we reverse the bias, then the opposite tendencies should hold. If the energy spectra on both sides are the same, the *I–V* curves must be antisymmetric. This case can be regarded as a *generalized Ohm's law*:

$$I = \frac{V}{R} \qquad \text{(small } V\text{)} \tag{10.6.2}$$

where R is a resistance, a material constant independent of the polarity of the voltage; R may depend on V, which is the said generalization.

Let us now derive a basic formula for quantum tunneling. Assume that a + pairon having charge $q = 2e$ tunnels rightward from S_1 to S_2. Such a pairon in S_1 must arrive

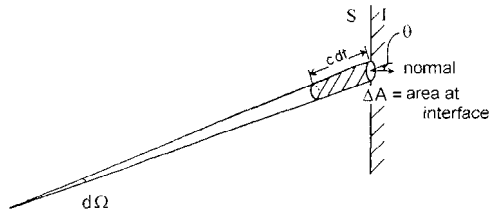

Figure 10.6. A pairon proceeding in the solid angle $d\Omega$ and located within the quasi-cylinder reaches the interface area ΔA in the time dt.

at the interface (S_1, I) with the positive (rightward) velocity. Inside S_1 there are many excited pairons (bosons) moving independently in all directions and populated by the Planck distribution function:

$$f(\epsilon) = \frac{1}{e^{\beta\epsilon} - 1} \tag{10.6.3}$$

where ϵ is the pairon energy:

$$\epsilon = cp, \qquad c \equiv \frac{v_F}{2} \tag{10.6.4}$$

This condition is very similar to that of black-body radiation (inside an oven maintained at a temperature T), where photons move and are isotropically distributed.

We ask how many pairons arrive at the small interface element ΔA per unit time in a particular direction (θ, ϕ). The number density of pairons moving in the right direction within the solid angle:

$$d\Omega = \sin\theta \, d\theta \, d\phi \tag{10.6.5}$$

see Fig. 10.6, is given by

$$f(\epsilon)(2\pi\hbar)^{-3} p^2 \, dp \, d\Omega \tag{10.6.6}$$

Noting that all pairons move with the *same speed c,* we obtain

$$\text{pairon flux} = cf(\epsilon)(2\pi\hbar)^{-3} p^2 \, dp \, d\Omega = \frac{1}{2} v_F f(\epsilon)(2\pi\hbar)^{-3} p^2 \, dp \, d\Omega \tag{10.6.7}$$

We remark that this expression is the same as for the photon flux escaping from a small hole in the oven wall in a specified direction (θ, ϕ).

On arriving at the interface, some of the pairons may be kicked in rightward through the oxide, gain energy equal to $2eV$, and reach the second superconductor S_2. Quantum tunneling here is similar to the elastic potential scattering treated in Section 7.6, only the final state must have an energy higher by $2eV$ than the initial state, so that

$$\epsilon_f = \epsilon_i + 2eV \tag{10.6.8}$$

which takes care of the energy gain during its passage through the oxide. We may then describe quantum tunneling in terms of the following quantum transition rate:

$$R = \frac{2\pi}{\hbar} |\langle p_f | v | p_i \rangle|^2 \delta(\epsilon_f - \epsilon_i) \tag{10.6.9}$$

[see Eq. (7.6. 10.)], where v is a tunneling perturbation (energy). The precise nature of the perturbation does not matter; the perturbation's only role is to initiate a quantum-tunneling transition from p_i to p_f. Such perturbation may come from lattice defects, interface irregularities, and others. We assume that the matrix element $\langle p_f|v|p_i\rangle$ is a constant:

$$\langle p_f|v|p_i\rangle = M \tag{10.6.10}$$

which is reasonable because of the incidental nature of the perturbation. Equation (10.6.9) may be used if and only if the energy of the final state $\in_f$ is in an energy continuum. This may be satisfied by the excited pairon states in the final-state, depending on $\in_i, \in_f$, and $2eV$. If not, quantum tunneling should not occur. We multiply Eqs. (10.6.7) and (10.6.9) together and integrate with respect to $d\Omega$ over the right-half, then further integrate with respect to dp. Since the + pairon has charge $2e$, we multiply the result by $2e$ to obtain an expression for the current density J as

$$J = \frac{4\pi eM^2}{\hbar}\left(\frac{1}{2}v_F\right)\int_{p_x>0} f(\epsilon)\frac{p^2dp}{(2\pi\hbar)^3}d\Omega\,\delta(\epsilon_f - \epsilon - 2eV) \tag{10.6.11}$$

where we used Eq. (10.6.10). The Ω-integration equals one-half of the integration over all directions. Integration with respect to the initial-state $\mathbf{p}_i$ may be replaced by integration with the final-state $\mathbf{p}_f$. If we use the identity:

$$(2\pi\hbar)^{-3}\int d^3p_f\,\delta(\epsilon_f - \epsilon_i) = \mathcal{N}_f(\epsilon_i) \tag{10.6.12}$$

where $\mathcal{N}_f$ represents the density of states at the final state, we can reexpress Eq. (10.6.11) as

$$\boxed{J = \frac{2\pi}{\hbar}CM^2\left(\frac{1}{2}ev_F\right)f_i(\epsilon)[1 + f_f(\epsilon + 2eV)]\mathcal{N}_f(\epsilon + 2eV)} \tag{10.6.13}$$

Here we added two correction factors C (a constant) and $[\,1 + f_f(\in + 2eV)]$.

This is the desired expression for the current density due to + pairons tunneling from S_1 to S_2. The arguments $\in + 2eV$ in $\mathcal{N}_f$ and f_f represent energies measured relative to the energy level fixed in the superconductor S_i. Fermi's golden rule for a quantum transition rate [see Eq. (7.6.13)] is given by

$$R(\mathbf{p}, \mathbf{p}_0) = \frac{2\pi}{\hbar}|\langle\mathbf{p}|v|\mathbf{p}_0\rangle|^2\mathcal{N}_f(\epsilon) \tag{10.6.14}$$

Thus Eq. (10.6.13) can be interpreted simply in terms of this rate R. Bardeen pointed out this important fact[7] right after Giaever's experiments[3] for the quasi-electron transport model; a further discussion of this topic is given in Section 10.10. The appearance of the Planck distribution function $f_i(\epsilon)$ is significant. Since this factor arises from consideration of the initial-state pairon flux, we attach a subscript i. In the derivation we tacitly assumed that all pairons arriving at the interface (S_1, I) can tunnel to S_2 and

that tunneling can occur independently of the incident angle relative to the positive x-direction. Both assumptions may lead to an overestimate. To compensate for this, we put the correction factor:

$$C\ (< 1) \tag{10.6.15}$$

to Eq. (10.6.13). In consideration of the boson-nature of the pairons, we also inserted the *quantum statistical factor* (see Section 7.8)

$$1 + f_f(\epsilon) \tag{10.6.16}$$

Let us summarize the results of our theory of quantum tunneling.

1. The predominant charge carriers are moving pairons of charge (magnitude) $2e$.
2. In the rightward bias ($V_1 > V_2$), + (–) pairons move preferentially right (left) through the oxide.
3. The bias voltage $V \equiv V_1 - V_2$ allows excited (or moving) pairons to gain or lose an energy equal to $2eV$ at the oxide.
4. Quantum tunneling occurs at $\in_f = \in_i \pm 2eV$ and it does so if and only if the final state is in a continuous range of pairon energy.
5. Moving pairons (bosons) are distributed according to the Planck distribution law, which makes the tunneling current temperature dependent.
6. Some condensed pairons may separate from the supercondensate and directly tunnel through the oxide.
7. Ground pairons may gain energy from the bias voltage to become excited pairons, which requires energy equal to twice the energy gaps $\in_j$ or greater. The resulting excited pairons may then tunnel through the barrier.

Statements 1–6 are self-explanatory. Statement 7 arises as follows. The minimum energy required to raise one pairon from the ground state to the excited state in S_i is equal to the energy gap $\in_g$. But to keep the supercondensate neutral, another pairon of the opposite charge must be taken away, which requires an extra energy equal to $\in_g$ (or greater). Thus the minimum energy required to move one pairon from the ground state to an excited state and keep the supercondensate intact is $2\in_g$. In the steady-state experimental condition, initial and final states must be maintained and constantly repaired with the aid of external forces (bias voltages). Repairing the supercondensate is therefore a necessity. The oxide is used to generate a bias. If the oxide layer is too thick, tunneling currents are too small to measure.

We now analyze the *S–I–S* tunneling as follows. For a small bias V below the threshold bias V_t such that

$$V < V_t \equiv \frac{c_g(T)}{e} \tag{10.6.17}$$

the excited pairons already present in S_1 and S_2 may tunnel through the oxide layer. The current I is small, since the number density of excited pairons is small. It should reach a plateau where all excited pairons, whose total number is fixed at a given temperature, contribute; this explains feature B.

A more elaborate explanation using Eq. (10.6.13) is as follows. First we note that Eq. (10.6.13) applies for the specific energy $\in$ corresponding to the initial momentum **p**. Integration with respect to $d\in$ yields the observed current. Assume the case of + pairons contributing to the charge transport. For a small bias V, the rightward current I_1^+ and the leftward current I_2^+ are calculated to be

$$\text{(right)} \qquad I_1^+ \propto A \int_0^\infty d\epsilon\, \epsilon^2 f(\epsilon)[1 + f(\epsilon + 2eV)] \qquad (f_i = f, \mathcal{N}(\epsilon) = A\epsilon^2)$$

$$\text{(left)} \qquad I_2^+ \propto -A \int_{2eV}^\infty d\epsilon\, \epsilon^2 f(\epsilon)[1 + f(\epsilon - 2eV)] \tag{10.618}$$

In the leftward tunneling, the + pairon loses an energy $2eV$, which is reflected in the arguments of f. The (final-state) density of states $\mathcal{N}_1(\epsilon - 2eV)$ in Eq. (10.6.13) indicates that if + pairons in S_1 do not have enough kinetic energies, they cannot contribute, yielding the lower limit $2eV$ on the last integral in Eq. (10.6.18). Thus the total current:

$$I^+ \equiv I_1^+ + I_2^+ \ (> 0) \tag{10.6.19}$$

is positive and increases with the bias V. As an internal check, let us consider the case of no bias: $V = 0$. In this case currents due to + pairons moving rightward from S_1 to S_2 and leftward are equal in magnitude but different in sign. Thus $I^+ = 0$.

The case of – pairons can be worked out in a similar manner. The total current:

$$I^- \equiv I_1^- + I_2^- \ (> 0) \tag{10.6.20}$$

is positive and increases with the bias V (Problem 10.6.1). Now

$$A \int_0^\infty d\epsilon\, \epsilon^2 f_1(\epsilon) = n_1 \tag{10.6.21}$$

represents the number density of excited + pairons in S_1 . Since this is a (temperature-dependent) constant, there is a plateau, which explains feature B.

Above the threshold V_t, some of the condensed pairons in the supercondensate may dissociate so that the resulting excited pairons tunnel through the oxide. The tunneling current is much greater, since the supercondensate is involved. Giaever *et al.*,[4,5] observed that the threshold voltage V_t depends on the temperature T and could determine the energy gap $\in_g(T)$ as a function of T. Figure 10.7 represents part of their results.

Above T_c there are no energy gaps, and so electrons may be excited more easily, since there are no energy gaps. There are moving pairons still above T_c. Since the number densities of electrons and holes outweigh the density of pairons far above T_c, the I–V curve should eventually approach the straight line, which explains feature D.

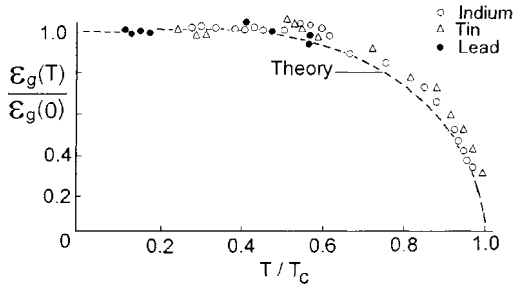

Figure 1 0.7. Variation of the measured energy gap $\in_g(T)$ with temperature.

Feature E supports our hypothesis that current passing through the oxide is carried by pairons. If quasi-electrons that become normal electrons above T_c were involved in the charge transport, the current I would have followed the ideal (Ohm's law) straight line immediately at T_c or above, in disagreement with the experimental observation.

Quantum tunneling is a relatively easy experiment to perform. It is remarkable that the energy gap, whose appearance is one of the most distinct features in a superconductor below T_c, can be obtained directly with no further calculations.

Giaever *et al.* assumed that the energy gap observed correspond to the quasi-electron energy gap $\Delta(T)$. The present authors take the view that the energy gap observed is the pairon energy gap $\in_g(T)$ As we see in Fig. 10.7, experimental data match well either of the theoretical curves in Figs. 10.1 or 10.2. We further discuss differences between the two models and the two interpretations in Section 10.10.

The energy gap $\in_g(T)$ can also be measured in photoabsorption experiments. These experiments [8] were done before tunneling experiments and give similar curves but with greater errors, particularly near T_c. We briefly discuss this case. First consider the case of $T = 0$. As we saw in Section 8.5, the ground-state energy W_0 is equal to the pairon ground-state energy w_0 times the number of pairons $N_0 = \hbar\omega_D \mathcal{N}(0)$. Thus the binding energy per pairon is equal to $|w_0|$. This can be probed in the photoabsorption experiments at the lowest temperatures. The threshold photon energy $\Delta\in$ above which a sudden increase in absorption is observed is found to be twice the binding energy $|w_0|$:

$$\Delta\epsilon = 2w_0 \ [= 2\epsilon_g(0)] \qquad (0 \text{ K}) \tag{10.6.22}$$

The photon is electrically neutral and therefore cannot change the charge state of the system. Thus each photon, when absorbed, may cause a *pair dissociation* in the supercondensate. Thus the factor 2 in Eq. (10.6.22) arises from the dissociation of *two* pairons of different charges $\pm 2e$. This is similar to the pair creation of an electron and a positron by a γ-ray, where the threshold energy is $2mc^2$ (c = light speed). The threshold energy $\Delta\in$ was found to be temperature-dependent. This can be interpreted simply by assuming that threshold energy corresponds to twice the pairon energy gap:

$$\Delta\in = 2\in_g(T) \tag{10.6.23}$$

Problem 10.6.1. Verify Eq. (10.6.21) by explicitly writing the contributions similar to Eq. (10.6.18).

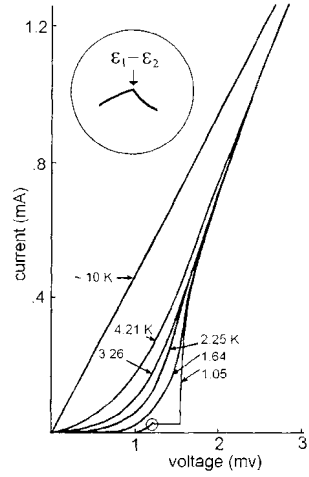

Figure 10.8. The *I–V* curves of the Al–Al_2O_3–Pb sandwich at various temperatures [after Giaever and Megerle (Ref. 4)].

10.7. QUANTUM TUNNELING EXPERIMENTS 2; S_1–*I*–S_2 AND S–*I*–N

Giaever and his group[3–5] carried out various tunneling experiments. The case in which two *different* superconductors are chosen for (S_1, S_2) is quite revealing. We discuss this case here. Figure 10.8 shows the *I–V* curves of an Al–Al_2O_3–Pb sandwich at various temperatures, reproduced from Ref. 4. The main features are:

A') The curves are generally similar to those for *S–I–S,* shown in Fig. 10.4, and they exhibit the same qualitative behaviors (features B–E).

B') There is a distinct maximum at

$$2eV_a = \epsilon_{g1} - \epsilon_{g2} \equiv \epsilon_1 - \epsilon_2 \tag{10.7.1}$$

where ϵ_i are the energy gaps for superconductors *i.* Above this maximum there is a *negative resistance* region ($dI/dV < 0$) (see the inset in Fig. 10.8).

C') Below T_c for both conductors, there is a major increase in current at

$$2eV_b = \epsilon_{g1} + \epsilon_{g2} \equiv \epsilon_1 + \epsilon_2 \tag{10.7.2}$$

The *I–V* curves will now be interpreted with the aid of diagrams in Fig. 10.9. There are *two* energy gaps (ϵ_1,ϵ_2). We assume that $\epsilon_1 > \epsilon_2$. No right-left symmetry with respect to the oxide exists, which means no antisymmetry in the *I–V* curve (see the following discussion).

Consider first the case of no bias. On entering in the oxide, excited pairons may move right or left with no preference. Therefore there is no net current:

$$I = 0 \quad \text{if } V = 0 \tag{10.7.3}$$

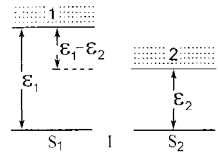

Figure 10.9. Pairon energy diagrams for S_1–*I*–S_2.

Suppose we apply a small voltage. We assume that the voltage at S_1 is higher than at S_2. Now the preferred direction for the + pairon having $2e$ is right, while that for the – pairon (having $-2e$) is left. From the diagram in Fig. 10.9, we see that the + pairons from S_1 can preferentially move (tunnel) to S_2, which contributes a small electric current running right. The – pairons from S_2 can preferentially move to S_1, which also contributes a tiny electric current running right. This contribution is tiny, since the excited pairons in S_2 must have energies greater by at least $\in_1 (> \in_2)$; therefore by the Boltzmann principle, the number of excited pairons must be extremely small.

We now increase the bias and examine the behavior of the net current. Earlier we enumerated a set of conditions for quantum tunneling. Below the threshold bias V_a defined by $\in_1 - \in_2 = 2eV_a$, the main contribution is due to the + pairons tunneling from S_1, to S_2. Above the threshold V_a, – pairons may preferentially tunnel from S_2 to S_1 with the aid of the bias voltage $V(> V_a)$. Their contribution should be much greater than that coming from those + pairons because the number of excited pairons in S_2 should be much greater than that of excited pairons in S_1 if $\in_1 > \in_2$. This is the main cause of the distinct current maximum in feature B' The total number of excited pairons in S_2 is fixed, and therefore there should be a second plateau.

Why a negative resistance region? We may explain this most unusual feature by using Eq. (10.6.13) as follows. First we note that Eq. (10.613) applies at a specific energy $\in$ corresponding to the initial momentum **p.** Integration with respect to $d\in$ yields the observed current. As the bias voltage V reaches and passes V_a, the extra current starts to appear and increase because more and more pairons can participate in the new process. The current density of the participating pairons is proportional to

$$A \int_0^\infty d\epsilon\, \epsilon^2 f_2(\epsilon)[1 + f_1(\epsilon + 2eV)] \tag{10.7.4}$$

For great values of V (not exceeding V_b), the Planck distribution $f_1(\in + 2eV)$ vanishes and the integral in Eq. (10.7.4) equals the total number density of the excited pairons n_2 in S_2:

$$A \int_0^\infty d\epsilon\, \epsilon^2 f_2(\epsilon) = n_2 \tag{10.7.5}$$

For an intermediate range between V_a and V_b but near V_a, the Planck distribution function $f_f(\in + 2eV)$ does not vanish, and therefore it should generate a maximum, as observed in the experiment. A more detailed discussion is given in Section 10.10.11. We emphasize

that this maximum arises because of the boson nature of pairons. If we assume a quasi-electron (fermion) transport model, expression (10.6.13) for the quantum-tunneling current must be modified with the quantum statistical factors[7]:

$$f_F^{(i)}(\epsilon)[1 - f_F^{(f)}(\epsilon + eV)] \tag{10.7.6}$$

where f_F represents the Fermi distribution function. The modified formula cannot generate a maximum because of the negative sign.

If the bias voltage is raised further and passes the threshold voltage V_b defined by

$$\epsilon_1 - \epsilon_2 + 2\epsilon_2 = \epsilon_1 + \epsilon_2 = 2eV_b \tag{10.7.7}$$

a new process 7 becomes active. Since this process originates in the supercondensate, the resulting current is much greater, which explains the observed feature C'

The major current increases in S–I–S and S_1–I–S_2 systems both originate from the supercondensate. Threshold voltages represented in terms of the energy gaps $\in_j$ are different. Current increases occur at $2\in$ for S–I–S and at $\in_1 + \in_2$ for S_1–I–S_2. Using several superconductors for S_j, one can make a great number of S_1–I–S_2 systems. Giaever and his group[3–5] and others[9] studied these systems and found that I–V curves have the same features as those for A1–$A1_2O_3$–Pb. Extensive studies confirm the main finding that the energy gap $\in_g(T)$ can be obtained directly from quantum-tunneling experiments. Taylor, Burstein and others[9] who carried out systematic measurements, reported that in such systems as Sn–I–T1, there are excess currents starting at $\in_{Tl}$ and $\in_{Sn}$ in addition to the principal exponential growth at $\in_{Tl} + \in_{Sn}$. These excess currents representing extra tunneling mechanisms can be accounted for by applying the rule 6 to nonpredominant pairons, which have been neglected in our discussion.

As noted earlier the right-left symmetry is broken for the S_1–I–S_2 system. Thus the I–V curve will not be antisymmetric. This can be shown as follows. Consider two cases:

$$A: \text{ rightward bias } V_1 > V_2, \qquad B: \text{ leftward bias } V_1 < V_2 \tag{10.7.8}$$

Then + (–) pairons move through the oxide preferentially right (left) in A, while + (–) pairons move preferentially left (right) in B. We assume the same voltage difference $|V_1 - V_2|$ for both cases and compute the total currents. For A the total current I_A is the sum of the current I^+ arising preferentially from the + pairons originating in S_1 and the current I^- arising from the – pairons originating in S_2. Both currents effectively transfer the positive charge right (in the positive direction): $I^{+(1)}, I^{-(2)} > 0$. For B there are two similar contributions, which are both negative. In summary:

$$\begin{aligned} A: &\qquad I_A = I^{+(1)} + I^{-(2)} > 0, \quad I^{+(1)}, \quad I^{-(2)} > 0 \\ B: &\qquad I_B = I^{+(2)} + I^{-(1)} < 0, \quad I^{+(2)}, \quad I^{-(1)} < 0 \end{aligned} \tag{10.7.9}$$

If the same superconductors are used for the two sides ($S_1 = S_2$), then from generalized Ohm's law as discussed in Section 10.6, we have

$$I^{+(1)} = -I^{+(2)}, \qquad I^{-(2)} = -I^{-(1)} \tag{10.7.10}$$

$$I_A = -I_B \quad \text{if } S_1 = S_2 \tag{10.7.11}$$

indicating that the *I–V* curve is antisymmetric. If different superconductors are used, Eqs. (10.7.10) do not hold. Then

$$|I_A| \neq |I_B| \quad \text{if } S_1 \neq S_2 \qquad \text{q.e.d.} \tag{10.7.12}$$

The preceding proof may be extended to any type of charge carrier including quasi-electrons.

Let us now discuss *I–V* curves for S_1–*I*–S_2 systems. For elemental superconductors, both ± pairons have the same energy gaps. Therefore magnitudes of threshold voltages (V_a, V_b) are independent of the bias direction. But by inequality (10.7.8), the magnitudes of tunneling currents (at the same voltage) should be unequal. For a high-T_c cuprate superconductor, there are two energy gaps ($\in_1, \in_2$) for ± pairons. The *I–V* curves for S_1–*I*–S_2 systems are found to be asymmetric (see Section 13.5).

10.8. DENSITY OF THE SUPERCONDENSATE

Below T_c there are a large number of pairons condensed at zero momentum. We discuss the temperature dependence of the supercondensate density in the present section.

At 0 K all pairons are condensed at zero momentum. At a finite temperature there are excited pairons and quasi-electrons. Pairons by construction are in negative-energy states, while quasi-electrons have positive kinetic energies. Thus by the Boltzmann principle, pairons are more numerous at the lowest temperatures. In the following we assume that there are only excited pairons. There are pairons of two charge types. The predominant pairons are composed of electrons or holes, whichever has smaller effective mass and higher Fermi velocity. These dominate the B–E condensation and again the supercurrent flow. [For Pb, the predominant pairons are (–) pairons, that is, pairons having negative charge ($-2e$). The predominant (–) pairons have about six times higher speeds than the nonpredominant (+) pairons.] The supercondensate is composed of an *equal* number of predominant and nonpredominant ground pairons. Because of this predominance, the B–E condensation of pairons can be discussed by looking at the predominant pairons only. The number density of ground predominant pairons $n_0(0)$ is given by

$$n_0(0) = n_0 \equiv \frac{\hbar\omega_D \mathcal{N}(0)}{2V} \equiv n, \qquad T = 0 \tag{10.8.1}$$

Hereafter in this section, we drop the subscript 0 on n to avoid confusion with n_0. As temperature is raised, the number density of the ground pairons $n_0(T)$ decreases and vanishes at the critical temperature T_c. The sum of the density of ground pairons $n_0(T)$ and the density of moving pairons $n_x(T)$ is equal to n:

$$n_0(T) + n_x(T) = n \tag{10.8.2}$$

Our task then is to find $n_x(T)$. [There is no way of finding $n_0(T)$ directly in the theory of B–E condensation.]

Let us recall that pairons do exist above T_c, and they have a linear energy–momentum relation [see Eq. (8.4.24)]:

$$w_q = w_0 + \frac{1}{2}v_F q < 0, \qquad w_0 \equiv \frac{-2\hbar\omega_D}{\exp[2/v_0\mathcal{N}(0)] - 1} \qquad T > T_c \tag{10.8.3}$$

Below T_c excited pairons exhibit the T-dependent energy–momentum relation in Eq. (10.5.11):

$$\tilde{w}_q = \tilde{w}_0(T) + \frac{1}{2}v_F q < 0, \qquad T < T_c \tag{10.8.4}$$

where $\tilde{w}_0(T)$ is the solution of

$$1 = \mathcal{N}(0)v_0 \int_0^{\hbar\omega_D} d\epsilon\, [|\tilde{w}_0| + 2(\epsilon^2 + \Delta^2)^{1/2}]^{-1} \tag{10.8.5}$$

The quasi-electron energy gap $\Delta(T)$ is given by Eq. (10.4.9) and the critical temperature T_c is defined by Eq. (10.4.10). Note: $\Delta = 0$ at T_c. Then from Eq. (10.8.5), we obtain $\tilde{w}_0(T_c) = w_0$. Thus:

$$\tilde{w}_q - w_0 = \tilde{w}_0 - w_0 + \frac{1}{2}v_F q \equiv \epsilon_g + \frac{1}{2}v_F q > 0 \tag{10.8.6}$$

Excited pairons in equilibrium are represented by the Bose distribution function:

$$f(\epsilon; \beta, \mu) \equiv \frac{1}{e^{\beta(\epsilon-\mu)} - 1} \equiv f(\epsilon) \qquad (\epsilon = \tilde{w}_q - w_0) \tag{10.8.7}$$

In the condensation region ($T < T_c$), the chemical potential μ vanishes

$$\mu = 0, \qquad T < T_c \tag{10.8.8}$$

Thus the number density of excited pairons, $n_x(T)$, below T_c, is given by

$$n_x(T) = (2\pi\hbar)^{-3} \int d^3q \left[\exp\left\{\beta\left[\epsilon_g(T) + \frac{v_F q}{2}\right]\right\} - 1\right]^{-1} \tag{10.8.9}$$

Let us assume a Fermi sphere. We then obtain (Problem 10.8.1):

$$n_x(T) = \left[\frac{4(k_B T)^3}{\pi^2\hbar^3 v_F^3}\right] \int_0^\infty \frac{x^2 dx}{\exp[\beta\epsilon_g(T) + x] - 1} \qquad \left(x \equiv \frac{1}{2}\beta v_F q\right) \tag{10.8.10}$$

Using the Bose–Einstein integral [see Eqs. (9.2.7) and (9.2.10)]

$$\phi_\nu(\lambda) \equiv \frac{1}{\Gamma(\nu)} \int_0^\infty dx \frac{x^{\nu-1}}{\lambda^{-1}e^x - 1} \equiv \sum_{j=1}^\infty \frac{\lambda^\nu}{j^\nu} \tag{10.8.11}$$

where $\Gamma(\nu)$ is the gamma function, we can reexpress Eq. (10.8.10) as

$$n_x(T) = \pi^{-2}\left[\frac{2k_B T}{\hbar v_F}\right]^3 \phi_3[\exp(-\epsilon_g/k_B T)] \tag{10.8.12}$$

At the critical temperature T_c, where $\tilde{w}_0(T_c) = w_0, \epsilon_g = 0$,

$$n_x(T_c) = \pi^{-2}\left[\frac{2k_B T_c}{\hbar v_F}\right]^3 \phi_3(1) = n \tag{10.8.13}$$

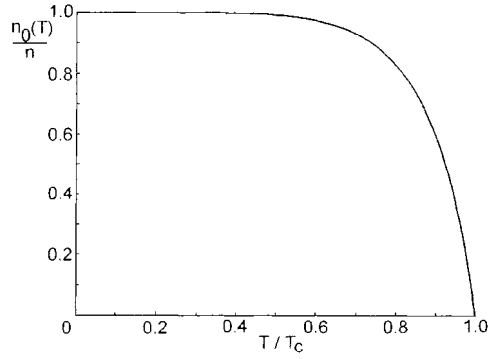

Figure 10.10. The reduced supercondensate density $n_0(T)/n$ monotonically declines with increasing temperature.

Therefore the desired $n_0(T)$ is given by

$$\begin{aligned} n_0(T) &= n - n_x(T) \\ &= \pi^{-2}\left[\frac{2k_B T_c}{\hbar v_F}\right]^3 \phi_3(1)\left\{1 - \left(\frac{T}{T_c}\right)^3 \frac{\phi_3[\exp(-\epsilon_g/k_B T)]}{\phi_3(1)}\right\} \end{aligned} \tag{10.8.14}$$

After introducing the reduced variables:

$$\frac{T}{T_c} \equiv x, \qquad \frac{\epsilon_g}{k_B T_c} \equiv y \tag{10.8.15}$$

we can then reexpress Eq. (10.8.14) as

$$\frac{n_0(T)}{n} = 1 - x^3 \frac{\phi_3[\exp(-y/x)]}{\phi_3(1)} \tag{10.8.16}$$

The temperature dependence of $n_0(T)/n$ is shown in Fig. 10.10. If there were no energy gap in the pairon energy [$\epsilon_g(T) = 0$] as in the Cooper system, Eq. (10.8.16) simplifies to

$$\frac{n_0(T)}{n} = 1 - x^3 = 1 - \left(\frac{T}{T_c}\right)^3, \qquad [\epsilon_g(T) = 0] \tag{10.8.17}$$

which is a known result for a system of free bosons moving with the linear energy–momentum relation $\epsilon = cp$ [see Eq. (9.3.6) and Fig. 9.3]. Note: The effect of a nonzero energy gap $\epsilon_g(T)$ is quite appreciable. The number density of excited pairons $n_x(T)$ drops off exponentially a little below T_c, as seen from Eq. (10.8.14). The existence of a macroscopic condensate is the most distinct feature of a system of bosons. Yet the temperature-dependent supercondensate density $n_0(T)$ is not subject to direct experimental observation. Elementary excitations in the presence of a supercondensate contribute to the heat capacity of the system, which is discussed in the following section.

Problem 10.8.1. Verify Eqs. (10.8.10) and (10.8.12).

10.9. HEAT CAPACITY

In this section we calculate the heat capacity of a superconductor under the assumption that there are no quasi-electrons and there are only predominant pairons.

For the Cooper system the energy–momentum relation for pairons is given by

$$w_q - w_0 = \frac{1}{2} v_F q \tag{10.9.1}$$

for all (low) temperatures. We calculated the heat capacity C in Sections 9.3 and 9.4. Below T_c C is proportional to T^3. For our generalized BCS system, the energy–momentum relation above T_c is the same as Eq. (10.9.1). But below T_c the relation is altered to

$$\tilde{w}_q - w_0 = \epsilon_g(T) + \frac{1}{2} v_F q \tag{10.9.2}$$

[see Eq. (10.8.6)]. The internal energy density $u(T)$ can be calculated as follows (Problem 10.9.1)

$$\begin{aligned} u(T) &= \frac{1}{(2\pi\hbar)^3} \int d^3q \left(\frac{1}{2} v_F q\right) \frac{1}{\exp\{[\epsilon_g(T) + v_F q/2]/k_B T\} - 1} \\ &= \frac{24(k_B T)^4}{\pi^2 \hbar^3 v_F^3} \frac{1}{\Gamma(4)} \int_0^\infty dx \frac{x^3}{e^{\beta\epsilon_g} e^x - 1} \\ &= 3nk_B T_c \left(\frac{T}{T_c}\right)^4 \frac{\phi_4[\exp(-\epsilon_g/k_B T)]}{\phi_3(1)} \end{aligned} \tag{10.9.3}$$

Comparing Eq. (10.9.3) with Eq. (9.3.7) and noting that $\epsilon_g(T_c) = 0$, we observe that the internal energy is continuous at T_c. Note: $u(T)$ is a sole function of T_c. Differentiating $u(T)$ with respect to T, we obtain (Problem 10.9.2)

$$\begin{aligned} C(T) = \frac{du(T)}{dT} &= 12nk_B \left(\frac{T}{T_c}\right)^3 \frac{\phi_4[\exp(-\epsilon_g/k_B T)]}{\phi_3(1)} \\ &\quad - 3n \left(\frac{T}{T_c}\right)^2 \frac{\phi_3[\exp(-\epsilon_g/k_B T)]}{\phi_3(1)} \left\{ \left(\frac{T}{T_c}\right) \frac{d\epsilon_g(T)}{dT} - \frac{\epsilon_g(T)}{T_c} \right\} \quad T < T_c \end{aligned} \tag{10.9.4}$$

Above T_c heat capacity C is the same as for the Cooper system [see Eq. (9.3.10)]:

$$C(T) = 12nk_B \left(\frac{T}{T_c}\right)^3 \frac{\phi_4(\lambda)}{\phi_3(1)} - 9nk_B \frac{\phi_3(\lambda)}{\phi_2(\lambda)}, \quad T > T_c \tag{10.9.5}$$

where the fugacity λ is implicitly given by [see Eq. (9.3.5)]:

$$\left(\frac{1}{8}\right) \pi^2 \hbar^3 v_F^3 n = k_B^3 T^3 \phi_3(\lambda) \qquad T > T_c \tag{10.9.6}$$

Comparing Eqs. (10.9.4) and (10.9.5), we observe that heat capacity C has a *discontinuity* at T_c. The magnitude of the discontinuous jump ΔC at T_c is given by (Problem 10.9.3)

$$\Delta C = 3nk_B \left[\frac{3\phi_3(1)}{\phi_2(1)} - \frac{1}{k_B} \frac{d\epsilon_g}{dT}\right]_{T=T_c} \tag{10.9.7}$$

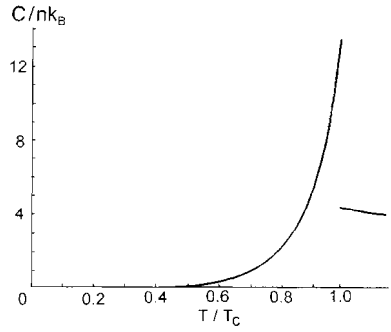

Figure 10.11. The (reduced) heat capacity C/nk_B versus temperature.

Figure 10.11 shows a plot of reduced heat capacity C/nk_B as a function of T/T_c. The effect of the pairon-energy gap $\in_g$ on heat capacity C appears prominently. The $C(T)$ falls more rapidly compared to the T^3-law for the auxiliary Cooper system. From Eq. (10.9.4), the behavior of $C(T)$ far below T_c may be represented analytically by

$$C(T) \sim \text{constant} \left(\frac{T}{T_c}\right)^3 \exp(-\epsilon_g/k_B T) \tag{10.9.8}$$

because $\phi_4(x)$ is a smooth function of x.

There is also a small but nonnegligible correction on the maximum heat capacity $C_{\max}$ [see Eq. (10.9.7)] because

$$\frac{d\epsilon_g}{dT} < 0 \tag{10.9.9}$$

The jump ΔC over the maximum $C_{\max}$ is given by

$$\frac{\Delta C}{C_{\max}} = \left[\frac{3\phi_3(1)}{\phi_2(1)} - \frac{d\epsilon_g}{d(k_B T_c)}\right] \Big/ \left[\frac{4\phi_4(1)}{\phi_3(1)} - \frac{d\epsilon_g}{d(k_B T_c)}\right] \tag{10.9.10}$$

If we neglect $d\epsilon_g(T)/dT$, we have [see Eq. (9.5.8)]:

$$\frac{\Delta C}{C_{\max}} = \frac{3}{4}\left[\frac{\phi_3(1)^2}{\phi_2(1)\phi_4(1)}\right] = 0.609 \tag{10.9.11}$$

which is quite close to the value obtained by the finite-temperature BCS theory[1]:

$$\left.\frac{\Delta C}{C_{\max}}\right)_{\text{BCS}} = 0.588 \tag{10.9.12}$$

The numerical calculation from Eqs. (10.9.5)–(10.9.7) and (10.9.10) yields the following ratio

$$\frac{\Delta C}{C_{\max}} = 0.702 \tag{10.9.13}$$

The experimentally observed ratios of heat capacity jump ΔC to the maximum $C_{\max}$ at T_c for several superconductors were given in Table 9.1. The ratios are in the range 0.6–0.7. Thus our theoretical results in Eqs. (10.9.11) and (10.9.13) are in very good agreement with experiments. Further discussion on our results are given in the following section.

Problem 10.9.1. Verify Eq. (10.9.3).

Problem 10.9.2. Verify Eq. (10.9.4).

Problem 10.9.3. Verify Eq. (10.9.7).

10.10. DISCUSSION

In the present chapter we studied the thermodynamic properties of a superconductor below T_c from the quantum statistical point of view. The equation-of-motion method is repeatedly used to study the energy spectra of quasi-electrons, ground and excited pairons. Quasi-electrons and pairons are found to have gaps ($\Delta_j, \in_{gj}$) in their spectra. These gaps depend on temperature. Both $\Delta_j(T)$ and $\in_{gj}(T)$ are greatest at 0 K and monotonically decrease to zero as temperature is raised to T_c. For elemental superconductors, energy gaps are the same for both charge types: $\Delta_1 = \Delta_2 \equiv \Delta$ and $\in_{g1} = \in_{g2} \equiv \in_g$. The temperature behavior of $\Delta(T)$ and $\in_g(T)$ are shown, respectively, in Figs. 10.1 and 10.2. In the range $(0, T_c)$, $\in_g(T) < \Delta(T)$. Pairons have negative energies, while quasi-electrons have positive energies. Thus, by the Boltzmann principle, pairons are more numerous than quasi-electrons, and the former dominate the low-temperature behavior. Pairon energy gaps $\in_g$ can be measured directly by the quantum-tunneling techniques. Data for *S–I–S* and S_1–*I*–S_2 systems are interpreted by the pairon transport model. Excited pairons move like massless bosons, with the common speed equal to $v_F/2$. Under the assumption that excited pairons are the only elementary excitations in the superconductor, we computed the density of condensed pairons $n_0(T)$, which is shown in Fig. 10.10. Under the same assumption, we calculated the heat capacity $C(T)$, which is shown in Fig. 10.11. The overall agreement with experimentation is very good. Our description of the superconducting state is quite different from the original BCS description, in particular regarding the choice of elementary excitations: excited pairons versus quasi-electrons. Whenever relevant we point out differences. In the following subsections, we enumerate and discuss a number of important results obtained in this chapter.

10.10.1. Ground State

The supercondensate at 0 K is composed of great and equal numbers of ground pairons of both charge types, with the total number of ground pairons $N_0(0)$ being $N_0(0) = N_0 \equiv \hbar\omega_D \mathcal{N}(0)$. Each ground pairon contributes energy equal to the ground-state energy of a Cooper pair w_0 to the system ground-state energy W:

$$W = N_0 w_0, \qquad w_0 \equiv \frac{-2\hbar\omega_D}{\exp[(2/v_0)\mathcal{N}(0)] - 1} \tag{10.10.1}$$

which is in agreement with the BCS formula (8.5.22). This is a significant result. In statistical mechanics we try to derive everything, starting with an assumed Hamiltonian. The generalized BCS Hamiltonian H in Eq. (9.4.9) satisfies the applicability condition [Eq. (6.5.1)] of the equation-of-motion method with respect to pairons. Thus by using this method and solving energy-eigenvalue problems for ground pairons, we can obtain the ground-state energy W rigorously. The mathematical steps are more numerous in our approach than in the BCS-variational approach based on the minimum-energy principle. However our statistical mechanical theory has a major advantage: There is no need to guess the form of the trial wave function Ψ, which requires a great intuition. This methodological advantage of statistical mechanical theory becomes clear in the finite-temperature theory (see Section 10.10.7).

10.10.2. Supercondensate Density

The most distinct feature of a system of bosons is the possibility of a B–E condensation. The total number density of condensed pairon (supercondensate) density $n_0(T) \equiv N_0/V$ is equal to n_0 at 0 K and decreases to zero as temperature is raised to T_c. The temperature dependence of $n_0(T)$ is shown in Fig. 10.10. The condensation in equilibrium occurs at zero momentum. Thus the intensive property of the supercondensate cannot change with temperature because there is no distribution. But its content (density) changes with temperature. Unpaired electrons in the system hinder formation of the supercondensate, therefore the supercondensate density $n_0(T)$ decreases as the temperature T is raised (see Section 10.10.5). As we see in Chapter 11, the supercurrent is generated by the supercondensate in motion, which is composed of great and equal numbers of $\pm$ pairons condensed at one and the same momentum **q.** The moving supercondensate produces the most striking superconducting properties: zero resistance, Meissner effect, flux quantization, and Josephson effects.

10.10.3. Quasi-Electrons; Energy $\Delta(T)$ Gap

In the presence of the supercondensate, unpaired (or quasi-) electrons move differently from Bloch electrons. Their energies are different:

$$E_p^{(j)} \equiv \left[\epsilon_p^{(j)^2} + \Delta(T)^2\right]^{1/2} \quad \text{(quasi-electron)}, \qquad \epsilon_p^{(j)} \quad \text{(Bloch electron)} \tag{10.10.2}$$

The energy gap $\Delta(T)$ is temperature-dependent, and its behavior is shown in Fig. 10.1. The energy $E_p^{(j)}$ is the energy of an unpaired electron relative to the hypothetical superelectron forming the ground pairon. Thus the gap $\Delta(T_c)$ must vanish at T_c, where there is no supercondensate. The actual calculations of $\Delta(T)$ are carried out from the energy-gap equations, which are discussed in the following sections.

10.10.4. Energy Gap Equations at 0 K

In Section 8.5, we saw that the energy gap Δ at 0 K mysteriously appears in the minimum-energy-principle calculation. The starting Hamiltonian H_0 in Eq. (8.6.9) and the trial wave function Ψ in Eq. (8.5.1) are both expressed in terms of the pairon operators b's only. Yet, the variational calculation based on Eq. (8.5.5) leads to energy-gap equations (8.5.13) or (8.5.20), which contain the quasi-electron variables. Using the

equation-of-motion method, we discovered that the energy-eigenvalue equation (10.3.7) for the ground pairons is equivalent to the energy-gap equations, indicating that the formation of the supercondensate is influenced by the presence of unpaired electrons.

10.10.5. Energy Gap Equations below T_c

As temperature is raised, some quasi-electrons are excited in the system. These quasi-electrons disrupt formation of the supercondensate, making the supercondensate density and the energy gaps Δ smaller. This in turn makes quasi-electron excitation easier. This cooperative effect is most apparent near T_c, which can be seen in Figs. 10.1 and 10.10. In the original paper [1] BCS obtained the temperature-dependent energy gap equation Eq. (10.4.9) by the free-energy minimum principle based on the assumption that quasi-electrons are predominant elementary excitations in the superconductor. We have reproduced the same result Eq. (10.4.9) and its generalization Eq. (10.4.6) by the equation-of-motion method. In the process of doing so, we found that the energy gap $\Delta(T)$ and supercondensate density $n_0(T)$ arise from the correlation between quasi-electrons and the supercondensate.

10.10.6. Excited Pairons; Pairon Energy Gap $\in_g$

The phonon-exchange attraction acts at all time and at any temperature. Thus two quasi-electrons may be bound to form excited pairons. Since quasi-electrons have an energy gap $\Delta(T)$, excited pairons also have an energy gap $\in_g(T)$. The energy–momentum relation for the excited pairon is

$$\tilde{w}_q = w_0 + \epsilon_g(T) + \frac{1}{2} v_F q < 0 \qquad (w_0 < 0) \tag{10.10.3}$$

The temperature behavior of the gap $\in_g(T)$ is shown in Fig. 10.2. In the entire domain of condensation, this gap $\in_g(T)$ is less than the quasi-electron energy gap:

$$\epsilon_g(T) < \Delta(T) \tag{10.10.4}$$

10.10.7. Elementary Excitations in a Superconductor

BCS obtained many thermodynamic properties, including the critical temperature T_c, the energy gap $\Delta(T)$, and heat capacity under the assumption that quasi-electrons are predominant elementary excitations. This assumption is necessary if the free-energy minimum principle is used to determine the thermal distribution of quasi-electrons. In our statistical mechanics theory, all thermodynamic properties are computed, starting with the Hamiltonian in Eq. (8.2.1). The question of whether excited pairons or quasi-electrons are predominant elementary excitations answered logically by examining energies of the quasi-particles. Excited pairons having negative energies are more numerous than quasi-electrons, and the former dominate the low-temperature behavior of the superconductor.

10.10.8. Quantum-Tunneling Experiments and Energy Gaps

The temperature-dependent pairon energy gap $\in_g$ can be observed directly in quantum-tunneling experiments. In an *S–I–S* sandwich, the threshold voltage V_t above

which a major current increase occurs gives the value of the energy gap $\in_g(T)$ through

$$eV_t = \epsilon_g \tag{10.10.5}$$

In an S_1–I–S_2 sandwich, where different superconductors (S_1, S_2) are used, the major current increase occurs at the voltage V_b defined by

$$2eV_b \equiv \epsilon_1 + \epsilon_2 \tag{10.10.6}$$

Thus by performing a number of quantum-tunneling experiments, we can measure pairon energy gaps $\in_j$ directly in a systematic manner. Figure 10.7 represents the variation of the measured gap $\in_g$ with the temperature T. The law of corresponding states works very well here. In our interpretation of the experiments, we used the pairon transport model in which excited pairons tunnel through the oxide layer. At a very low bias, a small number of excited pairons may preferentially tunnel through the thin oxide layer. If the bias voltage V is raised beyond the threshold voltage V_t, part of the supercondensate dissociates and the resulting excited pairons move through the oxide. This explains the major current increase in the I–V curve shown in Fig. 10.4.

10.10.9. Antisymmetry in the I–V Curves in Quantum Tunneling for Any S–I–S System

For S–I–S systems I–V curves are antisymmetric, which represents a generalized Ohms's law. For S_1–I–S_2 or S–I–N, where N represents the normal-state metal, the I–V curves are asymmetric. This rule also holds for a p–n junction in semiconductors.

10.10.10. Negative Resistance

The most unusual feature of the I–V curve for an S_1–I–S_2 system is the appearance of a negative resistance region above (or on the high-voltage side of) the maximum at $2eV_a = \in_1 - \in_2$, where *the current I decreases with increasing voltage.* This can be interpreted in terms of the quantum statistical factor $1 + f(\in + 2eV)$ in Eq. (10.7.4). Here the boson nature of pairons appears explicitly. Detailed calculations based on Eq. (10.6.13) show[10] that the current maximum at $2eV_a = \in_1 - \in_2$ is a *cusp* having a discontinuous slope; this is in agreement with experiments.[3] Because of this special shape (cusp), the values of $\in_1 - \in_2$ can be measured much more accurately than the values of $\in_1 + \in_2$ obtained from the second threshold, where the current I rises sharply but continuously (see Section 10.10.11).

10.10.11. Shape of the Major Current Rise

The major increase in the tunneling current arises from the dissociation of the supercondensate. The linear increase with the voltage V cannot be continued indefinitely because of the critical-current limitation on the supplier supercurrent. The tunneling current I should therefore behave like that above T_c. This explains the behavior of the I–V curves shown in Fig. 10.4 and 10.8. The I–V curves have a smooth transition through the critical temperature, since excited pairons are present below and above T_c.

10.10.12. The Ground-Pairon Density n_0 at 0 K

The energy gap $\epsilon_g(0)$ at 0 K is equal to the binding energy $|w_0|$ of a Cooper pair. We can obtain the values of $|w_0|$ through quantum tunneling or photoabsorption experiments. Since total binding energy W is given by

$$\frac{W}{V} = n_0|w_0| = \frac{B_c^2}{2\mu_0} \tag{10.10.7}$$

we can estimate the pairon density n_0. For Al (Pb) B_c = 105 (803) G and ϵ_g = 0.34 (2.73) meV. The values of n_0 calculated from Eq. (10.10.7) are 0.73 (5.29) × $10^{18} cm^{-3}$. Thus estimated pairon density is about 10^{-4} of the conduction electron density. This means that the great majority of electrons do not participate in the Cooper pair formation. Only those electrons near the hyperboloidal Fermi surface (necks and/or double caps) can form Cooper pairs.

10.10.13. Quasi-Electron Energy Δ Gap

According to our study in Section 8.6.3 the gap Δ is equal to the energy difference between the *real* unpaired electron and the *hypothetical* superelectron. Thus the quasi-electron energy gap Δ is not a real energy gap unlike the pairon energy gap ϵ_g. This means that the gap Δ cannot be observed in photoabsorption experiments. This is a major discrepancy with the prevalent theory, where the observed energy gaps in superconductors are identified as quasi-electron energy gaps.

A crucial test between the two theories may be set up as follows. Let us consider an *S–I–N* system, where one side of the conductors is made up of the true normal metal (*N*) like Cu. Such a metal, which remains normal down to 0 K, does not allow pairons to be formed. (This is in contrast to the normal state above T_c of a superconductor like Al where there are moving pairons.) Thus this metal *N* cannot supply pairons to the oxide (*I*). Moreover it cannot receive pairons through quantum tunneling because there are no continuous pairon energy levels. In other words no pairon charge transport is possible for this system. Any electrons that enter from either side can however be accelerated by the bias, and they can contribute to the net current. The major current increase should occur if the bias voltage is higher than the threshold voltage V_c defined by.

$$eV_c \equiv 2\epsilon_g + \epsilon_g = 3\epsilon_g, \qquad V_c = 3V_a \tag{10.10.8}$$

Here the rhs represents the minimum energy required for the dissociation of a pairon from the supercondensate ($2\epsilon_g$) and the subsequent break-up of the pairon into two electrons (ϵ_g); the lhs is the energy gain by one electron through the oxide. This threshold voltage V_c is three times higher than V_a. (In Section 13.6 we discuss *I–V* curves for *S–I–N* systems with *S* = high-T_c superconductors.)

10.10.14. Heat Capacity

Heat capacity is one of the most revealing properties of any many-particle system. Precise heat capacity measurements often contribute to a basic understanding of underlying physical phenomenon. We saw earlier in Chapter 9 that the superconducting transition is a B–E condensation of pairons independently moving with a linear energy–momentum

relation. The condensation phase transition is of the second-order. Below T_c the presence of the supercondensate generates an energy gap in the pairon energy–momentum relation. In the strong predominant pairon limit, we calculated the heat capacity $C(T)$; the result is shown in Fig. 10.11. The effect of $\in_g$ on $C(T)$ is apparent for all temperatures below T_c. Far below T_c, $C(T)$ falls almost exponentially as $\exp[-\in_g(T)/k_BT]$ [see Eq. (10.9.8)]. Since $d\in_g/dT < 0$ near T_c, the maximum $C_{\max}$ is greater for the generalized BCS system than the Cooper system. Thus the ratio $\Delta C/C_{\max}$ is greater for the generalized BCS system (0.702) than for the Cooper system (0.608). Experimental values for $\Delta C/C_{\max}$ for several elemental superconductors are in the 0.6–0.7 range. Agreement between theory and experiment is better than the BCS prediction of 0.588. Our numerical calculations are performed on the assumption of strong predominance. In real metals the ratio of absolute effective masses for electrons and holes $|m_1/m_2|$ may be far from unity. It varies from material to material. Thus if we include the finiteness of $|m_1/m_2|$ in the calculations, we may account for the material dependence of $\Delta C/C_{\max}$. The BCS theory is based on the assumption that quasi-electrons are the only elementary excitations, while our calculations are carried out on the assumption that excited pairons are predominant. It is quite remarkable that the calculated $C(T)$ is not dissimilar in spite of the fact that Bose (Fermi) distribution functions are used for excited pairons (quasi-electrons).

REFERENCES

1. J. Bardeen, L. N. Cooper, and J. R. Schrieffer, *Phys. Rev.* **108,** 1175 (1957).
2. S. Fujita and S. Watanabe, *J. Supercond.* **5,** 219 (1992).
3. I. Giaever, *Phys. Rev. Lett.* **5,** 147 (1960); **5,** 464 (1960).
4. I. Giaever and K. Megerle, *Phys. Rev.* **122,** 1101 (1961).
5. I. Giaever, H. R. Hart, and K. Megerle, *Phys. Rev.* **126,** 941 (1961).
6. J. R. Schrieffer, *Theory of Superconductivity* (Benjamin, New York, 1964).
7. J. Bardeen, *Phys. Rev. Lett.* **6,** 57 (1961).
8. R. E. Glover III and M. Tinkham, *Phys. Rev. Lett.* **108,** 243 (1957); M. A. Biondi and M. Garfunkel, *Phys. Rev.* **116,** 853 (1959).
9. B. N. Taylor and E. Burstein, *Phys. Rev. Lett.* **10,** 14 (1963); C. J. Adkins, *Phil. Mag.* **8,** 1051 (1963); P. Townsend and J. Sutton, *Proc. Phys. Soc.* (*London*) **78,** 309 (1961).
10. G. H. Kim, "Thermodynamic Properties of type I Superconductors," Ph.D. dissertation, State University of New York at Buffalo.

11

Supercurrents, Flux Quantization, and Josephson Effects

The moving supercondensate, which is made up of ± pairons all condensed at a finite momenturn **p**, generates a supercurrent. Flux quantization and Josephson effects are, respectively, first- and second-quantization effects manifested on a macroscopic scale. A close analogy emerges between a supercurrent and a laser. Supercurrents, not lasers, respond to electromagnetic fields, however. The phase of a macro-wave function can change due to particle motion and the magnetic field, leading to London's equation. The penetration depth λ based on the pairon flow model is given by $\lambda = (c/e)[p/4\pi n_0|v_F^{(2)} - v_F^{(1)}|]^{1/2}$. Quasi-wave function $\Psi_\sigma(\mathbf{r})$ [Ginzburg–Landau wave function $\Psi'_\sigma(\mathbf{r})$] can be expressed in terms of the pairon density operator n as $\Psi_\sigma(\mathbf{r}) = \langle \mathbf{r}|n|\sigma\rangle$ [$\Psi'_\sigma(\mathbf{r}) = \langle \mathbf{r}|n^{1/2}|\sigma\rangle$], where σ denotes the condensed pairon state. Both wave functions change in time, following a Schrödinger-like equation of motion. Basic equations for the current passing a Josephson junction are derived. They are used to discuss SQUID and AC Josephson effects. Analyses of Shapiro steps in the *V–I* diagram show that the quasi-wave function ψ represents correct pairon dynamics.

11.1. RING SUPERCURRENT; FLUX QUANTIZATION 1

The most striking superconducting phenomenon is a never-decaying ring supercurrent.[1] Why is the supercurrent not hindered by the impurities that must exist in any superconductor? We discuss this basic question and flux quantization in this section.

Let us take a ring-shaped superconductor at 0 K. The *ground state* for a pairon (or any quantum particle) in the absence of electromagnetic fields can be characterized by a *real* wave function $\psi_0(\mathbf{r})$ having no nodes and vanishing at the ring boundary:

$$\psi_0(\mathbf{r}) = \begin{cases} \text{nearly constant} & \text{inside the body} \\ 0 & \text{at tge boundry} \end{cases} \tag{11.1.1}$$

Such a wave function corresponds to the zero-momenturn state, and it cannot carry current. As we saw in Section 9.1, pairons move as bosons. They neither overlap in space nor interact with each other. At 0 K a collection of free pairons therefore occupy the same zero-momentum state ψ_0. The many-pairon ground state Ψ so constructed is

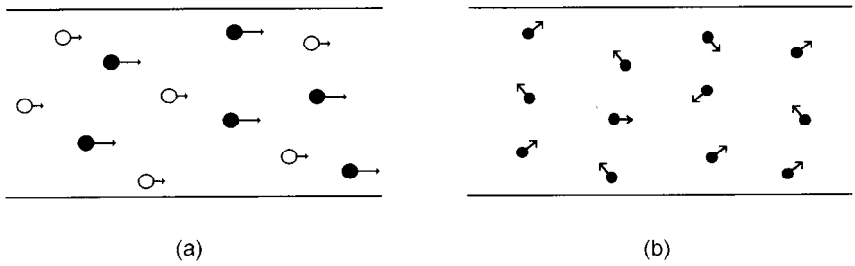

Figure 11.1. (a) Supercurrent; (b) normal current.

precisely the supercondensate discussed earlier in Chapter 8. There we saw that the supercondensate is composed of equal numbers of ± pairons with the total number being

$$N_0 = \hbar\omega_D \mathcal{N}(0) \tag{11.1.2}$$

We now consider current-carrying single-particle and many-particle states. There are many nonzero momentum states whose energies are very close to ground-state energy 0. These states may be represented by the wave functions $\{\psi_n\}$ having a finite number of nodes n along the ring. A typical state ψ_n is represented by

$$\psi_n(\mathbf{r}) = u \exp(iq_n x/\hbar) \tag{11.1.3}$$

$$q_n = \frac{2\pi\hbar n}{L}, \qquad n = \pm 1, \pm 2, \ldots \tag{11.1.4}$$

where x is the coordinate along the ring circumference of length L; the factor u is real and nearly constant inside, but vanishes at the boundary. When a macroscopic ring is considered, the wave function ψ_n represents a state having linear momentum q_n along the ring. For small n the value of $q_n = 2\pi\hbar n/L$ is very small, since L is a macroscopic length. The associated energy eigenvalue is also very small.

Suppose the system of free pairons of both charge types occupy the same state ψ_n. The many-pairon system-state Ψ_n so specified can carry a macroscopic current along the ring. In fact a pairon has charge $\pm 2e$ depending on charge type, there are equal numbers of ± pairons, and their speeds $c_j \equiv v_F^{(j)}/2$ are different. Thus total electric current density j, calculated by the rule: (charge) × (number density) × (velocity):

$$\boxed{j = (-2e)\left(\frac{n_0}{2}\right)(c_1 - c_2) = \frac{1}{2} e n_0 (v_F^{(2)} - v_F^{(1)})} \tag{11.1.5}$$

does not vanish. A schematic drawing of a supercurrent is shown in Fig. 11.1 (a). For comparison the normal current due to random electron motion is shown in Fig. 11.1 (b). Notice the great difference between the two.

In their classic paper,[2] BCS assumed that there were electrons and holes in a model superconductor, but they also assumed a spherical Fermi surface. (The contradictory nature of these two assumptions was mentioned earlier in Section 8.2.) In their model

electrons and holes have the same effective mass (magnitude) m^* and the same Fermi velocity $v_F^{(2)} = v_F^{(1)} = (2\epsilon_F/m^*)^{1/2}$. Then we obtain a vanishing supercurrent according to Eq. (11.1.5). Thus a finite supercurrent cannot be treated within the framework of the original BCS theory.

The supercurrent arises from a *many-boson state of motion.* This *many-particle* state is not destroyed by impurities, phonons, etc. This is somewhat similar to the situation in which a flowing river (large object) cannot be stopped by a small stick (small object). Microscopically, the elementary excitations in a superconductor are excited pairons. To generate an excited pairon, an energy greater than twice the energy gap $\in_g(T)$ must be supplied. Thus the supercurrent is stable with respect to small perturbations. Earlier in Section 8.6, we saw that because of charge and momentum conservation, the phonon exchange simultaneously pair creates ± pairons of the same momentum **q** from the physical vacuum. This means that the condensation of pairons can occur at *any* momentum state $\{\psi_n\}$. In the absence of electromagnetic fields, the zero-momentum state having minimum energy is the equilibrium state. In the presence of a magnetic field, the minimum-energy state is not necessarily the zero-momentum state, but it can be a finite momentum state, see below.

The supercurrent, generated by a *neutral* supercondensate in motion, is very stable against an applied voltage since no Lorentz electric force can act on it.

Let us now consider the effect of a magnetic field. In flux quantization experiments[3] a minute flux is trapped in the ring, and this flux is maintained by the ring supercurrent (see Fig. 1.4). Earlier in Section 5.6, we discussed dHvA oscillations in the susceptibility *versus* field diagram. According to Onsager's hypothesis,[4] the flux generated by a circulating electron carrying the charge $-e$ is quantized: in units of

$$\Phi_{el} \equiv \frac{h}{e} \equiv \frac{2\pi\hbar}{e}$$

[see Eq. (5.6.3)]. Experiments in superconductors,[3] (data are summarized in Fig. 1.5) show that the trapped flux Φ is quantized

$$\boxed{\Phi = n\Phi_0, \ (n = 0, 1, \ldots) \qquad \Phi_0 \equiv \Phi_{\text{pairon}} \equiv \frac{h}{2e} \equiv \frac{\pi\hbar}{e}} \tag{11.1.6}$$

From this Onsager concluded[5] that the particle circulating on the ring has a charge (magnitude) $2e$, in accord with the BCS picture of the supercondensate composed of pairons of charge (magnitude) $2e$. Flux quantization experiments were reported in 1961 by two teams, Deaver–Fairbank and Doll–Näbauer.[3] Their experiments are regarded as the most important confirmation of the BCS theory. They also show Onsager's great intuition about flux quantization. The integers n appearing in Eqs. (11.1.4) and (11.1.6) are the same, which can be seen by applying the Bohr–Sommerfeld quantization rule:

$$\oint p dx = 2\pi\hbar(n + \gamma) \tag{11.1.7}$$

to circulating pairons (Problem 11.1.1). The *phase* (number) γ is zero for the present ring (or periodic) boundary condition. A further discussion of flux quantization is given in Section 11.4.

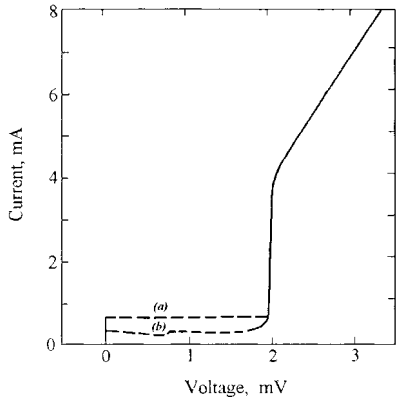

Figure 11.2. The *I–V* curves indicating a Josephson tunneling current; (a) $B = 0$, (b) $B = 0.4$ Gauss.

The supercurrent is generated by ± pairons condensed at a single momentum q_n and moving with different speeds $c_j \equiv v_F^{(j)}/2$. This picture explains why the supercurrent is unstable against a magnetic field **B**. Because of the Lorentz-magnetic force:

$$\pm 2e\mathbf{c}_j \times \mathbf{B} = \pm e\mathbf{v}_F^{(j)} \times \mathbf{B} \tag{11.1.8}$$

the B-field tends to separate ± pairons from each other. The (thermodynamic) *critical field* B_c should be higher for low-v_F materials than for high-v_F materials; this is in accord with experimental evidence. For example high-T_c superconductors have high B_c, reflecting the fact that they have low pairon speeds ($c_j \equiv v_F^{(j)}/2 \sim 10^5$ ms^{-1}). Since the supercurrent itself induces a magnetic field, there is a limit on the magnitude of the supercurrent, called a *critical current.*

Problem 11.1.1. Apply Eq. (11.1.7) to the ring supercurrent and show that $\gamma = 0$. Note: The phase γ does not depend on the quantum number n, suggesting a general applicability of the Bohr–Sommerfeld quantization rule with a high quantum number. Onsager used this rule to discuss the flux quantization, see Section 5.6.

11.2. JOSEPHSON TUNNELING; SUPERCURRENT INTERFERENCE

In 1962 Josephson predicted a supercurrent tunneling through a small barrier with no energy loss.[6] Shortly thereafter Anderson and Rowell[7] demonstrated this experimentally. Consider the circuit shown in Fig. 10.3. The circuit contains two superconductors S_1 and S_2 with a Josephson junction consisting of a very thin oxide film estimated to be of the order 10 Å. The two superconductors are made of the same material. The *I–V* curves observed are shown in Fig. 11.2. Finite current I_0 curve appears (a) even at $V = 0$, and its magnitude is of the order mA; it is very sensitive to the presence of a magnetic field. When a field $B = \mu_0 H$ (~ 0.4 Gauss) is applied, the current I_0 drops significantly as shown in (b). When voltage (~ mV) is raised high enough, the normal tunneling current

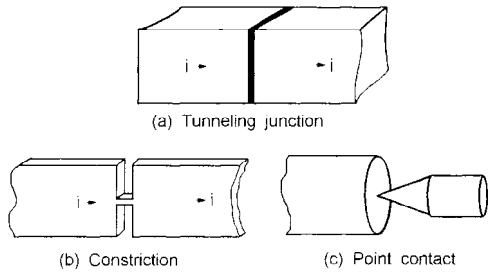

Figure 11.3. Three types of weak links.

appears; its behavior is similar to that of Giaever tunneling in the *S–I–S* system (see Fig. 10.4). To see the physical significance of Josephson tunneling, let us consider the same system above T_c. The two superconductors above T_c show potential drops, and the oxide layer generates a large potential drop. Below T_c the two superconductors having no resistance show no potential drops. Not only that, but the oxide layer exhibits no potential drop! This is an example of quantum tunneling, which we learn in elementary quantum theory. The quasi-wave functions $\Psi_j(\mathbf{r})$ in the superconductors S_j do not vanish abruptly at the S_j–I interfaces. If the oxide layer is small (10 Å), the two wave functions Ψ_1 and Ψ_2 may be regarded as a *single wave function* extending over both regions. Then pairons may tunnel through the oxide layer with no energy loss.

The oxide layer that allows supercurrent tunneling, shown in Fig. 11.3 (a), is called a *tunneling junction.* Similar effects can be produced by *constriction* and *point contact,* which are represented by (b) and (c). Any of the three is called a *weak link* or a *Josephson junction.*

We now take a ring-shaped superconductor with two Josephson junctions as shown in Fig. 1.11. Below T_c the current may split into two branches and rejoin. If a very weak magnetic field is applied normal to the ring and is varied, the current I has an oscillatory component, as shown in Fig. 1.12.[8] The oscillatory part can roughly be represented by

$$I = I_{\max} \cos(\pi\Phi/\Phi_0) \tag{11.2.1}$$

where Φ is the magnetic flux enclosed by the ring:

$$\Phi = BA, \qquad A = \pi r^2 \ (r \sim 1 \text{ mm}) \tag{11.2.2}$$

and $I_{\max}$ is a constant. This is a *supercurrent interference.* The two supercurrents separated by 1 mm can interfere just like two laser beams from the same source.

This interference can be explained as follows. We divide the steady supercurrents in two, as shown in Fig. 11.4, where (a) represents the current in the absence of **B**, and (b) the diamagnetic current going through two junctions. The diamagnetic current is similar to that appearing in the flux quantization experiment discussed in Section 11.1. Junctions allow the magnetic flux Φ to change continuously, which generates a continuous current. Detailed calculations (see Section 11.7) show that the period of oscillation is $\Phi/2\Phi_0$, as indicated in Eq. (11.2.1). To appreciate the physical significance, consider the same

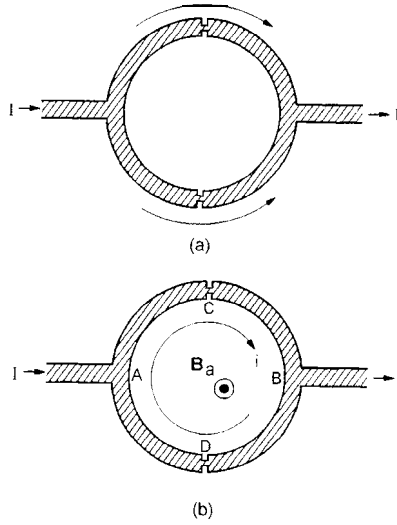

Figure 11.4. (a) The supercurrent at $B = 0$; (b) the diamagnetic supercurrent.

circuit above T_c. Application of a B-field generates a diamagnetic normal current around the ring, which dies out due to resistance, and cannot contribute to the steady current.

We close this section by pointing out a close analogy between supercurrent and laser. Both can be described by the wave function $U \exp(i\mathbf{k} \cdot \mathbf{r})$ (U = constant) representing a system of massless bosons all occupying one and the same momentum state $\hbar\mathbf{k}$. Such a monochromatic massless boson flux has a *self-focusing power* (capability). A flux of photons in a laser is slowed down by atomic electrons in a glass plate, but it can refocus itself to the original state due to the photon's boson nature. Similarly the pairon flux (supercurrent) becomes monochromatic after passing a Josephson junction. Thus both laser and supercurrent can interfere at a macroscopic distance. The self-focusing power comes from the quantum statistical factor

$$N_{\mathbf{p}} + 1 \tag{11.2.3}$$

with $N_{\mathbf{p}}$ denoting the number of condensed pairons associated with the condensation process in which a pairon joins the group numbering $N_{\mathbf{p}}$ in the state $\mathbf{p}$. This number $N_{\mathbf{p}} + 1$ is an enormous enhancement factor. But part of the enhancement is compensated for by the factor $N_{\mathbf{p}}$ associated with the decondensation process in which a pairon leaves the group. Feynman argued for such a *boson enhancement effect* in his provocative discussion of supercurrent.[9] He discussed this effect in terms of the probability amplitude, and therefore the factor $N_{\mathbf{p}}^{1/2}$ appears in his argument. It is interesting to note that such a self-focusing power is not known for a fermion (electron, neutron, proton) flux. Thus macroscopic interference may be observed for massless bosons (photons, pairons) only; quantum diffraction is observed for both fermions and bosons.

Supercurrents and lasers are however different. Pairons carry charge, but photons do not. Thus only pairons can contribute to the charge transport; moreover supercurrents generate magnetic fields and react against electromagnetic fields.

11.3. PHASE OF THE QUASI-WAVE FUNCTION

Earlier we saw that the supercurrent at a small section along the ring is represented by a plane wave:

$$\Psi_p(x) = A \exp(ipx/\hbar) \tag{11.3.1}$$

where A is a constant amplitude. We set $q_n \equiv p$; the pairon momentum is denoted by the more conventional symbol p. The quasi-wave function Ψ_p in Eq. (11.3.1) represents a system state of many pairons all condensed at $\mathbf{p}$ and the wave function ψ in Eq. (11.1.3) the single-pairon state. The Ψ_p and ψ_p are the same function except for the normalization constant (A). In this chapter we are mainly interested in the supercondensate quasi-wave function. We simply call Ψ the wave function hereafter (omitting quasi). In Section 11.2 we saw that two supercurrents macroscopically separated (~1 mm) can interfere just as two laser beams coming from the same source. In wave optics two waves are said to be *coherent* if they can interfere. Using this terminology two supercurrents are coherent within the *coherence range* of 1 mm. The coherence of the wave traveling through a region means that if we know the phase and amplitude at any space–time point, we can calculate the same at any other point from a knowledge of the k-vector ($\mathbf{k}$) and angular frequency (ω). In the present section, we discuss the phase of a general wave function and obtain an expression for the phase difference at two space–time points in the superconductor.

First consider a monochromatic plane wave running in the x-direction

$$\Psi = A \exp\left[i2\pi\left(\frac{x}{\lambda} - \frac{t}{T}\right)\right] = A \exp(ikx - i\omega t) = A \exp[i(px - Et)/\hbar] \tag{11.3.2}$$

where the conventional notations: $2\pi/\lambda \equiv k$, $2\pi/T \equiv \omega$, $p \equiv \hbar k$, $E \equiv \hbar\omega$ are used. We now take two points $(\mathbf{r}_1, \mathbf{r}_2)$. The phase difference $(\Delta\phi)_{12}$ between them

$$(\Delta\phi)_{12} = k(x_1 - x_2) - \omega(t_1 - t_2) \tag{11.3.3}$$

depends on the time difference $t_1 - t_2$ only. In the steady-state condition, this is a constant, which will be omitted hereafter. The positional phase difference is

$$(\Delta\phi)_{\mathbf{r}_1,\mathbf{r}_2} \equiv \phi(\mathbf{r}_1) - \phi(\mathbf{r}_2) = k(x_1 - x_2) \tag{11.3.4}$$

The phase difference $\Delta\phi$ for a plane wave proceeding in a $\mathbf{k}$ direction is given by

$$(\Delta\phi)_{\mathbf{r}_1,\mathbf{r}_2} = \int_{\mathbf{r}_2 \Rightarrow \mathbf{r}_1} \mathbf{k} \cdot d\mathbf{r} \tag{11.3.5}$$

where the integration is along a straight line path from $\mathbf{r}_2$ to $\mathbf{r}_1$. When the plane wave extends over the whole space; the line integral $\int_{\mathbf{r}_2 \to \mathbf{r}_2} \mathbf{k} \cdot d\mathbf{r}$ along *any* curved path joining the points $(\mathbf{r}_1, \mathbf{r}_2)$, see Fig. 11.5, has the same value (Problem 11.3.1):

$$(\Delta\phi)_{\mathbf{r}_1,\mathbf{r}_2} \equiv \int_{\mathbf{r}_2 \to \mathbf{r}_1} \mathbf{k} \cdot d\mathbf{r} = \int_{\mathbf{r}_2 \to \mathbf{r}_1} \mathbf{k} \cdot d\mathbf{r} \equiv \int_{\mathbf{r}_2}^{\mathbf{r}_1} \mathbf{k} \cdot d\mathbf{r} \tag{11.3.6}$$

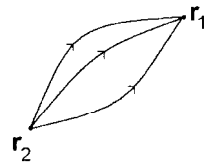

Figure 11.5. Directed paths from $\mathbf{r}_2$ to $\mathbf{r}_1$.

The line integral now depends on the end points only, and it will be denoted by writing out the limits explicitly as indicated in the last member of Eq. (11.3.6). Equivalently the same property can be expressed by (Problem 11.3.2):

$$\oint_C \mathbf{k} \cdot d\mathbf{r} = 0 \tag{11.3.7}$$

where integration is carried out along *any* closed directed path *C*.

We now consider the ring supercurrent shown in Fig. 11.6 (a). For a small section, the enlarged section containing point *A*, see (b), the supercurrent can be represented by a plane wave having momentum $\mathbf{p} = \hbar\mathbf{k}$. The phase difference $(\Delta\phi)_{\mathbf{r}_1,\mathbf{r}_2}$, where $(\mathbf{r}_1, \mathbf{r}_2)$ are any two points in the section, can be represented by Eqs. (11.3.6). If we choose a closed path ABA, the line integral vanishes

$$(\Delta\phi)_{\mathrm{ABA}} = \oint_{\mathrm{ABA}} \mathbf{k} \cdot d\mathbf{r} = 0 \tag{11.3.8}$$

Let us calculate the line integral along the ring circumference ARA indicated by the dotted line in (a). Note: The vector $\mathbf{k}$ changes its direction along the ring; for each small section, we can use Eq. (11.3.6). Summing over all sections, we obtain

$$(\Delta\phi)_{\mathrm{ARA}} = \oint_{\mathrm{ARA}} \mathbf{k} \cdot d\mathbf{r} = kL \tag{11.3.9}$$

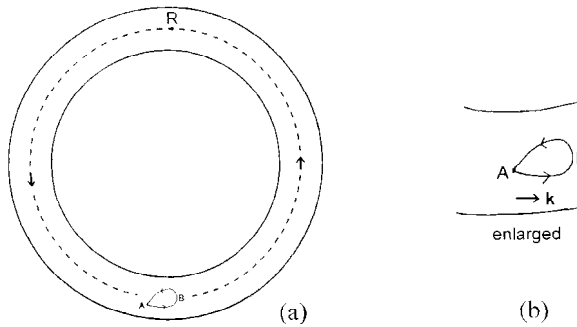

Figure 11.6. (a) A ring supercurrent, (b) an enlarged section.

where L is the ring length. Thus the line integral along the closed path ARA does not vanish. In fact if we choose a closed path C that circles the cavity counterclockwise N_1 times and clockwise N_2 times, the integral along the closed path is

$$\boxed{(\Delta\phi)_C \equiv \oint_C \mathbf{k}\cdot d\mathbf{r} = (N_1 - N_2)kL} \tag{11.3.10}$$

Note: Cases ABA (ARA), represented by Eq. (11.3.8) [(11.3.9)] can be obtained from this general formula by setting $N_1 = N_2 = 0$ ($N_1 = 1$, $N_2 = 0$). Since the momentum $\mathbf{p} \equiv \hbar\mathbf{k}$ is quantized such that $p_n = 2\pi n\hbar/L$, Eq. (11.3.10) can be reexpressed as

$$(\Delta\phi)_C = \oint_C \mathbf{k}\cdot d\mathbf{r} = 2\pi(N_1 - N_2)n \tag{11.3.11}$$

Problem 11.3.1. (a) Calculate the line integral in Eq. (11.3.6) by assuming a straight path from $\mathbf{r}_2$ to $\mathbf{r}_1$ and verify the equivalence of Eqs. (11.3.6) and (11.3.4). (b) Assume that the path is composed of two straight paths. Verify the equality. (c) Argue for a general curved path.

Problem 11.3.2. (a) Assume Eq. (11.3.6) and verify Eq. (11.3.7). (b) Assume Eq. (11.3.7) and verify Eq. (11.3.6).

11.4. LONDON'S EQUATION AND PENETRATION DEPTH; FLUX QUANTIZATION 2

In 1935 the brothers F. and H. London published classic papers[10] on the electrodynamics of a superconductor. By using the London equation (11.4.11) and Maxwell's equation (11.4.18), they demonstrated that an applied magnetic field $\mathbf{B}$ does *not* drop to zero abruptly inside the superconductor but penetrates to a certain depth. In this section we derive London equation and its generalization. We also discuss flux quantization once more.

In Hamiltonian mechanics the effect of electromagnetic fields $(\mathbf{E}, \mathbf{B})$ is included as follows: We replace the Hamiltonian without the fields $H(\mathbf{r},\mathbf{p})$ with

$$H' = H(\mathbf{r}, \mathbf{p} - q\mathbf{A}) + q\Phi \qquad (q = \text{charge}) \tag{11.4.1}$$

where $(\mathbf{A},\Phi)$ are the vector and scalar potentials generating the electromagnetic fields:

$$\mathbf{B} = \nabla \times \mathbf{A}, \qquad \mathbf{E} = -\nabla\Phi - \frac{\partial \mathbf{A}}{\partial t} \tag{11.4.2}$$

and then use Hamilton's equations of motion, equivalent to Newton's equations of motion. In quantum mechanics we may use the same Hamiltonian H'(the prime dropped hereafter) as a linear operator and generate Schrödinger's equation of motion. Detailed calculations show (Problem 11.4.1) that the phase difference $(\Delta\phi)_{\mathbf{r}_1,\mathbf{r}_2,\mathbf{B}}$ changes in the presence of the magnetic field such that

$$(\Delta\phi)_{\mathbf{r}_1,\mathbf{r}_2,B=0} = \hbar^{-1}\int_{\mathbf{r}_2}^{\mathbf{r}_1} \mathbf{p}\cdot d\mathbf{r} + q\hbar^{-1}\int_{\mathbf{r}_2}^{\mathbf{r}_1} \mathbf{A}\cdot d\mathbf{r} \equiv (\Delta\phi)^{(\text{motion})}_{\mathbf{r}_1,\mathbf{r}_2} + (\Delta\phi)^{(B)}_{\mathbf{r}_1,\mathbf{r}_2} \tag{11.4.3}$$

We call the first term on the rhs the phase difference due to particle motion and the second term, the phase difference due to the magnetic field. [The motion of charged particles generates an electric current, so $(\Delta\phi)^{(\text{motion})}_{\mathbf{r}_1,\mathbf{r}_2}$ may also be referred to as the phase difference due to the current.]

We now make a historic digression. Following London–London,[10,11] let us assume that the supercurrent is generated by hypothetical superelectrons. A superelectron has mass m and charge $-e$. Its momentum $\mathbf{p}$ is related to its velocity $\mathbf{v}$ by

$$\mathbf{v} = \frac{\mathbf{p}}{m} \tag{11.4.4}$$

The supercurrent density $\mathbf{j}_s$ is then:

$$\mathbf{j}_s = (-e)n_s\mathbf{v} = -en_s\mathbf{v} \tag{11.4.5}$$

Using the last two equations, we calculate the motional phase difference and obtain

$$(\Delta\phi)^{(\text{motion})}_{\mathbf{r}_1,\mathbf{r}_2} \equiv \hbar^{-1}\int_{\mathbf{r}_2}^{\mathbf{r}_1}\mathbf{p}\cdot d\mathbf{r} = -\int_{\mathbf{r}_2}^{\mathbf{r}_1}\left(\frac{m}{e\hbar n_s}\right)\mathbf{j}_s\cdot d\mathbf{r} \tag{11.4.6}$$

Let us consider an infinite homogeneous medium, for which the line integral of the phase along any closed path vanishes [see Eq. (11.3.7)]

$$\oint\left(\mathbf{j}_s + e^2m^{-1}n_s\mathbf{A}\right)\cdot d\mathbf{r} = 0 \tag{11.4.7}$$

Employing Stoke's theorem (Problem 11.4.2):

$$\oint d\mathbf{r}\cdot\mathbf{C} = \int\int d\mathbf{S}\cdot\nabla\times\mathbf{C} \tag{11.4.8}$$

where the rhs is a surface integral with the differential vector element $d\mathbf{S}$ by the right-hand screw rule, we obtain from Eq. (11.4.7):

$$\mathbf{j}_s + e^2m^{-1}n_s\mathbf{A} + \nabla\chi = 0 \tag{11.4.9}$$

where $\chi(\mathbf{r})$ is an arbitrary scalar field. Now the connection between the magnetic field $\mathbf{B}$ and the vector potential $\mathbf{A}$, as represented by $\mathbf{B} = \nabla\times\mathbf{A}$, has a certain arbitrariness; we may add the gradient of the scalar field χ to the original vector field $\mathbf{A}$, since

$$\nabla\times(\mathbf{A} + \nabla\chi) = \nabla\times\mathbf{A} \tag{11.4.10}$$

Using this *gauge-choice property* we may rewrite Eq. (11.4.9) as

$$\mathbf{j}_s = -e^2m^{-1}n_s\mathbf{A} \equiv -\Lambda_{el}\mathbf{A} \qquad \Lambda_{el} \equiv e^2m^{-1}n_s \tag{11.4.11}$$

This is known as *London's equation.* The negative sign indicates that the supercurrent is diamagnetic. The physical significance of Eq. (11.4.11) will be discussed later.

Let us go back to the condensed pairon picture of the supercurrent. First consider a + pairon having charge +2*e*. Since the pairon has the linear energy–momentum relation:

$$\epsilon_2 = w_0 + \left(\frac{1}{2}\right) p v_F^{(2)} \equiv w_0 + c_2 p \tag{11.4.12}$$

the velocity $\mathbf{v}_2$ has magnitude $c_2 \equiv v_F^{(2)}/2$ and direction $\hat{\mathbf{p}}$ along the momentum $\mathbf{p}$:

$$\mathbf{v}_2 = c_2 \hat{\mathbf{p}} \tag{11.4.13}$$

Thus if $p \neq 0$, there is a partial supercurrent density equal to

$$\mathbf{j}_s^{(2)} = (2e)\left(\frac{n_0}{2}\right) c_2 \hat{\mathbf{p}} = e n_0 \mathbf{v}_2 \tag{11.4.14}$$

Similarly – pairons contribute

$$\mathbf{j}_s^{(1)} = -e n_0 \mathbf{v}_1 \tag{11.4.15}$$

Using the last three relations, we repeat the calculations to obtain

$$\boxed{\mathbf{j}_s = -\Lambda_{\text{pairon}} \mathbf{A}, \qquad \Lambda_{\text{pairon}} = 2e^2 n_0 (c_2 + c_1) p^{-1} \equiv \Lambda} \tag{11.4.16}$$

which we call a *generalized London equation* or simply *London's equation.* This differs from the original London's equation (11.4.11) merely by a numerical factor.

Let us now discuss a few physical consequences derivable from Eq. (11.4.16). Taking the curl of this equation, we obtain

$$\nabla \times \mathbf{j}_s = -\Lambda \nabla \times \mathbf{A} = -\Lambda \mathbf{B} \tag{11.4.17}$$

Using Eq. (11.4.17) and one of Maxwell's equations:

$$\nabla \times \mathbf{H} = \mathbf{j}_s, \qquad \left(\frac{\partial \mathbf{D}}{\partial t} = 0,\ \mathbf{j}_n = 0\right) \tag{11.4.18}$$

[where we neglect the time derivative of the dielectric displacement ($\mathbf{D}$) and the normal current ($\mathbf{j}_n$)], we obtain (Problem 11.4.3):

$$\lambda^2 \nabla^2 \mathbf{B} = \mathbf{B}, \qquad \lambda \equiv \left(\frac{c}{e}\right)\left[\frac{p}{8\pi n_0 (c_2 + c_1)}\right]^{1/2} \qquad (\epsilon_0 \mu_0 \equiv c^{-2}) \tag{11.4.19}$$

Here λ is called a *generalized London penetration depth.*

We consider the boundary of a semi-infinite slab (superconductor). When an external magnetic field $\mathbf{B}$ is applied parallel to the boundary, the B-field computed from Eq. (11.4.19) can be shown to fall off exponentially (Problem 11.4.4):

$$B(x) = B(0) \exp(-x/\lambda) \tag{11.4.20}$$

(This solution is shown in Fig. 1.13.) Thus the interior of the superconductor far from the surface shows the Meissner state: $B = 0$. Experimentally the penetration depth at lowest temperatures is of the order 500 Å.

We emphasize that London's equation (11.4.16) holds for the supercurrent $\mathbf{j}_s$ only. Since this is a strange equation, we rederive it by a standard calculation. The effective Hamiltonian H for a + pairon moving with speed $c_2 \equiv v_F^{(2)}/2$ is

$$\mathrm{H} = \mathrm{c}_2|\mathrm{p}| \tag{11.4.21}$$

In the presence of a magnetic field $\mathbf{B} = \nabla \times \mathbf{A}$, this Hamiltonian is modified as

$$\mathrm{H'} = \mathrm{c}_2\,|\,\mathbf{p} - q\mathbf{A}\,| \tag{11.4.22}$$

Assume now that momentum $\mathbf{p}$ points in the x-direction. The velocity $v_x \equiv \partial H'/\partial p_x$ is

$$v_x = c_2 p^{-1}(p_x - qA_x) \tag{11.4.23}$$

We calculate the quantum mechanical average of v_x, multiply the result by the charge $2e$ and the + pairon density $n_0/2$ and obtain

$$(2e)\left(\frac{n_0}{2}\right)\langle v_x\rangle = en_0c_2\left\langle\frac{p_x}{|\mathbf{p}|}\right\rangle - 2e^2n_0c_2p^{-1}A_x \tag{11.4.24}$$

Adding the contribution of – pairons, we obtain the total current density j_s:

$$j_s = en_0(c_2 - c_1)\left\langle\frac{p_x}{|\mathbf{p}|}\right\rangle - 2e^2n_0(c_2 + c_1)p^{-1}A_x \tag{11.4.25}$$

Comparing this with London's equation (11.4.16) we see that the supercurrent arises from the magnetic field term for the velocity **v.**

As another important application of Eq. (11.4.3), let us consider a supercurrent ring. By choosing a closed path around the central line of the ring and integrating $(\Delta\phi)_{\mathbf{B}}$ along the path ARA, we obtain from Eqs. (11.3.10) and (11.4.3)

$$(\Delta\phi)_{\mathrm{ARA}}^{\mathrm{motion}} + 2e\hbar^{-1}\oint_{\mathrm{ARA}}\mathbf{A}\cdot d\mathbf{r} = kL = 2\pi n \tag{11.4.26}$$

The closed path integral can be evaluated by using Stoke's theorem Eq. (11.4.8) as

$$\oint_{\mathrm{ARA}}\mathbf{A}\cdot d\mathbf{r} = \int\int d\mathbf{S}\cdot\nabla\times\mathbf{A} = \int\int dS\,B = BS \equiv \Phi \tag{11.4.27}$$

where S is the area enclosed by the path ARA, and $\Phi \equiv BS$ is the magnetic flux enclosed. The phase difference due to the pairon motion $(\Delta\phi)_{\mathrm{ARA}}^{\mathrm{motion}}$ is zero since there is no supercurrent along the central part of the ring. We obtain from Eqs. (11.4.26) and (11.4.27)

$$\Phi = \frac{n\pi\hbar}{e} \equiv n\Phi_0 \tag{11.4.28}$$

reconfirming the flux quantization discussed [see Eq. (11.1.6)] in Section 11.1.

Let us now choose a second closed path around the ring cavity but one where the supercurrent does not vanish. For example choose a path within a penetration depth

around the inner side of the ring. For a small section where the current runs in the x-direction (see Fig. 11.8), the current due to a + pairon is

$$(2e)c_2\left\langle \frac{p_x}{p} \right\rangle - 4e^2 c_2 p^{-1} A_x \tag{11.4.29}$$

where p_x/p is the component of the unit vector $\hat{\mathbf{p}}$ pointing along the momentum **p.** If we sum $\hat{\mathbf{p}}$ over the entire circular path, the net result is from Eq. (11.3.11)

$$\oint_{\text{ARA}} \hat{\mathbf{p}} \cdot d\mathbf{r} = 2\pi\hbar L \tag{11.4.30}$$

This example shows that the motional contribution to the supercurrent, part of Eq. (11.4.24), $en_0c_2\langle p_x/p\rangle$ does not vanish. Thus in this case, the magnetic flux Φ by itself is not quantized, but the lhs of Eq. (11.4.26), called the *fluxoid,* is quantized.

Problem 11.4.1. Derive Eq. (11.4.3).

Problem 11.4.2. Prove Stoke's theorem Eq. (11.4.8) for a small rectangle, and then for a general case.

Problem 11.4.3. Derive Eq. (11.4.19).

Problem 11.4.4. Solve Eq. (11.4.19) and obtain Eq. (11.4.20).

11.5. GINZBURG–LANDAU WAVE FUNCTION; MORE ABOUT THE SUPERCURRENT

In 1950 Ginzburg and Landau published a classic paper[12] on a theory of superconductivity. They proposed a *complex-order parameter* $\Psi(\mathbf{r})$, also called a G–L *wave function,* to describe the superconducting state and introduced the concept of a coherence length ξ to discuss the thermodynamic properties of an interface between super and normal conductors. In fact the G–L wave function properly redefined can describe the many-pairon supercondensate existing below T_c. In the present section we discuss this revised G–L wave function.

The basic assumptions of the G–L theory are:

- There is a single (macroscopic) wave function $\Psi(\mathbf{r})$ for the supercondensate, which is in general complex and depends on the position **r.**
- Its absolute square is normalized to the density of the supercondensate:

$$|\Psi(\mathbf{r})|^2 d^3r = \text{the number of condensed pairons in } d^3r \text{ at } \mathbf{r} \tag{11.5.1}$$

- The $\Psi(\mathbf{r})$ cannot change appreciably within a distance ξ, called a *coherence length.*
- The function Ψ obeys a certain quantum mechanical equation.

First we note that $\Psi(\mathbf{r})$ is similar to the familiar wave function $\psi(\mathbf{r})$ for a quantum particle; thus the name wave function is used. But unlike the latter, this Ψ represents a state of the condensate, as reflected in the normalization condition Eq. (11.5.1).

In their original work[12] the absolute square of Ψ was equated with the number density of superelectrons n_s:

$$|\Psi(\mathbf{r})|^2 = n_s \tag{11.5.2}$$

As we saw in Section 11.1, the supercondensate in motion is represented by a single current-carrying state ψ_n. Since electrons are fermions, no two electrons can occupy the same state ψ_n. Thus Eq. (11.5.2) presents a fundamental difficulty. (Recall that the G–L theory was developed in 1950 before the BCS theory, which was reported in 1957). This difficulty can simply be removed by equating $|\Psi(\mathbf{r})|^2$ with the *density of pairons* (bosons), as postulated in Eq. (11.5.1). This is the revision mentioned earlier.

In Section 6.6 we introduced and discussed the one-body density operator n and density matrix n_{ab} for the treatment of a many-particle system. The density operator n, like the system density operator ρ, can be expanded in the form [see Eq. (6.6.11)]:

$$n = \sum_{\mu} |\mu\rangle P_{\mu} \langle\mu|, \qquad P_{\mu} \geq 0 \tag{11.5.3}$$

where $\{P_{\mu}\}$ denote the relative probabilities that particle-states $\{\mu\}$ are occupied. It is customary in quantum many-body theory to adopt the following normalization condition:

$$\sum_{\mu} P_{\mu} = \langle \hat{N} \rangle \tag{11.5.4}$$

where $\hat{N}$ is the number operator. We define a *root density operator* $n^{1/2}$ by

$$n^{1/2} \equiv \sum_{\mu} |\mu\rangle P_{\mu}^{1/2} \langle\mu| \qquad [= (n^{1/2})^{\dagger}] \tag{11.5.5}$$

which is Hermitian and satisfies (Problem 11.5.1):

$$(n^{1/2})^2 = n \tag{11.5.6}$$

The revised G–L wave function $\Psi_{\sigma}(\mathbf{r})$ can be related to the pairon density operator n by

$$\boxed{\Psi_{\sigma}(\mathbf{r}) = \langle \mathbf{r}|n^{1/2}|\sigma\rangle} \tag{11.5.7}$$

where σ represents the condensed pairon state. For a ring supercurrent we may choose

$$\sigma = q_n \tag{11.5.8}$$

Using Eqs. (11.5.6) and (11.5.7) we see that

$$\int d^3r |\Psi_{\sigma}(\mathbf{r})|^2 = \int d^3r \langle\sigma|n^{1/2}|\mathbf{r}\rangle\langle\mathbf{r}|n^{1/2}|\sigma\rangle = \langle\sigma|n|\sigma\rangle = \langle N_{\sigma}\rangle \tag{11.5.9}$$

which is equal to the average number of condensed pairons in the state σ, $\langle N_\sigma \rangle$. Note: We chose n to be the one-pairon (boson) density operator rather than the superelectron (fermion) density operator. For a system of any fermions and any state σ

$$\langle \sigma | n | \sigma \rangle \leq 1 \qquad \text{(fermions)} \tag{11.5.10}$$

due to Pauli's exclusion principle. Thus Eq. (11.5.9) holds only for a system of bosons.

The superconducting state characterized by q_n is in a state of motion very far from the equilibrium (zero-momentum) system ground state. As explained in Section 11.1, the energy difference between zero-momentum and q_n states is vanishingly small, since q_n is vanishingly small. They are quite different however, since only the q_n-state can carry a current along the ring. The direct evidence that the supercondensate is composed of massless bosons comes from the supercurrent interference, discussed in Section 11.2.

In Section 6.6 we discussed the main properties of the density operator n. If an observable X for a many-particle system is the sum of the corresponding single-particle observable ξ such that $X = \sum_j \xi^{(j)}$, then the grand-ensemble average $\langle X \rangle$ can be calculated from

$$\langle X \rangle \equiv \mathrm{TR}\{X\rho\} = \mathrm{tr}\{\xi n\} \tag{11.5.11}$$

where the lhs means the many-particle average and the rhs, the single-particle average. Using $n = (n^{1/2})^2$, we can reexpress $\mathrm{tr}\{\xi n\}$ as

$$\begin{aligned} \mathrm{tr}\{\xi n\} &= \mathrm{tr}\{n^{1/2}\xi n^{1/2}\} = \int d^3r \sum_a \langle a|n^{1/2}|\mathbf{r}\rangle\langle \mathbf{r}|\xi n^{1/2}|a\rangle \\ &= \sum_a \int d^3r \Psi_a^*(\mathbf{r})\xi(\mathbf{r}, -i\hbar\nabla)\Psi_a(\mathbf{r}) \end{aligned} \tag{11.5.12}$$

[use of Eq. (11.5.7)], where we assumed that ξ is a function of position $\mathbf{r}$ and momentum $\mathbf{p}$: $\xi = \xi(\mathbf{r}, \mathbf{p})$. Thus the average $\langle X \rangle$ for the many-particle system can be calculated in terms of the G–L wave function Ψ by the same rules as for a qauantum particle.

Problem 11.5.1. Verify Eq. (11.5.6).

11.6. QUASI-WAVE FUNCTION: ITS EVOLUTION IN TIME

In the present section, we discuss the interrelation between the G–L wave function, and the quasi-wave function and derive their evolution equations.

The quasi-wave function $\Psi_\nu(\mathbf{r})$ for a quasi-particle in the state ν is defined by Eq. (6.8.5):

$$\Psi_\nu(\mathbf{r}) \equiv \mathrm{TR}\{\psi_\nu^\dagger \phi(\mathbf{r})\rho\} \tag{11.6.1}$$

or

$$\boxed{\Psi_\nu(\mathbf{r}) = \langle \mathbf{r}|n|\nu\rangle} \tag{11.6.2}$$

[see Eq. (6.7.15)]. The G–L wave function $\Psi'_\sigma(\mathbf{r})$ (the prime is introduced for distinction) is defined by

$$\Psi'_\sigma(\mathbf{r}) = \langle \mathbf{r}|n^{1/2}|\sigma\rangle \tag{11.6.3}$$

where σ represents the condensed pairon state. Here and in Eq. (11.6.2), *n* represents the pairon density operator. The corresponding density matrix elements are given by

$$\langle \mu|n|\nu\rangle \equiv \mathrm{TR}\{\psi^\dagger_\nu \psi_\mu \rho\} \tag{11.6.4}$$

By choosing ν = σ, we see from Eqs. (11.6.2) and (11.6.3) that the two wave functions $\Psi(\mathbf{r})$ and $\Psi'(\mathbf{r})$ are closely related; they differ only in the normalization.

The system-density operator ρ(*t*) changes according to the quantum Liouville equation:

$$i\hbar \frac{\partial \rho}{\partial t} = [H, \rho] \tag{11.6.5}$$

Using Eq. (11.6.5) we now study the time evolution of the quasi-wave function $\Psi_\sigma(\mathbf{r}, t)$.

First we consider the supercondensate at 0 K. The supercondensate at rest can be constructed by using the reduced Hamiltonian H_0 in Eq. (8.6.9):

$$\begin{aligned} H_0 = &\sum_{\mathbf{k}}{}' 2\epsilon_k^{(1)} b_{\mathbf{k}}^{(1)\dagger} b_{\mathbf{k}}^{(1)} + \sum_{\mathbf{k}}{}' 2\epsilon_k^{(2)} b_{\mathbf{k}}^{(2)\dagger} b_{\mathbf{k}}^{(2)} \\ &- \sum_{\mathbf{k}}{}' \sum_{\mathbf{k}'}{}' [v_{11} b_{\mathbf{k}'}^{(1)\dagger} b_{\mathbf{k}}^{(1)} + v_{12} b_{\mathbf{k}'}^{(1)\dagger} b_{\mathbf{k}}^{(2)\dagger} + v_{21} b_{\mathbf{k}}^{(2)} b_{\mathbf{k}'}^{(1)} + v_{22} b_{\mathbf{k}'}^{(2)} b_{\mathbf{k}}^{(2)\dagger}] \end{aligned} \tag{11.6.6}$$

where electron kinetic energies are expressed in terms of the ground pairon operators *b*'s. Let us recall (see Section 8.6) that the supercondensate is generated from the physical vacuum by a succession of pair creation, pair annihilation, and pair correlation via phonon exchanges. In this condition, the electrons (and holes) involved are confined to a shell of energy width $\hbar\omega_D$ about the Fermi surface, and up- and down-spin electrons are always paired ($\mathbf{k}\uparrow, -\mathbf{k}\downarrow$) to form ground pairons. This static supercondensate cannot generate a supercurrent.

The moving supercondensate can also be generated from the physical vacuum via phonon exchanges. The relevant reduced Hamiltonian $H_\mathbf{q}$ is

$$\begin{aligned} H_\mathbf{q} \equiv &\sum_{\mathbf{k}}{}' \sum_j \left[\epsilon^{(j)}\left(|\mathbf{k}+\mathbf{q}/2|\right) + \epsilon^{(j)}\left(|-\mathbf{k}+\mathbf{q}/2|\right)\right] B_{\mathbf{kq}}^{(j)\dagger} B_{\mathbf{kq}}^{(j)} \\ &- \sum_{\mathbf{k}}{}' \sum_{\mathbf{k}'}{}' \left(v_{11} B_{\mathbf{k}'\mathbf{q}}^{(1)\dagger} B_{\mathbf{kq}}^{(1)} + v_{12} B_{\mathbf{k}'\mathbf{q}}^{(1)\dagger} B_{\mathbf{kq}}^{(2)\dagger} + v_{21} B_{\mathbf{kq}}^{(2)} B_{\mathbf{k}'\mathbf{q}}^{(1)} + v_{22} B_{\mathbf{k}'\mathbf{q}}^{(2)} B_{\mathbf{kq}}^{(2)\dagger}\right) \end{aligned} \tag{11.6.7}$$

which reduces to Eq. (11.6.6) when $\mathbf{q} = 0$. Supercondensation can occur at any momentum **q.** The quasi-wave function $\Psi_\mathbf{q}$ is a plane wave represented by

$$\Psi_\mathbf{q} = A \exp[i(\mathbf{q}\cdot\mathbf{r}\hbar^{-1} - \omega t)] \tag{11.6.8}$$

where the angular frequency ω is given by

$$\omega = \frac{q(v_F^{(1)} - v_F^{(2)})}{2} \tag{11.6.9}$$

a relation arising from the fact that ± pairons have energies:

$$\epsilon^{(j)} = w_0 + q v_F^{(j)}/2 \tag{11.6.10}$$

and they are always present in pair. The Hamiltonian $H_{\mathbf{q}}$ in Eq. (11.6.7) is a sum of single-pairon energies. Thus according to our study in Sections 6.5–6.6, we can describe the system in terms of a one-pairon density operator n. This operator $n(t)$ changes in time, following the one-body quantum Liouville equation

$$\boxed{i\hbar \frac{\partial n}{\partial t} = [h, n]} \tag{11.6.11}$$

Let us now take a mixed representation of Eq. (11.6.11). Introducing the quasi-wave function for the moving supercondensate:

$$\Psi_\sigma(\mathbf{r}) \equiv \langle \mathbf{r}|n|\sigma\rangle \tag{11.6.12}$$

we obtain [see Eq. (6.8.6)]

$$\boxed{i\hbar \frac{\partial}{\partial t}\Psi_\sigma(\mathbf{r}, t) = h(\mathbf{r}, -i\hbar\nabla t)\Psi_\sigma(\mathbf{r}, t)} \tag{11.6.13}$$

which is formally identical with the Schrödinger equation for a quantum particle; only the normalization is different.

The root density operator $n^{1/2}$, defined by Eq. (11.5.5), obeys the same evolution law as the density operator n (Problem 11.6.1)

$$i\hbar \frac{\partial n^{1/2}}{\partial t} = [h, n^{1/2}] \tag{11.6.14}$$

From Eq. (11.6.14) it follows that the G–L wave function $\Psi'_\sigma(\mathbf{r}, t) \equiv \langle \mathbf{r}|n^{1/2}(t)|\sigma\rangle$ also changes, following the same equation of motion (11.6.13).

Equation (11.6.13) was obtained under the condition that the system Hamiltonian H is the sum of particle Hamiltonians h. If a pairing Hamiltonian $(1/2)\sum_{i\neq j}\sum v(\mathbf{r}_i - \mathbf{r}_j)$ is present, the evolution equation of the field operator $\psi(\mathbf{r}, t)$ is nonlinear, see Eq. (6.5.18). In such a case nonlinear terms will appear on the rhs of Eq. (11.6.13). The original G–L equations[12] contain nonlinear terms:

$$\alpha\Psi'(\mathbf{r}) + \beta|\Psi'(\mathbf{r})|^2\Psi'(\mathbf{r}) + \frac{1}{2m}(-i\hbar\nabla - q\mathbf{A})^2\Psi'(\mathbf{r}) = 0$$

($\alpha < 0$, $\beta > 0$). The nonlinear term arises from the *pairon size effect* represented by $v(\mathbf{r}_1 - \mathbf{r}_2) = \beta\delta^{(3)}(\mathbf{r}_1 - \mathbf{r}_2)$.

Since the G–L wave function was intuitively introduced for a stationary state problem, it is not immediately clear how to describe its time evolution. Our quantum statistical calculations show that the *G–L wave function as well as the quasi-wave function satisfy the Schrödinger-like equation of motion.* This is a significant result, and some applications of Eq. (11.6.13) will be discussed in the following sections.

The normalization condition for the quasi-wave function $\Psi_\sigma(\mathbf{r})$ is

$$\langle N_\sigma \rangle = \langle \sigma | n | \sigma \rangle = \int d^3r \, \langle \sigma | \mathbf{r} \rangle \langle \mathbf{r} | n | \sigma \rangle = \int d^3r \, \psi_\sigma^*(\mathbf{r}) \Psi_\sigma(\mathbf{r}) \tag{11.6.15}$$

where:

$$\psi_\sigma^*(\mathbf{r}) \equiv \langle \sigma | \mathbf{r} \rangle \qquad \psi_\sigma(\mathbf{r}) = \langle \mathbf{r} | \sigma \rangle \tag{11.6.16}$$

is the wave function for a single pairon. The normalization condition Eq. (11.5.9) for $\Psi'_\sigma(\mathbf{r})$ is more symmetric than Eq. (11.6.15). However the probability amplitude A' in $\Psi_\sigma(\mathrm{r}) = A' \exp(i\phi)$ is burdened by the factor $A' \propto \langle N_\sigma \rangle^{1/2}$, while the amplitude A in $\Psi_\sigma(\mathrm{r}) = A \exp(i\phi)$ is proportional to $\langle N_\sigma \rangle$. This difference is insignificant when stationary state problems are considered. When dynamic problems are considered, the quasi-wave function $\psi_\sigma(\mathrm{r},t)$ gives a better physical representation, as we shall see in Section 11.8.

Problem 11.6.1. Derive Eq. (11.6.14).

11.7. BASIC EQUATIONS GOVERNING A JOSEPHSON JUNCTION CURRENT

In this section we derive basic equations governing the supercurrent passing through a Josephson junction. Our derivation essentially follows Feynman's in his lecture on supercurrent.[9,13] Our theory however is based on the independent pairon model, while Feynman assumed the superelectron model.

Consider an insulator of width Δx sandwiched between two identical superconductors as shown in Fig. 11.7. If the width Δx is large, the two superconductors do not affect each other, and the Schrödinger equations of motion in each superconductor are uncoupled:

$$i\hbar \frac{d}{dt} \Psi_1(t) = E_1 \Psi_1, \qquad i\hbar \frac{d}{dt} \Psi_2(t) = E_2 \Psi_2 \tag{11.7.1}$$

where E_j are energies of the supercondensate, with E_1 differing from E_2 if there is a voltage across the insulator, say

$$E_2 - E_1 = qV (= 2eV) \tag{11.7.2}$$

Now if the width Δx is very small ($\sim$ 10 Å), then Josephson tunneling can occur, so the two wave functions may be correlated. We represent this by

$$i\hbar \frac{d}{dt} \Psi_1(t) = E_1 \Psi_1 + K \Psi_2, \qquad i\hbar \frac{d}{dt} \Psi_2(t) = E_2 \Psi_2 + K \Psi_1 \tag{11.7.3}$$

where K is a real coupling (energy) constant. If there is no bias voltage, we have a single energy $E_1 + K$ for the combined system. Thus in this case, the reality of the energy constant K can be justified. The wavelength $\lambda = 2\pi/k$ characterizing the supercurrent

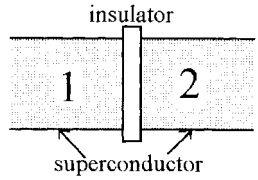

Figure 11.7. Insulator sandwiched by two superconductors.

is of the order of the ring circumference L, and therefore it is very much greater than the junction width Δx:

$$\lambda \gg \Delta x \tag{11.7.4}$$

Then the phase of the quasi-wave function:

$$\phi(x) = kx \equiv \frac{2\pi x}{\lambda} \tag{11.7.5}$$

does not change much when x is measured in units (lengths) of the order of Δx. We may simply assume that each superconductor has a position-independent phase θ_j.

Let us assume a wave function of the form:

$$\Psi_j(t) = n_j(t) \exp[i\theta_j(t)] \tag{11.7.6}$$

where the n_j are the pairon densities of superconductors j; these are position-independent for each superconductor. Substituting Eq. (11.7.6) in Eq. (11.7.3), we obtain (Problem 11.7.1)

$$\begin{aligned} i\hbar\dot{n}_1 + \hbar n_1\dot{\theta}_1 &= E_1 n_1 + K n_2 \exp[i(\theta_2 - \theta_1)] \\ i\hbar\dot{n}_2 + \hbar n_2\dot{\theta}_2 &= E_2 n_2 + K n_1 \exp[-i(\theta_2 - \theta_1)] \end{aligned} \tag{11.7.7}$$

Equating real and imaginary parts of Eqs. (11.7.7), we find that (Problem 11.7.2)

$$\hbar\dot{n}_1 = K n_2 \sin(\theta_2 - \theta_1) \equiv K n_2 \sin\delta, \qquad \hbar\dot{n}_2 = -K n_1 \sin\delta \tag{11.7.8}$$

$$\hbar\dot{\theta}_1 = E_1 + K\frac{n_2}{n_1}\cos\delta, \qquad \hbar\dot{\theta}_2 = E_2 + K\frac{n_1}{n_2}\cos\delta \tag{11.7.9}$$

where

$$\delta \equiv \theta_2 - \theta_1 \tag{11.7.10}$$

is the *phase difference across the junction.*

Let us introduce a steady-state condition. We may then assume that

$$n_1 = n_2 = n_0 \tag{11.7.11}$$

The bias voltage determines the direction of the electric current i, which should be proportional to the time rate of change in pairon density:

$$i \propto -\dot{n}_1 = \dot{n}_2 = K\hbar^{-1} n_0 \sin\delta \tag{11.7.12}$$

where we used Eqs. (11.7.8), (11.7.10), and (11.7.11). The proportionality factor should depend on the charge $2e$ of the carrier (pairon). Thus we may write

$$\boxed{i = i_0 \sin\delta, \qquad i_0 \equiv 2eK\hbar^{-1}n_0} \tag{11.7.13}$$

where i_0 is the maximum current, which is linear in the pairon density n_0 and in the junction energy constant K. Using Eqs. (11.7.2) and (11.7.9)–(11.7.11), we obtain

$$\boxed{\hbar\frac{d\delta}{dt} = 2eV} \tag{11.7.14}$$

These two equations are the basic equations, called the *Josephson–Feynman equations*, governing the tunneling supercurrent. Their physical meaning becomes clear after solving them explicitly, which we do in the next section.

As a first application, we complete the discussion of the SQUID with more quantitative calculations. The basic set-up of the SQUID is shown in Figs. 1.11 and 11.4. Consider first the current path ACB. The phase difference $(\Delta\phi)_{\mathrm{ACB}}$ along this path is

$$(\Delta\phi)_{\mathrm{ACB}} = \delta_C + 2e\hbar^{-1}\int_{\mathrm{ACB}} \mathbf{A}\cdot d\mathbf{r} \tag{11.7.15}$$

Similarly for the second path ADB, we have

$$(\Delta\phi)_{\mathrm{ADB}} = \delta_D + 2e\hbar^{-1}\int_{\mathrm{ADB}} \mathbf{A}\cdot d\mathbf{r} \tag{11.7.16}$$

Now the phase difference between A and B must be independent of the path:

$$(\Delta\phi)_{\mathrm{ACB}} = (\Delta\phi)_{\mathrm{ADB}} \tag{11.7.17}$$

from which we obtain

$$\delta_C - \delta_D = 2e\hbar^{-1}\oint_{\mathrm{ADBCA}} \mathbf{A}\cdot d\mathbf{r} = 2e\hbar^{-1}\Phi \tag{11.7.18}$$

where Φ is the magnetic flux through the loop. The total current I is the sum of I_C and I_D. For convenience we write

$$\delta_C \equiv \delta_0 + e\hbar^{-1}\Phi, \qquad \delta_D \equiv \delta_0 - e\hbar^{-1}\Phi \tag{11.7.19}$$

where δ_0 is a constant. Note: This set satisfies Eq. (11.7.18). Then using Eq. (11.7.13) we obtain

$$I \equiv I_C + I_D = I_0[\sin(\delta_0 + e\hbar^{-1}\Phi) + \sin(\delta_0 - e\hbar^{-1}\Phi)] = I_0 \sin\delta_0 \cos(e\hbar^{-1}\Phi) \tag{11.7.20}$$

The constant δ_0 introduced in Eq. (11.7.19) is an unknown parameter and it may depend on the applied voltage and other conditions. However $|\sin\delta_0|$ is bounded by unity. Thus

the maximum current has amplitude $I_{max} = I_0|\sin\delta_0|$, and the total current I is expressed as

$$I = I_{max}\cos(e\hbar^{-1}\Phi) = I_{max}\cos(\pi\Phi/\Phi_0), \qquad \Phi_0 \equiv \pi\hbar/e \tag{11.7.21}$$

proving Eq. (11.2.1).

Problem 11.7.1. Derive Eq. (11.7.7).

Problem 11.7.2. Verify Eqs. (11.7.8) and (11.7.9).

11.8. AC JOSEPHSON EFFECT; SHAPIRO STEPS

Josephson predicted[6] that on applying a constant voltage V_0, the supercurrent passing through a junction should have an oscillatory component characterized by the *Josephson (angular) frequency:*

$$\omega_J \equiv 2e\hbar^{-1}V_0 \tag{11.8.1}$$

We discuss this *AC Josephson effect* in the present section.

Assume that a small voltage V_0 is applied across a Josephson junction. Solving Eq. (11.7.14), we obtain

$$\delta(t) = \delta_0 + 2e\hbar^{-1}V_0 t = \delta_0 + \omega_J t \tag{11.8.2}$$

where δ_0 is the initial phase. Note: The phase difference δ changes linearly with the time t. Using Eq. (11.8.2) we calculate the supercurrent i_s from Eq. (11.7.13) to obtain

$$i_s(t) = i_0\sin(\delta_0 + \omega_J t) \tag{11.8.3}$$

For the ordinary (laboratory) voltage and time, the sine oscillates very rapidly, and the time-averaged current vanishes:

$$\langle i_s\rangle_{\text{time}} \equiv \lim_{T\to\infty}\frac{1}{T}\int_0^T dt\, i_s(t) = 0 \tag{11.8.4}$$

This is quite remarkable. The supercurrent does *not* obey Ohm's law familiar in the normal conduction: i_n (normal current) α V_0 (voltage). According to Eq. (11.8.3) the *supercurrent flows back and forth* across the junction with a (high) frequency ω_J under the action of a *DC* bias. Most importantly the supercurrent passing through the junction does not gain energy from the bias voltage. (The fact that the supercurrent in general cannot be accelerated was discussed earlier in Section 8.6.) Everything is consistent with our physical picture of *the supercondensate composed of independently moving ± pairons and electrically neutral.* In practice, since temperature is not zero, there is a small current i_n due to the moving charged quasi-particles (quasi-electrons, excited pairons).

Let us now apply a small AC voltage in addition to the DC voltage V_0. The AC voltage can be supplied by a microwave. We assume that

$$V = V_0 + v\cos\omega t \qquad (v \ll V_0) \tag{11.8.5}$$

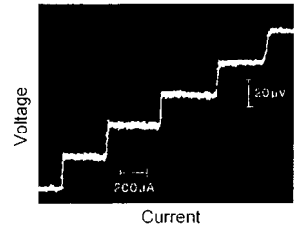

Figure 11.8. Shapiro steps in the *V–I* diagram [after Hartland (Ref. 15)].

where ω is the microwave frequency on the order of 10^{10} cycles/sec = 10 GHz. Solving Eq. (11.7.14) with respect to t, we obtain

$$\delta(t) = \delta_0 + \int_0^t dt\, q\hbar^{-1}[V_0 + v\cos\omega t] = \delta_0 + q\hbar^{-1}V_0 t + \frac{qv}{\hbar\omega}\sin\omega t \qquad (11.8.6)$$

Because $v \ll V_0$, the last term is small compared with the rest. We use Eqs. (11.7.13) and (11.8.6) to calculate the supercurrent i (the subscript s is dropped) and obtain (Problem 11.8.1):

$$i = i_0 \sin\delta(t) = i_0[\sin(\delta_0 + \omega_J t) + \left(\frac{2ev}{\hbar\omega}\right)\sin\omega t\cos(\delta_0 + \omega_J t)] \qquad (11.8.7)$$

The first term is zero on the average as before, but the second term is nonzero if

$$\omega = 2e\hbar^{-1}V_0 n = \omega_J n, \qquad n = 1, 2, \ldots \qquad (11.8.8)$$

(Problem 11.8.2). Thus there should be a *DC* current if the microwave frequency ω matches the Josephson frequency ω_J or its multiples $n\omega_J$. In 1963 Shapiro[14] first demonstrated such a resonance effect experimentally. If data are plotted in the *V–I* diagram, horizontal strips (currents) form steps of equal height $\hbar\omega/2e$ called *Shapiro steps*. Typical data for a Pb–PbO_x–Pb tunnel junction at ω = 10 GHz obtained by Hartland[15] are shown in Fig. 11.8. (Shapiro's original paper[14] contains steps, but later experimental data, such as those shown here, allow a more delicate interpretation of the AC Josephson effect.) The clearly visible steps are most remarkable. Further Fig. 11.8 indicates that horizontal (current) strips decrease in magnitude with increasing n, which will be explained below.

We first note that the DC bias voltage V_0 applied to the junction generates no change in the energy of the moving supercondensate. Thus we may include the effect of this voltage in the unperturbed Hamiltonian H_0 and write the total Hamiltonian H as

$$H = H_0 + 2ev\cos\omega t, \qquad q = 2e \qquad (11.8.9)$$

where the second term represents perturbation energy due to the microwave. We may write the wave function corresponding to the unperturbed system in the form:

$$\Psi_0(\mathbf{r}, t) = A(\mathbf{r})\exp(-iEt/\hbar) \qquad (11.8.10)$$

where E is the energy. In the presence of the microwave field, we may assume a steady-state wave function of the form:

$$\Psi(\mathbf{r}, t) = A \exp(-iEt/\hbar) \left[\sum_{n=-\infty}^{\infty} B_n \exp(in\omega t) \right] \tag{11.8.11}$$

Substituting Eq. (11.8.11) into the equation of motion $i\hbar\partial\Psi/\partial t = H\Psi$ [see Eq. (11.6.13)], we obtain

$$2nB_n = \frac{ev}{\hbar\omega}(B_{n-1} + B_{n+1}) \tag{11.8.12}$$

(Problem 11.8.3). The solution of this difference equation can be expressed in terms of the nth-order Bessel function of the first kind[16]:

$$B_n = J_n(\alpha), \qquad \alpha \equiv \frac{2ev}{\hbar\omega} \tag{11.8.13}$$

We thus obtain

$$\Psi(\mathbf{r}, t) = A \exp(-iEt/\hbar) \left[\sum_{n=\infty}^{\infty} J_n(\alpha) \exp(in\omega t) \right] \tag{11.8.14}$$

This steady-state solution in the presence of a microwave indicates that condensed pairons (supercondensate) can have energies E, $E \pm \hbar\omega$, $E \pm 2\hbar\omega$, ... Now from Eq. (11.7.13), we know that the supercurrent i is proportional to the condensed pairon density n_0. The amplitude of the quasi-wave function Ψ is also linear in this density n_0. Thus from Eq. (11.8.14), we deduce that the (horizontal) lengths of the Shapiro steps at n are proportional to $J_n(\alpha)$ and decrease with increasing n in agreement with experiments.

In the preceding discussion, we used the quasi-wave function Ψ. If we adopt the G–L wave function Ψ' instead, we obtain the same solution Eq. (11.8.14) from the Schrödinger-like equation of motion, but the physical interpretation is different. We would have concluded that the horizontal lengths of the Shapiro steps decrease with n in proportion to $J_n^2(\alpha)$.Experiments support the linear J_n-dependence. In other words the quasi-wave function Ψ, which is proportional to the supercondensate density n_0, gives a physically correct description of pairon dynamics.

Problem 11.8.1. Verify Eq. (11.8.7). Use Taylor's expansion.

Problem 11.8.2. Show that the averaged current i in Eq. (11.8.7) is finite if Eq. (11.8.8) is satisfied.

Problem 11.8.3. Verify Eq. (11.8.12).

11.9. DISCUSSION

Supercurrents exhibit many unusual behaviors. We enumerate their important features in the following subsections.

11.9.1. Super and Normal Currents

The supercurrent is generated by a moving supercondensate. The latter is composed of great and equal numbers of ± pairons condensed at a finite momentum **p.** Since ± pairons having charges ±2*e* and momentum **p** move with different speeds $c_i = v_F^{(i)}/2$, the net electric current density:

$$j = \frac{1}{2} e n_0 (v_F^{(2)} - v_F^{(1)}) \tag{11.9.1}$$

does not vanish. The supercurrent flowing in the surface of a straight wire is shown in Fig. 11.1 (a). Supercurrents totally dominate normal currents because of the Boltzmann principle; condensed pairons have lower energies by at least the gap $\in_g$ than noncondensed pairons; accordingly they are stable and predominant.

11.9.2. Supercurrents Are Not Hindered by Impurities

The macroscopic supercurrent generated by a moving supercondensate is not hindered by impurities that are microscopic by comparison. The fact that no microscopic perturbation causes a resistance (energy loss) is due to the quantum statistical nature of the macroscopic supercondensate; the change in the many-pairon state occurs only if a transition from one (supercondensate) state to another is induced. However large lattice imperfections and constrictions can affect the supercurrent significantly.

11.9.3. The Supercurrent Cannot Gain Energy from a DC Voltage

The supercondensate is electrically neutral and therefore it is stable against Lorentz-electric force. Thus the superconductor cannot gain energy from the applied voltage (see Section 11.9.13).

11.9.4. Instability against a Magnetic Field; Critical Fields and Critical Currents

In the superconducting state, ± pairons move in the same direction (because they have the same momentum) with different speeds. If a magnetic field **B** is applied, the Lorentz-magnetic force tends to separate ± pairons. Thus there must be a critical (magnetic) field B_c. The magnetic force is proportional to pairon speeds $v_F^{(i)}/2$. Thus superconductors having lower Fermi velocities, like high-T_c cuprates, are much more stable than elemental superconductors, and the former have higher critical fields. Since supercurrents themselves generate magnetic fields, there are critical currents J_c.

11.9.5. Supercurrent Ring; Flux Quantization

A persistent supercurrent ring exhibits striking superconducting properties: resistanceless surface supercurrent, Meissner state, and flux quantization.

The superconducting state Ψ_n is characterized by a momentum state wave function:

$$\Psi_n(x) = A \exp(-i\hbar^{-1} p_n x), \qquad p_n \equiv \frac{2\pi\hbar n}{L} \tag{11.9.2}$$

Since the ring circumference *L* is macroscopic, the quantized momentum p_n is vanishingly small under normal experimental conditions ($n \sim$ 1–10). The actual value of *n* in the

flux quantization experiments is determined by the Onsager–Yang's rule:

$$\Phi = n\Phi_0 \equiv n\frac{\pi\hbar}{e} \tag{11.9.3}$$

Each condensed pairon has an extremely small momentum p_n and therefore an extremely small energy $\epsilon = v_F^{(i)} p_n/2$. Under the usual experimental condition ($n < 100$), it appears that the supercurrent carries no kinetic energies.

11.9.6. Meissner Effect; Surface Supercurrent

A macroscopic superconductor expels an applied magnetic field **B** from its interior; this is the Meissner effect. Closer examination however reveals that the *B*-field within the superconductor vanishes excluding the surface layer. In fact a finite magnetic field penetrates the body within a thin layer of the order of 500 Å, and in this layer diamagnetic surface supercurrents flow such that the *B*-field in the main body vanishes, as shown in Fig. 1.17. Why does such a condition exist? The stored magnetic field energy for the system in the Meissner state is equal to $VB^2/2\mu_0$. This may be pictured as magnetic pressure acting near the surface and pointing inward. This is balanced by a Meissner pressure pointing outward that tries to keep the state superconductive. This pressure is caused by the difference in the Gibbs free energy between super and normal states $G_N - G_S$. Thus if

$$G_N - G_S > (2\mu_0)^{-1} V B^2 \tag{11.9.4}$$

the Meissner state is maintained in the interior with a sharp but continuously changing *B*-field near the surface. If the *B*-field is raised beyond the critical field B_c, the inequality (11.9.4) no longer holds, and the normal state should return. Note: The kinetic energy of the supercurrent is neglected here.

11.9.7. Penetration Depth; London's Equation

The existence of a penetration depth λ was predicted in 1935 by the London brothers[10] and it was later confirmed by experiments; this is regarded as an important step in understanding superconductivity. The qualitative agreement between theory and experiment established a tradition that electromagnetism as represented by Maxwell's equations can, and must, be applied to describe the superconducting state.

The steady-state supercurrent in a small section can be represented by a plane wave function: $\Psi_{\mathbf{p}}(\mathbf{r}) = A\exp(i\hbar^{-1}\mathbf{p}\cdot\mathbf{r}) = A\exp(i\hbar^{-1}px)$. The momentum **p** appears in the phase. The Londons assumed, based on the Hamiltonian mechanical consideration of a system of superelectrons, that the phase difference at two points ($\mathbf{r}_1$, r_2) in the presence of a magnetic field **B** has motional and field components, and obtained London's equation:

$$\mathbf{j}_s = -e^2 m^{-1} n_s A \tag{11.9.5}$$

The Londons used Eq. (11.9.5) and Maxwell's equation to obtain an expression for the penetration depth:

$$\lambda_{\text{London}} = \frac{c}{e}\left(\frac{m}{4\pi n_s}\right)^{1/2} \tag{11.9.6}$$

If we adopt the pairon flow model, we obtain instead

$$\lambda = \frac{c}{e}\left(\frac{p}{8\pi n_0(c_2 + c_1)}\right)^{1/2} \tag{11.9.7}$$

There is no mass in this expression, since pairons move as massless particles. The $n_0^{-1/2}$ dependence is noteworthy. The supercondensate density n_0 approaches zero as temperature is raised to T_c. The penetration depth λ therefore increases indefinitely as $T \to T_c$, which is in agreement with experiment.

11.9.8. Ginzburg–Landau Theory

In 1950 Ginzburg and Landau proposed the revolutionary idea that below T_c a superconductor has a complex order parameter Ψ' (G–L wave function) just as a ferromagnet possesses a real spontaneous magnetization below T_c. This means in particular that a superconductor below T_c has an additional thermodynamic state variables. In other words, the superconducting state is characterized by the presence of the G–L wave function Ψ'. The wave function Ψ' is meant to represent a many-particle supercondensate, and it obeys a *quantum* mechanical equation. They introduced the concept of a coherence length ξ to discuss thermodynamic properties of an interface between super and normal conductors. One of the most successful results based on the G–L theory is the prediction by Abrikosov,[17] and the subsequent confirmation,[18] of the mixed state of a type II superconductor, which will be discussed in Chapter 12. Ginzburg and Landau assume the superelectron (fermion) model to describe the supercondensate. In particular the absolute square of Ψ' is equated with the number density of superelectrons n_s:

$$|\Psi'(\mathbf{r})|^2 = n_s \tag{11.9.8.}$$

This assumption however presents difficulties related to Pauli's exclusion principle. All difficulties can be removed simply by assuming that $|\Psi'(r)|^2$ is equated with the number density of condensed pairons:

$$|\Psi'(\mathbf{r})|^2 = n_0 \tag{11.9.9}$$

The revised G–L wave function Ψ' can be connected with the pairon density operator, see Section 11.9.11.

11.9.9. DC Josephson Effect

In 1962 Josephson predicted that if two superconductors are connected by a weak link (Josephson junction), a supercurrent passes through the link without energy loss at zero bias voltage. This is Josephson tunneling. The quasi-wave functions Ψ on either side join smoothly across the junction, so there is no energy loss. Josephson current is typically very small (of the order mA), and it is very sensitive to an applied magnetic field (of the order mG). The Josephson junction allows a bias voltage to be created between the two superconductors. (The effect of the bias on the Josephson current will be discussed in Section 11.9.12.)

11.9.10. Interference; Analogy between Laser and Supercurrent

In a SQUID two supercurrents separated by 1 mm can exhibit an interference pattern just like two laser beams from the same source. There is a close analogy between laser and supercurrent. Both are described by the wave function $A\exp(-i\hbar^{-1}\mathbf{p}\cdot\mathbf{r})$ representing a state of condensed bosons with a linear energy–momentum relation. Such a boson flux has self-focusing power. A laser beam becomes self-focused after passing a glass plate (disperser); likewise the condensed pairon flux becomes monochromatic after passing a Josephson junction. Thus both laser and supercurrent can interfere at a macroscopic distance. Supercurrents can however carry electric currents. It is interesting to observe that no self-focusing power is known for fermion flux.

11.9.11. G–L Wave function, Quasi-Wave Function, and Pairon Density Operator

The G-L wave function $\Psi'_\sigma(\mathbf{r})$ and the pairon density operator n are related by

$$\Psi'_\sigma(\mathbf{r}) = \langle \mathbf{r}|n^{1/2}|\sigma\rangle \tag{11.9.10}$$

where σ represents the condensed pairon state. In a ring supercurrent, we simply choose $\sigma = p_m = 2\pi\hbar L^{-1}m$, $(m = 0, \pm1, \pm2, \ldots)$. Since there is only one condensed state, there is one G–L wave function. For $m = 0$, $p_m = 0$. The $\Psi'_0(\mathbf{r})$ corresponds to the ground supercondensate, which carries no currents. For $m \neq 0$, $\Psi'_p(\mathbf{r})$ represents a current-carrying momentum state $p = p_m$. This state is *material-independent.* That is, all supercurrents in *any* superconductors behave in the same manner. This state is qualitatively *the same for all temperatures* below T_c, since there is only one quantum state. Only the density of condensed pairons changes with temperature.

The quasi-wave function $\Psi\sigma(\mathbf{r})$ for condensed pairons is related to the pairon density operator n by

$$\Psi_\sigma(\mathbf{r}) = \langle \mathbf{r}|n|\sigma\rangle \tag{11.9.11}$$

This $\Psi_\sigma(\mathbf{r})$ and the G–L wave function $\Psi'_\sigma(\mathbf{r})$ are different only in the normalization. Both functions (Ψ', Ψ) can represent the state of the supercondensate.

The density operator $n(t)$ changes in time, according to a quantum Liouville equation. From this we found that both (Ψ', Ψ) obey the Schrödinger-like equation of motion:

$$i\hbar\frac{\partial}{\partial t}\Psi_\sigma(\mathbf{r}, t) = h(\mathbf{r}, -i\hbar\nabla)\Psi_\sigma(\mathbf{r}, t) \tag{11.9.12}$$

11.9.12. Josephson–Feynman Equations

The wave length $\lambda = h/p_m = L/m$ characterizing a supercurrent is much greater than the Josephson junction size (10 Å). Thus the phase of the quasi-wave function $\phi(x) = kx = 2\pi\lambda^{-1}x$ measured in units of the junction size is a very slowly varying function of x. We may assume that superconductors right and left of the junction have position-independent phase θ_j. Josephson proposed two basic equations governing the supercurrent running through the junction[6]:

$$i = i_0 \sin\delta, \qquad \delta \equiv \theta_2 - \theta_1 \tag{11.9.13}$$

$$\hbar \frac{d\delta}{dt} = 2eV \tag{11.9.14}$$

We derived these equations in Section 11.7 by using Eq. (11.9.12) and following Feynman's arguments.[9] Note: The response of the supercurrent to the bias voltage V is very different from that of normal current (Ohm's law). Supercurrent does not gain energy from a DC bias. This behavior is compatible with our picture of a neutral supercondensate in motion.

11.9.13. AC Josephson Effect; Shapiro Steps

Josephson predicted[6] that on applying a constant voltage V_0, the supercurrent passing through a junction should have an oscillatory component characterized by the Josephson frequency:

$$\omega_J \equiv 2e\hbar^{-1}V_0 \tag{11.9.15}$$

This *AC Josephson effect* was dramatically demonstrated by Shapiro.[14] By applying a microwave of a matching frequency:

$$\omega = n\omega_J, \qquad n = \pm 1, \pm 2, \ldots \tag{11.9.16}$$

steplike currents were observed in the *V–I* diagrams, as shown in Fig. 11.8. The step from Eq. (11.9.15) is

$$V_0 = \frac{\hbar}{2e}\omega_J \tag{11.9.17}$$

Since the microwave frequency ω can accurately be measured, and $(\hbar, e)$ are constants, Eq. (11.9.17) can be used to define a *voltage standard* just as a meter stick is used to define a meter standard. The horizontal (current) strips in the *V–I* diagram decrease in magnitude with increasing n. We studied this behavior in Section 11.8 using the quasi-wave function Ψ and the G–L wave function Ψ'. We found that the quasi-wave function Ψ whose amplitude is proportional to the pairon density gives the correct pairon dynamics.

11.9.14. Independent Pairon Picture

In the present treatment of the supercurrent, we assumed that ± pairons (bosons) having linear energy–momentum (Cooper–Schrieffer) relations move *independently* of each other. Thus the analogy between supercurrent and laser is nearly complete except that pairons have charges $\pm 2e$ and therefore interact with electromagnetic fields. The supercurrent interference at macroscopic distances is the most remarkable; it supports a B–E condensation picture of free pairons with linear energy–momentum relations. The excellent agreement between theory and experiment also supports our starting generalized BCS Hamiltonian in Eq. (8.2.1).

REFERENCES

1. J. File and R. G. Mills, *Phys. Rev. Lett.* **10,** 93 (1963).

2. J. Bardeen, L. N. Cooper, and J. R. Schrieffer, *Phys. Rev.* **108,** 1175 (1957).
3. B. S. Deaver and W. M. Fairbank, *Phys. Rev. Lett.* **7,** 43 (1961); R. Doll and M. Näbauer, *Phys. Rev. Lett.* **7,** 51 (1961).
4. L. Onsager, *Phil. Mag.* **43,** 1006 (1952).
5. L. Onsager, *Phys. Rev. Lett.* **7,** 50 (1961); N. Byers and C. N. Yang, *Phys. Rev. Lett.* **7,** 46 (1961).
6. B. D. Josephson, *Phys. Lett.* **1,** 251 (1962); *Rev. Mod. Phys.* **36,** 216 (1964).
7. P. W. Anderson and J. M. Rowell, *Phys. Rev. Lett.* **10,** 486 (1963).
8. R. C. Jaklevic, *et al.*, *Phys. Rev.* **140,** A1628 (1965).
9. R. P. Feynman, R. B. Leighton and M. Sands, *Feynman Lectures on Physics*, vol. 3, Chapter 21 (Addison-Wesley, Reading, MA, 1965), pp. 21–28.
10. H. London and F. London, *Proc. Roy. Soc.* (*London*) **A149,** 71 (1935); *Physica* **2,** 341 (1935).
11. F. London, *Superfluids*, vol. 1 (Wiley, New York, 1950).
12. V. L. Ginzburg and L. D. Landau, *J. Exptl. Theor. Phys.* (*USSR*) **20,** 1064 (1950).
13. R. P. Feynman, *Statistical Mechanics* (Addison-Wesley, Redwood City, CA, 1972).
14. S. Shapiro, *Phys. Rev. Lett.* **11,** 80 (1963).
15. A. Hartland, *Precis. Meas. Fundam. Constants*, **2,** 543 (1981).
16. D. H. Menzel, ed.; *Fundamental Formulas of Physics* (Dover, New York, 1960), p. 59.
17. A. A. Abrikosov, *J. Exptl. Theor. Phys.* (*USSR*) **32,** 1442 (1957).
18. U. Essmann and H. Täuble, *Phys. Lett.* **24A,** 526 (1967).

This page intentionally left blank.

12

Compound Superconductors

Compound superconductors exhibit type II magnetic behavior, and they tend to have higher critical fields than elemental superconductors. Otherwise they show the same superconducting behavior. The Abrikosov vortex lines, each consisting of a quantum flux and circulating supercurrents, are explained in terms of a supercondensate made up of condensed pairons. Exchange of optical and acoustic phonons are regarded as responsible for type II behavior.

12.1. INTRODUCTION

A great number of metallic compounds are found to be superconductors. Most of the experimental discoveries were made by Matthias and his group.[1] A common feature of these superconductors is that they exhibit type II magnetic behavior, which we explain more fully in Section 12.2. Briefly these superconductors show the four main properties: zero resistance below the critical temperature T_c, Meissner state below the lower critical field H_{c1}, flux quantization and Josephson effects, and energy gap $\in_g$ in the elementary excitation spectrum. The critical temperatures T_c tend to be higher for compounds than for elemental superconductors; the highest T_c ($\sim$ 23 K) found is found for Nb_3Ge. The upper critical fields H_{c2} for some compounds including Nb_3Sn can be very high, some reaching 2×10^5 G $\equiv$ 20 T, compared with typical 500 G for elemental superconductors. This feature makes compound superconductors very useful in devices and applications. In fact large-scale application and technology are carried out by using type II compound superconductors. Physics of compound superconductors is complicated because of their intrinsically involved lattice structures and associated electron and phonon band structures. But the superconducting state characterized by the four main properties, is essentially the same for both elemental and compound superconductors. For this reason the microscopic theory can be developed in a unified manner. In Chapter 12 we briefly outline our theory.

12.2. TYPE II SUPERCONDUCTORS; THE MIXED STATE

The magnetic properties of type I and type II superconductors are quite different. A type I superconductor repels a weak magnetic field from its interior at $T < T_c$, while a type II superconductor allows partial penetration of the field immediately below T_c;

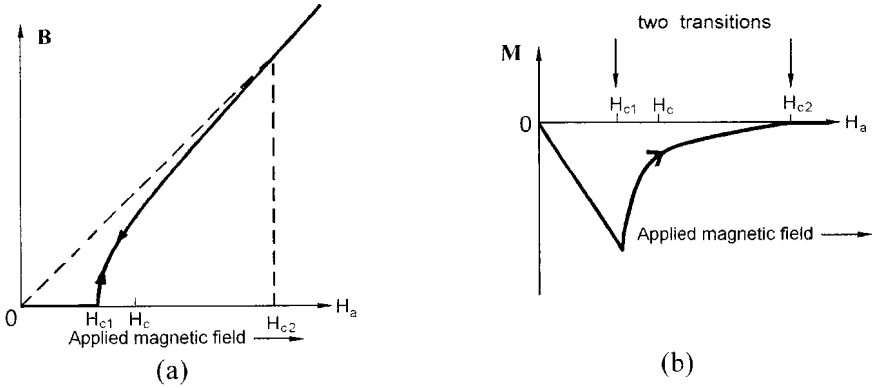

Figure 12.1. Magnetization curves of type II superconductors. Below the lower critical field H_{c1}, type II exhibit the same Meissner state ($B = 0$) as type I.

this behavior was shown in Fig. 1.14. Due to penetration of the magnetic field **B,** the superconducting state is more stable, making the upper critical fields in type II higher. The magnetization M and the B-field versus the H-field for type II are shown in Fig. 12.1. Note: The (dia)magnetization $M(< 0)$ is continuous at the lower critical field H_{c1} and also at the upper critical field H_{c2}. When the applied field H_a is between H_{c1} and H_{c2}, there is a penetration of magnetic flux B, and the sample develops a complicated structure having both normal and super regions. In this so-called *mixed state,* a set of quantized flux lines penetrate, and each flux line is surrounded by diamagnetic supercurrents. See Fig. 12.2. A quantized flux line and the surrounding supercurrents is called a *vortex line.* The B-field is nonzero within each vortex line, and it is nearly zero in the background (except for the surface layer). Such a peculiar structure was predicted by Abrikosov in 1957[3] on the basis of an extension of the G–L theory.[4] This *Abrikosov vortex structure* was later confirmed by experiments[5] as shown in Fig. 12.3. Each vortex line contains a flux quantum $\Phi_0 = \pi\hbar/e$. Penetration of these flux lines does not destroy the superconducting state if the flux density is not too high. If the applied magnetic field H_a is raised further, it eventually destroys the superconducting state at H_{c2}; there flux densities inside and outside become the same, and the magnetization M vanishes.

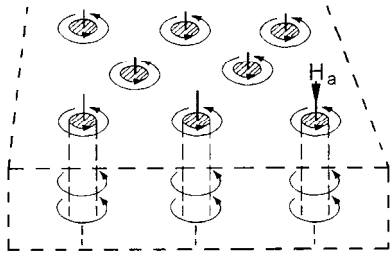

Figure 12.2. Quantized flux lines are surrounded by diamagnetic supercurrents.

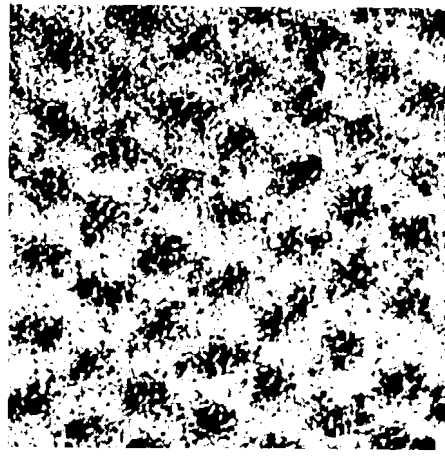

Figure 12.3. Abrikosov structure in Nb.

Why does such a structure occurs only for a type II superconductor? To describe the actual vortex structure, we need the concept of a coherence length ξ, which was first introduced by Ginzburg and Landau.[4] In fact the distinction between the two types can be made by the relative magnitudes of the coherence length ξ and the penetration depth λ:

$$\xi > 2^{1/2}\lambda \text{ (type I)}, \qquad \xi < 2^{1/2}\lambda \text{ (type II)} \tag{12.2.1}$$

Both ξ and λ depend on materials, temperature, and concentration of impurities. The penetration depth λ at 0 K is about 500 Å in nearly all superconductors. The BCS coherence length $\xi \equiv \hbar v_F/\pi\Delta$ has a wider range: 25–10^4 Å.

We now explain the phenomenon piece by piece.

1. We note the importance of flux quantization. Otherwise there is no vortex line.
2. Any two magnetic fluxes repel each other, as is well-known in electromagnetism, thus each vortex line should contain one flux quantum $\Phi_0 = \pi\hbar/e$.
3. Each magnetic flux is surrounded by a supercurrent with no energy loss, forming a vortex line. As a result the B-field is practically zero outside the vortex line.

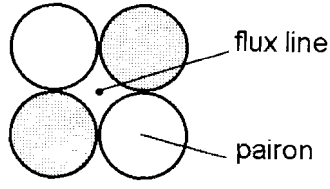

Figure 12.4. Closely packed circular disks (pairons) rotate around the flux.

4. Because of the surface supercurrent within the penetration depth λ, the B-field vanishes everywhere in the background where the supercondensate is in equilibrium.

5. The supercondensate is composed of condensed pairons; and therefore the minimum distance over which the pairon density is defined is the pairon size. Because of the Meissner pressure, each vortex may be compressed to this size. To see this, let us consider a set of four circular disks representing two + and two – pairons, as shown in Fig. 12.4. The four disks rotate around the fixed flux line, keeping the surrounding background stationary. From Fig. 12.4, we see that the vortex line represented by the flux line and the moving disks (pairons) has a radius of the order of the pairon size.

6. Vortices are round, and they weakly repel each other. This generates a hexagonal closed-pack structure as observed.

7. If the applied field H_a is raised to H_{c2}, the number density of vortex lines increases, so the magnetic flux density eventually becomes equal inside and outside of the superconductor. Then the super part is reduced to zero, see Fig. 12.1.

8. If the field H is lowered to H_{c1}, the number of vortex lines decreases to zero, and the magnetic fluxes pass through the surface layer. These fluxes and the circulating supercurrents maintain the Meissner state in the interior of the superconductor. This perfect Meissner state is kept below H_{c1} (> 0).

9. The surface region where fluxes penetrate and supercurrents run appears to be the same for $H < H_{c1}$. We may postulate that this region remains the same for all fields $0 < H < H_{c2}$, and it is characterized by the penetration depth λ.

10. Creating vortex lines (normal part) within a superconductor lowers the magnetic energies $B^2V/2\mu_0$ but raises the Meissner energies $G_N - G_S$ due to the decrease in the super part. This thermodynamic competition generates a phase transition of the first order at H_{c1}, see Fig. 12.5.

11. Penetration of the vortices lightens the magnetic pressure (see Section 11.9.6). Thus the superconducting state is much more stable against the applied field, making H_{c2} much greater than the ideal *thermodynamic critical field* H_c defined by

$$\frac{1}{2}\mu_0 H_c^2 \equiv \frac{G_N - G_S}{V} \tag{12.2.2}$$

12. Since the magnetization approaches zero near $H = H_{c2}$ [see Fig. 12.1 (b)], the phase transition is of the second order. This is in contrast with type I, where the phase transition at $H = H_c$ is of the first order (see Section 1.3.8 and Fig. 1.14). Data on heat capacity C in Nb by McConville and Serin,[6] shown in Fig. 12.5, support the second-order phase transition. Heat capacity at the higher critical temperature T_{c2} has a jump just like the heat capacity at T_c for a type I superconductor at $B = 0$, see Fig. 10.11.

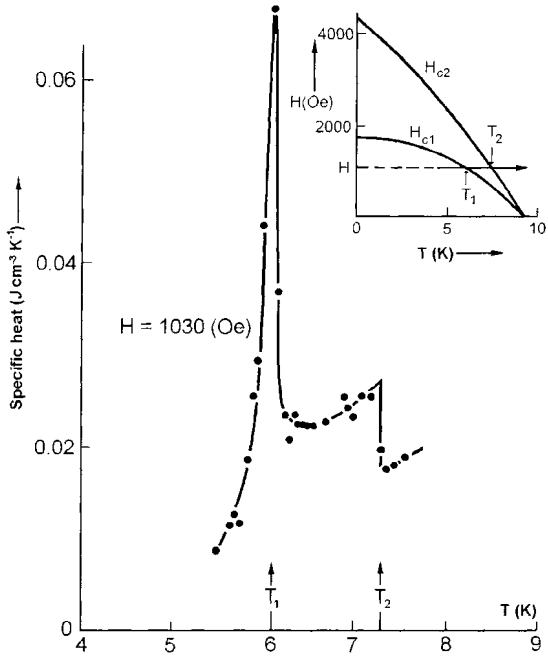

Figure 12.5. Specific heat of type II superconductor (Nb) in a constant applied magnetic field H [after McConville and Serin (Ref. 6)].

13. Why does a type I superconductor not develop the Abrikosov structure? Type I supercondensate is made up of large-size pairons on the order of 10^4 Å. Vortex lines having such a large size would cost too much Meissner energy to compensate for the possible gain in magnetic energy.

In summary a type II superconductor can, and does, develop a set of vortex lines of a radius on the order of ξ_0 in its interior. These vortices lower the magnetic energy at the expenses of their Meissner energy. They repel each other slightly and form a two-dimensional hexagonal lattice. At Abrikosov's time of work in 1957, flux quantization and Cooper pairs, which are central to the preceding arguments, were not known. The coherence length ξ_0 in the G–L theory is defined as the minimum distance below which the G–L wave function Ψ' cannot change appreciably. This ξ_0 is interpreted here as the Cooper pair size. The distinction between type I and type II as represented by Eq. (12.2.1) is equivalent to different signs in the interface energy between normal and super parts. Based on such nonmicroscopic physical ideas, Abrikosov predicted the now-famous Abrikosov structure.

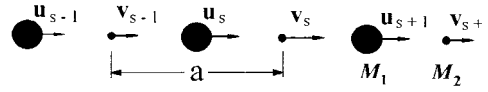

Figure 12.6. A ditomic one-dimensional lattice with masses M_1, M_2 bound by a force constant C.

12.3. OPTICAL PHONONS

A compound crystal has two or more atoms in a unit cell; so it therefore has optical modes of lattice vibration. We discuss this topic in the present section.

Consider a rock salt, a NaCl crystal whose lattice structure is shown in Fig. 3.1. In the ⟨111⟩ directions, planes containing Na ions and planes containing Cl ions alternate with a separation equal to $3^{1/2}/2$ times the lattice constant a_0. Thus we may imagine a *density wave* proceeding in this direction. This condition is similar to what we saw earlier in Section 7.4 for the lattice-vibrational modes in a sc crystal. We assume that each plane interact with its nearest neighbor planes and that the force constants C are the same between any pairs of nearest neighbor planes. We may use a one-dimensional representation as shown in Fig. 12.6. The displacements of atoms with mass M_1 are denoted. by $u_{s-1}, u_s, u_{s+1}, \ldots$, and those of atoms with mass M_2 by $v_{s-1}, v_s, v_{s+1}, \ldots$, From the figure, we obtain

$$M_1 \frac{d^2 u_s}{dt^2} = C(v_s + v_{s-1} - 2u_s), \qquad M_2 \frac{d^2 v_s}{dt^2} = C(u_{s+1} + u_s - 2v_s) \tag{12.3.1}$$

We look for a solution in the form of a traveling wave with amplitudes (u, v):

$$u_s = u \exp(isKa - i\omega t), \qquad v_s = v \exp(isKa - i\omega t) \tag{12.3.2}$$

where a is the repeat distance. Introducing Eqs. (12.3.2) into Eqs. (12.3.1), we obtain

$$\begin{aligned} -\omega^2 M_1 u &= Cv[1 + \exp(-iKa)] - 2Cu \\ -\omega^2 M_2 v &= Cu[1 + \exp(+iKa)] - 2Cv \end{aligned} \tag{12.3.3}$$

From the secular equation

$$\begin{vmatrix} 2C - M_1\omega^2 & -C[1 + \exp(-iKa)] \\ -C[1 + \exp(+iKa)] & 2C - M_2\omega^2 \end{vmatrix} = 0$$

we obtain

$$M_1 M_2 \omega^4 - 2C(M_1 + M_2)\omega^2 + 2C^2(1 - \cos Ka) = 0 \tag{12.3.4}$$

which can be solved exactly. The dependence of ω on K is shown in Fig. 12.7 for $M_1 > M_2$. Let us consider two limiting cases: $K = 0$ and $K = K_{max} = \pi/a$. For small K, $\cos Ka \simeq 1 - K^2a^2/2$, and the two roots from Eq. (12.3.4) are (Problem 12.3.1)

$$\begin{aligned} \omega_1 &= \left[\frac{2C(M_1 + M_2)}{M_1 M_2}\right]^{1/2} \left(1 - \frac{M_1 M_2 a^2}{8(M_1 + M_2)^2} K^2\right) \qquad \text{(optical branch)} \\ \omega_2 &= \left[\frac{C}{2(M_1 + M_2)}\right]^{1/2} Ka \qquad \text{(acoustic branch)} \end{aligned} \tag{12.3.5}$$

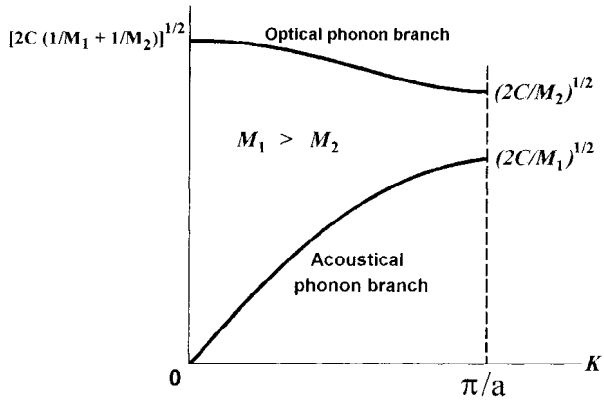

Figure 12.7. Optical and acoustic branches of the dispersion relation. The limiting frequencies at $K = 0$ and $K = \pi/a$ are shown.

At $K = \pi/a$, the roots are (Problem 12.3.2)

$$\omega_1 = \left(\frac{2C}{M_2}\right)^{1/2} + C_1\left(\frac{\pi}{a} - K\right)^2 \qquad \text{(optical branch)}$$

$$\omega_2 = \left(\frac{2C}{M_1}\right)^{1/2} - C_2\left(\frac{\pi}{a} - K\right)^2 \qquad \text{(acoustic branch)} \qquad (12.3.6)$$

where C_1 and C_2 are constants. These limiting cases are indicated in Fig. 12.7. Note: the dispersion relation is linear only for the low-K limit of the acoustic mode. Otherwise the energy–momentum relations have quadratic terms.

For a real three-dimensional crystal there are transverse and longitudinal wave modes. The particle displacements in the *transverse acoustic (TA)* and *optical (TO)* modes are shown in Fig. 12.8. The ω–k or dispersion relations can be probed by neutron-scattering experiments, whose results are in a good agreement with those of the simple theory discussed.[7]

Problem 12.3.1. Verify Eq. (12.3.5).

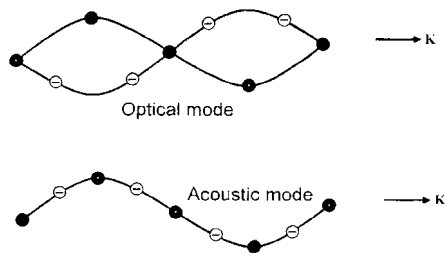

Figure 12.8. TO and TA waves in a linear diatomic lattice; $\lambda = 4a$.

Problem 12.3.2. Verify Eq. (12.3.6). Find (C_1, C_2) explicitly.

12.4. DISCUSSION

Compound superconductors show all of the major superconducting features found in elemental superconductors. We therefore expect the superconducting state to be characterized by the presence of a supercondensate and the superconducting transition to be a B–E condensation of pairons. We may assume the same generalized BCS Hamiltonian in Eq. (8.2.1) and derive all of the properties based on this Hamiltonian. From its lattice structure, a compound conductor should provide a medium in which optical phonons as well as acoustic phonons are created and annihilated. Moreover it is most likely to have two or more sheets of the Fermi surface; one of the sheets is electron like (of a negative curvature) and the other hole like. If other conditions are right, a supercondensate may be formed from electrons and holes on the different Fermi-surface sheets mediated by optical phonons. Acoustic phonons of small k-vectors may not do the intermediary because pair creation and pair annihilation of $\pm$ pairons can be done only by a phonon having a momentum (magnitude) greater than $\hbar$ times the minimum k-distance between electron and hole Fermi-surface sheets. (See Section 13.6 where a two-dimensional analogue is discussed and demonstrated.) Attraction by exchange of optical phonons having a quadratic energy–momentum relation [see Eqs. (12.3.5) and (12.3.6)] is short-ranged just as attraction by exchanging a massive π-meson is short-ranged as show by Yukawa.[8] Thus pairon size should be on the order of the lattice constant (5 Å) or greater. In fact compound superconductors have correlation lengths of the order 50 Å, much shorter than penetration depths (~ 500 Å). They are therefore type II superconductors.

REFERENCES

1. B. T. Matthias, *Progress in Low-Temperature Physics*, C. J. Gorter, ed. vol. 2 (North-Holland, Amsterdam, 1957), p. 138; B. T. Matthias *et al., Rev. Mod. Phys.* **36,** 155 (1964).
2. D. Saint-James, E. D. Thomas, and G. Sarma, *Type II Superconductivity* (Pergamon, Oxford, 1969).
3. A. A. Abrikosov, *J. Exp. Theor. Phys.* (*USSR*) **5,** 1174 (1957).
4. V. L. Ginzburg and L. D. Landau, *J. Exp. Theor. Phys.* (*USSR*) **20,** 1064 (1950).
5. U. Essman and H. Träuble, *Scientific American* (March 1971).
6. T. McConville and B. Serin, *Rev. Mod. Phys.* **36,** 112 (1964).
7. A. D. B. Woods, *et al., Phys Rev.* **131,** 1025 (1963).
8. H. Yukawa, *Proc. Math. Soc. Japan* **17,** 48 (1935).

13

High-T_c Superconductors

High-T_c superconductors exhibit the main superconducting properties, including zero resistance, Meissner effect, flux quantization and Josephson effects, and gaps in the excitation energy spectra. In addition they are characterized by a two-dimensional structure, a short coherence length ξ_0 (~ 10 Å) a high T_c (~ 100 K) and two energy gaps. These properties are discussed based on the generalized BCS model with two-dimensional band structures, optical phonon exchange attraction, and different interaction strengths V_{ij}.

13.1. INTRODUCTION

In 1986 Bednorz and Müller[1] reported their discovery of the first of the high-T_c cuprate superconductors (Ba–La–Cu–O, $T_c > 30$ K). Since then many investigations[2–5] have been carried out on high-T_c superconductors including Y–Ba–Cu–O with $T_c \approx 94$ K.[6] These compounds possess all of the main superconducting properties, indicating that there is the same kind of superconducting state in high-T_c as in elemental superconductors. In addition these cuprate superconductors are characterized by[7] (i) two-dimensional conduction, (ii) short zero-temperature coherence length ξ_0 (~ 10 Å), (iii) high critical temperature T_c (~ 100 K), (iv) two energy gaps, and (v) the transport behaviors above T_c are significantly different from those of a normal metal. In this chapter we present a theory of high-T_c superconductivity, starting with a generalized BCS Hamiltonian [Eq. (8.2.1)] taking account of crystal and energy band structures.

13.2. THE CRYSTAL STRUCTURE OF YBCO; TWO-DIMENSIONAL CONDUCTION

Cuprate superconductors have *layered structures* such that the copper plane comprising Cu and O are separated by a great distance (e.g., $a = 3.88$ Å, $b = 3.82$ Å, $c = 11.68$ Å for $YBa_2Cu_3O_{7-\delta}$). The lattice structure of YBCO is shown in Fig. 13.1. The succession of layers along the c-axis can be represented by

$$CuO–BaO–CuO_2–Y–CuO_2–BaO–CuO–\ldots$$

The buckled CuO_2 plane where Cu-plane and O-plane are separated by a short distance as shown is called the *copper planes*. The two copper planes separated by yttrium (Y)

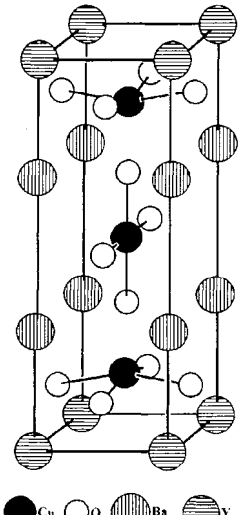

Figure 13.1. Arrangement of atoms in a crystal of $YBa_2Cu_3O_7$; superconducting YBCO has some missing oxygens.

are about 3 Å apart, and they are believed to be responsible for superconductivity.

The conductivity measured is estimated to be a few orders of magnitude smaller along the *c*-axis than perpendicular to it.[8] This appears to contradict the prediction based on the naive application of the Bloch theorem. This puzzle may be solved as follows.[9] Suppose an electron jumps from one conducting layer to its neighbor. This generates a change in the charge states of the layers involved. If each layer is macroscopic in dimension, we must assume that the charge state Q_n of the *n*th layer can change without limits: $Q_n = \ldots, -2, -1, 0, 1, 2, \ldots$ in units of the electron charge *e*. Because of unavoidable short circuits between layers due to lattice imperfections, these Q_n may not be large. At any rate if Q_n are distributed at random over all layers, periodicity of the potential for the electron along the *c*-axis is destroyed. Then the Bloch theorem based on the electron potential periodicity does not apply even though the lattice is periodic along the *c*-axis. As a result there are no *k*-vectors along the *c*-axis. This means that the effective mass in the *c*-axis direction is infinity, so that *the Fermi surface for a layered conductor is a right cylinder with its axis along the c-axis.*

The torque-magnetometry experiment by Farrel *et al.*[8] in $Tl_2Ba_2CaCu_2O_x$ indicates an effective-mass anisotropy of at least 10. Other experiments[10] in thin films and single crystals also suggest a high anisotropy. The most direct way of verifying the two-dimensional structure however is to observe the orientation dependence of the cyclotron resonance (CR) peaks. The peak position (ω) should follow Shockley's formula [see Eq. (5.10.10)]:

$$\frac{\omega}{eB} = \left\{ \frac{[m_2 m_3 \cos^2(\mu, x_1) + m_3 m_1 \cos^2(\mu, x_2) + m_1 m_2 \cos^2(\mu, x_3)]}{m_1 m_2 m_3} \right\}^{1/2} \tag{13.2.1}$$

where (m_1, m_2, m_3) are effective masses in the Cartesian axes (x_1, x_2, x_3) taken along the (a, b, c) crystal axes and $\cos(\mu, x_j)$ is the direction cosine relative to the field **B** and the

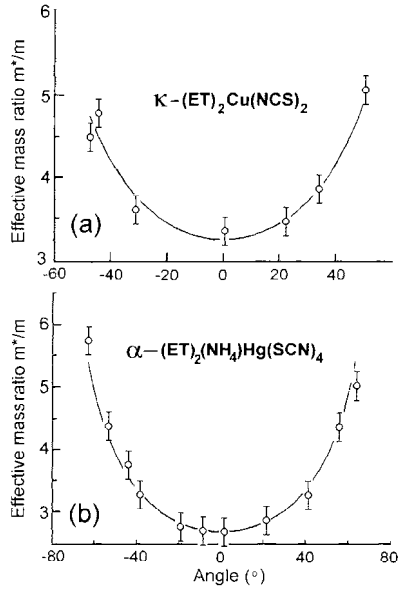

Figure 13.2. Angular dependence of the reduced effective mass in (a) k-$(ET)_2Cu(NCS)_2$ and (b) α-$(ET)_2(NH_4)Hg(SCN)_4$. An angle of 0 deg means **H** is perpendicular to the conducting plane. The solid fits are obtained using Eqs. (13.2.2) and (13.2.3) [after Wosnitza *et al.* (Ref. 12)].

axis x_j. If the electron motion is plane-restricted, so that $m_3 \rightarrow \infty$, Eq. (13.2.1) is reduced to the *cosine law* formula:

$$\omega = eB(m_1 m_2)^{-1/2} \cos\theta \equiv (eB/m^*)\cos\theta \tag{13.2.2}$$

where θ is the angle between the field and the c-axis. A second and much easier way of verifying two-dimensional conduction is to measure the de Hass–van Alphen (dHvA) oscillations and analyze the orientation dependence of the dHvA frequency with the help of Onsager's formula[11] (5.6.2), which may be reexpressed by

$$\Delta\left(\frac{1}{B}\right) = \frac{2\pi e}{\hbar}\frac{1}{A} \tag{13.2.3}$$

where A is the extremum inter-sectional area of the Fermi surface and the planes normal to the applied magnetic field **B**. Recently Wosnitza *et al.*[12] reported the first direct observation of the orientation dependence (cos θ law) of the dHvA oscillations in k-$(ET)_2Cu(NCS)_2$ and α-$(ET)_2(NH_4)Hg(SCN)_4$, both layered organic superconductors, confirming a right cylindrical Fermi surface. Their data and theoretical curves are shown in Fig. 13.2. Notice the excellent agreement between theory and experiment. Measurements of orientation-dependent magnetic or magneto-optical effects in high-T_c superconductors are highly desirable, since no transport measurements can give a conclusive test for two-dimensional conduction because of unavoidable short circuits between layers.

13.3. OPTICAL-PHONON-EXCHANGE ATTRACTION; THE HAMILTONIAN

Since electric current flows in the copper planes, there are continuous k-vectors and the Fermi energy ϵ_F. Many experiments [2–5] indicate that singlet pairs with antiparallel spins (pairons) form a supercondensate.

Let us examine the cause of electron pairing. We first consider attraction via the longitudinal acoustic phonon exchange. Acoustic phonons of lowest energies have long wavelengths λ and a linear energy-momentum relation may be assumed:

$$\epsilon = c_s \hbar K \tag{13.3.1}$$

The attraction generated by the exchange of longitudinal acoustic phonons is long-ranged. This mechanism is good for a type I superconductor whose pairon size is of the order of 10^4 Å. This attraction is in action also for a high-T_c superconductor, but it alone is unlikely to account for the much smaller pairon size.

Second we consider the optical phonon exchange. Roughly speaking each copper plane has Cu and O, and two-dimensional lattice vibrations of optical modes are expected to be important. Optical phonons of lowest energies have short wavelengths of the order of the lattice constants, and they have a quadratic dispersion relation [see Eq. (12.3.6)]

$$\epsilon = \epsilon_0 + A_1 \left(K_1 - \frac{\pi}{a_1} \right)^2 + A_2 \left(K_2 - \frac{\pi}{a_2} \right)^2 \tag{13.3.2}$$

where ϵ_0, A_1, and A_2 are constants. The attraction generated by the exchange of a massive boson is short-ranged just as the short-ranged nuclear force between two nucleons generated by the exchange of massive pions, first shown by Yukawa.[13] Lattice constants for YBCO are given by $(a_1, a_2) = (3.88, 3.82)$ Å, and the limit wavelengths ($\lambda_{\min}$) at the Brillouin boundary are twice these values. The observed coherence length ξ_0 is of the same order as $\lambda_{\min}$:

$$\xi_0 \sim \lambda_{\min} \cong 8 \text{ Å} \tag{13.3.3}$$

Thus an electron–optical-phonon interaction is a viable candidate for the cause of the electron pairing. To see this in more detail, let us consider the copper plane. With the neglect of a small difference in lattice constants along the a- and b-axes, Cu atoms form a square lattice of a lattice constant $a_0 = 3.85$ Å, as shown in Fig. 13.3. Twice as many oxygen atoms (O) as Cu atoms occupy midpoints of the nearest neighbors (Cu, Cu) in the x_1–x_2 plane.

First let us look at the motion of an electron wave packet that extends over more than one Cu-site. This wave packet may move easily in [110] or $[1\bar{1}0]$ because the O-sublattice charged uniformly and weakly favors such a motion over the possible motion in [100] and [010]. In other words easy axes of motion for the electron are the second nearest (Cu–Cu) neighbor directions [110] and $[1\bar{1}0]$ rather than the first neighbor directions [100] and [110]. The Bloch wave packets are superposable; therefore the electron can move in any direction characterized by the two-dimensional k-vectors with bases taken along [110] and $[1\bar{1}0]$. If the number density of electrons is small, the Fermi surface should then be a small circle as shown in the central part in Fig. 13.4.

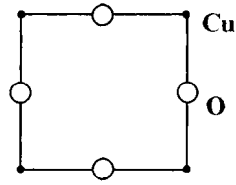

Figure 13.3. The idealized copper plane contains twice as many O's as Cu's.

Second we consider a hole wave packet that extends over more than one O-site. It may move easily in [100] or [010] because the Cu-sublattice of a uniform charge distribution favors such a motion. If the number of holes is small, the Fermi surface should consists of the four small pockets shown in Fig. 13.4. Under the assumption of such a Fermi surface, pair creation of ± pairons via an optical phonon may occur as shown in the figure. Here a single-phonon exchange generates an electron transition from A in the O-Fermi sheet to B in the Cu-Fermi sheet and another electron transition from A' to B', creating the – pairon at (B,B') and the + pairon at (A, A'). From momentum conservation the momentum (magnitude) of a phonon must be equal to $\hbar$ times the k-distance AB, which is approximately equal to the momentum of an optical phonon of the smallest energy. Thus an almost insulator-like layered conductor should have a Fermi surface comprising a small electron circle and small hole pockets, which are quite favorable for forming a supercondensate by exchanging an optical phonon.

Generally speaking any and every possible cause for electron pairing, including spin-dependent ones should be enumerated, and its importance be evaluated. However if the net interaction between two electrons due to all causes is attractive, pairons will be formed. Then a BCS-like Hamiltonian can be postulated generically irrespective of specific causes. Because of this nature of theory, we can set up a generalized BCS Hamiltonian as follows. We assume that:

1. there exists a well-defined Fermi energy $\in_F$ for the normal state[14];
2. the electron–phonon interaction generates pairons near the Fermi surface within a distance (energy) $\hbar\omega_D$.
3. the conduction electrons move in two dimensions;

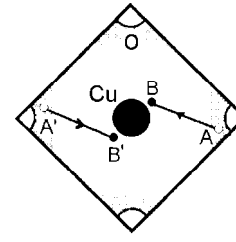

Figure 13.4. The proposed two-dimensional Fermi surface of a cuprate model has a small circle (electrons) at the center and a set of four small pockets (holes) at the Brillouin boundary. Exchange of a phonon can create the electron pairon at (B, B') and the hole pairon at (A, A'). The phonon must have a momentum equal to $\hbar$ times the k-distance AB, which is greater than the minimum k-distance between the electron circle and hole pockets.

4. there are electrons and holes with different effective masses; under these conditions we write down a generalized BCS Hamiltonian H [see Eq. (9.4.9)]

$$\begin{aligned} H = & \sum_{\mathbf{k},s} \epsilon_k^{(1)} n_{\mathbf{k},s}^{(1)} + \sum_{\mathbf{k},s} \epsilon_k^{(2)} n_{\mathbf{k},s}^{(2)} \\ & - \sum_{\mathbf{k}}{}' \sum_{\mathbf{q}}{}' \sum_{\mathbf{k}'}{}' [v_{11} B_{\mathbf{k}'\mathbf{q}}^{(1)\dagger} B_{\mathbf{k}\mathbf{q}}^{(1)} + v_{12} B_{\mathbf{k}'\mathbf{q}}^{(1)\dagger} B_{\mathbf{k}\mathbf{q}}^{(2)\dagger} + v_{21} B_{\mathbf{k}\mathbf{q}}^{(2)} B_{\mathbf{k}'\mathbf{q}}^{(1)} + v_{22} B_{\mathbf{k}'\mathbf{q}}^{(2)} B_{\mathbf{k}\mathbf{q}}^{(2)\dagger}] \\ & - \sum_{\mathbf{k}}{}' \sum_{\mathbf{k}'}{}' [v_{11} b_{\mathbf{k}'}^{(1)\dagger} b_{\mathbf{k}}^{(1)} + v_{12} b_{\mathbf{k}}^{(2)\dagger} b_{\mathbf{k}'}^{(1)\dagger} + v_{21} b_{\mathbf{k}}^{(2)} b_{\mathbf{k}'}^{(1)} + v_{22} b_{\mathbf{k}'}^{(2)} b_{\mathbf{k}}^{(2)\dagger}] \quad (13.3.4) \end{aligned}$$

5. the interaction strengths V_{ij} satisfy

$$V_{11} = V_{22} < V_{12} = V_{21} \quad (13.3.5)$$

since the Coulomb repulsion between two electrons separated by 10 Å is not negligible due to the incomplete screening.

Assumption 3 is explained in Section 13.2. All other assumptions are essentially the same as those for elemental superconductors, and detailed explanations were given in Section 8.2. In summary we assume the same generalized BCS Hamiltonian for cuprates. Only two-dimensional electron band structure, optical-phonon exchange attraction and inequalities (13.3.5) are newly introduced.

13.4. THE GROUND STATE

In Section 8.5 we studied the ground state of the generalized BCS system characterized by the Hamiltonian, Eq. (8.2.1). We can extend our theory to the cuprate model with a few changes. We simply summarize methods and results. At 0 K there are *ground pairons* only. The ground state Ψ for the system can be described by the *reduced* Hamiltonian per unit volume given by [see Eq. (8.2.6)]

$$\begin{aligned} H_0 = & \sum_{\mathbf{k}} \sum_{s} \epsilon_k^{(1)} n_{\mathbf{k}s}^{(1)} + \sum_{\mathbf{k}} \sum_{s} \epsilon_k^{(2)} n_{\mathbf{k}s}^{(2)} \\ & - \sum_{\mathbf{k}}{}' \sum_{\mathbf{k}'}{}' [v_{11} b_{\mathbf{k}'}^{(1)\dagger} b_{\mathbf{k}}^{(1)} + v_{12} b_{\mathbf{k}'}^{(1)\dagger} b_{\mathbf{k}}^{(2)\dagger} + v_{21} b_{\mathbf{k}}^{(2)} b_{\mathbf{k}'}^{(1)} + v_{22} b_{\mathbf{k}'}^{(2)} b_{\mathbf{k}}^{(2)\dagger}] \quad (13.4.1.) \end{aligned}$$

Folliwing BCS,[16] we assume the normalized ground-state ket $|\Psi\rangle$ of the form:

$$|\Psi\rangle \equiv \prod_{\mathbf{k}}{}' (u_{\mathbf{k}}^{(1)} + v_{\mathbf{k}}^{(1)} b_{\mathbf{k}}^{(1)\dagger}) \prod_{\mathbf{k}'}{}' (u_{\mathbf{k}'}^{(2)} + v_{\mathbf{k}'}^{(2)} b_{\mathbf{k}'}^{(2)\dagger}) |0\rangle \quad (13.4.2)$$

where u's and v's are probability amplitudes satisfying

$$u_{\mathbf{k}}^{(j)2} + v_{\mathbf{k}}^{(j)2} = 1 \quad (13.4.3)$$

We now determine u's and v's such that ground state energy

$$W \equiv \langle \Psi | H_0 | \Psi \rangle = \sum_{\mathbf{k}}{}' 2\epsilon_k^{(1)} v_{\mathbf{k}}^{(1)2} + \sum_{\mathbf{k}'}{}' 2\epsilon_{k'}^{(2)} v_{\mathbf{k}'}^{(2)2} - \sum_{\mathbf{k}}{}' \sum_{\mathbf{k}'}{}' \sum_i \sum_j v_{ij} u_{\mathbf{k}}^{(i)} v_{\mathbf{k}}^{(i)} u_{\mathbf{k}'}^{(j)} v_{\mathbf{k}'}^{(j)} \tag{13.4.4}$$

have a minimum value. After variational calculations, we obtain [see Eqs. (8.5.9)]

$$2\epsilon_k^{(j)} u_{\mathbf{k}}^{(j)} v_{\mathbf{k}}^{(j)} - (u_{\mathbf{k}}^{(j)2} - v_{\mathbf{k}}^{(j)2}) \sum_{\mathbf{k}'}{}' [v_{j1} u_{\mathbf{k}'}^{(1)} v_{\mathbf{k}'}^{(1)} + v_{j2} u_{\mathbf{k}'}^{(2)} v_{\mathbf{k}'}^{(2)}] = 0 \tag{13.4.5}$$

To simply treat these equations subject to Eq. (13.4.3), we introduce a set of energy parameters:

$$\Delta_j, \qquad E_k^{(j)} \equiv \left(\epsilon_k^{(j)2} + \Delta_j^2 \right)^{1/2} \tag{13.4.6}$$

such that

$$u_{\mathbf{k}}^{(j)2} - v_{\mathbf{k}}^{(j)2} = \frac{\epsilon_k^{(j)}}{E_k^{(j)}}, \qquad u_{\mathbf{k}}^{(j)} v_{\mathbf{k}}^{(j)} = \frac{\Delta_j}{2E_k^{(j)}} \tag{13.4.7}$$

Then Eq. (13.4.5) can be reexpressed as

$$\boxed{\Delta_j = \sum_{\mathbf{k}}{}' \sum_i v_{ij} \frac{\Delta_i}{2E_{k'}^{(i)}}} \tag{13.4.8}$$

[see Eq. (8.5.13)], which are generalized energy gap equations. These equations can alternatively be obtained by using the equation-of-motion method (see Sections 10.2–10.3).

Using Eqs. (13.4.7) and (13.4.8), we calculate the ground state energy W from Eq. (13.4.4) and obtain [Eq. (8.5.14)]

$$\begin{aligned} W &\equiv \sum_{\mathbf{k}}{}' \sum_j 2\epsilon_k^{(j)} v_{\mathbf{k}}^{(j)2} - \sum_{\mathbf{k}}{}' \sum_{\mathbf{k}'}{}' \sum_i \sum_j v_{ij} u_{\mathbf{k}}^{(i)} v_{\mathbf{k}}^{(i)} u_{\mathbf{k}'}^{(j)} v_{\mathbf{k}'}^{(j)} \\ &= \sum_{\mathbf{k}}{}' \sum_{j=1}^{2} \left\{ \epsilon_k^{(j)} \left[1 - \frac{\epsilon_k^{(j)}}{E_k^{(j)}} \right] - \frac{\Delta_j^2}{2E_k^{(j)}} \right\} \end{aligned} \tag{13.4.9}$$

The ground-state ket $|\Psi\rangle$ in Eq. (13.4.2) is a superposition of many-pairon states. Each component state can be reached from the physical vacuum state $|0\rangle$ by pair creation and/or pair annihilation of ± pairons and by pair correlation via a succession of phonon exchanges. Since phonon exchange processes are charge-conserving, the supercondensate is composed of equal numbers of ± pairons. The greatest possible numbers of + [–] pairons are given by $(1/2)\hbar\omega_D \mathcal{N}_1(0)$ [$(1/2)\hbar\omega_D \mathcal{N}_2(0)$]. We must then have

$$\mathcal{N}_1(0) = \mathcal{N}_2(0) \equiv \mathcal{N}(0) \tag{13.4.10}$$

In the bulk limit, sums over **k** can be converted into energy integrals; we obtain [Eq. (8.5.17)]

$$W = \sum_{j=1}^{2} \mathcal{N}(0) \int_0^{\hbar\omega_D} d\epsilon \left[\epsilon - \frac{\epsilon^2}{\left(\epsilon^2 + \Delta_j^2\right)^{1/2}} - \frac{\Delta_j^2}{2\left(\epsilon^2 + \Delta_j^2\right)^{1/2}} \right] = \frac{1}{2} N_0 (w_1 + w_2)$$

or

$$\boxed{W = \frac{1}{2} N_0 (w_1 + w_2)} \tag{13.4.11}$$

$$\boxed{w_i \equiv \hbar\omega_D \left\{ 1 - \left[1 + \left(\frac{\Delta_i}{\hbar\omega_D} \right)^2 \right]^{1/2} \right\} \ (< 0), \qquad N_0 \equiv \hbar\omega_D \mathcal{N}(0)} \tag{13.4.12}$$

Binding energies $|w_i|$ for ± pairons are different. To proceed further we must find Δ_j from the gap equations (13.4.8). In the bulk limit, these equations are simplified to [see Eq. (8.5.18)]

$$\begin{aligned} \Delta_j &= \frac{1}{2} v_{j1} \mathcal{N}(0) \int_0^{\hbar\omega_D} d\epsilon \frac{\Delta_1}{\left(\epsilon^2 + \Delta_1^2\right)^{1/2}} + \frac{1}{2} v_{j2} \mathcal{N}(0) \int_0^{\hbar\omega_D} d\epsilon \frac{\Delta_2}{\left(\epsilon^2 + \Delta_2^2\right)^{1/2}} \\ &= \frac{1}{2} v_{j1} \mathcal{N}(0) \Delta_1 \sinh^{-1}(\hbar\omega_D/\Delta_1) + \frac{1}{2} v_{j2} \mathcal{N}(0) \Delta_2 \sinh^{-1}(\hbar\omega_D/\Delta_2) \end{aligned} \tag{13.4.13}$$

whose solution will be discussed in Section 13.6.

13.5. HIGH CRITICAL TEMPERATURE; HEAT CAPACITY

In a layered superconductor, pairons move in a copper plane with a linear energy–momentum relation [see Eq. (8.4.25)]:

$$\epsilon = \frac{2 v_F p}{\pi} = cp \tag{13.5.1}$$

Earlier in Section 9.2, we saw that free bosons moving in two dimensions with a linear energy–momentum relation $\epsilon = cp$ undergoes a B–E condensation at [Eq. (9.2.11)]

$$T_c = 1.954\, \hbar c n^{1/2} k_B^{-1} \tag{13.5.2}$$

After using $c = 2v_F/\pi$, we obtain

$$\boxed{k_B T_c = 1.24\, \hbar v_F n_0^{1/2} = 1.24\, \hbar v_F r_0^{-1}} \tag{13.5.3}$$

where n_0 represents the number density of pairons in the superconductor and $r_0 \equiv n_0^{-1/2}$ is the average interpairon distance in two dimensions.

Let us compare our results with the case of elemental superconductors. The critical temperature T_c for three-dimensional superconductors can be expressed by

$$k_B T_c = 1.01\,\hbar v_F n_0^{1/3} = 1.01\,\hbar v_F r_0^{-1} \tag{13.5.4}$$

[Eq. (9.4.24)]. The similarity between Eqs. (13.5.3) and (13.5.4) is remarkable; in particular T_c depends on (v_F, r_0) in nearly the same way. Now the interpairon distance r_0 is different by the factor $10^2 \sim 10^3$ between type I and high-T_c. The Fermi velocity v_F is different by the factor $10 \sim 10^2$. Thus the *high* critical temperature can be explained by the very short interpairon distance, partially compensated by a smaller Fermi velocity. The critical temperature T_c is much lower than the Fermi temperature T_F. The ratio T_c/T_F can be computed from Eq. (13.5.3) and

$$k_B T_F = \frac{1}{2} m^* v_F^2 = \frac{\hbar^2 (2\pi n_{el})}{2m^*} = \frac{\pi \hbar^2}{m^* R_0^2} \tag{13.5.5}$$

yeilding

$$\boxed{\frac{T_c}{T_F} = 1.24 \left(\frac{2}{\pi}\right)^{1/2} \frac{R_0}{r_0} = 0.99 \frac{R_0}{r_0}} \tag{13.5.6}$$

which represents the law of corresponding states for T_c in two-dimensional superconductors. Note: Eq. (13.5.6) is remarkably close to the three-dimensional formula (9.5.13).

If we assume a two-dimensional Cooper system having a circular Fermi surface, we can calculate the ratio R_0/r_0 and obtain

$$R_0/r_0 = \left(\frac{\Theta_D}{2T_F}\right)^{1/2} \tag{13.5.7}$$

Introducing the pairon formation factor α (see Section 9.5.10), we can rewrite Eq. (13.5.6) as

$$\boxed{T_c = 0.70\,\alpha (\Theta_D T_F)^{1/2}} \tag{13.5.8}$$

which indicates that T_c is high if the Fermi temperature T_F and the Debye temperature Θ_D are both high. But the power laws are different compared to the corresponding three-dimensional Eq. (9.5.19). The observed pairon formation factor α for high-T_c cuprates are in the range $\sim 10^{-2}$, much greater than those for elemental superconductors. This is understandable, since the two-dimensional Fermi cylinders are intrinsically more symmetric than the three-dimensional Fermi surface, and the pairon formation is therefore more favorable.

We saw earlier in Section 8.6.6 that the interpairon distance r_0 in three dimensions is several times greater than the coherence length $\xi_0 = \hbar v_F/\pi\Delta$. For two dimensions, we obtain from Eq. (13.5.3)

$$r_0 = 6.89\,\xi_0 \tag{13.5.9}$$

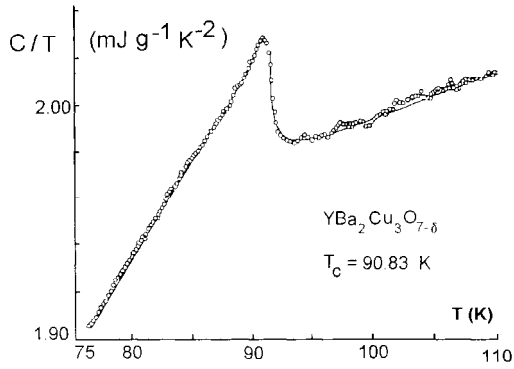

Figure 13.5. The electronic heat capacity near the critical temperature in YBCO [after Fisher *et al.* (Ref. 17)].

Experiments indicate that $\xi_0 = 14$ Å and $T_c = 94$ K for YBCO. Using these values, we estimate the value of the Fermi velocity v_F from Eq. (13.5.3) to obtain

$$v_F = 10^5 \text{ ms}^{-1} \tag{13.5.10}$$

The smallness of v_F partly explains the high thermodynamic critical field H_c of these materials, since $H_c \propto v_F$; see Eq. (11.1.8) and the following paragraph.

We now examine the heat capacity C near the superconducting transition. Since T_c is high, the electron contribution is very small compared to the phonon contribution. Systematic studies by Fisher *et al.*[17] of heat capacities of high-T_c materials (polycrystals) with and without applied magnetic fields indicate that there is a distinct maximum near T_c. A summary of the data is shown in Fig. 13.5. Since materials are polycrystals with a size distribution, the maximum observed is broader compared to those observed for pure metals. But the data are consistent with what is expected of a B–E condensation of free massless bosons in two dimensions, a peak with no jump at T_c with the T^2-law decline on the low temperature side. Compare Fig. 13.5 to Fig. 9.2.

13.6. TWO ENERGY GAPS; QUANTUM TUNNELING

The pairon size represented by the coherence length ξ_0 for YBCO is 14 Å. The density of conduction electrons that controls the screening effect is not high. Then the Coulomb repulsion between the constituting electrons is not negligible, so interaction strengths satisfy the inequalities:

$$v_{11} = v_{22} < v_{12} = v_{21} \tag{13.6.1}$$

As a result there are *two* quasi-electron energy gaps (Δ_1, Δ_2) satisfying [Eq. (13.4.13)]

$$\Delta_j = \frac{1}{2} \sum_i v_{ji} \mathcal{N}(0) \sinh^{-1}(\hbar\omega_D / \Delta_i) \tag{13.6.2}$$

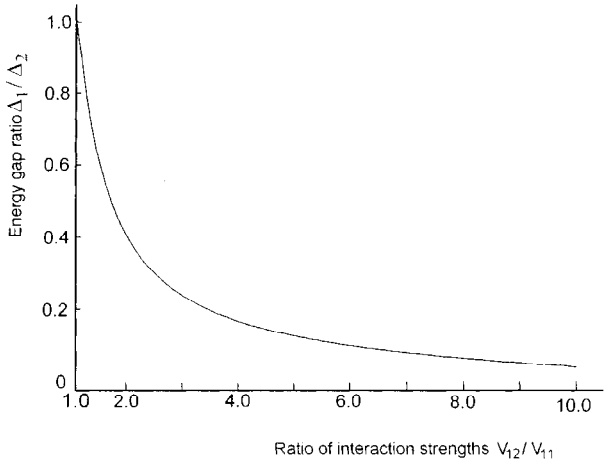

Figure 13.6. Variation of the ratio Δ_1/Δ_2 as a function of the ratio v_{12}/v_{11}.

The ratio Δ_1/Δ_2 of the two solutions of Eqs. (13.6.2) and its inverse Δ_2/Δ_1 satisfy the same equation. This means that we cannot determine from Eqs. (13.6.2) alone which types of pairons have the higher energy gaps $\in_j \equiv \in_{gj}$. To answer this question, we must examine the behavior of excited pairons. At any rate the ratio Δ_1/Δ_2 (or Δ_2/Δ_1) varies with the ratio of the interaction strengths v_{12}/v_{11}. This behavior is shown in Fig 13.6. Values of the ratio Δ_1/Δ_2 are sensitive near $v_{12}/v_{11} = 1$. Examining Eqs. (13.4.12) reveals that the greater the gap Δ_j, the greater is the binding energy $|w_j|$. Pairons with a greater Δ_j make a predominant contribution to ground-state energy. Quasi-electron energy gaps Δ_j generate the pairon energy gaps $\in_j$, which can be computed from Eqs. (10.5.9), (10.5.13), and (10.5.14). Examining these equations indicates that the greater the quasi-electron gap Δ_j, the greater the pairon gaps $\in_j$. Pairons with smaller gaps $\in_j$ are easier to excite, and these come from smaller gaps with smaller Δ_j. In summary pairons with greater Δ_j are major contributors to ground-state energy, but they are minor contributors to elementary excitations. The situation is thus rather complicated. In any event there are two energy gaps ($\in_1, \in_2$). Using this fact we now discuss the behavior of pairon energy gaps in quantum tunneling experiments. The appearance of energy gaps is one of the most important signatures of a superconducting state. A great number of quantum-tunneling studies have been made.[2–5,18] Since cuprate superconductors are ceramics and contain many imperfections, a wide range of scattered data were reported. The following general features however stand out: asymmetric *I–V* curve for *S–I–N* systems, a wide scatter of energy gaps data, and complicated conductance (dV/dI)–voltage (V) curves. We comment on these features separately.

13.6.1. Asymmetric I-V Curves for S–I–N

In Section 10.7 we showed that the *I–V* curve for a S_1–*I*–S_2(*N*) must in general be asymmetric. Briefly if the bias voltage is reversed, different charge carriers are involved in the quantum tunneling. Since moving pairons have two energy gaps ($\in_1, \in_2$), threshold

energies (V_{t1}, V_{t2}) are different, generating easily recognizable asymmetries. For a type I superconductor, there is a single energy gap ($\epsilon_1 = \epsilon_2$) and a single threshold voltage V_t for both polarities. In actual data for several types of cuprate superconductors, the difference between V_{t1} and V_{t2} is less than 3%, indicating

$$\frac{|\epsilon_1 - \epsilon_2|}{\epsilon_1} < 0.03 \tag{13.6.3}$$

13.6.2. Scattered Data for Energy Gaps

In Section 10.10.13, we showed that threshold voltage V_t for an *S–I–N* depends on the nature of the metal *N*. Consider two cases: *N* is a normal state superconductor and *N* is a true normal metal like Na and Pt. The threshold voltages are then different by a factor of 3 [see Eq. (10.10.8)]:

$$3V_a = V_c \tag{13.6.4}$$

which is consistent with most of the data on high-T_c superconductors. For *S* = YBCO:

$$2V_a = 8 \sim 10 \text{ mV and } 2V_c \text{ (Pt)} = 20 \sim 25 \text{ mV} \tag{13.6.5}$$

All experiments were done without knowledge of Eq. (13.6.4). Therefore no efforts were made to use different metals intentionally for *N*. Further systematic experiments are required to see how well Eq. (13.6.4) is observed.

13.6.3. Complicated I–V Curves

As previously stated, energy gaps (ϵ_1, ϵ_2) have a small difference. This means that pairons of both charge types are likely to be excited, generating complicated *I–V* curves.

In summary data for quantum tunnelings in high-T_c superconductors show more complicated features compared to the case of type I superconductors. All of the features coming from the existence of two pairon energy gaps (ϵ_1, ϵ_2) appear to be in agreement with experiment.

13.7. SUMMARY

High-T_c cuprates are conducting *layered* compounds. Thus the charge transport occurs only in the copper planes. Under the favorable condition, pairons of both charge types may be formed via optical phonon exchanges, bridging between electron-like and hole-like Fermi surface sheets. Since optical phonons exhibit quadratic energy–momentum relations of a massive boson type, the phonon-exchange attraction has a short range. As a result the pairon size is much smaller (~ 10 Å) in a cuprate than in a type I superconductor (~ 10^4 Å). Because of this smaller size, pairons can be packed much more densely. In fact the B–E condensation of pairons independently moving in two dimensions 2D with the Cooper–Schrieffer relation:

$$\epsilon = \epsilon_0 + \frac{2v_F}{\pi}p \tag{13.7.1}$$

occurs at

$$T_c = 1.24\hbar v_F n_0^{1/2} = 1.24\hbar v_F r_0^{-1} \qquad \text{(2D)} \tag{13.7.2}$$

which is similar to

$$T_c = 1.01\hbar v_F n_0^{1/3} = 1.01\hbar v_F r_0^{-1} \qquad \text{(3D)} \tag{13.7.3}$$

The (average) interpairon distance r_0 differs by the factor $10^2 \sim 10^3$ between elemental and high-T_c superconductors. The Fermi velocity v_F differs by the factor $10 \sim 10^2$. Therefore the critical temperature T_c in the cuprate superconductors is higher by factor of $10 \sim 10^2$ than in elemental superconductors. The B–E condensation in 2D is a phase transition of the second order. Heat capacity C has a maximum characterized by the T^2-law on the low-temperature side, and it is continuous at T_c, but the slope $\partial C/\partial T$ has a discontinuity, all in rough agreement with experiment. Since pairon size and conduction electron density are both small, the Coulomb repulsion between the constituting electrons is not negligible. Thus interaction strengths $\{v_{ij}\}$ between and among electron (1) and hole (2) pairons are different. Because of this, there are two gaps (Δ_1, Δ_2) in the quasi-electron energy spectra and again two gaps $(\in_1, \in_2)$ in the pairon energy spectra. The I–V curves for the quantum tunneling in S_1–I–N are asymmetric with more complicated features. The pairon speeds $c_i = 2v_F^{(i)}/\pi$ are much lower in high-T_c than in elemental superconductors. The thermodynamic critical field H_c ($\propto v_F$) is therefore much higher. The high-T_c cuprate is a type II superconductor, since $\xi_0 < \lambda$ (penetration depth); the upper critical field H_{c2} is high. These properties are favorable in devices and applications. The critical currents however are small. Currently great efforts are being made to raise critical currents (see Section 14.2).

The transport behaviors above T_c are found to be quite different from those of a normal metal, indicating that moving pairons contribute significantly in competition with normal electrons. Quantitative studies of these interesting behaviors are still lacking.

In summary, high-T_c cuprates can be treated within the framework of the present generalized BCS model.

REFERENCES

1. J. G. Bednorz and K. A. Müller, *Z. Phys. B. Cond. Matt.* **64,** 189 (1986).
2. J. W. Halley, ed., *Theory of High-Temperature Superconductivity* (Addison-Wesley, Redwood City, CA, 1988).
3. S. Lundquist, *et al.*, eds., *Towards the Theoretical Understanding of High-T_c Superconductivity*, Vol. 14 (World Scientific, Singapore, 1988).
4. D. M. Ginsberg, ed., *Physical Properties of High- Temperature Superconductors* (World Scientific, Singapore, 1989).
5. S. A. Wolf and W. Z. Kresin, *Novel Superconductivity* (Plenum, New York, 1989); Kitazawa, K. and Ishiguro, T. eds., *Advances in Superconductivity* (Springer, Tokyo, 1989).
6. M. K. Wu, *et al., Phys. Rev. Lett.* **58,** 908 (1987).
7. See, e.g., Ginsberg's overview, Ref. 4, pp. 1–38.
8. D. E. Farrell, *et al., Phys. Rev.* **B42,** 6758 (1990).
9. S. Godoy and S. Fujita, *J. Eng. Sci.* **29,** 1201 (1991).
10. J. H. Kang, R. T. Kampwirth, and K. E. Gray, *Appl. Phys. Lett.* **52,** 2080 (1988); M. J. Naughton, *et al., Phys. Rev.* **B 38,** 9280 (1988).
11. L. Onsager, *Phil. Mag.* **43,** 1006 (1952).

12. J. Wosnitza, *et al., Phys. Rev. Lett.* **67,** 263 (1991).
13. H. Yukawa, *Proc. Phys. Math. Soc. Jpn.* **17,** 48 (1935).
14. L. D. Landau, *Sov Phys. JETP,* **3,** 920 (1975); **5,** 101 (1975); **8,** 70 (1959).
15. L. N. Cooper, *Phys. Rev.* **104,** 2289 (1956).
16. J. Bardeen, L. N. Cooper, and J. R. Schrieffer, *Phys. Rev.* **108,** 1175 (1957).
17. R. A. Fisher, J. E. Gordon, and N. E. Phillips, *J. Supercond.* 1, 231 (1988).
18. T. Ekino, *et al., Physica C* **218,** 387 (1993); P. J. M. van Bentum, *et al., Phys. Rev.* B **36,** 843 (1987); F. Frangi, *et al., Sol. State Commun.* **81,** 599 (1992).

14

Summary and Remarks

14.1. SUMMARY

The most important properties of a superconductor are: (i) zero resistance, (ii) Meissner effect, (iii) flux quantization and Josephson effects, and (iv) excitation-energy gaps. These properties all arise from the motion of a supercondensate in the conductor below T_c. In the present text, we examined these and other superconductor properties from a quantum statistical mechanical point of view by taking pure elemental (type I) superconductors as primary examples.

The microscopic cause of type I superconductivity is well-established: It is caused by the phonon exchange attraction. Under certain conditions, conduction electrons near the Fermi surface form Cooper pairs (pairons) by exchanging acoustic phonons. Let us take a typical elemental superconductor such as lead (Pb). Such a metal has only acoustic phonons. These phonons are of course neutral, and therefore the states of two electrons between which a phonon is exchanged must have the same charge before and after the exchange. The virtual phonon exchange can generate an attraction if kinetic energies of the electrons involved are all close to each other. Thus this exchange generates an attractive correlation between electron (or hole) pair states whose energies are separated by twice the limit phonon energy $\hbar\omega_D$. Exchanging a phonon can also pair-create ± pairons from the physical vacuum. Because of this, if the Fermi surface is favorable, large and equal numbers of ± pairons are formed in the conductor. The phonon-exchange attraction is a quantum field theoretical effect, and therefore it cannot be explained by considering the potential energy alone. In fact the attraction depends on the kinetic energy of electrons.

Pairons move independently with a linear energy–momentum (Cooper–Schrieffer) relation:

$$w_q = w_0 + \frac{1}{2} v_F q < 0 \tag{14.1.1}$$

where

$$w_0 \equiv \frac{-2\hbar\omega_D}{\exp[2/v_0\mathcal{N}(0)] - 1} \tag{14.1.2}$$

is the ground-state energy of a pairon. In these respects they are very similar to photons. Unlike photons however pairons have charges of $\pm 2e$, and the total number of ± pairons

in a superconductor is limited. At 0 K the stationary conductor may contain great and equal numbers of ± pairons all condensed at zero momentum.

The most striking superconducting phenomenon is a never-decaying supercurrent ring, where the first three properties (i)–(iii) appear. In a flux quantization experiment, a weak supercurrent goes around the ring, enclosing the magnetic flux. This may be interpreted as follows. Macroscopic numbers of ± pairons are condensed at a single momentum:

$$q_n \equiv \frac{2\pi n\hbar}{L} \tag{14.1.3}$$

where L is the ring length and n a quantum number (0, ± 1, ±2, …) such that the flux Φ enclosed by the ring is n times the flux quantum $\Phi_0 \equiv h/2e$:

$$\Phi = n\Phi_0 \equiv n\frac{h}{2e} \tag{14.1.4}$$

The appearance of the factor $2e$ means that the charge (magnitude) of the current-carrying particle is twice the electron charge e, supporting the BCS picture of a supercondensate composed of pairons of charge (magnitude) $2e$.

The macroscopic supercurrent generated by the supercondensate in motion is not destroyed by microscopic impurities. This condition is somewhat similar to the situation in which a flowing river (large object) is perturbed but cannot be stopped by a stick (small object). The fact that small perturbations cause no energy loss comes from the quantum nature of the superconducting state. The change in the many-boson-condensed state requires redistributing a great number of pairons. Furthermore the supercurrent state can refocus by itself if the perturbation is not too strong. This is a quantum statistical effect peculiar to condensed bosons moving in space with a linear energy–momentum relation. This self-focusing power is most apparent in the Josephson interference, where two supercurrents macroscopically separated up to 1 mm can interfere with each other as do two laser beams from the same source. Thus there is close similarity between supercurrent and laser.

In the steady state, as realized in a circuit containing superconductor, resistor, and battery, all flowing currents in the superconductor are supercurrents. These supercurrents run in the thin surface layer characterized by the penetration depth λ (~500 Å), and they keep the magnetic field off the interior (Meissner effect). The current density j in a superconducting wire can be represented by

$$j = \frac{1}{2}en_0(v_F^{(2)} - v_F^{(1)}) \tag{14.1.5}$$

where n_0 is the total density of condensed pairons. The ± pairons move in the same direction, but their speeds, $v_F^{(j)}/2$, are different, and therefore the net current does not vanish. If a magnetic field **B** is applied, the Lorentz-magnetic force tends to separate ± pairons. Thus there is a critical magnetic field B_c. The supercurrent by itself generates a magnetic field, so there must be a critical current. The picture of a neutral moving supercondensate explains why the superconducting state of all materials is similar, and why the superconducting state is not destroyed by an applied electric field **E.** Since there is no net charge, $Q = 0$, no Lorentz-electric force F_E can act on the supercondensate:

$F_E \equiv QE = 0$. Thus the supercurrent is not accelerated, so it cannot gain energy from the applied voltage.

The system of free pairons (bosons) moving in three dimensions with the linear energy–momentum relation [Eq. (14.1.1)] undergoes B–E condensation at the critical temperature T_c given by

$$k_B T_c = 1.01\,\hbar v_F n_0^{1/3} \tag{14.1.6}$$

$$n_0 \equiv \frac{\hbar\omega_D \mathcal{N}(0)}{V} \tag{14.1.7}$$

The condensation transition is a phase change of second order. The heat capacity has a jump at T_c. Below T_c there is a supercondensate made up of ± pairons condensed at zero momentum. The density of condensed pairons increases to the maximum n_0 as temperature is lowered toward 0 K. Quasi-electrons in the presence of the supercondensate show an energy gap Δ. This gap Δ is temperature-dependent, and it reaches its maximum Δ_0 at 0 K. The maximum gap Δ_0 can be connected to the critical temperature T_c by

$$2\Delta_0 = 3.53\,k_B T_c \tag{14.1.8}$$

in the weak coupling limit. Phonon exchange is in action at all time and at all temperatures. Thus two quasi-electrons may be bound to form excited or moving pairons. Since quasi-electrons have an energy gap Δ, excited pairons also have an energy gap ϵ_g, which is temperature-dependent. The pairon energy gap $\epsilon_g(T)$ grows to its maximum equal to the binding energy of a Cooper pair $|w_0|$ as temperature is lowered toward 0 K.

Excited pairons have negative energies, while quasi-electrons have positive energies. By the Boltzmann principle, excited pairons are therefore more numerous than quasi-electrons, and they are the predominant elementary excitations below T_c. Pairon energy gaps strongly influence heat capacity $C(T)$ below T_c. The $C(T)$ far from T_c shows an exponential-decay-type T-dependence due to the energy gap ϵ_g; the maximum heat capacity $C_{\max}$ at T_c is modified by a small but nonnegligible amount. The energy gap ϵ_g between excited and condensed pairons can be probed by quantum-tunneling experiments. The threshold voltage V_a in the *I–V* curve for an *S–I–S* system can be connected simply with ϵ_g:

$$V_a = \frac{\epsilon_g(T)}{e} \tag{14.1.9}$$

This allows direct observation of the energy gap ϵ_g as a function of T.

From their intrinsic lattice structures, compound superconductors have optical and acoustic phonons. The Cooper pairs formed, mediated by optical phonons bridging between electron-like and hole-like Fermi surfaces, have smaller linear sizes ξ_0 (~ 50 Å). Thus these superconductors show type II behavior. The critical temperature T_c tends to be higher, since pairons can be packed more densely [see Eq. (14.1.6)].

High-T_c cuprate superconductors have layered lattice structures. Conduction electrons move only perpendicular to the *c*-axis. Since they are compounds, ± pairons can be generated with the aid of optical phonons bridging between electron-like and hole-like two-dimensional Fermi surfaces. The pairon size is small (~ 14 Å for YBCO), and

pairons may be packed even more densely. The critical temperature T_c, based on the model of free massless bosons moving in two dimensions, is given by

$$T_c = 1.24\,\hbar k_B^{-1} v_F n_0^{1/2} \tag{14.1.10}$$

The interpairon distance $r_0 \equiv n_0^{-1/2}$ is much smaller in cuprates than in elements, and the Fermi velocity v_F is smaller, making the critical temperature T_c higher. Since pairon size is small, the Coulomb repulsion between two electrons is not negligible. This generates two energy gaps (Δ_1, Δ_2) for quasi-electrons and two energy gaps (ϵ_1, ϵ_2) for moving pairons. Thus *I–V* curves for high T_c are more complicated.

We have treated all superconductors in a unified manner, starting with a generalized BCS Hamiltonian *H* in Eq. (8.2.1) and taking electron and phonon energy bands into consideration. The underlying assumption is that ± pairons are generated from the physical vacuum by emission and absorption of virtual phonons under favorable conditions. Alkali metals like Na have nearly spherical Fermi surfaces, such metals have electrons only; they cannot therefore be superconductors. Multivalent nonmagnetic metallic elements may generate ± pairons near hyperboloidal Fermi surfaces, so they are most often superconductors.

14.2. REMARKS

In the text we have discussed primarily chemically-pure, lattice-perfect, bulk-size superconductors. Many important superconducting properties arise in imperfect superconductors. We briefly discuss some of these properties in the following subsections.

14.2.1. Thin Films

If the dimension of a sample in some direction is less than the penetration depth λ, as in a thin film, the superconductor sample's critical temperature is a little higher than in a bulk sample. This may be explained as follows. Consider a very thin cylindrical supercurrent ring. The superconducting sample tends to expel any magnetic field at the expense of stored magnetic field energy. This expulsion is not complete because of the sample dimension; therefore stored magnetic energy is less than in bulk sample, making the superconducting state more stable and rendering T_c a little higher.

14.2.2. Nonmagnetic Impurities

A little amount of nonmagnetic impurities neither hinder the supercurrent nor alter the supercondensate density. This means that adding nonmagnetic impurities should not change T_c drastically. The impurities however significantly affect the coherence length ξ and the penetration depth λ. These effects are often described by

$$\frac{1}{\xi} = \frac{1}{\xi_0} + \frac{1}{l}, \qquad \lambda = \lambda_0 \left(\xi_0/\xi\right)^{1/2} \tag{14.2.1}$$

where *l* is the electron mean free path and (ξ_0, λ_0,) represent the values of (ξ, λ) for pure superconductor. According to Eq. (14.2.1), the addition of impurities makes ξ smaller and λ greater. This is experimentally supported by the fact that alloys like Pb–In_x show type II behavior if the fraction *x* is made high enough.

14.2.3. Magnetic Impurities

Ferromagnetic elements, such as iron (Fe) and nickel (Ni), are not superconductors. These metals of course have electrons and phonons. Thus spontaneous magnetization and the associated magnetic field are thought to be detrimental to the formation of Cooper pairs. Injection of magnetic ions in a superconductor lowers T_c significantly. This may be understood as follows. A Cooper pair is made up of electrons with up and down spins. The internal magnetic field destroys the symmetry between up and down spins; this makes the pairon formation less favorable, which lowers pairon density and the critical temperature.

14.2.4. Intermediate State

When a magnetic field $\mathbf{H}_a$ is applied along the axis of a cylindrical superconductor, surface supercurrents are generated to shield the B-field from the body with no loss of energy. If the superconductor has a poor geometrical shape and/or the H_a-field lies in the wrong direction, then it will be in the *intermediate state*, where normal and superconducting domains are formed side-by-side. The actual domain structures can be very complicated. We have avoided this complication completely in the text by assuming the ideal condition where the H_a-field is directed along the axis of a long cylindrical superconductor.

14.2.5. Critical Currents; Silsbee's Rule

How much current can be passed through a superconductor without generating resistance? This is an important question in devices and applications. As we mentioned in Subsection 14.2.4, the actual supercurrent configuration may be very complicated. It is recognized that a superconductor loses its zero resistance when at any point on the surface, the total magnetic field due to the transport current and the applied field exceeds the critical field B_c. This is often called the generalized *Silsbee's rule.*[1] (The original Silsbee's rule, proposed by this author in 1916, refers to the case of zero external field.) In our condensed pairon picture, a supercurrent is generated by ± pairons moving in the same direction with different speeds (c_1, c_2). Any B-field tends to separate these ± pairons with a magnetic force. Silsbee's rule is in accord with this picture.

14.2.6. Mixed State; Pinning Vortex Lines

Type II superconductors are more useful in devices and applications than type I because the upper (or superconducting) critical field H_{c2} can be much higher. Between the lower and upper critical fields (H_{c1}, H_{c2}), a type II superconductor allows partial penetration of elementary magnetic flux lines (vortices), which forms a two-dimensional lattice. Such a state is called a *mixed state*, distinct from the intermediate state discussed earlier. Elementary vortices repel each other. If the vortex lattice is perfect, there is no net current. In the actual current-carrying state, vortices are *pinned* by various lattice imperfections, and the resulting inhomogeneous vortex configuration generates a net supercurrent. In practice lattice imperfections are purposely introduced in the fabrication processes, and details of the flux (vortex) pinning are very complicated.

14.2.7. Critical Currents in Type II Superconductors

If the applied magnetic field H_a is less than the lower critical field H_{c1}, the critical current tends to decrease linearly with increasing field H_a. (The same behavior is observed in type I superconductors.) The associated B-field in the surface layer tends to disrupt the motion of ± pairons by the Lorentz force, causing a linear H_a-decrease in the critical current. The practically important case however is the one where the applied field H_a is higher than H_{c1} so that vortex lines penetrate the body. Experiments indicate that the more imperfect the sample, the higher is the critical current. This behavior arises from flux pinning by imperfections; besides the transport current appears to flow throughout the whole body. The phenomena are therefore quite complicated; but since this is very important in devices and application, extensive researches is currently being carried out.

14.2.8. Concluding Remarks

The traditional statistical mechanical theory deals with equilibrium thermodynamic properties and steady-state transport and optical properties of a macroscopic system. When a system contains super and normal domains or inhomogeneous pinning of vortex lines, theories must be developed case by case. In fact there is no unified theory dealing with such cases. Future challenging research includes seeking higher and higher T_c-materials and raising critical currents for larger-scale applications. Such research requires a great deal of efforts and creative minds. The authors hope the elementary quantum statistical theory of superconductivity presented here will be a useful guide for the exciting future developments.

REFERENCE

1. F. B. Silsbee, *J. wash. Acad. Sci.* **6,** 597 (1916).

Appendix A

Quantum Mechanics

The principles of quantum mechanics for a particle are briefly surveyed in this appendix. Schrödinger and Heisenberg pictures are discussed.

A.1. FUNDAMENTAL POSTULATES OF QUANTUM MECHANICS

Five fundamental quantum postulates are summarized below:

1. It is postulated that *to each quantum state of a system there corresponds a unique column vector* to within the normalization constant for length. Such a vector, denoted by $|\psi\rangle$, is called a *ket vector*. It is assumed that the ket $|\psi\rangle$ and the ket $c|\psi\rangle$, c = a nonzero complex number, correspond to the same quantum state. This same state can also be represented by the *bra vector* $\langle\psi|$, which is the Hermitian conjugate of $|\psi\rangle : \langle\psi| = (|\psi\rangle)^\dagger$. In simple terms $\langle\psi|$ is a *row vector* having the same elements complex-conjugated (denoted by the asterisk) as the column ket vector $|\psi\rangle$. The null ket (see below) does not correspond to any quantum state. If $|A\rangle$ and $|B\rangle$ are kets, then so is the vector sum $|A\rangle + |B\rangle$ (superposition). The scalar product of a ket $|A\rangle$ and a bra $\langle B|$ can be defined, and it is denoted by $\langle B| \cdot |A\rangle \equiv \langle B|A\rangle$. The length of a vector is given by $(\langle A|A\rangle)^{1/2}$. If $\langle A|A\rangle = 0$, then $|A\rangle$ is the null ket. The following properties are postulated (Problem A. 1.1):

$$\begin{aligned} |A\rangle + |B\rangle &= |B\rangle + |A\rangle \\ |A\rangle + (|B\rangle + |C\rangle) &= (|A\rangle + |B\rangle) + |C\rangle \qquad \text{(A.1.1)} \\ \langle A|(c|B\rangle) &= c\langle A|B\rangle \\ (c|A\rangle)^\dagger|B\rangle &= [c^*\langle A|]|B\rangle \equiv c^*\langle A|B\rangle \qquad \text{(A.1.2)} \\ (\langle A|B\rangle)^* &= \langle B|A\rangle, \qquad \langle A|A\rangle \geq 0 \\ \langle A|(|B\rangle + |C\rangle) &= \langle A|B\rangle + \langle A|C\rangle \end{aligned}$$

2. A *linear operator* α is defined by the relations:

$$\begin{aligned} |B\rangle &= \alpha|A\rangle \\ \alpha(|A\rangle + |C\rangle) &= \alpha|A\rangle + \alpha|C\rangle \\ \alpha(c|A\rangle) &= c\alpha|A\rangle \qquad \text{(A. 1.3)} \end{aligned}$$

where the first equation defines a ket $|B\rangle$ as a function of another ket $|A\rangle$, and the last two define the linearity of the operator α. (Problem A.1.2)

Linear operators can be added and multiplied together. If α and γ are two linear operators, the sum $\alpha + \gamma$ and the product $\alpha\gamma$ are defined, respectively, by

$$(\alpha + \gamma)|A\rangle \equiv \alpha|A\rangle + \gamma|A\rangle \tag{A.1.4}$$

$$(\alpha\gamma)|A\rangle \equiv \alpha(\gamma|A\rangle) \equiv \alpha\gamma|A\rangle \tag{A.1. 5}$$

The product $\alpha\gamma$ is not in general equal to the product of the reversed order $\gamma\alpha$:

$$\alpha\gamma \neq \gamma\alpha \tag{A. 1.6}$$

A linear operator α may also be defined relative to bra vectors such that

$$(\langle A_m|\alpha)|A_n\rangle = \langle A_m|(\alpha|A_n\rangle) \equiv \langle A_m|\alpha|A_n\rangle \equiv \alpha_{mn} \tag{A.1.7}$$

for any $|A_n\rangle$ and $\langle A_m|$. The *Hermitian conjugate* of α, denoted by $\alpha^\dagger$, is defined by

$$\langle A_m|\alpha^\dagger|A_n\rangle = (\langle A_n|\alpha|A_m\rangle)^* \quad \text{or} \quad (\alpha^\dagger)_{mn} = \alpha^*_{nm} \tag{A.1.8}$$

for every A_m and A_n. A linear operator equal to its adjoint:

$$\alpha^\dagger = \alpha \tag{A.1.9}$$

is called a *Hermitian operator.*

Such quantities as Hamiltonian, position, velocity, momentum, and angular momentum are called physical variables. *All observable physical variables are, by postulate, represented by Hermitian operators.*

If ξ is a Hermitian operator, then we can set up an *eigenvalue equation*:

$$\xi|\xi'\rangle = \xi'|\xi'\rangle \tag{A.1.10}$$

where $|\xi'\rangle \neq 0$ is an *eigenket* (vector), and the *eigenvalue* (number) ξ' can be shown to be real (Problem A.1.4). It is assumed that eigenvectors $|\xi'\rangle$ form a complete orthonormal set of vectors. Orthonormal means that

$$\langle\xi'|\xi''\rangle = \delta_{\xi'\xi''} \tag{A.1.11}$$

where the right-hand term is the Kronecker delta for the case of discrete spectra and the Dirac delta function [see Eq. (A.2.4)] for continuous spectra. *Completeness* means that any ket vector can be expanded in terms of $|\xi'\rangle$ as follows:

$$|\psi\rangle = \sum_{\xi'} |\xi'\rangle\langle\xi'|\psi\rangle \quad \text{or} \quad \mathbf{1} = \sum_{\xi'} |\xi'\rangle\langle\xi'| \tag{A.1.12}$$

3. It is postulated that by means of experiment, we can recognize and isolate a complete set of compatible observables represented by a set of commuting Hermitian operators $\xi, \eta, \ldots$, whose eigenvalues determine the possible quantum states of the system uniquely. We can then expand an arbitrary state represented by $|\psi\rangle$ as follows:

$$|\psi\rangle = \sum_{\xi'} \sum_{\eta' \ldots} |\xi'\eta' \ldots\rangle\langle\xi'\eta' \ldots|\psi\rangle \tag{A.1.13}$$

$$|\xi'\eta' \ldots\rangle \equiv |\xi'\rangle|\eta'\rangle \ldots \tag{A.1.14}$$

If $|\psi\rangle$ represents a state of the system at the moment when measurement takes place, the *probability of finding the system in the state* ξ', η', . . . , by postulate is given by

$$|\langle\xi'\eta' \ldots|\psi\rangle|^2 \equiv \langle\xi'\eta' \ldots|\psi\rangle\langle\psi|\xi'\eta' \ldots\rangle \geq 0 \tag{A.1.15}$$

4. In the *Schrödinger picture* the dynamic state of a system changes with time *t*. It is postulated that the temporal change of the Schrödinger state represen ted by a ket $|\psi,t\rangle$ is d etermined from the *Schrödinger equation of motion*:

$$i\hbar\frac{d}{dt}|\psi,t\rangle = H|\psi,t\rangle \tag{A.1.16}$$

where H is the Hamiltonian operator characterizing the system; the operator in many cases has the same functional form as the Hamiltonian in classical mechanics. The *expectation value* of an observable ξ at time t by postulate is given by

$$\langle\xi\rangle_t \equiv \langle\psi,t|\xi|\psi,t\rangle \tag{A.1.17}$$

5. Physical variables do not necessarily commute with each other. To make the description complete, we must supply commutation rules. If the three-dimensional motion of a particle is described by Cartesian coordinates q_r and momenta p_r, $r = 1, 2, 3$, the commutation rules are

$$[q_r, p_s] \equiv q_r p_s - p_s q_r = i\hbar\delta_{rs} \tag{A.1.18}$$

In dealing with spin angular momentum operators, special rules are required.

Problem A. 1.1. Assume

$$|A\rangle = \begin{pmatrix} a_1 \\ a_2 \end{pmatrix}$$

Then $\langle A| = (a_1^*, a_2^*)$. Show that (a) $\langle A|A\rangle \geq 0$, (b) $(\langle A|B\rangle)^* = \langle B|A\rangle$.

Problem A. 1.2. Assume

$$\alpha = \begin{pmatrix} a_{11} & a_{12} \\ a_{21} & a_{22} \end{pmatrix}, \qquad |A\rangle = \begin{pmatrix} a_1 \\ a_2 \end{pmatrix}, \qquad |B\rangle = \begin{pmatrix} b_1 \\ b_2 \end{pmatrix}$$

Verify the linearity of operator α.

Problem A.1.3. Pauli's spin matrices ($\sigma_x, \sigma_y, \sigma_z$) are defined by

$$\sigma_x = \begin{pmatrix} 0 & 1 \\ 1 & 0 \end{pmatrix}, \qquad \sigma_y = \begin{pmatrix} 0 & -i \\ i & 0 \end{pmatrix}, \qquad \sigma_z = \begin{pmatrix} 1 & 0 \\ 0 & -1 \end{pmatrix}$$

By inspection these are Hermitian. Show that (a) $\sigma_x^2 = \sigma_y^2 = \sigma_z^2 = 1$. (b) $[\sigma_y, \sigma_z] \equiv \sigma_y\sigma_z - \sigma_z\sigma_y = 2i\sigma_x$. (c) $\{\sigma_y, \sigma_z\} \equiv \sigma_y\sigma_z + \sigma_z\sigma_y = 0$.

Problem A.1.4. (a) Write down the eigenvalue equations for ($\sigma_x, \sigma_y, \sigma_z$). (b) Find the eigenvalues of ($\sigma_x, \sigma_y, \sigma_z$).

A.2. POSITION AND MOMENTUM REPRESENTATIONS; SCHRÖDINGER'S WAVE EQUATION

A.2.1. Position Representation

In the present appendix quantum mechanics of a single particle is reviewed. A system of many identical particles is treated in Appendix C.

Let us consider a particle moving on a line of an infinite length. The system is characterized by the Hamiltonian:

$$h(x,p) = \epsilon(p) + v(x) \tag{A.2.1}$$

where x and p are Hermitian operators representing the position and the momentum of the particle; $\epsilon(p) = p^2/2m$ is the kinetic energy and $v(x)$ a potential.

One of the basic observables of the system is the position x. The eigenvalue equation for this observable is

$$x \mid x' \rangle = x' \mid x' \rangle \tag{A.2.2}$$

The spectrum of its eigenvalues x' is continuous and covers the infinite line. If we take any two eigenstates x' and x'' and form their scalar product, we obtain the orthonormality relation

$$\langle x' \mid x'' \rangle = \delta(x' - x'') \tag{A.2.3}$$

where $\delta(y)$ is a Dirac *delta function.* The latter is defined by the relations:

$$\delta(y) = 0 \text{ if } y \neq 0; \qquad \int_{-\infty}^{\infty} f(y)\delta(y)dy = f(0) \tag{A.2.4}$$

where $f(y)$ is an arbitrary function continuous at $y = 0$ and the integration passes through the point $y = 0$ from the negative to the positive. This definition is meaningful only when we consider the integration.

The matrix representation of the position operator x using the base x' is

$$\langle x''|x|x'\rangle = \langle x''|x'|x'\rangle = x'\langle x''|x'\rangle = x'\delta(x' - x'') \tag{A.2.5}$$

The matrix representation using eigenstates of the position operator as base is called the *position representation.* In this representation every variable $f(x)$ that depends only on the position is diagonal:

$$\langle x''|f(x)|x'\rangle = \langle x''|f(x')|x'\rangle = f(x')\delta(x' - x'') \tag{A.2.6}$$

The basic vectors form a complete set:

$$\int_{-\infty}^{\infty} |x'\rangle dx' \langle x'| = 1 \tag{A.2.7}$$

If an observable is a function $f(x,p)$ of the momentum and the position, it is not diagonal in the position representation. By postulate 5, p and x do not commute but satisfy the relation:

$$xp - px = i\hbar \tag{A.2.8}$$

We can show from this (Problem A.2.1) that the operator p is equivalent to the following operator except for an unimportant phase factor:

$$p = \frac{\hbar}{i}\frac{d}{dx} \tag{A.2.9}$$

where the latter is defined by (Problem A.2.2):

$$\left\langle x' \left| \frac{d}{dx} \right| \psi \right\rangle \equiv \frac{d}{dx'}\langle x'|\psi\rangle, \qquad \left\langle \psi \left| \frac{d}{dx} \right| x' \right\rangle = -\frac{d}{dx'}\langle \psi|x'\rangle \tag{A.2.10}$$

Using the last few equations, we obtain

$$\langle x'|f(x,p)|\psi\rangle = f\left(x', -i\hbar\frac{d}{dx'}\right)\langle x'|\psi\rangle \tag{A.2.11}$$

A.2.2. Momentum Representation

The momentum p of a particle is another basic observable. It is as important as the position x, as seen in the fundamental commutation rule Eq. (A.2.8).

We enumerate the following important properties:

Eigenvalue equation:

$$p\,|\,p'\rangle = p'\,|\,p'\rangle, \qquad -\infty < p' < +\infty \tag{A.2.12}$$

Orthonormality:

$$\langle p''\,|\,p'\rangle = \delta(p'' - p') \tag{A.2.13}$$

Completeness:

$$\int_{-\infty}^{\infty} |p'\rangle dp' \langle p'| = \mathbf{1} \tag{A.2.14}$$

Equivalent relations:

$$x = i\hbar \frac{d}{dp} \tag{A.2.15}$$

$$\langle p'|f(x,p)|\psi\rangle = f\left(i\hbar \frac{d}{dp'}, p'\right) \langle p'|\psi\rangle \tag{A.2.16}$$

The representation in which the momentum is diagonal is called the *momentum representation.*

From Eqs. (A.2.11) and (A.2.12), we obtain

$$\langle x'|p|p'\rangle = p' \langle x'|p'\rangle = -i\hbar \frac{d}{dx'} \langle x'|p'\rangle \tag{A.2.17}$$

whose solution is

$$\langle x'|p'\rangle = c(p') e^{ip'x'/\hbar}$$

where $c(p')$ is a function of p'. From the symmetry between x and p and the orthonormality:

$$\langle p''|p'\rangle = \int_{-\infty}^{\infty} \langle p''|x'\rangle dx' \langle x'|p'\rangle = \delta(p'' - p') \tag{A.2.18}$$

we can determine $c(p')$ so that

$$\langle x'|p'\rangle = \frac{1}{(2\pi\hbar)^{1/2}} e^{ip'x'/\hbar} \tag{A.2.19}$$

If the particle is confined on a line of period L, the momentum eigenvalues become discrete:

$$p' = \frac{2\pi\hbar}{L} n \equiv p_n, \qquad n = \ldots, -1, 0, 1, 2, \ldots \tag{A.2.20}$$

Equations (A.2.18) and (A.2.19) will be replaced by (Problem A.2.3)

$$\langle p''|p'\rangle = \int \langle p''|x'\rangle dx' \langle x'|p'\rangle = \delta_{p''p'} \tag{A.2.21}$$

$$\langle x'|p'\rangle = \frac{1}{L^{1/2}} e^{ip'x'/\hbar} \tag{A.2.22}$$

A.2.3. Schrödinger's Energy Eigenvalue Equation

In many cases we are interested in the energy of the system. The problem is then to solve the energy eigenvalue equation:

$$h \mid E\rangle = E \mid E\rangle \tag{A.2.23}$$

where h is the Hamiltonian and E its eigenvalue. Multiplying Eq. (A.2.20) from the left by bra $\langle x' \mid$, we obtain

$$\langle x'|h(x,p)|E\rangle = h\left(x', -i\hbar\frac{d}{dx'}\right)\langle x'|E\rangle = E\langle x'|E\rangle \tag{A.2.24}$$

If we regard the numbers $\langle x \mid E\rangle$ as a function of x, where we dropped the primes indicating position eigenvalues, and write

$$\langle x|E\rangle \equiv \psi_E(x) \tag{A.2.25}$$

then Eq. (A.2.24) reads

$$h\left(x, -i\hbar\frac{d}{dx}\right)\psi_E(x) = \left(-\frac{\hbar^2}{2m}\frac{d^2}{dx^2} + v(x)\right)\psi_E(x) = E\psi_E(x) \tag{A.2.26}$$

This is *Schrödinger's energy eigenvalue equation.* The function $\psi_E(x)$ defined in Eq. (A.2.25) is called the *wave function.* Its absolute square $|\psi_E(x)|^2$ gives by postulate the (relative) probability of finding the particle in the neighborhood of x when the particle is in the energy eigenstate E.

A.2.4. Schrödinger's Equation of Motion

Define

$$\langle x, \mid \psi, t\rangle \equiv \psi(x, t) \tag{A.2.27}$$

which is an ordinary (c-number) function of (x, t). We multiply Eq. (A.1.16) from the left by $\langle x \mid$ and obtain

$$i\hbar\frac{\partial}{\partial t}\psi(x,t) = H\left(x, -i\hbar\frac{\partial}{\partial x}\right)\psi(x,t) = \left(-\frac{\hbar^2}{2m}\frac{\partial^2}{\partial x^2} + v(x)\right)\psi(x,t) \tag{A.2.28}$$

which is called *Schrödinger's equation of motion.* It describes how the wave function $\psi(x, t)$ changes in time. The wave function $\psi(x, t)$ is normalized such that

$$\int dx\, \psi^*(x,t)\psi(x,t) = \langle\psi, t|\psi, t\rangle = 1 \tag{A.2.29}$$

The preceding equations can be extended immediately to the three-dimensional case.

Problem A.2.1. Show that $\langle x'|[x(-i\hbar d/dx) - (-i\hbar d/dx)x]|\psi\rangle = i\hbar\langle x'|\psi\rangle$

Problem A.2.2. Show the equivalence between the two in Eqs. (A.2.10).

Problem A.2.3. Verify Eqs. (A.2.21) and (A.2.22). Use Eqs. (A.1.11) and (A.1.12).

A.3. SCHRÖDINGER AND HEISENBERG PICTURES

In the preceding sections, the quantum mechanical equation of motion is set up for the dynamic state in the *Schrödinger picture.* It is possible to describe the temporal evolution of the system from other points of view. (The discussions in this section can be extended to a many-particle system.)

The expectation value of an arbitrary observable ξ at time t is, by postulate 4, given by $\langle \psi, t | \xi | \psi, t \rangle$. In the quantum mechanical description, it is the most important kind of quantity that can be tested experimentally. In general there is a number of possible descriptions in which the expectation value has the same numerical value as $\langle \psi,t | \xi | \psi,t \rangle$. Every one of them is then regarded as equivalent to the Schrödinger description. A very important description due to Heisenberg is discussed in this section. By postulate the Schrödinger ket $|\psi, t\rangle$satisfies the equation of motion Eq. (A.1.16). The two kets $|\psi, 0\rangle$ and $|\psi, t\rangle$, representing the two Schrödinger states at two different times 0 and t, are related by

$$|\psi, t\rangle \equiv |\psi, t\rangle_S = U(t,0)|\psi, 0\rangle_S \equiv U(t)|\psi\rangle_S \tag{A.3.1}$$

where $U(t)$ is the solution of the differential equation:

$$i\hbar \frac{d}{dt} U(t) = H(t)U(t) \tag{A.3.2}$$

with the initial condition

$$U(0) = 1 \tag{A.3.3}$$

The U has the *unitary* property:

$$UU^\dagger = U^\dagger U = 1 \tag{A.3.4}$$

Let us prove part of Eq. (A.3.4) by mathematical induction for a continuous variable. The proof proceeds in two steps:

Step 1: At the initial time 0, we verify

$$U(0)U^\dagger(0) = 1 \cdot 1 = 1$$

Step 2: We assume that the property is valid for an arbitrary time t: $U(t)U^\dagger(t) = 1$. We then prove that this property is also valid for time $t + dt$: $U(t + dt)U^\dagger (t+ dt) = 1$. This means that the time derivative of $U(t)U^\dagger(t)$ must vanish. In fact

$$\frac{d}{dt}\left(U(t)U^\dagger(t)\right) = \frac{dU}{dt}U^\dagger + U\frac{dU^\dagger}{dt} = \frac{1}{i\hbar}HUU^\dagger + U\left(\frac{-1}{i\hbar}\right)U^\dagger H = 0 \qquad \text{q.e.d.}$$

The unitary property of U assures conservation of normalization condition (Problem A.3.1):

$$\langle \psi, t | \psi, t \rangle = {}_S\langle \psi | U^\dagger(t)U(t) | \psi \rangle_S = {}_S\langle \psi | \psi \rangle_S = 1 \tag{A.3.5}$$

Let us now introduce a ket $|\psi\rangle_H$, called a Heisenberg ket, defined by

$$|\psi\rangle_H \equiv U^\dagger(t)|\psi,t\rangle_S = U^\dagger(t)U(t)|\psi,0\rangle_S = |\psi,0\rangle_S \tag{A.3.6}$$

which does not change with time t. We also define the Heisenberg observable $\xi_H(t)$ by

$$\xi_H(t) \equiv U^\dagger(t)\xi U(t) \tag{A.3.7}$$

which is time-dependent. In terms of these new quantities, the expectation value of the observable at time t can be expressed by

$${}_H\langle\psi|\xi_H(t)|\psi\rangle_H = {}_S\langle\psi,0|U^\dagger(t)\xi U(t)|\psi,0\rangle_S = \langle\psi,t|\xi|\psi,t\rangle \tag{A.3.8}$$

Differentiating Eq. (A.3.7) with respect to t and using Eq. (A.3.2) and its adjoint, we obtain the following differential equation (Problem A.3.3):

$$i\hbar\frac{d\xi_H(t)}{dt} = [\xi_H(t), H_H(t)] \tag{A.3.9}$$

$$H_H(t) \equiv U^\dagger(t)H(t)U(t) \tag{A.3.10}$$

We may interpret the last five equations as follows. Instead of having temporally fixed observables ξ and moving state vectors $|\psi, t\rangle$, in the new picture we have moving dynamic variables $\xi_H(t)$ and fixed state vectors $|\psi\rangle_H$. The evolution of new variables is governed by the equation of motion Eq. (A.3.9). The expectation value is now given by Eq. (A.3.8). This new picture of motion is called the *Heisenberg picture.*

Problem A.3.1. By using the completeness relation Eq. (A.2.7), show that

$$\langle\psi,t|\psi,t\rangle = \int_{-\infty}^{\infty} dx\,\psi^*(x,t)\psi(x,t)$$

Problem A.3.2. By using mathematical induction, prove that the normalization condition Eq. (A.2.29) is maintained in time. Hint: use Eq. (A.2.28).

Problem A.3.3. Verify Eq. (A.3.9).

This page intentionally left blank.

Appendix B

Permutations

In this appendix elementary discussions of permutation operators are given.

B.1. PERMUTATION GROUP

Let us consider the set of ordered numerals [1, 2, 3]. Exchanging 1 and 2 we obtain [2, 1, 3]. Let us denote this operation by

$$(2, 1)[1, 2, 3] = (1, 2)[1, 2, 3] = [2, 1, 3] \tag{B.1.1}$$

operator $(2, 1) \equiv (1, 2)$ is called the *exchange* between 1 and 2. We can express the same operation in another way:

$$\begin{pmatrix} 1 & 2 & 3 \\ 2 & 1 & 3 \end{pmatrix} [1, 2, 3] = [2, 1, 3] \tag{B.1.2}$$

where

$$\begin{pmatrix} 1 & 2 & 3 \\ 2 & 1 & 3 \end{pmatrix}$$

indicates the change in order from [1, 2, 3] to [2, 1, 3]; it is called a *permutation.* The order of writing the numerals in columns is immaterial, so that

$$\begin{pmatrix} 1 & 2 & 3 \\ 2 & 1 & 3 \end{pmatrix} = \begin{pmatrix} 1 & 3 & 2 \\ 2 & 3 & 1 \end{pmatrix} = \begin{pmatrix} 2 & 1 & 3 \\ 1 & 2 & 3 \end{pmatrix} = \begin{pmatrix} 2 & 3 & 1 \\ 1 & 3 & 2 \end{pmatrix} = \begin{pmatrix} 3 & 1 & 2 \\ 3 & 2 & 1 \end{pmatrix} = \begin{pmatrix} 3 & 2 & 1 \\ 3 & 1 & 2 \end{pmatrix} \tag{B.1.3}$$

Distinct permutations of three numerals are given by

$$\begin{pmatrix} 1 & 2 & 3 \\ 1 & 2 & 3 \end{pmatrix}, \begin{pmatrix} 1 & 2 & 3 \\ 2 & 3 & 1 \end{pmatrix}, \begin{pmatrix} 1 & 2 & 3 \\ 3 & 1 & 2 \end{pmatrix}, \begin{pmatrix} 1 & 2 & 3 \\ 2 & 1 & 3 \end{pmatrix}, \begin{pmatrix} 1 & 2 & 3 \\ 1 & 3 & 2 \end{pmatrix}, \begin{pmatrix} 1 & 2 & 3 \\ 3 & 2 & 1 \end{pmatrix} \tag{B.1.4}$$

which may be denoted symbolically by $\{P_1, P_2, \ldots, P_6\}$. The product of any P_j and P_k is defined by

$$(P_j P_k)[1, 2, 3] \equiv P_j (P_k [1, 2, 3]) \tag{B.1.5}$$

The set of six elements $\{P_1, P_2, \ldots, P_6\}$ in Eq. (B.1.4) has the group properties; it is called the *permutation group* of degree 3. The said *group properties* are:

1. Composition

Any two members of the set, P_j and P_k, have the composition property such that the product $P_j P_k$ is also a member of the set, say, P_i:

$$P_j P_k = P_i \tag{B.1.6}$$

We demonstrate this property by examples. Let us choose

$$P_j = \begin{pmatrix} 1 & 2 & 3 \\ 2 & 1 & 3 \end{pmatrix} \quad \text{and} \quad P_k = \begin{pmatrix} 1 & 2 & 3 \\ 1 & 3 & 2 \end{pmatrix}$$

By direct calculations, we obtain

$$\begin{aligned} \left\{ \begin{pmatrix} 1 & 2 & 3 \\ 2 & 1 & 3 \end{pmatrix} \begin{pmatrix} 1 & 2 & 3 \\ 1 & 3 & 2 \end{pmatrix} \right\} [1,2,3] &\equiv \begin{pmatrix} 1 & 2 & 3 \\ 2 & 1 & 3 \end{pmatrix} \left\{ \begin{pmatrix} 1 & 2 & 3 \\ 1 & 3 & 2 \end{pmatrix} [1,2,3] \right\} \\ &= \begin{pmatrix} 1 & 2 & 3 \\ 2 & 1 & 3 \end{pmatrix} [1,3,2] = [2,3,1] \end{aligned} \tag{B.1.7}$$

We also obtain

$$\begin{pmatrix} 1 & 2 & 3 \\ 2 & 3 & 1 \end{pmatrix} [1,2,3] = [2,3,1] \tag{B.1.8}$$

We can therefore express the product

$$\begin{pmatrix} 1 & 2 & 3 \\ 2 & 1 & 3 \end{pmatrix} \begin{pmatrix} 1 & 2 & 3 \\ 1 & 3 & 2 \end{pmatrix}$$

by a single permutation

$$\begin{pmatrix} 1 & 2 & 3 \\ 2 & 3 & 1 \end{pmatrix}$$

which is a member of the set. We can obtain the same result by examining the permutations directly as follows: Start with the permutation

$$P_k = \begin{pmatrix} 1 & 2 & 3 \\ 1 & 3 & 2 \end{pmatrix}$$

This moves 1 to 1. Then the permutation

$$P_j = \begin{pmatrix} 1 & 2 & 3 \\ 2 & 1 & 3 \end{pmatrix}$$

moves 1 to 2. The net move is then $1 \rightarrow 1 \rightarrow 2$. Similarly, $2 \rightarrow 3 \rightarrow 3$ and $3 \rightarrow 2 \rightarrow 1$. We can thus represent the net move by the permutation

$$\begin{pmatrix} 1 & 2 & 3 \\ 2 & 3 & 1 \end{pmatrix}$$

2. Association

If P_i, P_j and P_k are any three elements of the set, then

$$(P_i P_j)P_k = P_i(P_j P_k) \equiv P_i P_j P_k \tag{B.1.9}$$

For example by applying the second method of calculation, we obtain

$$\left\{\begin{pmatrix}1&2&3\\2&1&3\end{pmatrix}\begin{pmatrix}1&2&3\\1&3&2\end{pmatrix}\right\}\begin{pmatrix}1&2&3\\3&2&1\end{pmatrix} = \begin{pmatrix}1&2&3\\2&3&1\end{pmatrix}\begin{pmatrix}1&2&3\\3&2&1\end{pmatrix} = \begin{pmatrix}1&2&3\\1&3&2\end{pmatrix}$$

$$\begin{pmatrix}1&2&3\\2&1&3\end{pmatrix}\left\{\begin{pmatrix}1&2&3\\1&3&2\end{pmatrix}\begin{pmatrix}1&2&3\\3&2&1\end{pmatrix}\right\} = \begin{pmatrix}1&2&3\\2&3&1\end{pmatrix}\begin{pmatrix}1&2&3\\3&2&1\end{pmatrix} = \begin{pmatrix}1&2&3\\1&3&2\end{pmatrix}$$

Thus we obtain

$$\left\{\begin{pmatrix}1&2&3\\2&1&3\end{pmatrix}\begin{pmatrix}1&2&3\\1&3&2\end{pmatrix}\right\}\begin{pmatrix}1&2&3\\3&2&1\end{pmatrix} = \begin{pmatrix}1&2&3\\2&1&3\end{pmatrix}\left\{\begin{pmatrix}1&2&3\\1&3&2\end{pmatrix}\begin{pmatrix}1&2&3\\3&2&1\end{pmatrix}\right\}$$

3. Identity

There exists a unique element, called the *identity E*, that has the property:

$$P_i E = P_i = E P_i \tag{B.1.10}$$

for any P_i. In the present case

$$E = \begin{pmatrix}1&2&3\\1&2&3\end{pmatrix} \tag{B.1.11}$$

4. Inverse

For every element P_i, there exists an element P_i^{-1}, called the *inverse* of P_i, in the set, that satisfies

$$P_i P_i^{-1} = E = P_i^{-1} P_i \tag{B.1.12}$$

For example if

$$P = \begin{pmatrix}1&2&3\\2&3&1\end{pmatrix}, \qquad P^{-1} = \begin{pmatrix}1&2&3\\3&1&2\end{pmatrix}$$

The four group properties refer to the principal operation defined by Eq. (B.1.5).

Let us consider all integers 0, ± 1, ± 2, ... With respect to the summation $j + k$, the four group properties are satisfied; the identity is represented by 0, and the inverse of j is $-j$. Therefore the set of integers form a group with respect to the summation. The same set does not however form a group with respect to multiplication, since the inverse of 2 for example cannot be found within the set.

Note: The product $P_j P_k$ is not in general equal to the product of the reversed order:

$$P_j P_k \neq P_k P_j \tag{B.1.13}$$

For example

$$\begin{pmatrix} 1 & 2 & 3 \\ 1 & 3 & 2 \end{pmatrix}\begin{pmatrix} 1 & 2 & 3 \\ 2 & 1 & 3 \end{pmatrix} = \begin{pmatrix} 1 & 2 & 3 \\ 3 & 1 & 2 \end{pmatrix}$$

$$\begin{pmatrix} 1 & 2 & 3 \\ 2 & 1 & 3 \end{pmatrix}\begin{pmatrix} 1 & 2 & 3 \\ 1 & 3 & 2 \end{pmatrix} = \begin{pmatrix} 1 & 2 & 3 \\ 2 & 3 & 1 \end{pmatrix}$$

$$\begin{pmatrix} 1 & 2 & 3 \\ 1 & 3 & 2 \end{pmatrix}\begin{pmatrix} 1 & 2 & 3 \\ 2 & 1 & 3 \end{pmatrix} \neq \begin{pmatrix} 1 & 2 & 3 \\ 2 & 1 & 3 \end{pmatrix}\begin{pmatrix} 1 & 2 & 3 \\ 1 & 3 & 2 \end{pmatrix}$$

The number of elements in a group is called the *order* of the group. The order of the permutation group of degree N is $N!$. To see this, let us write a permutation in the form

$$\begin{pmatrix} 1 & 2 & \dots & N \\ j_1 & j_2 & \dots & j_n \end{pmatrix}$$

where $\{j_k\}$ are different numerals taken from (1, 2, . . . N). Clearly there are $N!$ ways of ordering j's. Such ordering generates $N!$ permutations.

Problem B.1.1. Reduce each of the following into a single permutation.

(a) $\begin{pmatrix} 1 & 2 & 3 \\ 1 & 3 & 2 \end{pmatrix}\begin{pmatrix} 1 & 2 & 3 \\ 2 & 3 & 1 \end{pmatrix}$ (b) $\begin{pmatrix} 1 & 2 & 3 \\ 1 & 3 & 2 \end{pmatrix}\begin{pmatrix} 1 & 2 & 3 \\ 3 & 2 & 1 \end{pmatrix}$

(c) $\begin{pmatrix} 1 & 2 & 3 \\ 2 & 1 & 3 \end{pmatrix}\begin{pmatrix} 1 & 2 & 3 \\ 2 & 1 & 3 \end{pmatrix}$

Problem B.1.2. Find the inverses of the following permutations:

(a) $\begin{pmatrix} 1 & 2 & 3 \\ 3 & 1 & 2 \end{pmatrix}$ (b) $\begin{pmatrix} 1 & 2 & 3 & 4 \\ 2 & 3 & 4 & 1 \end{pmatrix}$

(c) $\begin{pmatrix} A & B & C & D \\ B & C & D & A \end{pmatrix}$

Problem B.1.3. The set of permutations of degree 3 is given in Eq. (B.1.4). (a) Multiply each permutation by (1, 2) from the left, then reduce it to a single permutation. Confirm that the set of all permutations so obtained is the same as the original set. (b) The property (a) can be verified no matter what permutation is used to construct the new set. Explain the reason for this.

Problem B.1.4. Refer to Problem B.1.1. Construct the product of the reversed order for each case and reduce it to a single permutation. For each case if the two permutations are commutative or not.

B.2. ODD AND EVEN PERMUTATIONS

As we can see from the two alternative expressions Eqs. (B.1.1) and (B.1.2) for the same operation, permutations and exchanges are related. The relation can be summarized by the following two theorems.

Theorem B.1. Any permutation can equivalently be expressed as a product of exchanges. For example:

$$\begin{pmatrix} 1 & 2 & 3 \\ 2 & 1 & 3 \end{pmatrix} = (2,1), \qquad \begin{pmatrix} 1 & 2 & 3 \\ 2 & 3 & 1 \end{pmatrix} = (2,3)(3,1) = (1,3)(1,2) = (1,2)(2,3)$$

This theorem is intuitively obvious. As we see in the second example, there are in general a number of equivalent expressions for a given permutation. However these expressions are not arbitrary but subject to an important restriction. If a permutation P is expressed in terms of an odd (even) number of exchanges, all of the equivalent decompositions of P have odd (even) numbers of exchanges. We may rephrase this property as Theorem B.2.

Theorem B.2. Any permutation may be classified as an odd or even permutation according to whether it can be built up from odd or even numbers of exchanges.

We demonstrate this as follows. Let us call a permutation of the form,

$$\begin{pmatrix} i_1 & i_2 & \cdots & i_n \\ i_2 & i_3 & \cdots & i_1 \end{pmatrix}$$

which transforms $i_1 \to i_2, i_2 \to i_3, \ldots i_n \to i_1$, a *cycle*, and we denote it by $(i_1, i_2, \ldots, i_n)$:

$$(i_1, i_2, \ldots, i_n) \equiv \begin{pmatrix} i_1 & i_2 & \cdots & i_n \\ i_2 & i_3 & \cdots & i_1 \end{pmatrix} \tag{B.2.1}$$

The number n is called the length of the cycle. Such a cycle can be decomposed into a product of exchanges (cycles of length 2); for example

$$(i_1, i_2, \ldots, i_n) = (i_1, i_2)(i_2, i_3) \ldots (i_{n-1}, i_n) \tag{B.2.2}$$

which shows that a cycle of length n can be decomposed into a product of $n-1$ exchanges. Therefore a cycle is even or odd according to whether its length n is odd or even. Any permutation can be expressed as a product of cycles whose arguments are mutually exclusive; for example

$$\begin{pmatrix} 1 & 2 & 3 & 4 & 5 \\ 5 & 3 & 2 & 1 & 4 \end{pmatrix} = \begin{pmatrix} 1 & 5 & 4 \\ 5 & 4 & 1 \end{pmatrix} \begin{pmatrix} 2 & 3 \\ 3 & 2 \end{pmatrix} = (1,5,4)(2,3)$$

The parity of the permutation can now be determined by finding the parity of each cycle and applying the rules:

$$\text{(even)(even)} = \text{(odd)(odd)} = \text{even}, \qquad \text{(odd)(even)} = \text{odd} \tag{B.2.3}$$

which follows simply from the definition of parity. Thus the parity of (1, 5, 4) is even and the parity of (2, 3) odd. Therefore the parity of

$$\begin{pmatrix} 1 & 2 & 3 & 4 & 5 \\ 5 & 3 & 2 & 1 & 4 \end{pmatrix}$$

is odd according to the rule (even)(odd) = odd. Clearly the parity of any permutation determined in this manner is unique. q.e.d.

The sign δ_P of the parity of a permutation P is defined by

$$\delta_P = \begin{cases} +1 & \text{if } P \text{ is even,} \\ -1 & \text{if } P \text{ is odd.} \end{cases} \tag{B.2.4}$$

From this definition we obtain

$$\delta_P^2 = (\pm 1)^2 = 1 \tag{B.2.5}$$

We can further establish that

$$\delta_P^{-1} = \delta_P \tag{B.2.6}$$

$$\delta_{PQ} = \delta_P \delta_Q \tag{B.2.7}$$

The last equation can be proved as follows. If P and Q are both odd, then $\delta_P \delta_Q = (-1)(-1) = 1$. By definition P and Q can be expressed in terms of odd numbers of exchanges. Using these expressions for P and Q, we can express the product PQ in terms of exchanges. The number of exchanges here is even, since the sum of two odd numbers is even. Hence $\delta_{PQ} = 1$. We can apply similar arguments to each of the other possibilities.

Let us now consider a function of several variables, $f(x_1, x_2, \ldots, x_n)$. If this function satisfies

$$Pf(x_1, x_2, \ldots, x_n) = f(x_1, x_2, \ldots, x_n) \quad \text{for all } P \tag{B.2.8}$$

where P's are permutations of n indices, it is called a symmetric function. For example $x_1 + x_2 + x_3, x_1^2 + x_2^2 + x_3^2$ and $x_1 x_2 x_3$ are all symmetric functions. If a function $f(x_1, x_2, \ldots, x_n)$ satisfies

$$Pf(x_1, x_2, \ldots, x_n) = \delta_P f(x_1, x_2, \ldots, x_n) \quad \text{for all } P \tag{B.2.9}$$

then f is called an antisymmetric function. For example $(x_1 - x_2)(x_2 - x_3)(x_3 - x_1)$ is antisymmetric. Note: Some functions satisfy neither Eq. (B.2.8) nor Eq. (B.2.9) (see Problem B.2.4).

Consider now two functions $f(x_1, x_2)$ and $g(x_1, x_2)$. Applying the permutation

$$\begin{pmatrix} 1 & 2 \\ 2 & 1 \end{pmatrix}$$

on the product $f(x_1, x_2)g(x_1, x_2)$ we obtain

$$\begin{pmatrix} 1 & 2 \\ 2 & 1 \end{pmatrix} \{f(x_1, x_2)g(x_1, x_2)\} = f(x_2, x_1)g(x_2, x_1) \tag{B.2.10}$$

We may write the last member as

$$\left[\begin{pmatrix} 1 & 2 \\ 2 & 1 \end{pmatrix} f(x_1, x_2)\right] \left[\begin{pmatrix} 1 & 2 \\ 2 & 1 \end{pmatrix} g(x_1, x_2)\right] = f(x_1, x_2)g(x_1, x_2)$$

where angular brackets mean that the permutation must be completed within the brackets. We then obtain from Eq. (B.2.10)

$$\left[\begin{pmatrix} 1 & 2 \\ 2 & 1 \end{pmatrix} f(x_1, x_2) g(x_1, x_2)\right] = \left[\begin{pmatrix} 1 & 2 \\ 2 & 1 \end{pmatrix} f(x_1, x_2)\right] \left[\begin{pmatrix} 1 & 2 \\ 2 & 1 \end{pmatrix} g(x_1, x_2)\right]$$

This example indicates that for a general P

$$[P(fg)] = [Pf][Pg] \tag{B.2.11}$$

The restriction indicated by the angular brackets can be removed by the following device. With the understanding that permutations act rightward, we may write Eq. (B.2.11) as

$$P(fg) = [Pf]Pg \tag{B.2.12}$$

But

$$fg = fP^{-1}Pg \tag{B.2.13}$$

[from Eq. (B.1.12)]. Multiplying Eq. (B.2.13) from the left by P, we obtain

$$PfP^{-1}Pg = P(fg) = [Pf]Pg \tag{B.2.14}$$

[from Eqs. (B.2.13) and (B.2.12)]. Comparing the first and last members, we obtain

$$PfP^{-1} = [Pf] \tag{B.2.15}$$

Using this result we may reexpress Eq. (B.2.11) as

$$P(fg)P^{-1} = (PfP^{-1})(PgP^{-1}) \tag{B.2.16}$$

Note: The the rhs term can be obtained from $P(fg)P^{-1}$ by inserting the identity $P^{-1}P$ between f and g, then reassociating the resulting factors:

$$P(fg)P^{-1} = Pf(P^{-1}P)gP^{-1} = (PfP^{-1})(PgP^{-1}) \tag{B.2.17}$$

Equation (B.2.16) means that the symmetry property of the product fg can be determined by studying each factor separately. Thus if a quantity to be studied appears as a factor, it is more convenient to define the permutation-symmetry property in the following form:

$$Pf(x_1, x_2, \ldots, x_n)P^{-1} = f(x_1, x_2, \ldots, x_n) \qquad \text{(symmetric)} \tag{B.2.18}$$

$$Pf(x_1, x_2, \ldots, x_n)P^{-1} = \delta_P f(x_1, x_2, \ldots, x_n) \qquad \text{(antisymmetric)} \tag{B.2.19}$$

Multiplying Eq. (B.2.18) from the right by P, we obtain

$$Pf = fP \quad \text{or} \quad [P, f] \equiv Pf - fP = 0 \qquad \text{(symmetric)} \tag{B.2.20}$$

This commutator form can also be used to define symmetry.

Problem B.2.1. Decompose the following permutations into products of exchanges.

(a) $\begin{pmatrix} 1 & 2 & 3 & 4 \\ 2 & 3 & 1 & 4 \end{pmatrix}$ (b) $\begin{pmatrix} 1 & 2 & 3 & 4 & 5 \\ 3 & 1 & 2 & 5 & 4 \end{pmatrix}$

Problem B.2.2. Find the parities of the following permutations.

$$\text{(a)} \begin{pmatrix} 1 & 2 & 3 & 4 \\ 2 & 3 & 1 & 4 \end{pmatrix} \qquad \text{(b)} \begin{pmatrix} 1 & 2 & 3 & 4 & 5 \\ 3 & 1 & 2 & 5 & 4 \end{pmatrix}$$

$$\text{(c)} \begin{pmatrix} 1 & 2 & 3 & 4 & 5 \\ 5 & 4 & 3 & 2 & 1 \end{pmatrix}$$

Problem B.2.3. For any permutation group, the number of even permutations is equal to the number of odd permutations. (a) Confirm this statement for $N = 2$ and $N = 3$. (b) Prove this statement for a general N.

Problem B.2.4. Let $f(x_1, x_2)$ be an arbitrary function of x_1 and x_2. (a) Show that $f(x_1, x_2) + f(x_2, x_1)$ and $f(x_1, x_2) - f(x_2, x_1)$ are, respectively, symmetric and antisymmetric. (b) Express f as a sum of symmetric and antisymmetric functions.

Appendix C

Bosons and Fermions

Quantum particles are either bosons or fermions. Bosons (fermions) can (cannot) multiply occupy the same particle-state. Indistinguishability and symmetric (antisymmetric) states for a system of bosons (fermions) are defined in terms of particle permutation symmetries.

C.1. INDISTINGUISHABLE PARTICLES

Consider a system composed of identical particles. If numbered particle coordinates are used in a theoretical formulation, a prediction from the theory must be independent of numbering the particles. For example the N-particle distribution function for the system must be invariant under permutations of N particle indices. Such a concept of indistinguishability can be applied to both classical and quantum mechanical systems.

Let us take a classical system of three identical particles moving in one dimension. The dynamic state of the system can be represented by three points in the phase space, as shown in Fig. C.1. Let us denote the location of these points by $(x_1, p_1, x_2, p_2, x_3, p_3)$. Consider an infinitesimal phase area $dx_j\, dp_j$ surrounding each point (x_j, p_j). The probability of finding the system in a state in which three particle points are within the element

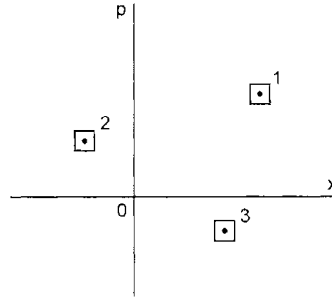

Figure C.1. The dynamic state for three identical classical particles can be represented by three particle points in the phase space.

$dx_1 dp_1 dx_2 dp_2 dx_3 dp_3$ can be written in the form:

$$\frac{\rho(x_1,p_1,x_2,p_2,x_3,p_3)dx_1dp_1dx_2dp_2dx_3dp_3}{(2\pi\hbar)^3(3!)}$$

$$\equiv \frac{\rho(1,2,3)dx_1dp_1dx_2dp_2dx_3dp_3}{(2\pi\hbar)^3(3!)} \tag{C.1.1}$$

where ρ represents the distribution function for the system. For identical particles, we require that the distribution function ρ (1, 2, 3) to be *symmetric*

$$\begin{aligned} P\rho(1,2,3) &= \rho(1,2,3) \qquad \text{for all } P \\ \rho(1,2,3) &= \rho(1,3,2) = \ldots = \rho(2,3,1) \end{aligned} \tag{C.1.2}$$

Physical variables ξ, such as the Hamiltonian and the total momentum depend on the particle variables:

$$\xi = \xi(x_1,p_1,x_2,p_2,x_3,p_3) \equiv \xi(1,2,3) \tag{C.1.3}$$

For identical particles, we require ξ to be symmetric:

$$P\xi(1,2,3) = \xi(1,2,3) \quad \text{for all } P \tag{C.1.4}$$

Equations (C.1.2) and (C.1.4) ensure that the average of ξ:

$$\langle\xi\rangle \equiv \frac{1}{(2\pi\hbar)^3}\frac{1}{3!}\int\ldots\int dx_1dp_1\ldots dp_3\,\xi(x_1,p_1,\ldots,p_3)\rho(x_1,p_1,\ldots,p_3) \tag{C.1.5}$$

is independent of numbering the particles.

In general the distribution function ρ changes with time. However the symmetry of the distribution function is maintained if the Hamiltonian H of the system is symmetric:

$$PH = H \text{ for all } P \tag{C.1.6}$$

Note: Equation (C.1.6) is a special case of Eq. (C.1.4). The theorem means that the *indistinguishability* of particles defined by Eqs. (C.1.2) and (C.1.4) is a time-independent (or permanent) property. This can be shown by using the Liouville equation.

In summary a system of identical particles can be properly treated if the distribution function is symmetric [Eq. (C.1.2)] and all physical variables are symmetric [see Eqs. (C.1.4) and (C.1.6)].

The significance of the symmetry requirements can be understood by considering distinguishable particles. Let us take a hydrogen atom, which consists of an electron with mass $m_e$and a proton with mass m_p. The Hamiltonian H for this system is

$$H(\mathbf{r}_1,\mathbf{p}_1,\mathbf{r}_2,\mathbf{p}_2) \equiv H(1,2) = \frac{1}{2m_e}p_1^2 + \frac{1}{2m_p}p_2^2 + V(|\mathbf{r}_1-\mathbf{r}_2|) \tag{C.1.7}$$

We apply exchange (1,2) to Eq. (C.1.7) and obtain

$$(1,2)H(1,2) = \frac{1}{2m_e}p_2^2 + \frac{1}{2m_p}p_1^2 + V(|\mathbf{r}_2-\mathbf{r}_1|) \neq H(1,2) \tag{C.1.8}$$

which indicates that this Hamiltonian H is *not* symmetric. Our example shows that if particles have different masses, then the Hamiltonian H is not symmetric. The important point however is that the Hamiltonian H can, and must, contain the built-in permutation symmetry appropriate for the system.

The symmetry requirements for identical particles can simply be extended to quantum mechanical many-particle systems as follows:

Let us consider a quantum system of N identical particles. We require that the Hamiltonian of the system be a symmetric function of particle-variables, $\zeta_j = (\mathbf{r}_j, \mathbf{p}_j)$:

$$PH(\zeta_1, \zeta_2, \ldots, \zeta_N)P^{-1} = H(\zeta_1, \zeta_2, \ldots, \zeta_N) \quad \text{or} \quad PH = HP \tag{C.1.9}$$

Since the quantum Hamiltonian is a linear operator and appears as a factor in the definition equation, the symmetry requirement must necessarily be expressed in the form of Eq. (C.1.9) instead of Eq. (C.1.3). We further require all observables ξ and the density operator ρ to be symmetric:

$$P\xi = \xi P, \qquad P\rho = \rho P \tag{C.1.10}$$

which are quantum analogs of Eqs. (C.1.4) and (C.1.2), respectively. By virtue of Eqs. (C.1.9)–(C.1.10), the expectation value $\langle \xi \rangle = \mathrm{Tr}\{\xi\rho\}$ is independent of numbering the particles (see Section C.3).

C.2. BOSONS AND FERMIONS

Every elementary particle is either a boson or a fermion. This is known as the *quantum statistical postulate.* It is distinct from the five quantum mechanical postulates stated in Section A.1, and it should be treated as an independent postulate.

For a quantum particle moving in one dimension, the eigenvalues for the momentum are

$$p_k = \left(\frac{2\pi\hbar}{L}\right)k, \qquad k = \ldots, -1, 0, 1, \ldots \tag{C.2.1}$$

The corresponding normalized eigenkets are denoted by $\{|\, p_k\rangle\}$, which satisfy the orthonormality condition $\langle p_i | p_j \rangle = \delta_{ij}$.

When a system contains two different particles, say A and B, we can construct a ket for the system from the *direct product* of the single-particle kets for A and B. Such a ket

$$|p_i^{(A)}\rangle|p_j^{(B)}\rangle = |p_j^{(B)}\rangle|p_i^{(A)}\rangle \equiv |p_i^{(A)}p_j^{(B)}\rangle \tag{C.2.2}$$

represents a state in which particles A and B occupy momentum states p_i and p_j, respectively. The ket $|p_i^{(A)}p_j^{(B)}\rangle$ is normalized to unity, since

$$\begin{aligned}\langle p_i^{(A)}p_j^{(B)}|p_i^{(A)}p_j^{(B)}\rangle &= \left(\langle p_j^{(B)}|\langle p_i^{(A)}|\right)\left(|p_i^{(A)}\rangle|p_j^{(B)}\rangle\right) \\ &= \langle p_j^{(B)}|\left(\langle p_i^{(A)}|p_i^{(A)}\rangle\right)|p_j^{(B)}\rangle \\ &= \langle p_j^{(B)}|p_j^{(B)}\rangle = 1\end{aligned} \tag{C.2.3}$$

We now consider a system of two identical particles. Let us construct a new ket:

$$|p_i p_j\rangle_S \equiv \frac{1}{2^{1/2}}\{|p_i^{(A)}\rangle|p_j^{(B)}\rangle + |p_i^{(B)}\rangle|p_j^{(A)}\rangle\} \tag{C.2.4}$$

By postulate the new ket represents the system-state in which two states p_i and p_j are occupied by two particles with no further specifications. The factor $2^{-1/2}$ is given to facilitate normalization. We now extend our theory to the case of N bosons. Let $|\alpha_a^{(j)}\rangle, |\alpha_b^{(j)}\rangle, \ldots$ be kets for the jth particle occupying single-particle states $\alpha_a, \alpha_b, \ldots$. We construct an N-particle ket by taking the product of particle kets:

$$|\alpha_a^{(1)}\rangle|\alpha_b^{(2)}\rangle \ldots |\alpha_g^{(N)}\rangle \tag{C.2.5}$$

By multiplying Eq. (C.2.5) from the left by the *symmetrizing operator*:

$$S \equiv \frac{1}{(N!)^{1/2}} \sum_P P \tag{C.2.6}$$

we obtain a symmetric ket for the system:

$$S(|\alpha_a^{(1)}\rangle|\alpha_b^{(2)}\rangle \ldots |\alpha_g^{(N)}\rangle) \equiv |\alpha_a \alpha_b \ldots \alpha_g\rangle_S \tag{C.2.7}$$

where particle labels are omitted on the rhs, since they are no longer relevant. The ket in Eq. (C.2.7) is obviously symmetric:

$$PS(|\alpha_a^{(1)}\rangle|\alpha_b^{(2)}\rangle \ldots |\alpha_g^{(N)}\rangle) = S(|\alpha_a^{(1)}\rangle|\alpha_b^{(2)}\rangle \ldots |\alpha_g^{(N)}\rangle) \qquad \text{for any } P \tag{C.2.8}$$

By postulate the symmetric ket Eq. (C.2.7) represents the system-state of N bosons in which the particle-states $\alpha_a, \alpha_b, \ldots, \alpha_g$ are occupied.

Let us next define the *antisymmetrizing operator* A by

$$A \equiv \frac{1}{(N!)^{1/2}} \sum_P \delta_P P \tag{C.2.9}$$

where δ_P is the *sign of parity of permutation* P defined by

$$\delta_P = \begin{cases} +1 & \text{if } P \text{ is even} \\ -1 & \text{if } P \text{ is odd.} \end{cases} \tag{C.2.10}$$

Applying the operator A on the ket in Eq. (C.2.5), we obtain a new ket

$$A(|\alpha_a^{(1)}\rangle|\alpha_b^{(2)}\rangle \ldots |\alpha_g^{(N)}\rangle) \equiv |\alpha_a \alpha_b \ldots \alpha_g\rangle_A \tag{C.2.11}$$

where the subscript A denotes the *antisymmetric* ket. The fact that this is antisymmetric can be shown as follows. Multiply Eq. (C.2.11) by an arbitrary permutation P:

$$PA(|\alpha_a^{(1)}\rangle|\alpha_b^{(2)}\rangle \ldots |\alpha_g^{(N)}\rangle) = \frac{1}{(N!)^{1/2}} \sum_Q \delta_Q PQ(|\alpha_a^{(1)}\rangle|\alpha_b^{(2)}\rangle \ldots |\alpha_g^{(N)}\rangle) \tag{C.2.12}$$

where we denote the summation variable by Q. According to the composition property [Eq. (B.1.6)], the product PQ is another element, say, R, of the permutation group:

$$PQ = R \tag{C.2.13}$$

Multiplying Eq. (C.2.13) from the left by P^{-1}, we obtain

$$P^{-1}PQ = P^{-1}R = Q \tag{C.2.14}$$

Using Eq. (C.2.14), (B.2.7), and (B.2.6), we now express δ_Q as follows:

$$\delta_Q = \delta_{(P^{-1}R)} = \delta_{P^{-1}}\delta_R = \delta_P\delta_R \tag{C.2.15}$$

Using Eq. (C.2.15) and Eq. (C.2.13), we can rewrite the rhs of Eq. (C.2.12) as

$$\begin{aligned} &\frac{1}{(N!)^{1/2}}\sum_Q \delta_Q PQ(|\alpha_a^{(1)}\rangle|\alpha_b^{(2)}\rangle\ldots|\alpha_g^{(N)}\rangle) \\ &= \frac{1}{(N!)^{1/2}}\sum_R \delta_P\delta_R R(|\alpha_a^{(1)}\rangle|\alpha_b^{(2)}\rangle\ldots|\alpha_g^{(N)}\rangle) \\ &= \delta_P A(|\alpha_a^{(1)}\rangle|\alpha_b^{(2)}\rangle\ldots|\alpha_g^{(N)}\rangle) \end{aligned} \tag{C.2.16}$$

which establishes the desired antisymmetric property:

$$P\left[A(|\alpha_a^{(1)}\rangle|\alpha_b^{(2)}\rangle\ldots|\alpha_g^{(N)}\rangle)\right] = \delta_P\left[A(|\alpha_a^{(1)}\rangle|\alpha_b^{(2)}\rangle\ldots|\alpha_g^{(N)}\rangle)\right] \tag{C.2.17}$$

We postulate that the antisymmetric ket in Eq. (C.2.11) represents the system state of N fermions in which particle-states $a, b, \ldots, g$ are occupied. For illustration let us take the case of two fermions moving in one dimension. Corresponding to the state in which momentum states p_i and p_j are occupied, we construct the ket

$$|p_ip_j\rangle_A \equiv \frac{1}{2^{1/2}}\{|p_i^{(1)}\rangle|p_j^{(2)}\rangle - |p_i^{(2)}\rangle|p_j^{(1)}\rangle\} = -|p_jp_i\rangle_A \tag{C.2.18}$$

If $p_i = p_j$, we obtain

$$|p_ip_i\rangle_A = 0 \tag{C.2.19}$$

By postulate the null ket does not correspond to any quantum state. Thus *two fermions must not occupy the same state.* This is known as *Pauli's exclusion principle.*

Pauli's principle applies to *any* particle state. For example except for the spin degeneracy, two fermions can occupy neither the same momentum state nor the same space point. Historically Pauli's exclusion principle was discovered from the study of atomic spectra. The original statement referred to atomic orbitals: No two electrons can occupy the same orbital with identical quantum numbers.

C.3. MORE ABOUT BOSONS AND FERMIONS

In quantum mechanics theory and experiment are compared only through expectation values for observables. For a system of identical particles, these values must then be independent of particle numbering. We study this theoretical requirement in the present section. Let us first consider the case of fermions. In Section C.2 we saw that the

quantum state for a system of identical fermions by postulate is represented by the antisymmetric ket $|\alpha_a\alpha_b\ldots\alpha_g\rangle_A$, or equivalently by the antisymmetric bra ${}_A\langle\alpha_a\alpha_b\ldots\alpha_g|$. We also saw in Section C.1 that any observable ξ for the system is symmetric. By the quantum postulate the expectation value of the observable ξ is given by

$$ {}_A\langle\alpha_a\alpha_b\ldots\alpha_g|\xi|\alpha_a\alpha_b\ldots\alpha_g\rangle_A \tag{C.3.1}$$

We now examine the permutation symmetry of this quantity. By multiplying Eq. (C.3.1) by an arbitrary permutation P from the left and by its inverse P^{-1} from the right, we have $P({}_A\langle\alpha_a\alpha_b\ldots\alpha_g|\xi|\alpha_a\alpha_b\ldots\alpha_g\rangle_A)P^{-1}$, which can be calculated as follows:

$$\begin{aligned}
&P({}_A\langle\alpha_a\alpha_b\ldots\alpha_g|\xi|\alpha_a\alpha_b\ldots\alpha_g\rangle_A)P^{-1}\\
&= ({}_A\langle\alpha_a\alpha_b\ldots\alpha_g|P^{-1})(P\xi P^{-1})(P|\alpha_a\alpha_b\ldots\alpha_g\rangle_A P^{-1}) \qquad \text{[from Eq. (B.2.16)]}\\
&= (\delta_P\,{}_A\langle\alpha_a\alpha_b\ldots\alpha_g|)(\xi)(\delta_P|\alpha_a\alpha_b\ldots\alpha_g\rangle_A) \qquad \text{[from Eqs. (C.1.10) and (C.2.12)]}\\
&= {}_A\langle\alpha_a\alpha_b\ldots\alpha_g|\xi|\alpha_a\alpha_b\ldots\alpha_g\rangle_A
\end{aligned} \tag{C.3.2}$$

[from Eq. (C.2.10)]. Thus Eq. (C.3.1) is *invariant under permutation* of particle indices.

Next we consider the case of identical bosons. The expectation value of ξ for this system is given by

$$ {}_S\langle\alpha_a\alpha_b\ldots\alpha_g|\xi|\alpha_a\alpha_b\ldots\alpha_g\rangle_S \tag{C.3.3}$$

which is clearly symmetric:

$$P({}_S\langle\alpha_a\alpha_b\ldots\alpha_g|\xi|\alpha_a\alpha_b\ldots\alpha_g\rangle_S)P^{-1} = {}_S\langle\alpha_a\alpha_b\ldots\alpha_g|\xi|\alpha_a\alpha_b\ldots\alpha_g\rangle_S \tag{C.3.4}$$

In summary symmetric (antisymmetric) vectors for bosons (fermions) satisfy the necessary invariance requirement, Eq. (C.3.4) [Eq. (C.3.2)]. In principle other vectors that satisfy the invariance requirement can be constructed, but they are irrelevant because of the quantum statistical postulate. Once assumed at an initial time, the invariance properties are maintained indefinitely. This can be demonstrated as follows. If the ket $|\psi, t\rangle_S$ is symmetric at time t, the ket $H|\psi, t\rangle_S$, where H represents the symmetric Hamiltonian, is also symmetric. In the Schrödinger picture, the ket $|\psi, t\rangle_S$ varies in time, following the equation of motion:

$$i\hbar\frac{\partial}{\partial t}|\psi,t\rangle_S = H|\psi,t\rangle_S \tag{C.3.5}$$

Therefore $(\partial/\partial t)|\psi,t\rangle_S$ is also symmetric. By mathematical induction for a continuous variable t, the symmetry of the ket $|\psi, t\rangle_S$ is maintained for all time t. In a similar manner, if the ket $|\psi, t\rangle_A$ is initially antisymmetric, then $H|\psi, t\rangle_A$is antisymmetric, ensuring that the ket will still be antisymmetric later. Thus a state that is initially symmetric (antisymmetric) will always remain symmetric (antisymmetric). Equations (C.3.2) and (C.3.4) are maintained separately for fermions and bosons. Therefore the distinction between bosons and fermions is permanent.

As we saw in Section C.2, the number of fermions occupying any particle state is limited to one or zero. This leads to a special statistics called *Fermi–Dirac statistics*. Fermi first studied the statistics, then Dirac established that particles subject to Pauli's

principle are precisely those for which antisymmetric states must be prescribed. No restriction on the occupation number is imposed for bosons. The statistics of bosons is not the same as the Boltzmann statistics because quantum states are different from classical dynamic states. Quantum statistics for massless bosons were first studied by Bose, and this theory was extended for massive bosons by Einstein; this statistics is called the *Bose–Einstein statistics.*

This page intentionally left blank.

Appendix D

Laplace Transformation; Operator Algebras

Laplace transformation and operator algebras are discussed. Proofs of Eqs. (7.9.19) and (7.10.15) are given.

D.1. LAPLACE TRANSFORMATION

Many time-dependent problems can be handled simply by using Laplace transformation techniques. We briefly review these techniques in this section.

Let us consider a function $f(t)$ of time t defined in $(0, \infty)$. Its Laplace transform $F(s)$ is defined by

$$F(s) \equiv \int_0^\infty e^{-st} f(t) dt \tag{D.1.1}$$

Symbolically, we may write

$$F(s) = \mathcal{L} f(t) \tag{D.1.2}$$

For derivatives we obtain after simple calculations (Problem D.1.1)

$$\mathcal{L} f' = -f(0+) + s\mathcal{L} f \tag{D.1.3}$$

$$\mathcal{L} f'' = -f'(0+) - sf(0+) + s^2 \mathcal{L} f \tag{D.1.4}$$

and so on. The arguments 0+ mean that we approach 0 from the positive side; $f(t)$ is undefined for negative t. By using Eqs. (D.1.1)–(D.1.4), we can reduce a linear time differential equation with constant coefficients to an algebraic equation in the Laplace space, a major advantage. By direct calculation we obtain (Problem D.1.2)

$$\mathcal{L}(1) = \frac{1}{s}, \qquad \mathcal{L} \frac{t^n}{n!} = \frac{1}{s^{n+1}} \tag{D.1.5}$$

where s^{-1} and s^{-n-1} are analytic (differentiable) in the right-half plane:

$$\text{Real part of } s \equiv \text{Re}(s) > 0 \tag{D.1.6}$$

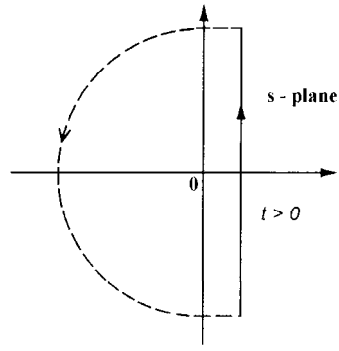

Figure D.1. A closed contour for evaluating Eq. (D. 1.8).

The original function $f(t)$ can be obtained from its transform $F(s)$ by the inverse Laplace transformation $\mathcal{L}^{-1}$:

$$f(t) \equiv \mathcal{L}^{-1}F(s) = \frac{1}{2\pi i}\int_{c-i\infty}^{c+i\infty} ds e^{st}F(s) \tag{D.1.7}$$

where c is chosen such that $F(s)$ is analytic on the right of the integration path.

For example take

$$X \equiv \frac{1}{2\pi i}\int_{c-i\infty}^{c+i\infty} ds e^{st}\frac{1}{s} \tag{D.1.8}$$

We may choose c to be a small positive number, which is often denoted by 0+. The integrand e^{st}/s is vanishingly small if $s \equiv Re^{i\theta}$ has an argument θ such that $\pi/2 < \theta < 3\pi/2$ and R is far away from the origin:

$$\frac{e^{st}}{s} = \frac{e^{Rt(\cos\theta + i\sin\theta)}}{R(\cos\theta + i\sin\theta)} \to 0 \quad \text{as} \quad R \to \infty \tag{D.1.9}$$

We may then choose a closed semicircle of an infinite radius C as shown in Fig. D.1. There is a pole of order one at the origin inside the closed path. By using the *residue theorem*, we then obtain

$$X = \frac{1}{2\pi i}\oint_C ds\frac{e^{st}}{s} = \frac{1}{2\pi i} \times (2\pi i) \text{ Residue of } \frac{e^{st}}{s} = 1$$

Note: We obtained the desired result without carrying out the integration in Eq. (D.1.8).

As we see in this example, an elementary knowledge of the theory of functions of complex variables is very useful. The reader is strongly recommended to acquire such a knowledge. If

$$h(t) \equiv \int_0^\infty f(\tau)g(t-\tau)d\tau \tag{D.1.10}$$

then

$$\mathcal{L}h = [\mathcal{L}f][\mathcal{L}g] \tag{D.1.11}$$

This is known as the *convolution theorem.* (Problem D.1.4)

Problem D.1.1. Derive Eqs. (D.1.3) and (D.1.4).

Problem D.1.2. Verify Eqs. (D.1.5) and (D.1.6).

Problem D.1.3. Show that the Laplace inverse of $s^{-(n+1)}$ is equal to $t^n/n!$ Use Eq. (D.1.7).

Problem D.1.4. Prove Eq. (D.1.11) using Eq. (D.1.7).

D.2. LINEAR OPERATOR ALGEBRAS

Quantum linear operators do not in general commute. Furthermore they may not have inverses; we must therefore treat these operators with a proper care. The perturbation theory developed in Section 7.5 can be applied to a general case in which the perturbation V depends on time; there is considerable simplification if V is time-independent. We treat such a special case in which the total Hamiltonian H of a system is time-independent.

The evolution operator $U(t)$ for the system satisfies the Schrödinger equation:

$$i\hbar\frac{d}{dt}U(t) = HU(t) \tag{D.2.1}$$

The formal solution of this equation with the initial condition that $U(0) = 1$

$$U(T) = \exp(-it\hbar^{-1}H) \tag{D.2.2}$$

This solution holds as though H were an ordinary algebraic variable instead of a linear operator because there is no quantity that does not commute with H. If the system had a time-dependent Hamiltonian, the solution of Eq. (D.2.1) is more complicated.

To proceed in a general manner, we assume that a function of a linear operator ξ is defined by either a polynomial or an infinite series in powers of some parameters (numbers). For example we may regard $\exp(-ith^{-1}H)$ as a series in powers of t:

$$\exp(-ith^{-1}H) \equiv 1 - it\hbar^{-1}H + (1/2)(it\hbar^{-1})^2H^2 + \ldots \tag{D.2.3}$$

The evolution operator $U_D(t)$ in the Dirac Picture (DP), defined by Eq. (7.5.9), can be reexpressed as

$$U_D(t) \equiv e^{itH_0/\hbar}U(t) = e^{itH_0/\hbar}e^{-itH/\hbar} \tag{D.2.4}$$

$$V_D(t) = e^{itH_0/\hbar}Ve^{-itH_0/\hbar} \tag{D.2.5}$$

Multiplying Eq. (7.5.15) from the left by $\exp(-it\hbar^{-1}H_0)$ and using Eqs. (D.2.4)–(D.2.5), we obtain

$$e^{-itH/\hbar} = e^{-itH_0/\hbar} - i\lambda\hbar^{-1}\int_0^t d\tau e^{-i(t-\tau)H_0/\hbar}Ve^{i\tau H/\hbar} \tag{D.2.6}$$

By Laplace transformation, we obtain (Problem D.2.1):

$$\frac{1}{H_0 + \lambda V - z} = \frac{1}{H_0 - z} - \lambda \frac{1}{H_0 - z} V \frac{1}{H_0 + \lambda V - z} \tag{D.2.7}$$

Equation (D.2.7) is a special case of the general identity (Problem D.2.2):

$$\frac{1}{a+b} = \frac{1}{a} - \frac{1}{a} b \frac{1}{a+b} \tag{D.2.8}$$

where a and b are arbitrary operators that may not commute; in addition the existence of a^{-1} is assumed. This identity may be proved by multiplying from the right by $a + b$.

We solve Eq. (D.2.7) by iteration:

$$\frac{1}{H_0 + \lambda V - z} = \frac{1}{H_0 - z} - \lambda \frac{1}{H_0 - z} V \frac{1}{H_0 - z} + \lambda^2 \frac{1}{H_0 - z} V \frac{1}{H_0 - z} V \frac{1}{H_0 - z} + \ldots \tag{D.2.9}$$

Thus, the perturbation expansion in Laplace space can be handled concisely.

Problem D.2.1. Verify Eq. (D.2.7). Use the convolution theorem (D.1.9).

Problem D.2.2. (a) Prove Eq. (D.2.8). (b) Prove

$$\frac{1}{a+b} = \frac{1}{a} - \frac{1}{a+b} b \frac{1}{a}$$

D.3. LIOUVILLE OPERATOR ALGEBRAS; PROOF OF EQ. (7.9.19)

Calculation of matrix elements containing commutator-generating *quantum Liouville operators* $\mathcal{H}$ can be handled systematically by using a *P–k representation.* In this representation we can develop quantum and classical dynamics in a parallel manner, a great advantage.

Let us specify the (p_1, p_2) element of an arbitrary density operator n by

$$\langle p_1 | n | p_2 \rangle = n_{p_1 - p_2}\left(\frac{p_1 + p_2}{2}\right) \tag{D.3.1}$$

If we introduce a pair of variables (P, k) replacing the original pair (p_1, p_2) such that

$$P \equiv \frac{p_1 + p_2}{2}, \qquad k \equiv p_1 - p_2; \qquad p_1 = P + \frac{k}{2}, \qquad p_2 = P - \frac{k}{2} \tag{D.3.2}$$

we can express Eq. (D.3.1) as

$$n_k(P) = \left\langle P + \frac{k}{2} \middle| n \middle| P - \frac{k}{2} \right\rangle \tag{D.3.3}$$

We call this specification the P–k representation. So far we used one-dimensional notation. The extension to a higher dimension is straightforward. We further note that the

pair (P, k) is defined differently from the pair specification **(k, q)** of the electron-pair operator:

$$B_{\mathbf{p}_1\mathbf{p}_2} = B'_{\mathbf{k},\mathbf{q}}$$

see Eqs. (8.4.5) and (8.4.6).

Consider now $\hbar n \equiv hn - nh$. After simple calculations In the P–k representation we obtain (Problem D.4.1)

$$(\hbar n)_k(P) = \sum (k|\hbar(P)|k')n_{k'}(P) \tag{D.3.4}$$

$$(k|\hbar(P)|k') \equiv \eta^{k'} h_{k-k'}(P)\eta^{-k} - \eta^{-k'} h_{k-k'}(P)\eta^{k} \tag{D.3.5}$$

where η^k is a displacement operator acting on a function of P such that

$$\eta^k f(P) = f\left(P + \frac{k}{2}\right)\eta^k \tag{D.3.6}$$

We can further show that (Problem D.4.2)

$$(\hbar_1\hbar_2 n)_k(P) = \sum_{k'}\sum_{k''}(k|\hbar_1(P)|k')(k'|\hbar_2(P)|k'')n_{k''}(P) \tag{D.3.7}$$

Equations (D.3.4) and (D.3.7) show that calculations in the P–k representation proceed according to the ordinary rule of matrix multiplication with quantum Liouville operators acting like matrices in k and the density operator like a vector.

Using an explicit Hamiltonian:

$$h \equiv \epsilon(\mathbf{p}) + \lambda\sum_\alpha \tilde{v}(\mathbf{r} - \mathbf{R}_\alpha) \equiv h_0 + \lambda\sum_\alpha \tilde{v}_\alpha \tag{D.3.8}$$

we obtain (Problem D.4.3)

$$(\mathbf{k}|\hbar_0(\mathbf{P})|\mathbf{k}') = \left[\epsilon\left(\mathbf{P} + \frac{\mathbf{k}}{2}\right) - \epsilon\left(\mathbf{P} - \frac{\mathbf{k}}{2}\right)\right]\delta_{\mathbf{k},\mathbf{k}'} \tag{D.3.9}$$

$$(\mathbf{k}|v_\alpha(\mathbf{P})|\mathbf{k}') = \tilde{v}(\mathbf{k} - \mathbf{k}')\exp[-i\hbar^{-1}(\mathbf{k} - \mathbf{k}')\cdot\mathbf{R}\alpha](\eta^{\mathbf{k}-\mathbf{k}'} - \eta^{-\mathbf{k}+\mathbf{k}'}) \tag{D.3.10}$$

The Liouville operator $\hbar_0(\mathbf{P})$ is diagonal in **k** just as the corresponding Hamiltonian operator h_0 is diagonal in the momentum **p.**

Using the P–k representation we now derive Eq. (7.9.19) from Eq. (7.9.18). Consider first

$$\frac{1}{\hbar_0 - z} = -\frac{1}{z} + \frac{1}{z^2}\hbar_0 - \frac{1}{z^3}\hbar_0^2 + \ldots \qquad (z \equiv ia) \tag{D.3.11}$$

We take **k – k'** matrix elements of this to obtain (Problem D.4.4)

$$(\mathbf{k}|[\hbar_0 - z]^{-1}|\mathbf{k}') = \left[\epsilon\left(\mathbf{P} + \frac{\mathbf{k}}{2}\right) - \epsilon\left(\mathbf{P} - \frac{\mathbf{k}}{2}\right) - z\right]^{-1}\delta_{\mathbf{k},\mathbf{k}'} \tag{D.3.12}$$

Second we consider the impurity average:

$$\left\langle \left(\mathbf{k} \left| \sum_{\alpha} \sum_{\alpha'} \tilde{v}_{\alpha} \frac{1}{\hbar_0 - z} \tilde{v}_{\alpha'} \right| \mathbf{k}' \right) \right\rangle_{\text{av}} \equiv X \tag{D.3.13}$$

The average of the double sum with $\alpha \neq \alpha'$ can be equated with zero since the impurity potential $\tilde{v}$ is defined up to a constant and this constant can be chosen to vanish. Applying Eq. (7.9.15) and using Eqs. (D.3.9) and (D.3.11), we obtain in the bulk limit:

$$X = n_I (2\pi\hbar)^3 \left(\mathbf{k} \left| \sum_{\alpha} \tilde{v}_{\alpha} \frac{1}{\hbar_0 - z} \tilde{v}_{\alpha} \right| \mathbf{k}' \right) \delta_{\mathbf{k},\mathbf{k}'} \tag{D.3.14}$$

Finally consider

$$\begin{aligned} &\left\langle \mathbf{p}_1 \left| \left\langle \sum_{\alpha} \tilde{v}_{\alpha} \frac{i}{\hbar_0 - ia} \tilde{v}_{\alpha} \right\rangle_{\text{av}} n \right| \mathbf{p}_2 \right\rangle \\ &\equiv \int d^3k' \left(\mathbf{k} \left| \left\langle \sum_{\alpha} \tilde{v}_{\alpha} \frac{i}{\hbar_0 - ia} \tilde{v}_{\alpha} \right\rangle_{\text{av}} \right| \mathbf{k}' \right) n_{\mathbf{k}'}(\mathbf{P}) \equiv Y \end{aligned} \tag{D.3.15}$$

By using Eqs. (D.3.10), (D.3.12), (D.3.14), and (7.9.14), we obtain

$$\begin{aligned} Y &= \lim_{a \to 0} n_I (2\pi\hbar)^3 \int d^3k |\tilde{v}(k)|^2 \frac{2a}{[\epsilon(\mathbf{P}+\mathbf{k}) - \epsilon(\mathbf{P})]^2 + a^2} (\eta^{2\mathbf{k}} - 1) n_k(\mathbf{P}) \\ &= 2\pi (2\pi\hbar)^3 n_I \int d^3k |\tilde{v}(k)|^2 \delta(\epsilon_{P+k} - \epsilon_P) [n_{\mathbf{k}}(\mathbf{P}+\mathbf{k}) - n_{\mathbf{k}}(\mathbf{P})] \end{aligned} \tag{D.3.16}$$

In the last step we used the formal identity:

$$\lim_{a \to 0} \frac{a}{\epsilon^2 + a^2} = \pi \delta(\epsilon) \tag{D.3.17}$$

Substituting Eq. (D.3.16) into Eq. (7.9. 18), we obtain Eq. (7.9.19).

Problem D.3.1. Verify Eq. (D.3.4).

Problem D.3.2. Verify Eq. (D.3.7).

Problem D.3.3. Verify Eq. (D.3.9) and Eq. (D.3.10).

Problem D.3.4. Verify Eq. (D.3.12).

D.4. THE v–m REPRESENTATION; PROOF OF EQ. (7.10.15)

The quantum state for the electron–phonon system may be represented by the electron occupation number states $\{N_{\mathbf{p}}\}$ and the phonon occupation number states $\{N_{\mathbf{q}}\}$. The electron–phonon interaction generates no change in spin states; therefore we omit

the spin variables hereafter. Techniques of the *P–k* representation are extended to all quantum numbers $\{N_{\mathbf{p}}\ N_{\mathbf{q}}\}$.

For each phonon state **q,** we introduce new specifications of the matrix elements as follows:

$$\langle N_1|\rho|N_2\rangle \equiv \rho_{N_1}\left[\frac{1}{2}(N_1+N_2)\right] \tag{D.4.1}$$

$$\nu \equiv \frac{1}{2}(N_1+N_2), \quad m \equiv N_1-N_2, \quad N_1=\frac{1}{2}\nu+m, \quad N_2=\frac{1}{2}\nu-m \tag{D.4.2}$$

$$\rho_m(\nu) = \left\langle \nu+\frac{1}{2}m\middle|\,\rho\,\middle|\nu-\frac{1}{2}m\right\rangle \tag{D.4.3}$$

which are generalizations of Eqs. (D.3.1)–(D.3.3). We call the new specification the ν–*m* representation. We omitted the state-designation **q.** We make this specification for all **q.** Occupation numbers $N_{\mathbf{p}}$ for electrons are limited to 0 or 1; otherwise the same ν–*m* representation can also be defined and applied.

Consider now $\mathcal{H}\rho \equiv H\rho - \rho H$. In the ν–*m* representation (for each state **q**), we obtain

$$(\mathcal{H}\rho)_m(\nu) = \sum_{m'}(m|\mathcal{H}(\nu)|m')\rho_{m'}(\nu) \tag{D.4.4}$$

$$(m|\mathcal{H}(\nu)|m') \equiv \eta^{m'}H_{m-m'}(\nu)\eta^{-m} - \eta^{-m'}H_{m-m'}(\nu)\eta^{m} \tag{D.4.5}$$

$$\eta^m f(\nu) = f\left(\nu+\frac{m}{\gamma}\right)\eta^m \tag{D.4.6}$$

$$(\mathcal{H}_1\mathcal{H}_2\rho)_m(\nu) = \sum_{m_1}\sum_{m_2}(m|\mathcal{H}_1(\nu)|m_1)(m_1|\mathcal{H}_2(\nu)|m_2)\rho_{m_2}(\nu) \tag{D.4.7}$$

which are generalizations of Eqs. (D.3.4)–(D.3.7).

In summary occupation number states can be handled simply in the ν–*m* representation where calculations proceed in the same manner as in the *P–k* representation.

Let us consider the unperturbed Hamiltonian, see Eqs. (7.10.1):

$$H_0 = \sum_{\mathbf{p}}\epsilon_p n_{\mathbf{p}} + \sum_{\mathbf{q}}\hbar\omega_q\left(\frac{1}{2}+n_{\mathbf{q}}\right) \tag{D.4.8}$$

which is diagonal in momentum occupation number states. Because of this property, the corresponding Liouville operator $\mathcal{H}_0$ is diagonal in m (Problem D.4.1):

$$(m|\mathcal{H}_0(\nu)|m') = \left(\sum_{\mathbf{p}}\epsilon_p m_{\mathbf{p}} + \sum_{\mathbf{q}}\hbar\omega_q m_{\mathbf{q}}\right)\delta^{(\mathrm{all})}_{m,m'} \tag{D.4.9}$$

$$\delta^{(\mathrm{all})}_{m,m'} \equiv \prod_{\mathbf{p}}\delta_{m_{\mathbf{p}}m'_{\mathbf{p}}}\prod_{\mathbf{q}}\delta_{m_{\mathbf{q}}m'_{\mathbf{q}}} \tag{D.4.10}$$

Next consider part of the perturbation Hamiltonian V in Eqs. (7.10.1):

$$V_q c^\dagger_{\mathbf{k}+\mathbf{q}} c_{\mathbf{k}} a_{\mathbf{q}} \equiv v(\mathbf{k}+\mathbf{q}, \mathbf{k}, \mathbf{q}) \tag{D.4.11}$$

which generates a change in electron numbers at $(\mathbf{k}+\mathbf{q}, \mathbf{k})$ and phonon numbers at $\mathbf{q}$. In ν–m representations the corresponding Liouville operator $v(\mathbf{k}+\mathbf{q}, \mathbf{k}, \mathbf{q})$ is nondiagonal only in these states indicated. By using Eq. (D.4.5) we obtain (Problem D.4.2):

$$\begin{aligned}
&(m_{\mathbf{k}+\mathbf{q}}, m_{\mathbf{k}}, m_{\mathbf{q}} | v(\nu_{\mathbf{k}+\mathbf{q}}, \nu_{\mathbf{k}}, \nu_{\mathbf{q}}) | m'_{\mathbf{k}+\mathbf{q}}, m'_{\mathbf{k}}, m'_{\mathbf{q}}) \\
&= V_{\mathbf{q}} \delta_{m_{\mathbf{k}}, m'_{\mathbf{k}}+1} \left(\eta^{m'_{\mathbf{k}}-m_{\mathbf{k}}} - \eta^{-m'_{\mathbf{k}}+m_{\mathbf{k}}} \right) \delta_{m_{\mathbf{k}+\mathbf{q}}, m'_{\mathbf{k}+\mathbf{q}}+1} \\
&\times \left(\eta^{m'_{\mathbf{k}+\mathbf{q}}-m_{\mathbf{k}+\mathbf{q}}} - \eta^{-m'_{\mathbf{k}+\mathbf{q}}+m_{\mathbf{k}+\mathbf{q}}} \right) \delta_{m_{\mathbf{q}}, m'_{\mathbf{q}}-1} \left(\eta_{(ph)}^{m'_{\mathbf{q}}-m_{\mathbf{q}}} - \eta_{(ph)}^{-m'_{\mathbf{q}}+m_{\mathbf{q}}} \right)
\end{aligned} \tag{D.4.12}$$

The operator v is diagonal in all of the other m's. The Hermitian conjugate of the perturbation v in Eq. (D.4.11) is given by

$$v^\dagger = V_q^* c^\dagger_{\mathbf{k}} c_{\mathbf{k}+\mathbf{q}} a^\dagger_{\mathbf{q}} \tag{D.4.13}$$

The corresponding Liouville operator in the ν–m representation has the following matrix elements:

$$\begin{aligned}
&(m_{\mathbf{k}+\mathbf{q}}, m_{\mathbf{k}}, m_{\mathbf{q}} | v^\dagger(\nu_{\mathbf{k}+\mathbf{q}}, \nu_{\mathbf{k}}, \nu_{\mathbf{q}}) | m'_{\mathbf{k}+\mathbf{q}}, m'_{\mathbf{k}}, m'_{\mathbf{q}}) \\
&= V_{\mathbf{q}}^* \delta_{m_{\mathbf{k}}, m'_{\mathbf{k}}-1} \left(\eta^{m'_{\mathbf{k}}-m_{\mathbf{k}}} - \eta^{-m'_{\mathbf{k}}+m_{\mathbf{k}}} \right) \delta_{m_{\mathbf{k}+\mathbf{q}}, m'_{\mathbf{k}+\mathbf{q}}-1} \\
&\times \left(\eta^{m'_{\mathbf{k}+\mathbf{q}}-m_{\mathbf{k}+\mathbf{q}}} - \eta^{-m'_{\mathbf{k}+\mathbf{q}}+m_{\mathbf{k}+\mathbf{q}}} \right) \delta_{m_{\mathbf{q}}, m'_{\mathbf{q}}+1} \left(\eta_{(ph)}^{m'_{\mathbf{q}}-m_{\mathbf{q}}} - \eta_{(ph)}^{-m'_{\mathbf{q}}+m_{\mathbf{q}}} \right)
\end{aligned} \tag{D.4.14}$$

All of the calculational tools in the ν–m representation are now defined. Actual calculations are aided greatly by drawing Feynman diagrams.

By using the ν–m representation, we derive Eq. (7.10.15) from Eq. (7.10.13). Consider first

$$\frac{1}{\mathcal{H}_0 - z} = -\frac{1}{z} + \frac{1}{z^2}\mathcal{H}_0 - \frac{1}{z^3}\mathcal{H}_0^2 + \dots \tag{D.4.15}$$

We take m–m' matrix elements to obtain (Problem D.4.3)

$$\langle m | [\mathcal{H}_0 - z]^{-1} | m' \rangle = \left[\sum_{\mathbf{p}} \epsilon_p m_{\mathbf{p}} + \sum_{\mathbf{q}} \hbar\omega_q m_{\mathbf{q}} - z \right]^{-1} \delta^{(\text{all})}_{m,m'} \tag{D.4.16}$$

At 0 K there are no phonons: $N_q = 0$; virtual phonons appear only in intermediate states. This allows us to consider the phonon vacuum average of collision operators. In the weak coupling limit, we may consider only second-order processes represented by diagrams in Fig. 7.7. Let us now consider

$$Y = \lim_{a \to 0} i \langle \mathbf{k}_1, \mathbf{k}_2 | \langle \mathcal{V} [\mathcal{H}_0 - ia]^{-1} \mathcal{V} \rangle_{\text{av}} \rho | \mathbf{k}_3, \mathbf{k}_4 \rangle \tag{D.4.17}$$

Using Eqs. (D.4.9), (D.4.12), (D.4.14), and (D.4.16) we obtain after lengthy but straightforward calculations (Problem D.4.4)

$$Y - \sum_{\mathbf{k}_5 s_5} \sum_{\mathbf{k}_6 s_6} -i\hbar^{-1}[\langle 1,2|v_e|5,6\rangle \rho_2(5,6;3,4,t) - \langle 5,6|v_e|3,4\rangle \rho_2(1,2;5,6,t)] \tag{D.4.18}$$

$$\langle 3,4|v_e|1,2\rangle \equiv |V_q|^2 P \frac{\hbar\omega_q}{(\epsilon_3 - \epsilon_1)^2 - \hbar^2\omega_q^2} \delta_{\mathbf{k}_1+\mathbf{k}_2,\mathbf{k}_3+\mathbf{k}_4} \delta_{\mathbf{k}_3-\mathbf{k}_1,\mathbf{q}} \delta_{s_3 s_1} \delta_{s_4 s_2} \tag{D.4.19}$$

where we used the formal identity:

$$\lim_{a\to 0} \frac{i}{\epsilon - ia} = \pi\delta(\epsilon) + iP\left(\frac{1}{\epsilon}\right) \tag{D.4.20}$$

In Eqs. (D.4.19) and (D.4.20) the symbol P denotes that Cauchy's principal values are taken on integrating. Using Eq. (D.4.18) and putting back spin variables, we obtain from Eq. (7.10.13) the final results given in Eqs. (7.10.15) and (7.10.16).

Problem D.4.1. Verify Eq. (D.4.9).

Problem D.4.2. Verify Eqs. (D.4.12) and (D.4.14).

Problem D.4.3. Verify Eq. (D.4.16).

Problem D.4.4. Verify Eq. (D.4.18).

This page intentionally left blank.

Bibliography

SUPERCONDUCTIVITY

Introductory and Elementary Books

Lynton, E. A.: *Superconductivity* (Methuen, London, 1962).

Vidali, G.: *Superconductivity* (Cambridge University Press, Cambridge, England, 1993).

General Textbooks at about the Same Level

Feynman, R. P., Leighton R. B., and Sands, M.: *Feynman Lectures on Physics*, Vol 3 (Addison-Wesley, Reading, MA, 1965), pp. 1–19.

Feynman, R. P.: *Statistical Mechanics* (Addison-Wesley, Reading, MA, 1972), pp. 265–311.

Rose-Innes, A. C., and Rhoderick, E. H.: *Introduction to Superconductivity*, 2d ed. (Pergamon, Oxford, England, 1978).

More Advanced Texts and Monographs

Abrikosov, A. A.: *Fundamentals of the Theory of Metals*, A. Beknazarov, trans. (North Holland-Elsevier, Amsterdam, 1988).

Bardeen, J., and Schrieffer, J. R.: *Progress in Low-Temperature Physics*, ed. de Gorter (North-Holland, Amsterdam, 1961), p. 171.

Gennes, P.: *Superconductivity of Metals and Alloys* (Benjamin, Menlo Park, CA, 1966).

Rickayzen, G.: *Theory of Superconductivity* (Interscience, New York, 1965).

Saint-James, D., Thomas, E. J., and Sarma, G.: *Type II Superconductivity* (Pergamon, Oxford, England, 1969).

Schafroth, M. R.: *Solid-State Physics*, Vol. 10, eds. F. Seitz and D. Turnbull (Academic, New York, 1960), p. 488.

Schrieffer, J. R.: *Theory of Superconductivity* (Benjamin, New York, 1964).

Tilley, D. R., and Tilley, J.: *Superfluidity and Superconductivity*, 3d ed. (Adam Hilger, Bristol, England, 1990).

Tinkham, M.: *Introduction to Superconductivity* (McGraw-Hill, New York, 1975).

BACKGROUNDS

Solid-State Physics

Ashcroft, N. W., and Mermin, N. D.: *Solid-State Physics* (Saunders, Philadelphia, 1976).

Harrison, W. A.: *Solid-State Theory* (Dover, New York, 1979).

Haug, A.: *Theoretical Solid-State Physics, I* (Pergamon, Oxford, England, 1972).

Kittel, C.: *Introduction to Solid-State Physics*, 6th ed. (Wiley, New York, 1986).

Mechanics

Goldstein, H.: *Classical Mechanics* (Addison Wesley, Reading, MA, 1950).

Kibble, T. W. B.: *Classical Mechanics* (McGraw-Hill, London, 1966).

Marion, J. B.: *Classical Dynamics* (Academic, New York, 1965).

Symon, K. R.: *Mechanics*, 3d ed. (Addison-Wesley, Reading, MA, 1971).

Quantum Mechanics

Alonso, M., and Finn, E. J.: *Fundamental University Physics, III Quantum and Statistical Physics* (Addison-Wesley, Reading, MA, 1989).

Dirac, P. A. M.: *Principles of Quantum Mechanics*, 4th ed. (Oxford University Press, London, 1958).

Gasiorowitz, S.: *Quantum Physics* (Wiley, New York, 1974).

Liboff, R. L.: *Introduction to Quantum Mechanics* (Addison-Wesley, Reading, MA, 1992).

McGervey, J. D.: *Modern Physics* (Academic Press, New York, 1971).

Pauling, L., and Wilson, E. B.: *Introduction to Quantum Mechanics* (McGraw-Hill, New York, 1935).

Powell, J. L., and Crasemann, B.: *Quantum Mechanics* (Addison-Wesley, Reading, MA, 1961).

Electricity and Magnetism

Griffiths, D. J.: *Introduction to Electrodynamics*, 2d ed. (Prentice-Hall, Englewood Cliffs, NJ, 1989).

Lorrain, P., and Corson, D. R.: *Electromagnetism* (Freeman, San Francisco, 1978).

Wangsness, R. K.: *Electromagnetic Fields* (Wiley, New York, 1979).

Thermodynamics

Andrews, F. C.: *Thermodynamics: Principles and Applications* (Wiley, New York, 1971).

Bauman, R. P.: *Modern Thermodynamics with Statistical Mechanics* (Macmillan, New York, 1992).

Callen, H. B.: *Thermodynamics* (Wiley, New York, 1960).

Fermi, E.: *Thermodynamics* (Dover, New York, 1957).

Pippard, A. B.: *Thermodynamics: Applications* (Cambridge University Press, Cambridge, England, 1957).

Statistical Physics (undergraduate)

Fujita, S.: *Statistical and Thermal Physics, I and II* (Krieger, Malabar, FL, 1986).

Kittel, C., and Kroemer, H.: *Thermal Physics* (Freeman, San Francisco, CA, 1980).

Mandl, F.: *Statistical Physics* (Wiley, London, 1971).

Morse, P. M.: *Thermal Physics*, 2d ed. (Benjamin, New York, 1969).

Reif, F.: *Fundamentals of Statistical and Thermal Physics* (McGraw-Hill, New York, 1965).

Rosser, W. G. V.: *Introduction to Statistical Physics* (Horwood, Chichester, England, 1982).

Sears, F. W., and Salinger, G. L.: *Thermodynamics, Kinetic Theory, and Statistical Thermodynamics* (Addison-Wesley, Reading, MA, 1975).

Terletskii, Ya. P.: *Statistical Physics*, N. Froman, trans. (North-Holland, Amsterdam, 1971).

Zemansky, M. W.: *Heat and Thermodynamics*, 5th ed. (McGraw-Hill, New York, 1957).

Statistical Physics (graduate)

Davidson, N.: *Statistical Mechanics* (McGraw-Hill, New York, 1969).

Finkelstein, R. J.: *Thermodynamics and Statistical Physics* (Freeman, San Francisco, CA, 1969).

Goodstein, D. L.: *States of Matter* (Prentice-Hall, Englewood Cliffs, NJ.

Heer, C. V.: *Statistical Mechanics, Kinetic Theory, and Stochastic Processes* (Academic Press, New York, 1972).

Huang, K.: *Statistical Mechanics*, 2d ed. (Wiley, New York, 1987).
Isihara, A.: *Statistical Physics* (Academic, New York, 1971).
Kestin, J., and Dorfman, J. R.: *Course in Statistical Thermodynamics* (Academic, New York, 1971).
Landau, L. D., and Lifshitz, E. M.: *Statistical Physics*, 3d ed. Part 1 (Pergamon, Oxford, England, 1980).
Lifshitz, E. M., and Pitaevskii, L. P.: *Statistical Physics*, Part 2 (Pergamon, Oxford, England, 1980).
McQuarrie, D. A.: *Statistical Mechanics* (Harper and Row, New York, 1976).
Pathria, R. K.: *Statistical Mechanics* (Pergamon, Oxford, England, 1972).
Wannier, G. H.: *Statistical Physics* (Wiley, New York, 1966).

This page intentionally left blank.

Index